THE UNIVERSITY OF
SYDNEY

Shoreface Response to Sea Level Change and the Evolution of Barrier Coasts

Michael A. Kinsela

School of Geosciences

The University of Sydney

A thesis submitted in fulfilment of the requirements for the degree of

Doctor of Philosophy

April, 2014

Statement of Originality

I declare that the research presented in this thesis is my own original work, except where duly acknowledged in the text, and has not been submitted to any other institution for the award of a degree.

Michael A. Kinsela

14 April, 2014

Cover: Coastal barrier systems at Myall Lakes, NSW (M.A. Kinsela, 2012).

Abstract

This thesis investigates shoreface response to sea level change and the evolution of wave-dominated barrier coasts, for environmental conditions that are typical of late-Quaternary and potential future coastal evolution. A numerical stratigraphic model was calibrated and applied to explore shoreface response rates, using geological records from barrier coasts of southeastern Australian. First, the origins and evolution of preserved coastal barrier systems were examined using an inverse modelling approach, in which the geological evidence was used to constrain aggregated system forcing and morphological response rates. In particular, the role of sea level change in the development and preservation of coastal barrier systems, throughout the last glacial-interglacial cycle and Holocene sea-level highstand, was examined. The site-calibrated models were then applied in hypothetical forward simulations to assess the sensitivity of shoreface response and coastal evolution to sea level change. Variations in overall shoreface geometry, active-shoreface extent and depth-dependent lower-shoreface response, were compared between sea level scenarios and settings. The implications of shoreface response to sea level change for key problems and approaches in stratigraphy, geomorphology and coastal engineering and management were then considered.

Investigation of the origins of Holocene coastal strandplains supported previous suggestions that strandplain progradation was primarily sourced from disequilibrium-stress-induced shoreface sand supply. The simulated contribution from mid- to late-Holocene sea-level fall within the bounds of existing evidence was shown to be insufficient to supply the observed strandplain progradation. Furthermore, dominant external sand supply resulted in barrier deposition well beyond the depth of the present-day barrier toe. The erosion of lower-shoreface sand bodies (e.g. drowned coastal barriers that were overstepped during late transgression) were shown to adequately supply the observed strandplain progradation. Simulation experiments also demonstrated the sensitivity of highstand coastal barrier stratigraphy to late-Quaternary sea level change. The occurrence and stratal architecture of highstand coastal barriers were shown to vary with prior transgressive-barrier behaviour. The interaction between sea level change and substrate physiography controlled barrier-overstepping and barrier-rollover behaviours, which resulted in alternative highstand-barrier stacking. The model experiments also suggested that sea levels in southeastern Australia during Marine Isotope

Stage (MIS) 5a and MIS 3 were 10-15 m higher than indicated by global records from dated relative-sea-level indicators (e.g. corals) and marine oxygen isotope data.

Active-shoreface response made a significant contribution to coastal sediment budgets in all hindcast simulations through provision of an autochthonous sediment supply. The forward simulations demonstrated that for rates of sea level change typical of late-Quaternary coastal evolution and projected sea-level rise, shoreface activity varied from complete time-invariant response to complete depth-dependent response. Specifically, for increasing rates of sea level change from 0.05 to 10 mm/a, the active-shoreface depth limit (h_a) was shown to decrease from the lower shoreface depth limit (h_i) to the surf zone in the simulations considered. Despite marking a conspicuous break in shoreface response to varied forcing over observational timescales, the upper-shoreface depth limit (h_c) did not mark the limit of time-invariant shoreface geometry across the spectrum of forcing scenarios considered. The influence of depth-dependent lower-shoreface response on coastal sediment budgets increased for both decreasing h_a and reduced shelf gradient. For coastal sediment budgets during sea level change, depth-dependent lower-shoreface response was most significant for mesoscale coastal evolution, which is characterised by partial shoreface activity (i.e. $h_c < h_a < h_i$).

Morphokinematic models predict coastal evolution using the migration and geometric evolution of the shoreface feature. Without a sufficient understanding of shoreface response to dynamic forcing, equilibrium-profile models that assume complete time-invariant shoreface geometry are widely used. However, both late-Quaternary coastal change and future coastal response to sea-level rise are mesoscale coastal evolution problems. Thus the reliability of equilibrium-profile models depends on the use of a representative closure depth, which accounts for both variable active-shoreface extent, and depth-dependent lower-shoreface response. In the context of observed and projected sea level rise from 1880-2100, an equilibrium-profile model with a closure depth of h_c best approximated active shoreface response predicted by the dynamic shoreface models. This was attributed to rapidly accelerating sea level rise beyond 1990, resulting in contraction of the active shoreface to h_c. However, the equilibrium model did not consider the potential for enhanced or moderated shoreline retreat due to depth-dependent shoreface response beyond h_a, which depends on the nature of shoreface-shelf disequilibrium beyond h_c. The findings suggest that depth- and timescale-dependent shoreface response limit the reliability of equilibrium-profile models for mesoscale problems.

Acknowledgements

This thesis would not have been possible without the encouragement, assistance, and support that has been provided by many people. First thanks go to my primary supervisor Peter Cowell, for the entertaining and educational discussions from which many of the ideas expressed in this thesis have emerged, and for always encouraging and supporting the development and diversification of my academic experience.

Secondly, thanks must go to Joep Storms from Delft University of Technology, for introducing me to BARSIM and facilitating a visit to Delft early during my candidature. Further thanks are also due to other staff members of the Geocoastal Research Group, who have enriched my academic experience and contributed useful commentary on my work, including, Ana Vila Concejo, Jody Webster and Thomas Hubble. Thanks are also due to Bruce Thom and David Karoly, for the inspiration, awareness and opportunities provided through the Wentworth Group mentoring program.

To my fellow student colleagues (and ex-students) from the Geocoastal Research Group, many thanks are due for the healthy mix of thesis-related musings, venting frustrations, and social distractions along the way. In particular, I am sure that it could not have taken this amount of time to finish without lunchtime research gatherings and field trips to the beach. I am also thankful for the adventures and experiences provided through participation in your research projects. Best wishes to you all!

To my family, I cannot thank all of you enough for providing unconditional support and understanding throughout all of my academic experience. From start to finish, your support has allowed me to indulge in the uncertain and selfish task of a PhD, with the unabating assurance that regardless of any adversities encountered along the way, everything will be alright.

Finally, to my wife Lucie, you have always made every effort to encourage and support the completion of this thesis. From inspiring me with gifts of motivation such as David Branagan's masterful book - *TW Edgeworth David: A Life*, to marrying me during the final, and somewhat stressful, stage of this thesis, and, for copy editing the final document when I could read no more. Above all, your unrivalled ability to distract me from the work, when necessary, has no doubt ensured the conservation of my mind. This thesis would not have happened without you.

To my parents,
for providing a childhood by the coast
and a thirst for lifelong learning.

Contents

List of Figures **xi**

List of Tables **xv**

1 Introduction **1**

1.1 Subject 1

1.2 Objectives 5

1.2.1 Thesis aims and scope 5

1.2.2 Significance of the research 9

1.3 Controls on wave-dominated coastal evolution 10

1.3.1 Geohistorical variables 10

1.3.2 Antecedent substrate 11

1.3.3 Shoreface morphodynamics 12

1.4 Modelling coastal evolution 16

1.4.1 Timescale and model complexity 16

1.4.2 Mesoscale coastal evolution: shoreface dynamic equilibrium . . . 18

1.4.3 Evidence from stratigraphic records 21

1.5 BARSIM model 22

1.5.1 Model overview 22

1.5.2 Shoreface erosion 24

1.5.3 Deposition 26

1.5.4 Previous applications 27

1.6 Thesis organisation 28

2 Barrier Coasts of Southeastern Australia **31**

2.1 Introduction 31

2.2 Regional Setting 33

2.3 Coastal barrier deposition and sea level change 36

2.3.1 Highstand 37

2.3.2 Falling Stage 42

2.3.3 Lowstand 45

2.3.4 Transgression 45

2.4 Late-Quaternary highstand barrier stacking 47

2.4.1 Composite Pleistocene barrier system 50

2.4.2 Horizontally-stacked barrier systems 51

2.4.3 Vertically-stacked barrier systems 55

2.4.4 Solitary Holocene barrier system 56

2.5 Sampling methods 56

2.5.1 Geophysical surveys 57

2.5.2 Drilling and coring 57

2.5.3 Dating methods 58

2.6 Moruya 59

2.6.1 Coastal geomorphology 59

2.6.2 Age data 62

2.6.3 Sediments, stratigraphy and age structure 65

2.7 Forster-Tuncurry 66

2.7.1 Coastal geomorphology 68

2.7.2 Age data 69

2.7.3 Sediments, stratigraphy and age structure 72

2.7.3.1 Northern (Tuncurry) embayment 72

2.7.3.2 Cape Hawke shelf 82

2.7.3.3 Southern (Wallis Lake) embayment 84

2.7.4 Updrift-sink regional sedimentation model 89

2.8 Conclusions 91

3 Shoreface Sand Supply or Sea Level Change? The Origins of Holocene Coastal Strandplains **93**

3.1 Introduction . . . 93
3.1.1 Background . . . 93
3.1.2 Aims . . . 95
3.2 Holocene sea levels and coastal barrier deposition . . . 97
3.2.1 Evidence for mid- to late-Holocene sea level change . . . 97
3.2.2 Shoreface disequilibrium-stress (D-S) response . . . 100
3.3 Methods . . . 103
3.3.1 BARSIM model calibration . . . 104
3.3.1.1 Model assumptions . . . 104
3.3.1.2 Wave climate and substrate characteristics . . . 104
3.3.1.3 Local erosion efficiency . . . 105
3.3.2 Model experiments . . . 110
3.3.2.1 Shoreface disequilibrium-stress response . . . 111
3.3.2.2 External sediment supply . . . 113
3.3.2.3 Relative sea-level fall . . . 114
3.3.2.4 Combined forcing . . . 116
3.4 Results . . . 117
3.4.1 Shoreface disequilibrium-stress (D-S) response . . . 117
3.4.2 External sediment supply . . . 124
3.4.3 Relative sea-level fall . . . 127
3.4.4 Combined forcing . . . 133
3.5 Discussion . . . 139
3.5.1 Sources of mid- to late-Holocene strandplain deposition . . . 139
3.5.1.1 Shoreface disequilibrium-stress response . . . 139
3.5.1.2 External sediment supply . . . 141
3.5.1.3 Relative sea-level fall . . . 144
3.5.1.4 Combined forcing . . . 149
3.5.2 Implications for shoreface response . . . 150
3.5.3 Potential for model dependence . . . 152
3.6 Conclusions . . . 155

4 Origins and Controls of Stacked Coastal Barrier Systems: Lessons From Numerical Experiments at Forster-Tuncurry 159

4.1 Introduction . . . 159
4.1.1 Background . . . 159
4.1.2 Aims . . . 160
4.2 Late-Quaternary sea levels . . . 161
4.3 Methods . . . 167
4.3.1 Sea-level/barrier-age correlation . . . 167
4.3.2 Stratigraphic modelling . . . 167
4.3.2.1 Sea level scenarios . . . 167
4.3.2.2 Simulation experiments . . . 170
4.4 Results . . . 172
4.4.1 Sea-level/barrier-age correlation . . . 172
4.4.2 Simulated coastal barrier stratigraphy . . . 174
4.4.2.1 Fitted sea level (LG-W) . . . 174
4.4.2.2 Modified sea level (LG-M1) . . . 177
4.4.2.3 Modified sea level (LG-M2) . . . 180
4.5 Discussion . . . 183
4.5.1 Last-glacial sea levels and coastal barrier deposition . . . 183
4.5.2 Transgression: barrier overstepping vs. barrier rollover . . . 187
4.5.3 Shoreface response and onshore sand supply . . . 192
4.5.4 Potential for model dependence . . . 193
4.6 Evolution of the coastal barrier systems at Forster-Tuncurry . . . 194
4.6.1 Middle Pleistocene . . . 195
4.6.2 Late Pleistocene . . . 197
4.6.2.1 MIS 5e . . . 197
4.6.2.2 MIS 5c . . . 198
4.6.2.3 MIS 5a . . . 198
4.6.2.4 MIS 3 . . . 200
4.6.3 Holocene . . . 202
4.6.3.1 Post-glacial transgression . . . 202
4.6.3.2 Highstand . . . 203
4.7 Conclusions . . . 204

5 Shoreface Response to Sea Level Change 1: Concepts **207**
5.1 Introduction . . . 207
5.1.1 Background . . . 207
5.1.2 Aims . . . 208
5.2 Shoreface definitions . . . 209
5.2.1 Upper shoreface . . . 211
5.2.2 Lower shoreface . . . 213
5.2.3 Active shoreface . . . 216
5.3 Methods . . . 217
5.4 Simulation results . . . 220
5.4.1 Rate of sea-level change . . . 220
5.4.2 Substrate gradient . . . 227
5.4.3 Site morphodynamic efficiency . . . 232
5.5 Discussion . . . 234
5.5.1 R-dependent shoreface response . . . 234
5.5.1.1 Active shoreface depth limit . . . 234
5.5.1.2 Depth-dependent shoreface response . . . 238
5.5.2 Scale-transcending shoreface definition . . . 243
5.5.3 Implications for late-Quaternary coastal barrier evolution . . . 245
5.5.4 Potential for model dependence . . . 246
5.6 Conclusions . . . 247

6 Shoreface Response to Sea Level Change 2: Examples **251**
6.1 Introduction . . . 251
6.2 Predicting coastline response to climate change . . . 251
6.2.1 Methods . . . 253
6.2.1.1 Accelerating sea-level rise scenario . . . 253
6.2.1.2 Simulation experiments . . . 256
6.2.2 Results . . . 260
6.2.3 Discussion . . . 265
6.3 Falling-stage coastal barrier deposition . . . 271
6.3.1 Methods . . . 271
6.3.1.1 MIS-3 sea-level rise scenarios . . . 271

6.3.1.2 Simulation experiments 275
6.3.2 Results 275
6.3.3 Discussion 279
6.4 Shoreline trajectories and highstand barrier stacking 285
6.4.1 Methods 285
6.4.2 Results 286
6.4.3 Discussion 290
6.5 Conclusions 292

7 Conclusions and Future Work **295**
7.1 Research conclusions 295
7.1.1 Evolution of barrier coasts 296
7.1.2 Sensitivity of shoreface response to sea level change 298
7.2 Limitations and opportunities for future research 302
7.2.1 Available datasets 302
7.2.2 Modelling approach 303
7.2.3 Potential for model dependence 305

References **307**

A BARSIM Model Configurations **327**

B Holocene Relative Sea-Level Fall Simulation Outputs **329**

C Holocene Combined Forcing Simulation Outputs **337**

D Highstand Barrier Deposition at Forster-Tuncurry **345**

List of Figures

1.1 Spatial and temporal scales of coastal evolution 4
1.2 Geometric equilibrium-profile model of coastal evolution 11
1.3 Coastal morphodynamic systems and shoreface response 15
1.4 Schematic of BARSIM model domains and sediment fluxes 24

2.1 Southeast Australian margin setting 35
2.2 Systems Tract classification of shallow-marine stratigraphy 36
2.3 Coastal barrier deposition during sea-level highstand 38
2.4 Rates of Holocene strandplain progradation in SE Australia 40
2.5 General model of transgressive and falling-stage deposition on barrier coasts 44
2.6 Stratigraphy of highstand barrier-stacking relationships 48
2.7 Highstand barrier-stacking relationships in southeastern Australia . . . 49
2.8 Coastal geomorphology of the Port Stephens-Myall Lakes region 52
2.9 Stratigraphy of the Newcastle Bight embayment 54
2.10 Geomorphology and Quaternary geology of the Moruya region 60
2.11 Legend for Quaternary subsurface sediment distributions 61
2.12 Age structure of the Holocene barrier system at Moruya from radiocarbon dating 63
2.13 Geomorphology and Quaternary geology of the Forster-Tuncurry region 67
2.14 Interpreted drill holes from the Forster-Tuncurry region 73
2.15 GPR profile across the Tuncurry composite strandplain 74
2.16 Tuncurry Holocene barrier sedimentology and age data 77
2.17 GPR profile across the Tuncurry Holocene strandplain 79
2.18 Forster-Tuncurry shallow-marine seismic profiles 1 and 13 81

2.19 Forster-Tuncurry shallow-marine seismic profiles 24/25, 28 and 31 . . . 83
2.20 Forster-Tuncurry shallow-marine seismic profiles 39, 48 and 51 86
2.21 Interpreted stratigraphic sections from the Forster-Tuncurry region . . . 88
2.22 Updrift-sink sedimentation model for the Forster-Tuncurry region 90

3.1 Revised Holocene sea level curve for SE Australia 99
3.2 Sediment accommodation in graded, under-fit and over-fit shelf settings 102
3.3 Moruya BARSIM erosion efficiency calibration 108
3.4 Tuncurry BARSIM erosion efficiency calibration 109
3.5 Sea level scenarios applied in Holocene highstand models 116
3.6 MR-ST-DS simulation experiment, see Table 3.1 118
3.7 TC-ST-DS simulation experiment, see Table 3.1 120
3.8 TC-ST-DS-Q2 simulation experiment, see Table 3.1 122
3.9 BARSIM grain-size distributions: MR-ST-DS and TC-ST-DS-Q2 123
3.10 MR-ST-Q10 simulation experiment, see Table 3.1 125
3.11 TC-ST-Q7 simulation experiment, see Table 3.1 126
3.12 MR-ST simulation experiment, see Table 3.1 128
3.13 Simulated strandplain progradation due to relative sea-level fall at Moruya 129
3.14 TC-ST simulation experiment, see Table 3.1 131
3.15 Simulated strandplain progradation due to relative sea-level fall at Tuncurry 132
3.16 Initial shoreface morphology for combined forcing experiments at Moruya 134
3.17 Simulated strandplain progradation due to combined forcing at Moruya 135
3.18 Initial shoreface morphology for combined forcing experiments at Tuncurry 136
3.19 Simulated strandplain progradation due to combined forcing at Tuncurry 137
3.20 Volume difference between initial shoreface sand bodies 138
3.21 Stratigraphic evidence for location of shoreface toe at Tuncurry 143
3.22 MR-SL-EQ geometric-equilibrium sea-level fall models for Moruya . . . 146
3.23 TC-SL-EQ geometric-equilibrium sea-level fall models for Tuncurry . . . 147

4.1 Late-Quaternary sea level records from coral datasets 164
4.2 Continuous late-Quaternary sea level records 165
4.3 Speleothem evidence for MIS-5a sea levels near PMSL 166
4.4 Sea level scenarios applied in Tuncurry last-glacial cycle models 169

4.5 Late-Quaternary sea levels and coastal barrier deposition at Forster-Tuncurry . . . 173
4.6 Simulated stratigraphy for last-glacial LG-W sea level at Tuncurry . . . 176
4.7 Simulated stratigraphy for last-glacial LG-M1 sea level at Tuncurry . . . 179
4.8 Simulated stratigraphy for last-glacial LG-M2 sea level at Tuncurry . . . 182
4.9 Interpreted and simulated last-glacial stratigraphy at Tuncurry . . . 186
4.10 Highstand barrier establishment by transgressive-barrier overstepping and rollover . . . 191

5.1 Morphodynamic definition of the shoreface . . . 211
5.2 Limits of timescale- and depth-dependent shoreface response . . . 215
5.3 Tuncurry 80-m sea level fall at -10 mm/a for shelf gradient 0.15° . . . 222
5.4 Tuncurry 80-m sea level fall at -5 mm/a for shelf gradient 0.15° . . . 223
5.5 Tuncurry 80-m sea level fall at -2.5 mm/a for shelf gradient 0.15° . . . 224
5.6 Tuncurry 80-m sea level fall at -1 mm/a for shelf gradient 0.15° . . . 225
5.7 Tuncurry 80-m sea level fall at -0.5 mm/a for shelf gradient 0.15° . . . 226
5.8 Tuncurry 80-m sea level fall at -2.5 mm/a for shelf gradient 0.225° . . . 228
5.9 Tuncurry 80-m sea level fall at -2.5 mm/a for shelf gradient 0.30° . . . 229
5.10 Tuncurry 80-m sea level fall at -10 mm/a for surveyed shelf . . . 230
5.11 Tuncurry 80-m sea level fall at -1 mm/a for surveyed shelf . . . 231
5.12 Moruya 80-m sea level fall at -2.5 mm/a for shelf gradient 0.30° . . . 233
5.13 Controls on shoreface response to sea-level change . . . 236
5.14 Influence of substrate slope on coastal barrier deposition during sea-level fall . . . 242

6.1 Historical record of global mean sea-level change . . . 254
6.2 Projected global mean sea-level rise relative to measurement data . . . 255
6.3 Accelerating sea level scenario applied in sea-level rise models . . . 256
6.4 Simulated coastline response at Moruya, 1880-2100 . . . 261
6.5 Predicted shoreline retreat at Moruya, 1880-2100 . . . 262
6.6 Simulated coastline response at Tuncurry, 1880-2100 . . . 263
6.7 Prediction shoreline retreat at Tuncurry, 1880-2100 . . . 264
6.8 Extrapolated shoreface response timescales from Gold Coast dataset . . . 269
6.9 Sea level scenarios applied in Tuncurry MIS-3 falling-stage models . . . 274

6.10 Simulated falling-stage coastal barrier deposition at Tuncurry 278
6.11 Lagrangian shoreface profiles from Tuncurry MIS-3 simulations 279
6.12 Interpreted and simulated MIS-3 stratigraphy at Tuncurry 281
6.13 Seismic reflection line across the continental shelf off Ballina 284
6.14 Depositional response to 60-m sea-level fall based on complete time-invariant and dynamic shoreface responses 288
6.15 Depositional response to 60-m sea-level rise based on complete time-invariant shoreface response 289

B.1 MR-HL1 simulation experiment, see Table 3.1 330
B.2 MR-HL2 simulation experiment, see Table 3.1 331
B.3 MR-HL3 simulation experiment, see Table 3.1 332
B.4 TC-HL1 simulation experiment, see Table 3.1 333
B.5 TC-HL2 simulation experiment, see Table 3.1 334
B.6 TC-HL3 simulation experiment, see Table 3.1 335

C.1 MR-HL1-DS simulation experiment, see Table 3.1 338
C.2 MR-HL2-DS simulation experiment, see Table 3.1 339
C.3 MR-HL3-DS simulation experiment, see Table 3.1 340
C.4 TC-HL1-DS-Q2 simulation experiment, see Table 3.1 341
C.5 TC-HL2-DS-Q2 simulation experiment, see Table 3.1 342
C.6 TC-HL3-DS-Q2 simulation experiment, see Table 3.1 343

D.1 Highstand barrier deposition at Forster-Tuncurry: Stages 1-3 346
D.2 Highstand barrier deposition at Forster-Tuncurry: Stages 4-7 347

List of Tables

2.1 Radiocarbon age data for the Moruya strandplain 64
2.2 Thermoluminescence age data for the Forster-Tuncurry region 70
2.3 Radiocarbon age data for the Forster-Tuncurry region 71

3.1 BARSIM Holocene simulations matrix 111
3.2 BARSIM onshore sand supply due to relative sea-level fall 144
3.3 Equilibrium onshore sand supply due to relative sea-level fall 148

5.1 Residual shoreface response volumes 240
5.2 Scales of coastal evolution and indicative shoreface response 244

6.1 Shoreface dimensions applied in the dynamic shoreface models 259

A.1 BARSIM model configurations for Moruya and Tuncurry 328

Glossary

AAR - Amino-acid racemisation
A1FI - IPCC scenario A1 Fossil-fuel Intensive
AR4 - Assessment Report Four
BP - Before present
DH - Drill hole
D-S - Disequilibrium stress
FSST - Falling-stage systems tract
FT - Forster-Tuncurry
GPR - Ground-penetrating radar
HL - Holocene
HST - Highstand systems tract
IPCC - Intergovernmental Panel on Climate Change
LG - Last glacial
LIG - Last interglacial
LST - Lowstand systems tract
MIS - Marine Isotope Stage
M-L - Mid to late (prefix)
MR - Moruya
NSW - New South Wales
OSL - Optically-stimulated luminescence
PGMT - Post-glacial marine transgression
PMSL - Present mean sea level
RSL - Relative sea level
ST - Static
TC - Tuncurry
TL - Thermoluminescence
TST - Transgressive systems tract

List of Notations

Morphodynamic systems:

f - system forcing

r - morphological relaxation (response)

t - time

T_r - shoreface relaxation timescale

T_f - system forcing timescale

Geohistorical variables:

R - rate of sea level change

Q - rate of external sediment supply

M - texture of supplied sediments

D - rate of sediment dispersal

P - available fluid power

Morphodynamic setting:

H_{sig} - significant wave height

T_{sig} - significant wave period

D - sediment grain size

BarSim variables:

E - erosion rate

F - sediment flux

F_{add} - external sediment supply

F_{BB} - flux for backbarrier deposition

F_{SF} - flux for shoreface deposition

F_t - total sediment flux volume

G - local erosion efficiency

H - model surface elevation

H_s - model shoreline/sea level height

H_w - model wave base height

S - sedimentation rate

T - total rate of subsidence

α_r - reference shoreface gradient

α_s - mean shoreface gradient

c_d - local dissipation constant

c_e - erosion efficiency rate constant

c_g - local wave climate constant

c_w - event-driven wave climate

d - sediment travel distance

d^* - empirical sediment travel distance

k - shoreface sediment fall-out rate

m - erosion efficiency scaling exponent

w - sampled wave height

w_{fw} - fair-weather reference wave height

x_s - model shoreline position

x_w - model wave base position

z_w - absolute wave base

Shoreface definitions:

d_l - Hallermeier inner limit

d_i - Hallermeier outer limit

x - shoreface distance (positive seaward)

h - shoreface depth (positive depth)

h_c - upper shoreface limiting depth

h_a - active shoreface limiting depth

h_i - lower shoreface limiting depth

h_w - wave base

1

Introduction

1.1 Subject

From a coastal morphodynamics perspective, the shoreface feature [*Johnson*, 1919] is the morphological manifestation of the dynamic relationship between fluid processes and coastal geomorphology [*Wright and Thom*, 1977; *Cowell and Thom*, 1994; *Cowell et al.*, 1999]. The shoreface controls coastal evolution and shoreline migration on wave-dominated barrier coasts by modulating sediment exchanges between the coast and inner-continental shelf [*Oertel*, 1985; *Swift et al.*, 1985; *Roy et al.*, 1994]. Any change in system boundary conditions (e.g. sea level, wave climate, sediment supply) can be expected to instigate a response from the morphodynamic system, in which sediment exchanges across the shoreface drive the evolution of coastal morphology and shoreline migration [*Cowell et al.*, 2003a]. For stable sea level conditions, and where a sedimentary substrate prevails, the geometry of the shoreface profile describes the relationship between the hydrodynamic and sedimentary regimes, within the context of the inherited continental-shelf surface [*Dean*, 1977; *Niedoroda et al.*, 1985a; *Dean*, 1991; *Inman et al.*, 1993]. In response to a change in *allochthonous* (external) sediment supply, enhanced deposition or erosion across the upper shoreface drives shoreline progradation and retrogradation respectively [*Curray*, 1964]. In response to changing sea level, the migration of an erosional shoreface environment across the continental shelf may also generate an autochthonous sediment supply [Sec. 1.3.1] through reworking of the shelf substrate [*Swift and Thorne*, 1991; *Roy et al.*, 1994].

The fundamental role of the shoreface in the generation and exchanges of sediment

volumes that drive wave-dominated coastal evolution has two implications central to the ideas and approaches presented in this thesis. These include:

1. Where the nature of past boundary conditions (i.e. system forcing) can be constrained, preserved depositional records may provide evidence of the migration and geometric evolution of the shoreface in response to dynamic forcing.

2. Where the nature of future boundary conditions can be estimated, the shoreface provides a means by which to predict coastal evolution and shoreline migration.

The first point alludes to the significance of geological records as a potential source of evidence for constraining the nature and rates of shoreface response to changing boundary conditions. Coastal barrier systems contain geological records of wave-dominated coastal evolution that represent the depositional outcome of the interaction between dynamic boundary conditions and internal system responses [*Roy et al.*, 1994]. These records comprise distinctive morphostratigraphy that is characteristic of different depositional conditions, as defined by rates of sea level change and sediment supply [*Thom et al.*, 1981a; *Thom*, 1984]. At a broad scale, the volumes of preserved barrier deposits represent the lumped outcome of all depositional and erosional processes. At a finer scale, the geometries of buried palaeo-shorefaces and their stratigraphic relationships may provide direct insight to the system boundary conditions at any point in time [*Hampson and Storms*, 2003; *Grossman et al.*, 2006; *Kim et al.*, 2006; *Charvin et al.*, 2009]. Between both scales, the stratigraphy of coastal barrier systems may be used to explore coastal dynamics in response to past environmental conditions. That is, where the behaviour of system boundary conditions and the depositional record are known, coastal barrier systems may provide an opportunity to constrain the nature of internal system dynamics, including rates of shoreface response.

Prospects raised by the second point have been demonstrated previously through the use of geometric models founded on sediment-volume conservation principles (i.e. morphokinematic models). In such models, a user-prescribed shoreface profile is used to predict coastal evolution and shoreline migration in response to changes in sea level and/or external sediment supply rates [*Cowell et al.*, 1995, 2003b; *Stolper et al.*, 2005; *Tortora et al.*, 2009a,b; *Wolinsky and Murray*, 2009; *Moore et al.*, 2010]. The most simplistic geometric models are equilibrium profile models, which are based on the cross-shelf translation of an time-invariant shoreface profile, of geometry defined by the

equilibrium relationship between the hydrodynamic and sedimentary regimes [*Bruun*, 1962, 1983; *Dean and Maurmeyer*, 1983; *Komar et al.*, 1991]. Implicit in equilibrium profile models is the assumption that time-invariant shoreface geometry adequately represents shoreface sediment transport processes for the range of potentially time-varying system forcing considered. That is, it is assumed that timescales of shoreface morphological relaxation are small relative to the timescales of system forcing.

However, the relationship between depth-diminishing shoreface response rates and rates of sea level change (R) remains poorly understood for mesoscale problems [Fig. 1.1], which include unravelling late-Quaternary coastal evolution and predicting future coastal change over decades and centuries to come. For example, timescales of lower shoreface relaxation are anticipated to be on the order of millennia [*Stive and de Vriend*, 1995; *Wright*, 1995; *Cowell et al.*, 2003a], which suggests that time-invariant shoreface geometry may not be a sound assumption across the entire shoreface, for the rates of sea level change that characterise mesoscale problems. Thus the application of morphokinematic models to mesoscale coastal evolution remains problematic due to the potential significance of unconstrained R-dependent lower-shoreface erosion residuals on the inferred cross-shore sediment-volume exchanges.

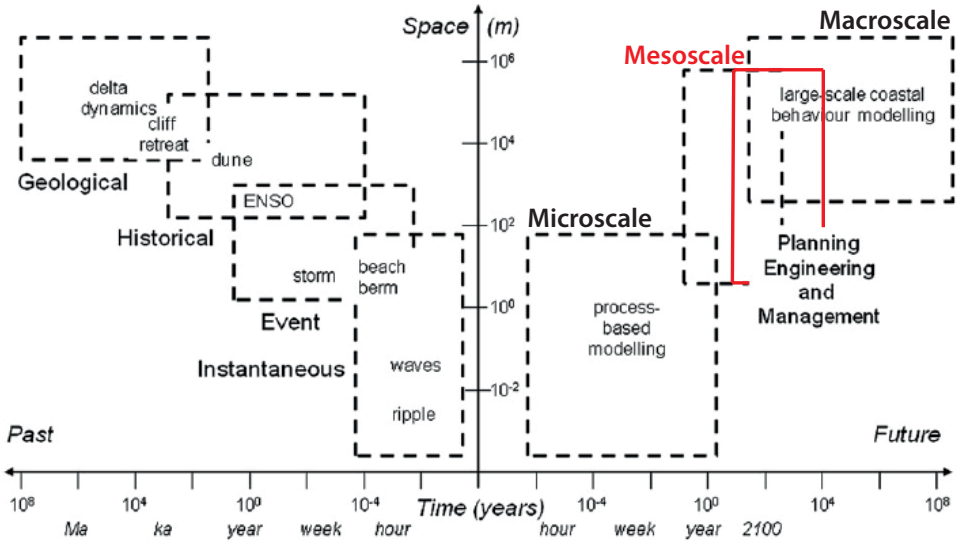

Figure 1.1: Spatial and temporal scales of coastal evolution - Scale classification for coastal depositional systems indicating the physical processes, sedimentary features and modelling approaches characteristic of each domain. The microscale, mesoscale and macroscale domains of *Wolinsky* [2009] are shown to represent natural breaks in spatial and temporal scales and modelling approaches. Modified from *Woodroffe and Murray-Wallace* [2012], after *Gelfenbaum and Kaminsky* [2010].

1.2 Objectives

1.2.1 Thesis aims and scope

The general objectives of this thesis are to investigate shoreface response to sea level change across the timescales of coastal evolution, and to resolve the contribution of shoreface erosion to past and future coastal evolution and shoreline migration. The objectives are explored for wave-dominated barrier-coast settings typical of southeastern Australia, and environmental forcing scenarios typical of the late-Quaternary and projected future conditions. The two general objectives have emerged from the proposition that the evolution of barrier coasts is intrinsically related to the behaviour of the shoreface depositional feature, which regulates sediment exchanges between the coast and shelf [Sec. 1.1].

Isolating shoreface response to sea level change first requires a satisfactory understanding of the environmental setting and the nature of boundary conditions for the system and period of interest [Sec. 1.1]. Depositional records from coastal barrier systems of southeastern Australia provide the physical evidence that is applied in this thesis to constrain the numerical models that are used to explore shoreface response to sea level change. Thus the first part of the thesis discusses the origins of these coastal barrier systems, and the environmental forcing that contributed to their evolution. An inverse stratigraphic modelling approach [Sec. 1.4.3] is applied to constrain rates of sea level change, external sand supply and disequilibrium-stress induced onshore shoreface sand supply, throughout the late-Pleistocene glacial-interglacial cycle and the Holocene sea-level highstand.

Regarding the origins and evolution of Holocene coastal strandplains in tectonically stable accommodation-dominated barrier-coast settings, and the nature of depositional controls during that period, the following questions are considered:

1. Was mid- to late-Holocene (6-0 ka BP) strandplain progradation in southeastern Australia primarily a response to onshore shoreface sand supply driven by morphodynamic disequilibrium, relative sea level fall, or external sand supply from the alongshore transport system?

2. Which conceptual model of onshore shoreface sand supply is most consistent with shoreface processes and the age structures of Holocene strandplains - i.e. depth-

diminishing or depth-constant shoreface lowering? What does this suggest about the origins of onshore shoreface sand supply?

3. Considering the range of potential mid to late-Holocene sea level scenarios, is it likely that shoreface lowering due to relative sea level fall made a significant contribution to Holocene strandplain progradation?

4. Which potential mid to late-Holocene sea level scenario is most consistent with glacio- and hydro-isostatic responses and relative sea level indicators from southeastern Australia? What does this suggest about the contribution of relative sea level fall to Holocene strandplain progradation?

5. What role did the regional northward-directed alongshore transport system play in the Holocene progradation of coastal strandplains? If rates of onshore shoreface sand supply diminished through the late Holocene, were sustained rates of strandplain progradation primarily a response to alongshore sand supply or relative sea level fall?

Regarding barrier-coast evolution in response to late-Quaternary sea level change, and the nature of depositional controls during that period, the following questions are considered:

1. The age structures of composite Pleistocene highstand coastal strandplains in southeastern Australia (and elsewhere) suggest multiple phases of progradation, associated with multiple sea-level highstands, with no preserved evidence of intervening transgression [Sec. 2.4.1]. In contrast, Holocene barrier systems preserve well-developed transgressive and backbarrier facies [Sec. 2.4.2]. Is it possible that composite coastal strandplains formed by recurrent progradation during consecutive sea-level highstands, without the preservation of significant transgressive and backbarrier facies?

2. What depositional conditions favour the deposition and preservation of transgressive and backbarrier facies within highstand coastal barrier systems? Alternatively, what depositional conditions allow for preservation of only regressive strandplain facies?

3. Where both Pleistocene- and Holocene-age coastal barrier systems are preserved in southeastern Australian, they may be arranged in horizontal or vertical stacking arrangements [Sec. 2.4]. What conditions favour the development of horizontally- and vertically-stacked barrier systems?

4. The age structures of drowned barrier systems preserved at inner- to mid-shelf depths suggest deposition during Marine Isotope Stage (MIS) 3, although their origins remain largely unconstrained. What roles did MIS-3 sea level change, disequilibrium-stress induced shoreface sand supply, and alongshore sand supply play in the deposition of drowned barrier systems?

5. Are the age structures and elevations of coastal barrier systems in southeastern Australia consistent with existing late-Quaternary relative sea level records? If not, what does the distribution of barrier systems suggest about late-Quaternary sea levels in southeastern Australia?

Addressing the above questions builds upon the existing state of knowledge regarding late-Quaternary coastal barrier systems, and the simulation experiments provide further evidence to resolve the depositional controls contributing to alternative coastal barrier stratigraphies in southeastern Australia. The geological evidence was first used to calibrate the stratigraphic modelling approach [Sec. 1.4.3] for the sites of interest. The stratigraphic models were then applied to investigate shoreface kinematic response to sea level change in a series of hypothetical exploratory simulations. In those experiments, depositional conditions were controlled in order to test the sensitivity of shoreface response for a range of idealised settings and scenarios. Consideration of all findings then allows for an assessment of the significance of shoreface response in the context of late-Quaternary coastal barrier evolution and future coastal change.

For the investigation of shoreface response to sea level change, this thesis aims to determine for what conditions, if any, is shoreface response [Sec. 1.3.3] sensitive to the rate of sea level change (R). In particular, for conditions typical of late-Quaternary coastal evolution and potential future coastal change, do rates of system forcing exceed depth-dependent shoreface response rates? The following questions are considered:

1. Beyond what typical depth did disequilibrium shoreface morphologies (due to incomplete morphological relaxation) likely persist at the onset of Holocene sea-level highstand in southeastern Australia?

2. Given the age structures of Holocene strandplains in southeastern Australia, and potential mid- to late-Holocene sea level scenarios, what rates of shoreface response were required to generate observed strandplain progradation?

3. Does the nature of contributions from onshore shoreface sand supply, relative sea level fall and alongshore sand supply, to Holocene strandplain progradation, suggest that a significant disequilibrium-induced onshore sand supply persists today?

4. The active shoreface is defined by full time-invariant response for a given value of R. Is the active shoreface limiting depth (h_a) sensitive to rates of sea level change characteristic of the late Quaternary and projected future sea level rise? Is h_a sensitive to between-site variations in shelf geomorphology and morphodynamic efficiency?

5. Is depth-dependent shoreface response between h_a and wave base sensitive to the rate of sea level change and shelf geomorphology? How significant is depth-dependent shoreface response beyond h_a for timescales of relevance to late-Quaternary coastal evolution and predicting future coastal change?

6. Is the assumption of full time-invariant shoreface geometry satisfied for late-Quaternary coastal barrier evolution in southeastern Australia? If not, what was the range of R-dependent shoreface response?

7. Considering the potential for R-dependent shoreface response, are geometric equilibrium models capable of reliable predictions of late-Quaternary evolution?

8. Is the assumption of time-invariant shoreface geometry satisfied for the case of future coastal change in response to accelerated sea level rise? If not, do the predictions of models that take into account dynamic shoreface response differ from those based on geometric equilibrium profile models?

9. Are shoreline trajectories sensitive to R-dependent shoreface response? Is there a more suitable geometric measure for describing shoreface response to sea level change?

1.2.2 Significance of the research

Regardless of increased efforts in field and laboratory studies of coastal processes, and technological advances in measuring and monitoring capabilities, little remains known about shoreface change beyond the surf zone [*Cowell et al.*, 1999]. Whilst it has been proposed that shoreface relaxation timescales (T_r) increase with water depth [*Stive and de Vriend*, 1995; *Storms et al.*, 2002], a quantitative general relationship for lower-shoreface T_r is yet to be established. Complex hydrodynamics, as well as gradual rates of residual sand transport and surface response, impair empirical investigations of shoreface response beyond the upper shoreface [*Nicholls et al.*, 1998; *Hinton and Nicholls*, 2007], limiting our understanding of sediment-volume exchanges across the shoreface using present approaches and tools [*Niedoroda and Swift*, 1991; *Cowell et al.*, 1999]. For engineering applications such as beach nourishment programs, shore-normal sediment exchanges outside of the surf zone may be beyond the scope or assumed to be negligible for the project timescale [*Dean*, 2002]. For coastal management problems that manifest at decadal and longer timescales, however [Fig. 1.1], such as planning for coastal response to projected sea level rise, cross-shelf sediment exchanges associated with shoreface response remain a source of uncertainty with indistinct bounds. Analogous to constraining future sea level scenarios, resolving uncertainties relating to internal coastal system responses may improve the reliability of advice available to decision makers responsible for coastal planning and management.

In addressing the above questions [Sec. 1.2.1] using a stratigraphic modelling approach [Sec. 1.4.3], an attempt is made here to constrain the bounds of sensitivity in shoreface response and onshore shoreface sand supply under both stable and dynamic sea level conditions. Computer modelling can be used as a tool to explore coastal dynamics, supplementing field studies that provide the physical evidence suitable for calibrating model configurations [*Cowell et al.*, 2003b; *Storms et al.*, 2008]. For cases where depositional controls (e.g. sea level, alongshore sediment budget) can be resolved to a reasonable level of confidence, computer modelling provides a means by which to explore internal system behaviour, such as depth-dependent shoreface response rates. The research reported in this thesis considers the range of sensitivity of shoreface response and coastal evolution, for sea level conditions typical of the recent geological past and potential future scenarios. In this way the approaches and findings of this

thesis aim to provide initial boundaries for shoreface response to sea level change, from which future efforts employing additional datasets and improved techniques may work to further advance our understanding of wave-dominated coastal morphodynamics.

1.3 Controls on wave-dominated coastal evolution

1.3.1 Geohistorical variables

Extending earlier work on the relationship between key depositional controls and patterns of continental shelf sedimentation [*Sloss*, 1962; *Curray*, 1964], *Swift and Thorne* [1991] proposed a general model in which accommodation-dominated and supply-dominated sedimentary regimes were defined based on the interaction of four geohistorical variables. The variables describe the dominant depositional controls on shelf sedimentation, and include; the rate of sediment supply (Q), the texture of supplied sediments (M), the rate of relative sea level change (R), and the rate of dispersive sediment transport (D). Applying their regime concept, accommodation-dominated settings are simply defined by $RD/QM > 1$ and supply-dominated settings by $RD/QM < 1$. The sedimentary regime has implications for the nature of coastal deposition during sea level change, with accommodation-dominated settings characterized by *autochthonous* (i.e. of *in situ* origin) sedimentation, and supply-dominated settings characterized by *allochthonous* (of far-travelled origin) sedimentation. The regime model provides a simple framework to guide the design of quantitative stratigraphic models.

According to the general model of *Swift and Thorne* [1991], a fifth variable fluid power (P) controls sediment transport rates across the shelf and thus modulates rates of sediment input at a given location. For wave-dominated settings the magnitude of P diminishes with increasing depth, contributing to the classical concave-up geometry of the shoreface-inner shelf profile [*Wright*, 1995]. The regime concept may be applied quantitatively using the simple assumption that an equilibrium shoreface profile is maintained regardless of any change in the geohistorical variables. That is, shoreface processes allow for instantaneous profile adjustment, and thus coastal deposition and shoreline migration may be described by sea level change and the cross-shelf translation of a time-invariant shoreface profile [Fig. 1.2]. These principles are fundamental to the application of geometric equilibrium profile models in coastal engineering [*Bruun*, 1962, 1983, 1988; *Dean*, 1991] and stratigraphy [*Posamentier et al.*, 1988; *Cant*, 1991;

Nummedal et al., 1993]. As demonstrated in Figure 1.2, the regime concept implies that shoreface migration may be forced by either relative sea level change (R-dependent case) or the rate of sediment supply (Q-dependent case). In each case coastal evolution and shoreline migration are driven by the dominant geohistorical variable, and shoreface response to the change in system forcing is assumed to be instantaneous [Fig. 1.2].

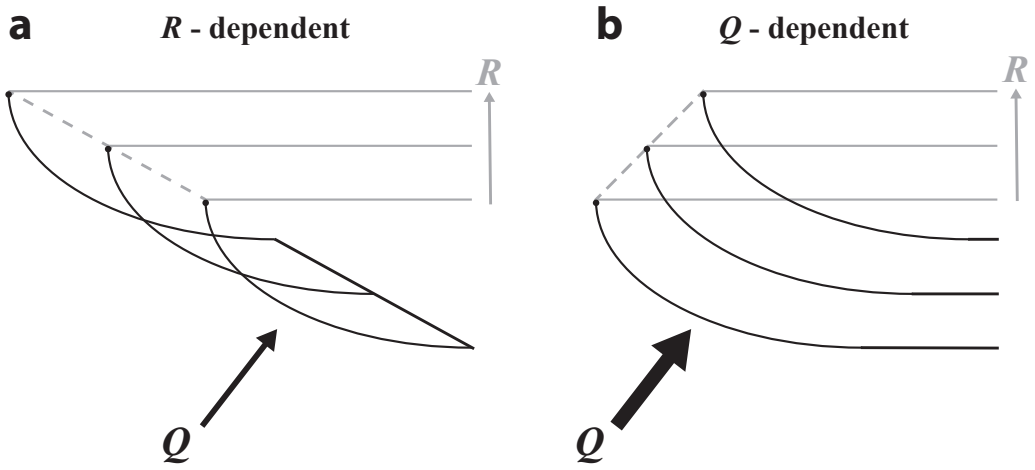

Figure 1.2: Geometric equilibrium-profile model of coastal evolution - Deposition and shoreline migration is driven by translation of the shoreface environment in response to altered system forcing. In the R-dependent case, sea level rise and low rates of external sediment supply (thin arrow) drives erosional shoreface retreat. In the Q-dependent case, a high rate of external sediment supply (thick arrow) drives progradation under the same rising sea level conditions. Modified from *Thorne and Swift* [1991].

1.3.2 Antecedent substrate

The antecedent substrate controls the balance between geohistorical variables in any depositional system through its influence on both the available and potential sediment accommodation [*Sloss*, 1962]. On the other hand, the antecedent substrate may also contribute a significant autochthonous sediment supply through the process of shoreface erosion [*Swift et al.*, 1991]. For barrier coastlines, the antecedent substrate is a determining factor in the development and preservation of coastal barrier systems [*Roy et al.*, 1994]. For example the nature of coastal barrier systems on contemporary highstand

coasts has been shown to vary depending on geological framework of the coastline [*Roy and Thom*, 1981; *Belknap and Kraft*, 1985; *Evans et al.*, 1985]. Furthermore, during marine transgression and regression [*Curray*, 1964] the antecedent substrate represents a basic control on shoreline trajectories [*Helland-Hansen and Martinsen*, 1996; *Helland-Hansen and Hampson*, 2009], imposing gross boundaries on shoreline migration, within which the geohistorical variables and system dynamics interact to determine coastal evolution. Numerical stratigraphic models have been used to demonstrate the significance of substrate slope as a depositional control during sea level change, influencing both the development and preservation of coastal barrier systems [*Roy et al.*, 1994; *Dillenburg et al.*, 2000; *Tortora et al.*, 2009b].

1.3.3 Shoreface morphodynamics

In this thesis, 'shoreface response' refers to the kinematic behaviour of the shoreface profile in response to a change in system forcing (e.g. sea level change). Depending on the nature of both forcing and the antecedent substrate, shoreface response may involve either the active or passive adjustment of the shoreface profile, or both. *Active shoreface response* refers to the wave-driven adjustment of the shoreface profile, in response to morphodynamic disequilibrium between the ambient hydrodynamic regime and the inherited substrate. This may be distinguished from *passive shoreface response*, which refers to adjustments of the shoreface profile that are driven by passive inheritance of the antecedent substrate. In a closed system, active shoreface response generates an autochthonous sediment supply volume [*Swift et al.*, 1991], which may result in a positive contribution to the coastal sediment budget where net shoreface sediment transport is onshore. Here this is referred to as (onshore) shoreface sand supply, in recognition of the net shoreward transfer of sediments to the coast under stable conditions for the settings considered here [*Cowell et al.*, 2001, 2003b]. Whilst passive shoreface response does not contribute directly to the sediment budget, it acts as a depositional control through modification of the hydrodynamic regime and accommodation volume, resulting in the internal sediment redistributions within the sediment-sharing system.

Consideration of only the geohistorical variables [Sec. 1.3.1] and the antecedent shelf substrate [Sec. 1.3.2] paints an overly simplistic picture of coastal evolution and the formation of shallow-marine stratigraphy. This is because rather than being directly affected by the geohistorical variables, the inherited antecedent substrate is embedded

within the coastal morphodynamic system [*Wright and Thom*, 1977]. The additional complexities of coastal evolution that are not captured within simple geometric equilibrium profile models arise due to feedback between dynamic topography and fluid motions. The relationship between the geohistorical variables and the morphodynamic system is described in Figure 1.3a, in which the antecedent substrate is denoted by 'Topography and Stratigraphy'. Feedback may be negative (self regulating) or positive (self organising), with reversals in behaviour marking thresholds between different system responses [*Cowell and Thom*, 1994]. The outcome of feedback within the morphodynamic system is state-determining morphological behaviour, in which the continuous evolution of 'initial conditions' (e.g. antecedent substrate) determines the subsequent behaviour of the system [*Cowell and Thom*, 1994]. Coupled with the stochastic nature of the geohistorical variables [Sec. 1.3.1] in reality, state-determining behaviour gives rise to Markovian inheritance of the antecedent substrate by subsequent morphodynamic states [*Wright and Thom*, 1977].

Although the qualitative mechanics of coastal morphodyamic systems are relatively well documented in the literature, quantitative predictions remain problematic due to uncertainties regarding morphological relaxation timescales (T_r): i.e. the time required for morphological adjustment to attain a new equilibrium with altered boundary conditions. The required time is dependent on sediment transport rates and is constrained by the frequency-response characteristics of the system [*Cowell and Thom*, 1994]. Unfortunately uncertainties regarding T_r appear to be most acute for mesoscale problems, which are of particular relevance to coastal planning and management [Fig. 1.1]. Figure 1.3b shows the hypothesised implications of the relationship between T_r and the forcing timescale (T_f) for shoreface response as depicted in morphokinematic models [Fig. 1.2]. Considering sea level fall in this example, for $T_r \leq T_f$ the equilibrium shoreface form is maintained and the model is analogous to a geometric equilibrium model [Fig. 1.2a]. For $T_r > T_f$ however, morphological relaxation time exceeds the rate of system forcing, and equilibrium profile geometry is not maintained across the entirety of the shoreface. Specifically, rates of surface response (i.e. sediment transport) across the lower shoreface are insufficient to sustain equilibrium profile geometry for the rate of system forcing. This is most apparent in the difference in migration of the shoreface toe between the two cases [Fig. 1.3b]. Borrowing from *Thorne and Swift* [1991], the term 'R-dependent shoreface response' is used in this thesis to describe the situation

where $T_r > T_f$. That is, where shoreface response is sensitive to the rate of sea level change (R).

Whilst Monte Carlo modelling techniques and Bayesian frameworks provide a means to explore the statistical probabilities of system outcomes under a stochastic forcing climate [*Cowell et al.*, 2006; *Gutierrez et al.*, 2011], model predictions remain subject to assumed morphological relaxation timescales. For wave-dominated coasts the most significant uncertainty relates to shoreface response timescales, and in particular, rates of depth-dependent lower shoreface response [*Cowell et al.*, 1999]. For example, whilst upper shoreface response timescales may be considered instantaneous in the context of large-scale coastal behaviour, unconstrained depth-dependent lower shoreface response varies with the timescale of the problem [*Stive and de Vriend*, 1995; *Cowell et al.*, 2003a]. In practice, rates of active shoreface response may be estimated across the upper shoreface through repeat surveys of profile morphology, although anticipated lower shoreface response timescales imply that rates of profile adjustment are imperceptible in historical datasets. Rather, active shoreface response across the lower shoreface has been inferred empirically from geological records for cases where geohistorical variables are known to have been relatively stable [*Cowell et al.*, 2001]. During sea level change however, interactions between the translating shoreface environment and complex shelf physiography suggests that palaeo-shorefaces represent a combination of active and passive shoreface responses, which may be difficult to isolate. Thus in the context of all controls on wave-dominated coastal evolution, the role of shoreface response is difficult to isolate because it is often subordinate to the influences of more basic and observable controls. The potential significance of shoreface response to coastal evolution across the spectrum of morphodynamic scales is considered in Section 1.4.1.

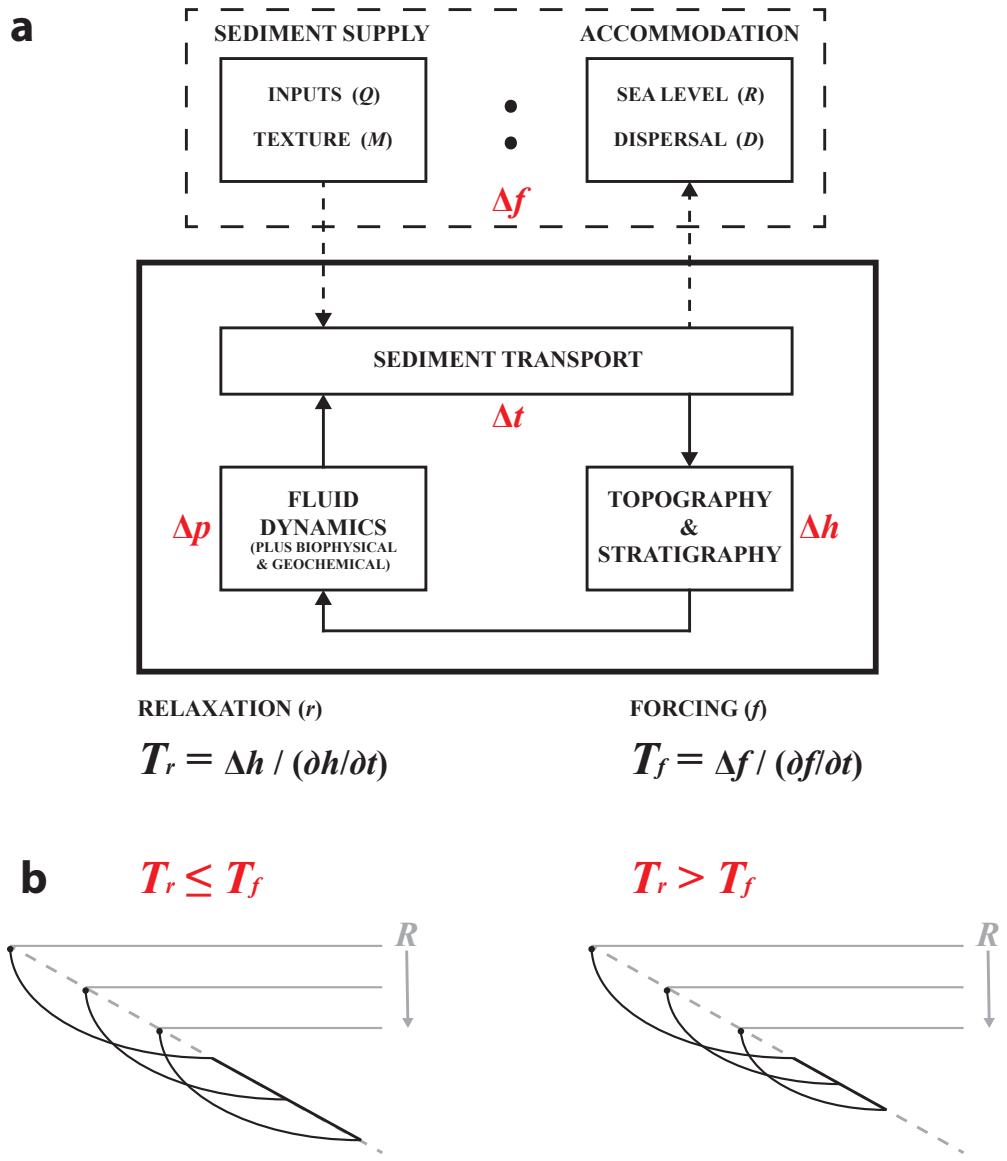

Figure 1.3: Coastal morphodynamic systems and shoreface response - (a) The system is forced by the geohistorical variables (f), which together with coastal topography define the balance between sediment supply (Q) and accommodation (A). Feedback between fluid dynamics (p) and morphology (h) is regulated by time-dependent (t) sediment transport, which controls morphological relaxation time (T_r). Altered system forcing causes mutual change in both morphology and fluid dynamics through the morphodynamic system. Modified from *Cowell and Thom* [1994]. (b) The relationship between T_r and the forcing timescale (T_f) is hypothesised to control shoreface geometry during sea level change, due to the frequency-response characteristics of coastal morphodynamic systems. For $T_r \leq T_f$, the time-invariant shoreface assumption is satisfied. For $T_r > T_f$, geometric equilibrium profile models may over-predict sediment exchanges between coast and shelf, and thus shoreline migration.

1.4 Modelling coastal evolution

1.4.1 Timescale and model complexity

Acknowledging the hierarchical nature of coastal geomorphic systems [*Cowell et al.*, 2003a], *Wolinsky* [2009] developed a unifying framework for shoreline migration to reconcile interrelated problems that transcend the disciplines of coastal engineering (microscale), geomorphology (mesoscale) and stratigraphy (macroscale). More specifically, Wolinsky used a common quantitative basis - the Exner equation - to describe shoreline migration and coastal evolution, and suitable modelling approaches, across the continuum of morphodynamic scales [Fig. 1.1]. He concluded that whilst process-based morphodynamic models could be suitable for solving microscale problems, the unresolved complexity of coastal evolution at longer timescales was best represented by geometric behaviour models.

Beginning with microscale problems, extensive efforts have been made to solve coastal change from first principles using theoretical and semi-empirical hydrodynamic and sediment transport relationships, which have been calibrated and evaluated through field and laboratory experiments [*Komar*, 1998; *Dean and Dalrymple*, 2002]. In the most complex morphodynamic models, many such relationships are consolidated to predict time-dependent two-dimensional surface evolution by simulating flow-driven sediment exchanges across a regular grid or irregular mesh [*Hanson et al.*, 2003; *Fagherazzi and Overeem*, 2007; *Roelvink et al.*, 2009]. However, simpler profile-based theoretical and empirically-derived models have also been developed to predict shoreline response to periodic variations in wave and sea level forcing [*Larson and Kraus*, 1991; *Aagaard and Sorensen*, 2012]. Whilst intensive calibration of process-based models may improve predictions of short-term coastal response to storm events [*Vousdoukas et al.*, 2012], the timescales of reliable application remain limited by the accumulation of error residuals in sediment transport relationships [*Cowell et al.*, 2003b], and the absence of long-term measurement datasets for model calibration and verification [*Thieler et al.*, 2000; *Amoudry and Souza*, 2011].

Although a tantalising prospect, the up-scaling of findings from morphodynamic models to address medium- to long-term coastal evolution problems (that exceed observational timescales) faces further complications, in addition to the accumulation of error residuals associated with inaccurate predictions of sediment transport. That

is, as described in Section 1.3.3, non-linear morphodynamic feedback implies that the cumulative effects of internal system feedback and state-determining morphological behaviour remain unresolved. Considering these constraints, process-based morphodynamic models are not yet capable of addressing some important questions relevant to coastal management and planning: for example, how will coastlines respond to future energy climate variations and sea level change at decadal to centennial timescales?

On the other hand, *Wolinsky* [2009] identified untapped potential in geometric-behaviour (i.e. morphokinematic) approaches, due to the capacity for reliable predictions of macroscale shoreline trajectories and shelf sedimentation using simple and efficient functions. In morphokinematic models, time-integrated processes and morphodynamic feedback are implicit within surface evolution, which is parameterised as a function of shoreline position [*Cowell et al.*, 1995; *Wolinsky*, 2009]. That is, shore-normal sediment transport and shoreline migration are inferred from the behaviour of the model surface, which is constrained by the cross-shore sediment control volume. The control volume itself need not be held constant, but may vary with external sediment exchanges and the evolution of the shoreface surface. This approach has been applied previously to model the morphostratigraphic evolution of coastal sedimentary systems in diverse settings, due to forcing from dynamic sediment budgets and sea level change [*Cowell et al.*, 1995, 2003b; *Stolper et al.*, 2005; *Tortora et al.*, 2009a,b; *Wolinsky and Murray*, 2009; *Moore et al.*, 2010].

Across all disciplines and timescales [Fig. 1.1], however, the application of morphokinematic models has been largely limited to equilibrium-profile models, which are a special case of geometric model in which time-invariant shoreface geometry is assumed [*Wolinsky*, 2009]. Enforced migration of the time-invariant profile, in response to sea level change or variable sediment supply, determines the shoreline trajectory and stratigraphic evolution [Fig. 1.2] through the application of sediment conservation principles. This concept has been widely applied by coastal engineers to predict shoreline retreat in response to sea level rise using the so-called Bruun rule of coastal erosion [*Bruun*, 1962, 1983, 1988]. Equilibrium-profile models have also been applied by stratigraphers to describe and predict sequence architecture and facies migration [*Cant*, 1991; *Nummedal et al.*, 1993; *Posamentier et al.*, 1988].

Whilst morphokinematic models hold the potential to avoid the issues associated with up-scaling temporally limited field studies and process-based simulations [*Cowell*

et al., 1995, 2003b; *Wolinsky*, 2009], implicit in such approaches is the abstraction of coastal processes within surface behaviour, which, depending on the availability of site-specific measurements and the timescale of the problem, may not provide a reliable description of cross-shore sediment transport [*Aagaard and Sorensen*, 2012]. Where a short timescale negates the significant accumulation of sediment transport residuals associated with the depth-dependent shoreface responses, the time-invariant (equilibrium) shoreface assumption may be appropriate. For example, an equilibrium-profile model may be applied to estimate the sand volume required for beach nourishment, where significant cross-shore transport is restricted to the vicinity of the surf zone for the project timescale [*Dean and Dalrymple*, 2002; *Dean*, 2002]. Beyond microscale problems however, some understanding of the extent and rate of surface adjustment for the timescale of interest may be required to constrain depth-dependent rates of shoreface response. Thus in practice the reliability of morphokinematic models may depend on user expertise and the availability of data for model calibration and verification.

Because depth-dependent shoreface relaxation timescales remain poorly resolved [Sec. 1.3.3] the application of morphokinematic models to large-scale coastal behaviour may at first seem questionable. However, for macroscale coastal evolution problems considered by stratigraphers, the timescales of geological records generated by low-order forcing (e.g. tectonically-driven basin-volume adjustments, isostacy, and shifting sedimentation regimes) typically dwarf deposition associated with higher frequency system forcing from climate-driven fluctuations in wave energy and sea level [*Cowell et al.*, 2003a]. Thus for true macroscale problems, the stratigraphic response to prolonged and steady fluxes in boundary conditions may be reasonably estimated using a time-invariant profile [*Sen et al.*, 1999]; and, at the resolution of ancient stratigraphic records, the entire delta foreslope may exhibit time-invariant geometry [*Kim et al.*, 2006], and thus shoreline trajectories may only be sensitive to gross changes in margin geometry [*Helland-Hansen and Hampson*, 2009].

1.4.2 Mesoscale coastal evolution: shoreface dynamic equilibrium

For intermediate (mesoscale) problems, including the societal need to anticipate shoreline retreat due to projected sea level rise over the coming decades and centuries [*Stive*, 2004; *FitzGerald et al.*, 2008; *Nicholls and Cazenave*, 2010], morphokinematic models

appear to have the greatest prospects for success and caveats on reliability [*Wolinsky*, 2009]. Whilst depth-dependent shoreface response may be ignored for macroscale problems [Sec. 1.4.1], for mesoscale coastal evolution shoreface response is characterised by dynamic equilibrium arising from depth-dependent response rates [*Kooi and Beaumont*, 1996] - i.e. $T_r > T_f$ [Sec. 1.3.3]. Thus for high-resolution stratigraphic records of more recent deposition, equilibrium profile models may only describe gross stratal relationships [*Nummedal et al.*, 1993].

Where rates of higher frequency forcing exceed rates of shoreface response, time-varying shoreface geometry may be required to describe shore-normal sediment exchanges that contribute to the observed stratigraphic response [*Storms and Swift*, 2003; *Storms and Hampson*, 2005]. The restriction of equilibrium profile response to the surf zone may ignore significant erosion and/or deposition across the lower shoreface. On the other hand, an assumption of time-invariant profile response across the entire inner shelf may overestimate shore-normal sediment exchanges. In reality, the closure depth (which defines the limit of the time-invariant profile) probably varies with the rate of relative sea level change, through control of the rate of translation of the shoreface environment. Thus it cannot be assumed that shore-normal sediment fluxes beyond closure depth are negligible for intermediate timescales [*Hallermeier*, 1981; *Nicholls et al.*, 1998]. Instead, depth-dependent rates of surface adjustment may become important, and for such cases, slight variations in the geometry of the inherited shelf may be expected to have a more pronounced effect on erosion and sedimentation volumes, and shoreline trajectories.

The time-invariant shoreface assumption places fundamental importance on the existence of, and the ability to identify, an absolute profile 'closure depth' [*Komar et al.*, 1991]. Beyond the closure depth, shore-normal sediment exchanges are considered to be negligible for the setting and timescale of interest [*Dean and Dalrymple*, 2002]. Therefore an inaccurate closure depth will result in an over or under prediction of shore-normal sediment exchanges, with associated implications for predicted shoreline migration and stratal formation. This issue is exemplified in coastal engineering, where considerable effort has been spent on field measurements of closure depth [*Birkemeier*, 1985; *Nicholls et al.*, 1998] and the development of general rules to estimate closure depth for a given wave climate and sediment characteristics [*Hallermeier*, 1981]. Furthermore, considering the influence of the hydrodynamic and sedimentary regimes on

equilibrium profile geometry [*Dean*, 1991], equilibrium profile models are incapable of accommodating changes in hydrodynamics or sedimentary regime within a given scenario. Given these limitations, it appears that the applicability of equilibrium profile models may be restricted to microscale and macroscale problems.

There have been few attempts to consider depth-dependent shoreface response in morphokinematic models, or in any other large-scale modelling approaches. A notable exception is the GEOMBEST model first described by *Stolper et al.* [2005]. GEOMBEST predicts shoreline migration and stratigraphic evolution in response to input forcing (e.g. sea level, sediment supply) and shoreface profile evolution. The shoreface profile is defined by a series of points interpolated by straight lines, which approximate the surveyed shoreface profile or estimated equilibrium profile. GEOMBEST features two notable improvements on earlier morphokinematic models - e.g. Shoreface Translation Model (STM) [*Cowell et al.*, 1995, 2006]: (1) a flexible series of stratigraphic units characterised by varying sand/mud ratios and an erodibility index between 0 (fully-erodible) and 1 (non-erodible); and, (2) a user-defined depth-dependent shoreface response function that allows for instantaneous or depth-decaying shoreface response to the selected closure depth [*Stolper et al.*, 2005]. Whilst depth-dependent shoreface response may be considered using the flexible profile geometry of the STM, the implementation is manual and remains unconstrained by the model morphology.

Moore et al. [2010] applied GEOMBEST to investigate the sensitivity of barrier island evolution in North Carolina to substrate slope and composition, the rate of sea level change, and the sediment supply rate, for Holocene sea level change. The depth-dependent (shoreface) response rate (DDRR) parameter in GEOMBEST is a function of cross-shore distance from the shoreline, and defines the maximum rate of net vertical erosion or accretion that can occur within a specified period of time. In the GEOMBEST models applied by *Moore et al.* [2010], the DDRR decreased linearly from the point of definition at the shoreline to zero at the shoreface toe. They considered DDRR values between 1 and 0.01 m/a in a series of sensitivity experiments. For the setting and Holocene sea level histories considered, they found that for diminishing rates of shoreface erosion below a threshold of DDRR = 0.07 m/a, simulations became unstable due to insufficient shoreface sand supply to the barrier island, which drowned in situ. Of particular interest, the barrier island migration rate, substrate erosion depth and barrier island volume were not sensitive to variations in the DDRR above 0.07 m/a.

Most recently, *Lorenzo-Trueba and Ashton* [2014] presented a simple morphodynamic model that features a time-invariant profile that considers shoreface dynamic equilibrium. Simulated coastal barrier evolution is driven by sea level rise, storm overwash and disequilibrium shoreface response. Simulation experiments carried out using their model suggested that internal system dynamics may lead to previously unidentified complex barrier behaviour. Of particular interest, their model predicted that barriers drown vertically when overwash flux is insufficient to maintain the subaqueous portion of the barrier, and horizontally when shoreface response is insufficient to maintain barrier geometry during landward migration. The simulation experiments further suggested that barrier coasts may experience periodic shoreline retreat in response to constant sea level rise, due to time lags in the shoreface response to barrier overwash. Although highly relevant to the research presented here, the findings of *Lorenzo-Trueba and Ashton* [2014] only became available following the finalisation of this thesis. Thus while they are briefly mentioned here for completeness, their investigation is not considered in the interpretation of the research findings presented here.

1.4.3 Evidence from stratigraphic records

It has been established that whilst morphokinematic models present an attractive approach to solving coastal evolution and shoreline migration problems, uncertainty regarding shoreface response timescales limits their reliability for mesoscale applications [Sec. 1.4.2]. However, coastal barrier systems contain depositional records of shoreface response that may be used as evidence to calibrate shoreface response timescales for geomorphic modelling [*Storms et al.*, 2008]. Such evidence may be accessed using inverse modelling techniques, where environmental variables and system boundary conditions are known [*Charvin et al.*, 2009]. Late Quaternary depositional records are a particularly promising place to search for evidence of the relationship between shoreface response and sea level change, due to the abundance of preserved coastal barrier deposits and relatively well-constrained boundary conditions. Furthermore, both the range and rates of sea level change during that time, and the geological context, are representative of past and potential future mesoscale problems relevant to the geomorphology and coastal management disciplines [*Church et al.*, 2008].

A stratigraphic modelling approach is adopted here to investigate the significance of scale-dependent shoreface response to mesoscale coastal evolution. Depositional records

from coastal barrier systems of southeastern Australia provide the geological evidence that is used to constrain model dynamics and shoreface response rates. First, inverse modelling techniques are applied to constrain model parameters and system boundary conditions during the time of deposition. A forward modelling approach is then applied to explore the sensitivity of shoreface response to rates of sea level change that are typical of late-Quaternary coastal evolution and potential future coastal change. The influences of antecedent substrate and internal system dynamics are also explored. The BARSIM stratigraphic model [Sec. 1.5] is used as a tool to investigate both the relationship between system forcing and shoreface response rates, and the implications for coastal evolution, shoreline migration and stratigraphic preservation.

1.5 BARSIM model

The profile-based numerical stratigraphic model BARSIM (developed by J. E. A. Storms, Delft University of Technology) is used here to investigate late-Quaternary coastal evolution in response to a range of forcing scenarios, and to explore the sensitivity of shoreface response to sea level change. The BARSIM model algorithms have been described in detail previously by *Storms et al.* [2002], *Storms* [2003] and *Storms et al.* [2008]. However, considering that the BARSIM model is a fundamental aspect of the methodology presented in this thesis, on which many of the research findings and major conclusions depend, a concise but comprehensive description is warranted. This section describes the fundamental BARSIM equations that govern the simulated coastal dynamics and depositional responses presented in this thesis. Therefore, the material presented in this section is largely derived from the papers cited above.

1.5.1 Model overview

BARSIM uses process-response behaviour rules, which describe time-averaged sediment transport in a computationally efficient manner, to model coastal evolution without the use of geometric principles [*Storms et al.*, 2002]. Coastal sediment transport processes are considered within lumped parameters and simplifying functions, which control depth-dependent rates of erosion and grain-size-dependent sediment travel distances. The simulated morphostratigraphic evolution is driven by the nature of boundary conditions (e.g. sea level, inherited coastal physiography, external sediment supply) and

internal system dynamics, which manifest in the spatial derivative of shore-normal sediment flux residuals. The latter are constrained by a sediment control-volume, which is a function of the substrate and any external supplies or losses. The primary advantage of using BARSIM to address the research questions considered here [Sec. 1.2.1], is that assumptions regarding time-invariant (or time-varying) shoreface geometry are not needed to predict shoreline migration and coastal evolution. That is, the geometric evolution of the shoreface profile emerges from the interaction between the depth-dependent erosion function and grain-size dependent sediment travel distances.

First and foremost, similar to the morphokinematic models described in Section 1.4, BARSIM uses sediment-mass conservation principles to calculate morphological response to system forcing:

$$\frac{\delta H}{\delta t} = -\frac{\delta F}{\delta x} + T \tag{1.1}$$

where t is time, x is horizontal distance, H is topographic elevation relative to a constant reference level, F is the sediment flux, and T is the rate of subsidence due to the combined effects of compaction, loading and vertical movements of the basin floor. The mass conservation constraint allows for the calculation of morphostratigraphic evolution in response to system forcing through the redistribution of a finite sediment volume (although external sediment supplies are also considered).

Second, the evolution of coastal morphology, shoreline migration, and development of the stratigraphic record, all result from the interaction between the depth-dependent erosion function and grain-size-dependent sedimentation function. Specifically, surface evolution is defined by the spatial derivative of the sediment flux (F), which is calculated as follows:

$$\frac{\delta F}{\delta x} = E(x,t) - S(x,t) \tag{1.2}$$

where $E(x,t)$ is the rate of erosion and $S(x,t)$ is the rate of sedimentation (deposition).

The process-response approach avoids calculating spatially dependent and time-varying sediment exchanges between each element of the coastal profile from first principles, which is a computationally intensive approach. Rather, net volumes of erosion and deposition are calculated across the profile using the spatially varying erosion and deposition functions. In practice, net shoreface erosion, backbarrier deposition and shoreface deposition are calculated and applied in three phases to simulate the generation and redistribution of the sediment flux at each model timestep [Fig. 1.4].

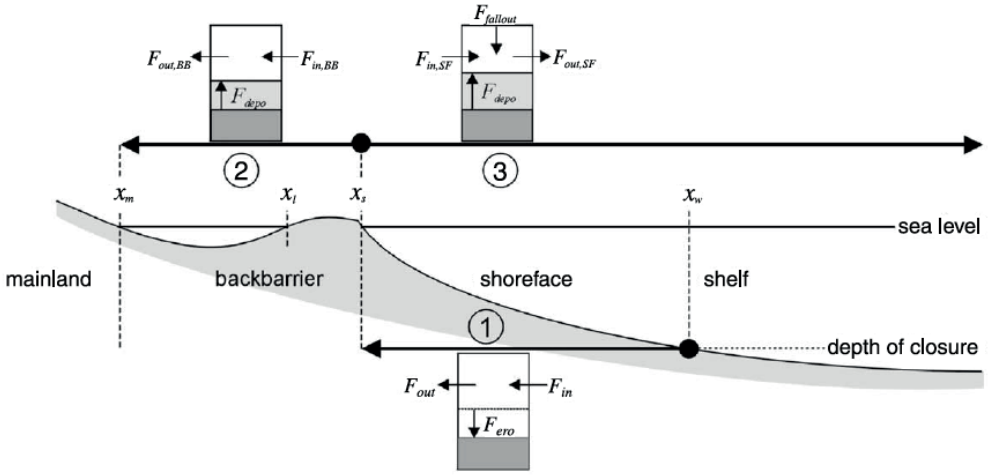

Figure 1.4: Schematic of BARSIM model domains and sediment fluxes - The model algorithm includes three phases of sediment dispersal to describe coastal and shallow-marine deposition: (1) shoreface erosion by wave action, (2) deposition in the backbarrier environment (if present) by tidal inlet and overwash processes, and (3) deposition across the shoreface-inner shelf environment by fallout. From *Storms* [2003].

1.5.2 Shoreface erosion

In Phase 1 the shoreface erosion volume (i.e. the *autochthonous* component of the sand supply volume) is calculated for each grid cell between the shoreline and wave base, using the following erosion function:

$$E(x,t) = c_e \cdot c_d(t) \cdot c_w(t) \cdot G(x,t) \text{ (Phase 1)} \tag{1.3}$$

In Equation 1.3: c_e is the erosion efficiency rate constant (independent of the unconsolidated substrate properties); c_d is the local wave-energy dissipation constant; c_w is the time-dependent wave energy parameter; and, $G(x,t)$ describes local erosion efficiency [Eq. 1.4]. Thus shoreface erosion is both depth and time dependent.

Local erosion efficiency refers to depth-dependent shoreface erosion rates between the shoreline and wave base, and is a function of distance from the shoreline (x) and time (t), as follows:

$$G(x,t) = \left(\frac{H(x,t) - H_w(t)}{H_s(t) - H_w(t)} \right)^m \text{ for } x_s < x < x_w(t) \tag{1.4}$$

$$G(x,t) = 0 \text{ for } x \leq x_s(t) \text{ and } x \geq x_w(t) \tag{1.5}$$

where $x_s(t)$ corresponds to the shoreline defined by the intersection of sea level, $H_s(t)$, and the topographic profile [Fig. 1.4]. Location $x_w(t)$ is defined by the intersection of the wave base ($H_w(t)$) and the topographic profile.

The wave base depth is defined as: $H_w(t) = H_s(t) - z_w(t)$, where $z_w(t)$ is the maximum water depth at which waves affect the seabed. The value of $z_w(t)$ is a function of wave height: $z_w(t) = c_c w(t)$, where c_c is a constant. Thus erosion is restricted to the shoreface domain between $x_s(t)$ and $x_w(t)$. Furthermore, local erosion efficiency at a point $H(t)$ on the shoreface decreases with increasing proximity to wave base ($H_w(t)$), in a manner defined by the local erosion efficiency scaling exponent (m).

The local wave-energy dissipation constant in Equation 1.3 is defined as:

$$c_d(t) = 1 + \frac{\alpha_s(t) - \alpha_r}{\alpha_r} \tag{1.6}$$

where $\alpha_s(t)$ is the mean gradient of the shoreface, and α_r is a reference shoreface gradient. A shallow value of $\alpha_s(t)$ relative to α_r leads to increased wave-energy dissipation and reduced erosion potential between wave base and the coastline.

The time-dependent wave energy parameter in Equation 1.3 scales the sampled wave height $w(t)$ against the fair-weather reference wave height w_{fw}, as follows:

$$c_w(t) = \frac{w(t)}{w_{fw}} \tag{1.7}$$

Large waves relative to w_{fw} increase the erosion potential.

An event-driven wave climate was implemented by *Storms* [2003] to enable the simulation of intra-parasequence stratigraphic architecture. The event-driven wave climate features periods of fair-weather conditions characterised by gradual sediment transport, which are interspersed with high-energy events during which large sediment volumes are transported. Wave heights ($w(t)$) are sampled stochastically. Storm conditions, defined by waves exceeding w_{fw}, last for short periods only, during which washover and shoreface deposition are dominant. On the other hand, fair-weather conditions between successive storms may last for several years in BARSIM, and are characterised by lower rates of erosion and deposition.

The total sediment volume (in cubic metres) available for deposition (F_t) in Phase 2 & Phase 3 is the sum of the shoreface erosion volume (i.e. the *autochthonous* supply)

and any *allochthonous* supply (or loss) (F_{add}), derived from external sediment sources such as the littoral drift system:

$$F_t(t, D) = \sum_{x=x_s}^{x=x_w} [E(x, t) \cdot (x_s(t) - x_w(t))] + F_{add}(t, D) \tag{1.8}$$

1.5.3 Deposition

Deposition in BARSIM is divided into two discrete phases, in which the available sediment volume $F_t(t)$ [Eq. 1.8] is distributed between the backbarrier (Phase 2) and shoreface (Phase 3) environments. To satisfy Equation 1.1, the total $F_t(t)$ volume must be deposited between Phase 2 & Phase 3. That is, $F_t(t) = F_{BB} + F_{SF}$.

If backbarrier accommodation exists, a proportion of F_{BB} that varies with BARSIM tidal deposition parameters is deposited in the lagoon. The Phase 2 backbarrier deposition function is as follows:

$$S(x, t, D) = \frac{F_{BB}(x, t, D)}{d(D)} \text{ for } x \leq x_s \text{ (Phase 2)} \tag{1.9}$$

where F_{BB} is the flux of sediment that is available for deposition, and d is the sediment travel distance (grain-size dependent), which depends on the grain size and the environment of deposition (i.e. the flow properties of the transporting medium).

The rate of tidal backbarrier deposition is a linear function of tidal prism (tidal amplitude x basin width) [*Storms et al.*, 2008]. In the absence of washover processes during fair-weather wave conditions, all sediment eroded from the shoreface is potentially available for tidal deposition. However, the grain-size distribution of sediments available for tidal deposition is different from that of the shoreface sediment. In BARSIM, it is assumed that deposition of the sand fraction is limited to the tidal channel, and tidal-flat deposits are much finer grained. The proportion of F_{BB} sand-size sediment that is available for tidal deposition can be varied with a user-defined parameter.

Following backbarrier deposition, the remainder of the total sediment flux (F_{SF}) is deposited across the shoreface and shelf as follows:

$$S(x, t, D) = \frac{F_{SF}(x, t, D)}{d(D)} + k(t, D) \text{ for } x > x_s \text{ (Phase 3)} \tag{1.10}$$

where k is a steady fall-out rate of fine sediment in calm water across the shoreface-shelf domain. If included, k essentially represents a uniform shoreface-shelf aggradation rate that is independent of $F_t(t)$.

The net effects of size-selective transport are simulated through the size dependence of the travel distance (d) in the deposition functions. Cross-shore sediment dispersal is described by the following relationship between the nominal grain diameter (D) and sediment travel distance, for the case of a 50-m profile grid increment (d^*):

$$d^*(D) = c_g(x) \cdot c_w(t)[110 + 590(\frac{D_{ref}}{D})^{2.5}] \text{ for } D > D_{ref} \tag{1.11}$$

$$d^*(D) = c_g(x) \cdot c_w(t)[500 + 200(\frac{D_{ref}}{D})^{0.6}] \text{ for } D \leq D_{ref} \tag{1.12}$$

where $D_{ref} = 0.125$ mm, as the dominant mode of transport in fully turbulent unidirectional flows of sediment below this size is in suspension, whereas sediments above this size are transported mostly as traction load. Sediment transport capacity depends on wave height as waves generate onshore-directed currents during storms. However, these currents lack during fair-weather conditions. The constant $c_w(t)$ accounts for the temporal variability of wave height [Eq. 1.7], whilst the constant $c_g(x)$ accounts for local conditions. The value of $c_g(x)$ varies for deposition across the shoreface-shelf and backbarrier domains. Where the user-defined profile grid increment varies from 50 m an additional transformation is applied, such that:

$$d^*_{adj}(D) = \frac{\Delta x}{[1 - (1 - \frac{50}{d^*(D)})^{0.02\Delta x}]} \tag{1.13}$$

The travel distances have been calibrated with data from Terschelling, The Netherlands.

1.5.4 Previous applications

Following development of the process-response modelling approach [*Storms et al.*, 2002], and the implementation of event-drive erosion and deposition [*Storms*, 2003], BARSIM has been applied as a modelling tool in numerous studies. For example, BARSIM has been used to unravel the intricacies of fine-scale deposition in shoreface-shelf environments, as observed in high-resolution stratigraphy [*Hampson and Storms*, 2003; *Storms and Swift*, 2003; *Storms and Hampson*, 2005], and to investigate coastal dynamics during rapid sea-level rise [*Storms et al.*, 2008]. More recently, BARSIM has been applied within an inverse modelling framework to investigate key environmental parameters (e.g. sea level change, sediment supply) that control stratigraphy [*Charvin et al.*, 2009]. The reproduction of high-resolution stratigraphy in model well logs suggests that the

simulated interaction between depth-dependent shoreface erosion and grain-size dependent sedimentation in BARSIM is capable of predicting coastal and shallow-marine deposition due to poorly constrained coastal dynamics.

1.6 Thesis organisation

This thesis is organised into seven chapters that document the development and application of the computer simulation experiments that were carried out to address the research questions defined in Section 1.2.1. To the extent possible in an integrated work such as this, the chapters of this thesis that document experimental approaches and findings are structured as stand-alone research articles in preparation for subsequent submission to academic journals.

Chapter 2 begins by considering the spectrum of coastal barrier systems within a sequence stratigraphy framework, which provides a convenient structure for considering coastal barrier evolution and shoreline migration in response to sea level change. The coastal barrier systems of southeastern Australia are used as a natural laboratory that showcases the diversity of wave-dominated barrier coastlines, and from which a rich array of chronostratigraphic records have been retrieved that support the investigation of depositional controls using computer simulation experiments. Varying stratigraphic relationships between coastal barriers that are associated with successive late-Quaternary sea-level highstands are then considered as evidence for alternative evolutionary behaviour under comparable forcing scenarios. Lastly, the geological datasets from which many of the research questions have emerged are introduced as evidence that is subsequently used to constrain the stratigraphic forward modelling approach and evaluate the research questions.

The first of these questions is addressed in Chapter 3, which considers the role of shoreface kinematic response in coastal deposition under near-stable highstand sea-level conditions. Specifically, the disputed roles of disequilibrium-induced shoreface erosion, late-Holocene sea level change and external sediment supply regimes are examined in the context of the origins of mid- to late-Holocene highstand coastal strandplains at two sites in southeastern Australia. Chapter 4 delves deeper into the evolution of wave-dominated barrier coastlines by examining the roles of the basic controls of sea level change and inherited antecedent physiography in the origins of coastal barrier

systems at Forster-Tuncurry, on the central southeast Australian coast. There, the influences of these basic controls relative to shoreface kinematic response and modest rates of external sediment supply are demonstrated as a determining factor in the general stratigraphic evolution of highstand coastal barrier systems, through control of transgressive barrier behaviour.

Whilst the simulation experiments documented in Chapters 3 and 4 address a number of outstanding questions regarding the origins of coastal barrier systems, they also highlight the difficulties of isolating the often subordinate but fundamental role of shoreface kinematic response in the evolution of wave-dominated barrier coasts. In Chapter 5 the role of shoreface kinematic response is isolated using a series of idealised experimental designs in which other depositional controls are isolated. Specifically, the proposition of an 'active shoreface' characterised by time-invariant profile geometry that gives way to depth-dependent lower-shoreface response is examined for a range of scenarios, in which the rate of sea level change, substrate gradient and site morphodynamics are individually manipulated.

In Chapter 6 the scope and implications of the shoreface behaviour demonstrated in Chapter 5 are explored for a selection of problems relevant to the stratigraphy, geomorphology, and coastal management disciplines. The nature of shoreface response to projected sea level rise over the next few centuries is a question of fundamental importance to human settlements in coastal areas worldwide [*Stive*, 2004; *FitzGerald et al.*, 2008; *Nicholls and Cazenave*, 2010], and remains largely unconsidered in coastal management practice. The implications of the findings from the simulation experiments in Chapters 3, 4 and 5 are considered in an investigation of the significance of shoreface response in predictions of shoreline retreat due to sea level rise. Specifically, an attempt is made to constrain future shoreface response over the coming few centuries for settings typical of southeastern Australia. Accelerating rates of sea level rise and latency in shoreface response are considered in terms of change in active shoreface dimensions and depth-dependent lower-shoreface response.

Chapter 7 presents a synthesis of the major findings of this thesis with a particular focus on the implications of shoreface response for problems of late-Quaternary coastal evolution and potential future coastal change. The limitations of the approach, and future directions for the refinement and extension of the research methodologies and findings presented in this thesis are also discussed.

2

Barrier Coasts of Southeastern Australia

2.1 Introduction

The southeast Australian continental margin contains an array of contrasting coastal barrier systems that span the length of the margin along the modern highstand coastline, and in some cases coastal barriers associated with interstadial sea levels extend across the margin to the edge of the continental shelf. Coastal barrier systems, characterised by their depositional architecture, formed within embayments of the contemporary coastline during mid- to late-Pleistocene and Holocene sea-level highstands, and have been preserved to varying degrees depending on the nature of shelf physiography, energy climate, accommodation space, and the available sediment supply [*Roy et al.*, 1980; *Roy and Thom*, 1981; *Thom et al.*, 1981a; *Thom*, 1984]. Across the inner to mid shelf, coastal barriers from lower sea levels were preserved in palaeo-embayments, where rates of sea level change and sediment supply permitted the burial of transgressed deposits [*Schluter*, 1982; *Browne*, 1994; *Boyd et al.*, 2004]. On the outer shelf, lowstand deposits comprising cool-water carbonate sands, which contain fossil mollusc species characteristic of the shoreface environment, date to MIS 2, MIS 6 and MIS 8 glacial stages [*Ferland et al.*, 1995; *Murray-Wallace et al.*, 1996, 2005]. Considering the gently sloping geometry of the outer shelf, and the wave-dominated setting, these shoreface deposits might represent remnants of coastal barrier systems that were subsequently reworked at the onset of transgression.

2. BARRIER COASTS OF SOUTHEASTERN AUSTRALIA

The relatively high preservation and diversity of coastal barrier systems in southeastern Australia has inspired the development of qualitative regional coastal-deposition models [*Roy and Thom*, 1981; *Roy et al.*, 1994]. However, detailed sampling investigations form a patchwork of studies along the margin, and thus our understanding of the role of late-Quaternary depositional controls and time-dependence in the evolution of coastal barrier stratigraphic architecture remains incomplete. Whilst mean sea level change and the ambient energy climate may have been relatively uniform along the margin, margin physiography, sedimentary regime and the nature of shoreface response may have varied with latitude. The outcome of regional-scale and site-specific variation in depositional controls is readily observed today in the variable occurrence and diverse assortment of coastal barrier systems preserved on the contemporary highstand coastline. The origins of different highstand coastal barrier systems are considered later in this thesis through simulation experiments that extend interpretations of existing geological datasets. The context for the research questions and experimental simulations described in later chapters is provided here through a review of coastal barrier evolution at different sea level stages and the evidence for alternative depositional responses [Sec. 2.3]. Furthermore, the sampling methods [Sec. 2.5], geological datasets and previous evolutionary interpretations are described for the study sites [Secs. 2.6 & 2.7].

The primary objective of this chapter is to present the geological evidence from southeastern Australia from which the research questions have emerged and on which the simulation experiments are based. In doing so this chapter provides both a description of the empirical datasets applied in this thesis, and the necessary context to establish the significance of the research questions in regard to evolutionary principles of wave-dominated barrier coasts. This chapter has the following specific objectives:

1. Describe the geology and physiography of the southeast Australian regional setting, which has given rise to a diverse range of coastal barrier systems.

2. Review the role of varying depositional controls (sea level change in particular) in the evolution of different coastal barrier types, and locate coastal barrier stratigraphies within a 'systems tract' framework.

3. Classify varying highstand coastal barrier stacking relationships as observed in southeastern Australia, and investigate their distribution in the context of the regional setting.

4. Describe geological datasets from coastal barrier systems at Moruya and Forster-Tuncurry, which provide the physical evidence that underpins the development of the modelling approach and simulation experiments.

5. Review previously proposed evolutionary histories of these coastal barrier systems to identify unresolved questions in regard to coastal barrier evolution and shoreface kinematic response.

2.2 Regional Setting

The southeast Australian continental margin extends about 2000 km NNE from the entrance of Bass Strait to Breaksea Spit at the northern tip of Fraser Island [Fig. 2.1]. The greater East Australian margin was initiated around 110 Ma by gradual thinning and rifting of continental crust associated with opening of the Tasman Sea [*Persano et al.*, 2005]. Seafloor spreading between 85-52 Ma resulted in separation of the Lord Howe Rise from the Australian mainland and formation of the contemporary Tasman Sea basin [*Hayes and Ringis*, 1973; *Gaina et al.*, 1998]. The contemporary margin is tectonically passive by global standards, and has gradually subsided since formation, experiencing only limited volcanism that may be related to the passage of the continent over a mantle hot spot [*Lister et al.*, 1986; *Roy and Thom*, 1991; *Thom et al.*, 2010]. The margin is atypical of classic passive margin settings (e.g. US Atlantic margin), however, being unusually narrow (30-50 km wide), relatively old and characterised by a comparatively thin sediment cover [*Roy and Thom*, 1981; *Boyd et al.*, 2004].

Latitudinal and depth-based variations in margin geomorphology have been described by *Roy and Thom* [1981], and more recently by *Boyd et al.* [2004]. Briefly, the inner margin is predominantly a quartz sand province, with reworked siliciclastic sands grading into an outer shelf plain that is dominated by carbonate sands [*Boyd et al.*, 2004]. Coastal and shallow-marine sediments are relatively uniform, and comprise well-rounded and well-sorted quartz-rich sands that suggest a history of prolonged reworking [*Roy and Thom*, 1981]. Carbonate content is locally variable on the inner to mid shelf, and immature lithic-rich sands of recent fluvial origins are restricted to estuaries and the vicinities of larger rivers [*Boyd et al.*, 2004]. The margin is bordered to the north by the Great Barrier Reef carbonate province. The coast is embayed with conspicuous bedrock promontories separating the individual compartments in which

coastal barrier estuaries and drowned river valleys have formed during the present and previous sea-level highstands [*Roy et al.*, 1980; *Roy and Thom*, 1981]. In general, the northern sector is characterised by low coastal relief, long and broad embayments and a shallow shelf, whilst the southern sector is characterised by rugged hinterland, smaller pocket embayments, steep inner- and mid-shelf regions, and a deep outer shelf plain [*Roy and Thom*, 1981]. A transition zone around Newcastle exhibits elements typical of both sectors.

The inner shelf is exposed to a moderately high-energy wave climate with a strong winter season energy bias in which storm and swell waves originate predominantly from the south to southeast [*Short and Trenaman*, 1992]. Historical observations and geological records also demonstrate that the southeast Australian wave climate is characterised by significant variability at inter-annual to multi-decadal timescales in association with southern hemisphere climatic phenomena including the Southern Annular Mode, El Nino Southern Oscillation, and Interdecadal Pacific Oscillation [*Ranasinghe et al.*, 2004; *Goodwin*, 2005; *Goodwin et al.*, 2006; *Harley et al.*, 2010]. Due to the oblique SSW-NNE orientation of the coast, net northward littoral drift of sediments prevails along the upper shoreface where headland bypassing permits, which is believed to have contributed to an accumulation of coastal sediments in the northern sector throughout the late Quaternary [*Roy and Thom*, 1981].

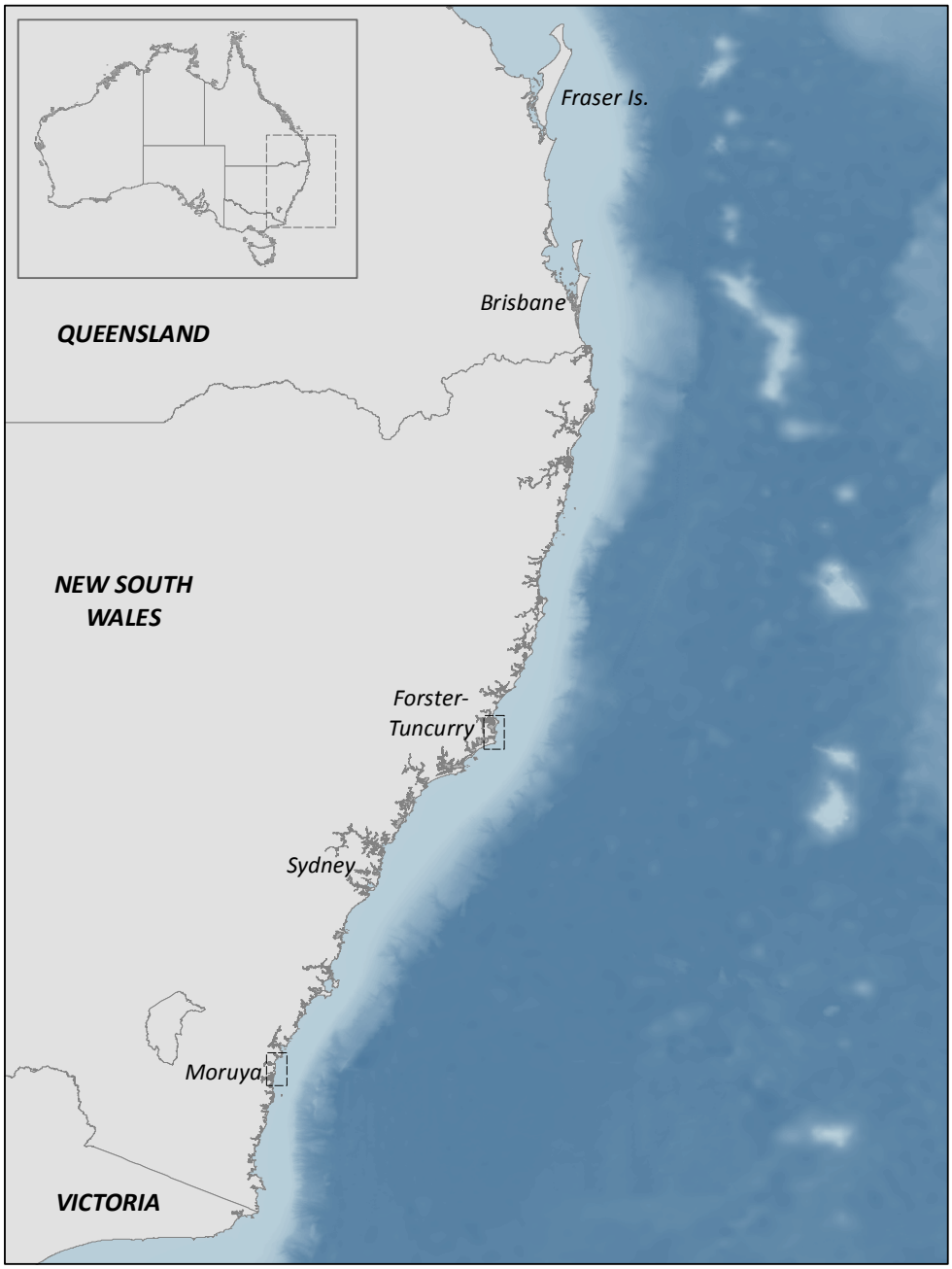

Figure 2.1: Southeast Australian margin setting - Location and morphology of the southeast Australian continental margin. The locations of the Moruya and Forster-Tuncurry study areas are also shown.

2.3 Coastal barrier deposition and sea level change

A sequence stratigraphy framework was adopted here to relate the morphostratigraphic variants of the coastal barrier depositional system to the range of sea level conditions experienced during late-Quaternary times. Figure 2.2 shows the systems-tract models that are the building blocks of the sequence stratigraphy approach [*Posamentier and Vail*, 1988; *Plint and Nummedal*, 2000], which provide a natural and established framework for classifying depositional responses to variations in geohistorical variables such as sea level change [Sec. 1.3.1].

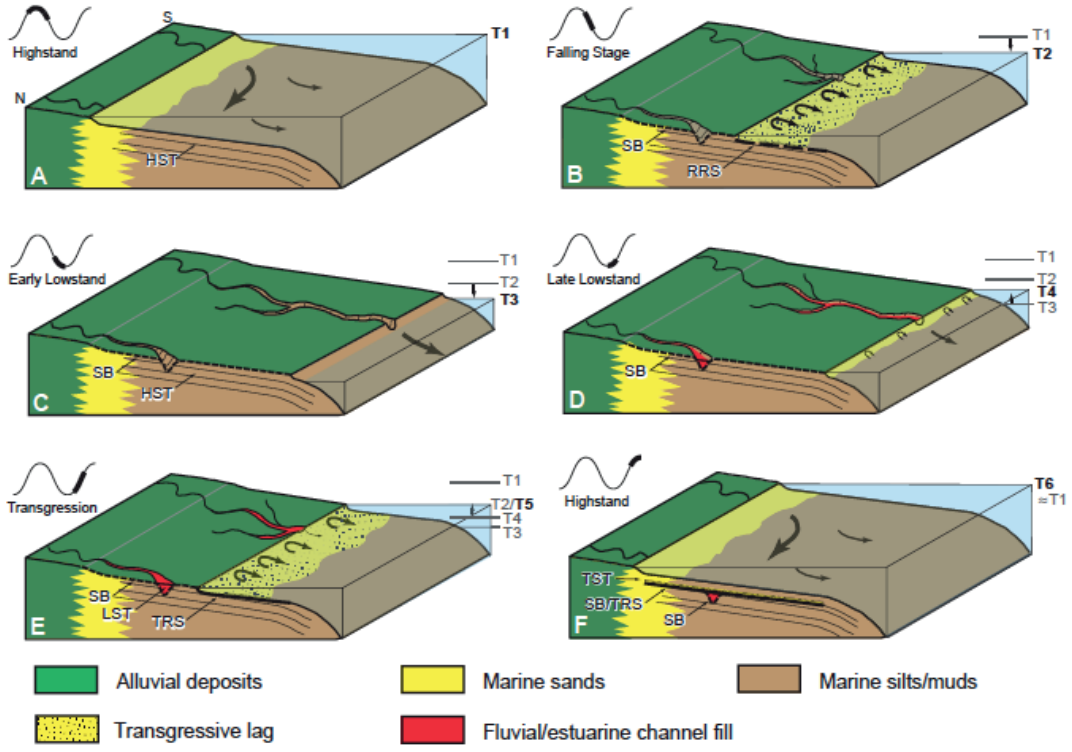

Figure 2.2: Systems Tract classification of shallow-marine stratigraphy - Typical patterns of coastal and shallow-marine deposition associated with highstand, falling stage, lowstand and transgression sea-level stages. The regressive ravinement surface (RRS) and transgressive ravinement (TRS) surface are shown. From *Mountain et al.* [2007]

Although systems-tract models were originally developed from ancient macroscale examples, the characteristic stratal architecture of the models is equally relevant to late-Quaternary coastal and shallow-marine deposition. The secondary objective of

this approach to the classification of coastal barrier variants is to transcend the scale division between the paradigms and terminology of the stratigraphy, geomorphology and engineering disciplines. This is particularly relevant for the subsequent investigation of shoreface response to sea level change and the implications for coastal and shallow-marine deposition, which are considered later in this thesis. That is, shoreface response may vary continuously across the morphodynamic scales, and different types of response may not always fit comfortably within discrete scale divisions.

2.3.1 Highstand

Highstand coastal barrier systems have developed under relatively stable highstand sea-level conditions such as those prevailing during late-Quaternary interglacials. The Highstand Systems Tract (HST) is generally characterised by one or more aggradational parasequence sets that are succeeded by progradational parasequence sets, and is variably expressed within a range highstand coastal barrier types on contemporary barrier coasts [*Posamentier and Vail*, 1988]. Highstand barriers are restricted to tectonically quiet settings where slow rates of vertical adjustment support more or less stable relative sea level conditions for prolonged periods of time [*Inman and Nordstrom*, 1971; *Roy et al.*, 1994]. Most coasts do not experience absolute 'stillstand' sea level conditions due to the dynamic nature of forcing mechanisms that control regional sea level anomalies and tectonic adjustments. Rather, the term 'stillstand' describes the case where relative sea level is stable or subtly varying, and its influence on coastal deposition is subordinate to other depositional controls (e.g. shoreface response, littoral sediment budget). Figure 2.3 shows the range of potential coastal sedimentary bodies during sea-level highstand, including four barrier types that may be differentiated by variable development and preservation of coastal barrier deposits [*Thom*, 1984]. The four barrier types described below represent alternative morphostratigraphic responses to decreasing rates of sub-aerial coastal deposition. The development and preservation of typical offlapping (i.e. prograding) HST stratal architecture increases with available sediment supply, whether *autochthonous* or *allochthonous* in nature.

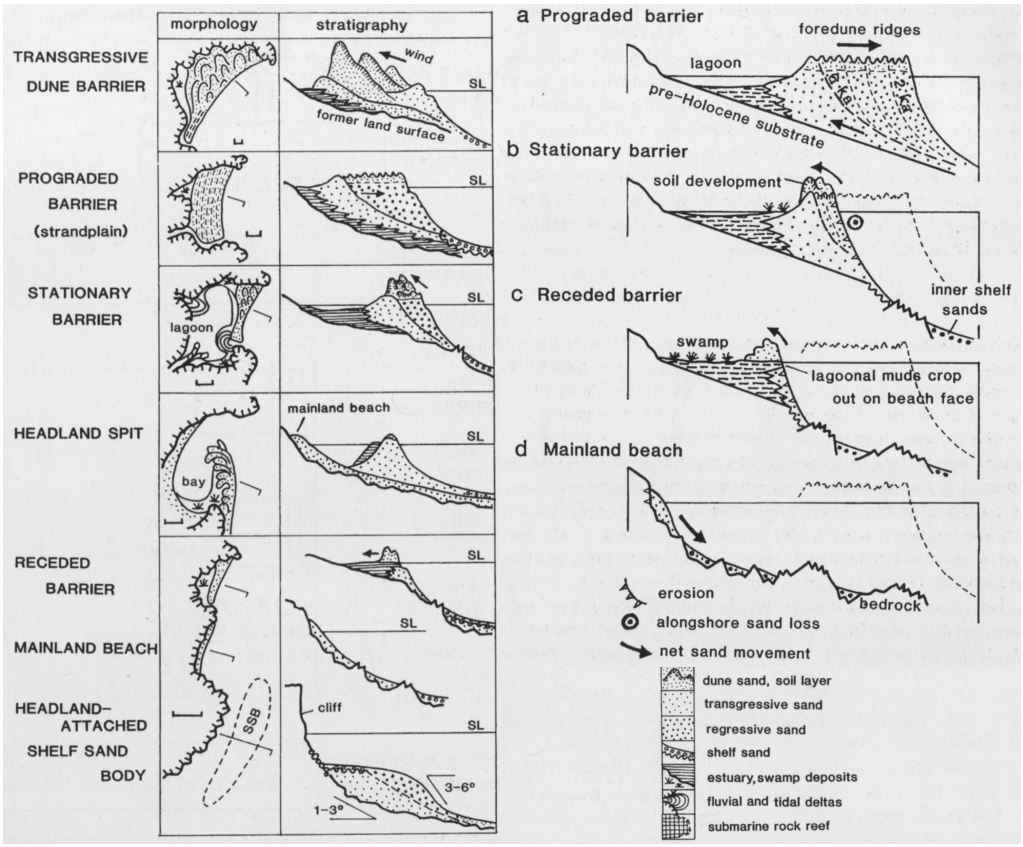

Figure 2.3: Coastal barrier deposition during sea-level highstand - Types of coastal barrier deposits that form during relatively stable highstand sea level conditions. Four highstand barrier types (prograded barrier, stationary barrier, receded barrier and mainland beach) are differentiated by the volume of deposition at the coast, and develop in response to regionally variations in geomorphology, energy climates and sedimentary regimes. From *Roy et al.* [1994].

Prograded barriers have been ambiguously termed 'regressive barriers' in the past. Traditionally, the term 'regression' refers to the emergence of the submerged coast above sea level, which may arise due to the seaward advance (i.e. progradation) of the coastline in response to high sediment supply, falling relative sea level, or a combination of both [*Curray*, 1964]. Within sequence stratigraphy nomenclature, these distinctly different processes are termed *normal regression* where high sediment supply drives progradation under stable or subtly rising sea levels, and *forced regression* where relative sea level fall is the dominant depositional control [*Posamentier et al.*, 1992]. In both cases the resulting depositional feature is a strandplain that is characterised by offlapping strata, although forced-regressive strandplains are organised into down-stepping stratal sets [*Posamentier and Morris*, 2000]. Whilst the term 'strandplain' is more strictly correct, under 'stable' highstand sea level conditions, coastal strandplains are a product of high sediment supply, and thus the term 'prograded barrier' is preferred here [*Roy et al.*, 1994]. The term 'forced-regressive strandplain' is used here to describe the depositional response to falling sea level [Sec. 2.3.2]. Thus the requirement of a sediment supply that exceeds the rate of accommodation generation is emphasised as the dominant control on prograded barrier deposition.

Deposition of prograded barriers is by means of shoreface progradation, in which high rates of deposition across the upper shoreface progressively extend the sub-aerial component of the barrier seaward [Fig. 2.4]. Prolonged shoreface progradation ultimately leads to the development of a coastal strandplain, which comprises a series of relict foredune-beach ridges that is fronted by the active foredune and beachface [Fig. 2.3a]. The elevations of the beach ridges may increase with proximity to the shoreline and thus decreasing age. In contrast, progressively younger beach ridges are typically organised in a down-stepping arrangement within forced-regressive strandplains [*Posamentier and Morris*, 2000]. The stratigraphic implication of shoreface progradation is that sub-aerial barrier facies (e.g. beach and dunes) come to overlie buried nearshore marine facies [Fig. 2.3a].

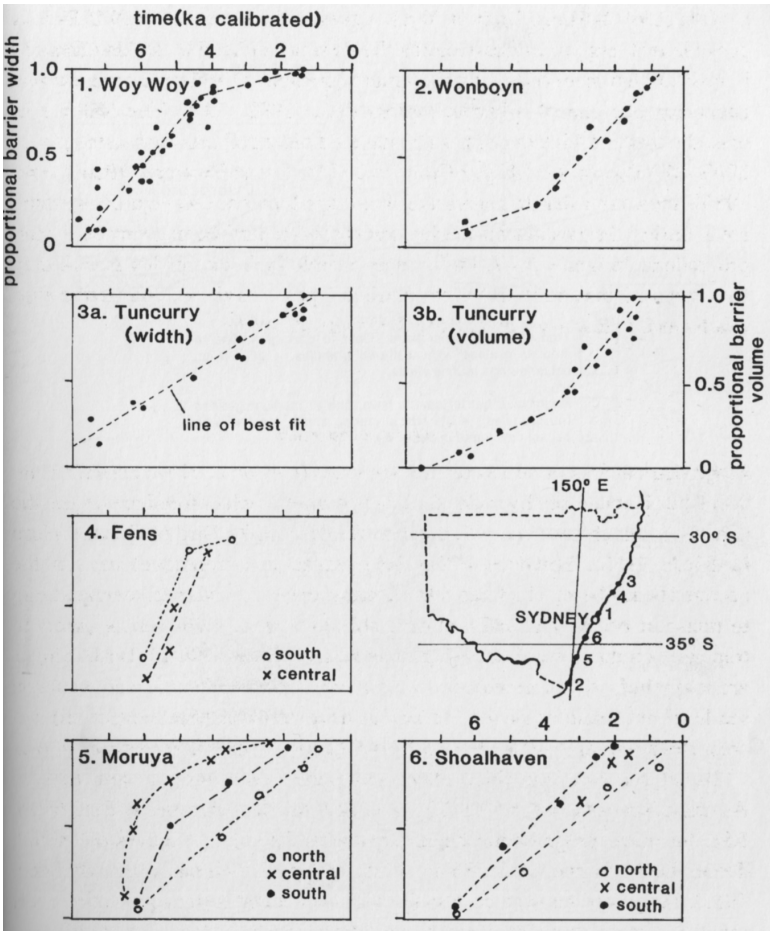

Figure 2.4: Rates of Holocene strandplain progradation in SE Australia - Proportional rates of Holocene strandplain progradation at various sites in southeastern Australia. Note the diminishing rates of late-Holocene barrier progradation at Moruya relative to the more steady rate at Tuncurry. From *Roy et al.* [1994].

Stationary barriers or 'aggraded barriers' are named for their stationary behaviour regarding shore-normal migration. They occur where subtly rising relative sea level occurs with moderate rates of sediment supply to the coast, such that the barrier accumulates vertically [*Roy et al.*, 1994]. In this case, the increased accommodation space offered by gradually rising sea level is contemporaneously filled by sediment, such that the shoreline maintains a constant position and does not undergo transgression. Under these conditions, shore-normal migration of coastal barrier depositional environments is absent, resulting in the deposition of relatively thick sedimentary units and vertical uniformity in facies [Fig. 2.3b]. Stationary barriers may also occur under stable sea level where rates of erosion and sediment supply at the coast are in balance and aeolian processes drive barrier aggradation [*Thom*, 1984].

Receded barriers are characterised by shoreline recession in response to a littoral sediment budget deficit. That is, the volume of sediments removed from the subaerial barrier by coastal processes exceeds that being deposited at the beach. This results in landward retreat of the shoreline. Although the term 'retrogradation' is the linguistic counterpart to 'progradation' [*Cowell et al.*, 2003b], the term 'receded barrier' is preferred here as retrogradational stacking is commonly used in sequence stratigraphy to describe transgressive parasequence sets [*Cattaneo and Steel*, 2003]. Thus the use of 'retrogradation to describe barrier deposition under stable sea level and a sediment-budget deficit may be ambiguous. Unlike the case of transgression in which accommodation is generated by rising sea level, receded barrier shorelines migrate landward in response to the net erosion of the coast, and thus are poorly preserved in stratigraphic records [Fig. 2.3c]. Where rising relative sea level drives shoreline retreat, coastal barrier deposits may be preserved in the stratigraphic record as thin retrogradational parasequence sets [*Storms et al.*, 2002].

Mainland beaches represent the least developed highstand sand body on barrier coasts and occur due to the near-absence of coastal accommodation space. In south-eastern Australia mainland beaches occur along comparatively steep coastal sectors and feature a thin veneer of shoreface deposits that mantles the underlying bedrock [Fig. 2.3d]. *Cowell et al.* [1995] demonstrated that transgression over steep coastal terrain is characterised by deposition at the toe of the shoreface, thereby restricting the opportunity for coastal barrier development. During sea-level highstand, steep coastal terrain restricts the width of coastal accommodation thereby prohibiting the development of

backbarrier environments. On the steepest coasts sub-aerial coastal barrier deposition is absent altogether, and barrier deposits are restricted to submerged shelf sand bodies [Fig. 2.3].

2.3.2 Falling Stage

Prolonged and steady relative sea-level fall may occur due to falling global sea levels or due to tectonic or isostatic adjustments. Until recently, deposition during sea-level fall remained largely overlooked and poorly formalised within sequence stratigraphy models. For example, strata associated with falling sea level were only considered in the context of the early deposition of the lowstand systems tract (LST) [*Posamentier and Vail*, 1988]. However, acknowledging the clear and systematic consistencies in coastal deposition during sea level fall, *Plint and Nummedal* [2000] introduced the falling-stage systems tract (FSST). The FSST is initiated at the first instance of sea-level fall following the stable sea level conditions associated with the HST, and is the lowest systems tract in a sequence [*Plint and Nummedal*, 2000]. The basal surface of the FSST is a diachronous sequence boundary that caps the HST, and is identified by a subaerial erosive surface updip and the basal surface (marine erosion) of forced regression. By definition, the FSST is characterised by offlapping stratal geometry [*Plint and Nummedal*, 2000]. That is, successively younger strata extend less farther landward, thereby leaving exposed a portion of the older unit upon which they lie. This results in a forestepping and downstepping stacking-pattern of higher order sequences, which are progressively deposited as the shoreline translates basinward. This should not be confused with the stratal architecture associated with 'normal regression' that characterises prograded barriers [Sec. 2.3.1]. The beginning of the LST [Sec. 2.3.3] marks the termination of the FSST, although this may potentially be difficult to define if deposition occurs within previously incised valleys.

The 'forced-regressive deposit' is the key depositional unit of the FSST, and takes the form of a down-stepping strandplain [*Hunt and Gawthorpe*, 2000; *Posamentier and Morris*, 2000]. It may be distinguished from the prograded strandplain associated with 'stillstand' deposition by a basinward decrease in beach ridge elevation - a direct response to falling relative sea level. Continuously falling sea level ensures that back-barrier accommodation is minimal or absent. Instead, incised streams are cut into the HST and earlier FSST deposits to deliver coastal run-off from the coastal plain directly

to the nearshore. Depending on the volume and intensity of terrestrial drainage, deposition of the forced-regressive strandplain may be predominantly sourced from fluvial input. Alternatively, forced-regressive strandplain deposition may be sourced from autochthonous sources, such as the reworking of unconsolidated shelf deposits by shoreface erosion [*Roy et al.*, 1994; *Cowell et al.*, 1995].

Remnants of the FSST have been preserved in late-Quaternary sequences. In south-eastern Australia, buried strandplain deposits that appear to show forced-regressive stratal architecture occur in seismic stratigraphy records from inner- to mid-shelf depths [*Jones et al.*, 1982; *Schluter*, 1982; *Searle*, 1982; *Browne*, 1994; *Roy et al.*, 1997], particularly along the low-relief and gently sloping northern sector of the margin [Sec. 2.2]. The best documented examples occur in the Forster-Tuncurry region, where down-stepping barrier sands between 10-15 m thick occur in water depths from 30 to 90 m [*Roy et al.*, 1997]. Figure 2.5b shows planform and profile illustrations of forced-regressive deposits associated with coastal barrier deposition during sea level fall. Stratal architecture is characterised by an offlapping relationship between seismic reflectors, which slope seawards at an angle comparable to that of the current shoreface, and are arranged in a progressively down-stepping manner. The geomorphology and stratigraphy of the Forster-Tuncurry region is considered in detail in Section 2.7.

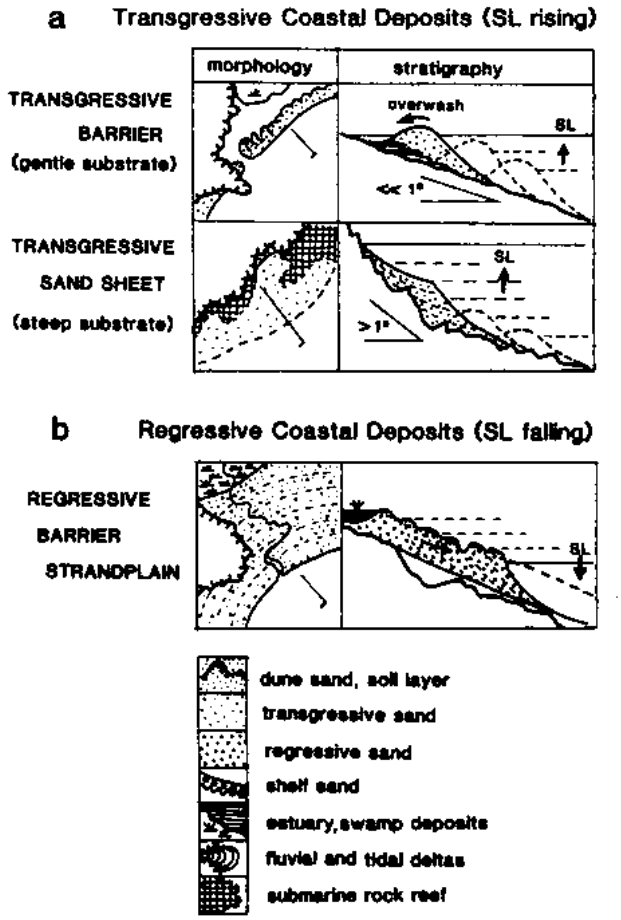

Figure 2.5: General model of transgressive and falling-stage deposition on barrier coasts - Coastal barrier morphologies characteristic of (a) transgression on gentle and steep substrates, and (b) falling sea level conditions. Here, the 'regressive barrier strandplain' of *Roy et al.* [1994] is referred to as a 'forced-regressive strandplain' to emphasise the role of sea-level fall in coastal deposition. From *Roy et al.* [1994].

2.3.3 Lowstand

The LST is characterised by a lowstand wedge complex comprising progradational and/or aggradational parasequence stacking comparable to that of the HST [Sec. 2.3.1]. However, the backstepping of younger strata onto antecedent forced-regressive deposits may be more pronounced [*Posamentier et al.*, 1992]. Lowstand deposition is thought to be characterised by limited generation of accommodation perhaps associated with a small sea level rise during essentially stillstand conditions. Thus sedimentary units are typically less developed relative to the HST. The lower boundary of the LST is defined as the first onlap onto the forestepping clinoforms of the late FSST, and the upper boundary is represented by the transgressive surface associated with the first significant flooding event of resumed sea level rise [*Posamentier and Vail*, 1988].

Comparatively little is known about the morphology of lowstand coastlines given that there are no contemporary examples to observe. Thus geological datasets and computer modelling are the only means of investigating coastal deposition during sea-level lowstand. In southeastern Australia carbonate sands on the outer shelf that date to MIS 2, MIS 6 and MIS 8 glacial stages and contain fossil assemblages characteristic of shoreface environments provide evidence of lowstand shorelines [*Ferland et al.*, 1995; *Murray-Wallace et al.*, 1996; *Ferland and Roy*, 1997; *Murray-Wallace et al.*, 2005], although no barrier systems have been identified. However, the mapping and sampling of drowned barrier systems from the Gulf of Mexico and the Adriatic Sea suggests that the morphology of low-gradient lowstand barrier coastlines may have been strikingly similar to contemporary highstand barrier coastlines [*Gardner et al.*, 2005, 2007; *Storms et al.*, 2008].

2.3.4 Transgression

The transgressive systems tract (TST) is initiated by the first significant flooding event after a prolonged period of lowstand conditions, during which the basal boundary surface (i.e. the transgressive surface) is created [*Posamentier and Vail*, 1988]. The initial flooding event may coincide with the breaching of the lowstand barrier complex, perhaps during a low-frequency high-magnitude storm event, and initiates conditions where sediment supply is insufficient for the barrier to maintain its position (via aggradation or progradation) given the rate of sea level rise. That is, the rate of accommodation

generation exceeds the rate of deposition. The subsequent landward migration of the barrier system as sea level rises results in backstepping (retrogradational) parasequence sets, which successively onlap younger strata [*Cattaneo and Steel*, 2003]. Dune, beach and shoreface facies come to overlie estuarine or lagoonal facies in typically coarsening upward parasequences [*Cattaneo and Steel*, 2003]. The TST is bounded at its upper extent by the maximum flooding surface, which corresponds to the surface of deposition at the time that the shoreline reaches its most landward position [*Posamentier and Vail*, 1988].

Transgressive coasts are subject to rising relative sea level due to rising global sea level, subsidence, or a combination of both. Within late-Quaternary stratigraphic records, transgressive barrier deposits are generally associated with rapid and high-magnitude global sea-level rises that occurred in response to the sudden melting of polar ice caps at the termination of glacial periods. On the other hand, contemporary coastlines undergoing transgression occur in tectonically active areas that are experiencing subsidence [*Inman and Nordstrom*, 1971]. Transgressive barriers are usually characterised by a low-relief sub-aerial barrier and well-developed backbarrier complex [Fig. 2.5], although the deposition and preservation of the depositional environments depends on the rate of sea level change and setting [*Tortora et al.*, 2009a,b]. They migrate landward in response to rising sea level through process of barrier roll-over, which is the time-averaged net sediment transport associated with the episodic accumulation of overwash and flood-tide delta facies [*Leatherman*, 1983; *Niedoroda et al.*, 1985b]. Deposition is concentrated in the backbarrier complex, which is continually afforded additional accommodation as sea level rises, thereby maintaining an accommodation-dominated sedimentation regime [*Swift et al.*, 1991]. Barrier island, barrier spit and bay barrier morphologies are all possible under transgression over relatively gently sloping substrates, and depend largely on the setting. In general, low-gradient shelf settings with low-relief coastal plains are more conducive to barrier islands and spits, moderate sloping substrates and more embayed settings favour bay barriers, whilst steep substrates are characterised by transgressive sand sheets [*Roy et al.*, 1994].

2.4 Late-Quaternary highstand barrier stacking

An early observation from the study of coastal barriers in southeastern Australian was that many embayments contain multiple barrier systems that appear to be associated with different sea-level highstands [*Thom*, 1965; *Langford-Smith and Thom*, 1969]. Typically, a Pleistocene-age 'inner barrier' is preserved landward of a Holocene-age 'outer barrier' [*Thom et al.*, 1981a]. However, the occurrence of, and stacking relationships between, Pleistocene and Holocene barrier systems is not consistent along the coastline, but varies both regionally and in some cases between neighbouring embayments. Despite a range of stacking relationships having been identified, their origins remain to be explored in detail. Although previous authors have proposed general models of late-Quaternary margin sedimentation in southeastern Australia [*Roy and Thom*, 1981], there has been little attempt to investigate the role of sea-level change and varying margin physiography on highstand barrier stacking.

Based on both the deposition of coastal barriers during Pleistocene and Holocene sea-level highstands, and the preservation of barrier deposits during intervening periods of erosion and reworking, four distinct barrier stacking relationships can be identified [Fig. 2.6]:

1. Composite Pleistocene barrier system
2. Horizontally stacked inner Pleistocene and outer Holocene barriers
3. Vertically stacked buried Pleistocene and exposed Holocene barriers
4. Solitary Holocene barrier system

It should be noted that the coastal barrier stacking relationships defined here refer to the occurrence and arrangement of coastal *barrier systems*. This does not always indicate that coastal barrier deposits of Pleistocene or Holocene age are absent from solitary-barrier settings, but that the deposits are neither sufficiently extensive nor diverse to constitute a coastal barrier system. Figure 2.7 shows the distribution of documented highstand barrier stacking relationships in southeastern Australia.

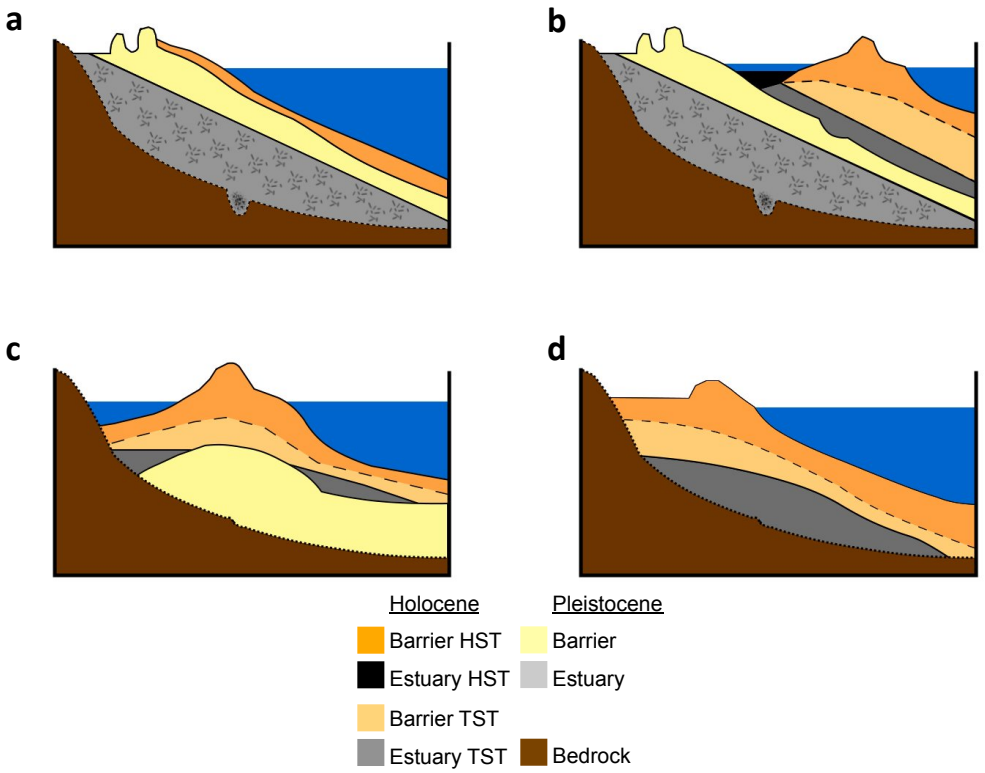

Figure 2.6: Stratigraphy of highstand barrier-stacking relationships - Highstand coastal-barrier stacking relationships of southeastern Australia as shown in Figure 2.7. (a) composite Pleistocene barrier, (b) horizontally-stacked Pleistocene 'inner barrier' and Holocene 'outer barrier', (c) vertically-stacked buried Pleistocene barrier and exposed Holocene barrier and (d) solitary Holocene barrier.

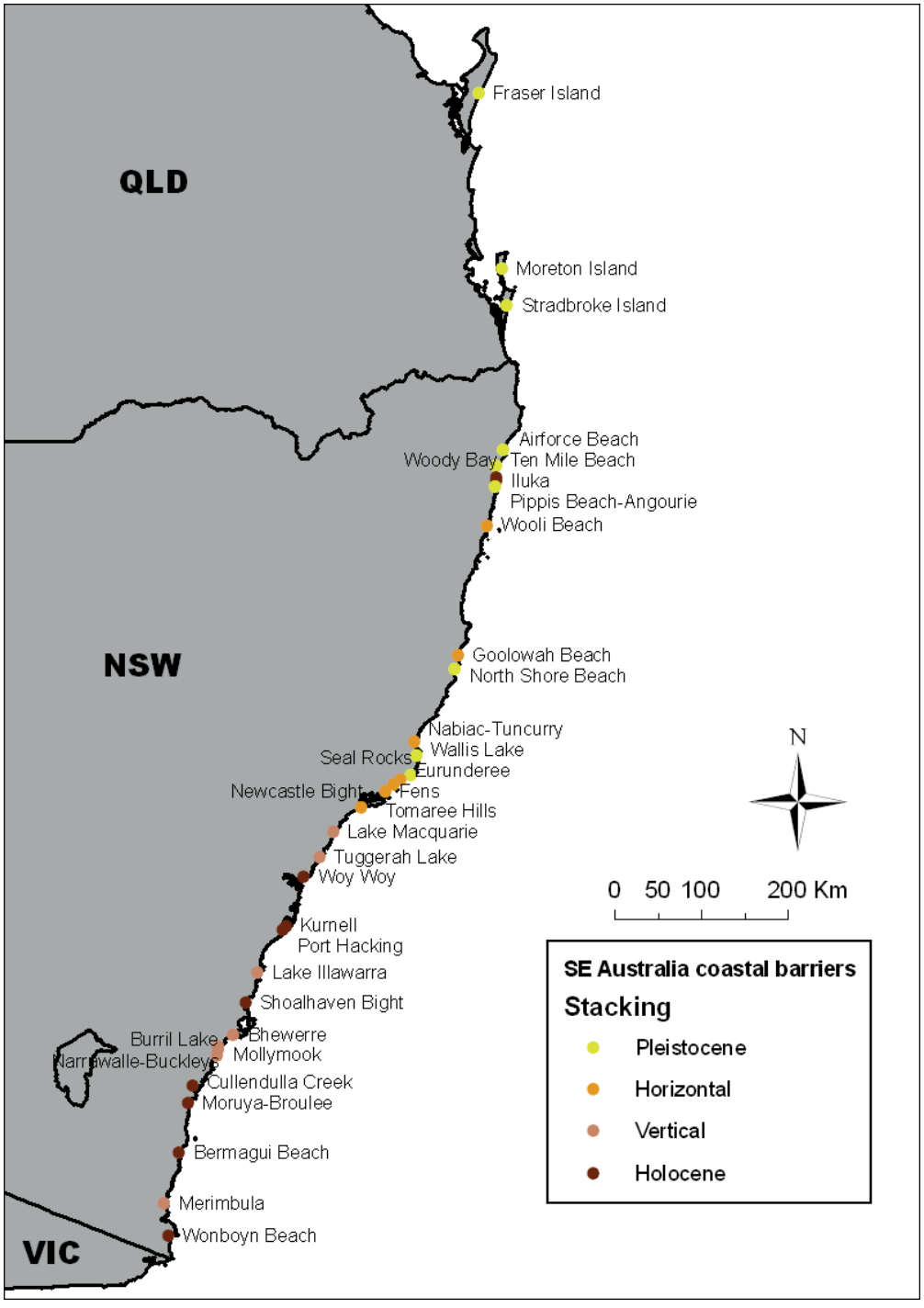

Figure 2.7: Highstand barrier-stacking relationships in southeastern Australia - Distribution of composite Pleistocene barrier, horizontally-stacked barrier systems, vertically-stacked barrier systems and solitary Holocene barrier stacking relationships along the southeast Australian margin. The characteristic stratigraphies of the different stacking relationships are shown in Figure 2.6.

2.4.1 Composite Pleistocene barrier system

The first type of stacking relationship is restricted to the northern half of the SE Australian coastline, and describes the case where preserved barrier deposits are (almost) exclusively associated with highstand deposition prior to and/or during the last interglacial. The typical stratigraphy of composite Pleistocene barrier systems is shown in Figure 2.6a. The Pleistocene barrier deposits have been subject to aeolian reworking during the last cycle, and in some cases marine erosion during the Holocene highstand. Extensive vegetated beach-ridge strandplains may be preserved where minimal reworking has occurred. Coastal barrier deposits of Holocene age are either absent or poorly developed, generally being restricted to thin shoreface veneers and estuarine flood-tide deltas. In cases where fluvial deposition has been significant, backbarrier environments may contain surficial Holocene estuarine deposits atop Pleistocene backbarrier muds.

Composite Pleistocene barrier systems occur from the barrier islands of southeastern Queensland [*Hails*, 1964; *Ward and Little*, 1975] as far south as Seal Rocks [*Thom et al.*, 1981a]. For example, the coastal embayments immediately south of the Clarence River, and north from Woody Bay to Evans Head (i.e. Ten Mile Beach) are almost entirely filled with Pleistocene barrier and backbarrier deposits [*Walsh and Roy*, 1983]. Where present, Holocene beach sediments are restricted to a narrow lens of shoreface facies (less than 3 m thick) seaward of scarped Pleistocene dunes. Holocene backbarrier facies are limited to flood-tide delta sands, thin estuarine muds, and lakeshore and tidal inlet sandy muds [*Walsh and Roy*, 1983]. Although historically shoreline recession is characteristic of some embayments in that region [*Goodwin et al.*, 2006], there is no evidence to suggest that more substantial Holocene barrier deposits existed previously [*Walsh and Roy*, 1983]. An anomaly is the section of coastline north from the Clarence River inlet to Woody Bay, which is predominantly composed of Holocene prograded barriers, which have accumulated entirely within the past few thousand years [*Walsh and Roy*, 1983; *Goodwin et al.*, 2006]. However, this anomaly has been attributed to the behaviour of the Clarence River inlet (e.g. breaching earlier barrier deposits) and the influence of late-Holocene wave climate variation on sediment transport within the region [*Goodwin et al.*, 2006]. Further south in the highly exposed Seal Rocks embayment [Fig. 2.7], the Pleistocene barrier system is completely buried beneath an extensive Holocene transgressive dune system. Stratigraphic investigations of this

embayment indicate that only a thin Holocene beach exists seaward of the buried Pleistocene barrier system, and there is no evidence to suggest the existence of a Holocene barrier system in the past [*Thom et al.*, 1981a, 1992].

2.4.2 Horizontally-stacked barrier systems

The second type of stacking relationship refers to the situation where an inner Pleistocene-age barrier is bordered to seaward by an adjacent outer Holocene-age barrier system that developed during mid- to late-Holocene transgression and highstand. The typical stratigraphy of horizontally-stacked barrier systems is shown in Figure 2.6b. An inter-barrier depression comprising Holocene-age fluvial or estuarine backbarrier deposits often separates the two barriers at the surface. Depending on the degree of development and preservation of both barrier systems, a variety of coastal barrier facies and depositional features of both age groups may be present. In well-developed cases, backbarrier deposits, beach-ridge strandplains and coastal dunes associated with both barrier systems may be preserved.

The most conspicuous and documented examples of horizontal barrier stacking in southeastern Australia reside within the Port Stephens-Myall Lakes region on the NSW mid-north coast. There, the coastal geomorphology of six adjacent embayments from Newcastle Bight in the south to Seal Rocks in the north has been investigated in detail [Fig. 2.8], beginning with *Thom* [1960]. Numerous subsequent studies have been synthesised into a regional investigation by *Thom et al.* [1992]. The initial identification of adjacent Pleistocene and Holocene barrier systems inspired the terminology 'inner' and 'outer' barriers [*Thom*, 1965]. Given the preservation of both Pleistocene and Holocene barrier systems, the horizontal stacking arrangement was referred to as a 'composite barrier' by *Thom et al.* [1978]. However, as both composite Pleistocene barrier systems [Sec. 2.4.1] and vertically-stacked Pleistocene and Holocene barrier systems [Sec. 2.4.3] are also recognised here, the term 'composite barrier' is not used to describe horizontally-stacked barrier systems.

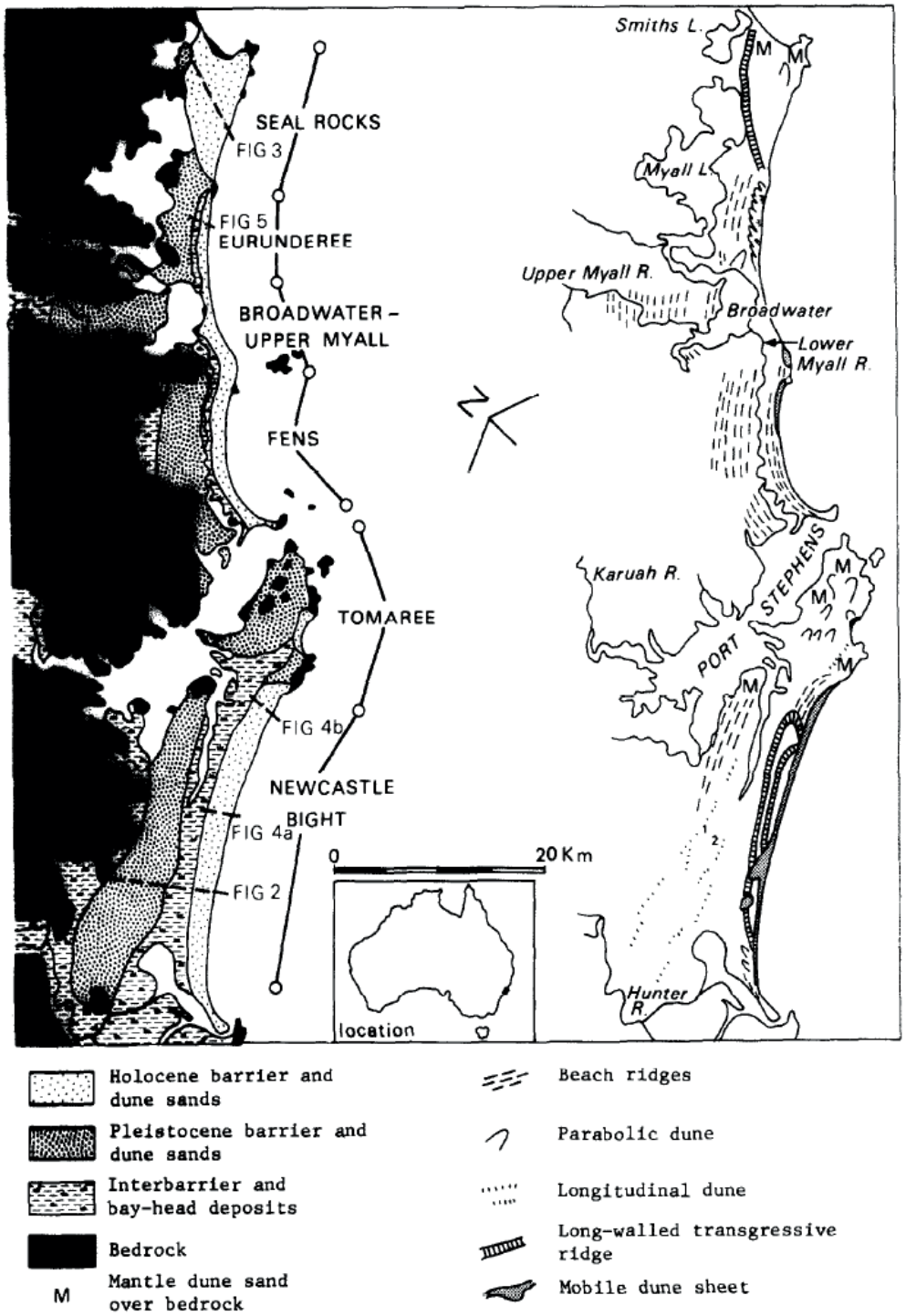

Figure 2.8: Coastal geomorphology of the Port Stephens-Myall Lakes region - Distribution of inner and outer coastal barrier systems in the Port Stephens-Myall Lakes region, which is immediately south of the Forster-Tuncurry region [Fig. 2.13]. Horizontal barrier stacking is most developed in the Newcastle Bight embayment, where the interbarrier depression is occupied by Holocene backbarrier deposits. From *Thom et al.* [1981a].

Horizontally-stacked barrier systems have developed to varying degrees within four of the six embayments (Newcastle Bight, Fens, Upper Myall-Broadwater and Eurunderee), which may be differentiated on the basis of geology and exposure to the wind and wave climates [Fig. 2.8]. In the most exposed Newcastle Bight embayment, extensive Pleistocene and Holocene barrier systems that each contain successions of beach ridges and reworked (aeolian) coastal dunes, are clearly distinguished from one another by an interbarrier depression, which contains backbarrier estuarine deposits of Holocene age [Fig. 2.9]. Similar stacking relationships are observed in the other embayments although features are generally developed to lesser degrees. The remaining two embayments (Tomaree Hills and Seal Rocks) are characterised by the development of only one barrier system and extensive dune deposits [Fig. 2.8]. The absence of an interbarrier depression and Holocene backbarrier deposits at Seal Rocks suggest that a Holocene barrier system did not develop there. Instead, Holocene beachface deposits have been reworked into an extensive transgressive dune system. In the Tomaree Hills embayment, Pleistocene and Holocene deposits are restricted to cliff-top dunes and a mainland beach respectively [Fig. 2.8]. Variation in the development of Holocene barrier systems in the Port Stephens-Myall Lakes region highlights the fundamental roles of antecedent geology, coastal sediment budgets and energy regime in controlling highstand barrier stacking relationships.

Horizontally-stacked barrier systems are by no means unique to the Port Stephens-Myall Lakes region. For example, similar coastal barrier stratigraphy has been documented in the East Gippsland region of Victoria [*Bird*, 1965; *Jenkin*, 1968]. Both inner Pleistocene and outer Holocene barrier systems are preserved there, which collectively impound numerous large coastal lakes and smaller lagoons. Relict barrier deposits believed to be of pre-last-interglacial age have also been preserved landward of the inner barrier [*Bird*, 1965]. In contrast to the Port Stephens-Myall Lakes region, contemporary backbarrier lagoons and lakes are much more extensive along the lower gradient East Gippsland coast. At the other end of the size spectrum, horizontally-stacked barriers have been observed within the comparatively minute Wyvuri embayment to the south of Cairns in northeastern Australia [*Gagan et al.*, 1994]. Along the southeast Australian margin, examples of horizontally-stacked barrier systems are most common along the NSW mid-north coast [Fig. 2.7]. Further north the development of Holocene

barrier systems appears to have been restricted, whilst further south the preservation of intact and exposed Pleistocene barrier systems is not observed.

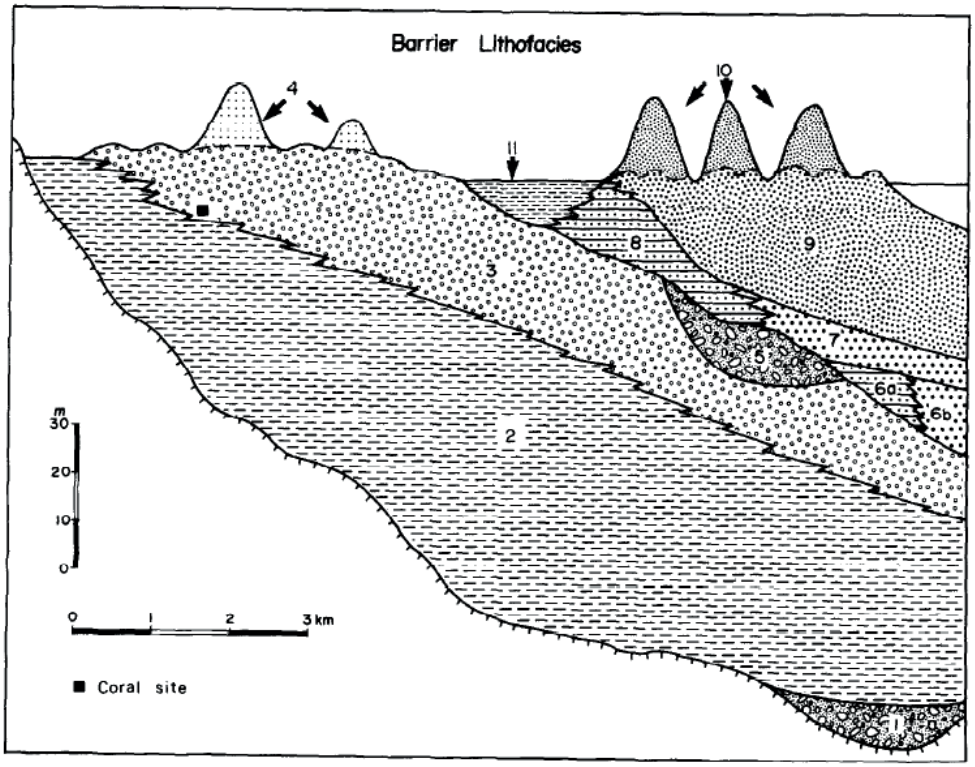

Figure 2.9: Stratigraphy of the Newcastle Bight embayment - Representative stratigraphy of horizontally-stacked barrier systems of the Newcastle Bight embayment [Fig. 2.8]. Facies shown include: (1) basal fluvial sands and gravels, (2) interbedded clays and sands (composite estuarine unit), (3) inner barrier marine sands, (4) Pleistocene dune sands, (5) fluvial sands and gravels (6) late-Pleistocene marine and estuarine sands, (7) marine transgressive sands, (8) backbarrier sands and muddy sands, (9) outer barrier marine sands, (10) outer barrier transgressive dune sands and (11) Holocene estuarine muds. From *Thom et al.* [1981a].

Globally, horizontally-stacked barrier systems are generally observed in passive margin settings. For example, the geomorphology of the Rio Grande do Sul coast in Brazil is not dissimilar to that of the East Gippsland coast, although on a much larger scale. There, multiple Pleistocene barrier systems and the Holocene barrier system impound

lagoons of varying dimensions that occupy the interbarrier depressions [*Dillenburg et al.*, 2000; *Tomazelli and Dillenburg*, 2007]. Similar barrier-stacking relationships are observed in the Wilderness barrier systems of South Africa [*Bateman et al.*, 2011]. On the other hand, the coastline of Georgia Bight on the US Atlantic margin is characterised by a series of Holocene barrier islands and spits, which are backed by relict Pleistocene barriers that are now attached to the mainland in most cases [*Hayes*, 1994]. There, a Holocene backbarrier lagoon filled with recent silt and clay deposits usually separates the contemporary barrier from its Pleistocene counterpart, although in some cases the older and younger barriers may be welded together [*Frey and Howard*, 1988].

2.4.3 Vertically-stacked barrier systems

Vertically-stacked barrier systems refers to the case where the antecedent (Pleistocene) barrier system occurs buried beneath the overlying Holocene barrier system [Fig. 2.6c]. Unlike in the case of horizontal stacking, corresponding facies associated with the Pleistocene and Holocene barrier systems are vertically concordant. That is, Holocene-age depositional environments overlie the corresponding Pleistocene-age depositional environments. In some cases, aeolian or fluvial erosion during lowstand conditions may have removed the upper section of the Pleistocene barrier prior to the subsequent burial of these deposits by the Holocene transgressive barrier. Vertically-stacked barrier systems are found along the central and southern NSW coastlines [Fig. 2.7].

Thom et al. [1978] first described a vertically-stacked barrier relationship in the stratigraphy at Bherwerre Beach (St Georges Basin), which they classified as a Holocene episodic dune bay barrier. Drilling of the surficial Holocene dune sands, however, revealed buried relict Pleistocene barrier deposits some 12 m below the surface, although no relict beach ridges were observed at the surface. Evidence of similar buried relict Pleistocene barrier deposits that are overlain by Holocene barrier deposits were also identified at Fingal Bay, Dee Why, Bermagui, Tuggerah Lake and Lake Macquarie [*Roy and Peat*, 1973; *Thom et al.*, 1978; *Roy*, 1994]. More recently, the application of amino-acid racemisation, radiocarbon and thermoluminescence dating techniques to new sediment samples, and the collection of estuarine seismic data, has provided a more detailed account of vertical barrier stacking in the incised valleys of the southern NSW coast [*Sloss et al.*, 2005, 2006a,b, 2010]. In general, remnant Pleistocene transgressive

deposits, which have been modified by lowstand fluvial incision, form the basal sedimentary unit of the incised valleys, and grade into Pleistocene barrier deposits toward the bay-mouth location of the current Holocene barrier in these embayments. The basal deposit may be overlain disconformably by a thin Holocene transgressive sand sheet, which is topped by Holocene barrier, flood-tide delta and estuarine deposits.

2.4.4 Solitary Holocene barrier system

The solitary Holocene barrier system arrangement refers to the case where only an individual Holocene-age coastal barrier system is preserved within the present-day embayment [Fig. 2.6d]. Coastal barrier deposits associated with Pleistocene sea-level highstands either did not accumulate in the embayment or were subsequently removed by fluvial erosion or shoreface reworking. The most documented solitary Holocene barrier system in southeastern Australia occupies a bay-head position within the Moruya embayment [Sec. 2.6]. Drilling and dating of barrier sands in the Moruya embayment depict the seaward progradation of the shoreline following the termination of Holocene transgression, giving rise to an extensive (c. 20-30 m deep, 2 km wide) beach-ridge strandplain [*Thom*, 1978; *Thom et al.*, 1981b; *Thom*, 1984; *Thom and Roy*, 1985]. Beneath the prograded barrier strandplain, a transgressive sand sheet deposited during the latter stages of the Holocene transgression overlies backbarrier estuarine mud associated with the Holocene transgressive barrier [Sec. 2.6]. Solitary Holocene barrier systems are restricted to the central and southern NSW coast, and have been identified in the Woy Woy, Merimbula and Wonboyn embayments [*Thom*, 1978; *Thom et al.*, 1981b].

2.5 Sampling methods

In this section a brief description of the field and laboratory techniques that have been used to sample the coastal barrier systems considered in this thesis is provided. The descriptions provide the detail required to interpret the geological evidence presented in Sections 2.6 and 2.7, which form the basis of the simulation experiments that are described in subsequent chapters. In many cases the sampling and analysis has been carried out as a collaborative effort between multiple institutions. To compile a comprehensive account of previous work on the coastal barrier systems at Moruya and

Forster-Tuncurry therefore, reference is made to the individual studies in which key datasets and interpretations have been previously published.

2.5.1 Geophysical surveys

Ground penetrating radar (GPR) has been used to image the subsurface of terrestrial coastal barrier systems. For example, [*Roy et al.*, 1997] carried out a number of GPR transects that collectively traversed the coastal strandplains of the northern embayment at Forster-Tuncurry. They used a Pulse Echo IV instrument operated at 50 MHz, which provided the most suitable balance of penetration and resolution. Marine seismic reflection techniques have also been used to image the subsurface of submerged barrier systems on the continental shelf. For example, *Roy et al.* [1997] imaged the inner shelf at Forster-Tuncurry using high-resolution marine seismic reflection, which was collected along a series of cross-shore profiles to a maximum water depth of 60 m using a monopulse boomer system. Aside from some limited examples of industry data [*Browne*, 1994], high-resolution marine seismic records such as the Forster-Tuncurry dataset are scarce along the southeast Australian margin. Although reconnaissance seismic traverses across the margin have been conducted by public authorities and research agencies, the resolution of such data is too low to resolve late-Quaternary deposition in detail.

2.5.2 Drilling and coring

Reverse-circulation drilling and coring has been carried out previously on the Pleistocene strandplains, the Holocene strandplain, and southern embayment Pleistocene barrier at Forster-Tuncurry [*Roy et al.*, 1997]. A Gemco H13B rotary rig with a 54 mm diameter core barrel and plastic liner assembly was used to retrieve core samples at the four locations [*Roy et al.*, 1997]. A series of short cores were also collected on the GPR traverse of the Pleistocene strandplains to obtain age data from quartz sand samples. These ages were first published by *Bryant et al.* [1994]. Drilling of the Holocene barrier system at Moruya was carried out along three transects using a Gemco 210B power auger [*Thom et al.*, 1981b]. Fifteen holes were also drilled across the Holocene barrier system at Forster-Tuncurry using a power auger, from which 28 ages were obtained from shell hash samples [*Nielsen and Roy*, 1981]. These ages were first published by [*Melville*, 1984]. To assist with the interpretation of high-resolution seismic data from

Forster-Tuncurry, vibrocore samples were collected at 90 sites in water depths between 16-100 m along the seismic profile transects. Vibrocoring in the predominantly sandy shelf sediments was reported to have achieved a maximum penetration of 6 m (average 4.75 m) and very good recovery [*Roy et al.*, 1997]). Sediment samples were subsequently analysed for both textural properties (grain-size, sorting) and mineralogy.

2.5.3 Dating methods

The age structures of many Holocene barriers systems of the southeast Australian coastline have been determined previously using radiocarbon dating techniques *Thom et al.* [1978, 1981b]; *Roy et al.* [1997]. A detailed description of the sampling and laboratory techniques used has been provided by *Thom et al.* [1981b]. The radiocarbon ages that are used to guide the model experiments in this study were derived by Beta Analytic, The University of Sydney, and Australian National University from in situ whole shells, shell fragments, shell hash, and wood materials. Briefly, conventional radiocarbon ages are based on isotopic-fractionation corrected C^{14} depletion with respect to 95% of the activity of isotopically-corrected oxalic acid count rate, using the C^{14} half life of 5,770 years (i.e. 5,730 $\pm$ 40 years) and assuming a δ-value of -1 $\pm$ 2% for shells or -25 $\pm$ 2% for wood. The oceanic environmental corrected ages are based on an Oceanic Reservoir Apparent Age of -450 $\pm$ 35 years. The calibrated radiocarbon ages reported here were derived using the procedure of *Clark* [1975].

Thermoluminescence (TL) dating techniques have been used previously to derive indicative ages for coastal barrier deposits from Forster-Tuncurry, where the limits of conventional radiocarbon dating were exceeded [*Bryant et al.*, 1994, 1997; *Roy et al.*, 1997]. Analyses have been carried out on quartz sand that was retrieved from the shallow cores taken across the Pleistocene strandplains, and offshore vibrocores from the drowned shelf barrier systems [*Roy et al.*, 1997]. The TL analyses were carried out at the University of Wollongong, and the derived ages and techniques used have been described in detail elsewhere [*Bryant et al.*, 1994; *Price et al.*, 2001]. Nonetheless, a brief account of the necessary details is provide below:

The TL signal from the 90-125 micron quartz fraction was measured over temperature plateaus spanning 300-500°C. Specific activity was measured by means of thick source alpha counting over a 42 mm scintillation screen. A cosmic contribution of 150 $\pm$ 50 μGra^{-1} was assumed for all samples except samples W1182-W1190 inclusive,

for which a value of 138 ± 25 μGra^{-1} was used. All samples with the exception of W1395-W1397 were saturated at the time of collection and moisture content measured in the lab was between 15-25%. Where the measured moisture content was assessed to vary from the long-term average water content, TL dates were adjusted to reflect long-term averages considering the locations of samples. This was the case for samples retrieved from the northern Pleistocene strandplain (W1182-W1190), for which in situ water content of 25% was assumed. However, the relatively deep burial of those samples (2-3 m) allowed for lower cosmic doses to be assumed, and thus the error bars for the older samples could be reduced. The error ranges of TL ages reported acknowledge the total experimental, environmental and statistical uncertainties associated with each parameter in the analysis, and not simply the statistical uncertainty of the measurement technique.

2.6 Moruya

2.6.1 Coastal geomorphology

The Moruya embayment is located to the south of Batemans Bay, about 300 km south from Sydney [Fig. 2.10]. The Holocene prograded barrier there spans approximately 7 km alongshore, stretches almost 2 km from the head of the embayment to the present-day shoreline, and is composed of 40-50 beach ridges [Fig. 2.10]. The average elevation of the strandplain is 4-5 m PMSL and the relief of the beach ridges varies between 1-3 m. The modern foredune is a complex feature that is formed of numerous mounds and depressions, and which exceeds 10 m elevation in parts. Iron-rich podzols are found underlying the entire strandplain and are heavily leached toward the landward end of the barrier, although there is no evidence of soil development beneath the modern foredune complex [*Thom et al.*, 1978]. The rock outcrops of Broulee Headland/Island at the northern end of the strandplain divide the Moruya embayment from the smaller Broulee embayment to the north. The Broulee Holocene strandplain is similar in morphology and age structure to the Moruya strandplain, and the two bays were likely connected during the early to mid Holocene [*Thom et al.*, 1981b]. The continental shelf fronting the Moruya embayment has an average slope of 0.45° to 70 m depth, a steep mid-shelf slope between 80-100 m depth, and a gently sloping outer shelf plain to the shelf break at 145 m depth.

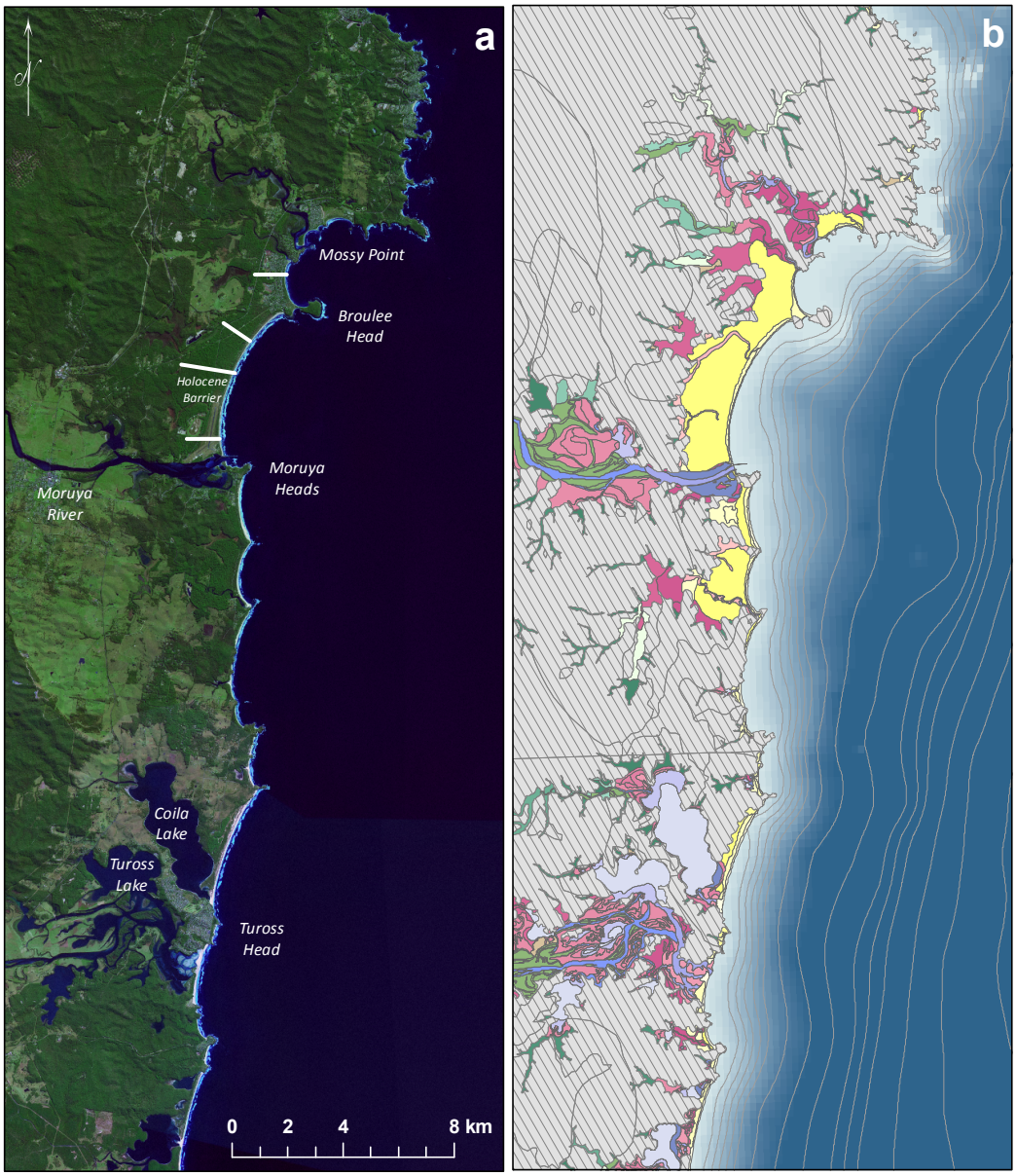

Figure 2.10: Geomorphology and Quaternary geology of the Moruya region - (a) Satellite imagery and (b) Quaternary subsurface sediment distributions of the Moruya region [Fig. 2.1]. The locations of the northern, central and southern Moruya drilling transects [Fig. 2.12] are shown with the individual Broulee transect to the north. Note the steep inner-continental shelf as indicated by 10-m bathymetry, and the limited development of coastal barrier deposits along the rocky coastline to the south of Moruya. See Figure 2.11 for a legend of Quaternary subsurface sediments shown in panel b.

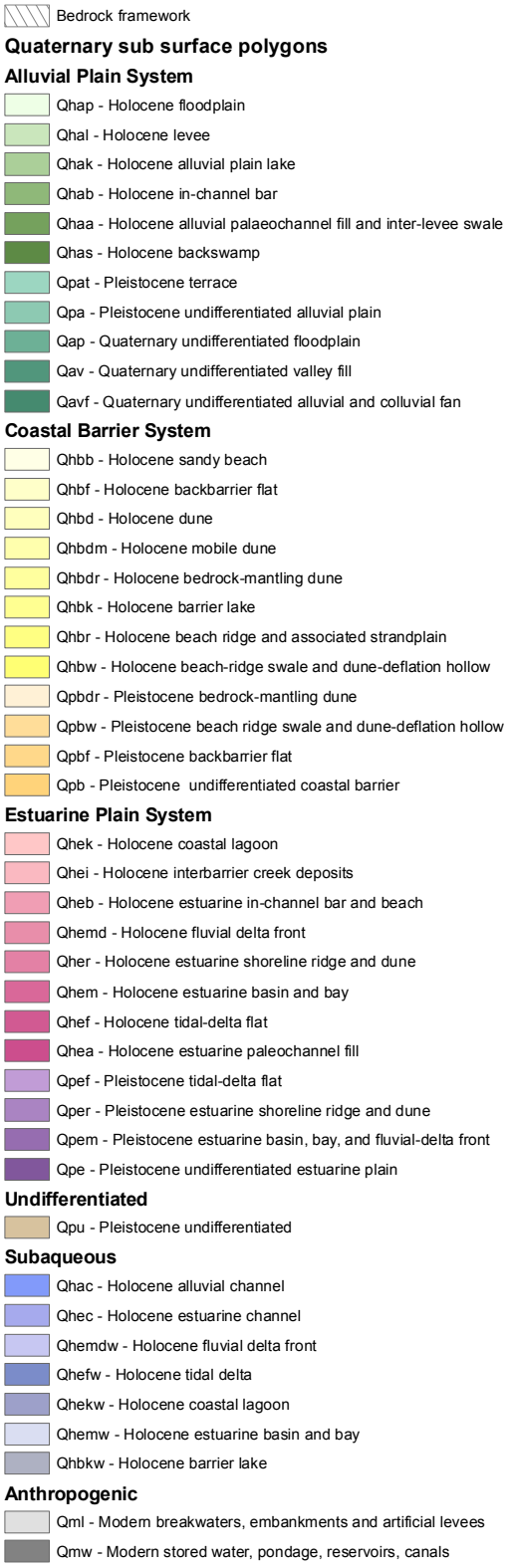

Figure 2.11: Legend for Quaternary subsurface sediment distributions - This legend accompanies Figures 2.10 and 2.13.

2.6.2 Age data

Radiocarbon ages derived using the methods described in Section 2.5.3 have been retrieved from three drilling transects in the Moruya embayment [Fig. 2.12], and one transect in the Broulee embayment, by *Thom et al.* [1981b]. Figure 2.12 shows the distribution of age data for the Moruya embayment. The details of the age data are provided in Table 2.1, and interpreted palaeo-shorefaces are shown in Figure 2.12 for the central Moruya transect. Proportional rates of strandplain progradation derived from the northern, southern and central Moruya transects are shown in Figure 2.4. Comparison of the proportional strandplain progradation rates within the Moruya embayment, in the context of all the evidence, suggests that Holocene strandplain progradation commenced around 6.5 ka BP and proceeded rapidly at first, before diminishing through the late Holocene.

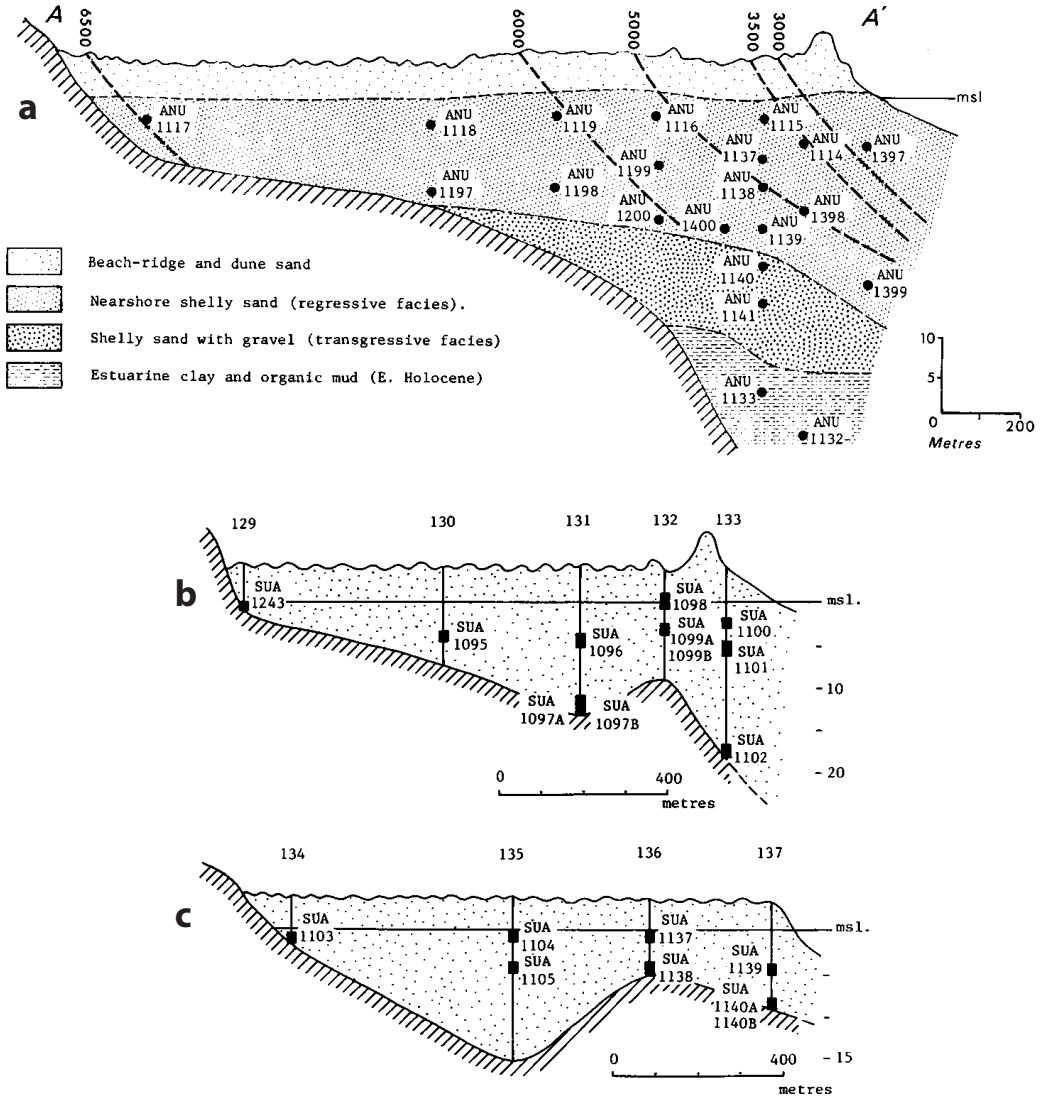

Figure 2.12: Age structure of the Holocene barrier system at Moruya from radiocarbon dating - Interpreted cross-sections for the three Moruya embayment drilling transects [Fig. 2.10]. The distribution of sediment facies and samples retrieved for radiocarbon dating are shown, along with interpreted mid- to late-Holocene palaeo-shorefaces for the central Moruya drilling transect. Modified from [*Thom et al.*, 1981b].

Table 2.1: Radiocarbon age data for the Moruya strandplain - Samples retrieved from the central, northern and southern Moruya transects [Fig. 2.10], as reported by *Thom et al.* [1981b]. An environmental correction of -450 ± 35 years was applied to each Apparent C^{14} age to derive the conventional ages. Absent Calibrated ages were beyond the range of the techniques used.

Lab code	Apparent C^{14} age (years)	Conventional age (years)	Calibrated age (years)
ANU-1117	6,100 ± 80	5.650 ± 90	6,480 ± 190
ANU-1118	5,920 ± 70	5,470 ± 80	6,270 ± 230
ANU-1197	5,860 ± 70	5,410 ± 80	6,220 ± 240
ANU-1119	5,820 ± 90	5,370 ± 100	6,180 ± 250
ANU-1198	5,830 ± 70	5,380 ± 80	6,190 ± 250
ANU-1200	6,290 ± 80	5,840 ± 90	6,690 ± 250
ANU-1116	4,930 ± 70	4,480 ± 80	5,200 ± 280
ANU-1199	5,120 ± 80	4,670 ± 90	5,430 ± 240
ANU-1400	5,410 ± 90	4,960 ± 100	5,740 ± 230
ANU-1138	5,180 ± 60	4,730 ± 70	5,500 ± 240
ANU-1139	5,150 ± 60	4,700 ± 70	5470 ± 240
ANU-1398	4,920 ± 80	4,470 ± 90	5,190 ± 280
ANU-1399	4,950 ± 100	4,500 ± 110	5,230 ± 300
ANU-1115	4,100 ± 60	3,650 ± 70	4,060 ± 310
ANU-1137	3,760 ± 60	3,310 ± 70	3,640 ± 270
ANU-1114	3,810 ± 80	3,360 ± 90	3,700 ± 270
ANU-1397	2,740 ± 70	2,290 ± 80	2,390 ± 280
ANU-1140	8,490 ± 170	8,040 ± 170	
ANU-1141	9,130 ± 210	8,680 ± 210	
ANU-1133		8,960 ± 100	
ANU-1132		9,700 ± 110	
SUA-1243	5,705 ± 80	5,260 ± 90	6,080 ± 270
SUA-1095	3,835 ± 80	3,390 ± 90	3,730 ± 270
SUA-1096	2,985 ± 80	2,540 ± 90	2,650 ± 260
SUA-1097A	4,055 ± 75	3,610 ± 80	4,000 ± 300
SUA-1098	1,885 ± 75	1,440 ± 80	1,400 ± 180
SUA-1099A	2,485 ± 70	2,040 ± 80	2,050 ± 280
SUA-1099B		2,360 ± 70	2,480 ± 260
SUA-1100	1,520 ± 75	1,070 ± 80	1,040 ± 200
SUA-1101	2,220 ± 80	1,770 ± 90	1,720 ± 190
SUA-1102	4,380 ± 80	3,930 ± 90	4,460 ± 350
SUA-1103	5,790 ± 85	5,340 ± 90	6,160 ± 260
SUA-1104	5,035 ± 85	4,590 ± 90	5,330 ± 270
SUA-1105	4,930 ± 80	4,480 ± 90	5,200 ± 280
SUA-1137	3,710 ± 75	3,260 ± 80	3,570 ± 260
SUA-1138	4,630 ± 80	4,180 ± 90	4,800 ± 330
SUA-1139	2,710 ± 75	2,260 ± 80	2,310 ± 250
SUA-1140A	3,785 ± 65	3,340 ± 70	3,670 ± 270
SUA-1140B		1,850 ± 65	1,810 ± 160

2.6.3 Sediments, stratigraphy and age structure

Thom et al. [1978] described the stratigraphy of the Moruya embayment from the sampling carried out on the central transect [Fig. 2.12a]. They described the lowest unit, which reaches -30 m PMSL at its highest elevation, as a compact dark-grey and organic-rich 'clay' containing thin layers of sand. Conventional C^{14} ages obtained from organic mud in that unit were 9,700 ± 110 (ANU-1132) and 8,960 ± 100 years (ANU-1133) [Tab. 2.1]. The 'clay' unit contained common estuarine mud in-fauna species, including *Nassarius sp.* and *Notospicular parva*, and was thus proposed to represent a backbarrier estuarine basin environment [*Thom et al.*, 1978]. A gravelly-sand unit overlies the basal 'clay' and bedrock, and was interpreted to be a transgressive sand sheet, on the basis of sediment sorting and biota [*Thom et al.*, 1978]. Conventional C^{14} ages obtained from the carbonate sand fraction in that unit were 8,680 ± 210 (ANU-1141) and 8,040 ± 170 years (ANU-1140) [Tab. 2.1].

A wedge-shaped unit of very shelly sand that thickens in a seaward direction occurs above the transgressive and estuarine faces [Fig. 2.12a]. The yellow-grey medium to coarse sand becomes finer with increasing depth, and is rich in both detrital shell and whole-shell specimens of *Bankivia fasciata*. On the basis of internal sediment grain-size distributions and preserved whole shells of nearshore species, that unit was interpreted as regressive shoreface sands typical of strandplain progradation [*Thom et al.*, 1978]. Seventeen calibrated C^{14} ages retrieved from the regressive unit suggest progradation at progressively decreasing rates between about 6.5 ka and 2 ka BP [Tab. 2.1]. Overlying the regressive sand unit, a tabular unit of fining-upwards sands of uniform thickness was interpreted as beachface and dune facies deposited by beach and aeolian processes [*Thom et al.*, 1978].

Whilst the Moruya stratigraphy is best constrained for the central transect, the additional northern and southern Moruya transects, and the Broulee transect, reported by *Thom et al.* [1981b], demonstrate that the regressive strandplain unit extends throughout the Moruya and Broulee embayments [Fig. 2.12]. This is further evident in the extension of roughly shore-parallel beach ridges throughout both embayments. Thus the central transect is assumed to be representative of the embayments.

2.7 Forster-Tuncurry

The Forster-Tuncurry region is located about 300 km north of Sydney in the central region of the southeast Australian margin [Fig. 2.1]. The coast is divided into northern and southern embayments, which are separated by the Cape Hawke promontory [Fig. 2.13]. Although the contemporary highstand embayments are bound alongshore and to landward by Palaeozoic to Mesozoic bedrock, the isolation of Cape Hawke from the mainland geology suggests that the northern and southern embayments were once joined prior to infilling with Quaternary sediments [Fig. 2.13b]. Thus Cape Hawke is believed to have acted as an offshore island during early to mid Pleistocene sea-level highstands [*Melville*, 1984]. The coastal geomorphology and stratigraphy of the Forster-Tuncurry region have been described previously by *Melville* [1984] and *Roy et al.* [1997]. *Melville* [1984] proposed a conceptual model for late-Quaternary coastal evolution at Forster-Tuncurry from the study of aerial photographs, surficial sediment samples and core samples collected during mineral exploration. He identified seven evolutionary stages during which the two embayments infilled with shallow-marine and fluvial deposits. Specifically, three stages of mid-late Pleistocene highstand deposition were identified, followed by an erosive phase during the last-glacial stage, and three subsequent stages of Holocene deposition. However, the absence of geophysical surveys and pre-Holocene age constraints precluded a comprehensive chronostratigraphic analysis. Subsequent dating of the northern embayment coastal strandplains appears to support the model of *Melville* [1984], with three Pleistocene age groups identified [*Bryant et al.*, 1994, 1997; *Roy et al.*, 1997]. The geophysical data, sediment samples and age data collected at Forster-Tuncurry form part of a comprehensive study carried out by *Roy et al.* [1997], who further described the timing, location and sources of coastal barrier deposition based on their stratigraphic interpretations.

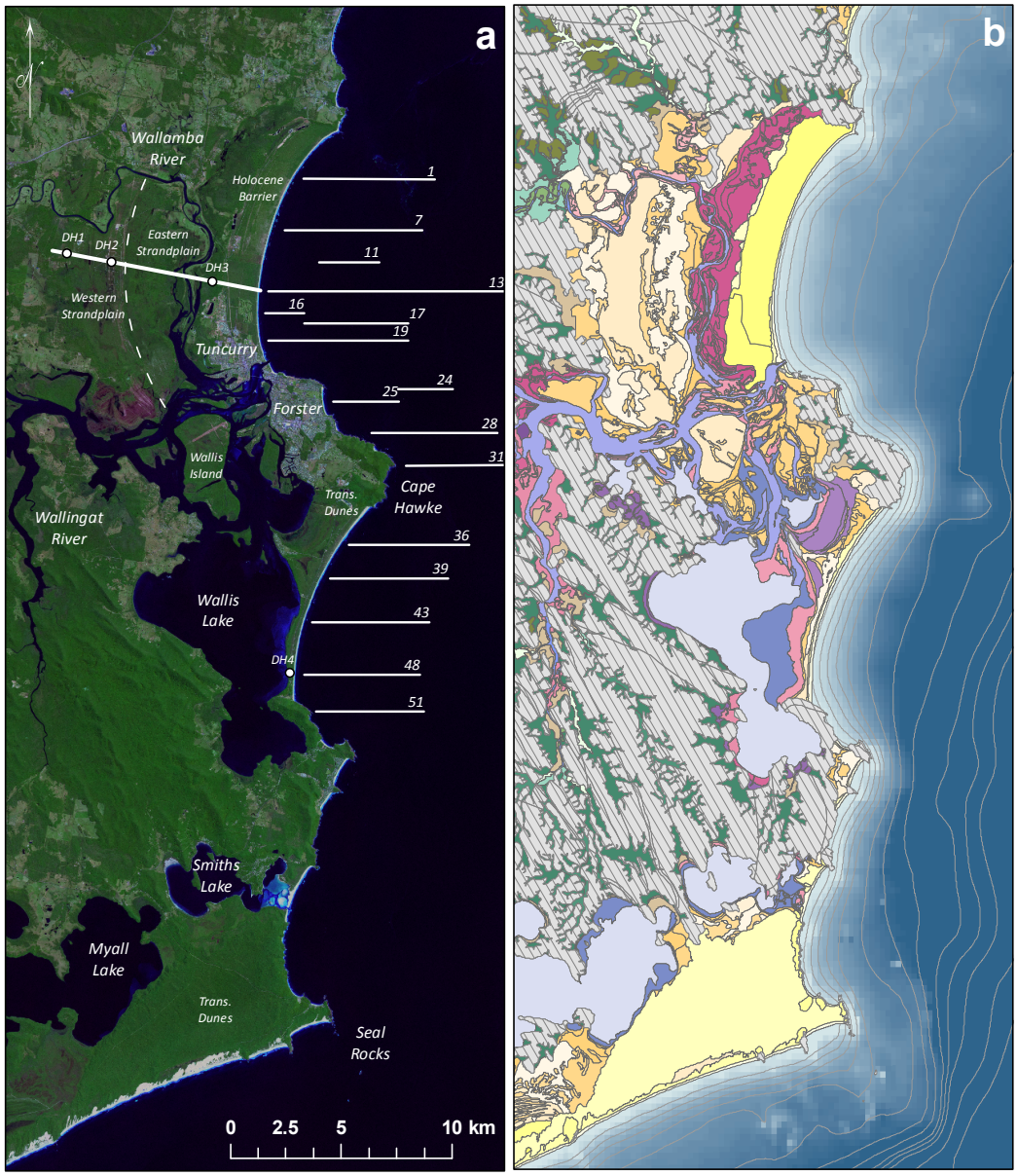

Figure 2.13: Geomorphology and Quaternary geology of the Forster-Tuncurry region - (a) Satellite imagery and (b) Quaternary subsurface sediment distributions of the Forster-Tuncurry region [Fig. 2.1]. The locations of ground penetrating radar (GPR) transects [Figs. 2.15 & 2.17] across the northern embayment barrier systems, and high-resolution marine seismic and vibrocore sampling lines across the inner shelf [Figs. 2.18, 2.19 & 2.20], are shown. Shallow-core sand samples for TL dating of the inner composite strandplain and drill cores for radiocarbon dating of the Holocene strandplain were retrieved along the GPR transect. The locations of the interpreted drill holes in Figure 2.14 are also shown. Note the shallower northern embalmment inner-continental shelf relative to the southern embayment, as indicated by 10-m bathymetry in panel b. See Figure 2.11 for a legend of Quaternary subsurface sediments shown in panel b.

2.7.1 Coastal geomorphology

Figure 2.13 shows the coastal geomorphology and Quaternary geology of the Forster-Tuncurry region. The northern (i.e. Tuncurry) embayment contains a series of coastal strandplains that span up to 8 km in width and 12 km alongshore. At the surface, the strandplains can be divided into three apparently distinct sections that are separated by a shore-parallel topographic discontinuity and the Wallamba River. West of the river, a composite Pleistocene-age strandplain reaches up to 6 km wide in the central part of the embayment, and is divided into western and eastern sections by the topographic discontinuity. The southern extremity of the composite strandplain is dissected where the Wallingat River joins the Wallis Lake estuary, isolating Wallis Island from the rest of the strandplains. East of the Wallamba River, a Holocene-age strandplain spans 12.5 km alongshore and is up to 2 km in width. The Holocene strandplain is composed of about 40 beach ridges at 5-8 m elevation. The Holocene barrier system is located adjacent and seaward of the composite strandplain that lies to the west of the Wallamba River. The Wallamba River fills the interbarrier depression between the composite strandplain and the Holocene barrier system. The continental shelf fronting the Tuncurry embayment has an average gradient of 0.225° to the shelf break at 140 m. Submerged bedrock reefs extend seaward from Hallidays Point and Cape Hawke.

In contrast, the southern embayment is narrower (5-7 km wide) and shorter in alongshore extent (9 km). It is dominated by the Wallis Lake estuary, which shares a common tidal inlet with the Wallamba and Wallingat Rivers in the southern corner of the northern embayment. The estuary is partially filled with Holocene backbarrier muds, and marine influences are restricted to a bi-lobed flood-tide delta located near the estuary mouth, which is 5-10 m thick. The estuary is impounded by a narrow apparently Pleistocene-age coastal barrier, which widens to the north where an estuarine strandplain has developed between a bedrock outcrop at Green Point and the Cape Hawke promontory. Aeolian deposits increase in volume toward the northern end of the embayment, where transgressive dunes at Cape Hawke are mid-Pleistocene in age [*Bryant et al.*, 1994]. On the ocean side of the barrier Holocene sediments are restricted to a thin shoreface veneer, and the inner shelf is approximately twice as steep relative to the northern embayment (0.45°).

2.7.2 Age data

The results for 12 unpublished TL ages from the Forster-Tuncurry region are presented in Table 2.2, along with previously published ages [*Bryant et al.*, 1994, 1997]. The unpublished ages were obtained from vibrocores retrieved from the northern embayment shelf, and drill hole DH4 from the southern embayment [Fig. 2.13]. The depths of samples from the composite strandplain were found to be sufficient to reach undisturbed sediments by dating shallower samples (c. 60-70 cm depth), which returned ages between 20-34 ka, and thus indicate partial re-zeroing of sediments [*Roy et al.*, 1997]. The TL ages from the northern embayment and shelf fall into four age groups (261-217, 147-131, 94-79 and 59-43 ka) which suggests multiple phases of mid to late Pleistocene deposition within the region, beginning from sometime during MIS 7. In the southern embayment, TL ages from drill-core DH4 span between 115-87 ka, suggesting late-Pleistocene deposition of the outer part of the barrier. Older TL ages (>390 to 256 ka) from the Cape Hawke transgressive dunes suggest that aeolian deposition pre-dates the preserved coastal barrier deposits [*Bryant et al.*, 1994].

Table 2.3 contains the details of 31 radiocarbon ages from vibrocores retrieved from the Forster-Tuncurry inner shelf and Wallis Lake estuary. The environmentally corrected ages span from 1.65 ka BP to the limits of laboratory techniques (i.e. >40 ka BP), suggesting that both pre- and post-last-glacial maximum deposits were sampled. The ages from the drowned shelf barrier and backbarrier deposits agree well with TL ages [Tab. 2.2], with those from the northern embayment reaching the limits of the dating technique and suggesting that the drowned barriers there were deposited prior to 40 ka BP [Tab. 2.3]. Radiocarbon ages from the drowned coastal barrier systems of the southern-embayment shelf fall between 37-30 ka BP, suggesting that these deeper deposits are younger than the coastal barrier deposits of the northern embayment shelf. Radiocarbon ages from drill cores retrieved from the Wallis Lake tidal inlet indicate that the progradation of the flood-tide delta into the estuary predominantly occurred between 4-2 ka BP [Tab. 2.3].

Table 2.2: Thermoluminescence age data for the Forster-Tuncurry region - Samples retrieved from the northern and southern Pleistocene barriers, the Cape Hawke dunes, and the drowned shelf barriers of the northern embayment [Fig. 2.13].

Location	Height (m)	Depth (cm)	Lab code	Palaeodose (Gy)	k (%)	Specific activity (Bg/Kg U+Th)	Annual dose (μGy)	Age (ka)	Reference
Northern barriers									
A3		170-220	W1182	52.4 ± 4.6	0.031	5.9 ± 0.2	241 ± 21	217 ± 27	*Bryant et al.* [1994]
B3		195-235	W1183	62.5 ± 8.3	0.036	7.4 ± 0.3	263 ± 21	238 ± 37	*Bryant et al.* [1994]
C3		180-220	W1184	71.8 ± 5.6	0.039	7.8 ± 0.3	275 ± 21	261 ± 28	*Bryant et al.* [1994]
D3		250-290	W1185	62.2 ± 12.6	0.054	15.6 ± 0.6	422 ± 22	147 ± 31	*Bryant et al.* [1994]
E3		140-190	W1186	52.6 ± 4.7	0.055	12.2 ± 0.5	360 ± 21	146 ± 16	*Bryant et al.* [1997]
F3		150-200	W1187	48.3 ± 5.5	0.039	21.5 ± 0.8	511 ± 23	94.4 ± 11.5	*Bryant et al.* [1997]
G3		150-200	W1188	46.5 ± 3.7	0.044	20.8 ± 0.8	533 ± 24	87.3 ± 8.0	*Bryant et al.* [1997]
H3		150-170	W1189	35.5 ± 5.0	0.066	12.3 ± 0.5	380 ± 22	93.3 ± 14.2	*Bryant et al.* [1997]
I3		350-400	W1190	40.0 ± 2.9	0.060	19.9 ± 0.8	502 ± 23	79.6 ± 6.8	*Bryant et al.* [1994]
J1		200-230	W1134	74.7 ± 7.9	0.035	19.7 ± 0.5	571 ± 26	131 ± 15	*Bryant et al.* [1997]
K1		-	W1270	91.6 ± 7.5	0.03	18.2 ± 0.6	468 ± 22	196 ± 19	*Bryant et al.* [1997]
FT13.3	-25.5	185-200	W1130	130.9 ± 17.2	0.580	48.8 ± 1.5	1368 ± 1.5	95.7 ± 13	*Bryant et al.* [1997]
Shelf barriers									
FT1.5	-35.6	230-240	W1287	56.6 ± 4.9	1.020	18.3 ± 4	1263 ± 59	44.8 ± 4.4	*Roy et al.* [1997]
FT1.5	-35.6	348-355	W1288	66.1 ± 6.1	0.990	21.6 ± 4	1313 ± 60	45.8 ± 5.1	*Roy et al.* [1997]
FT7.5	-36.8	387-404	W1289	67.5 ± 5.2	1.010	27.0 ± 4	1396 ± 59	48.4 ± 4.3	*Roy et al.* [1997]
FT7.7	-36.0	431-443	W1290	78.4 ± 12.9	1.145	24.0 ± 4	1478 ± 60	53.1 ± 9.0	*Roy et al.* [1997]
FT13.7	-38.3	345-370	W1131	55.4 ± 7.3	0.732	17.3 ± 0.7	1044 ± 41	53.1 ± 7.3	*Roy et al.* [1997]
FT13.8	-42.9	207-225	W1132	56.4 ± 6.6	0.696	14.7 ± 0.6	953 ± 40	59.2 ± 7.3	*Roy et al.* [1997]
FT24.1	-42.3	185-195	W1291	118 ± 12	0.695	114 ± 4	2628 ± 62	44.9 ± 4.7	*Roy et al.* [1997]
FT24.2	-48.0	315-340	W1292	73.4 ± 5.4	1.275	28.1 ± 4	1686 ± 61	43.5 ± 3.6	*Roy et al.* [1997]
FT24.2	-48.0	355-370	W1293	75.8 ± 6.4	1.265	25.2 ± 4	1627 ± 61	46.6 ± 4.3	*Roy et al.* [1997]
Cape Hawke									
CH1		-	W1375	>245 ± 61	0.03	23.4 ± 0.07	626 ± 49	>390 ± 100	*Bryant et al.* [1994]
CH2		-	W1376	117 ± 17	-	9.9 ± 0.4	344 ± 49	340 ± 68	*Bryant et al.* [1994]
CH2		-	W1378	58.1 ± 6.7	-	4.2 ± 0.2	227 ± 48	256 ± 62	*Bryant et al.* [1994]
Southern barriers		(m)							
BB DH1		26.0-28.5	W1395	105.5 ± 8.7	0.595	28.4 ± 4	1213 ± 67	87.0 ± 8.6	*Roy et al.* [1997]
BB DH1		48.1-48.7	W1396	160.5 ± 19.2	1.085	27.6 ± 4	1663 ± 67	96.5 ± 12.2	*Roy et al.* [1997]
BB DH1		49.0-50.2	W1397	217.7 ± 26.1	1.060	39.4 ± 4	1851 ± 67	115 ± 15	*Roy et al.* [1997]

Table 2.3: Radiocarbon age data for the Forster-Tuncurry region - Samples retrieved from shelf deposits within the northern and southern embayments and from the Wallis Lake flood-tide delta [Fig. 2.13], as reported by *Roy et al.* [1997]. Dated shell fragments from Wallis Lake were all estuarine species.

Site & core	Water depth (m)	Sample depth (cm)	Lab code	Dated material	Conventional age (ka)	Corrected age (ka)
Northern embayment						
FT7.7	36.0	290-300	Beta45165	Wood	9.90 ± 0.11	9.90 ± 0.11
FT11.1	29.0	60-70	Beta45428	Shells and fragments	3.15 ± 0.09	2.70 ± 0.09
FT11.1	29.0	460-480	Beta45429	Estuarine shells	30.99 ± 1.57	30.54 ± 1.57
FT13.1	14.0	317-327	Beta45166	Thin walled shells	7.14 ± 0.10	6.69 ± 0.10
FT13.3	23.5	510-524	Beta45431	Shell hash	37.45 ± 1.77	> 37.0
FT13.5	30.4	65-75	Beta45167	Shell hash	2.47 ± 0.06	2.02 ± 0.07
FT13.7	38.0	50-70	Beta45168	Shell hash	3.52 ± 0.07	3.07 ± 0.07
FT13.8	43.0	135-145	Beta45169	Shell hash	6.88 ± 0.08	6.43 ± 0.08
FT13.10	53.0	120-140	Beta45170	Thin walled shells	13.14 ± 0.08	12.69 ± 0.08
FT14.1	20.0	430-440	Beta45432	Andara shells	8.96 ± 0.09	8.51 ± 0.09
FT17.3	29.0	550-560	Beta45433	Estuarine shell	> 40.07	> 40.0
FT19.7	40.5	220-300	Beta45434	Bankivia shells	> 34.42	> 34.0
Wallis Lake						
RC6	3.6	430-490	SUA1340	Shell fragments	3.03 ± 0.12	2.58 ± 0.12
RC8	2.6	1080-1190	SUA1341	Shell fragments	3.49 ± 0.12	3.04 ± 0.13
RC9	4.3	180-240	SUA1342	Shell fragments	3.29 ± 0.09	2.84 ± 0.09
RC9	4.3	730-910	SUA1343	Shell fragments	4.05 ± 0.11	3.60 ± 0.11
Cape Hawke						
210 GS	36.0	0-200	SUA1697	Thin walled shells	2.10 ± 0.09	1.65 ± 0.10
210 GS	36.0	600-750	SUA1581	Thin walled shells	5.02 ± 0.09	4.57 ± 0.10
Southern embayment						
FT39.2A	30.6	128-145	SUA2992	Thin walled shells	2.73 ± 0.22	2.28 ± 0.23
FT39.4	43.5	55-65	Beta45440	Shell hash	5.16 ± 0.08	4.71 ± 0.08
FT39.4	43.5	160-180	Beta45441	Shell hash	10.50 ± 0.12	10.05 ± 0.12
FT39.4	43.5	240-250	Beta45442	Shell hash	9.60 ± 0.28	9.15 ± 0.28
FT39.4	43.5	510-525	Beta45171	Shell hash	30.24 ± 0.37	29.79 ± 0.37
FT39.4	43.5	550-570	Beta45443	Chalky shells	30.25 ± 0.91	29.80 ± 0.92
FT39.6	47.2	40-50	Beta45444	Shell fragments	6.49 ± 0.10	6.04 ± 0.10
FT39.6	47.2	130-140	Beta45172	Shell hash	7.95 ± 0.07	7.50 ± 0.07
FT39.6	47.2	205-215	Beta45445	Shell hash	13.62 ± 0.17	13.17 ± 0.17
FT39.8	56.9	80-95	Beta45446	Shell fragments	7.40 ± 0.10	6.95 ± 0.10
FT48.3	52.8	70-80	Beta45173	Shell hash	2.49 ± 0.07	2.04 ± 0.07
FT48.3	52.8	330-340	Beta45447	Chalky shell	> 37.57	> 37.00
FT48.3	52.8	391-400	Beta45174	Shell hash	35.98 ± 0.75	35.53 ± 0.75
FT48.3	52.8	490-496	Beta45175	Shell hash	37.35 ± 0.83	36.90 ± 0.83
FT51.3	50.2	90-100	Beta45448	Shells and fragments	3.67 ± 0.07	3.22 ± 0.07
FT51.3	50.2	255-265	Beta45449	Marine shell	8.69 ± 0.19	8.24 ± 0.19
FT51.3	50.2	450-455	Beta45450	Wood fragments	12.34 ± 0.10	12.34 ± 0.10

2.7.3 Sediments, stratigraphy and age structure

The following data and interpretations of late-Quaternary coastal barrier deposition at Forster-Tuncurry has been derived from the methodologies [Sec. 2.5] and findings of *Roy et al.* [1997]. As their work remains to be published in the general literature in detail, a summary is presented here to provide context for the thesis aims [Sec. 1.2.1] and evidence for the simulation experiments in subsequent chapters.

2.7.3.1 Northern (Tuncurry) embayment

Pleistocene composite strandplains. The central Pleistocene strandplains comprises a continuous succession of barrier sands, which span 5-6 km parallel to the modern coast between interfluves at the head of the embayment and the Wallamba River [Fig. 2.13]. The strandplains are a composite feature that is divided at the surface into western and eastern strandplains by a conspicuous topographic discontinuity that is oriented roughly parallel to the contemporary shoreline. The western strandplain appears to be further divided into two separate age groups of barrier deposits [Tab. 2.2]. The surface of the western strandplain is relatively flat at between 2-7 m PMSL, and comprises low relief and widely spaced shore-parallel ridges that appear to be the remnants of relict foredunes. The surface of the eastern strandplain is between 1-3 m PMSL, is swampy in places and surface lineations are less apparent compared with the western strandplain.

Barrier deposits of the western strandplain are between 10-14 m thick, up to 3 km wide, and the total volume is estimated at 44 x 10^3 m^3/m [Fig. 2.14]. The GPR profiles depict a near continuous succession of regressive barrier sands, which are characterised by concave-up, seaward dipping and offlapping reflectors that are indicative of palaeo-shorefaces that were buried during strandplain progradation [Fig. 2.15]. The tops of palaeo-shoreface reflectors are preserved to within 2 m of the contemporary surface. The oldest barrier sands date to between 261-217 ka [Tab. 2.2] and stretch 1.5-2 km east from the head of the embayment, whilst barrier sands further to the east but landward of the topographic discontinuity date to around 146 ka. There is no evidence of intervening backbarrier facies or an inter-barrier depression dividing barrier sands of the two age groups and the deposits appear to form a composite strandplain feature. The contact between barrier deposits from the two age groups is not apparent within GPR profiles and may have been obscured by heavy mineral mining [Fig. 2.15].

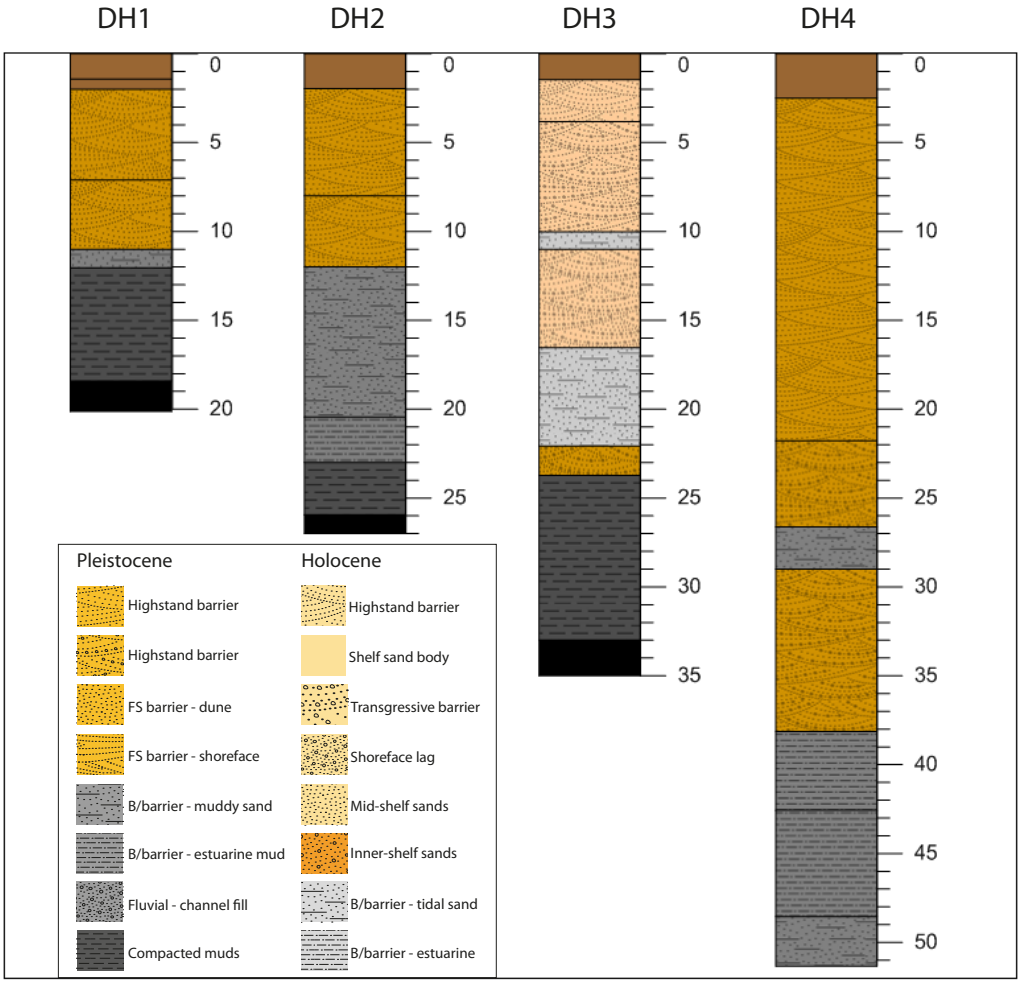

Figure 2.14: Interpreted drill holes from the Forster-Tuncurry region - Cored drill holes (a) DH1 and (b) DH2 from the northern embayment composite strandplain, (c) DH3 from the northern embayment Holocene strandplain, and (c) DH4 from the southern embayment Pleistocene barrier [Fig. 2.13]. Modified from *Roy et al.* [1997].

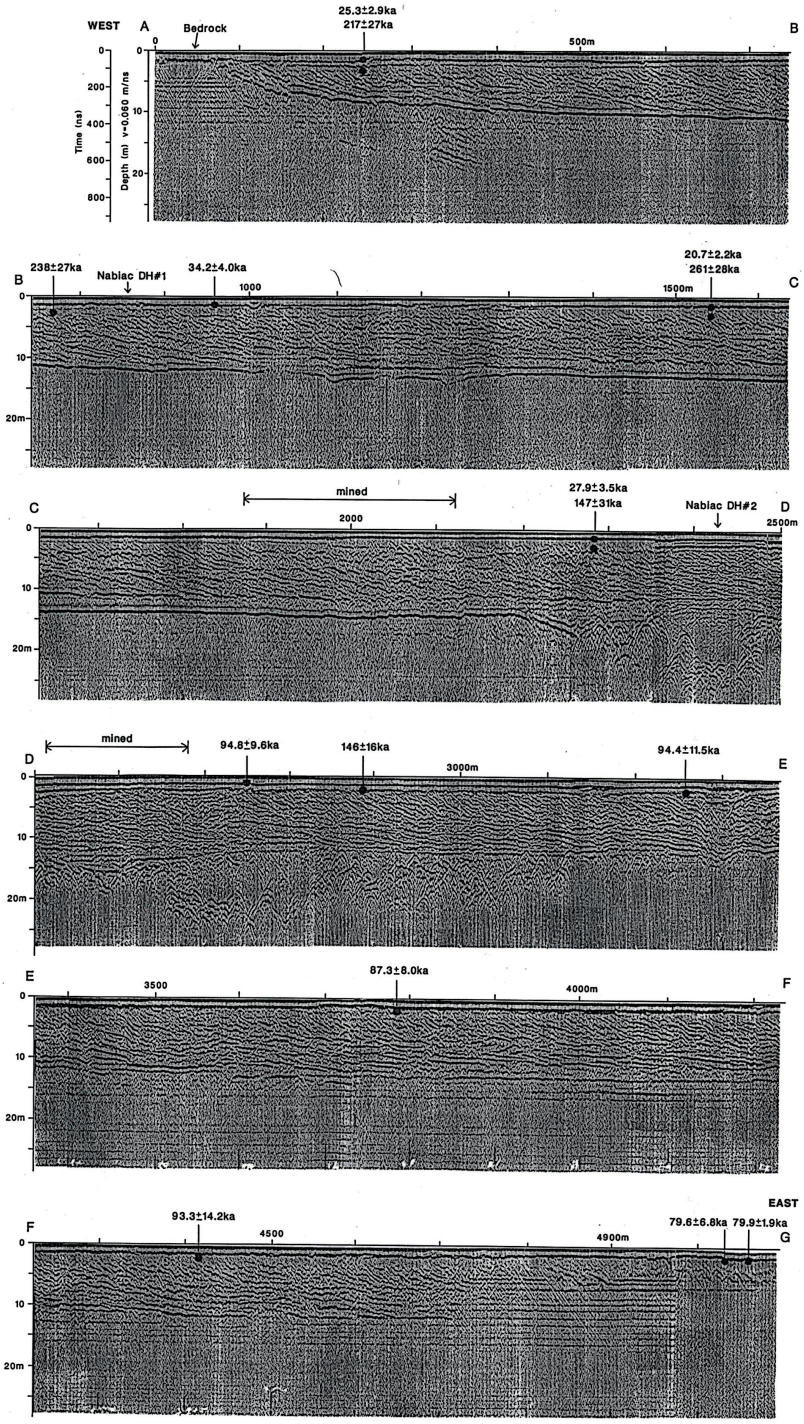

Figure 2.15: GPR profile across the Tuncurry composite strandplain - Ground penetrating radar (GPR) profile across the composite strandplain of the northern embayment. The locations of TL dates from both the A2 and B soil horizons are indicated along with sections that have been disturbed during heavy mineral mining. *Roy et al.* [1997].

The regressive barrier sands comprise quartz-rich, fine to medium grained and moderately well sorted sands of rounded to sub-rounded grains. Mud content is generally absent. From the surface to a maximum 2 m depth the barrier sands have been modified by soil development, and fine-grained and well-sorted sandy soils range in colour from grey to black where organic matter is concentrated to leached white elsewhere. The textural and compositional characteristics are typical of barrier dune sands and backbarrier (swale) infill. Beneath the soils barrier sands to 12 m depth are dark to light brown in colour, mostly fine-grained and well sorted, and indurated in the upper parts. Coarser granules are found towards the base of the unit, and in graded beds throughout. Sub-horizontal sedimentary structures are well defined in parts.

The eastern Pleistocene strandplain occurs between the older barrier deposits to the west of the topographic discontinuity and the Wallamba River and Holocene barrier system to the east. Barrier deposits of the eastern strandplain are between 12-15 m thick, up to 2 km wide, and the total volume is estimated at 29 x 10^3 m^3/m [Fig. 2.14]. The barrier sands date to between 94-79 ka [Tab. 2.2] and generally become younger to the east. The contact between the western and eastern strandplains is not clear with the GPR profile [Fig. 2.15], although the age data and sedimentology suggest distinctive origins. In contrast to the older barrier deposits of the western strandplain, which have been mined for heavy minerals that occur within beach facies 1-3 m below the surface (3-5 m PMSL), the younger deposits of the eastern strandplain are devoid of heavy mineral deposits. Pleistocene barrier sands that are associated with the eastern strandplain were also sampled in vibrocore FT13.3, at an outcrop at the toe of the Holocene barrier on the contemporary inner shelf. A TL age of 95.7 $\pm$ 13 ka was returned from sample FT13.3 [Tab. 2.2].

The barrier sands of the Pleistocene strandplains overlie bedrock, relict backbarrier deposits, and fine-grained quartz sands with lithic granules and graded layers that occur in palaeo-river channels. A weathered estuarine mud unit (observed at the base of DH1, DH2 and DH3) up to 9 m thick overlies Palaeozoic bedrock at the base of the sequence and appears to predate all strandplain deposits [Fig. 2.14]. The weathered mud ranges from green-grey at the top to mottled yellow and orange at the base. Sediments are partly oxidised and absent of any sedimentary structures or shell content. Evidence of subaerial weathering suggests that the palaeo-estuary system in which the weathered mud formed was exposed during lower sea levels prior to burial beneath the preserved

strandplains. Within palaeo-river channels (e.g. DH2) a dark grey backbarrier estuarine mud deposit lies disconformably atop the relict weathered mud unit [Fig. 2.14]. The backbarrier mud occurs as a relatively thin layer and is a firm, massive unit with traces of thin-walled estuarine shells present and no depositional structures.

Holocene highstand barrier system. East of the interbarrier depression and Wallamba River, DH3 shows that the Holocene coastal barrier system overlies relict barrier sands associated with the eastern component of the Pleistocene composite strandplain, and the basal weathered estuarine mud [Fig. 2.14]. In contrast to the Pleistocene strandplains, the Holocene barrier system features backbarrier, transgressive and highstand coastal barrier deposits. The highstand prograded barrier features a strandplain up to 2 km wide [Fig. 2.13]. The surface of the strandplain spans the length of the embayment (12.5 km) between Hallidays Point and Cape Hawke, and comprises about 40 beach ridges at 5-8 m elevation that measures up to 1.8 km in width. The Holocene barrier comprises a buried core of *transgressive barrier sands* that is overlain by the strandplain, which is composed of *regressive barrier sands*. In cross-section, the areas of transgressive and regressive facies are approximately 28 x 10^3 m^3/m and 26 x 10^3 m^3/m respectively. Figure 2.16 shows the lithological characteristics and age structure that differentiate the transgressive and regressive barrier sands.

Regressive barrier sands comprise beach and shoreface sands (250 μm) that are overlain by comparatively well-sorted dune sands of similar grain size. Within GPR profiles, reflectors are concave-up, seaward dipping and show offlapping relationships that are typical of buried palaeo-shoreface surfaces [Fig. 2.17]. The ages of dated shell hash range between 6.52-1.43 ka BP [Fig. 2.16], indicating deposition of the strandplain during the Holocene sea-level highstand. The age structure of the regressive barrier facies as determined from the distribution of dated specimens indicates variable rates of progradation during this period [Fig. 2.16]. Specifically, the rate of coastline progradation appears to have varied between 0.25 m/a for the period 6-4 ka BP, 0.15 m/a for the period 4-2 ka BP, and 0.20 m/a from 2 ka BP to present.

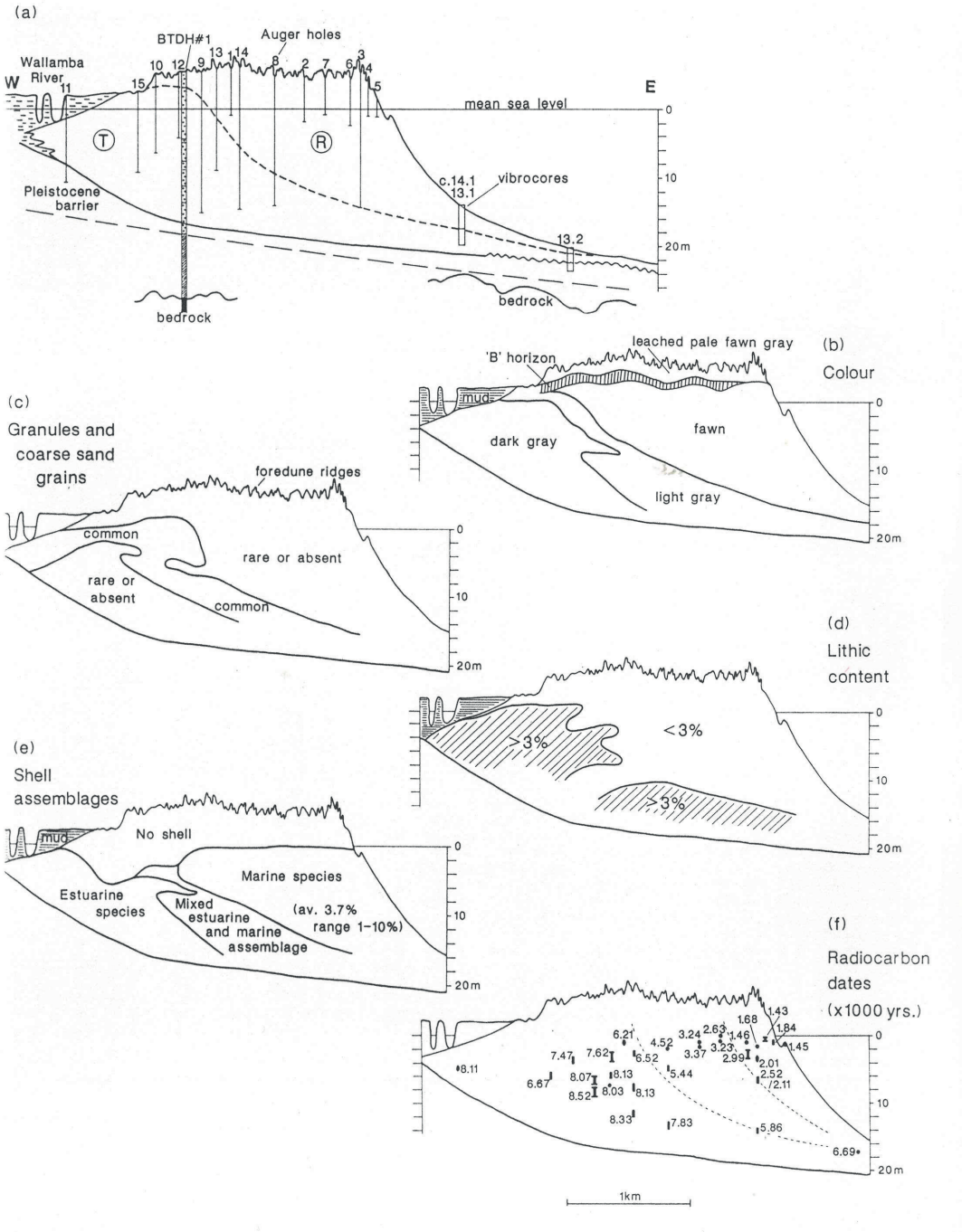

Figure 2.16: Tuncurry Holocene barrier sedimentology and age data - Sedimentology of the Holocene barrier in the northern embayment including (a) the location of drill holes and distribution of the transgressive (T) and regressive (R) facies, (b) colour and soil horizons, (c) relative abundance of granules and coarse grains, (d) lithic content, (e) shell assemblages, and (f) age distribution based on radiocarbon dates. See Figure 2.13 for sample locations. From *Roy et al.* [1997].

Transgressive barrier sands are readily identified within GPR profiles by sub-horizontal or gently landward-inclined reflectors that suggest deposition by washover and tidal inlet processes [Fig. 2.17]. Sediments comprise slightly coarser and less well-sorted barrier sands than the regressive facies, are dark to light grey, and in composition grade from a lithic-rich (> 3%) and granular top to finer muddy sands, both to landward and toward the bottom. Shell content is mixed marine and estuarine, although it becomes dominantly estuarine to landward. The ages of dated shell hash retrieved from drill holes range from 8.52 to 6.67 ka BP, with ages becoming younger to seaward and toward the top of the unit [Fig. 2.16]. The GPR records and sedimentological data suggest deposition in washover lobes and tidal inlet deposits toward the latter stages of the post-glacial transgression.

Backbarrier muddy sands that are associated with transgressive barrier deposition are divided into tidal inlet and estuarine facies. The former are medium grained quartz sands that are pale yellow-grey to fawn in colour, moderately sorted, and contain whole *Glycimeras sp.* and *Bankivia sp.* shells and shell fragments (<5%). Shell assemblages are mixed estuarine (e.g. *Anadara sp.*) and marine and angular shell fragments are common. Alternating fine and coarse-grained beds occur throughout the deposits and well-defined laminations and cross bedding are common. The estuarine facies are dark grey, fine-grained muddy sands (up to 50% mud), which comprise minor shell fragments of estuarine species and are heavily bioturbated. Comparable estuarine muddy sands dating to 12.3 ± 1 ka BP were sampled at the toe of the shelf sand body in the southern embayment [Sec. 2.7.3.3]. More recent fluvial-estuarine mud deposits associated with the Wallamba River overlie Holocene transgressive barrier sands and backbarrier muddy sands in the northern embayment.

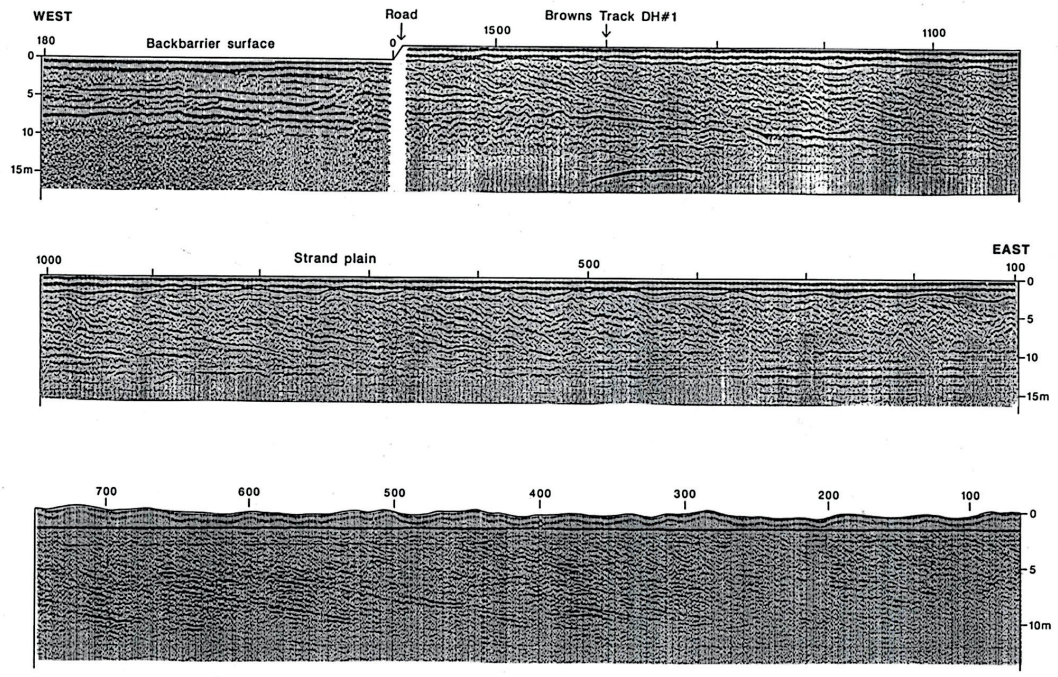

Figure 2.17: GPR profile across the Tuncurry Holocene strandplain - GPR profile across the Holocene barrier of the northern embayment. The upper two panels show the complete transect whilst the lower panel shows the eastern (seaward) half of the profile in higher resolution. See Figure 2.13 for sample locations. From *Roy et al.* [1997].

Drowned shelf barrier systems. Extensive drowned barrier systems span some 15 km across the contemporary inner to mid shelf of the northern embayment, from depths of about 30 m to well beyond 90 m. The drowned barriers are the most significant deposits of the last glacial sequence, having an estimated volume of 80 x 10^3 m^3/m. TL ages obtained from the barrier systems at 35-50 m water depth date to between 43-59 ka [Tab. 2.2]. On the inner shelf, the barriers occupy a shallow palaeo-embayment that is defined by submerged low-relief bedrock extensions of Hallidays Point and Cape Hawke. High-resolution seismic reflection to beyond 50 m water depth depicts extensive sets of concave-up, seaward dipping and offlapping reflectors, which downlap onto underlying channel fill deposits or Palaeozoic basement rocks near the coast [Fig. 2.18]. These well-defined prograded palaeo-shoreface reflector sets are arranged in a seaward down-stepping pattern, which is characteristic of falling-stage systems tract deposition [Sec. 2.3.2]. The homogenous palaeo-shoreface reflector sets are interspersed with prominent high-amplitude seaward-dipping double reflectors and beds of low-amplitude irregular reflectors in the upper section [Fig. 2.18].

Regressive barrier sands of the drowned barrier systems are comparable to those of the coastal strandplains. Although marginally finer in mean grain-size, they comprise an additional coarse mode that occurs as either discrete event beds or generally disseminated throughout the core. Dune and upper-shoreface facies were identified in regressive barrier sands retrieved in vibrocores from the northern shelf [Fig. 2.18]. Dune sands are very fine to fine grained, well sorted and structureless. Upper shoreface sands are fine to medium grained, and are characterised by coarser event beds and sub-horizontal bedding layers in parts. Bedrock and a basal weathered estuarine mud facies underlie the drowned barriers.

Pleistocene backbarrier muddy sands occur immediately landward and underlying the drowned barriers in cores retrieved between 20-30 m water depth [Fig. 2.18]. Sediments are dark grey to olive grey fine-grained sands and are typically well sorted. They comprise a slight mud fraction (<5%) and minor fine wood fragments occur in bands throughout the deposits. Shell assemblages range between estuarine, mixed and marine fauna, and include complete specimens and fragments. Bands of poorly sorted coarse sand and pebbles occur at various depths and the unit commonly features a lag deposit composed of gravel and/or shell. Depositional structures are absent and bioturbation is common with evidence of preserved burrows in parts.

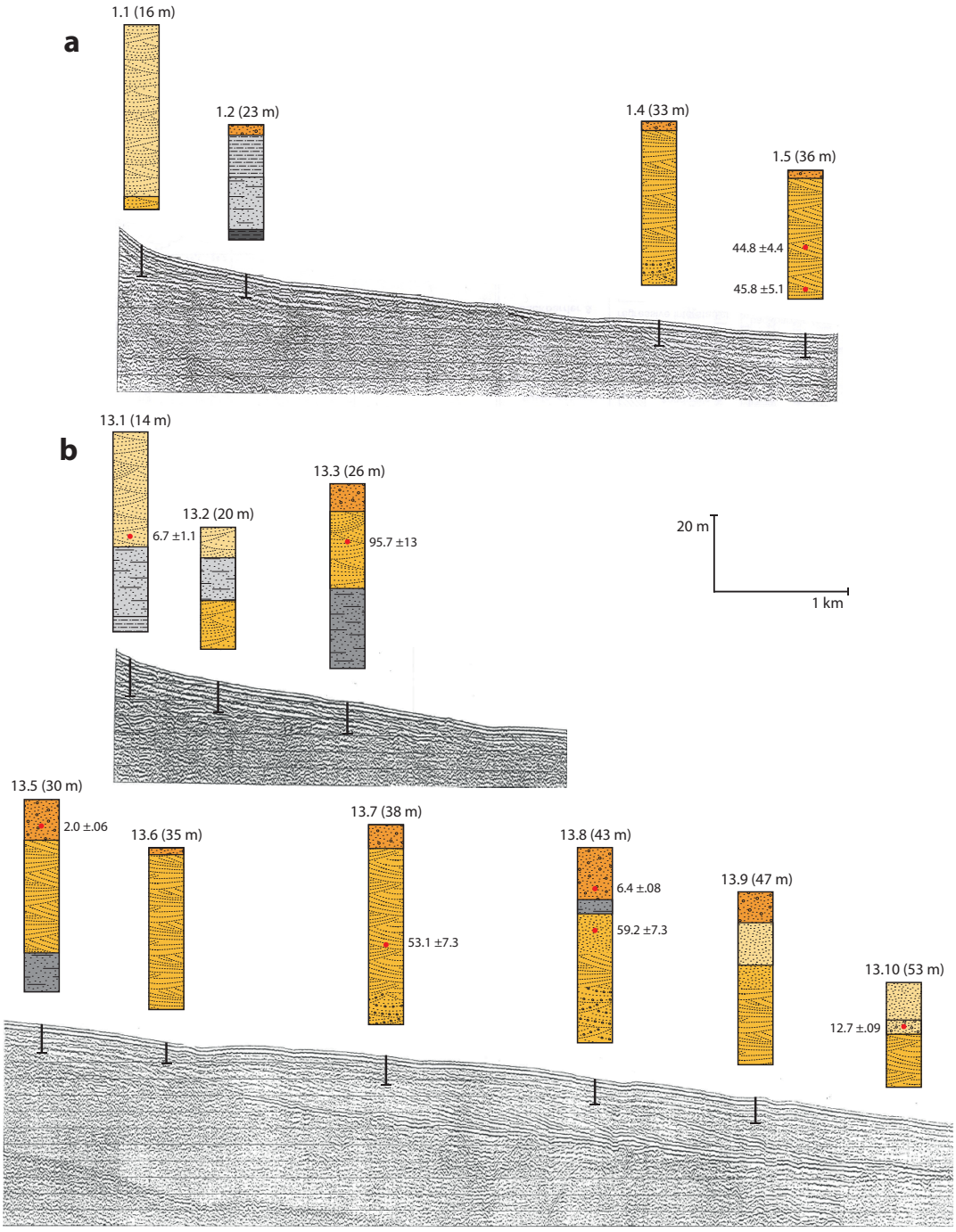

Figure 2.18: Forster-Tuncurry shallow-marine seismic profiles 1 and 13 - High-resolution seismic profiles and interpreted vibrocores of Lines (a) 1 and (b) 13 from the northern embayment [Fig. 2.13]. The locations and water depths of vibrocores are shown with the TL and radiocarbon ages reported in Tables 2.2 and 2.3. See Figure 2.14 for a legend of identified lithofacies. Modified from *Roy et al.* [1997].

Holocene shelf deposits. Inner shelf sands occur as a thin blanket (typically < 1 m thick) between 20-50 m depth within the northern embayment [Fig. 2.18]. Texture is highly variable and polymodal, with grain sizes ranging from fine to coarse sand (no mud present), and sediments are poorly sorted. Sand grains are frequently iron-stained giving the unit a characteristic orange-brown colour. Inner shelf sands are coarser and have higher shell content than the barrier sands of the upper shoreface, with abraded shell fragments making up 5-25% of the sediments. In some places the inner shelf sands also include a basal erosional lag that comprises a 0.1-0.4 m thick layer of fine to coarse poorly sorted sand, shells and occasional pebbles. The basal lag also features large estuarine shells that indicate erosional working of backbarrier estuarine sediments.

Mid shelf fine sands consisting of dark olive grey, fine to very fine calcareous sand and occasional traces of mud dominate mid shelf regions between 50-75 m depth [Fig. 2.18]. The sand is rich in lithic minerals (7-20%) and grains are angular to subrounded and not iron-stained. Biogenic sediments account for (10-40%) of mid shelf fine sands, and include thin-walled shells and foraminifera that live at mid shelf depths. Fine wood fragments are also present. Mid shelf sands are texturally uniform with unimodal grain-size distributions and are moderately well sorted.

2.7.3.2 Cape Hawke shelf

Shallow-marine deposits on the steep shelf seaward of Cape Hawke (and Charlotte Head) contrast with those of the northern embayment. Figure 2.19 shows that the most conspicuous depositional feature is a stratigraphically amorphous shelf sand body (SSB). Regressive barrier facies associated with falling-stage deposition are very limited or absent, and underly the SSB where present. In its entirety, the SSB stretches from the vicinity of One Mile Beach continuously south to Seal Rocks, although it is best developed along the steeper coastal sectors such as Cape Hawke, where its lens-shaped structure reaches 20 m in thickness [Fig. 2.19]. In contrast the SSB has a planar surface and forms a thinner drape (c. 6 m) over underlying barrier deposits in the southern embayment [Fig. 2.20]. Radiocarbon dating of samples retrieved from the SSB range from 10.1 ka BP toward the base of the unit on the shelf fronting the southern embayment, to 1.7 ka BP near the modern seabed off Cape Hawke [Tab. 2.3]. The age structure of sampled deposits suggests that the majority of SSB deposition occurred between 6.5-3.5 ka BP [Fig. 2.19].

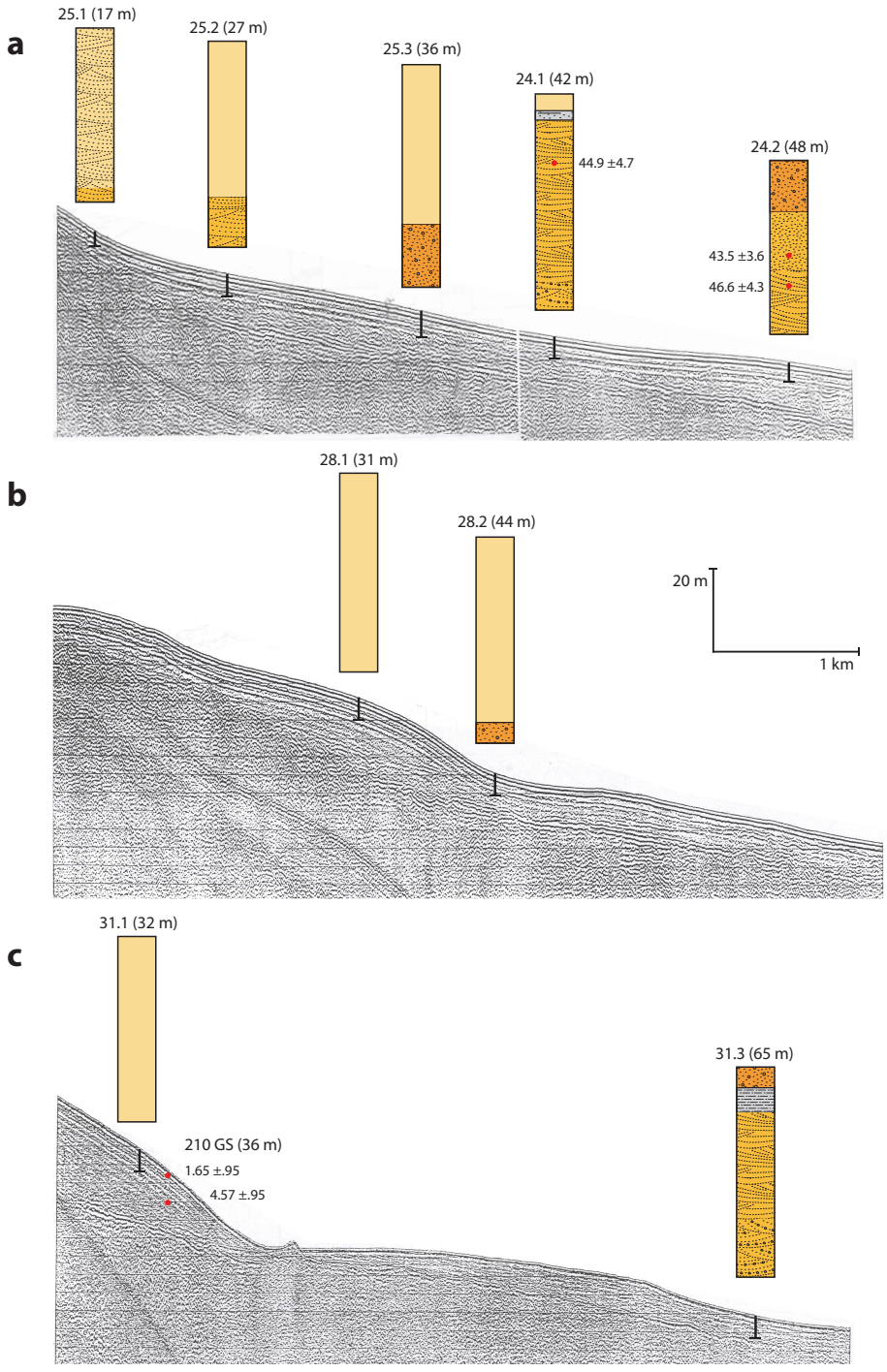

Figure 2.19: Forster-Tuncurry shallow-marine seismic profiles 24/25, 28 and 31 - High-resolution seismic profiles and interpreted vibrocores of Lines (a) 25, (b) 28 and (c) 31 from the Cape Hawke shelf [Fig. 2.13]. The locations and water depths of vibrocores are shown with the TL and radiocarbon ages reported in Tables 2.2 and 2.3. See Figure 2.14 for a legend of identified lithofacies. Modified from *Roy et al.* [1997].

The SSB overlies the coarser inner shelf sands and grades into mid shelf fine sands at the toe [Fig. 2.21c]. Depositional structures within the SSB are typically absent, with only faint seaward-dipping reflectors discernible in some seismic lines (e.g. Line 51) [Fig. 2.20]. The SSB comprises uniformly fine to medium grained sand that is moderately well sorted, and which is comparable to Holocene coastal barrier beach and upper shoreface facies and somewhat finer grained and less iron-stained than the inner shelf sand. Shell content ranges between 2-20% (10% mode) and the frequent occurrence of shoreface species such as *Bankivia faciata* at depths well beyond its contemporary range suggests offshore sand transport. At the toe of the SSB where sediments grade into mid shelf fine sands, the SSB sands become coarser grained and less well sorted, which appears to be associated with an increase in both shell detritus and a coarser clastic component.

2.7.3.3 Southern (Wallis Lake) embayment

Pleistocene highstand barrier system. In contrast to the extensive coastal strandplains of the northern embayment, the Wallis Lake estuary dominates the southern embayment and sub-aerial barrier deposits are limited to a narrow isthmus that connects the Cape Hawke promontory with the mainland to the south [Fig. 2.13]. However, Wallis Lake conceals a vast composite Pleistocene barrier system that is up to 5 km wide, 12-40 m thick, and which extends across the entirety of the deeply incised embayment [Fig. 2.21b]. The sand body forms a seaward-thickening wedge and has an irregular base. The total volume of the Pleistocene composite barrier has been estimated at 67 x 10^3 m^3/m from extensive seismic surveys and reverse circulation drilling within the estuary. The age structure of the composite barrier system is unclear as age data is limited to just three TL ages from drill hole DH4 [Tab. 2.2].

The description of Pleistocene barrier facies is based on drill hole DH4 [Fig. 2.14] and seismic traverses captured within Wallis Lake [*Roy et al.*, 1997]. Beneath a 2.5 m thick upper layer of reworked (Holocene) sands, Pleistocene barrier sands dominate DH4 to almost 40 m depth. The barrier sands are separated into two separate units by an intervening unit of muddy fine-grained estuarine sand. The upper unit is almost 25 m thick and comprises black-brown, fine to medium grained sand with some laminations and no shell. The sands are heavily impregnated with humic colloids above 8 m depth, and the lower 5 m of these barrier sands are grey to brown in colour and comprise

medium to coarse grains. The lower barrier sand unit is 9 m thick, mid brown in colour, and comprises predominantly fine to medium grained and uniformly well-sorted sands. Thin downward-coarsening beds occur around 30 m depth and humate occurs throughout with the exception of the bottom 0.5 m.

The Pleistocene composite barrier is underlain by deposits of weathered estuarine clay, and fluvial sands within the axes of the bedrock valley. Clay deposits are up to 15 m thick and a series of erosional discontinuities in seismic sections across the lake suggest that the deposit formed in multiple phases. Within DH4 the clay deposits are sampled between 38 and 48 m depth, where they are characterised by black to grey compacted muds with fine sand in parts, and contain degraded wood and other organic material [Fig. 2.14]. Beneath the compacted muds in DH4 lies an interbedded clay and sand tidal channel fill unit [Fig. 2.14]. The unit comprises dark grey clay and light-dark grey fine to very fine sand, and contains traces of shell fragments and bioturbation structures especially in the upper part of the unit.

Drowned shelf barrier systems. Regressive barrier deposits of comparable lithology to the northern embayment falling-stage barrier systems occur beneath the southern expanse of the Cape Hawke SSB. The characteristic seaward-dipping and offlapping reflectors of this unit are discernable in line 39 [Fig. 2.20]. The volume of the falling-stage barrier deposits in the southern embayment is much lower however, whilst the texture of the deposits is finer and typical of lower shoreface facies. Lower shoreface sands are uniformly fine grained and well sorted, with typically minor shell content (<5%) comprising marine species, faint bedding structures in parts, and traces of fine wood and charcoal fragments throughout.

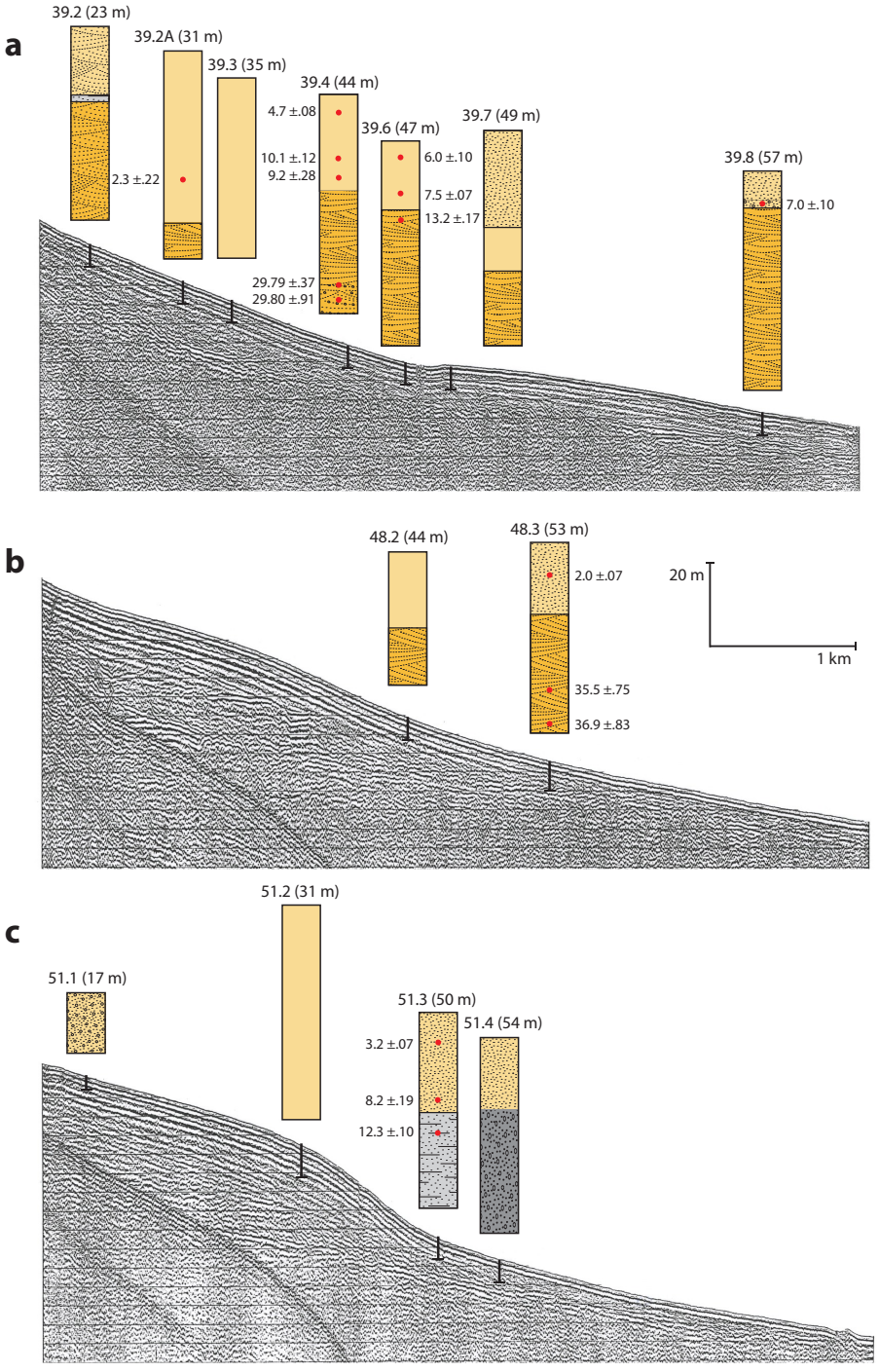

Figure 2.20: Forster-Tuncurry shallow-marine seismic profiles 39, 48 and 51 - High-resolution seismic profiles and interpreted vibrocores of Lines (a) 39, (b) 48 and (c) 51 from the southern embayment [Fig. 2.13]. The locations and water depths of vibrocores are shown with the TL and radiocarbon ages reported in Tables 2.2 and 2.3. See Figure 2.14 for a legend of identified lithofacies. Modified from *Roy et al.* [1997].

Holocene highstand barrier deposits. Holocene highstand barrier sands are limited to thin dune deposits and a shoreface veneer that disconformably onlaps the Pleistocene composite barrier below [Fig. 2.21b]. Holocene backbarrier muddy sands occur both within the contemporary Wallis Lake estuary system. Flood-tide delta facies fill the system of palaeochannels where the Wallamba and Walingat Rivers and Wallis Lake converge in the central part of the estuary system. Sediments are composed of shelly quartz sands that are comparable to modern shoreface sand, with varying but typically minor estuarine shell and mud content. Texturally, the modern backbarrier sands range from fine to coarse and sorting is variable, and no relationship between texture and proximity to the modern inlet mouth is evident. Distal from fluvial and tidal influences, the dominant surficial sedimentary unit within Wallace Lake is dark grey to black mud that typically includes slight to moderate silt and sand content. The upper few metres are typically rich in biogenic content (shell fragments) and heavily bioturbated. Below these shelly muds quartzose sands become increasingly prominent.

Holocene shelf deposits. Inner shelf depths between 30-50 m are dominated by the SSB. Beyond the SSB mid shelf sands overlie the regressive falling-stage deposits [Fig. 2.20], and are particularly lithic-rich, containing coarse-grained layers that are much more poorly sorted. The coarse material is a mixture of shell fragments and quartz grains that is comparable to that found at the base of the SSB. Fluvial gravelly sand associated with a palaeo-river channel that drained the southern embayment were sampled in vibrocore FT51.4 [Fig. 2.20], underlying the mid shelf fine sands on the shelf adjacent to Charlotte Head. This unit comprises orange-brown, iron-stained and heavily oxidised gravelly layers that are formed of subangular to well rounded clasts. The gravels are interspersed with layers of fine-grained laminated sand that comprise some granules. Cyclic fining and coarsening trends occur throughout the deposit, and coarsening-upward sequences are particularly pronounced. Rare traces of shell and burrows are found in the sandy layers.

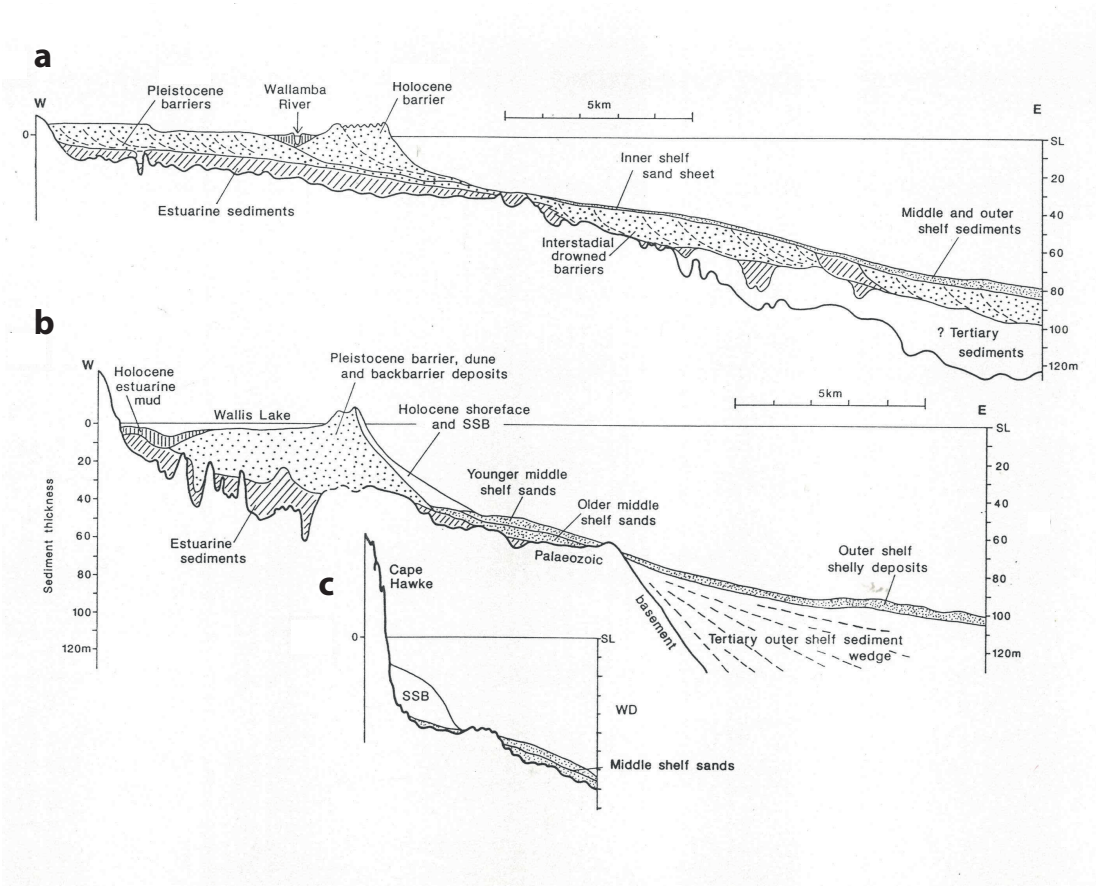

Figure 2.21: Interpreted stratigraphic sections from the Forster-Tuncurry region - Representative stratigraphic cross-sections of the (a) northern embayment, (b) southern embayment and (c) Cape Hawke shelf. From *Roy et al.* [1997].

2.7.4 Updrift-sink regional sedimentation model

The distribution of coastal barrier deposits and age data at Forster-Tuncurry inspired a regional sedimentation model [*Roy et al.*, 1997], which implies that barrier deposition between embayed and protruding coastal sectors is intimately related. The sedimentation model of *Roy et al.* [1997] is referred to as the 'updrift-sink' model throughout this thesis. Figure 2.22 shows an illustration of the updrift-sink model that describes the relationships between coastal barrier deposition within the region at different sea level stages. In particular, coastal barrier deposition within the northern (i.e. Tuncurry) embayment [Sec. 2.7.3.1] is closely related to the evolution of the Cape Hawke shelf sand body [Sec. 2.7.3.2]. The principals of the updrift-sink model also apply beyond the Forster-Tuncurry region. For example, the great volume of coastal barrier deposits in the updrift Port Stephens-Myall Lakes region [Fig. 2.8] is understood to relate to preferential trapping of sand from the alongshore transport system there.

Beginning with typical highstand sea level geomorphology representative of the last-interglacial (i.e. MIS 5e), a well-developed shelf sand body occurs off Cape Hawke and strandplain progradation occurs in the embayed Tuncurry compartment [Fig. 2.22a]. During falling-stage sea-level fall the updrift shelf sand body is exposed to the energetic upper shoreface environment and is subject to significant erosion[Fig. 2.22b]. The eroded sand is added to the northward-directed alongshore transport system and feeds deposition of the forced-regressive strandplain in the Tuncurry shelf palaeo-embayment [Fig. 2.22b]. Once the prograding coastline extends beyond the embayment alongshore sand transport bypasses the Tuncurry region and continues to the north [Fig. 2.22c]. During transgression the Cape Hawke shelf sand body is re-established once rising sea levels generate sufficient accommodation space [Fig. 2.22d]. Limited sand supply to the Tuncurry embayment during growth of the shelf sand body results in the partial reworking of the drowned forced-regressive strandplain by the transgressive barrier system [Fig. 2.22d]. During subsequent sea-level highstand the fully-developed shelf sand body stabilises, thus allowing headland bypassing of littoral sediments into the Tuncurry embayment [Fig. 2.22e]. Radiocarbon ages from the Wallis Lake flood-tide delta indicate that during the Holocene highstand, sediments supplied by the re-established alongshore transport system were sequestered into the delta complex until it attained an equilibrium morphology around 3 ka BP.

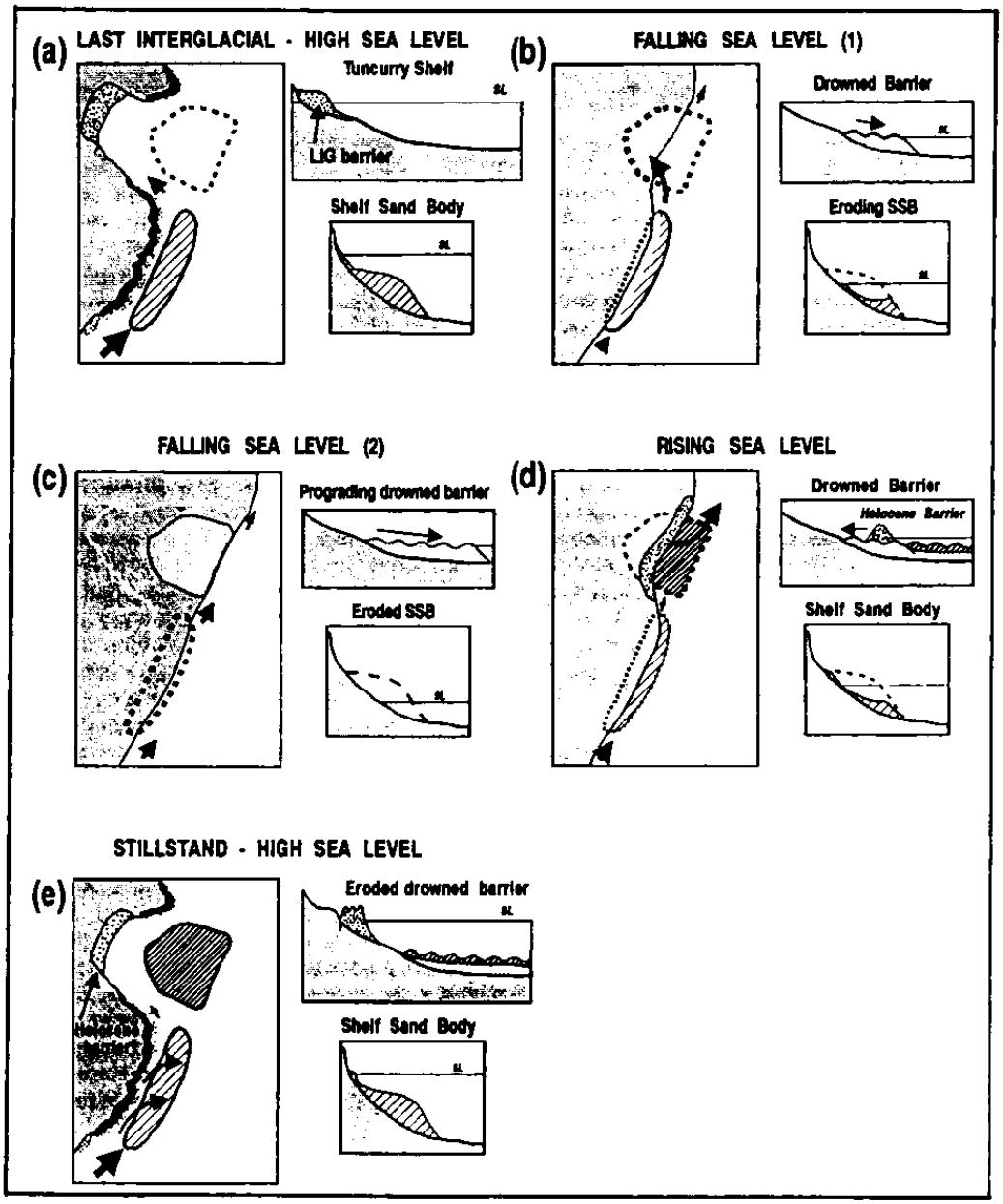

Figure 2.22: Updrift-sink sedimentation model for the Forster-Tuncurry region - Throughout late-Quaternary sea-level fluctuations, coastal deposition in the Forster-Tuncurry region involved the interrelated behaviour of shelf sand bodies and coastal barriers. From *Roy et al.* [1997]

2.8 Conclusions

This chapter has described the geological evidence that underlies the research questions of this thesis [Sec. 1.2.1] and the simulation experiments carried out in subsequent chapters. In particular, the variable occurrence and arrangement of highstand coastal barrier systems raises questions regarding controls on coastal barrier deposition during sea-level change that remain to be explored. The southeast Australian margin provides a natural laboratory where coastal barrier systems have developed during different sea level stages, and in response to varying depositional controls. Specifically, late-Quaternary sea-level change, regionally varying margin geology, and local sediment budget influences have contributed to the formation and preservation of coastal barrier systems covering the spectrum of barrier types. The resulting barrier systems provide case examples for experimentation using the stratigraphic modelling approach. In particular, the chronologically constrained stratigraphy of the coastal barrier systems at Moruya and Forster-Tuncurry provide suitable datasets on which to base the stratigraphic modelling experiments that are used here to address the research questions.

3

Shoreface Sand Supply or Sea Level Change? The Origins of Holocene Coastal Strandplains

3.1 Introduction

3.1.1 Background

Although it has long been accepted that wave-induced shoreface erosion may be a primary source for coastal sediment budgets during sea level change [*Curray*, 1964], the importance of onshore-directed shoreface sand supply under stable sea level conditions is a relatively recent proposition [*Cowell et al.*, 2001, 2003a]. Implicit in that proposition are the fundamental concepts of morphological relaxation and morphodynamic feedback [*Cowell and Thom*, 1994], which imply that the shoreface continues to adjust to dynamic forcing long after sea level has stabilised. This hypothesis emerges from the observation that rates of sediment entrainment and transport diminish across the shoreface with increasing water depth, due to the reduced intensity and availability of wave-driven fluid power, increased boundary layer effects, and the influence of complex interacting currents [*Niedoroda et al.*, 1984; *Niedoroda and Swift*, 1991; *Wright*, 1995]. Thus bed surface response rates and relaxation timescales increase with depth, and may be orders of magnitude longer across the lower shoreface than observed rates of upper shoreface response [*Stive and de Vriend*, 1995; *Cowell et al.*, 2003a].

3. SHOREFACE SAND SUPPLY OR SEA LEVEL CHANGE? THE ORIGINS OF HOLOCENE COASTAL STRANDPLAINS

The significant and rapid sea-level rise (i.e. 130 m in less than 10,000 years) following the last glacial maximum, and the relatively stable sea level conditions that ensued thereafter, suggest that mid- to late-Holocene (hereafter M-L Holocene) subaerial coastal depositional features may contain evidence of onshore shoreface sediment supply during times of stable sea level. The implication of this proposition is that rapid sea level change is likely to have exceeded lower shoreface response timescales, thereby inducing disequilibrium shoreface geometry. During the period of relative sea level stability that followed, the readjustment of shorefaces may have been recorded in the depositional records of coastal barriers. The southeast Australian coastline comprises numerous Holocene bay barrier systems that fill coastal embayments to varying degrees [*Roy and Thom*, 1981; *Roy et al.*, 1994]. Figure 2.3 shows the morphology and stratigraphy of the various coastal depositional features (including coastal barrier systems) that developed along this coastline during the Holocene in response to regional and site-specific variations in inherited coastal geomorphology, energy climate and sedimentation regime.

Prograded barriers (strandplains) are of particular interest here because they offer the potential for preservation of a relatively continuous depositional record that may contain evidence of changes in sea level, energy climate and sediment sources. The age structures of many strandplains are relatively well constrained by radiocarbon ages gained from shell specimens and other organic materials such as wood fragments, charcoal and mangrove stumps [*Thom et al.*, 1978, 1981b,a; *Thom*, 1984; *Thom and Roy*, 1985; *Roy et al.*, 1997]. Despite good agreement between sites that Holocene strandplain progradation commenced from between 6-7 ka BP, subsequent rates of strandplain accretion varied between sites [Fig. 2.4]. Furthermore, the cause of late-Holocene strandplain progradation remains disputed, with a number of forcing factors potentially having contributed to their deposition. The sedimentology of Holocene strandplains indicates that in most cases regressive coastal barrier sands were not sourced locally from recent fluvial systems [*Thom*, 1978; *Roy et al.*, 1994]. Rather the strandplain sediments are palimpsest 'marine sands' that are believed to have experienced multiple phases of reworking on the continental shelf during late Quaternary sea level oscillations [*Roy and Thom*, 1981, 1991]. Recently, the ultimate origins of the quartz marine sands have been traced back to basin deposition associated with the Central Transantarctic orogeny [*Sircombe*, 1999], and thus pre-date margin initiation [Sec. 2.2].

Uncertainty regarding the origins of Holocene strandplain deposition in southeastern Australia is embedded in the question of relative sea levels during this time. That is, were M-L Holocene times characterised by sea level stillstand or a slight but significant (c. 1-2 m) relative sea-level fall? Depending on the interpretation of sedimentary and biological relative sea level indicators that suggest higher than present sea levels, a range of possible sea level histories including fluctuating, gradually falling and stable M-L Holocene sea levels may be argued [Sec. 3.2.1]. Depending on the adopted sea level history, potential sources of Holocene barrier progradation that are considered here include:

1. rapid influx of sediments into highstand embayments following the post-glacial marine transgression (PGMT) that was driven by predominantly northward alongshore transport and the erosion of updrift shelf sand bodies stranded on steeper sections of the inner shelf;

2. shoreface lowering during M-L Holocene relative sea-level fall that contributed to strandplain progradation by forced regression, *sensu Posamentier et al.* [1992],

3. shoreface lowering from the onset of sea-level highstand associated with the morphodynamic disequilibrium-stress (D-S) response of the shoreface to the inherited coastal geomorphology.

3.1.2 Aims

Resolving the depositional histories and origins of Holocene coastal strandplains introduces a question of fundamental significance to understanding mesoscale coastal change (i.e. 10^2 to 10^5 years), which forms the basis of research for this thesis. That is, for a given energy climate and sedimentary substrate, how do rates of lower shoreface response vary with increased water depth under both stable and changing sea level conditions? A satisfactory answer to this question implicitly addresses the question of potential rates of onshore shoreface supply. Thus the purpose of this chapter is to constrain rates of lower shoreface response and onshore sediment supply for Holocene sea level conditions using known strandplain age structures and a stratigraphic forward modelling approach. The following questions are considered regarding the origins of Holocene strandplains:

3. SHOREFACE SAND SUPPLY OR SEA LEVEL CHANGE? THE ORIGINS OF HOLOCENE COASTAL STRANDPLAINS

1. Was mid- to late-Holocene (6-0 ka BP) strandplain progradation in tectonically stable southeastern Australia primarily a response to onshore shoreface sand supply driven by morphodynamic disequilibrium, relative sea-level fall, or external sand supply from the alongshore transport system?

2. Which conceptual model of onshore shoreface sand supply is most consistent with shoreface processes and the age structures of Holocene strandplains - i.e. depth-diminishing or depth-constant shoreface lowering? What does this suggest about the origins of onshore shoreface sand supply?

3. Considering the range of potential mid to late-Holocene sea level scenarios, is it likely that shoreface lowering due to relative sea-level fall made a significant contribution to Holocene strandplain progradation?

4. Which potential mid to late-Holocene sea level scenario is most consistent with glacio- and hydro-isostatic responses and relative sea level indicators from southeastern Australia? What does this suggest about the contribution of relative sea-level fall to Holocene strandplain progradation?

5. What role did the regional northward-directed alongshore transport system play in the Holocene progradation of coastal strandplains? If rates of onshore shoreface sand supply diminished into the late Holocene, was observed strandplain progradation primarily a response to alongshore sand supply or relative sea-level fall?

Furthermore, the following questions are considered regarding rates of lower shoreface response under stable and changing sea level conditions:

1. Beyond what typical depth did disequilibrium shoreface morphology likely persist at the onset of Holocene sea-level highstand in southeastern Australia?

2. Given the age structures of Holocene strandplains in southeastern Australia and potential mid- to late-Holocene sea level scenarios, what rates of shoreface response were required to generate observed strandplain progradation? Are the implied rates of onshore shoreface sand supply feasible in the context of shoreface processes?

3. Does the nature of contributions from onshore shoreface sand supply, relative sea-level fall and alongshore sand supply to Holocene strandplain progradation suggest that a significant onshore sand supply persists today?

The impracticalities of measuring rates of shoreface adjustment at the necessary spatial and temporal scales imply that these questions cannot be addressed using historical observational datasets. Although previous studies have considered some of the above questions [Sec. 3.2.2], the implications of Holocene sea level change are yet to be explored and time variable rates of shoreface response and external sediment supplies remain only loosely constrained. The answers to the questions posed here have the potential to inform both our understanding of past coastal change through refined stratigraphic interpretations, and the prediction of future coastal change in response to projected climate change. Section 3.2 provides the regional context and theoretical basis for the experimental design of stratigraphic simulation experiments and subsequent interpretation of model findings.

3.2 Holocene sea levels and coastal barrier deposition

3.2.1 Evidence for mid- to late-Holocene sea level change

The southeast Australian margin is considered a far field site and was not subject to direct glacio-isostatic loading during the last glacial maxiumum [*Lambeck and Nakada*, 1990]. Thus relative sea levels during the Holocene were primarily a product of eustatic sea level changes, hydro-isostatic responses, and any persisting tectonic responses. At Holocene timescales, passive margin subsidence at the anticipated rates would have had a negligible influence on relative sea levels [Sec. 2.2]. Evidence from radiocarbon dating of shell specimens and other organic materials such as wood fragments, charcoal, and mangrove stumps, suggests that relative sea level had reached near-present elevations in southeastern Australia between 7-7.5 ka BP [*Thom and Chappell*, 1975; *Jones et al.*, 1979; *Thom and Roy*, 1985]. Terminal PGMT sea levels may have then attained maximum heights up to 2 m PMSL between 5-6 ka BP, before gradually falling to present levels throughout the mid to late Holocene [*Bryant*, 1992; *Gill and Hopley*, 1972]. However, it has also been argued that relative sea level remained more or less stable at or near present levels from about 7 ka BP onwards [*Thom et al.*, 1969, 1972].

3. SHOREFACE SAND SUPPLY OR SEA LEVEL CHANGE? THE ORIGINS OF HOLOCENE COASTAL STRANDPLAINS

Recently, new and revised evidence for M-L Holocene sea levels in southeastern Australia has been interpreted as suggesting steady raised or fluctuating sea levels within the range of 0-2 m, from the termination of the PGMT until about 1.5-2 ka BP [*Sloss et al.*, 2007; *Lewis et al.*, 2008, 2013]. For example, intertidal fixed biological indicators including barnacles, oysters and tubeworms, which were retrieved from elevations above present intertidal extents, have been used to suggest both higher and fluctuating Holocene sea levels [*Baker and Haworth*, 1997; *Baker et al.*, 2001]. Furthermore, geomorphic evidence from elevated (c. +1-1.5 m) beach deposits at a sheltered site within Batemans Bay suggests slightly higher sea levels persisting until 2-2.5 ka BP [*Switzer et al.*, 2010]. Figure 3.1 shows a revised Holocene sea level envelope based on the ages and elevations of a range of relative sea level indicators. Constraining the precise nature of late Holocene sea level change based on these indicators is problematic however, with different analyses suggesting gradually falling or oscillating relative sea levels between 6 ka BP and present [*Baker and Haworth*, 2000a,b]. Moreover, intrinsic limitations of the above lines of evidence as reliable sea level indicators include the influences of exposure to the prevailing energy climate and estuarine impoundment on the inferred sea levels. Thus the evidence for fluctuating Holocene sea levels remains far from conclusive.

The rationale behind relative sea-level fall for far-field sites following the onset of eustatic sea-level highstand relates to the hydro-isostatic response of the continental shelf to water loading, which is believed to have caused regionally variable subsidence of the southeast Australian continental shelf and uplift along the coast [*Lambeck and Nakada*, 1990; *Lambeck et al.*, 2003]. Hydro-isostatic signals within the region are best constrained for the northeast Australian margin (the Great Barrier Reef Carbonate Province), where aggraded coral reefs provide reliable chronology and elevation controls for sea level change. At Orpheus Island for example, a relative sea-level fall of 1 m ($\pm$0.5 m) between 6.5-3 ka BP may have been associated with hydro-isostatic response [*Lambeck and Chappell*, 2001]. Such an adjustment implies mid Holocene stabilization of eustatic sea level and a near-instantaneous hydro-isostatic response. Along the comparatively narrow and deep southeast Australian margin hydro-isostatic signals are less well constrained due to poorer relative sea level control, although *Lambeck and Nakada* [1990] originally proposed up to 2 m sea fall between 6-0 ka BP.

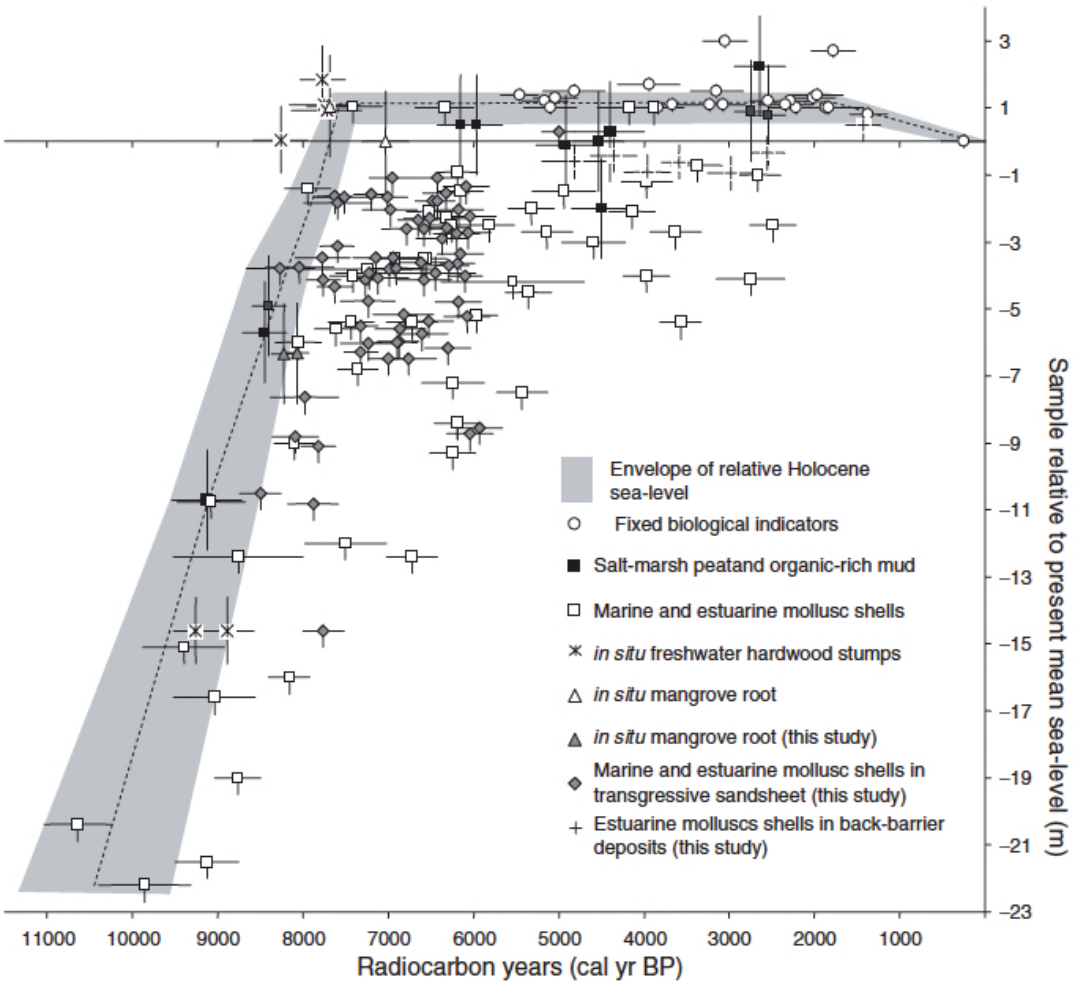

Figure 3.1: Revised Holocene sea level curve for SE Australia - Revised Holocene sea level curve for southeastern Australia based on existing and recent evidence from coastal deposits and fixed biological indicators. From *Sloss et al.* [2007].

Global glacio-isostatic adjustment theory implies that sea-level highstand conditions persisted at far-field sites until inputs of melt water from the disintegrating ice masses ceased. However, the timing of relative sea-level fall at far field sites may have been delayed if rates of meltwater input exceeded rates of hydro-isostatic response due to the equatorial ocean siphoning effect [*Mitrovica and Peltier*, 1991; *Mitrovica and Milne*, 2002]. The cessation of meltwater contributions is believed to have occurred post 3 ka BP [*Lambeck*, 2002], which supports the proposition of late Holocene sea-level fall.

This theory is more consistent with the distribution of fixed biological and sedimentary relative sea level indicators described above, and is further supported by more robust relative sea level indicators from other sites [*Lewis et al.*, 2008]. For example, *Goodwin and Harvey* [2008] present evidence from coral micro-atolls in the Southern Cook Islands that suggests relative sea-level fall commenced prior to 2.5 ka BP, and fell from 1.3 ± 0.1 m to 0.45 ± 0.15 m by 1 ka BP at a rate of -0.5 mm/a. Considering all of the potential sea level models discussed above, the general trend of M-L Holocene relative sea levels may be approximated by a gradual falling trend between 6-0 ka BP from a peak elevation of around 1.5 m, at rates between -0.25 and -1 mm/a.

3.2.2 Shoreface disequilibrium-stress (D-S) response

Considering lithological evidence from the coast and shelf, *Thom and Roy* [1985] proposed that Holocene barrier-strandplain progradation in southeastern Australia was driven by the readjustment of inner-shelf gradients. This concept was demonstrated by *Cowell et al.* [1995], who described the connection between highstand barrier progradation and inner-shelf lowering, which was attributed to a progressive increase in shoreface dimensions driven by latent surface adjustment and depth-dependent sediment transport rates [*Niedoroda et al.*, 1995; *Stive and de Vriend*, 1995]. *Cowell et al.* [2001], and later *Cowell et al.* [2003b], examined the concepts and evidence within a global context, carrying out simulations with a geometric model that were constrained by chronostratigraphic evidence from coastal barrier deposits of the southeast Australian, Dutch North Sea and Pacific United States coasts. The role of shoreface sand supply has since been considered in the evolutionary reconstructions of coastal dunes elsewhere [*Aagaard et al.*, 2004; *Anthony et al.*, 2010; *Schwab et al.*, 2013].

The problem was recently revisited in southeastern Australia, again using morphokinematic modelling. *Daley* [2012] considered the responses of over-fit (positive

accommodation), under-fit (negative accommodation) and graded (equilibrium) inherited shelf regimes under stable sea level conditions [Fig. 3.2]. Part of his work examined the case for inner-shelf lowering as a potential source of Holocene strandplain progradation, with the findings suggesting that strandplain progradation could have been sourced from inner-shelf lowering, longshore sand transport, or a combination of both. However, whilst the modelling approach of *Daley* [2012] generated barrier stratigraphy consistent with the age structures of coastal strandplains, shoreface response was manually controlled to calculate cross-shore sediment transport and coastal response. Although geological evidence was used to guide the extent of depth-dependent shoreface adjustment, rates of shoreface response applied in the geometric model remained abstract from shoreface sediment transport processes. Furthermore, a comprehensive appraisal of potential sources of strandplain progradation was beyond the scope of that study (e.g. time-varying rates of longshore sediment supply and alternative sea level histories were not considered).

The rationale behind shoreface sand supply to beaches and dunes has emerged from shoreface equilibrium theory. That is, the shoreface form as a morphodynamic feature represents a dynamic equilibrium response between the characteristics of the inner-shelf seabed (grain-size, shape, density) and the ambient energy climate [*Bruun*, 1954; *Dean*, 1977, 1991]. The geometry of the shoreface is further controlled by inherited margin geomorphology and the relationship between the frequency of change in boundary conditions (e.g. relative sea level, energy climate) and response timescales [*Cowell and Thom*, 1994; *Cowell et al.*, 1999]. A number of models have been proposed regarding the physical basis for such equilibrium, including concepts of uniform energy dissipation and convective transport processes [*Wright*, 1995]. In the context of highstand barrier progradation, the theory implies that for an underfit shelf regime in a given setting the shoreface profile is shallower than the equilibrium profile, and thus a time-averaged erosional response prevails in association with the lowering of the shoreface to wave base [*Cowell et al.*, 2003b; *Daley*, 2012]. Coastal tract concepts of cross-shelf continuity in sediment transport pathways then imply that the outcome of erosion across the inner shelf under such conditions should be deposition at the shoreline, which may be recorded by preserved prograded coastal strandplains [*Cowell et al.*, 2003a].

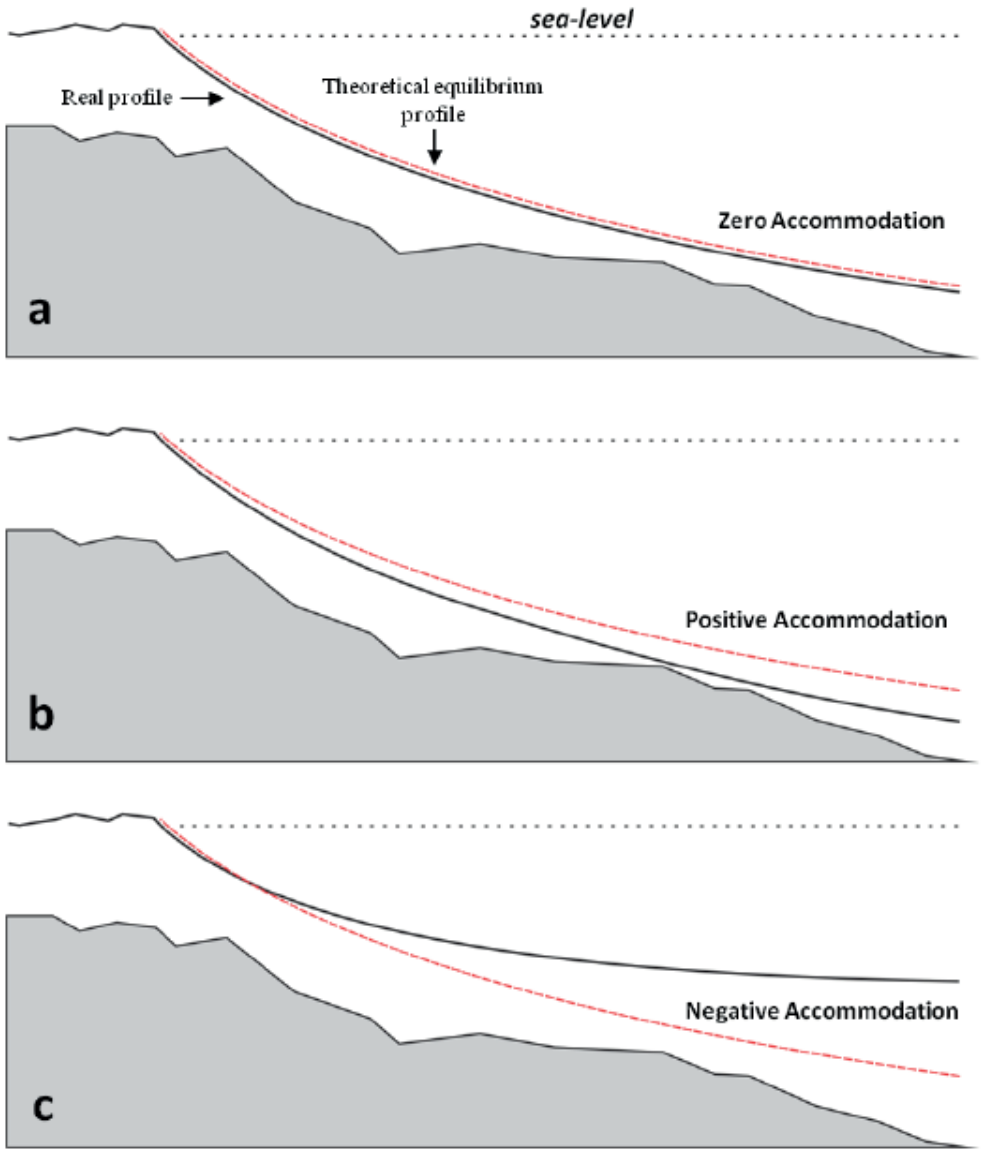

Figure 3.2: Sediment accommodation in graded, under-fit and over-fit shelf settings - (a) Graded shelf settings are characterised by a shoreface-inner shelf surface that is in equilibrium with the modal energy regime and sediment type. (b) Under-fit shelf settings refer to the case where the shoreface-inner shelf surface is deeper than the theoretical equilibrium profile, and thus are typically accommodation-dominated. (c) Over-fit shelf settings occur where the shoreface-inner shelf surface is shallower than the theoretical equilibrium profile, and thus are typically supply-dominated. From [*Daley*, 2012].

Recently, consideration has been given to the importance of shoreface sand supply to sediment budgets at management timescales through the analysis of long-term survey datasets. For example, *Patterson* [2012] estimated rates of onshore supply from a 42-year record of shoreface profiles from the Gold Coast, Australia. From the analysis of that dataset he concluded that shoreface response times increased from 4 years at 10 m depth to 300 years at 20 m depth, and millennia for depths greater than about 23 m. Furthermore, shoreface sand supply was also identified as a critical component of the sediment budget at Fire Island, New York [*Schwab et al.*, 2013]. Other researchers have endeavoured to identify the processes by which shoreface sediments are transported in large volumes to the shoreline. For example, *Aagaard et al.* [2004] demonstrated a mechanism for shoreface sand supply to beaches involving onshore bar migration from the analysis of a long-term survey dataset from the Skallingen barrier (Danish North Sea coast). Specifically, a long-term profile survey dataset and empirical measurements during high-energy dissipative conditions were considered. Their analysis demonstrated that onshore bar migration and net landward sediment transport processes ultimately resulted in the formation of welded bars in the intertidal zone, which provided a sediment source for subsequent aeolian transportation to the dune system. In that study, comparison of barrier progradation rates with rates of sediment supply from onshore bar migration supported the case for the shoreface as the dominant source of strandplain sediments [*Aagaard et al.*, 2004]. Considering the timescale of the study however, lower shoreface sand supply could not be considered.

3.3 Methods

A numerical stratigraphic model (BARSIM) was calibrated and applied to investigate the relationships between Holocene strandplain progradation and onshore sand supply due to shoreface D-S response, relative sea-level fall and alongshore sediment transport regimes. The BARSIM model has been described in Section 1.5, and as such, the methodology reported here focuses on the model calibration and application to the Moruya [Sec. 2.6] and Tuncurry [Sec. 2.7] embayments. This investigation represents the first application of the BARSIM model to a southeast Australian setting, and the selected sites provide useful comparative conditions with respect to magnitudes of littoral sand supply relative to sand supply from the shoreface.

3.3.1 BARSIM model calibration

3.3.1.1 Model assumptions

As is the case for any model, the BARSIM algorithm necessitates some assumptions regarding the representation of site hydrodynamics and geomorphology. Here, empirical datasets and a site calibration procedure are used in an attempt to optimise the model representation of site morphodynamics. The BARSIM parameter settings used are provided in Appendix A.

First, within-site variation in substrate erodibility is not supported in BARSIM, and thus isolated patches of hard substrate (e.g. bedrock outcrops) are not represented. However, for the case study sites examined here the distribution of bedrock was either restricted or captured in the substrate geometry, and thus this was not deemed to significantly influence model findings. Second, the erosion-efficiency scaling exponent (m) requires calibration so that simulated morphodynamic interactions between the model wave climate and substrate in BARSIM best approximate reality. That is, site-specific factors (e.g. grain-size distributions, sediment composition, wave transformation) may influence depth-dependent shoreface erosion rates for a given wave climate and model substrate. Here the value of m was determined from the calibration procedure described in Section 3.3.1.3, in which the erosion function was tuned using the known age structures of coastal strandplains.

Lastly, BARSIM does not simulate aeolian deposition, and thus the role of dune formation in the evolution of coastal barriers is not considered. That is, the extent of wave run-up (i.e. the beach berm) marks the vertical limit of simulated barrier deposition, although berm height does vary between fair-weather and event wave conditions and is correlated with storm intensity. Thus the vertical reach of the shoreface may restrict the elevations of simulated coastal barriers. During marine transgressions, when barrier rollover processes dominate, limited opportunities for dune formation imply that this is not likely to influence model findings. Under stable sea levels however, simulated barrier heights may be lower than in reality.

3.3.1.2 Wave climate and substrate characteristics

Long-term (20-30 years) wave climate statistics from a network of deep-water waverider buoys moored off the southeast Australian coast between 75-90 m water depths were

used to define model wave climates. Although some latitudinal variation has been noted in the regional wave climate, omissions of extreme events in some records due to instrument failure makes it difficult to demonstrate significant trends between sites. In any case, in this study the assumption of a uniform wave climate for the 6 ka simulation period is likely to be more of an issue than any spatial trend in historical measurement records. Considering the above, annual mean significant wave height of $H_{sig} = 1.6$ m ($\sigma = 0.47$), annual mean wave period of $T_{sig} = 8$ s ($\sigma = 0.53$), and a fair-weather/storm-event boundary of $H_{sig} = 2.5$ m were adopted for all models, after *Short and Trenaman* [1992]. These statistics are consistent with long-term investigations of the regional wave climate using both measurement records and model wave hindcast data based on atmospheric reanalysis [*Harley et al.*, 2010]. Although uniform wave climate parameters were maintained throughout each simulation, the BARSIM event-driven wave climate algorithm sampled fair-weather periods and intermittent storm events of variable magnitude from the input distributions [Sec. 1.5.2].

Sediment grain-size statistics of samples obtained from the Tuncurry coast and shelf [Sec. 2.7] were used to guide grain-size fractions for model substrates and regional sediment budgets at both sites. Four grain-size classes (125, 177, 250, 354 μm) were included at fractions consistent with averaged sampled grain-size distributions (i.e. 0.1, 0.2, 0.5, 0.2) according to *Roy et al.* [1997]. Considering that the southeast Australian margin is characterized by an autochthonous shelf sedimentary regime [*Roy et al.*, 1994], the composition of external sediment supply to the shoreface (where included in simulations) was assumed to be consistent with the initial model substrate. Subsequent distribution of sediment grain-size classes across the model domain was then determined by the BARSIM sediment transport rules. Temporal and volumetric variation in external sediment supply to the Tuncurry site was consistent with the updrift-sink regional sediment budget model determined from the distribution and age structures of coastal depositional features within the region [Sec. 2.7.4].

3.3.1.3 Local erosion efficiency

The erosion-efficiency scaling exponent, m [Sec. 1.5], requires calibration so that simulated morphodynamic interactions between the model wave climate and substrate in BARSIM best approximate reality. That is, because of site-specific factors that may influence shoreface erosion rates for a given wave climate and model substrate (e.g.

grain-size distributions, sediment composition, wave transformation), the BARSIM erosion function should be tuned for each site. The value of m indirectly controls shoreface concavity by scaling the maximum shoreface erosion rate in the BARSIM erosion function. If it is assumed that surface relaxation times during the Holocene have been sufficient for the Tuncury and Moruya shorefaces to attain approximate equilibrium forms based on the mean wave climate, local grain-size distributions, and the inherited inner-shelf gradient, then contemporary shoreface geometry may be used to guide the calibration. Although it may well be the case that lower shoreface D-S responses are ongoing at imperceptible rates, minimal change in sea level during the late Holocene should have allowed for complete upper to mid shoreface response. For the lower shoreface, equilibrium surface gradients will likely approach that of the contemporary inner to mid shelf.

A 6,000-year calibration simulation was carried out for each site to achieve reliable estimations of m for the Tuncurry and Moruya settings:

1. The substrates for the calibration simulations comprised a linear start-up surface of average gradient equal to that of the 6ka BP inner to mid shelf, and sediment grain-size fractions as defined above. The average 6 ka BP substrate gradients were calculated between the 6ka BP beach ridges and 70 m shelf depth contours at each site.

2. An iterative inversion procedure was then carried out to constrain the appropriate value of m for each site, with the optimal value being that which resulted in terminal shoreface geometry that most closely approximated that of the contemporary shoreface.

Figures 3.3 and 3.4 show the results of the optimal calibration simulation for the Moruya and Tuncurry sites, for which erosion efficiency values were $m = 2.7$ and $m = 4.7$ respectively. The dimensionless order-one shape index 'alpha' [*Wolinsky*, 2009] was also used to measure simulated shoreface geometry. For net shoreface relief (i.e. vertical distance between the shoreline and shoreface toe), H_{SF}, alpha is determine by:

$$\alpha = \frac{\overline{H}}{H_{SF}} \tag{3.1}$$

where $\overline{H}$ represents the average shoreface relief. It can be seen that for each case the model shoreface shape initially approached that of the measured shoreface rapidly and stabilised by about 3 ka BP [Figs. 3.3 & 3.4]. This calibration procedure increases confidence in the model representation of site morphodynamics.

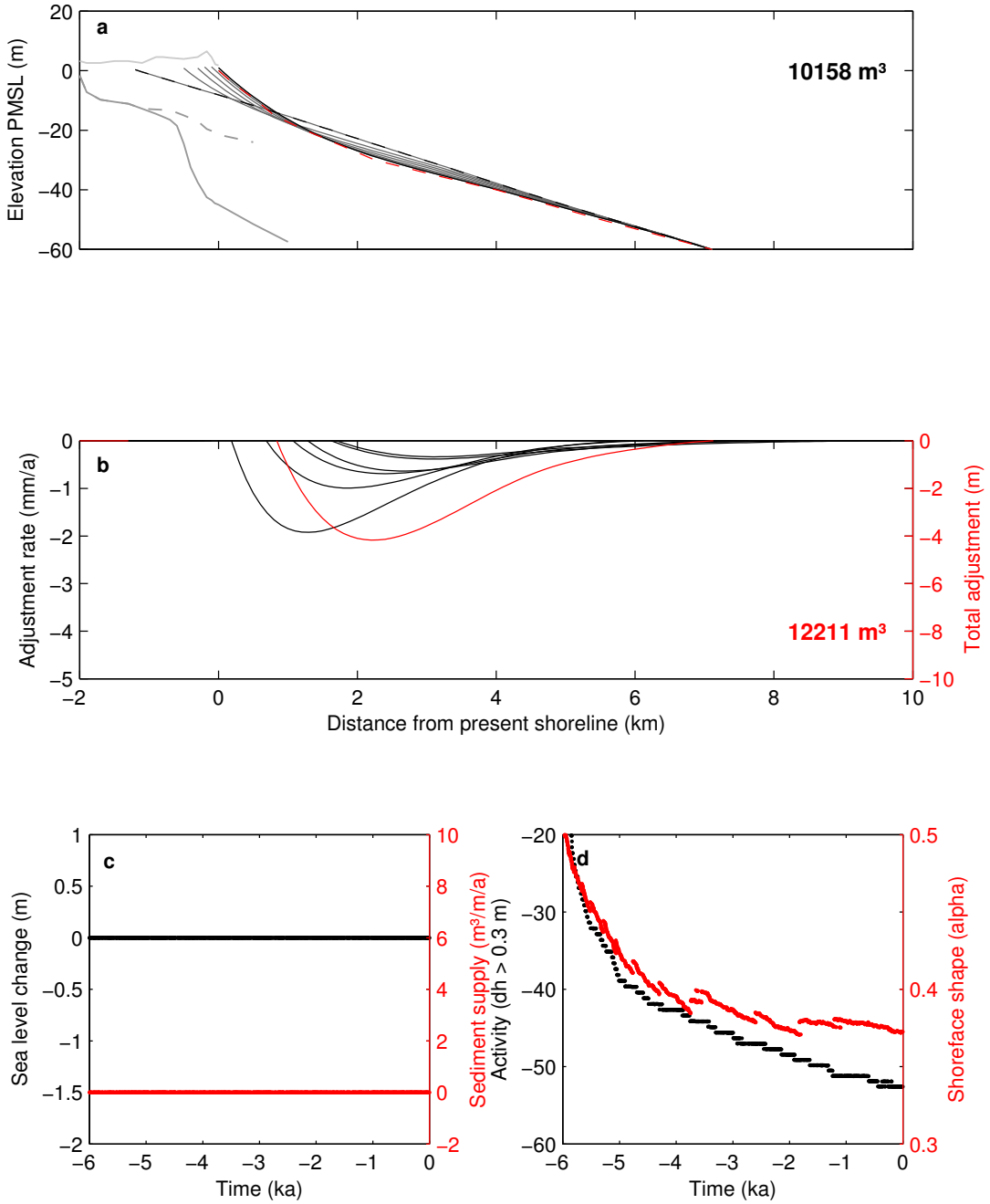

Figure 3.3: Moruya BARSIM erosion efficiency calibration - (a) Initial model morphology (dashed black), barrier and shoreface evolution at millennia-average time increments (grey solid), final model morphology (solid black) and surveyed shoreface profile (dashed red); total deposition at the coastline also shown; (b) millennia-average rates of depth-dependent shoreface lowering (black), total shoreface adjustment (red) and total shoreface erosion volume; (c) sea level change and external sediment supply scenarios; (d) fixed-magnitude depth limit of shoreface activity (black), and dimensionless shoreface shape (red) where alpha < 0.5 indicates concavity.

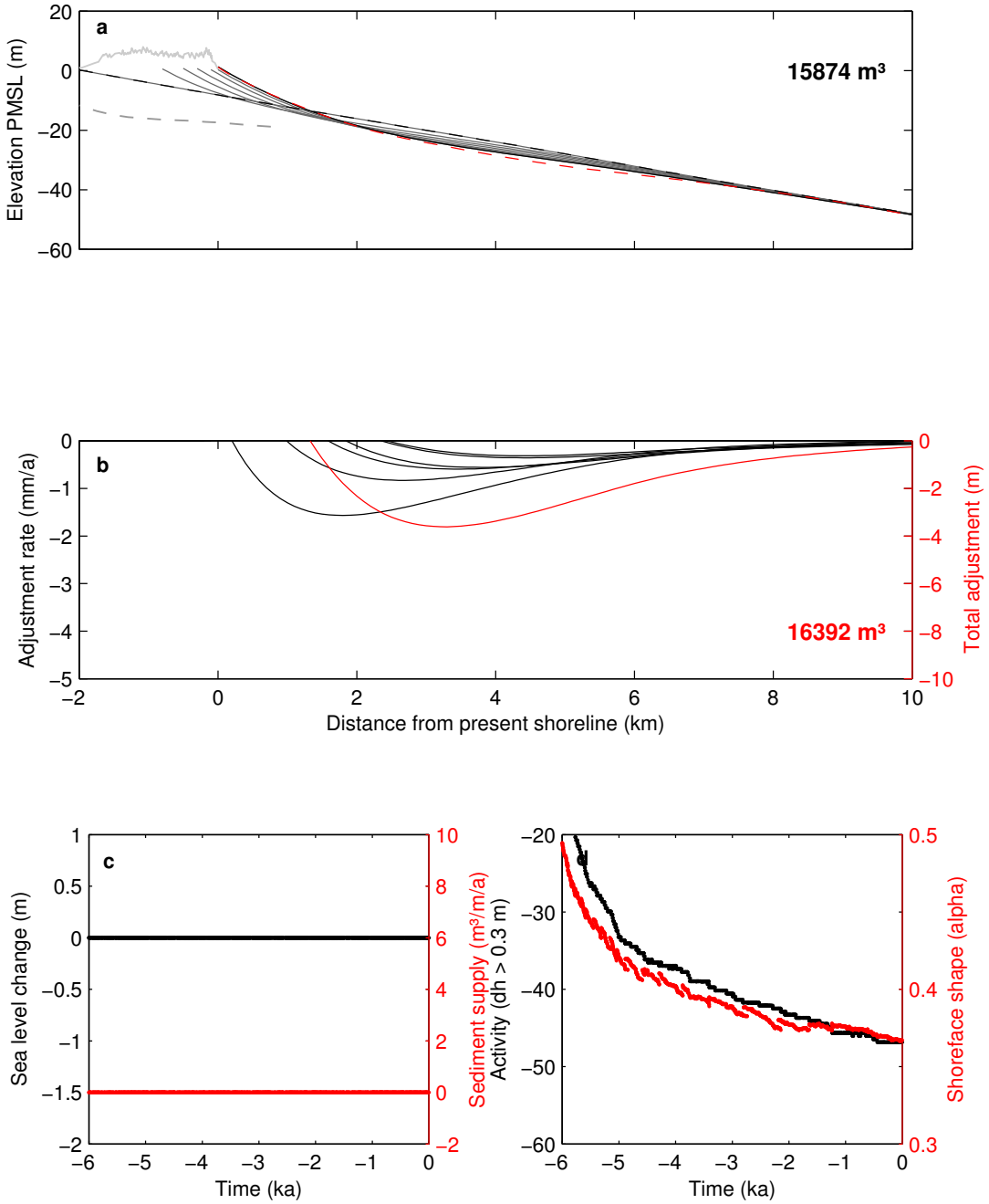

Figure 3.4: Tuncurry BARSIM erosion efficiency calibration - (a) Initial model morphology (dashed black), barrier and shoreface evolution at millennia-average time increments (grey solid), final model morphology (solid black) and surveyed shoreface profile (dashed red); total deposition at the coastline also shown; (b) millennia-average rates of depth-dependent shoreface lowering (black), total shoreface adjustment (red) and total shoreface erosion volume; (c) sea level change and external sediment supply scenarios; (d) fixed-magnitude depth limit of shoreface activity (black), and dimensionless shoreface shape (red) where alpha < 0.5 indicates concavity.

3.3.2 Model experiments

A range of model scenarios were examined using the site-calibrated BARSIM models to investigate the sensitivity of simulated strandplain progradation to the following:

1. Shoreface disequilibrium-stress (D-S) response
2. Potential external sediment supply from northward alongshore transport
3. Three alternative late-Holocene sea level scenarios
4. Combined forcing from all of the above

The objective of the simulations was to constrain the likely contribution of each potential sediment source to strandplain progradation at each site. Simulations were carried out for a 6,000-year time period (i.e. 6-0 ka BP), during which observed rates of strandplain progradation, as estimated from the barrier age structure at each site, were simulated by manipulating the sediment sources being assessed. Specifically, the response to shoreface disequilibrium-stress response and relative sea-level fall were first examined in isolation, with alongshore sediment transport introduced where the former modes of supply failed to meet the required demand (as specified by the barrier age structures). The effects of all three modes of supply were then considered simultaneously. All other model parameters and variables were maintained constant between each of the simulations.

A variety of initial (i.e. 6 ka BP) model substrates determined through inverse simulation were imposed as necessary start-up conditions for each scenario. Initial upper shoreface dimensions set identically for all simulations, determined empirically from the barrier age structures at each site. That is, the 6 ka BP model substrates were inferred from the distribution of radiocarbon ages in each strandplain [Chapter 2]. However, lower shoreface geometry was varied between simulations depending on the necessary required onshore sand supply volume from shoreface D-S response, with high rates of supply requiring greater shoreface disequilibrium at start up (i.e. 6 ka BP initial conditions). To achieve this, initial lower shoreface convexity was increased to satisfy the shoreface supply demand. For scenarios with an increased availability of supplementary sediment sources (e.g. sea-level-fall induced shoreface lowering or alongshore sediment transport), initial lower shoreface convexity was reduced accordingly. The simulation

matrix in Table 3.1 specifies the nature of model forcing by sea level, shoreface D-S response and external sediment supply (Q) for each of the simulation experiments.

Table 3.1: BARSIM Holocene simulations matrix - Matrix of simulation experiments carried out for Moruya (MR) and Tuncurry (TC) using the site-calibrated BARSIM models. Model forcing from the three relative sea level change scenarios (HL1, HL2, HL3), shoreface D-S response and external sediment supplies (Q) are shown.

Model Scenario	ST	Sea Level HL1	HL2	HL3	Shoreface D-S	Start Q-rate ($m^3/m/a$)	End Q-rate ($m^3/m/a$)
MR-ST-DS	Y				Y	0	0
TC-ST-DS	Y				Y	0	0
TC-ST-DS-Q2	Y				Y	0	2
MR-ST-Q10	Y				N	10	3
TC-ST-Q7	Y				N	7	4.5
MR-ST	Y				N	0	0
MR-HL1		Y			N	0	0
MR-HL2			Y		N	0	0
MR-HL3				Y	N	0	0
TC-ST	Y				N	0	0
TC-HL1		Y			N	0	0
TC-HL2			Y		N	0	0
TC-HL3				Y	N	0	0
MR-HL1-DS		Y			Y	0	0
MR-HL2-DS			Y		Y	0	0
MR-HL3-DS				Y	Y	0	0
TC-HL1-DS-Q2		Y			Y	0	2
TC-HL2-DS-Q2			Y		Y	0	2
TC-HL3-DS-Q2				Y	Y	0	2

3.3.2.1 Shoreface disequilibrium-stress response

Disequilibrium-stress induced shoreface lowering as the sole source of late Holocene strandplain progradation was the subject of the first set of experiments. In the absence of sea-level fall or an external sediment source, convex initial lower shoreface geometry was a necessary condition imposed at both sites to achieve strandplain volumes simulated with the calibrated BARSIM model consistent with the age structures of the barrier systems. Specifically, a lower shoreface sand body situated at about 20 m water depth was a necessary initial condition of site morphology. For each case, initial shoreface

geometry including the dimensions of the lower shoreface sand body was constrained by the following factors:

1. the strandplain progradation volume and interpreted barrier age structure;
2. the site erosion-efficiency factor as estimated in Section 3.3.1.3; and,
3. the present-day shoreface geometry determined from hydrographic surveys.

That is, the assumption that strandplain progradation was sourced entirely from shoreface lowering due to D-S response in these simulations meant that the dimensions of lower-shoreface sand bodies were guided by the following conditions, which are derived from the interpreted barrier age structures:

1. provide a sufficient sand supply to satisfy the interpreted strandplain progradation distance between 6-0 ka BP; and,
2. occupy suitable depths to support rates of strandplain progradation consistent with the barrier age structures.

Lower shoreface convexity was manipulated within the calibrated BARSIM models using an iterative inversion procedure to identify the initial shoreface geometry that resulted in strandplain progradation at rates consistent with the barrier age structure, and a final surface consistent with the contemporary shoreface geometry. Millennia average rates of shoreface lowering and total shoreface lowering over the 6-0 ka BP simulation period were calculated by measuring surface change within each model grid cell for each simulation time step. The evolution of shoreface geometry was also quantified throughout the simulations. First, a fixed-magnitude depth limit of shoreface activity, quantified as depth change $dh > 0.3$ m, was measured to investigate the dependence of the shoreface limiting depth on measurement timescale. Second, shoreface shape was measured (to $h = 35$ m) using the dimensionless order-one shape index (alpha), after *Wolinsky* [2009].

Strong evidence exists to suggest that late Holocene strandplain progradation at Tuncurry occurred in response to both shoreface lowering and external sediment supply to the embayment [*Roy et al.*, 1994, 1997]. Specifically, the age structures of an updrift headland-attached shelf sand body and estuarine tidal delta suggest that fluctuations in northward alongshore transport rates into the Tuncurry embayment were

regulated by the deposition of these sedimentary features. The depositional evidence is explored in detail in Chapter 2, and implies increasing rates of alongshore sediment supply to the embayment during the late Holocene. Specifically, *Roy et al.* [1997] estimated that approximately 20% of the total volume of the Tuncurry strandplain was supplied by alongshore transport from the coastline to the south, and reasoned that the rate of supply increased from about 1.5 ka BP onwards, coincident with the filling of updrift sinks. They further reasoned that northward alongshore drift into the Tuncurry embayment became the dominant source of strandplain progradation after 2 ka BP.

The implications of alongshore sediment supply at Tuncurry on shoreface response was investigated numerically by manipulating both the BARSIM initial shoreface convexity and external sediment supply in accordance with the depositional evidence, to achieve simulated strandplain progradation from combined shoreface-alongshore supply consistent with the measured barrier age structure.

Much lower rates of alongshore sediment supply to the Moruya embayment during the late Holocene are likely to have prevailed: steeper shelf gradients in that region suggest that once sea level flooded the coastal embayments and stabilised at near present elevations, the alongshore transport pathways present at lower sea levels were rapidly cut off. However, although it seems clear that strandplain progradation at Moruya between 6-0 ka BP was supplied by the adjacent shelf [*Cowell et al.*, 2001; *Daley*, 2012], initially significant (i.e. 6-4 ka BP) rates of alongshore sediment supply to the Moruya shoreface could have prevailed if concurrent erosion of updrift barriers and sand bodies, which may have become stranded on steep unembayed sections of the shelf, reached the Moruya shoreface. That is, notwithstanding that shoreface supply to the Moruya strandplain was well underway by 6 ka BP, realised rates of shoreface lowering may have been initially moderated relative to what is suggested by rates of strandplain progradation during this time, due to alongshore sediment supply from the south to the Moruya shoreface. Because there is no preserved depositional evidence to constrain alongshore transport rates at Moruya during that period, alongshore sediment supply to the Moruya embayment is not considered here.

3.3.2.2 External sediment supply

Considering the highly embayed nature of the coastlines at Moruya and Tuncurry at the onset of the Holocene sea-level highstand, the cases for overwhelming sand supply

from external sources such as alongshore drift are not particularly strong. However, hypothetical model scenarios that featured strandplain progradation solely by external sand supply were included here to investigate both time-dependent variations in the required supply volumes and the sensitivity of shoreface geometry to stable sea levels and high rates of external sand supply. To minimise the potential for shoreface D-S response in these scenarios, initial lower shoreface geometry was consistent with the present-day shoreface at each site. The external sand supply rates were then varied throughout the 6-0 ka BP simulation period to achieve simulated rates of strandplain progradation consistent with the barrier age structures at each site. In these scenarios therefore, all model parameters and variables were held constant with the exception of the external sand supply rate.

3.3.2.3 Relative sea-level fall

Although the nature of late Holocene sea level change in southeastern Australian remains unresolved due to the limitations of available relative sea level indicators, the review of evidence for late Holocene sea level change in Section 3.2.1 suggests three alternative scenarios that capture the range of proposed sea level histories. The scenarios considered here are shown in Figure 3.5 and include:

1. a sea-level fall from 1.5 m PMSL to 0 m occurring between 6-0 ka BP at a constant rate of 0.25 mm/a (HL1);

2. sea-level highstand at 1.5 m PMSL between 6-3 ka BP, followed by a sea-level fall from 1.5 m to 0 m between 3-0 ka BP at a constant rate of 0.5 mm/a (HL2); and,

3. sea-level highstand at 1.5 m PMSL between 6-1.5 ka BP, followed by a sea-level fall from 1.5 m to 0 m between 1.5-0 ka BP at a constant rate of 1.0 mm/a (HL3).

Scenario HL1 is based on the proposition that terminal PGMT sea levels reached a highstand level of up to 2 m PMSL prior to 6 ka BP, before gradually subsiding throughout the mid to late Holocene in response to the hydro-isostatic adjustment of the continental margin [*Lambeck and Nakada*, 1990]. Scenario HL2 derives from the more recent proposition that the effects of hydro-isostatic adjustment on relative sea levels may not have been realised until after 3 ka BP, when meltwater inputs are believed to have ceased [*Lambeck*, 2002; *Goodwin and Harvey*, 2008]. Scenario HL3 is based on

the revised Holocene sea level curve of *Sloss et al.* [2007], which was derived from a review of evidence from estuarine sediments and fixed biological indicators. Scenario 3 is consistent with the reasoning underpinning Scenario 2 for prolonged mid- to late-Holocene raised sea levels, although sea-level fall does not commence until 1.5-2 ka BP. The rationale for a delay in the commencement of sea-level fall following the cessation of meltwater input remains unclear.

Similar to the external sediment supply scenarios, in these simulations it was assumed that dynamic shoreface geometric equilibrium was attained rapidly following termination of the PGMT, and strandplain progradation between 6-0 ka BP was therefore driven solely by the falling sea level scenarios. This was achieved in the BARSIM models again by the application of present-day shoreface geometry in the initial conditions for each site. To control for latent shoreface D-S response associated with the contemporary shoreface morphology and model configuration for each site, a comparable simulation was also carried out with no sea level change. Thus any shoreface lowering that was attributable to ongoing D-S response in the model was quantified and subsequently subtracted from the strandplain volumes of the relative sea-level fall scenarios. In this manner an estimate of onshore sediment supply due to each sea level scenario alone was determined.

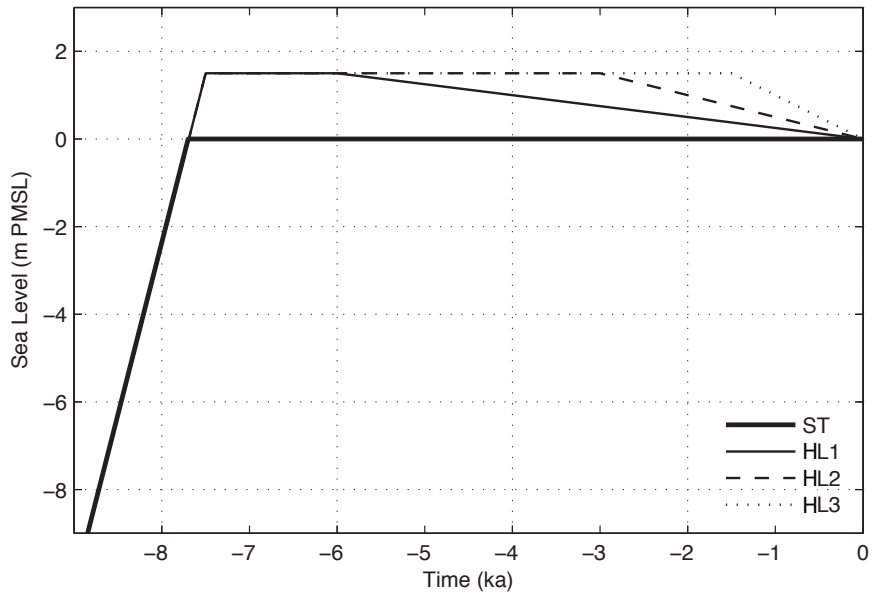

Figure 3.5: Sea level scenarios applied in Holocene highstand models - One stillstand (ST) and three sea-level fall scenarios were examined using the BARSIM models. Sea level fall at rates of -0.25 (HL1), -0.5 (HL2) and -1.0 (HL3) mm/a were considered.

3.3.2.4 Combined forcing

In the fourth set of scenarios the response to combined forcing from all of the above potential sources of Holocene strandplain progradation was examined. For each sea-level fall scenario [Fig. 3.5], the volume and geometry of the initial lower shoreface sand body was manipulated using an iterative inversion procedure to achieve simulated mid to late Holocene rates of strandplain progradation consistent with the barrier age structure at each site. Therefore these scenarios constrained rates of onshore sand supply associated with shoreface lowering due to concurrent relative sea-level fall and shoreface D-S response, and also rates of alongshore sand supply inferred from the regional geomorphology at Tuncurry.

3.4 Results

3.4.1 Shoreface disequilibrium-stress (D-S) response

Figure 3.6 shows that for the Moruya site, the total volume of disequilibrium-stress-induced shoreface lowering required to generate 900 m of strandplain progradation, was 23,746 m^3 per metre of embayment shoreline (i.e. m^3/m). The total volume of the prograded strandplain was 21,363 m^3/m, with the remaining 2,383 m^3/m of shoreface sand supply reworked *in situ* or deposited across the inner to mid shelf [Fig. 3.6a]. Strandplain progradation was sourced entirely from the erosion of a convex shoreface sand body located between 18-50 m depth [Fig. 3.6a], which lowered at progressively reduced rates [Fig. 3.6b], as the shoreface became deeper and more concave [Fig. 3.6f]. The rate of (onshore) shoreface sediment supply diminished throughout the simulation, with millennia average rates of strandplain progradation decreasing from 7.5 $m^3/m/a$ at the beginning of the simulation (i.e. 6-5 ka) to 2 $m^3/m/a$ by the end [Fig. 3.6d]. Rates of barrier growth were closely correlated with the rates of shoreface sand supply [Fig. 3.6d]. Figure 3.6c shows that based on the initial shoreface morphology, the model reproduced rates of strandplain progradation throughout the simulation period that were consistent with the distribution of radiocarbon dates, as seen in the spacing of simulated 1-ka (solid) and 0.5-ka (dashed) model shorefaces relative to the age data. That is, the majority of age samples are located within their corresponding 0.5-ka model increments.

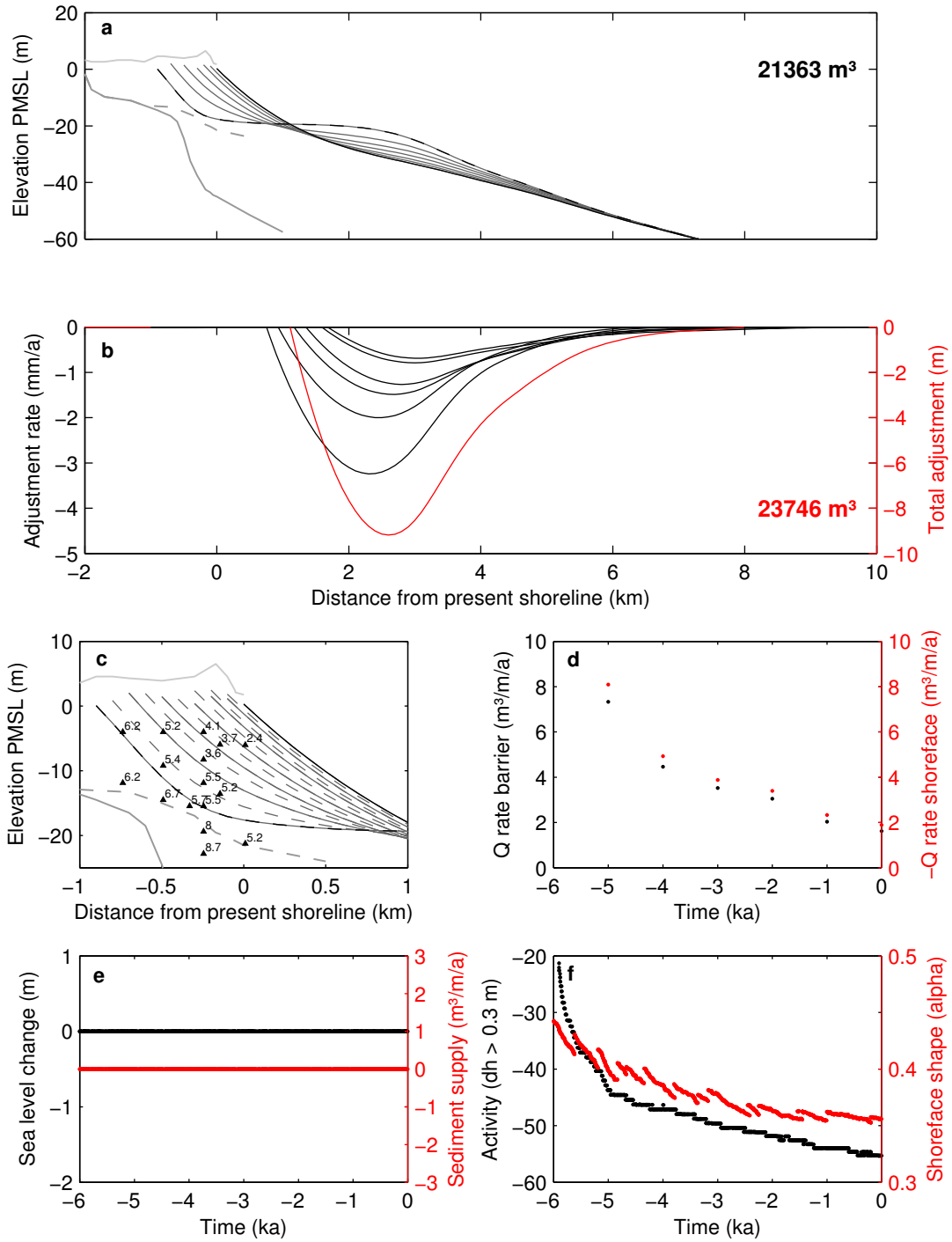

Figure 3.6: MR-ST-DS simulation experiment, see Table 3.1 - (a) Barrier & shoreface evolution at millennia-average increments & total barrier progradation volume; (b) millennia-average rates of depth-dependent shoreface lowering (black), total shoreface adjustment (red) & total shoreface erosion volume; (c) simulated evolution at 1-ka (solid) & 0.5-ka (dashed) increments with respect to C^{14} ages; (d) millennia-average rates of barrier deposition (black) & shoreface erosion (red); (e) sea level change & external sediment supply scenarios; (f) fixed-magnitude depth limit of shoreface activity (black) & dimensionless shoreface shape (red).

At Tuncurry the volume of disequilibrium-stress-induced shoreface lowering that was required to generate 1,100 m of strandplain progradation was 27,078 m^3/m [Fig. 3.7]. The total volume of the prograded strandplain was 26,176 m^3/m, with the remaining 902 m^3/m of shoreface sand supply reworked *in situ* or deposited across the inner to mid shelf [Fig. 3.7a]. Strandplain progradation was sourced entirely from the erosion of a convex inner-shelf sand body located between 16-40 m depth [Fig. 3.7a], which lowered at progressively reduced rates [Fig. 3.7b], as the shoreface became deeper and more concave [Fig. 3.7f]. Millennia-average rates of strandplain progradation decreased from 8.25 $m^3/m/a$ at the beginning of the simulation to 2 $m^3/m/a$ at the end [Fig. 3.7d]. Rates of barrier growth were closely correlated with the rates of shoreface sand supply [Fig. 3.7d]. However, Figure3.7c shows that based on the initial shoreface morphology, simulated rates of strandplain progradation were not consistent with the barrier age structure, as seen in the spacing of simulated 1-ka (solid) and 0.5-ka (dashed) model shorefaces relative to the age data. That is, whilst the simulated barrier volume was consistent with the geological evidence, the internal barrier age structure was not. For example, the 1.5 ka age sample is located closer to the 2.5 ka model shoreface.

Due to the depth-decaying BARSIM erosion function [Eq. 1.3], rates of onshore sediment supply from D-S induced shoreface lowering progressively diminished throughout the simulations in both the Moruya [Fig. 3.6d] and Tuncurry [Fig. 3.7d] examples. Whilst the age structure of the Moruya barrier is consistent with a diminishing rate of late-Holocene strandplain progradation, the distribution of radiocarbon ages from the Tuncurry Holocene barrier suggest a more constant rate of strandplain progradation between 6-0 ka BP [Fig. 2.4]. There is strong evidence from studies of the Quaternary geology of the Forster-Tuncurry region [Sec. 2.7] to suggest that the Tuncurry embayment received an additional sand supply via northward littoral drift from about 3 ka onwards [Sec. 2.7.4]. To investigate the potential influence of a longshore sand supply on strandplain progradation and shoreface response at Tuncurry, additional simulations were carried out that featured a supplementary external sediment supply volume [Sec. 3.3.2.1]. Time-varying external sand supply rates based on the updrift-sink model [Sec. 2.7.4] were evaluated in an iterative process to identify the best-fit model based on the distribution of age data.

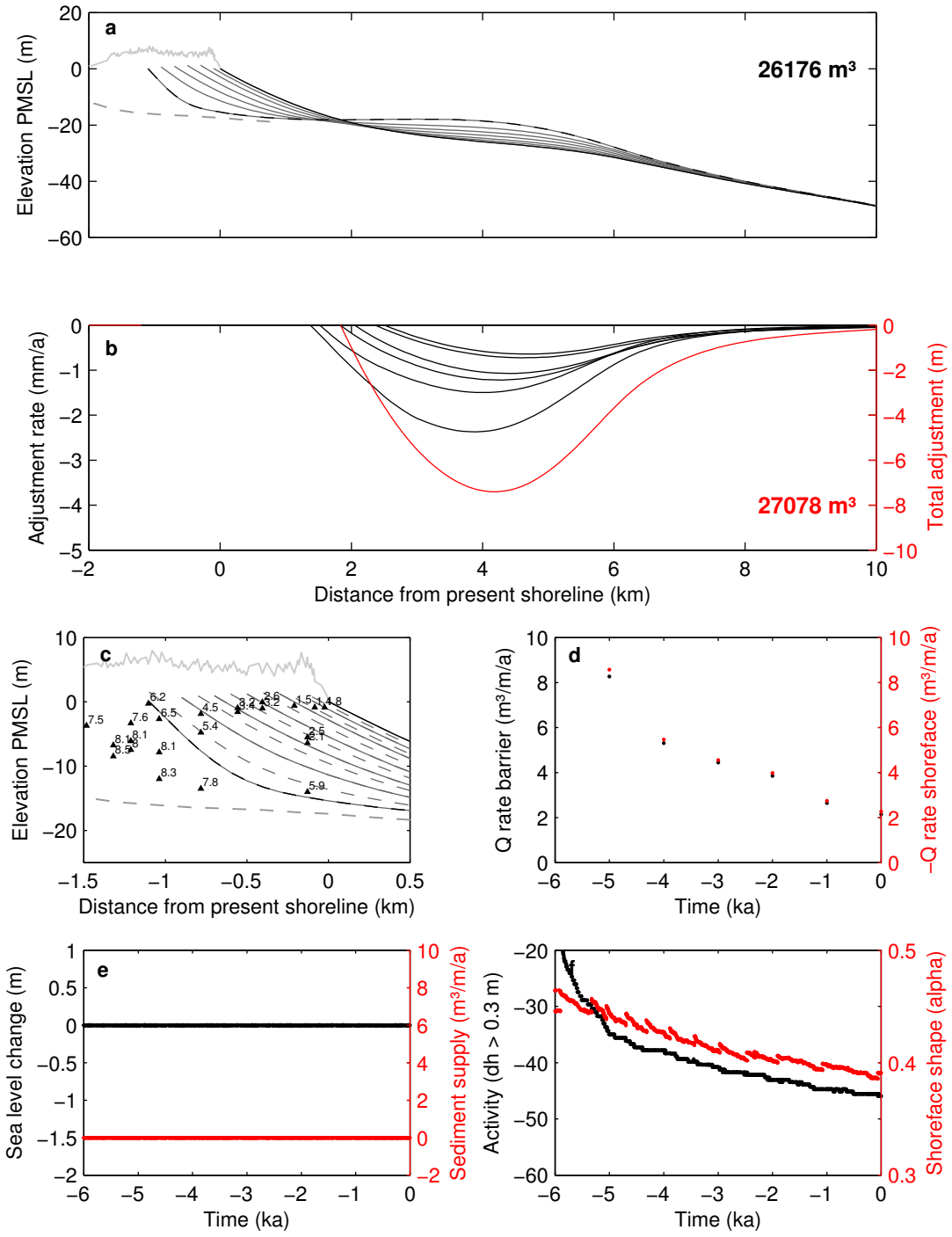

Figure 3.7: TC-ST-DS simulation experiment, see Table 3.1 - (a) Barrier & shoreface evolution at millennia-average increments & total barrier progradation volume; (b) millennia-average rates of depth-dependent shoreface lowering (black), total shoreface adjustment (red) & total shoreface erosion volume; (c) simulated evolution at 1-ka (solid) & 0.5-ka (dashed) increments with respect to C^{14} ages; (d) millennia-average rates of barrier deposition (black) & shoreface erosion (red); (e) sea level change & external sediment supply scenarios; (f) fixed-magnitude depth limit of shoreface activity (black) & dimensionless shoreface shape (red).

For the optimal simulation of Tuncurry strandplain progradation in response to shoreface disequilibrium-stress and longshore sand supply, the model strandplain prograded 1,100 m in response to the deposition of 25,091 m^3/m throughout the embayment [Fig. 3.8a]. In this scenario the volume of disequilibrium-stress-induced shoreface lowering was only 21,189 m^3/m [Fig. 3.8b]. The rate of longshore sand supply to the embayment increased throughout the simulation from 0 $m^3/m/a$ for the period 6-3 ka BP, 1 $m^3/m/a$ for the period 3-2 ka BP, and 2 $m^3/m/a$ for the period 1.5 ka BP to present [Fig. 3.8d]. The total volume of sediments supplied to the embayment by northward longshore sand transport between 3-0 ka BP was 4,740 m^3/m, which accounted for 19% of the total strandplain volume. In response to the combined sediment supply from diminishing disequilibrium-stress-induced shoreface sand supply, and increasing longshore sand supply, millennia-average rates of strandplain progradation between 5-0 ka BP remained more or less constant at 4 $m^3/m/a$ (decreasing from 7 $m^3/m/a$ between 6-5 ka BP) [Fig. 3.8d]. The divergence between the shoreface sand supply rate (red) and strandplain progradation rate (black) in Figure 3.8d indicates the influence of the additional longshore sand supply. The model reproduced rates of strandplain progradation that were consistent with the distribution of radiocarbon dates, as seen in the relatively uniform spacing of simulated 1-ka (solid) and 0.5-ka (dashed) model shorefaces, and improved model fit relative to the age data [Fig. 3.8c].

Figure 3.9 shows the sediment grain-size distributions simulated by BARSIM for strandplain progradation in response to the shoreface D-S response scenarios at Moruya [Fig. 3.6] and Tuncurry [Fig. 3.7]. Upper shoreface facies are characterised by coarser sand that is deposited as storm-event beds in response to the event-drive BARSIM wave climate. Lower shoreface facies are characterised by finer sands, which is consistent with the grain-size-dependent sediment travel distances of the BARSIM deposition function.

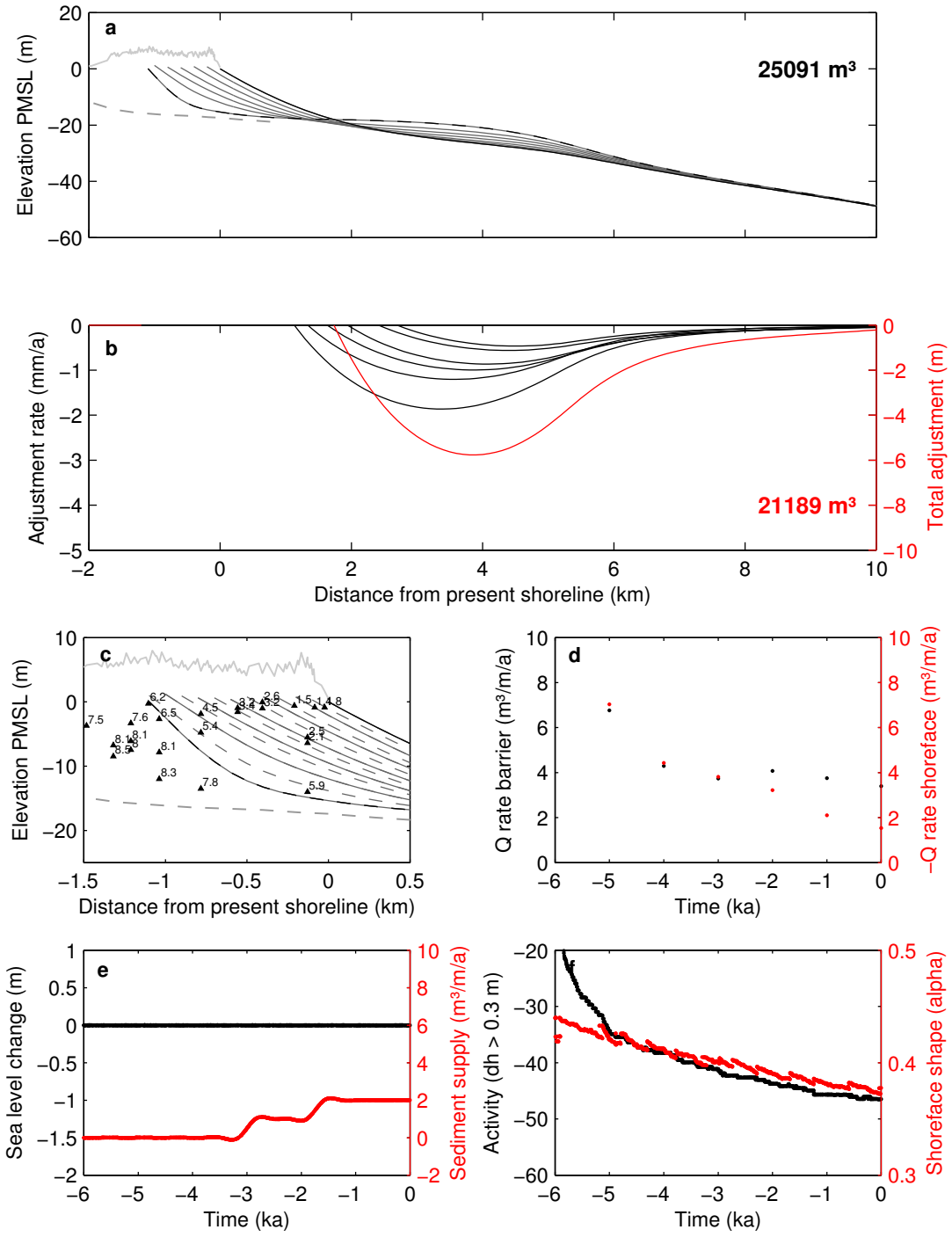

Figure 3.8: TC-ST-DS-Q2 simulation experiment, see Table 3.1 - (a) Barrier & shoreface evolution at millennia-average increments & total barrier progradation volume; (b) millennia-average rates of depth-dependent shoreface lowering (black), total shoreface adjustment (red) & total shoreface erosion volume; (c) simulated evolution at 1-ka (solid) & 0.5-ka (dashed) increments with respect to C^{14} ages; (d) millennia-average rates of barrier deposition (black) & shoreface erosion (red); (e) sea level change & external sediment supply scenarios; (f) fixed-magnitude depth limit of shoreface activity (black) & dimensionless shoreface shape (red).

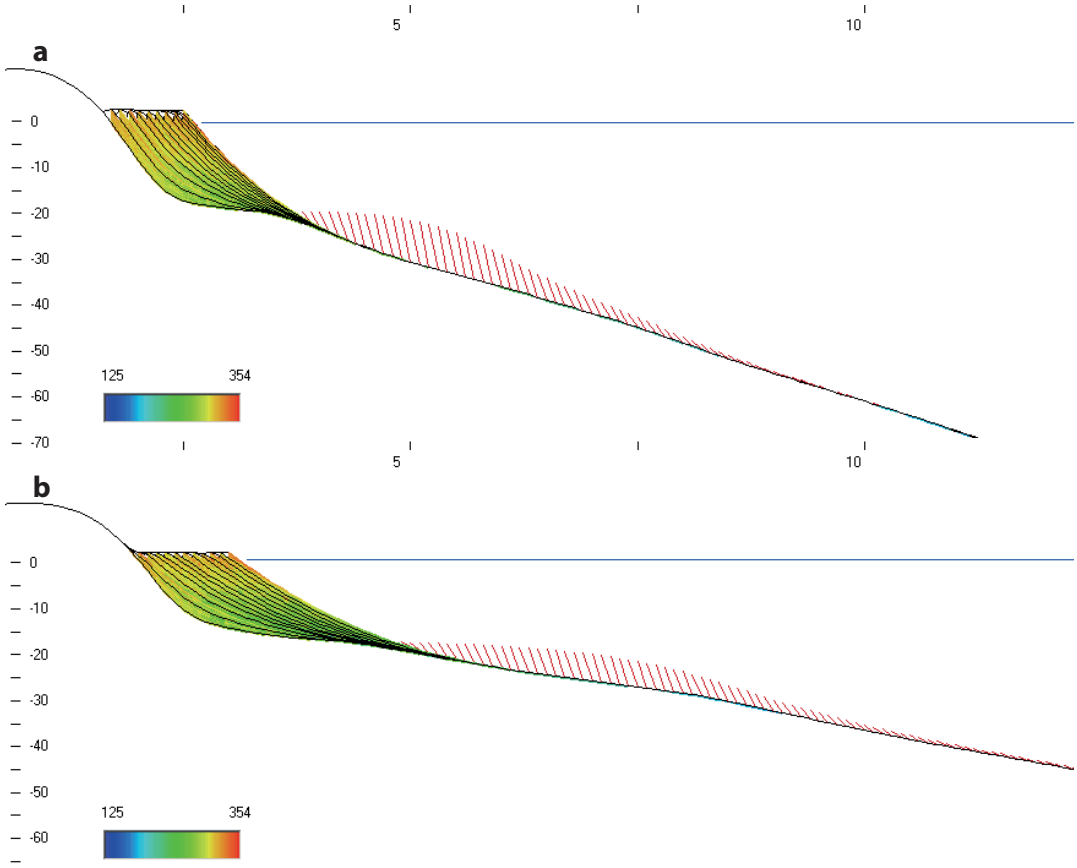

Figure 3.9: BARSIM grain-size distributions: MR-ST-DS and TC-ST-DS-Q2 - Sediment grain-size distributions for stillstand shoreface D-S response simulations for (a) Moruya and (b) Tuncurry. Note the concentration of coarser sediments (warmer colours) within upper-shoreface event-deposition beds and distribution of finer sediments (cooler colours) across mid- to lower-shoreface depths.

3.4.2 External sediment supply

Strandplain progradation in response to an external sand supply (longshore transport system) only was also simulated for both sites, to investigate the possibility that strandplain progradation was completely supplied by external sand sources.

To achieve simulated stratigraphy consistent with the barrier age structure at Moruya [Fig. 3.10c], a total sediment supply of 31,606 m^3/m was required [Fig. 3.10a]. The rate of sediment supply decreased linearly from 10 $m^3/m/a$ to 5 $m^3/m/a$ between 6-3 ka BP, and from 5 $m^3/m/a$ to 3 $m^3/m/a$ between 3-0 ka BP [Fig. 3.10d]. In contrast to the shoreface D-S response simulation in which barrier progradation occurred to 22 m water depth [Fig. 3.6a], in this simulation barrier progradation extended across the lower shoreface to 38 m depth [Fig. 3.10a].

At Tuncurry the total volume of external sediment supply required to achieve simulated stratigraphy consistent with the barrier age structure [Fig. 3.11c] was 32,011 m^3/m [Fig. 3.11a]. The necessary rate of sediment supply was was a step-wise decrease from 7 $m^3/m/a$ between 6-5 ka BP, to 6 $m^3/m/a$ between 5-4 ka BP, 5 $m^3/m/a$ between 4-2 ka BP and 4.5 $m^3/m/a$ between 2-0 ka BP [Fig. 3.11d]. Similar to the Moruya example, barrier progradation occurred to about 32 m water depth in this scenario [Fig. 3.11a], whereas barrier progradation only occurred to about 22 m depth in the shoreface disequilibrium-stress response simulation [Fig. 3.7a].

Total annual rates of longshore sand supply implied by the models can be determined by multiplying the external sand supply rates required in the BARSIM profile models by the embayment lengths. In this approach, both the Moruya (5.5 km length) and Broulee (1.5 km length) embayments [Fig. 2.10] should be considered together given that they would have remained connected for the majority of the simulation period [*Thom et al.*, 1981b]. Thus for the MR-ST-Q10 model the annual rate of sediment supply into the Moruya-Broulee embayment decreased from 70,000 m^3/a at 6 ka BP to 35,000 m^3/a at 3 ka BP, and 21,000 m^3/a by the end of the simulation. For the Tuncurry embayment (12.5 km length) annual rates of sediment supply in the TC-ST-Q7 model were 87,500 m^3/a, 75,000 m^3/a, 62,500 m^3/a and 56,250 m^3/a, for the 6-5 ka BP, 5-4 ka BP, 4-2 ka BP and 2-0 ka BP periods respectively. These longshore transport rates assume no leakage out of the north end of each embayment for the duration of the simulations.

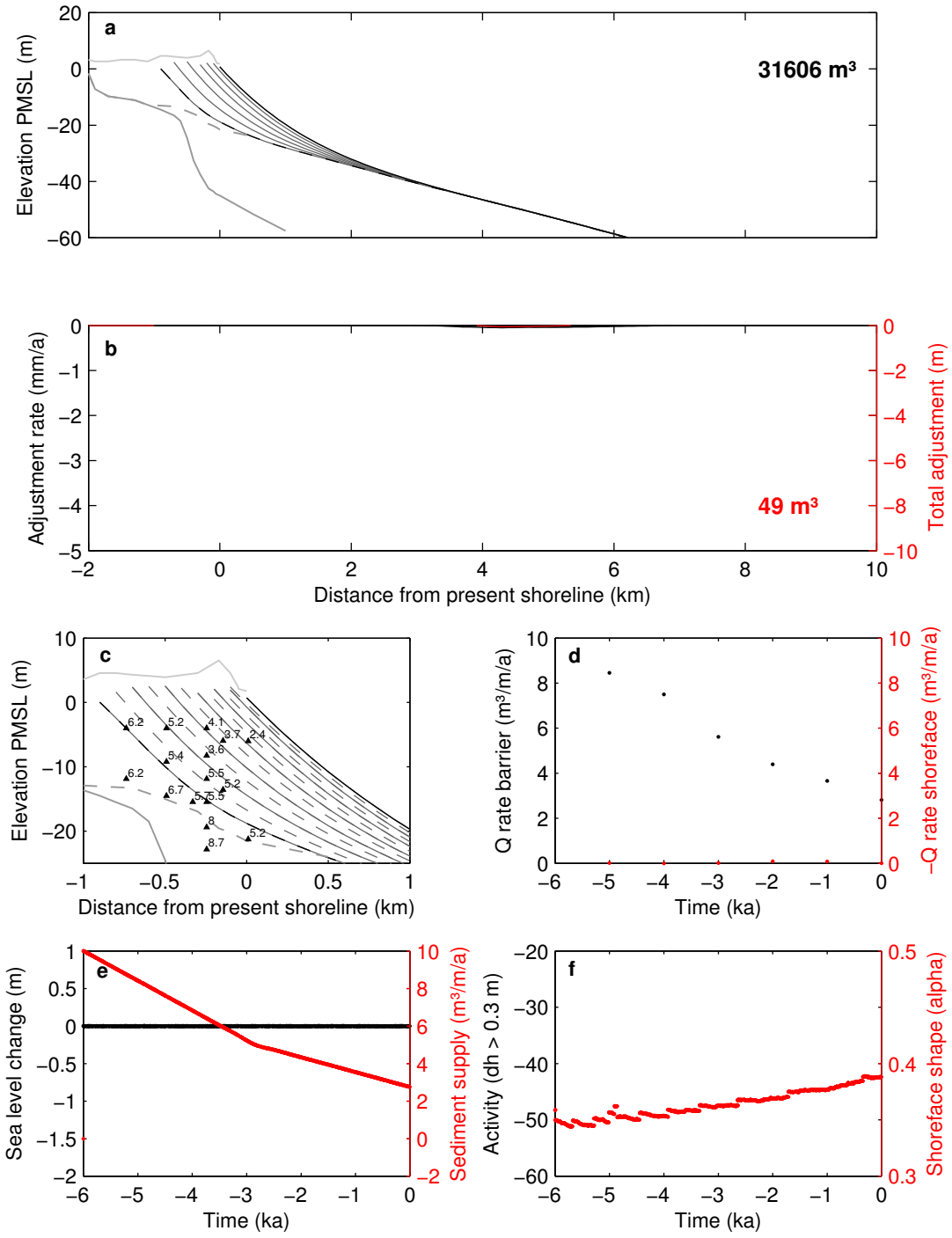

Figure 3.10: MR-ST-Q10 simulation experiment, see Table 3.1 - (a) Barrier & shoreface evolution at millennia-average increments & total barrier progradation volume; (b) millennia-average rates of depth-dependent shoreface lowering (black), total shoreface adjustment (red) & total shoreface erosion volume; (c) simulated evolution at 1-ka (solid) & 0.5-ka (dashed) increments with respect to C^{14} ages; (d) millennia-average rates of barrier deposition (black) & shoreface erosion (red); (e) sea level change & external sediment supply scenarios; (f) fixed-magnitude depth limit of shoreface activity (black) & dimensionless shoreface shape (red).

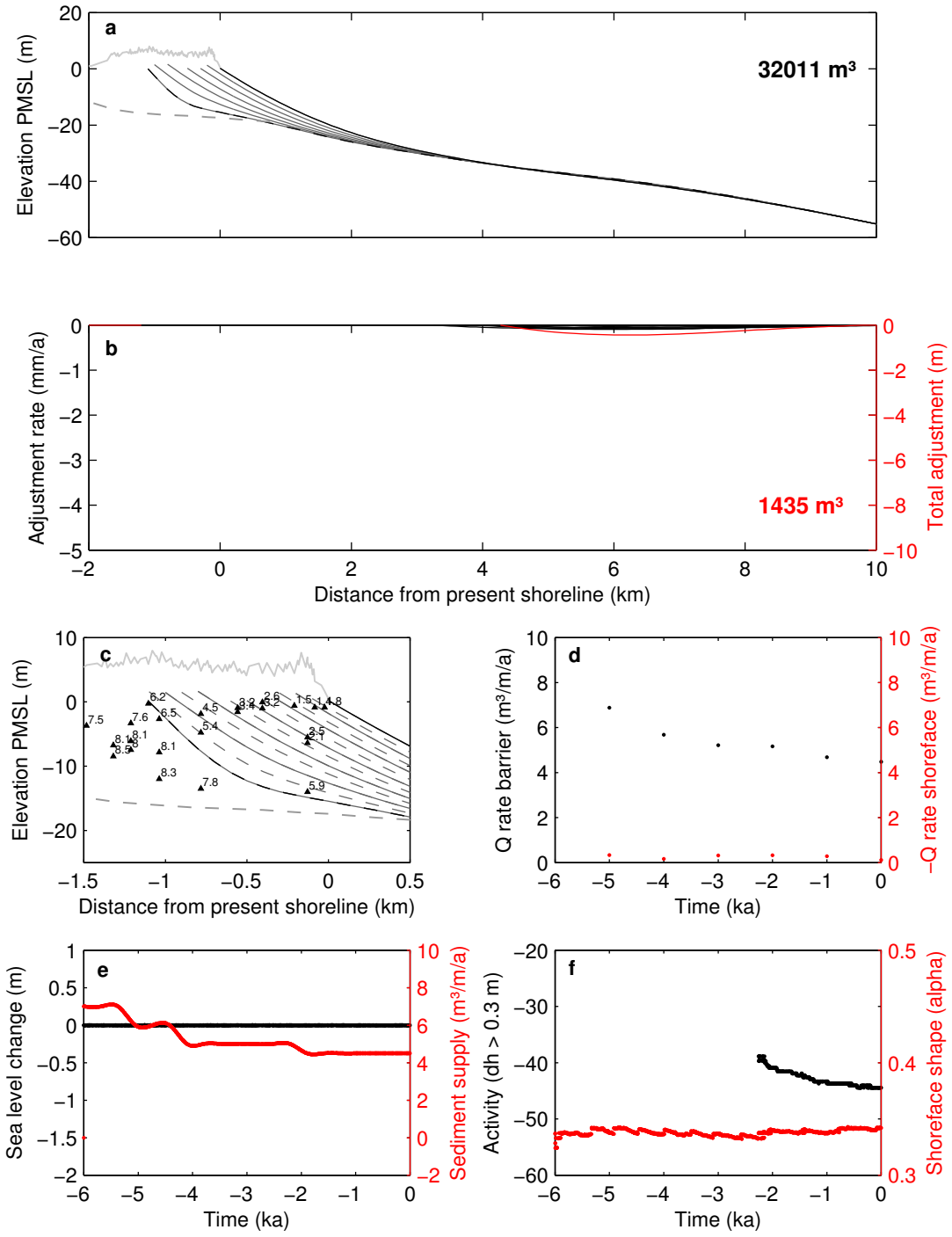

Figure 3.11: TC-ST-Q7 simulation experiment, see Table 3.1 - (a) Barrier & shoreface evolution at millennia-average increments & total barrier progradation volume; (b) millennia-average rates of depth-dependent shoreface lowering (black), total shoreface adjustment (red) & total shoreface erosion volume; (c) simulated evolution at 1-ka (solid) & 0.5-ka (dashed) increments with respect to C^{14} ages; (d) millennia-average rates of barrier deposition (black) & shoreface erosion (red); (e) sea level change & external sediment supply scenarios; (f) fixed-magnitude depth limit of shoreface activity (black) & dimensionless shoreface shape (red).

3.4.3 Relative sea-level fall

To investigate the potential contribution of sea-level fall to mid- to late-Holocene strandplain progradation, simulations were carried out using calibrated BARSIM models that featured present-day initial shoreface morphology (i.e. without shoreface sand bodies) and three alternative relative sea-level fall scenarios [Fig. 3.5]. In the absence of onshore sand supply due to shoreface D-S response, rates of strandplain progradation in response to the relative sea-level fall scenarios alone, were much lower.

At Moruya the control volume of strandplain progradation due to ongoing shoreface disequilibrium-stress response based on present-day initial shoreface morphology and no sea level change was 6,537 m^3/m [Fig. 3.12]. Addition of the HL1, HL2 and HL3 sea level fall scenarios to the control simulation had very little influence on strandplain progradation [Fig. 3.13]. A summary of the Moruya relative sea-level fall experiments is provided below (the full simulation outputs for the relative sea-level fall experiments can be found in Appendix B):

- For HL1, total strandplain progradation increased to 6,938 m^3/m, suggesting only 401 m^3/m of strandplain progradation could be attributed to a constant 1.5 m sea-level fall over the 6 ka simulation period.
- For HL2, total strandplain progradation increased to 6,744 m^3/m, suggesting only 207 m^3/m of strandplain progradation could be attributed to a constant 1.5 m sea-level fall over the 3 ka simulation period.
- For HL3, total strandplain progradation increased to 6,639 m^3/m, suggesting only 102 m^3/m of strandplain progradation could be attributed to a constant 1.5 m sea-level fall over the 1.5 ka simulation period.

Average rates of simulated onshore supply due to sea-level fall at Moruya were 0.067, 0.069 and 0.068 $m^3/m/a$ for the HL1, HL2 and HL3 scenarios respectively.

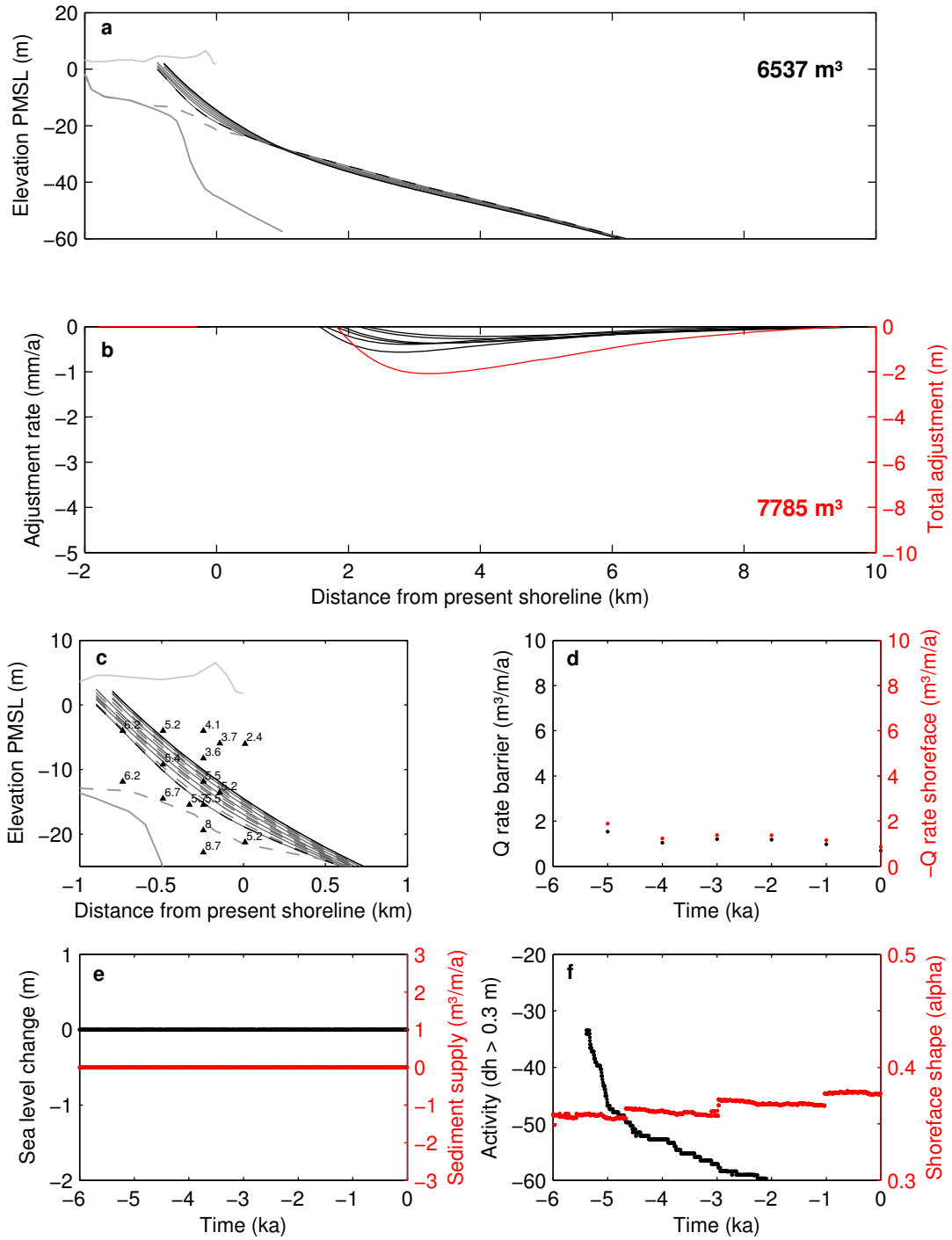

Figure 3.12: MR-ST simulation experiment, see Table 3.1 - (a) Barrier & shoreface evolution at millennia-average increments & total barrier progradation volume; (b) millennia-average rates of depth-dependent shoreface lowering (black), total shoreface adjustment (red) & total shoreface erosion volume; (c) simulated evolution at 1-ka (solid) & 0.5-ka (dashed) increments with respect to C^{14} ages; (d) millennia-average rates of barrier deposition (black) & shoreface erosion (red); (e) sea level change & external sediment supply scenarios; (f) fixed-magnitude depth limit of shoreface activity (black) & dimensionless shoreface shape (red).

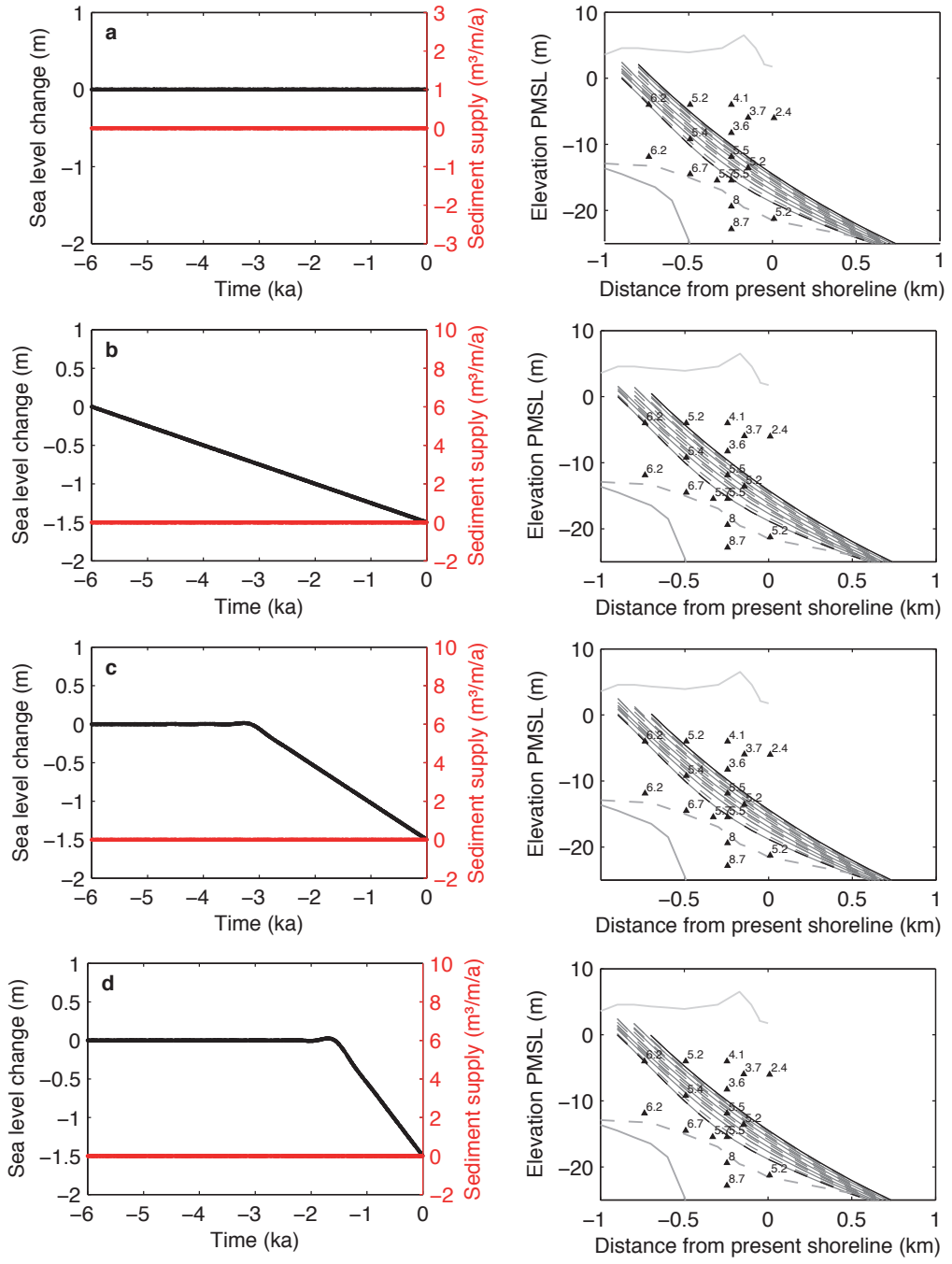

Figure 3.13: Simulated strandplain progradation due to relative sea-level fall at Moruya - Simulated strandplain progradation at Moruya in response to the sea level scenarios considered [Fig. 3.5]: (a) ST sea level scenario (i.e. no sea level change); (b) HL1 sea-level fall scenario; (c) HL2 sea-level fall scenario; and, (d) HL3 sea-level fall scenario. Full simulation outputs can be found in Appendix B.

At Tuncurry, the control volume of strandplain progradation due to ongoing shoreface disequilibrium-stress response based on present-day initial shoreface morphology and no sea level change was 5,013 m^3/m [Fig. 3.14]. Similar to the Mourya example, addition of the HL1, HL2 and HL3 sea level fall scenarios to the control simulation had very little influence on strandplain progradation [Fig. 3.15]. A summary of the Tuncurry relative sea-level fall experiments is provided below (the full simulation outputs for the relative sea-level fall experiments can be found in Appendix B):

- For HL1, total strandplain progradation increased to 5,365 m^3/m, suggesting only 352 m^3/m of strandplain progradation could be attributed to a constant 1.5 m sea-level fall over the 6 ka simulation period.
- For HL2, total strandplain progradation increased to 5,173 m^3/m, suggesting only 160 m^3/m of strandplain progradation could be attributed to a constant 1.5 m sea-level fall over the 3 ka simulation period.
- For HL3, total strandplain progradation increased to 5,089 m^3/m, suggesting only 76 m^3/m of strandplain progradation could be attributed to a constant 1.5 m sea-level fall over the 1.5 ka simulation period.

Average rates of simulated onshore supply due to sea-level fall at Tuncurry were 0.059, 0.053 and 0.051 m^3/m/a for the HL1, HL2 and HL3 scenarios respectively.

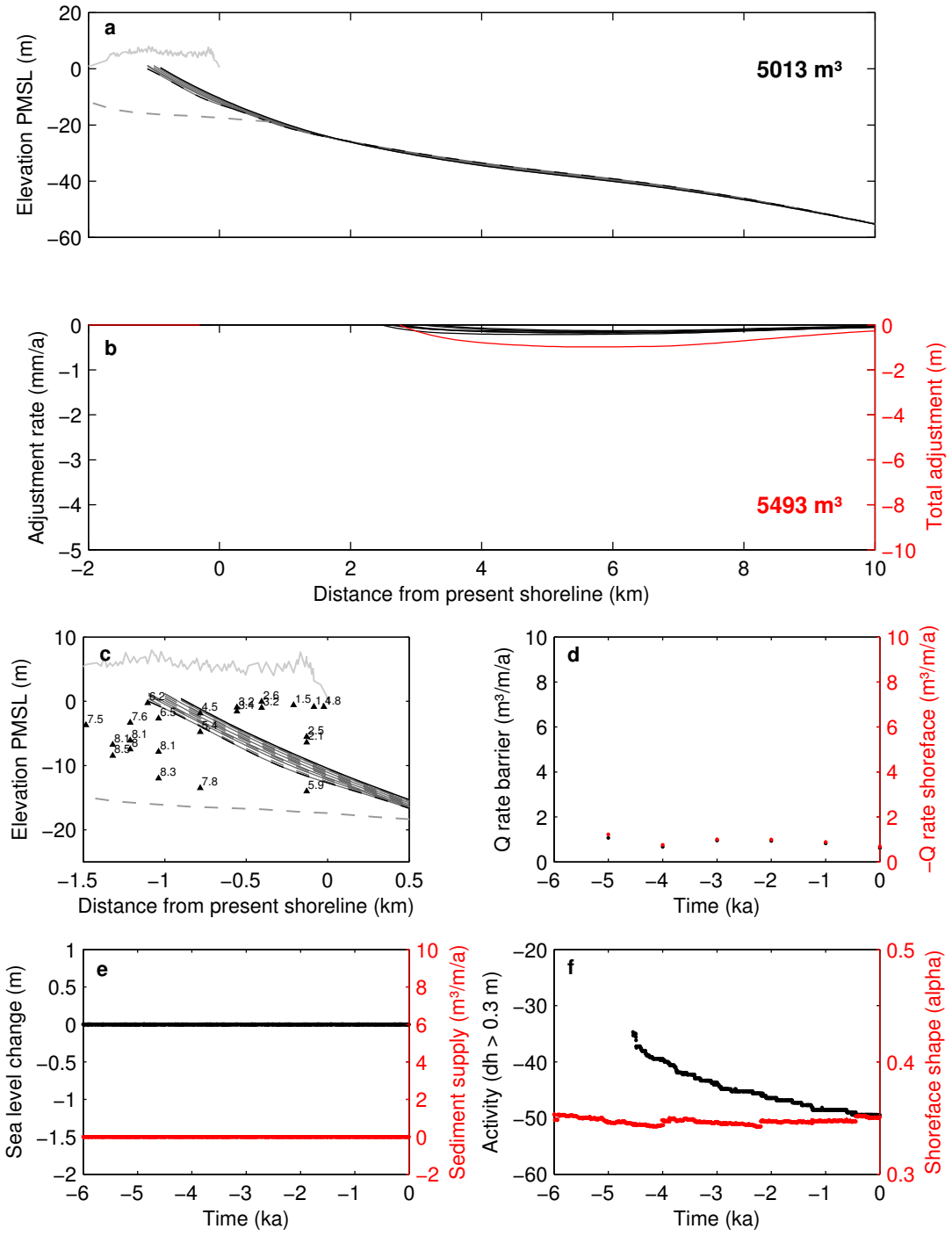

Figure 3.14: TC-ST simulation experiment, see Table 3.1 - (a) Barrier & shoreface evolution at millennia-average increments & total barrier progradation volume; (b) millennia-average rates of depth-dependent shoreface lowering (black), total shoreface adjustment (red) & total shoreface erosion volume; (c) simulated evolution at 1-ka (solid) & 0.5-ka (dashed) increments with respect to C^{14} ages; (d) millennia-average rates of barrier deposition (black) & shoreface erosion (red); (e) sea level change & external sediment supply scenarios; (f) fixed-magnitude depth limit of shoreface activity (black) & dimensionless shoreface shape (red).

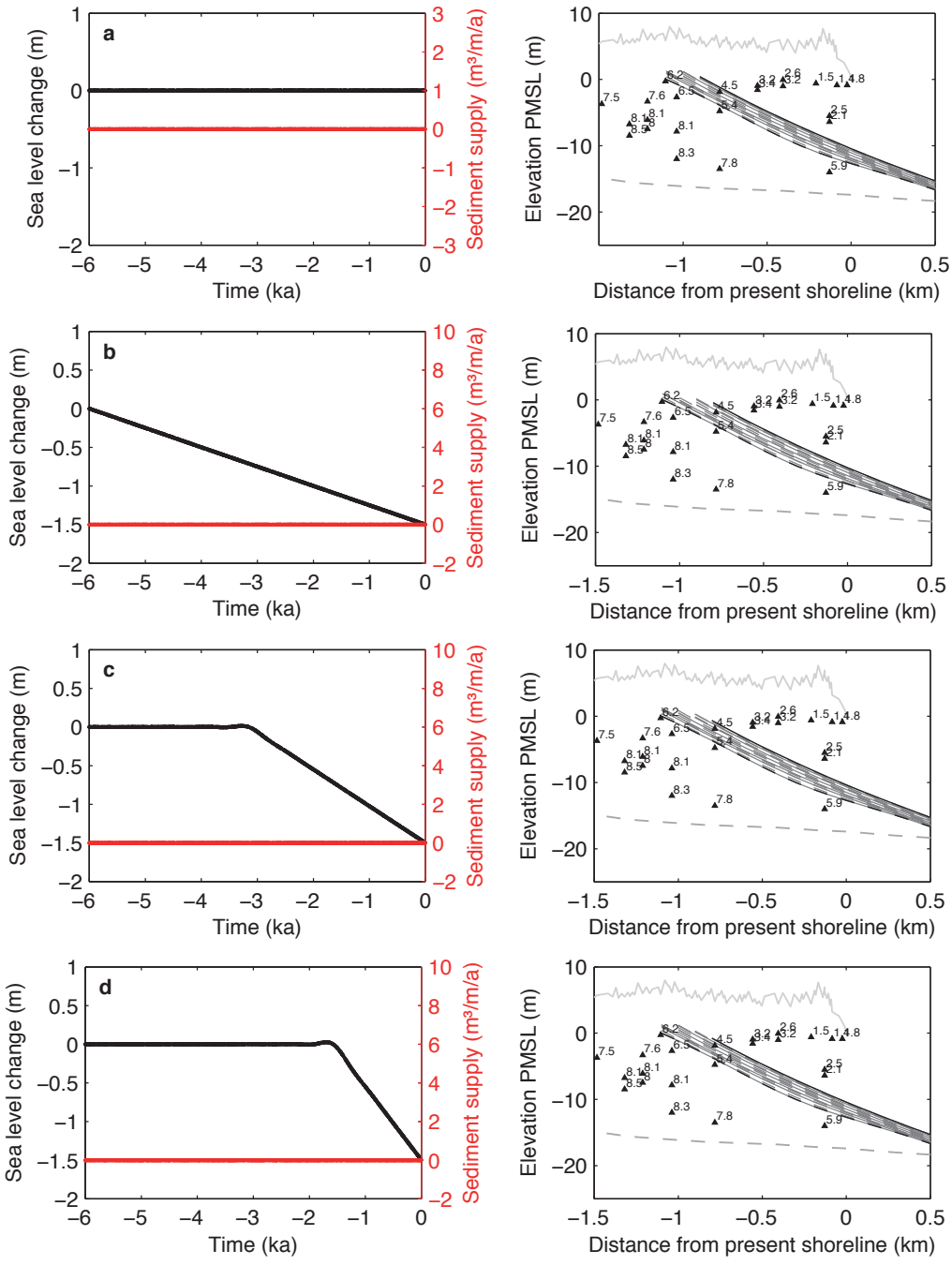

Figure 3.15: Simulated strandplain progradation due to relative sea-level fall at Tuncurry - Simulated strandplain progradation at Tuncurry in response to the sea level scenarios considered [Fig. 3.5]: (a) ST sea level scenario (i.e. no sea level change); (b) HL1 sea-level fall scenario; (c) HL2 sea-level fall scenario; and, (d) HL3 sea-level fall scenario. Full simulation outputs can be found in Appendix B.

3.4.4 Combined forcing

Strandplain response to combined forcing from onshore sand supply due to shoreface D-S response and relative sea-level fall was also considered by adding the three sea level scenarios [Fig. 3.5] to the shoreface D-S response simulations [Sec. 3.3.2.1]. For both sites, the effect of adding sea level forcing was to reduce the volume of the lower shoreface sand body that was required in the initial model morphology, to achieve strandplain progradation consistent with the barrier age structures. Without reducing the initial volume of the lower shoreface sand body, the simulated strandplains extended seaward beyond the present-day shorelines in all cases.

Figure 3.16 shows the necessary adjustments to initial shoreface morphology at Moruya with the addition of each of the three sea level scenarios, relative to the stable (ST) sea level case alone. Figure 3.17 shows that with the initial morphology adjustments, simulated strandplain progradation was comparable between each scenario. More specifically, strandplain progradation volumes for the HL1, HL2 and HL3 scenarios were between 21,000-21,500 m^3/m, and similarly shoreface lowering volumes were between 23-24,000 m^3/m [Appendix C].

Figure 3.18 shows the required adjustments to initial shoreface morphology at Tuncurry with the addition of each of the three sea level scenarios, relative to the stable (ST) sea level case alone. Figure 3.19 shows that with the initial morphology adjustments, simulated strandplain progradation was comparable between each scenario. More specifically, strandplain progradation volumes for the HL1, HL2 and HL3 scenarios were about 24,000 m^3/m, whilst shoreface lowering volumes and external sediment supply were about 20,000 m^3/m and 4,000 m^3/m respectively [Appendix C].

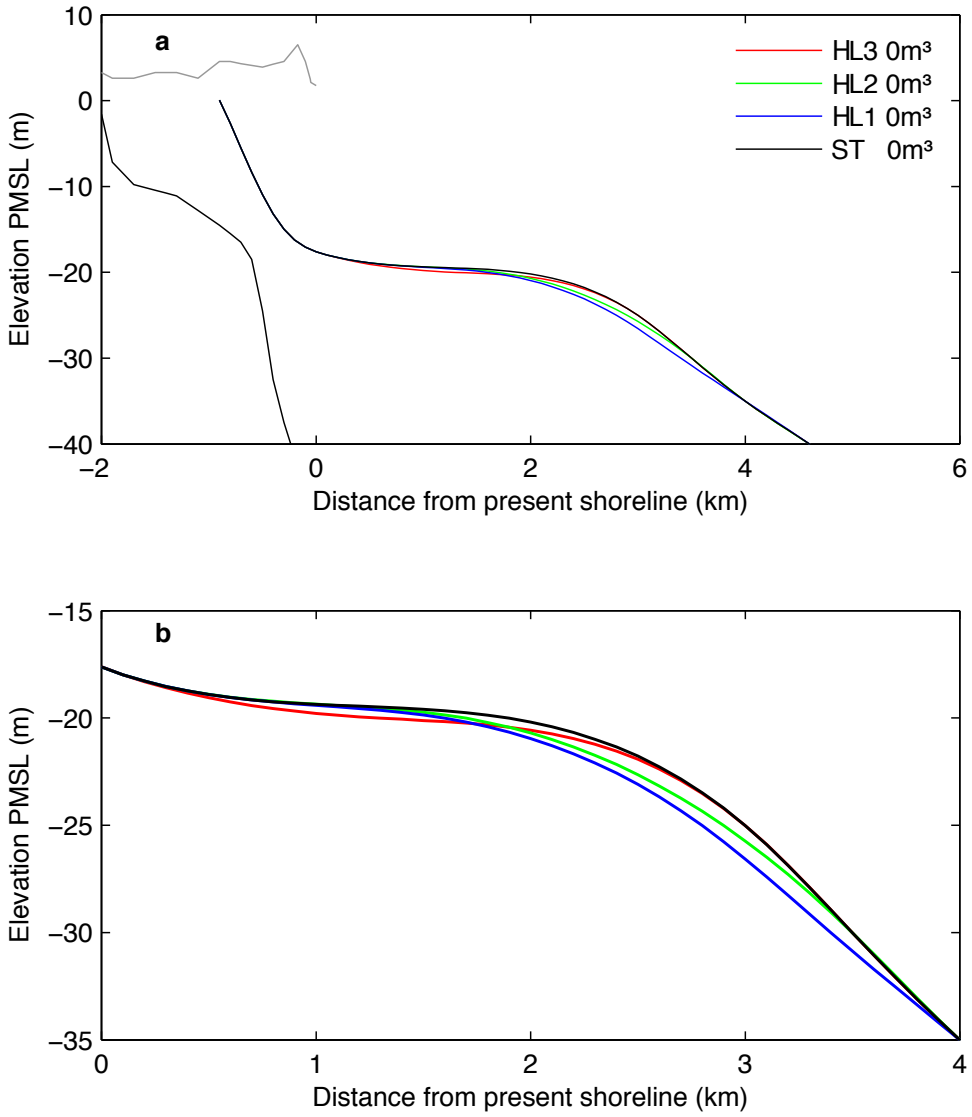

Figure 3.16: Initial shoreface morphology for combined forcing experiments at Moruya - Initial model profiles for combined SL-DS forcing experiments at Moruya, showing (a) entire shoreface and (b) shoreface sand body. Note the reduced shoreface sand body volume required for decreased rates of sea-level fall (i.e. HL3 to HL1) and increased depths at which the volume adjustment was applied.

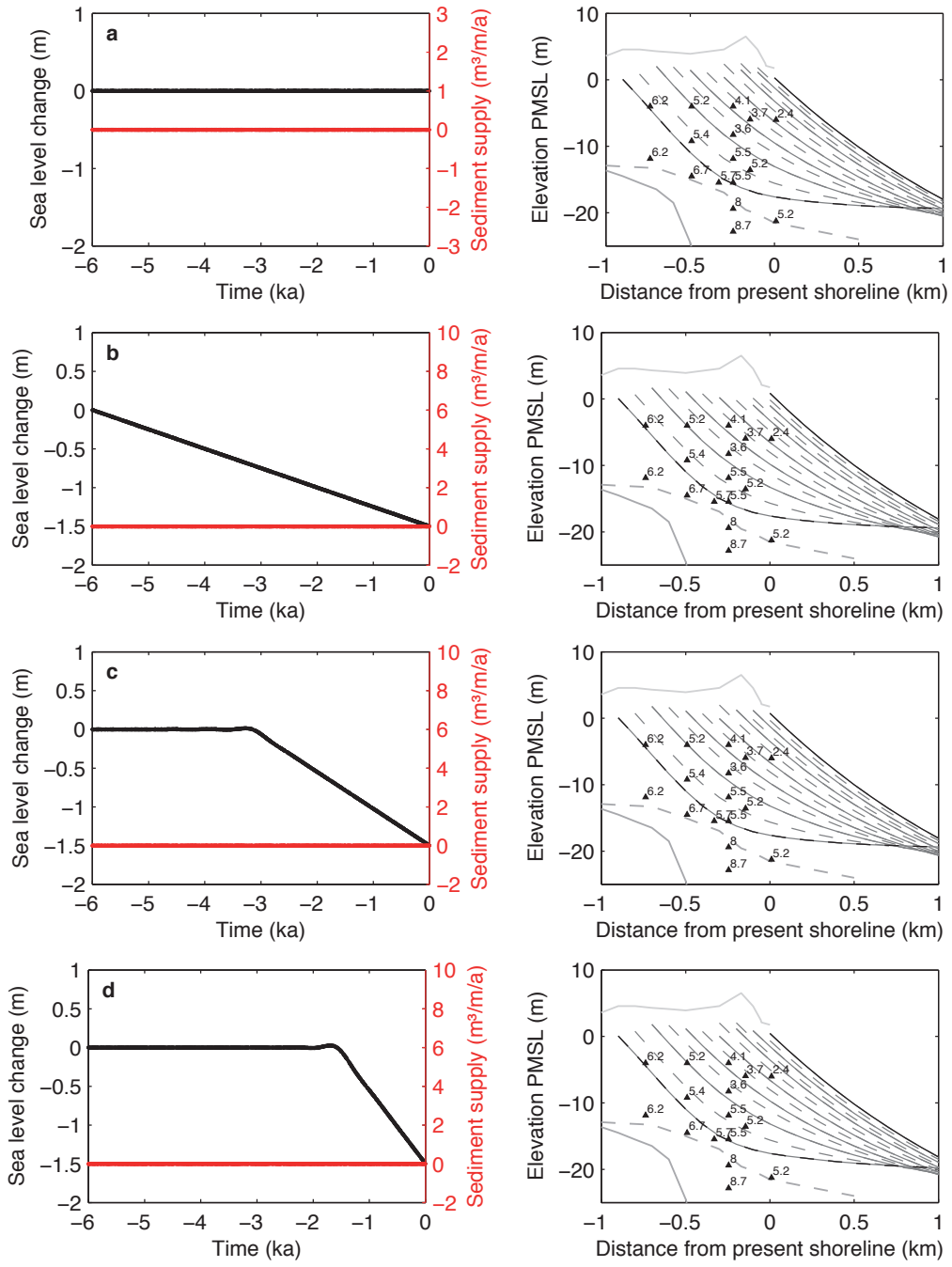

Figure 3.17: Simulated strandplain progradation due to combined forcing at Moruya - Simulated strandplain progradation at Moruya in response to shoreface D-S response and the sea level scenarios considered [Fig. 3.5]: (a) ST sea level scenario (i.e. no sea level change); (b) HL1 sea-level fall scenario; (c) HL2 sea-level fall scenario; and, (d) HL3 sea-level fall scenario. Full simulation outputs can be found in Appendix C.

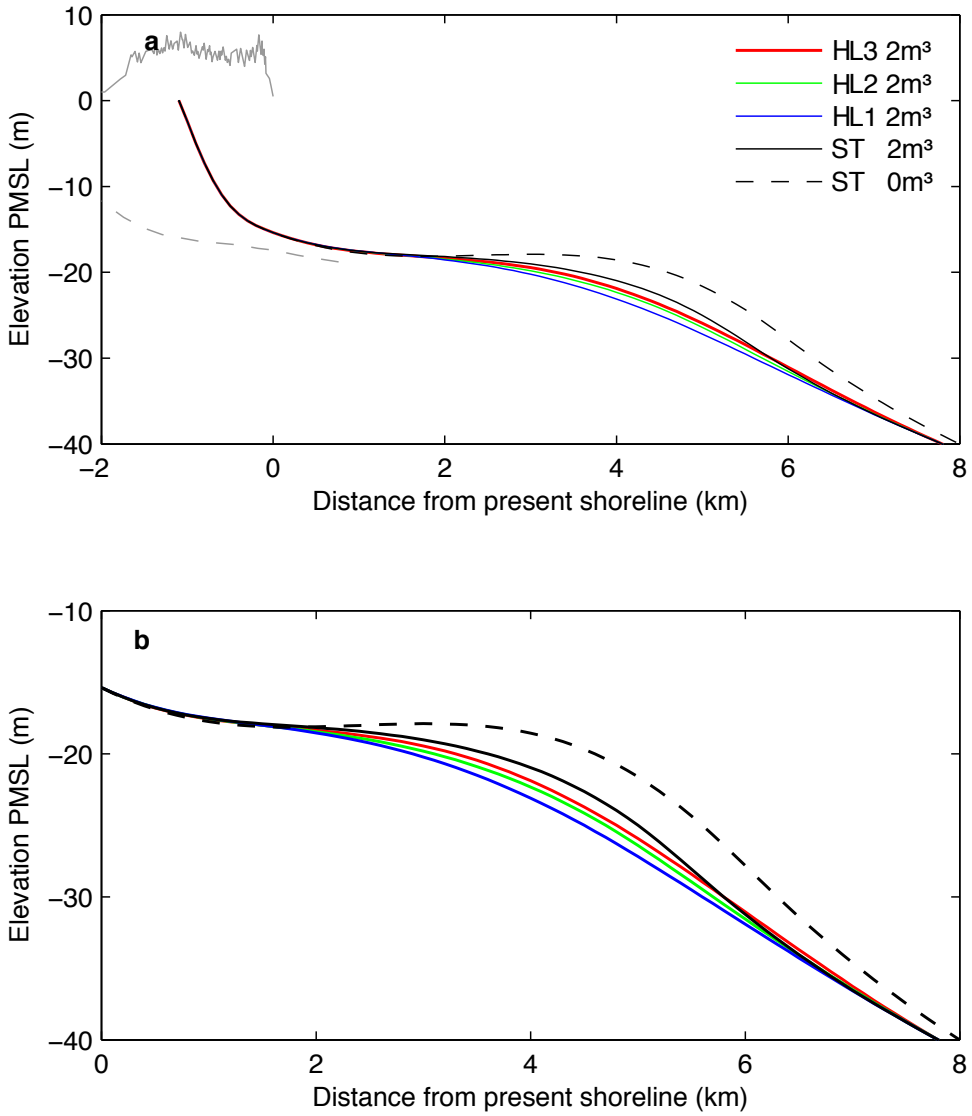

Figure 3.18: Initial shoreface morphology for combined forcing experiments at Tuncurry - Initial model profiles for combined SL-DS forcing experiments at Moruya, showing (a) entire shoreface and (b) shoreface sand body. Note the reduced shoreface sand body volume required for decreased rates of sea-level fall (i.e. HL3 to HL1) and increased depths at which the volume adjustment was applied.

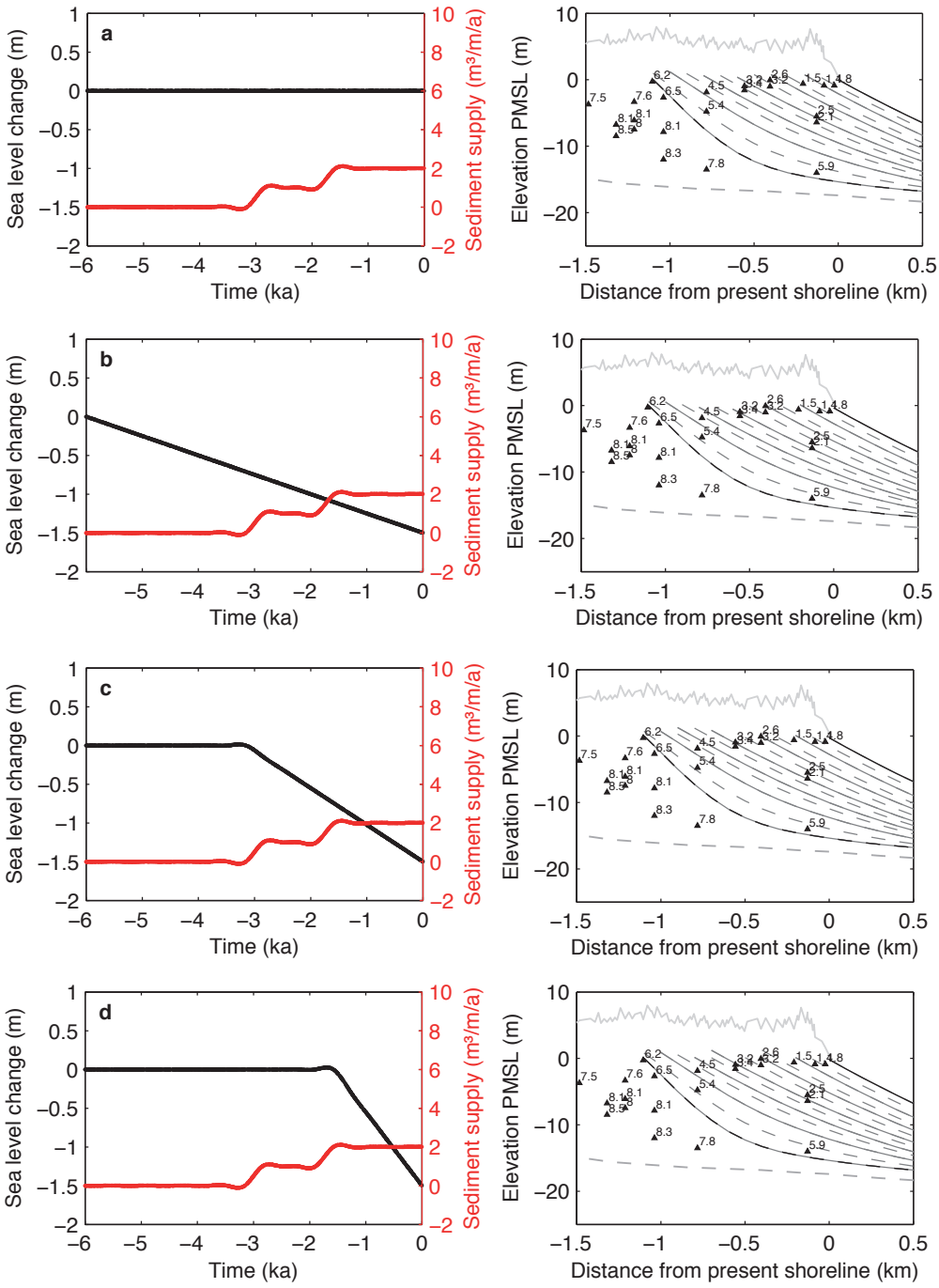

Figure 3.19: Simulated strandplain progradation due to combined forcing at Tuncurry - Simulated strandplain progradation at Tuncurry in response to shoreface D-S response and the sea level scenarios considered [Fig. 3.5]: (a) ST sea level scenario (i.e. no sea level change); (b) HL1 sea-level fall scenario; (c) HL2 sea-level fall scenario; and, (d) HL3 sea-level fall scenario. Full simulation outputs can be found in Appendix C.

Figure 3.20 shows the adjustments to the initial volume of the lower shoreface sand bodies (relative to shoreface D-S response simulations reported in Section 3.4.1), which were necessary to achieve simulated strandplain progradation consistent with barrier age structures, when sea level forcing was included. For both sites, the necessary adjustment to initial shoreface volume was greatest for HL1 (-0.25 mm/a) and decreased for the HL2 (-0.5 mm/a) and HL3 (-1.0 mm/a) scenarios [Fig. 3.20]. The adjustment did not decrease linearly for faster rates of sea-level fall; rather, a larger adjustment was required between the HL1 and HL2 scenarios relative to between HL2 and HL3 scenarios [Fig. 3.20]. That is, shoreface sand supply associated with the more gradual HL1 sea-level fall was disproportionately greater than that associated with the HL2 and HL3 scenarios. For both sites, the water depths at which the initial shoreface morphology adjustment was implemented to achieve strandplain progradation consistent with barrier age structures, increased with increased duration and decreased rates of sea level change [Figs. 3.16 & 3.18].

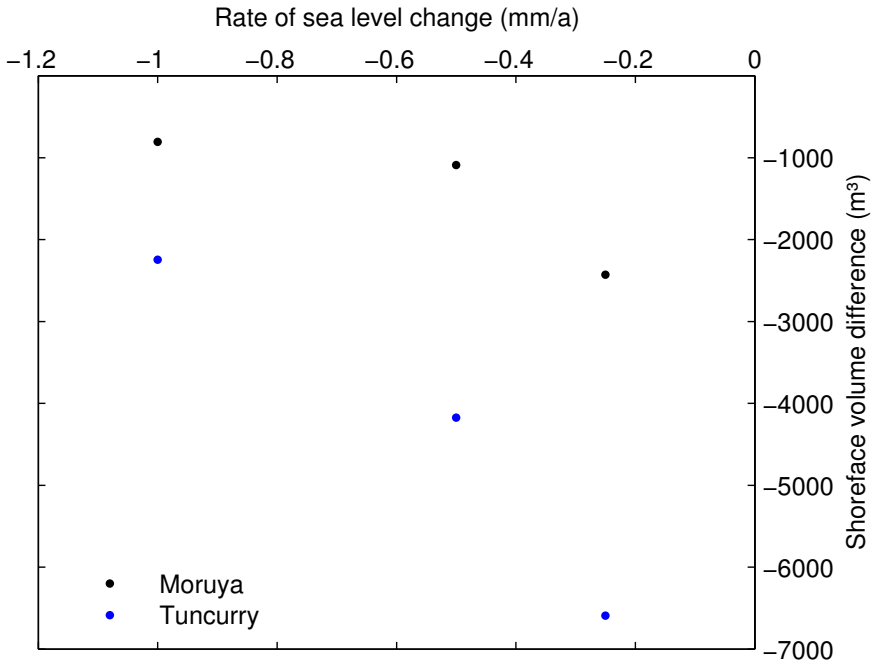

Figure 3.20: Volume difference between initial shoreface sand bodies - Reduction in initial shoreface sand body volume relative to stillstand (ST) simulations, which was required for each sea-level fall scenario to achieve simulated progradation rates consistent with the observed barrier age structures at Moruya and Tuncurry.

3.5 Discussion

3.5.1 Sources of mid- to late-Holocene strandplain deposition

On initial inspection, the results of model experiments at both sites suggested that multiple forcing scenarios (i.e. combination of shoreface sand supply, sea-level fall and external supply) could have generated strandplain progradation consistent with the barrier age structures, given the limited distribution and precision of age data. However, the models suggest that sensitivity of onshore shoreface sand-supply volumes to the examined sea level scenarios was relatively low. Specifically, the findings suggest a non-negligible but subtle onshore sand supply from relative sea-level fall, which increases for slower rates of change. In contrast, shoreface D-S response and external sediment supply from alongshore transport were demonstrated to potentially support strandplain progradation at rates consistent with the barrier age structures. However, further evaluation of shoreface D-S response, external sediment supply, and relative sea level fall scenarios against the geological evidence is necessary before conclusions may be drawn on the likely sources of strandplain progradation and rates of shoreface response. In the discussion below, the simulation results and scenarios are compared and contrasted with the potential inherited coastal geomorphology at each site following the Holocene transgression, and interpreted rates of external sand supply.

3.5.1.1 Shoreface disequilibrium-stress response

Rates of sand supply to the Holocene strandplains at Moruya and Tuncurry from shoreface D-S response progressively diminished throughout the 6,000 year simulations, which was consistent with an observed decrease in rates of shoreface surface adjustment [Figs. 3.6 & 3.8]. Considering the exponential form of the BARSIM shoreface erosion function [Sec. 1.5.2], which was calibrated here to estimate the local erosion efficiency at Moruya and Tuncurry [Sec. 3.3.1.3], it is implicit that rates of onshore shoreface sand supply diminish with the progressive lowering of the shoreface surface. This formulation is consistent with the diminishing capacity of wave-induced sediment entrainment and transport across the shoreface with increased depth [*Niedoroda and Swift*, 1991; *Cowell et al.*, 1999]. Rates of onshore sand supply due to shoreface D-S response have been quantified (based on the model configuration) and demonstrated for each sce-

nario in terms of millennia-average volumetric rates of shoreface lowering and barrier progradation, and total shoreface adjustment for each simulation.

Shoreface D-S response appears to be a viable sole source of M-L Holocene strandplain progradation at Moruya, where the barrier age structure is consistent with progressively diminishing rates of late-Holocene strandplain progradation [Fig. 3.6]. At Tuncurry however, it was demonstrated that an additional time-varying external sediment supply was required to achieve the near-uniform rates of strandplain progradation suggested by the barrier age structure there [Fig. 3.8]. For the case of forcing by shoreface D-S response alone, simulated progradation rates at Tuncurry were not consistent with the barrier age structure [Fig. 3.7]. The model findings support the regional sedimentation model of *Roy et al.* [1997], which implies that although alongshore sediment transport between embayments was limited along the southern section of the southeast Australian margin during the Holocene sea-level highstand, it has persisted along the northern section of the margin to the present day [Sec. 2.2].

To achieve simulated rates of strandplain progradation due to shoreface D-S response that were consistent with the barrier age structures, a lower shoreface sand body of comparable volume to the 6 ka strandplains was a necessary condition of the initial model morphologies. Specifically, initial shoreface geometry was characterised by a concave upper shoreface, a convex middle shoreface inflection, and a concave lower shoreface [as seen in Figures 3.16 & 3.18]. The maximum thickness of the shoreface sand bodies was 9 m at Moruya and 7 m at Tuncurry, and occurred at around 20 m water depth on the initial profiles [Figs. 3.6 & 3.8]. The offshore extent of the sand bodies was 50 m and 40 m water depth at Moruya and Tuncurry respectively. The comparative geometries of these lower shoreface sand bodies and terminal (i.e. present day) shoreface profiles are consistent with the inverse relationship between water depth and wave-induced sediment transport capacity.

Two hypotheses are offered regarding the origins of the shoreface sand bodies. First, the overstepping of an earlier transgressive barrier located closer to the mouths of the highstand embayments could have resulted in the stranding of convex lower shoreface sand deposits of adequate dimensions. In that case, late-transgressive deposition would have abruptly switched landward to the embayment head at Moruya, or to a subsequent transgressive barrier that was ultimately preserved within the Holocene barrier system at Tuncurry. This type of barrier-overstepping behaviour is further explored in

Chapter 4. The second case emerges from the hypothesis that the extent of shoreface erosion became substantially reduced during rapid sea level change, resulting in a low autochthonous supply and reduced barrier deposition. If erosion of the antecedent substrate were restricted to the upper shoreface during the rapid post-glacial transgression, upon reaching the highstand embayments the transgressive barriers would have featured a concave upper shoreface that had been maintained by wave processes, and which was cut into the pre-existing substrate. That is, a convex inflection would persist between the convex upper shoreface and poorly developed lower shoreface at the onset of the Holocene highstand. This hypothesis is addressed in Chapter 5 through more detailed model experiments regarding shoreface response to rapid sea level change.

3.5.1.2 External sediment supply

Simulated stratigraphy consistent with the age structures of the Tuncurry and Moruya barriers was also obtained by experimenting with rates of external sediment supply to the shoreface in each model. At Moruya, linear decreases in the external sediment supply rate from 10-5 m^3/m/a between 6-3 ka BP and 5-2.5 m^3/m/a between 3-0 ka BP was required to generate a progressively diminishing rate of strandplain progradation consistent with the barrier age structure [Fig. 3.10]. At Tuncurry a more complex stepped decrease between 7-4.5 m^3/m/a over the 6-ka simulation period was required to generate the more uniform rates of strandplain progradation suggested by the barrier age structure there [Fig. 3.11]. Although the rate of progradation near the Tuncurry strandplain surface (where age constraints were available) remained relatively constant from 5 ka BP onwards, a subtle decrease in the rate of external sand supply was required at 2 ka BP to accommodate the evolving shoreface geometry. Despite the different widths of the 6 ka strandplains at Moruya (0.9 km) and Tuncurry (1.1 km), the deeper barrier toe in the Moruya model resulted in the total volumes of required sediment input being comparable between sites (i.e. 31,606 and 32,011 m^3/m respectively).

Consideration of the total longshore transport rates calculated in Section 3.4.2, in the context of regional geomorphology, raises some questions regarding the likelihood of post-transgressive drift-dominated settings at Moruya and Tuncurry. Specifically, along the highly embayed southern and central sectors of the margin regional northward transport would have been attenuated by updrift sediment sinks upon the breaching of highstand embayments [Sec. 2.7.4]. This implies that longshore sand supply into the

embayments would have been greatly reduced following the termination of transgression, until the establishment of new pathways for headland bypassing in the form of submerged shelf sand bodies [*Roy et al.*, 1997].

Although the ST-Q models were consistent with the barrier age structures suggested by the distribution of radiocarbon ages, the simulated lower shoreface stratigraphy differed from that of the ST-DS models, and the interpreted site stratigraphy. Specifically, shoreface deposition and barrier-strandplain progradation extended to much greater depths in the absence of onshore sand supply due to shoreface D-S response (and the initial condition of a lower shoreface sand body). Consequently, volumetric rates of strandplain progradation in the ST-Q simulations were considerably greater than for the respective ST-DS models.

At Moruya for example, shoreface deposition occurred to 38 m depth in the MR-ST-Q experiment [Fig. 3.10], whilst strandplain progradation terminated at 22 m depth in the Moruya MR-ST-DS experiment [Fig. 3.6]. A similar relationship was observed in the Tuncurry simulations, with the depth limits of shoreface deposition for the TC-ST-Q and TC-ST-DS experiments being 32 m and 22 m respectively [Figs. 3.11 & 3.8]. The models thus suggest the potential for the entire shoreface to act as a sediment sink under conditions of high sediment supply and stable sea level. In comparison with the ST-DS models, the absence of an initial shoreface sand body in the ST-Q models affords a large volume of sediment-accommodation space across the shoreface, which was gradually filled by sand supplied to the embayments by the longshore transport system.

The interpreted stratigraphy of the coastal strandplains and shelf at Tuncurry support the shallower depth limit of barrier-strandplain progradation, as in the ST-DS models. For example, high-resolution seismic and vibrocoring across the Tuncurry inner shelf indicates that the toe of the Holocene barrier occurs between 19-23 m depth [*Roy et al.*, 1997]. An abrupt transition in surficial sediments is observed in the vicinity of the barrier toe, where finer shoreface sands meet coarser inner-shelf sands. To landward, the inner-shelf sands occur as an erosional lag that underlies the regressive barrier sands and eventually merge with transgressive barrier facies [Fig. 3.21]. To seawards the inner shelf sands form a thin veneer or sheet that overlies antecedent backbarrier deposits associated with lower sea levels [Fig. 3.21].

The coarser mode of the inner-shelf sand sheet facies suggests that the deposit has been subject to erosion during the late-Holocene [*Roy et al.*, 1997]. Furthermore, radiocarbon dating indicates that the inner-shelf sand sheet accumulated between 2-6.5 ka BP [Fig. 2.18]. Although the interface between surficial shelf sediment facies occurs between 18-19 m water depth at Tuncurry, the stratigraphic boundary that is evident in vibrocore samples [Fig. 2.18] occurs slightly seaward, between 20-23 m depth [Fig. 3.21]. Nonetheless, both lines of evidence suggest that the seaward extent of late-Holocene strandplain progradation was limited to around 20 m depth, which is supported by the ST-DS simulations and inconsistent with the ST-Q simulations.

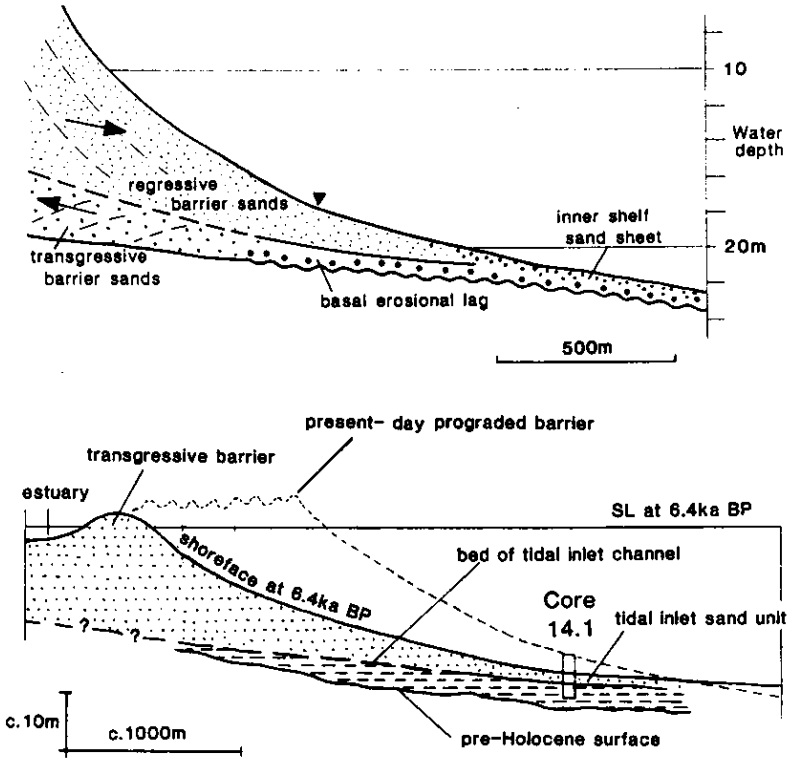

Figure 3.21: Stratigraphic evidence for location of shoreface toe at Tuncurry - Stratigraphic relationships between transgressive barrier sands, regressive barrier sands and the inner-shelf sand sheet, as interpreted by *Roy et al.* [1997] from vibrocores and shallow-marine seismic data. Holocene barrier morphology at 6.4 ka BP is also shown.

3.5.1.3 Relative sea-level fall

The simulated volumes of onshore sand supply due to shoreface lowering driven by relative sea-level fall accounted for only a fraction of the late-Holocene strandplain volumes at each site. The simulation experiments suggest that without a supplementary sediment source, a late Holocene sea-level fall of 1.5 m at rates between -0.25 mm/a to -1 mm/a [Fig. 3.5] would have been insufficient to supply progradation of the Tuncurry and Moruya strandplains alone. In the model experiments [Appendix B], shoreface lowering due to relative sea-level fall contributed a maximum of 350-400 m^3/m of onshore sand supply, which is equivalent to 1.5-2% of total late-Holocene strandplain progradation at each site. The model findings thus suggest that sea-level fall at the rates considered would have only had a small influence on late-Holocene strandplain progradation. Put into context, a shoreface sand supply of 350-400 m^3/m is less than twice the volume of the storm cut attributed to the largest historical erosion event (c. 200-250 m^3/m) observed on this coastline [*Thom and Hall*, 1991].

Simulated rates of onshore sand supply due to relative sea-level fall increased linearly and inversely with the rate and duration of sea-level fall. At Moruya, for example, a 1.5 m relative sea-level fall at rates of -1, -0.5 and -0.25 mm/a resulted in total onshore supply volumes of 102, 207 and 401 m^3/m, over 1.5, 3 and 6 ka respectively [Tab. 3.2]. A similar pattern was observed for Tuncurry [Tab. 3.2]. Thus halving the rate of a 1.5 m sea-level fall resulted in twice the volume of onshore sand supply. This indicates that whilst simulated shoreface lowering due to sea-level fall was minor, the magnitude of response was nonetheless sensitive to the rate of sea level change. Despite control experiments to quantify any ongoing shoreface D-S response associated with the modern shoreface geometry and model calibration, the capacity to isolate shoreface response to sea-level fall remained somewhat compromised by the ongoing shoreface D-S response.

Table 3.2: BARSIM onshore sand supply due to relative sea-level fall - Simulated onshore sand supply to the Moruya and Tuncurry strandplains by shoreface lowering due to relative sea-level fall for the scenarios in Figure 3.5.

Scenario	Duration (ka)	Rate (mm/a)	Volume (m^3/m) Moruya	Volume (m^3/m) Tuncurry
HL1	6	-0.25	401	352
HL2	3	-0.50	207	160
HL3	1.5	-1.00	102	76

The very low volumes of sea-level-fall induced shoreface sand supply suggest that a complete 'equilibrium' shoreface response was not achieved in any of the BARSIM experiments. To investigate the potential onshore sand supply volumes that would be generated by complete shoreface adjustment to a 1.5 m relative sea-level fall, a simple geometric model can be used to simulate time-invariant shoreface response and strandplain progradation. The geometric model uses sediment-mass conservation principles popularised by the so-called 'Bruun Rule' [*Bruun*, 1962, 1983, 1988]. According to the Bruun rule, sea level change drives the translation of a time-invariant shoreface profile, and the sediment-volume flux at the shoreline is equal to that across the active shoreface. The geometry of the time-invariant shoreface profile is defined by the fitted equilibrium shoreface profile, which considers that shoreface geometry is proportional to the mean wave climate and sediment characteristics [*Bruun*, 1954; *Dean*, 1977, 1991]. Although the Bruun Rule was intended for the estimation of beach erosion due to sea-level rise, if the assumption of time-invariant shoreface geometry holds true the rule should be equally applicable to sea-level fall, providing that the rate of sea-level fall does not exceed depth-dependent shoreface erosion rates.

Figures 3.22 and 3.23 show the results of a 1.5 m sea-level fall at Moruya and Tuncurry respectively using the geometric equilibrium model. The outcomes of complete shoreface response are shown for five cases at each site, in which the depth limit of time-invariant shoreface response was progressively extended from 25 m to 45 m water depth in 5-m increments. In each scenario, a linear shoreface-toe slope extended from the depth limit of time-invariant shoreface geometry (DoC) to the ultimate depth of shoreface response, which occurred 5 m deeper on the profile. This was to ensure a realistic interface between the inner-shelf and shoreface surfaces. The depth limit of the 'active shoreface' profile was defined using the outer shoal zone limit (d_i) relationship after *Hallermeier* [1981], which specifies the annual limit of significant cross-shore sediment transport by waves. The range of d_i values considered includes the full spectrum of relevant values within the constraints of Hallermeiers equation, and given the context of uncertainties regarding wave climate statistics and sediment grain size at Moruya and Tuncurry, [*Meleo*, 1994; *Cowell et al.*, 1999]. The volumes and distances of strandplain progradation that correspond to the tested depth limits of shoreface activity are shown in Table 3.3.

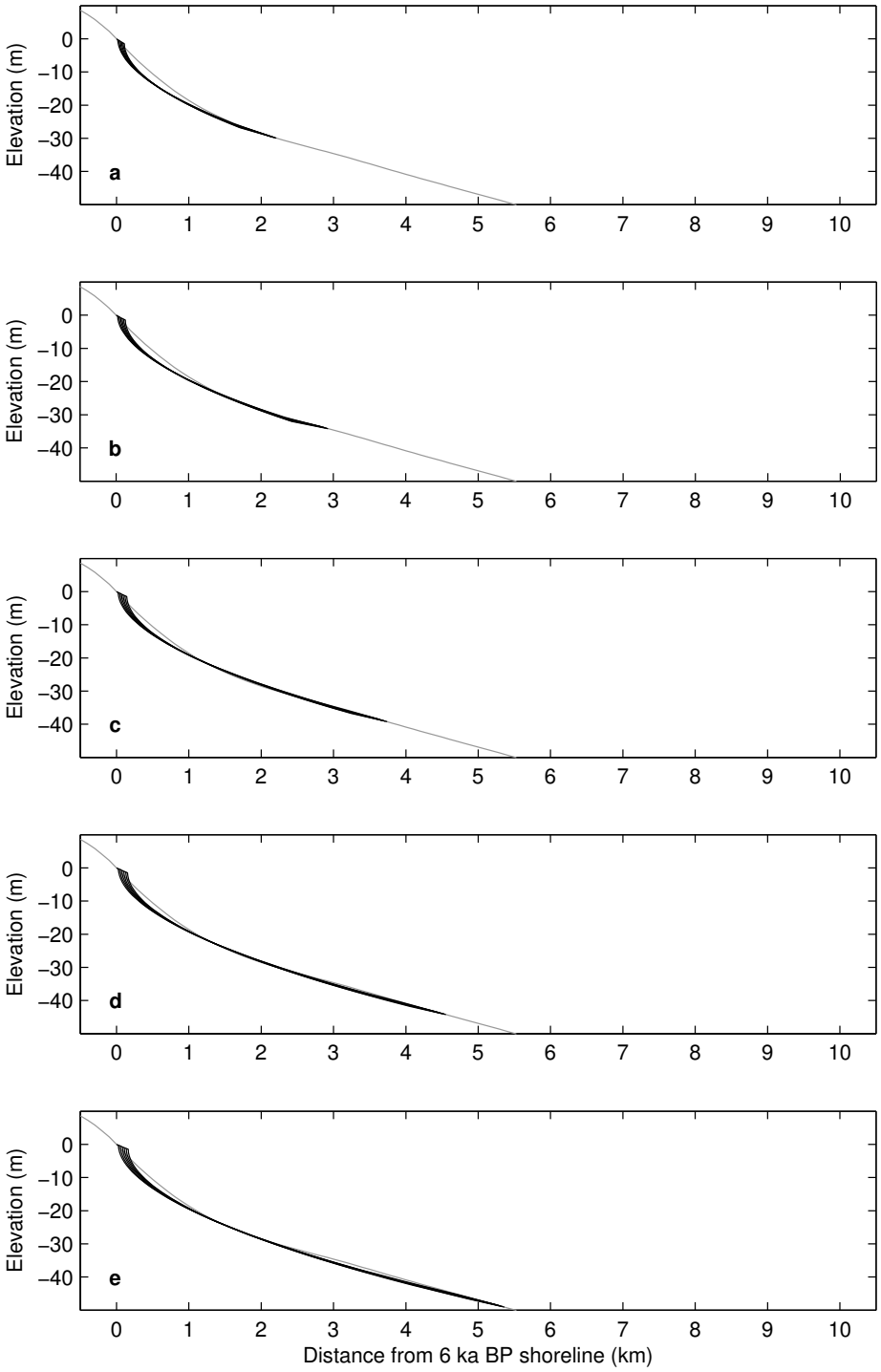

Figure 3.22: MR-SL-EQ geometric-equilibrium sea-level fall models for Moruya - Simulated shoreface lowering and strandplain progradation at Moruya predicted by a simple time-invariant shoreface geometry model, for shoreface outer depth limits of (a) 30 m, (b) 35 m, (c) 40 m, (d) 45 m, (e) 50 m.

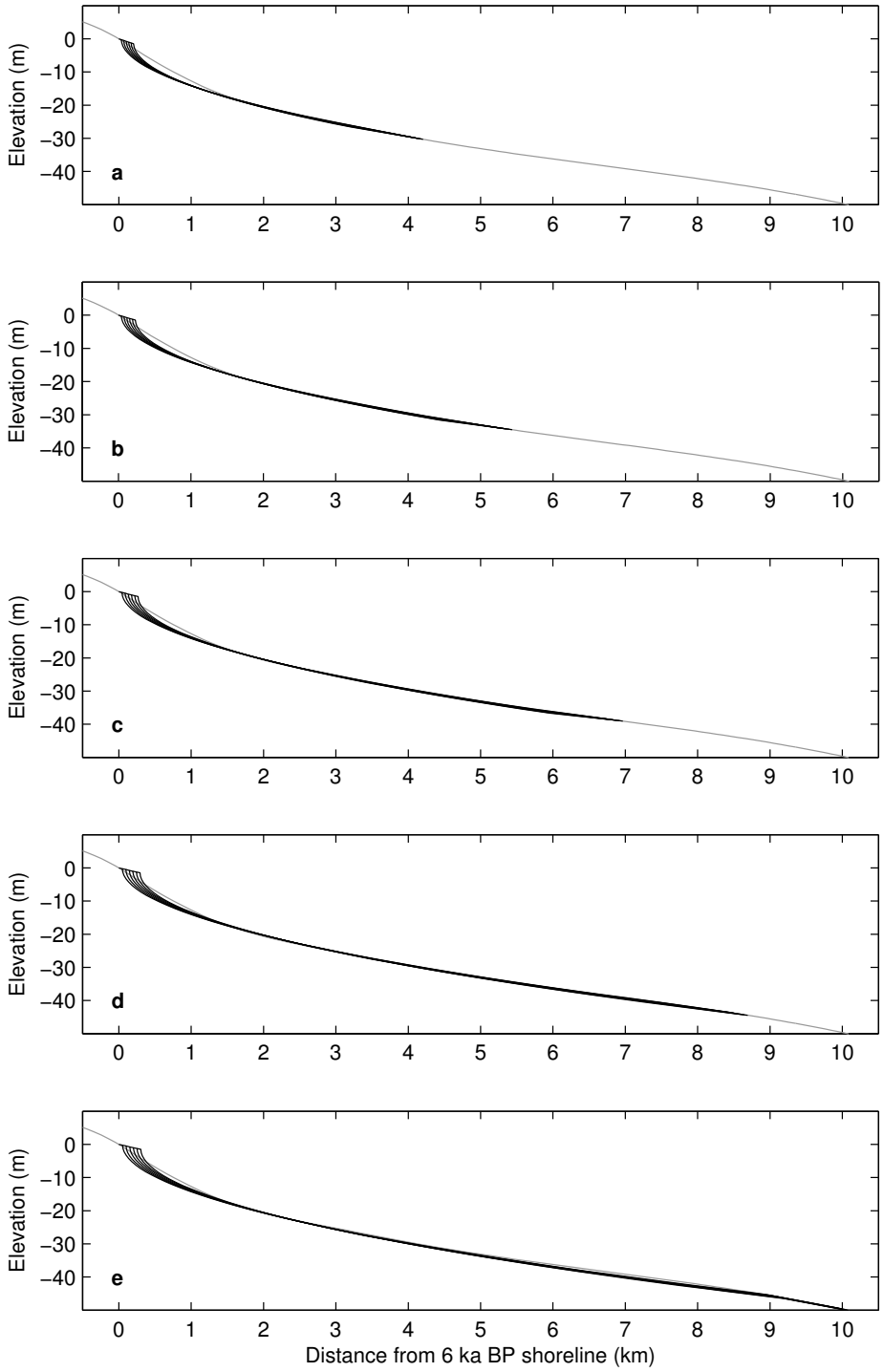

Figure 3.23: TC-SL-EQ geometric-equilibrium sea-level fall models for Tuncurry - Simulated shoreface lowering and strandplain progradation at Tuncurry predicted by a simple time-invariant shoreface geometry model, for shoreface outer depth limits of (a) 30 m, (b) 35 m, (c) 40 m, (d) 45 m, (e) 50 m.

Table 3.3: Equilibrium onshore sand supply due to relative sea-level fall - Sand volumes supplied to the Moruya and Tuncurry strandplains by shoreface lowering due to relative sea-level fall with the assumption of time-invariant shoreface geometry to the indicated shoreface outer depth limits.

DoC	d_i	Progradation (m^3/m)		Progradation (m)	
		Moruya	Tuncurry	Moruya	Tuncurry
25	30	720	1,443	109	205
30	35	1,000	1,877	126	233
35	40	1,236	2,426	142	264
40	45	1,498	3,005	153	292
45	50	1,781	3,701	163	302

The geometric equilibrium model demonstrates that for both sites, the seaward extension of the active shoreface provided an increased shoreface erosion volume [Figs. 3.22 & 3.23], which resulted in greater strandplain volumes and higher rates of progradation [Tab. 3.3]. Whilst seemingly intuitive, this may not be the case where shoreface width is not particularly sensitive to increased shoreface depth [*Moore et al.*, 2010]. The effects of the average shelf gradient being approximately twice as steep at Moruya relative to Tuncurry was that rates and volumes of strandplain progradation were roughly twice as high at Tuncurry [Tab. 3.3]. This is consistent with the simple geometric relationship applied in the equilibrium model that implies that shoreline migration is proportional to the slope of the shoreface profile [*Bruun*, 1962].

Importantly, even for the most generous case of $d_i = 50$ m, the simulated progradation distance at each site accounted for only a fraction of the late-Holocene strandplain widths. Progradation distances of 163 m and 302 m accounted for 18% and 27% of strandplain width at Moruya and Tuncurry respectively. However, comparison between progradation volumes in Table 3.3 and from the MR-ST-DS [Fig. 3.6] and TC-ST-DS-Q2 [Fig. 3.8] simulations indicates that onshore shoreface supply due to sea-level fall actually only accounted for 8% and 14% of the observed strandplain volumes. This discrepancy relates to the geometry of the strandplain surface and upper shoreface, and locations of barrier toes, between the BARSIM and geometric models. Nonetheless, the experiments clearly demonstrate that a relative sea-level fall of 1.5 m as suggested by some evidence [Sec. 3.2.1] could have supplied a maximum volume of about one-fifth of the interpreted late-Holocene strandplain progradation.

Based on the model configurations and scenarios considered here, the findings do not explicitly support any one particular M-L Holocene sea level curve [Fig. 3.5]. However, the results hint at the role played by the rate of sea level change in controlling *active* shoreface response. That is, given depth-diminishing shoreface erosion rates associated with diminishing wave influence at increased water depths, which was demonstrated here in the plots of shoreface adjustment rates and the fixed-magnitude limit of shoreface activity, lower rates of sea level change appear to generate higher volumes of shoreface sand supply. Although the findings are not sufficient to resolve the question of late-Holocene sea levels in southeastern Australia, it has been shown that a sea-level fall of 1.5 m magnitude during the last few thousand years may, perhaps, have had little more influence on overall strandplain volumes than any ongoing (present-day) shoreface D-S response. Whilst the onshore sand supply volumes suggested by the BARSIM models were roughly equivalent to that of the contemporary beach and foredune at each site, the geometric models suggest that M-L Holocene sea-level fall may have contributed up to 8% and 14% of Holocene strandplain volumes at Moruya and Tuncurry respectively.

3.5.1.4 Combined forcing

Simulations that featured combined onshore sand supply from shoreface lowering due to D-S response, and relative sea-level fall, also suggested that the effect of sea-level forcing was a non-negligible but secondary onshore supply volume, which varied with the rate and duration of sea-level fall. The addition of sea level scenarios HL1, HL2 and HL3 to the MR-ST-DS and TC-ST-DS-Q2 models resulted in strandplain progradation that exceeded the present-day shoreline position in all cases. To achieve simulated strandplain stratigraphy that was consistent with the barrier-age structures, and both present-day shorelines and shorefaces, the initial volume of the shoreface sand body had to be reduced. The requisite sand-body volume reduction was such that lower rate (longer duration) sea level scenarios required both a greater volume of the initial sand body to be removed, and from progressively lower on the shoreface [Figs. 3.16 & 3.18]. That is, the required contribution from shoreface D-S response was lowest for scenario HL1 and increased for scenarios HL2 and HL3. The findings thus suggest that a dominant contribution from shoreface D-S response or an external sediment

supply source is necessary to achieve the interpreted rates of late-Holocene strandplain progradation at Tuncurry and Moruya.

Of note, however, the requisite volume adjustment to the initial sand body for combined forcing simulations did not vary linearly with the rate of sea level change [Fig. 3.20]. Rather, an increase in the rate of sea level change from -0.25 mm/a (HL1) to -1 mm/a (HL3) required a logarithmic decrease in the onshore shoreface sand supply, as indicated by the initial shoreface dimensions required in each case to reproduce the observed stratigraphy of each strandplain. This finding indicates latency in lower shoreface adjustment to sea level change, which is implicit in the exponential decrease in surface response rates across the lower shoreface to wave base, as considered in the BARSIM erosion function [Sec. 1.5.2]. Latent shoreface response due to depth-dependent shoreface erosion rates is also evident in the reduction in startup shoreface convexity that was necessary at increasing depths for slower and more prolonged sea-level fall [Figs. 3.16 & 3.18]. Thus for slower rates of sea level change, sedimentary exchanges between the shoreline and lower shoreface/inner shelf may become increasingly significant for coastal sediment budgets. The relationship between sea level change and shoreface response is explored in further detail in Chapter 5.

3.5.2 Implications for shoreface response

The BARSIM models calibrated and applied here offer some insights on the potential extent and rates of M-L Holocene shoreface response. As described in Section 3.5.1.1, simulated shoreface lowering due to D-S response occurred between 18-50 m depth at Moruya and 16-40 m depth at Tuncurry. This was similarly the case for the combined forcing simulations albeit with slightly modified initial shoreface geometries [Sec. 3.5.1.4]. These source depths fall within the potential range of values for the *Hallermeier* [1981] outer shoal zone limit (d_i) [Tab. 3.3], based on the wave climate and shoreface sediments. Millennia-average shoreface response rates in the MR-ST and TC-ST models peaked at 3 and 2 mm/a respectively, and occurred between 5-6 ka BP across the shallowest parts of the shoreface sand bodies (i.e. < 20 m water depth) at Moruya [Fig. 3.12] and Tuncurry [Fig. 3.14]. That is, even the upper range of shoreface lowering rates required by the models to achieve strandplain progradation consistent with the barrier age structures would be imperceptible (i.e. < 10 cm) over the duration of the longest historical survey records. Therein lies the difficulty of resolving

depth-dependent lower-shoreface response rates from observation datasets [*Niedoroda and Swift*, 1991; *Cowell et al.*, 1999].

The MR-ST and TC-ST simulation experiments that featured stable sea level and present-day shoreface geometry suggest the persistence of a subtle but ongoing shoreface D-S response in the calibrated models [Figs. 3.12 & 3.14]. Specifically, the upper limit of ongoing surface adjustment across the lower shoreface at Moruya and Tuncurry is suggested to be 0.25 and 0.15 mm/a respectively. These figures equate to a total onshore sand supply of less than 1 m^3/m/a. The routinely adopted design storm-induced beach erosion volume (equivalent to the maximum observed historical storm bite) for this coastline is 200-250 m^3/m [*Thom and Hall*, 1991]. Thus any persisting onshore sand supply at rates suggested by the models is likely to be difficult to differentiate in the short term from low-frequency high-magnitude coastal change associated with episodic erosion events and subsequent beach recovery . Nonetheless, the significance of a 1-2 m^3/m/a alongshore sand supply at Tuncurry between 3 ka BP to present [Sec. 3.5.1.1], suggests that in the context of long-term sediment budgets shoreface lowering may remain a significant factor in future coastal change.

The requisite initial shoreface geometries for the simulations that included shoreface D-S response suggest that by between 5-6 ka BP equilibrium shoreface geometries were established to approximately -15 m and -12 m PMSL at Moruya and Tuncurry respectively [Figs. 3.16 & 3.18]. Interestingly, these depth limits correspond to the range of applicable values of the *Hallermeier* [1981] inner shoal zone depth limit (d_l) for south-east Australian settings [*Meleo*, 1994]. Thus the models are generally consistent with previous assertions of a time-invariant or equilibrium upper shoreface that extends to the depth limit of observable profile change, and progressively decreasing lower shoreface response rates that contribute to imperceptible but non-negligable coastal change [*Cowell et al.*, 1999]. Whilst this remains a preliminary and qualitative observation here, the sensitivity of time-invariant shoreface geometry to sea level change is examined in further detail in Chapter 5.

Comparison of the BARSIM model findings for relative sea-level fall simulations with predictions based on a time-invariant geometric model [Sec. 3.5.1.3] suggests that the BARSIM configuration was relatively insensitive to the sea level change scenarios considered. Nonetheless, the findings demonstrate the offshore extension of measurable shoreface change for relaxed rates of sea level change. It is difficult to distinguish the

relative influences of the rate of sea level change and any latency in response due to the progressive decrease in duration between the three Holocene sea level scenarios [Fig. 3.5]. This remains an interesting question of critical importance to predicting potential future coastal change in response to climate change, and is explored in further detail in Chapter 5. For example, considering the accelerating nature of sea-level rise projections, over what timescales may lower shoreface responses become perceptible in coastal sediment budgets? The preliminary results presented here suggest that application of the Bruun Rule to Hallermeier's outer shoal zone limit (d_i) may represent a conservative estimate of coastline retreat due to projected sea-level rise (i.e. it may over-estimate the response). The implications of simulated shoreface response rates for predictions of future coastal change are considered in Chapter 6.

3.5.3 Potential for model dependence

As for any geomorphic modelling exercise, the validity of the results presented in this chapter are contingent on the accuracy of the models in representing net sediment transport for the forcing scenarios and timescales considered. Section 1.4 considered the difficulties in modelling large-scale coastal behaviour, and in particular, bridging the gap between physics-based sediment transport rules derived from short-term empirical studies, and coastal evolution of interest to coastal managers/planners and geomorphologists. The research presented in this thesis attempts to further our understanding of mesoscale coastal behaviour using the BARSIM process-response model [Sec. 1.5], and geological records of coastal barrier evolution [Ch. 2]. Whilst this approach is promising in its capacity to consider the implications of depth-dependent shoreface response at the timescales of interest, the impression of the model formulation on the research findings must be critically evaluated.

Considering the temporal and logistical limitations of measuring coastal change, the preserved stratigraphy in coastal and shallow-marine environments provides the only record of coastal dynamics from which the evolution of coastal depositional landforms emerges. BARSIM uses observational and morphologic evidence of coastal dynamics, and stratigraphic evidence, to constrain model predictions through a process-response modelling approach [Sec. 1.5]. The following stratigraphic and observational evidence guided the calibration of BARSIM models applied here:

- interpreted stratigraphy and age structures of the Holocene barrier systems
- empirically derived shoreface sedimentation rules of BARSIM [Sec. 1.5]
- long-term wave climate measurement statistics
- site-specific sediment characteristics
- present-day shoreface geometry.

Considering the shape of the BARSIM erosion efficiency function [Eq. 1.4], and the concave shoreface geometry at Tuncurry and Moruya, the calibration procedure [Sec. 3.3.1.3] provides some confidence that the model configurations are somewhat representative of site-specific morphodynamic efficiency for the timescales considered. That is, the sensitivity testing was carried out to identify suitable values of m to fit the observed shoreface geometry. However, there of course remains considerable uncertainty regarding the nature of the initial (i.e. 6 ka BP) morphology at each site. The model experiments in this chapter suggest that simulated rates of shoreface erosion are very high for the case of disequilibrium shoreface conditions and decrease with shoreface lowering. Given that the calibration simulations ran for 6,000 year durations, the calibration procedure may not be overly sensitive to the initial (morphologic) conditions, for cases where initial conditions reflect the average substrate gradient. The initial shoreface geometry at each site was further explored within the shoreface D-S response simulation experiments, in which initial shoreface morphology was constrained by the need to achieve strandplain progradation consistent with both the observed barrier-age structures and present-day shoreface geometry (for the adopted m value).

Given uncertainties regarding initial conditions and the net shoreface sediment transport in response to complex forcing, none of the above implies that the simulated shoreface dynamics in BARSIM provide an accurate depiction of reality; only that the model configurations generate stratigraphy consistent with the interpreted geological records based on uncertain initial conditions. Although the BARSIM shoreface erosion function and sedimentation rules offer an elegant and intuitive solution, it should not be considered a unique solution. For example, comparable outcomes could be achieved using a more complex solution that considers differential upper and lower shoreface processes and response timescales [*Cowell et al.*, 1999] in greater detail. In that case, shoreface geometry would be markedly different and the quantitative predictions of

shoreface response considered here would undoubtedly differ. It is unlikely that a simple exponential function such as Equation 1.4 adequately describes net shore-normal sediment transport across the shoreface resulting from a complex array of wave- and current-driven transport processes [*Niedoroda et al.*, 1984; *Niedoroda and Swift*, 1991]. Thus the extents and rates of shoreface response suggested by the BARSIM modelling cannot be considered definitive. Rather, the modelling approach simply provides an experimental platform from which to consider the unknown shoreface dynamics that have contributed to preserved stratigraphic records of coastal barrier evolution.

The general behaviour simulated by an event-driven depth-decaying erosion function [Eq. 1.3] of a form consistent with observed shoreface geometry for relatively stable (e.g. Holocene) forcing conditions, and sediment dispersal rules derived from empirical observations, suggests that the BARSIM models applied here may offer a qualitatively reasonable representation of wave-dominated coastal behaviour for the settings considered. The absence of alternative equivalent approaches with which to compare model findings limits prospects for model verification beyond the stratigraphic records considered in this thesis. However, comparison with geometric model predictions, as demonstrated in this chapter, provides a means of evaluating BARSIM predictions against established (albeit contended) concepts of large-scale coastal behaviour. Where informative, comparisons with geometric models are used in this thesis to examine dynamic shoreface behaviour against time-invariant shoreface response.

In this chapter, comparison between coastal response to relative sea-level fall predicted by the BARSIM and geometric equilibrium-profile models suggested that the former were not particularly sensitive to sea level scenarios considered. That is, based on the model configurations, coastal response to the sea-level fall scenarios was largely obscured by ongoing shoreface D-S response. Nonetheless, the geometric model results demonstrate that relative sea-level fall was not the primary cause of M-L Holocene strandplain progradation in southeastern Australia. The BARSIM models did however suggest a subtle ongoing onshore sand supply due to shoreface D-S response, which is consistent with previous assertions [*Cowell et al.*, 2001, 2003b]. Although it remains unclear if the geometric model predictions are representative of shoreface response at the timescales of interest, the comparison suggests that subsequent BARSIM experiments into shoreface response to sea level change should consider larger scale and/or longer

term sea level change scenarios. Thus the findings presented in this chapter inform the design of the modelling experiments document in Chapters 5 & 6.

3.6 Conclusions

A methodology was developed in this chapter to investigate potential theoretical models of mid- to late-Holocene coastal evolution in southeastern Australia using process-response stratigraphic modelling and existing geological records. BARSIM experiments that considered a range of forcing scenarios provided new insights on the origins of Holocene coastal barrier systems by examining the evidence for strandplain progradation due to shoreface D-S response, relative sea-level fall, and potential external sand supply from longshore transport. The findings presented here extend previous investigations on the relationships between shoreface D-S response, onshore sand supply and Holocene coastal barrier evolution [Sec. 3.2.2]. Specifically, depth-dependent shoreface response, time-varying longshore sand transport rates and mid- to late-Holocene sea level fall have been considered for the first time.

Based on the review of geological records [Sec. 2.6 & 2.7] and the model experiments described in this chapter, the following conclusions are made regarding the origins of Holocene strandplains. Aspects of the conclusions that are potentially model dependent [see Sec. 3.5.3] have been *italicised*. This is not to imply that the suggested behaviours are incorrect, but that quantitative estimates are dependent on the BARSIM algorithms and model configurations.

1. The predominant sediment source for strandplain progradation at Moruya and Tuncurry was onshore sand supply driven by shoreface erosion, which persisted during morphodynamic disequilibrium-stress conditions following the abrupt termination of rapid sea-level rise between 7-8 ka BP.

2. Whilst the age structure of the Moruya strandplain is consistent with a diminishing onshore sand supply during the late Holocene, strandplain progradation at Tuncurry appears to have continued at relatively uniform rates (approximately 4 $m^3/m/a$). Rates of onshore sand supply have diminished during the late Holocene due to progressive shoreface deepening and the reduced capacity for onshore sand transport due to wave orbital-velocity skewness.

3. Assuming depth-diminishing capacities of onshore sand transport due to wave orbital-velocity skewness (as simulated by BARSIM), and the interpreted rates of Holocene strandplain progradation, onshore sand supply due to shoreface D-S response must have been sourced from mid- to lower-shoreface sand bodies.

4. *At Moruya and Tuncurry, the modelling suggests that the shoreface sand bodies had a maximum thickness of 7-9 m at about 20 m water depth.* This is consistent with geophysical and coring investigations of drowned inner-shelf coastal barrier deposits at Tuncurry, which, based on the geometries of preserved palaeo-shoreface reflectors, suggest that the upper 10 m of the drowned barrier deposits are missing from the stratigraphic record [*Roy et al.*, 1997].

5. Mid- to late-Holocene relative sea-level fall on the order of 1.5 m could not have been the primary source of strandplain progradation, but may have contributed a small supplementary onshore sand supply form 3-2 ka BP onwards. *Comparison of* BARSIM *model findings with geometric-equilibrium model predictions suggests that a 1.5-m late-Holocene sea-level fall would be difficult to discern from any ongoing shoreface D-S response.* Assuming full time-invariant shoreface response, geometric model predictions indicate that sea-level fall would not have supported the sustained rates of late-Holocene strandplain progradation at Tuncurry, thus implying that ongoing shoreface D-S response or an external sand supply must have contributed.

6. A review of the evidence for mid- to late-Holocene sea level change [Sec. 3.2.1] favours the commencement of sea-level fall after 3 ka BP, in conjunction with the decline of melt-water input rates below hydro-isostatic response rates. Whilst the range of potential onshore sand supply due to a 1.5-m relative sea-level fall has been resolved, it remains uncertain if complete shoreface morphological relaxation occurred (i.e. to Hallermeiers d_i), for the magnitude and timescales considered. This question is further explored in Chapter 5.

7. It is unlikely that external sand supply from the longshore transport system was the primary source of Holocene strandplain progradation. *Without the initial condition of a shoreface sand body in the initial model substrate (and associated onshore sand supply due to shoreface D-S response), sediment accommodation*

across mid-to -lower shoreface depths provided a sediment-sink for the external sand supply. In that case, strandplain progradation extended to 30-40 m water depth, which is inconsistent with geological evidence that indicates that the toe of prograded barriers is at approximately 20 m depth. At Tuncurry, the longshore transport system likely provided a supplementary late-Holocene sand supply that sustained rates of strandplain progradation. This is consistent with the updrift-sink regional sedimentation model [Sec. 2.7.4] of *Roy et al.* [1997].

Based on the model experiments described in this chapter, the following conclusions are made regarding the nature of mid- to late-Holocene shoreface response:

1. At the onset of the Holocene sea-level highstand (i.e. 7 ka BP), disequilibrium shoreface geometry likely persisted beyond the upper shoreface (12-15 m water depth). *Based on the* BARSIM *experiments, shoreface geometry at Moruya and Tuncurry would have featured convex mid- to lower-shoreface sand bodies beyond 18 m and 16 m water depth respectively*, which supplied the majority of mid- to late-Holocene strandplain progradation.

2. *To reproduce rates of Holocene strandplain progradation consistent with the measured barrier-age structures, millennia-average rates of simulated active shoreface response decreased from 2-3 mm/a (i.e. 2-3 m per millennia) between 6-5 ka BP, to less than 1 mm/a between 1-0 ka BP. Peak rates of shoreface lowering occurred at mid-shoreface depths of around 18 m and decreased with increasing depth across the lower shoreface. Rates of onshore sand supply from shoreface lowering rapidly decreased from up to 8 m^3/m/a between 6-5 ka BP to below 5 m^3/m/a from 5-4 ka BP onwards.*

3. It is likely that shoreface D-S response and onshore sand supply is ongoing today, although at imperceptible rates (i.e. < 1 m^3/m/a). Late-Holocene sea-level fall would have further contributed to any ongoing shoreface D-S response remaining from sea-level stabilisation at the onset of highstand.

This model experiments described in this chapter raise additional questions regarding the depth and timescale dependence of shoreface response to sea level change. In particular, the question of lagged shoreface response persists. That is, for a given

magnitude sea-level change, what is the required duration for noticeable shoreface response to occur? In this chapter, the timescales considered impaired the ability to draw decisive conclusions on the relationship between the rate of sea level change and depth-dependent rates of shoreface response. That is, because the three Holocene sea level scenarios featured different rates of sea level change over short durations, it was difficult to isolate the influence of sea-level fall on coastal deposition. This relationship is examined more thoroughly in Chapter 5. The model experiments in this chapter also demonstrate that, because of this timescale dependency, a fixed-magnitude measure of shoreface activity ($dh > 0.3$ m) is largely irrelevant for dynamic sea level.

4

Origins and Controls of Stacked Coastal Barrier Systems: Lessons From Numerical Experiments at Forster-Tuncurry

4.1 Introduction

4.1.1 Background

The nature of coastal barrier deposition in relation to sea-level change and the diversity of highstand barrier stacking relationships observed on the southeast Australian coastline were described in Sections 2.3 and 2.4. The coastal depositional features are by no means unique to that coastline, but are representative of barrier coasts in general. Collectively, the sensitivity of coastal barrier morphology to sea-level change and the distribution of barrier stacking relationships demonstrate the depositional response to the fundamental controls of sea level, inherited antecedent physiography and local sedimentary regime. However, it is difficult to isolate the significance of each control from consideration of the preserved depositional record alone. This is more so the case when the very nature of the depositional controls remains unknown or poorly constrained. At Forster-Tuncurry, spatial and temporal variations in these depositional controls have contributed to the development and preservation of a diverse variety of late-Quaternary coastal barrier systems [Sec. 2.7]. Although previous

chrono-stratigraphic investigations [*Roy et al.*, 1997] have somewhat constrained the timing and sources of deposition, the coastal dynamics responsible for the selective deposition and preservation of coastal barrier systems largely remains to be explored. In this chapter therefore, the site-calibrated Tuncurry BARSIM model is applied to investigate the nature of late-Quaternary depositional controls in southeastern Australia, and, the origins of highstand coastal-barrier morphologies and stacking relationships.

4.1.2 Aims

Chapter 3 considered the origins of mid- to late-Holocene coastal strandplains in the context of depositional controls, including disequilibrium-stress induced shoreface lowering, external sediment supply and minor relative sea-level change. In this chapter, the relationships between the depositional controls and late-Quaternary barrier-coast evolution are considered for large-scale eustatic sea level change typical of glacial-interglacial cycles. In particular, the influence of interacting depositional controls on highstand barrier deposition and resultant barrier-stacking arrangements is investigated. The following questions are considered:

1. Is it possible that Pleistocene-age composite strandplains [Sec. 2.4.1], such as at Tuncurry, developed in response to recurrent highstand barrier deposition associated with multiple late-Quaternary interglacial sea-level highstands?

2. What depositional conditions may support the commencement of highstand coastal strandplain progradation without the deposition or preservation of significant transgressive and backbarrier deposits?

3. Alternatively, what depositional conditions favour the development of transgressive and backbarrier deposits, during late transgression, and subsequent preservation during sea-level highstand?

4. What do the Tuncurry coastal barrier systems suggest about general principles of shoreface response and coastal barrier deposition during late-Quaternary sea level change?

5. What implications may the distribution and elevations of dated coastal barrier deposits at Tuncurry have for the applicability of widely accepted late-Quaternary global sea level records in southeastern Australia?

The Forster-Tuncurry region examined here offers a rich dataset against which to calibrate and evaluate the predictive model. Furthermore, in this chapter an opportunity arises to constrain late-Quaternary sea levels in southeastern Australia and the conditions in which the different coastal barrier stacking relationships identified in Section 2.4 might arise. However, the questions considered in this chapter have implications for general principles of coastal and shallow-marine deposition in barrier-coast settings. Specifically, the pursuit of solutions to the above questions examines the sensitivity of modes of coastal barrier evolution to various depositional controls during sea level change.

4.2 Late-Quaternary sea levels

In a geological context, sea level records during the last glacial-interglacial cycle are relatively well constrained, due to reasonable agreement between continuous records from indirect methods (e.g. marine oxygen isotopes), and dated relative sea level indicators from biological (e.g. corals, speleothems) and sedimentary records [*Chappell et al.*, 1996; *Lambeck and Chappell*, 2001; *Waelbroeck et al.*, 2002; *Siddall et al.*, 2003; *Thompson and Goldstein*, 2006; *Rohling et al.*, 2009]. Furthermore, recent developments in ice-sheet and Earth rheology models have constrained regional glacio-isostatic and hydro-isostatic signals, thereby allowing for the normalisation of relative sea level records and comparison between sites [*Lambeck et al.*, 1998; *Yokoyama et al.*, 2000, 2001; *Lambeck et al.*, 2002, 2003; *Lambeck and Purcell*, 2005]. However, despite good agreement between records on the general pattern of sea level change, in many cases the timing and magnitude of individual fluctuations remains contested.

In particular, peak sea levels attained during some interglacial and interstadial sea-level highstands remain debated, with an increasing body of evidence from more recent studies challenging earlier interpretations. For example, *Medina-Elizalde* [2013] presented a quality-controlled compilation of relative sea level indicators from U-Th dated corals, which suggested considerable scatter between datasets during MIS 5a in particular [Fig. 4.1]. *Caputo* [2007] also presented a comparison of continuous and derived relative sea level records [Fig. 4.2] that demonstrated the range of variability in late-Quaternary sea levels, and associated implications for end users. The recent evidence, along with the intrinsic errors associated with indirect records, biological

indicators, and dating techniques [*Walker*, 2005], implies persisting uncertainties in the magnitudes (and rates) of late-Quaternary sea level fluctuations. At present a lack of clarity regarding transparent and objective criteria for sub-setting late-Quaternary sea level datasets presents a challenge to end users [*Medina-Elizalde*, 2013], with the scope for variation in sea level histories potentially contributing to significant differences in evolutionary reconstructions of coastal environments [*Caputo*, 2007].

Peak sea levels during MIS-5a remain particularly contested, with recent evidence suggesting that global sea levels during this time may have been at or near PMSL. This conflicts with many previous records from uplifted coral terraces and marine oxygen isotopes, which suggest that both MIS-5c and MIS-5a sea levels peaked at between 15 and 25 m lower than PMSL [Figs. 4.1 & 4.2]. For example, *Dorale et al.* [2010] presented evidence from speleothem encrustations at an intermediate-field site in the Mediterranean Sea, which suggests that sea levels reached up to 1 m PMSL there at around 81 ka BP. Figure 4.3 shows that their findings are consistent with the reconstructed marine oxygen isotope record of *Shackleton* [2000], in which global sea levels during MIS 5a were close to present coincident with a peak in 60 North insolation. Furthermore, Uranium-series ages and morphosedimentary evidence from the Strait of Gibralter suggest that MIS-5a sea levels were above present-day levels there [*Abad et al.*, 2013]. In North America, Uranium-series ages from coral samples retrieved from near present sea level within a number of contemporary coastal plains along the US Atlantic margin date to between 80-85 ka BP [*Wehmiller et al.*, 2004]. More recently, [*Simms et al.*, 2009] presented further evidence for higher MIS-5a sea levels from a drowned coastal barrier system in the Gulf of Mexico. Their findings suggest that sea levels exceeded -12 m PMSL at the least during MIS 5a. Further evidence from nearby Bermuda suggests that sea levels were near PMSL there during MIS 5a [*Muhs et al.*, 2002]. Lastly, optical-stimulated luminescence (OSL) ages retrieved from highstand coastal barrier deposits in the Wilderness embayment, South Africa, also suggest that MIS 5a sea levels were near PMSL [*Bateman et al.*, 2011].

Similar to the case of MIS 5a, there is also evidence to suggest that peak MIS-3 sea levels were higher than depicted by many of the records shown in Figures 4.1 & 4.2. For example, relative sea level indicators from depositional records in southern Australia [*Cann et al.*, 1988; *Murray-Wallace et al.*, 1993; *Cann et al.*, 2000] and abroad [*Mauz and Hassler*, 2000; *Rodriguez et al.*, 2000; *Banfield and Anderson*, 2004] suggest that

peak MIS-3 sea levels may have reached up to -30 m PMSL. That evidence conflicts with many coral and deep-sea oxygen isotope records that place peak MIS-3 sea levels between -50 and -60 m PMSL, and is most consistent with the *Shackleton* [2000] reconstructed marine oxygen isotope record [Fig. 4.1]. Thus although the timing of the MIS-3 interstadial period is well constrained to between about 60 and 30 ka BP, the amplitude and timing of MIS-3 sea level oscillations remain in question [*Siddall et al.*, 2008]. For example, uncertainties regarding the role of ice sheets as active or responsive contributors to sea level change during abrupt Dansgaard-Oeschger climate change, and the dominant contribution of northern (Greenland) or southern (Antarctica) hemisphere ice sheets hinder the capacity to resolve global sea levels during MIS 3 [*Siddall et al.*, 2008]. Recent evidence supports four major sea level oscillations between 20-30 m magnitude during MIS 3, superimposed on a general falling trend from about -60 m PMSL during the first half of MIS 3 to -80 m PMSL for the remainder [*Rohling et al.*, 2008; *Siddall et al.*, 2008].

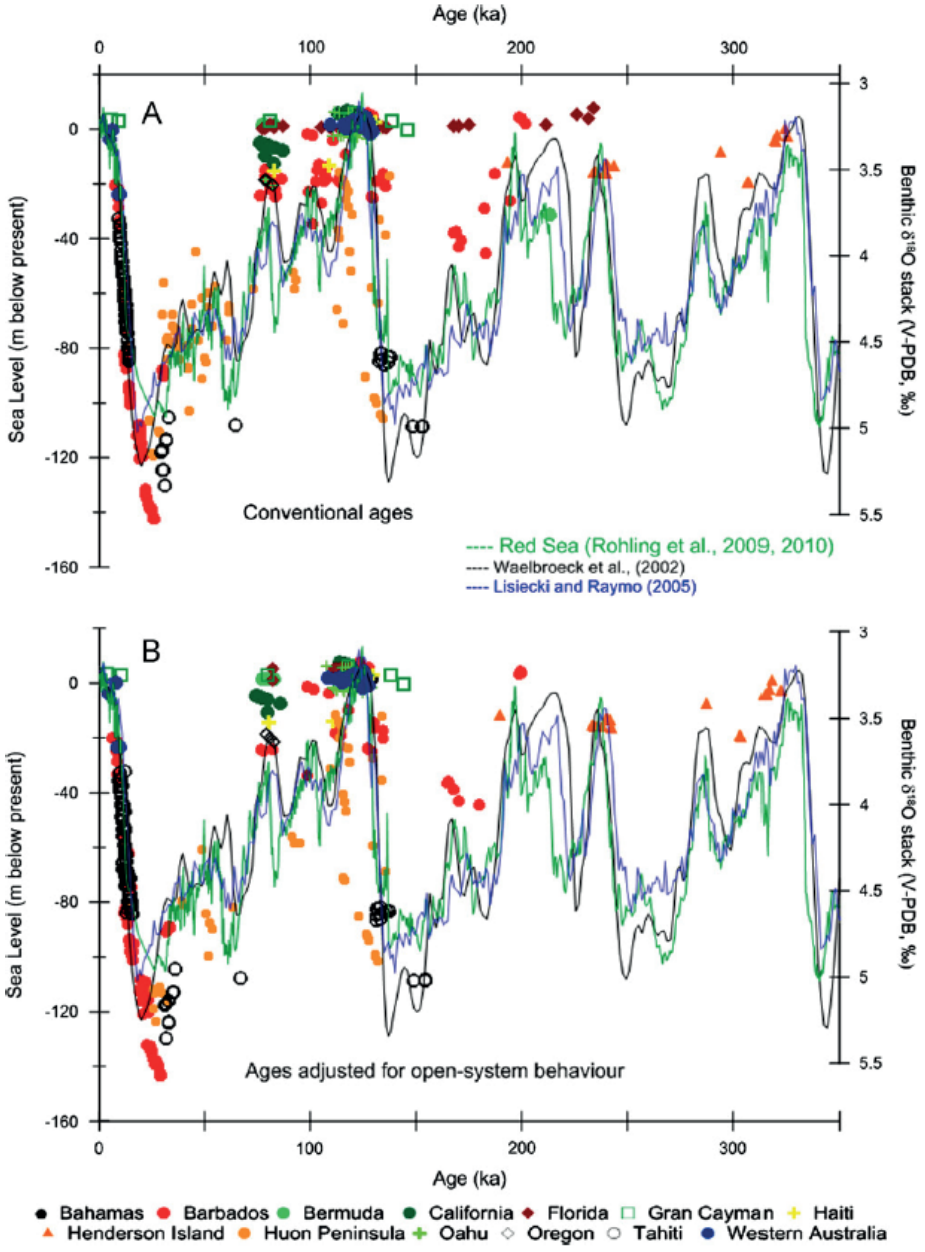

Figure 4.1: Late-Quaternary sea level records from coral datasets - Relative sea level records from coral data based on (a) conventional ages and (b) ages adjusted for open system behaviour. Selected continuous sea level records are also shown as indicated in figure. Note particular scatter in the data during MIS 5a. From *Medina-Elizalde* [2013].

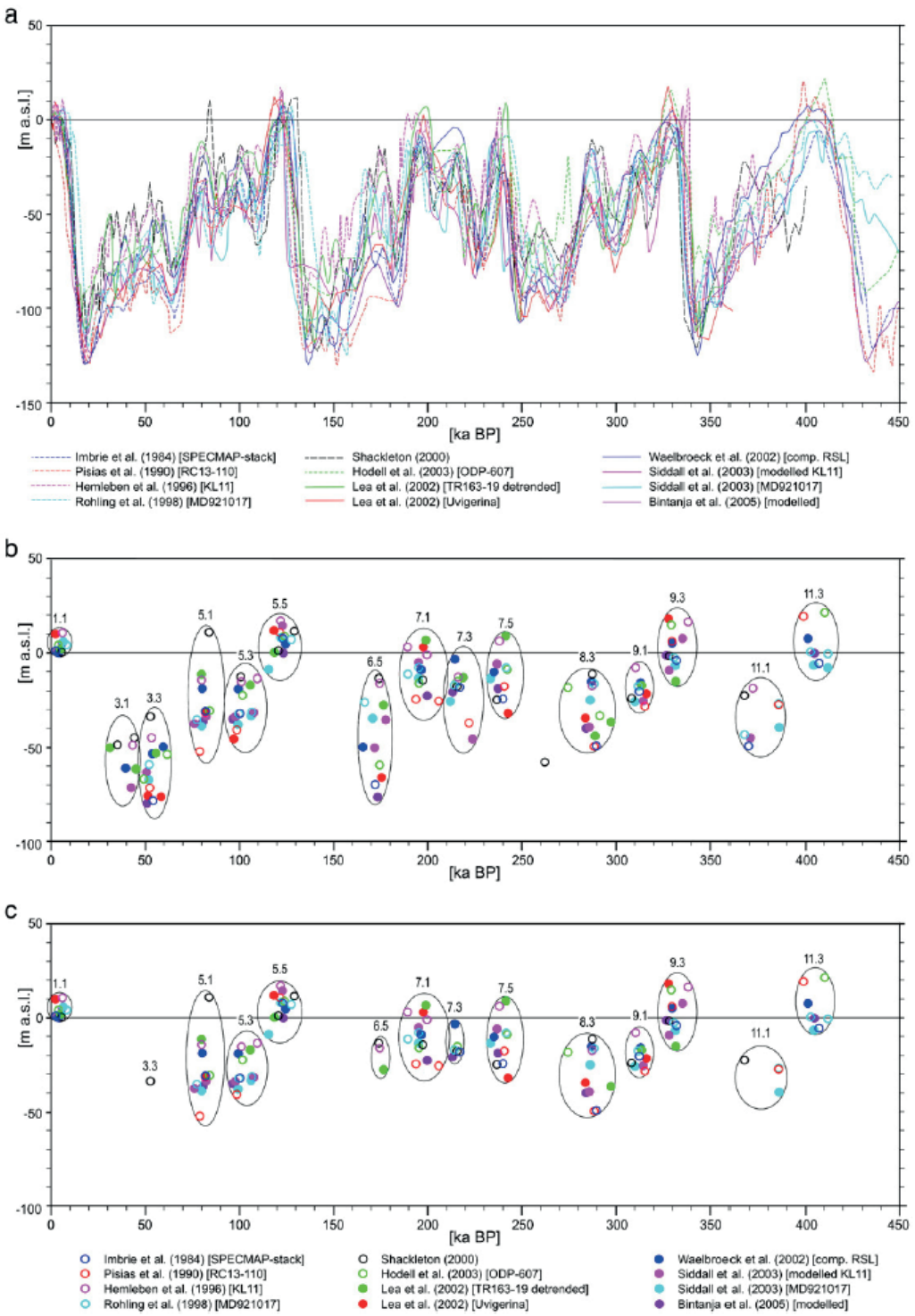

Figure 4.2: Continuous late-Quaternary sea level records - (a) Selected relative sea level (solid) and derived relative sea level (dashed) records for the last four glacial cycles. The distribution of highstand sea level peaks is also shown assuming (b) 2 mm/a and (c) 1 mm/a uplift rates. Note scatter in the data during MIS 5a. From *Caputo* [2007].

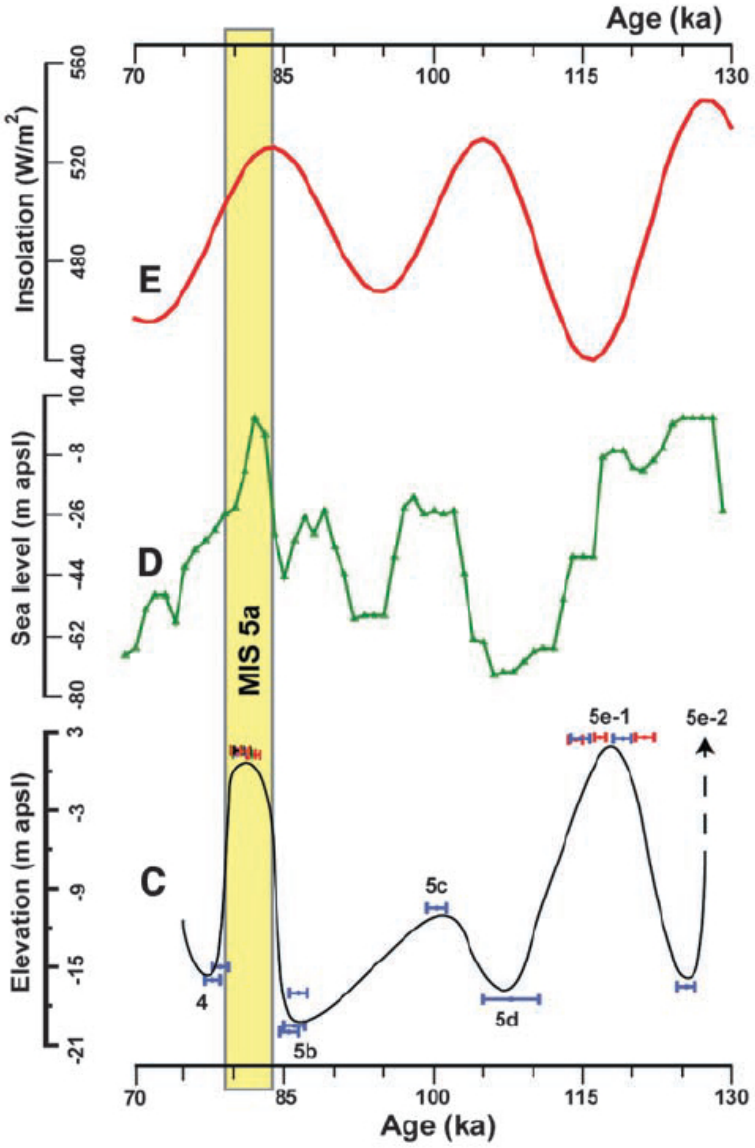

Figure 4.3: Speleothem evidence for MIS-5a sea levels near PMSL - (a) June insolation at 60°north, (b) reconstructed ocean-water oxygen isotope record of *Shackleton* [2000] scaled as sea level, and (c) sea level curve for Mallorca showing previous data (blue) and Speleothem relative sea-level indicators (red). From *Dorale et al.* [2010].

4.3 Methods

4.3.1 Sea-level/barrier-age correlation

To establish the chronologic relationships between late-Quaternary sea levels and dated coastal barrier deposits at Tuncurry, the thermoluminescence and radiocarbon age data collected from the Tuncurry barrier systems Section 2.7.2 was compared with a selection of representative sea level records. The sea level-barrier age correlation considered both continuous indirect records and relative sea-level indicators [Fig. 4.4]. The range of palaeo-sea-levels inferred from the present-day elevations of the samples were plotted against the age data (with error bounds), and superimposed on the sea level records shown in Figure 4.4.

4.3.2 Stratigraphic modelling

The sensitivity of last-glacial coastal barrier deposition to different sea level histories was examined using the Tuncurry BARSIM model described in Chapter 3. More specifically, the BARSIM numerical stratigraphic model was described in Section 1.5 and the erosion efficiency calibration procedure is documented in Section 3.3.1. In this chapter it is assumed that the model configuration established in Chapter 3 is appropriate for investigating late-Quaternary coastal barrier evolution at Tuncurry.

4.3.2.1 Sea level scenarios

Significant variability between published sea level records for the last glacial cycle [Sec. 4.2] implies a degree of subjectivity in selecting a suitable curve for sites distal from age-constrained relative sea level indicators. *Caputo* [2007] examined the difficulties and potential issues arising from the subjective selection of sea level records, and advocated the investigation of multiple records where age reconstructions or tectonic signals are poorly constrained at the site of interest. In the absence of a robust last-glacial relative sea level curve for southeastern Australia, to proceed here it is necessary to select a representative curve as a starting point for the simulation experiments. Age data from Tuncurry was compared with multiple sea level records in Section 4.3.1 to evaluate the applicability of indirect and derived last-glacial sea level curves to southeastern Australia. The *Waelbroeck et al.* [2002] composite sea level curve (and confidence interval) was adopted here for simulations of last-glacial coastal barrier evolution at Tuncurry.

Their record combined deep-sea benthic oxygen isotope ratios from the North Atlantic and Equatorial Pacific oceans with relative sea level indicators from corals and other sources, and is thus constrained by U-Th ages. Further to providing a representative and robust last-glacial sea level record, the resolution of the *Waelbroeck et al.* [2002] curve was consistent with the temporal resolution of the BARSIM stratigraphic models applied here [Fig. 4.4]. That is, a computational compromise between simulation duration and temporal resolution implied that is was not possible for the models to represent the *Lambeck and Chappell* [2001] sea level curve [Fig. 4.4] in full temporal detail.

Ultimately, both a fitted *Waelbroeck et al.* [2002] sea level curve and two modified curves, postulated through constraints drawn from local data discussed below, were applied in the simulations to examine the sensitivity of coastal barrier deposition to different sea level scenarios. The black line in Figure 4.4 shows that the fitted sea level model (i.e. LG-W) matches the *Waelbroeck et al.* [2002] sea level curve (thick grey line) closely, although omits some higher order oscillations. The dashed blue line in Figure 4.4 shows the first modified sea level curve (LG-M1), in which peak sea levels during MIS 3, MIS 5a and MIS 5c have been raised by between 12-15 m, constrained by the observed elevations of coastal barrier deposits at Tuncurry [Fig. 4.5]. The red line in Figure 4.4 shows the second modified sea level curve (LG-M2), in which peak sea levels during MIS 3 and MIS 5a have been raised only by between 12-15 m. That is, except for the MIS-5c sea-level highstand, the LG-M1 and LG-M2 sea level models were identical. The evidence for higher sea levels during MIS 3 and MIS 5 has been reviewed in Section 4.2, and the rationale for the LG-M1 and LG-M2 sea level curves is described in the context of the model experimental design [Sec. 4.3.2.2].

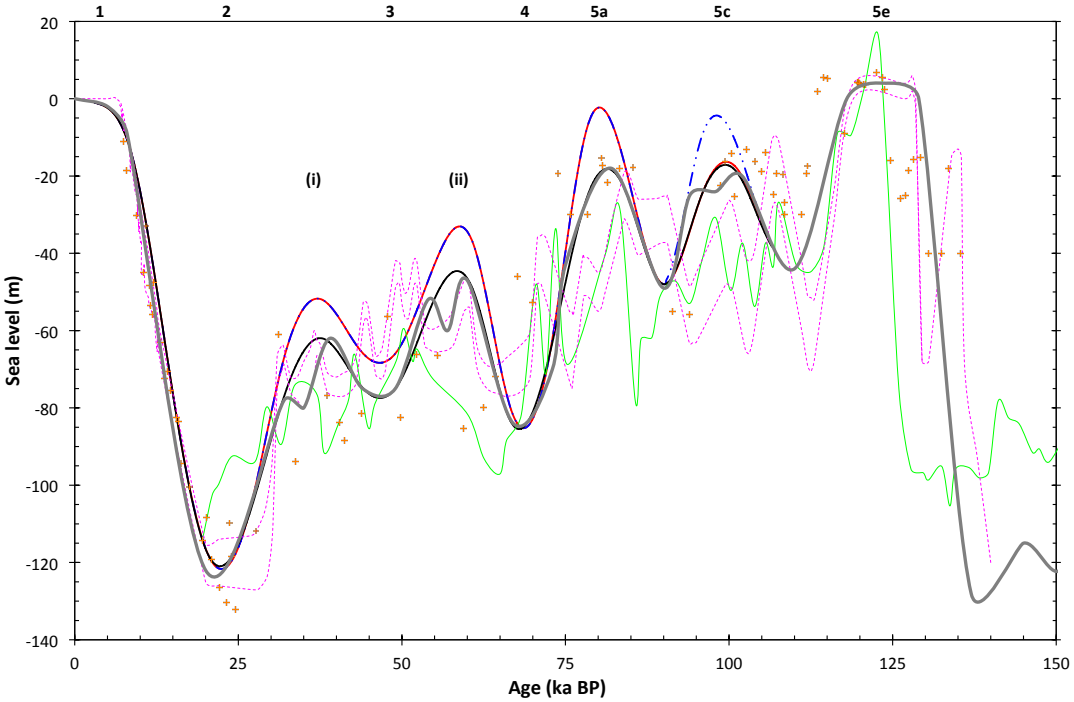

Figure 4.4: Sea level scenarios applied in Tuncurry last-glacial cycle models - Sea level scenarios applied in the last-glacial cycle stratigraphic models at Tuncurry, including the fitted LG-W (black), modified LG-M1 (dashed blue) and modified LG-M2 (red). Selected continuous sea level records shown for comparison include the *Waelbroeck et al.* [2002] composite curve (thick grey), the Red Sea curve from *Siddall et al.* [2003] (green), and the Huon sea level envelope of *Lambeck and Chappell* [2001] (dashed purple). Coral sea level indicators from *Thompson and Goldstein* [2006] (orange +) are also shown.

4.3.2.2 Simulation experiments

Coastal and shallow-marine deposition at Tuncurry throughout the last-glacial cycle was simulated from the termination of the MIS-5e sea-level highstand to the beginning of the Holocene highstand (i.e. 118-6 ka BP) using the Tuncurry BARSIM model. The simulated depositional sequence was then compared with the interpreted site stratigraphy from the Tuncurry coast and inner-continental shelf [Sec. 2.7.3]. The model was initially forced with the LG-W sea level curve to investigate coastal barrier deposition in response to the *Waelbroeck et al.* [2002] sea level curve [Fig. 4.4]. However, comparison between the simulated and site stratigraphy showed that the model was unable to reproduce the site stratigraphy using the LG-W sea level curve. Furthermore, discrepancies between the elevations of dated coastal barrier deposits and the selected sea level records of Figure 4.4 also suggested that the *Waelbroeck et al.* [2002] sea level curve was inconsistent with late-Quaternary coastal evolution at Tuncurry.

Although BARSIM does not include a capability to account for hard substrates, the Tuncurry site is largely free of such effects. More specifically, in the case of the central Tuncurry embayment, the MIS-5a shelf morphology is presumed to have been comparable to the Holocene situation, in which the inner shelf palaeo-embayment is partially filled with transgressive and falling-stage coastal barrier deposits. Although there are no bedrock outcrops at the seafloor in the Tuncurry embayment, shelf sediment cover is thinnest over the bedrock high that separates the highstand embayment from the inner-shelf palaeo-embayment (visible at about -30 m PMSL in Lines 1 and 13 in Figure 2.18). However, the topographic influence of the bedrock high on coastal barrier deposition was preserved in simulations, which is indicated by preservation of the convex inflection between the highstand embayment and inner-shelf palaeo-embayment. This suggests that the geometry and composition of the model substrate is representative of site geomorphology.

Following consideration of the sea-level/barrier-age correlation carried out in Section 4.3.1, the LG-W sea level curve was modified for the subsequent simulations. First, the sea level curve was modified by adjusting the peak sea levels attained during all highstands to be consistent with the elevations inferred from dated barrier deposits corresponding to each stage. Thus in scenario LG-M1, peak sea levels attained during MIS 3, MIS 5a and MIS 5c were raised by up to 15 m [Fig. 4.4]. However, the

comparison between simulated and site stratigraphy again indicated that model predictions were inconsistent with the observed site stratigraphy. As discussed in Section 4.2 there is reasonable evidence to suggest that peak sea levels attained during MIS-3 and MIS-5a sea-level highstands were on the order of -40 to -30 m PMSL and -12 to +1 m PMSL respectively. Furthermore, the age data from the youngest component of the inner-barrier strandplain suggests a closer association to MIS 5a than MIS 5c. Therefore, a second modified sea level curve (LG-M2) was tested. Specifically, the MIS-3 and MIS-5a peak sea levels of LG-M1 were retained, whilst MIS-5c peak sea level was maintained at -20 m PMSL, as implied by the *Waelbroeck et al.* [2002] sea level curve [Fig. 4.4].

To enable comparison between the simulated stratigraphy at different stages of the last-glacial sea level cycle, each model was run over three different durations, all commencing from the end of the MIS-5e sea-level highstand. Specifically, each model was run in separate simulations from 118 ka BP to the MIS-4 lowstand (i.e. 70 ka BP), the MIS-2 lowstand (20 ka BP) and the onset of the MIS-1 (Holocene) highstand (6 ka BP). External sediment supply was maintained at zero throughout each simulation, except for during MIS-5 and MIS-3 sea-level highstands, where external sediment supply was increased to 2 $m^3/m/a$. The rationale for this increase was to account for the trapping of northward littoral drift upon flooding of the highstand and shelf embayments. Evidence for this process has been described in Section 2.7.4. The external sediment supply scenario was identical for each of the three simulation experiments. The outputs of each model were then plotted together to create a time series of stratigraphic evolution for each of the three models. Synthetic well logs were generated within BARSIM for the full 112 ka models to compare simulated coastal barrier stratigraphy between the models and against the site stratigraphy described in Section 2.7.3. The synthetic well logs were plotted with the simulated depositional sequences to demonstrate both the cross-shelf and vertical variation in predicted barrier stratigraphy resulting from the three alternative sea level models.

4.4 Results

4.4.1 Sea-level/barrier-age correlation

The sea-level/barrier-age correlations show reasonable agreement within the bounds of dating error for coastal barrier deposits corresponding to MIS-7 sea-level highstands (red markers) and the MIS-5e highstand (orange markers) [Fig. 4.5]. These deposits were retrieved from the western Pleistocene strandplain [Fig. 2.13], and suggest two distinct age groups of barrier deposits. This is consistent with the interpretation of [*Roy et al.*, 1997], who proposed that the western strandplain was a composite feature, although did not find any stratigraphic evidence within GPR profiles of any intervening transgressive deposition between barrier deposits associated with the two age groups [Sec. 2.15].

The third oldest barrier age group (yellow markers in Figure 4.5) comes from samples retrieved from the eastern Pleistocene strandplain [Fig. 2.13]. The deposits date to between 94-79 ka BP and appear to correspond to the MIS-5a and/or MIS-5c sea-level highstand/s. However, relative to the MIS-7 and MIS-5e age groups there is poorer agreement between the sea level records and the elevations of these barrier deposits. Figure 4.5 shows that the eastern Pleistocene strandplain deposits suggest that sea levels were 10-20 m higher during MIS 5a and/or MIS 5c than implied by the sea level records. Barrier deposits that appear to be associated with the eastern Pleistocene strandplain were also sampled in vibrocore FT13.3 at the toe of the Holocene barrier on the contemporary inner shelf [Fig. 2.18]. A TL age of 95.7 $\pm$ 13 ka was returned from that sample [Tab. 2.2].

The TL age data returned from the shelf barrier samples [Tab. 2.2] suggests deposition during MIS 3. However, the elevations of samples associated with the first half of MIS 3 (-40 to -50 m PMSL), and elevations of samples associated with the second half of MIS 3 (-50 to -60 m PMSL), both suggest higher MIS-3 sea levels than the sea level records shown in Figure 4.5. The discrepancy between the elevations of shelf barrier deposits from the northern shelf (blue markers) and the southern shelf (green markers) relates to the absence of barrier deposits at shallower depths on the steeper southern shelf (Fig. 2.21). The sea level records shown in Figure 4.2 show a range of possible MIS 3 highstand sea levels, which have been discussed in Section 4.2.

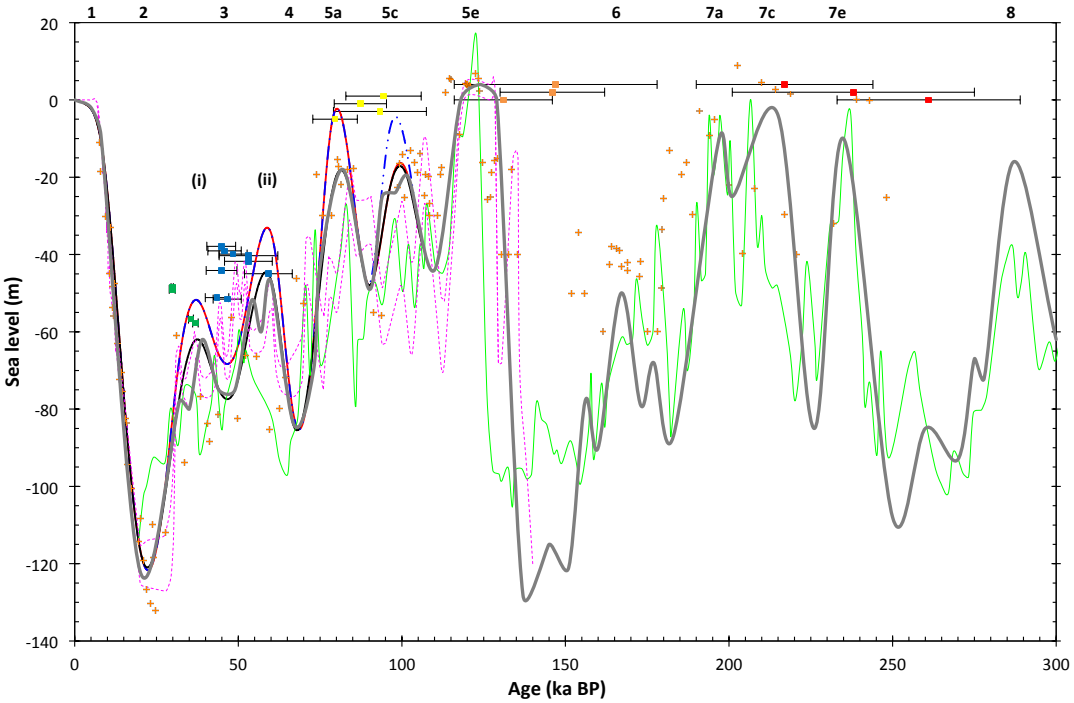

Figure 4.5: Late-Quaternary sea levels and coastal barrier deposition at Forster-Tuncurry - Ages and inferred sea levels at the time of deposition of sampled coastal barrier deposits at Forster-Tuncurry in relation to published sea level records for the last two glacial-interglacial cycles. Samples from the western inner-barrier strandplain (red, orange), eastern inner-barrier strandplain (yellow), northern embayment shelf barriers (blue) and southern embayment shelf barriers (green) are shown. See Figure 4.4 for a description of the sea level records shown.

4.4.2 Simulated coastal barrier stratigraphy

4.4.2.1 Fitted sea level (LG-W)

Figure 4.6 shows the simulated last-glacial stratigraphic sequence resulting from the LG-W sea level model. Sea level rise into MIS 5c was characterised by the landward migration of a transgressive barrier, which stalled at the mouth of the highstand embayment when sea level peaked at -20 m PMSL [Fig. 4.6a]. During the brief MIS-5c sea-level highstand, a backbarrier-fill deposit (U1a) composed of mud and fine sands accumulated throughout the highstand embayment behind the transgressive barrier (U1b). A thin forced-regressive strandplain (U1c) was deposited across the shoreface to about -50 m PMSL during the sea-level fall following MIS 5c. During MIS 5a sea level reached a comparable elevation as during MIS 5c. However backbarrier accommodation was restricted due to the presence of the MIS-5c barrier system, and thus the MIS-5a highstand barrier system was limited to a transgressive barrier [Fig. 4.6a]. The transgressive barrier (U2b) was composed of fine-coarse sands from combined barrier overwash and backbarrier deposition. Similarly to MIS 5c, a thin forced-regressive deposit (U2c) accumulated across the shoreface during sea-level fall following MIS 5a. Rapid sea-level fall across the mid-shelf embayment following MIS 5a was accompanied by limited deposition, until slowing rates of sea-level fall eventually permitted the development of a forced-regressive strandplain and lowstand barrier during MIS 4 [Fig. 4.6a].

During the MIS-3ii sea-level highstand (50-60 ka BP) a transgressive barrier (U3b) composed of medium-coarse sands formed at around -40 m PMSL in the mid-shelf embayment [Fig. 4.6b]. Synthetic core 1.3 shows the stratigraphy of the transgressive barrier [Fig. 4.6c]. Following the brief highstand a forced-regressive strandplain (U3c) was deposited to about -70 m PMSL, before sea level began to rise into the second MIS 3 sea-level highstand (30-40 ka BP). During the MIS-3i sea-level highstand barrier deposition occurred at about -60 m PMSL [Fig. 4.6b]. Backbarrier deposition was characterised by the accumulation of an estuarine fill (U4a) composed of fine-medium sands. Synthetic core 1.4 shows the stratigraphy of the MIS-3i barrier (U4b) overlying the earlier MIS-3ii barrier [Fig. 4.6c]. Deposition of a forced-regressive strandplain (U4c) followed the MIS-3i highstand. The volume of the strandplain was relatively low compared to post-MIS-3ii strandplain [Fig. 4.6b].

The simulated depositional response to rapid sea-level rise following MIS 2 was characterised by the formation, landward migration and overstepping of successive transgressive barriers. The remnants of this process can be seen in the convex deposits of medium-coarse sands that overlie the earlier deposits at various locations across the shelf [Fig. 4.6c]. Late transgression at the mouth of the highstand embayment was characterised by the reworking of much of the MIS-5c and MIS-5a highstand barrier systems. The reworked barrier deposits contributed to the development of a significant transgressive barrier at the mouth of the highstand embayment during MIS 1. Synthetic core 1.2 shows the stratigraphy of the MIS-1 transgressive barrier (U5b), which overlies earlier MIS-1 and MIS-5a backbarrier estuarine fills [Fig. 4.6c]. Deposition of backbarrier estuarine-fill (U5a) recommenced across much of the highstand embayment during MIS 1. Synthetic core W1.1 shows that a thin unit of coarser sands separates the MIS 1 (U5a) and MIS 5c (U1a) estuarine-fill units [Fig. 4.6c].

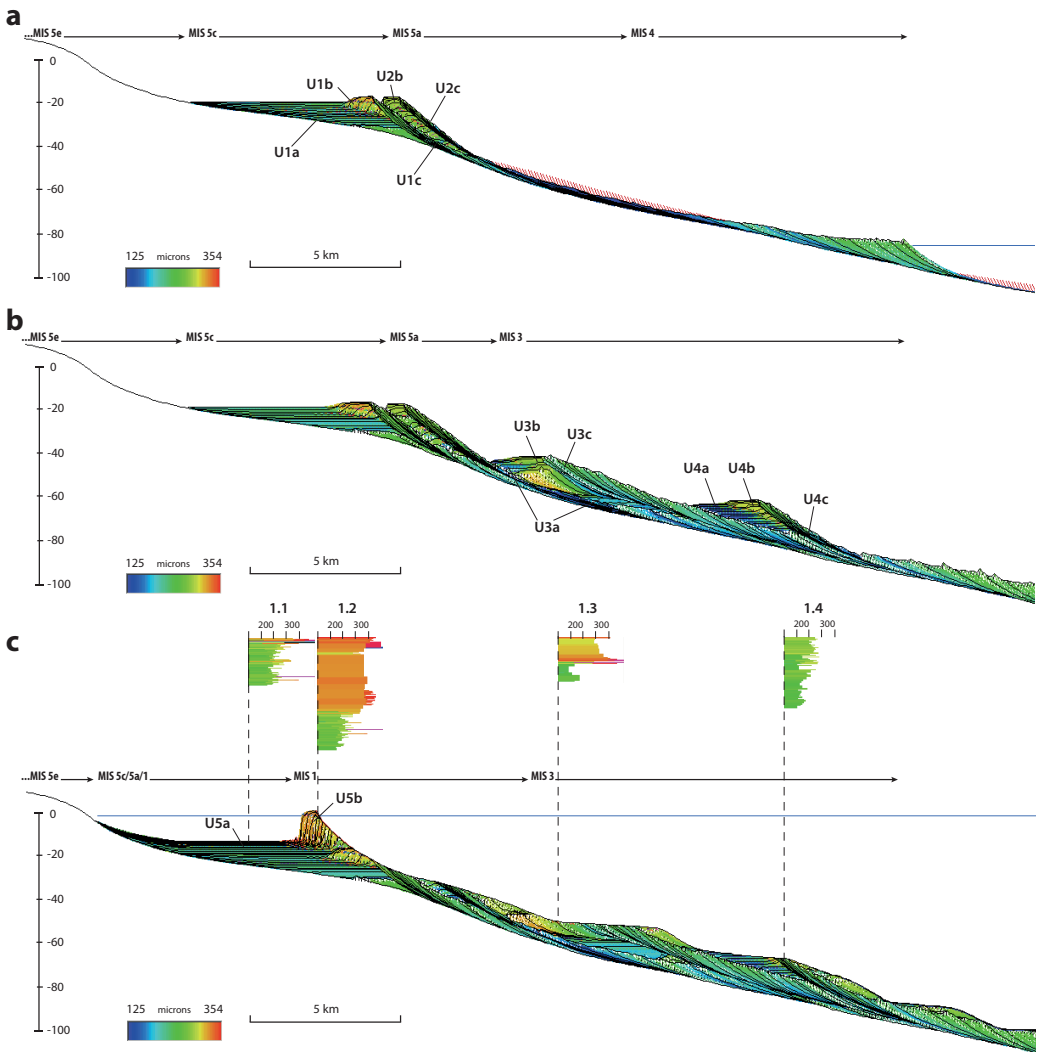

Figure 4.6: Simulated stratigraphy for last-glacial LG-W sea level at Tuncurry - Simulated coastal barrier deposition at Tuncurry over the last third-order sea level cycle using the Tuncurry BARSIM model and LG-W sea level curve. Modelled strata at (a) MIS 4 (70 ka BP), (b) MIS 2 (20 ka BP) and (c) MIS 1 (6 ka BP) are shown. Synthetic well logs show detailed stratigraphy at key locations of interest are for comparison with the interpreted vibrocores in Figure 2.18. The extents of barrier systems associated with each marine isotope stage are also indicated.

4.4.2.2 Modified sea level (LG-M1)

Figure 4.7 shows the simulated last-glacial stratigraphic sequence resulting from the LG-M1 sea level model. Higher sea levels during MIS 3, MIS 5a and MIS 5c resulted in barrier deposition at different locations compared with the LG-W model. Although the development and arrangement of barrier systems were generally comparable, the preserved stratigraphy was different, particularly in the highstand embayment [Fig. 4.7]. For example, Figure 4.7a shows that the general stratal architecture and stacking arrangement of the MIS-5c (U1) and MIS-5a (U2) barrier deposits were comparable to the LG-W model [Fig. 4.7a]. However, the higher sea levels of the LG-M1 model permitted barrier development within the highstand embayment, rather than at the mouth of the embayment. Upon breaching the embayment mouth, a significant transgressive unit that is related to U1b was deposited across much of the highstand embayment. This unit occurs at the base of W2.1, beneath younger transgressive barrier deposits [Fig. 4.7c]. A comparatively thick estuarine-fill unit (U1a) accumulated behind an MIS-5a transgressive barrier (U1b) of comparable dimensions to the corresponding unit of the LG-W model. Similarly, the MIS 5a barrier (U2b) was comparable to that of the LG-W model, although the associated estuarine fill (U2a) was more developed in the LG-M1 model [Fig. 4.7a].

The MIS-3ii (U3) and MIS-3i (U4) barrier systems also showed comparable stratal architecture and stacking arrangements to the LG-W model [Fig. 4.7b]. However, the barrier systems occurred at -30 m and -50 m PMSL respectively (c.f. -40 m and -60 m PMSL in the LG-W model). Furthermore, the MIS-3ii transgressive barrier (U3b) featured a more developed backbarrier-fill unit (U3a) relative to the LG-W model. This is evident in the lower fine-medium sand unit that is preserved in W2.3 [Fig. 4.7c]. The MIS-3ii barrier system also comprised a significant transgressive barrier, the remnants of which were preserved at the top of W2.3. Comparable simulated stratigraphy in W1.4 and W2.4 show that apart from the elevation of barrier deposition, the MIS-3i barrier systems (U4) were similar in the LG-W and LG-M1 models [Figs. 4.6c & 4.7c].

The simulated deposition of the MIS-1 barrier system (U5) occurred in more or less the same location in the LG-W and LG-M1 models. However, whereas the U1 and U2 barrier deposits were reworked into the U5 barrier system in the LG-W model, the U5 barrier system developed seaward of the U1 and U2 barrier deposits in the LG-M1

model [Fig. 4.7c]. The simulated stratigraphy in W2.2 shows that the MIS-1 barrier system overlies the MIS-5a and MIS-5c barrier systems, each of which is represented by transgressed fine-medium grained backbarrier deposits (U2a/U1a) that underlie forced-regressive deposits (U2c/U1c) composed of medium-grained sands. Relative to the LG-W model, backbarrier accommodation in the MIS-1 barrier system was restricted in the LG-M1 model due to the elevations of the preserved MIS-5c and MIS-5a barrier systems. This resulted in only comparatively negligible deposition of the U5a backbarrier-fill unit [Fig. 4.7c].

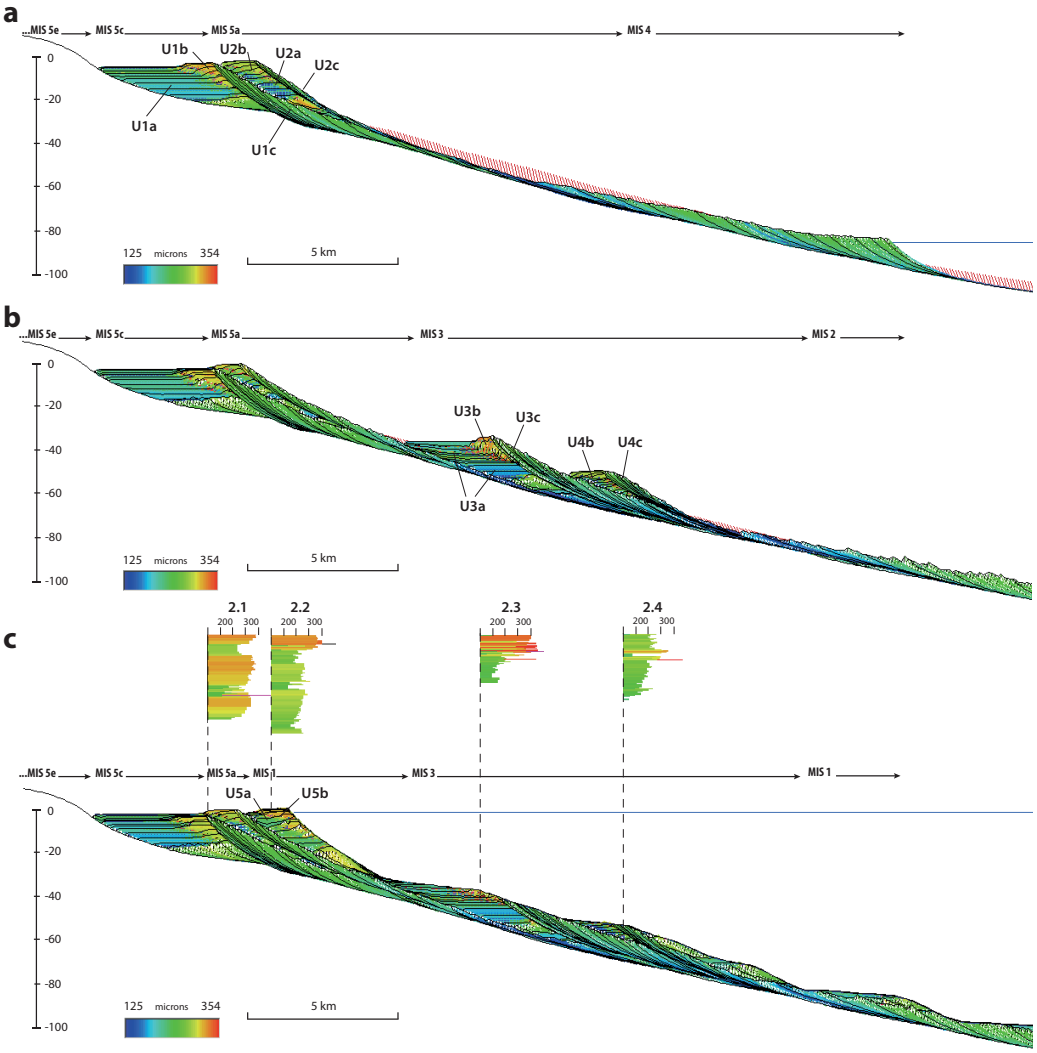

Figure 4.7: Simulated stratigraphy for last-glacial LG-M1 sea level at Tuncurry - Simulated coastal barrier deposition at Tuncurry over the last third-order sea level cycle using the Tuncurry BARSIM model and LG-M1 sea level curve. Modelled strata at (a) MIS 4 (70 ka BP), (b) MIS 2 (20 ka BP) and (c) MIS 1 (6 ka BP) are shown. Synthetic well logs show detailed stratigraphy at key locations of interest are for comparison with the interpreted vibrocores in Figure 2.18. The extents of barrier systems associated with each marine isotope stage are also indicated.

4.4.2.3 Modified sea level (LG-M2)

Figure 4.8 shows the simulated last-glacial stratigraphic sequence resulting from the LG-M2 sea level model, which differed from the LG-M1 model only in peak sea level reached during MIS-5c. Specifically, peak MIS-5c sea levels were -4 m and -18 m PMSL in the LG-M1 and LG-M2 sea level curves respectively [Fig. 4.4]. Figure 4.8a shows that MIS-5c barrier deposits (U1b) were not preserved in the LG-M2 model despite the MIS-5c barrier system developing as in the LG-W model [Fig. 4.6a], which shared an identical sea level curve prior to MIS 5a [Fig. 4.4]. As in the LG-W model the development of the MIS-5c barrier system included the deposition of a backbarrier fill (U1a), which is preserved at the bases of W3.1 and W3.2. During the rapid sea-level rise at the onset of MIS 5a, the MIS-5c barrier was briefly re-activated as a transgressive barrier, which stalled atop the remnant barrier and began to aggrade prior to the barrier system being overstepped by the shoreline at 82 ka BP. At this time the shoreline migrated instantaneously to the head of the highstand embayment where deposition of a regressive strandplain commenced (c.f. forced-regression). Deposition of the MIS-5a highstand strandplain (U2b) was supplied by shoreface reworking of the overstepped MIS-5c barrier system at the embayment mouth, which continued throughout the MIS-5a sea-level highstand. The simulated strata in W3.1 shows that U2b is up to 20 m thick and is separated from the underlying U1a by an erosional unconformity. Rapid sea-level fall following MIS 5a was initially characterised by the deposition of a forced-regressive strandplain (U2c) as sea level fell to -85 m PMSL.

The MIS-3ii and MIS-3i barrier systems showed comparable stratal architecture and stacking relationships as in the LG-M1 model. As the LG-M1 and LG-M2 models were forced with the same sea level curve following MIS 5a [Fig. 4.4], the MIS-3 barrier systems also developed at the same elevations and in similar locations [Fig. 4.8b]. The only notable difference in the MIS-3 barrier deposits in the LG-M2 model was that transgressive-barrier deposition was relatively limited, apparently at the expense of backbarrier-fill deposition. That is, the MIS-3 barrier systems of the LG-M2 model featured better developed backbarrier deposits, which can be seen in the greater extent of fine-grained horizontally-bedded deposits in Figure 4.8b compared with Figure 4.6b. The simulated strata in W3.4 [Fig. 4.8c] shows the backbarrier fill (U3a) associated

with the MIS-3ii barrier system, which is up to 15 m thick and is located landward of the forced-regressive strandplain deposits (U3c).

As in the LG-W and LG-M1 models, rapid sea-level rise into MIS 1 was characterised by the overstepping of numerous transgressive barriers as the shoreline migrated landward across the shelf, and shoreface reworking of the upper sections of earlier barrier deposits [Fig. 4.8c]. Ultimately the MIS-1 transgressive barrier (U5b) ceased migration at a position seaward of the MIS-5a highstand strandplain (U2b) atop of the MIS-5a forced-regressive strandplain (U2c). The stacking relationship can be seen in the simulated strata in W3.2, in which MIS-1 barrier (U5b) and backbarrier (U5a) deposits overlie MIS-5a barrier deposits (U2b) and MIS-5c backbarrier deposits (U1a). The simulated strata in W3.3 show that at -25 m PMSL U2b is buried below a thin deposit of transgressive barrier facies associated with U5b. Backbarrier fill (U5a) associated with late-Holocene transgression separates the MIS-5a highstand strandplain and MIS-1 transgressive barrier at the surface [Fig. 4.8c].

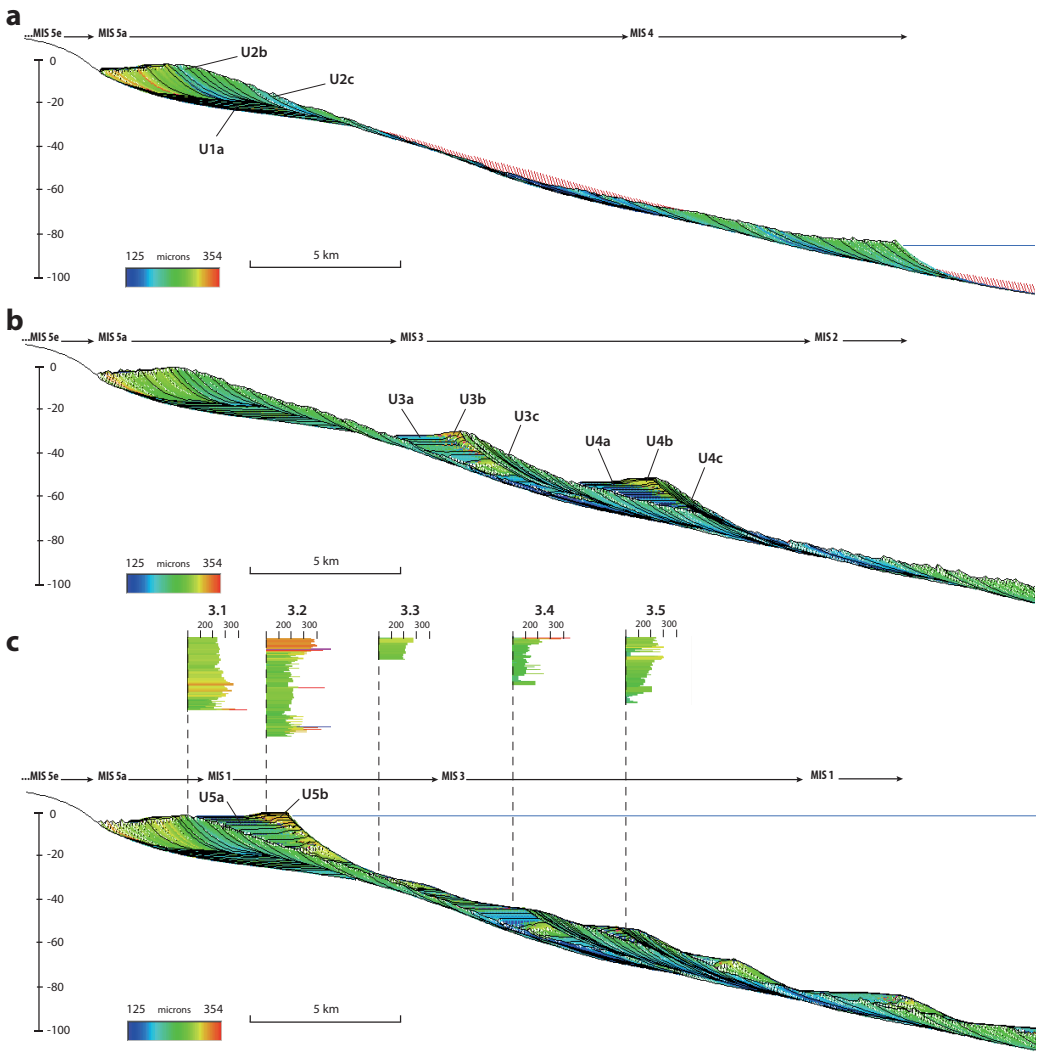

Figure 4.8: Simulated stratigraphy for last-glacial LG-M2 sea level at Tuncurry - Simulated coastal barrier deposition at Tuncurry over the last third-order sea level cycle using the Tuncurry BARSIM model and LG-M2 sea level curve. Modelled strata at (a) MIS 4 (70 ka BP), (b) MIS 2 (20 ka BP) and (c) MIS 1 (6 ka BP) are shown. Synthetic well logs show detailed stratigraphy at key locations of interest are for comparison with the interpreted vibrocores in Figure 2.18. The extents of barrier systems associated with each marine isotope stage are also indicated.

4.5 Discussion

Figure 4.9 shows that the simulated last-glacial depositional sequence of the LG-M2 model closely resembles the previous stratigraphic interpretation of the northern embayment [*Roy et al.*, 1997]. Both the stratal architecture and barrier stacking relationships compare well between the interpreted and simulated stratigraphy. Considering that the stratigraphic interpretation of the contemporary inner shelf is primarily based on seismic line FT-13 and vibrocores 13.1 to 13.10, that data is repeated in Figure 4.9 for reference. Excluding the subsequent deposition of the Holocene barrier after 6 ka BP (as seen in vibrocores 13.1 and 13.2), the simulated last-glacial sequence is consistent with the shallow-marine seismic and vibrocore datasets. For example, the mid-shelf embayment features a series of stacked forced-regressive strandplains, which overlie transgressed backbarrier-fill deposits comprising both coarse transgressive barrier facies and finer estuarine muddy sand facies. Coastal evolution observed in the LG-M2 model in response to varying depositional controls is used here to support and extend previous evolutionary reconstructions of the Forster-Tuncurry coastal barrier systems [*Roy et al.*, 1997], which were described in Chapter 2.

4.5.1 Last-glacial sea levels and coastal barrier deposition

The ages and elevations of coastal strandplain deposits of the northern embayment provide minimum constraints on relative sea levels at Forster-Tuncurry during late Quaternary sea-level highstands. The well-preserved stratigraphy of the northern embayment supports the LG-M2 sea level curve. Dated palaeo-shoreface deposits sampled from the Pleistocene composite strandplain imply that sea levels reached near-present elevations between 261-217, 147-131 and 94-79 ka. Accounting for dating error, these age groups roughly correspond to the MIS-7, MIS-5e and MIS-5a/MIS-5c interglacial sea-level highstands respectively [Fig. 4.5]. Elevated palaeo-shorefaces between 2-5 m PMSL within the suggested MIS-7 and MIS-5e western strandplain imply sea levels at the time of deposition at or slightly above present. This is consistent with the majority of recent sea level records [Sec. 4.2]. Although the younger Holocene beach ridges attain higher elevations between 5-8 m PMSL, the deeper position of the Pleistocene strandplains within the Tuncurry embayment (and thus wider and shallower nearshore zone prior to progradational fill) suggests that deposition may have occurred under

lower energy conditions due to higher attenuation of wave energy. Thus the relative elevations of Pleistocene beach ridges at the time of deposition may well have been a few meters lower than the Holocene ridges. Furthermore, chemical weathering and carbonate leaching may have contributed to a reduction in the sand volume of the Pleistocene strandplains.

Comparison of age and elevation data from the eastern Pleistocene strandplain with published sea level indicators favours deposition during MIS 5a. That is, although the error bars of the age data suggests that the deposits may be related to both MIS 5a and MIS 5c, the apparent tendency for the TL ages to slightly pre-date sea-level highstands suggests a preference for barrier deposition during MIS 5a, although this cannot be considered conclusive. The LG-M2 model demonstrated a mechanism by which strandplain deposition could occur during MIS 5a. However, the inferred MIS-5a sea levels are significantly higher than many existing sea level records [Fig. 4.5]. Elevated palaeo-shorefaces between -2 to 0 m PMSL within the eastern strandplain imply sea levels at the time of deposition between -3 to -5 m PMSL [*Roy et al.*, 1997]. Similarly, the ages and elevations of palaeo-shoreface deposits of the falling-stage coastal barrier systems suggest higher peak sea levels during MIS 3 than are observed in many published sea level records [Fig. 4.5]. Specifically, palaeo-shorefaces within the northern shelf embayment range from -30 to at least -60 m PMSL and date between 59-43 ka [Fig. 2.18]. Drowned barrier deposits of the steeper southern shelf embayment occupy similar depths and date to between 37-30 ka BP [Fig. 2.20]. Thus the drowned shelf barrier systems suggest that relative sea levels during the earlier and later stages of MIS 3 reached up to -32 m and -45 m PMSL at Forster-Tuncurry, which is about 10 m higher than estimated from most sea level indicators [Sec. 4.2].

The distribution of ages retrieved from the Pleistocene strandplains in the northern embayment [Tab. 2.2] suggests that barrier deposition was intermittent, involving multiple phases of deposition as sea levels fluctuated throughout the MIS-7 and MIS-5 interglacials. Considering the absence of notable stratigraphic variation between the suggested MIS-7, MIS-5e and MIS-5a strandplains, it also remains a possibility that each strandplain age component developed during multiple phases of highstand deposition. For example, *Bateman et al.* [2011] identified multiple phases of coastal barrier construction during MIS 7 and MIS 5 sea-level highstands within their investigation of the evolution of the Wilderness barrier systems of South Africa. They concluded

that the relatively steep shelf fronting the Wilderness barrier systems supported the formation of composite coastal barriers during rapid sea level fluctuations by compressing the zone of barrier migration. Accordingly, coastal barrier deposits associated with multiple MIS-5 sea-level highstands are both vertically and horizontally stacked within the Wilderness embayment.

Further to influencing the locations and elevations of highstand barrier deposition, the rate of sea level change at different stages during the last-glacial cycle controlled the volumes of barrier deposition and preservation across the shelf. Specifically, the best-preserved barrier systems that achieved the greatest volumes were deposited at times of briefly stable or slowly changing sea levels. For example, model findings show that the falling-stage shelf barrier systems predominantly formed during MIS-3 sea-level highstands, when rates of sea-level rise slowed and ultimately reversed [Fig. 4.8]. In contrast, reduced deposition occurred in the model when rates of sea level change accelerated during the rapid sea level fluctuations that intervened and followed. Thus rather than representing a continuous forced-regressive deposit, *sensu Posamentier and Morris* [2000], the falling-stage shelf barriers appear to have formed predominantly during MIS-3 interstadial highstands. The combination of both normal and forced regression has thereby resulted in a series of down-stepping barrier systems associated with progressively lower interstadial sea levels. This is consistent with evidence of thin intervening transgressive and backbarrier deposits in the seismic sections and cores (e.g. FT13.8 in Figure 4.9c), which were reproduced by the LG-M2 model (W3.5 in Figure 4.9b).

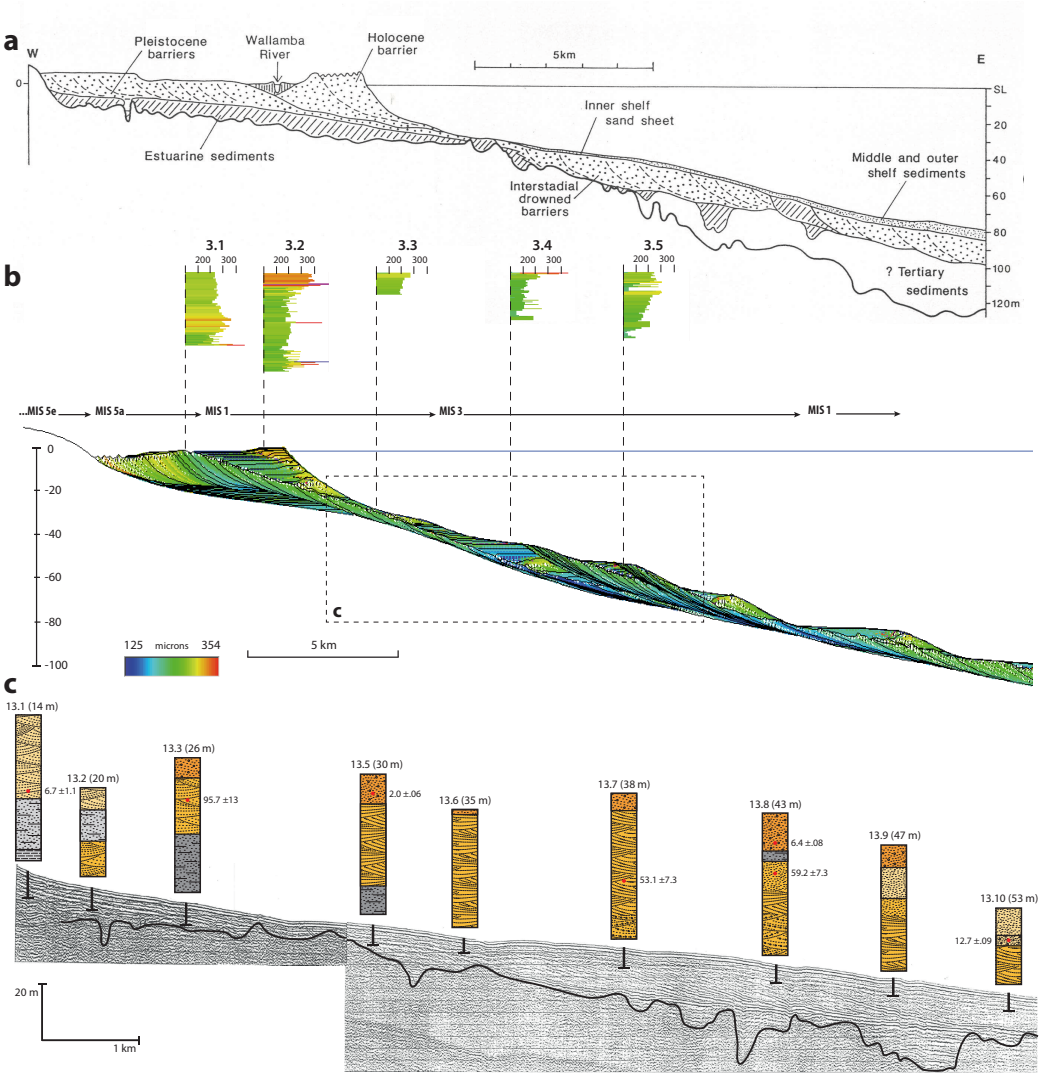

Figure 4.9: Interpreted and simulated last-glacial stratigraphy at Tuncurry - (a) Interpreted stratigraphy of the northern embayment from Roy et al. (1997) as shown in Figure 2.21, (b) simulated stratigraphy from the LG-M2 model as shown in Figure 4.8, and (c) shallow-marine seismic line FT13 with interpreted vibrocores as shown in Figure 2.18. The dashed box in (b) shows the approximate domain of the seismic profile in (c).

4.5.2 Transgression: barrier overstepping vs. barrier rollover

The absence of inter-barrier depressions or intervening transgressive or backbarrier facies between the MIS-7 and MIS-5e components of the western Pleistocene strandplain, and the MIS-5a eastern Pleistocene strandplain [Fig. 2.21], suggests an alternative mode of highstand barrier establishment compared to the Holocene barrier system. That is, the Holocene barrier system comprises a transgressive barrier core that accounts for about half (28 x 10^3 m^3/m) of the total barrier volume [Fig. 2.16]. The development and preservation of this transgressive barrier implies that prior to progradation of the Holocene strandplain during sea-level highstand, late transgression was characterised by the landward migration of a low-lying barrier system into the highstand embayment. This barrier rollover behaviour is illustrated in Figure 4.10d. The volume of the transgressive facies implies that the barrier experienced prolonged growth under rising sea levels [*Cowell et al.*, 1995] and thus was not overstepped by the shoreline during late transgression. The resultant stratigraphic relationship indicates that the transgressive barrier ultimately came to rest adjacent to and seaward of the antecedent MIS-5a strandplain [Fig. 4.9a]. This behaviour was captured in the LG-M2 model, where the MIS-1 transgressive barrier is separated from the earlier MIS-5a strandplain by transgressed backbarrier deposits [Fig. 4.9b]. The inter-fingering of backbarrier facies with the transgressive barrier as seen in the simulated stratigraphy is consistent with the observed barrier sedimentology that shows increasing estuarine influence at the landward end of the Holocene barrier [Fig. 2.16].

Further to being consistent with the Tuncurry site stratigraphy, the arrangement of the MIS-5a strandplain and MIS-1 transgressive barrier in the LG-M2 model [Fig. 4.9] reflects the horizontal stacking relationship of many other Holocene coastal barrier arrangements in southeastern Australia. For example, several coastal barrier systems that occupy the embayments between Newcastle and Seal Rocks to the immediate south of the study area feature similar Holocene-age outer barrier systems that are separated from Pleistocene-age inner barrier systems by inter-barrier topographic depressions [Sec. 2.4.2]. These inter-barrier depressions are similarly filled with Holocene backbarrier and transgressive barrier facies and are understood to have developed by the same means as the Tuncurry Holocene barrier [*Thom et al.*, 1981a; *Thom*, 1984]. The mode of barrier behaviour from which such stratigraphy emerges has been termed

barrier rollover, where shoreface erosion supplies shallow-marine sediments to back-barrier environments via wash-over and tidal inlet processes [*Leatherman*, 1983; *Swift et al.*, 1985; *Niedoroda et al.*, 1985b]. Therefore, it appears that transgression by barrier rollover was the dominant depositional mode of highstand barrier establishment during the Holocene.

In contrast, the stratigraphy of the Tuncurry Pleistocene strandplains suggests that shoreface progradation commenced instantaneously from the bedrock framework or relict surface of antecedent strandplain deposits upon flooding of the embayment at the onset of each highstand. If it is assumed that the rate of sea level change at the onset of the MIS-7 and MIS-5 sea-level highstands were comparable to the Holocene transgression, it seems reasonable to expect to find transgressive facies associated with barrier-rollover within the Pleistocene barrier systems. However, the stratigraphic record shows no such evidence of Pleistocene transgressive barrier facies [Sec. 2.7.3.1]. Rather, the LG-M2 model demonstrated an alternative barrier-overstepping mode of highstand barrier establishment, which resulted in a stratigraphic record consistent with the age structure and arrangement of coastal barrier deposits at Tuncurry [Fig. 4.9]. Figure 4.10c illustrates the simulated process of barrier-overstepping as it occurred during MIS 5a in the LG-M2 model. Specifically, a transgressive barrier (i) that stalled atop the antecedent MIS-5c highstand barrier (ii) at the embayment mouth was overstepped (iii) as MIS-5a sea level approached a peak of -3 m PMSL. Subsequently, strandplain progradation (iv) supplied by erosion of the overstepped bay-mouth barrier commenced from the head of the embayment. The absence of barrier overstepping within the highstand embayment in the LG-M1 model [Fig. 4.7] suggests that barrier overstepping is sensitive to both the rate of sea level change and antecedent topography.

Storms et al. [2008] used BARSIM to investigate coastal dynamics during rapid sea level change on the Italian northern Adriatic shelf. There they sampled drowned barrier island features that suggested barrier-overstepping occurred during the rapid Holocene post-glacial transgression. Their findings demonstrated that whilst the probability of barrier-island overstepping during transgression was inversely proportional to tidal amplitude (and thus rates of backbarrier deposition), complex substrate topography could cause an abrupt shift to disequilibrium depositional conditions during rapid sea-level rise, which could result in barrier-overstepping regardless of tidal conditions. Given

the open-ocean setting of the Forster-Tuncurry region and relatively uniform geometry of the shelf, palaeo-tidal amplitude during the last glacial period was most likely similar to present day and was maintained constant in simulations here. Rather, similar to the findings of *Storms et al.* [2008], barrier overstepping during MIS 5a was driven by the rapid expansion of backbarrier dimensions that occurred when sea level (and the transgressive barrier) breached the topographic inflection at the mouth of the highstand embayment. Upon overtopping of the composite MIS-5c bay-mouth barrier, backbarrier width in the model increased rapidly with rising sea level [Fig. 4.10c]. Due to the abrupt shift to disequilibrium conditions that followed, the width of the bay-mouth barrier could not be sustained, due to the low rates of fluvial sediment input to the backbarrier and the sequestration of shoreface sand through tidal inlets. Thus the bay-mouth barrier was drowned *in situ* and the shoreline (and location of barrier deposition) back-stepped to the head of the highstand embayment [Fig. 4.10c].

The review of highstand coastal barrier systems of southeastern Australia [Sec. 2.4] suggests that transgressive-barrier overstepping was not unique to Tuncurry, or to Pleistocene sea-level highstands. For example in the Port Stephens-Myall Lakes region immediately to the south of the Forster-Tuncurry region, a basal estuarine 'clay' unit similar to at Tuncurry underlies inner and outer barrier systems within a number of embayments [Fig. 2.9]. The clay unit reaches up to 50 m thickness in parts and contains up to five seismic discontinuities that represent a series of deposition/erosion cycles, most of which appear to predate MIS 5 [*Thom et al.*, 1981a, 1992]. Based on preserved barrier sands located beyond the toe of the modern shoreface (c. -40 m PMSL), *Roy and Crawford* [1980] hypothesised the existence of a proto-barrier located at the mouth of the Newcastle Bight embayment, which was proposed to have reformed during multiple Pleistocene sea-level highstands to support deposition of the thick basal clay unit [*Thom et al.*, 1981a]. Although the age structures of the Pleistocene-age inner barriers of those embayments are not known in detail, Uranium-series ages of 142-143 ka from corals found within the inner barrier [*Marshall and Thom*, 1976] suggest that deposition within the broad proto-estuary ceased during MIS-5. Therefore the evidence suggests that transgression into at least one MIS-5 highstand was likely characterised by the overstepping of an earlier bay-mouth barrier. Unlike at Tuncurry, the absence of pre-LIG age data makes it difficult to determine during which sea-level highstand barrier overstepping commenced.

Approximately 300 km to the south of Sydney, the Moruya Holocene barrier system appears to tell a different story. In a comparison of findings from drilling in several coastal barriers along the southeast Australian margin, [*Thom*, 1984] revealed that the deeply embayed Moruya compartment contains an extensive strandplain, which radiocarbon dates suggest is exclusively Holocene in age [Sec. 2.6]. Similar to the western Pleistocene strandplain of the northern embayment at Tuncurry, the Moruya strandplain is immediately abutted by the bedrock framework of the embayment. Beneath the regressive facies of the strandplain at the mouth of the Moruya embayment, a thin lens of transgressive barrier sands overlies a thick backbarrier lagoon-fill sequence. Thus Holocene strandplain deposition at Moruya appears to have commenced from the head of the embayment following *in situ* drowning of an antecedent bay-mouth barrier. Common to both examples is the provision of a deeply embayed and relatively shallow compartment that is breached by the sea during the latter stages of transgression. This suggests that the mode of highstand barrier initiation is controlled by antecedent topography.

The stratigraphic forward modelling carried out here suggests that the Holocene transgression may not have been exclusively characterised by the continuous landward migration of transgressive barrier systems by barrier rollover, but may have involved barrier overstepping as well. The last-glacial cycle simulations demonstrated that, although barrier rollover was the dominant depositional mode of late-transgression, earlier coastal barriers were overstepped during post-glacial sea-level rise across the continental shelf, where abrupt changes in substrate geometry associated with topographic inflections resulted in disequilibrium backbarrier dimensions [Fig. 4.10]. Such conditions were particularly prevalent on the lower mid to outer shelf where substrate gradients are lowest, and thus backbarrier dimensions and rates of barrier migration are greatest. For example, drowned transgressive barrier deposits containing mixed estuarine and shoreface facies preserved at -70 m and -80 m depth in the simulated sequence from the LG-M2 model [Fig. 4.8] represent the remnants of transgressive barriers that were overstepped during post-glacial sea-level rise.

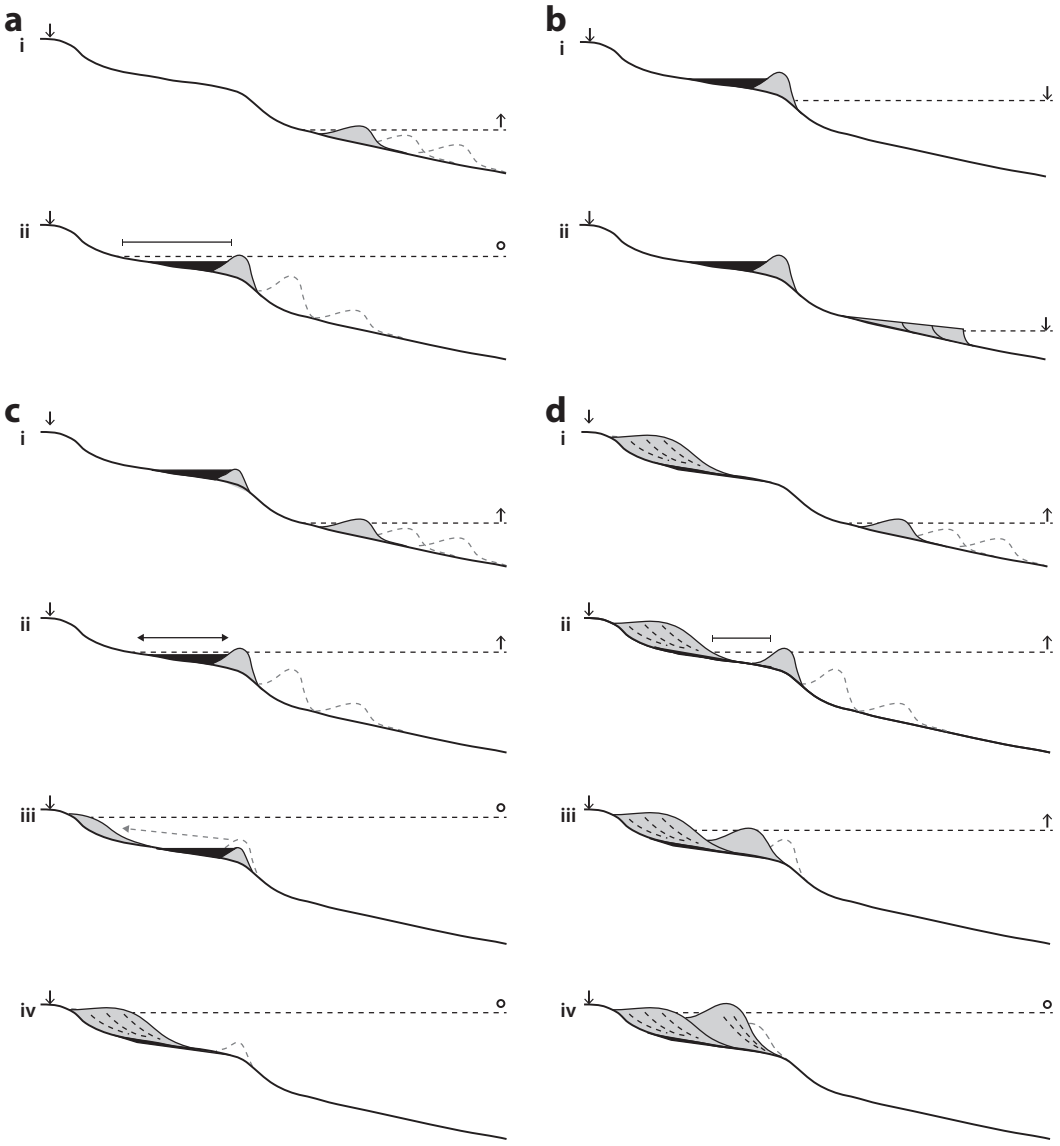

Figure 4.10: Highstand barrier establishment by transgressive-barrier overstepping and rollover - Continental subsidence and the direction of sea level change are indicated by arrows. (a) Prior to MIS 7 peak highstand relative sea levels were insufficient for barrier deposition to occur within present-day embayments. Rather, coastal barriers formed at the mouths of embayments, impounding broad lagoons that infilled with estuarine deposits. (b) During lower sea levels highstand barriers were abandoned as the shoreline migrated across the shelf. (c) Eventually, peak highstand sea levels were sufficient for the bay-mouth barrier systems to be overstepped during late transgression, due to the rapid expansion of backbarrier environments and low rates of coastal deposition. Transgressive-barrier overstepping caused instantaneous shoreline migration to embayment heads, where highstand strandplains were deposited. (d) During the late-Holocene transgression, the preserved highstand strandplains restricted backbarrier dimensions in semi-full compartments, allowing transgressive barriers to migrate into embayments by barrier rollover.

4.5.3 Shoreface response and onshore sand supply

The development and preservation of coastal barriers during the last-glacial cycle simulations was highly sensitive to the interaction between sea level and antecedent topography. Collectively, those depositional controls determined both the location of barrier formation and relative barrier growth during the various last-glacial sea level stages. In the LG-M2 model, coastal barrier systems associated with the MIS-5a, MIS-3 and MIS-1 interglacial and interstadial sea-level highstands were preserved [Fig. 4.8]. In contrast preserved deposits associated with rapidly changing sea level were limited to low-volume forced-regressive deposits and relict transgressive lags respectively [Fig. 4.8]. Considering the relatively uniform gradient of the Tuncurry shelf, and that autochthonous sand supply from shoreface reworking was the dominant sand supply in simulations, the models suggest that shoreface erosion volumes vary with the rate of sea level change. Specifically, sand supply volumes were only sufficient to support the deposition and preservation of significant coastal barrier systems during highstand stages, in which rates of sea level change slowed and reversed [Fig. 4.4].

Furthermore, the relative volumes of the barrier systems associated with each sea-level highstand varied. Simulated deposition of the comparatively large MIS-5a strandplain was supplied by high rates of onshore sand supply fuelled by shoreface reworking of the overstepped MIS-5c barrier system within the shallow highstand embayment. As demonstrated in Chapter 3, high rates of shoreface sand supply to the coast can be achieved whilst the shoreface sustains disequilibrium geometry due to the inheritance of a shallow substrate. The volume of the MIS-5a strandplain diminished with reduced rates of shoreface sand supply and resumed sea-level fall. Although rates of external sediment supply during the MIS-3 sea-level highstands were equivalent to MIS-5a, barrier volumes were much reduced [Fig. 4.8b]. Rather, backbarrier deposition dominated during transgressive-barrier rollover and increased in response to slowed rates of sea-level rise into the highstands. Given the deeper shoreface of the shelf embayment and the absence of an overstepped antecedent barrier, rates of shoreface erosion (and onshore sand supply) during highstand were comparatively lower than during MIS 5a. In a similar manner to the MIS-5a highstand, strandplain volumes diminished with the resumption of sea-level fall following each of the MIS-3 highstands [Fig. 4.8b].

Although the relationship between shoreface response and barrier deposition was investigated for stable and minor sea level change in Chapter 3, the shoreface response (and rates of autochthonous sand supply) remains to be explored for large-scale sea level change typical of the late Quaternary. The simulation findings presented in this chapter suggest that coastal deposition is limited during rapid sea level change, because net shoreface erosion volumes diminish for faster rates of sea level change. Reworking of the upper sections of antecedent deposits hints that upper shoreface erosion, at least, is maintained for the last-glacial rates of sea level change considered here. Rates of shoreface response are difficult to resolve in complex simulations featuring multiple depositional controls, each varying simultaneously, as for the simulation experiments described in this chapter. Thus outstanding questions regarding shoreface response to sea level change are addressed in Chapters 5 and 6 through a series of hypothetical simulation experiments using the Tuncurry and Moruya BARSIM models.

4.5.4 Potential for model dependence

No attempt was made to evaluate the sensitivity of simulated stratigraphy to the BARSIM model configuration in this chapter. Rather, it was assumed that the Tuncurry parameter values adopted and derived in Chapter 3 (including the erosion efficiency scaling exponent m) were appropriate for the model experiments described here. Given the limitations of the erosion efficiency calibration procedure (i.e. uncertain initial conditions, stable sea level), it is not likely that the model configuration provides the best representation of coastal dynamics for the range of boundary conditions (e.g. sea level change, external sand supply, antecedent substrates) considered in this chapter. As an extreme example, during lower sea levels, when the shoreline was located on the outer shelf plain, which is characterised by carbonate muds associated with highstand fall out, erosion efficiency undoubtedly varied. Here, the consideration of coastal barrier deposition within the highstand and inner-shelf embayments only, and the relatively uniform shelf slope, provides some confidence that the model configuration derived in Chapter 3 provides a reasonable approximation of late-Quaternary coastal dynamics. Other unknown variables, such as wave climate variation beyond what has been measured in historical records, was beyond the consideration of the model experiments presented here.

However, for the adopted model configuration, the model nonetheless demonstrates variability in coastal and shallow-marine deposition in response to dynamic boundary conditions. Whilst only the qualitative behaviour should be considered here given uncertainties in the model configuration, it is interesting that the relative volumes of the simulated coastal barrier deposits are reasonably consistent with the interpreted stratigraphy [e.g. Fig. 4.9]. At the least, this outcome provides additional confidence in the general reliability of qualitative model predictions.

4.6 Evolution of the coastal barrier systems at Forster-Tuncurry

The simulation findings presented above provide impetus for a revised model of coastal barrier evolution at Tuncurry. Although a site-specific evolutionary model is of no interest in the scientific quest for general principles, late-Quaternary coastal evolution at Tuncurry epitomises a range of depositional conditions in which alternative modes of coastal barrier development have emerged. That is, different highstand barrier stratigraphies and stacking relationships have arisen in response to varying depositional controls throughout the late Quaternary. Therefore the long record of coastal barrier evolution at Tuncurry may be used to demonstrate the influence of changing depositional controls on late-Quaternary coastal evolution in southeastern Australia. Study of the Tuncurry site has informed previous descriptions of general principles of coastal evolution [*Roy et al.*, 1994; *Cowell et al.*, 1995].

The evolution of the Tuncurry coastal barrier systems is revisited here, taking account of previous evidence [Sec. 2.7] and the findings of the simulation experiments described in Chapters 3 and 4. The previous evolutionary reconstructions of *Melville* [1984] and *Roy et al.* [1997] are revised and extended using the simulation findings. The evolutionary model of *Melville* [1984] can be found in Appendix D, whilst the updrift-sink model of *Roy et al.* [1997] has been described in Section 2.7.4. The focus remains on describing stratigraphic sensitivity to depositional controls, and the evolutionary model follows from the discussion of general principles in Section 4.5. The reconstruction focuses on the northern embayment where data is most abundant, although deposition in the southern embayment is considered where possible.

4.6.1 Middle Pleistocene

The oldest known coastal sand deposits at Forster-Tuncurry are tentatively interpreted as MIS 9 to MIS 8 in age [Tab. 2.2], and were retrieved from the Cape Hawke transgressive dune field [Fig. 2.13]. The dune sands pre-date all coastal barrier deposits within the region, which suggests that aeolian deposition was active prior to the development of coastal barriers within the highstand embayments, and the establishment of a highstand land connection between Cape Hawke and the mainland. The absence of coastal barrier deposits that pre-date MIS 7 in the northern highstand embayment may be explained using two fundamental controls on late Quaternary deposition: (1) the slow subsidence of the southeast Australian margin throughout the Quaternary; and (2) the preferential, and thus earlier, filling of updrift compartments by the northward littoral transport system.

First, passive margin subsidence associated with the post-extension phase of Tasman Sea formation has persisted throughout the Quaternary [*Lister et al.*, 1986; *Roy and Thom*, 1991]. This implies that for interglacial sea-level highstands where sea levels were at or near present, the elevation of shoreline during each successive highstand would be higher than on previous occasions. Second, the net northward transport of shallow-marine sands along the margin is considered to be a basic control on late Quaternary coastal deposition in southeastern Australia [*Roy and Thom*, 1981]. In the case of the Forster-Tuncurry region, a series of updrift southeast facing embayments between Newcastle and Seal Rocks [Fig. 2.8] acted as a significant trap for northward alongshore drift throughout the mid to late Pleistocene [*Thom et al.*, 1981a], thereby restricting coastal deposition north of Seal Rocks. Also, the deeper southern embayment houses a significant composite Pleistocene barrier (c. 70 x 10^3 m^3) that remains to be dated in detail. Therefore once relative sea levels were sufficient to flood the contemporary highstand embayments, coastal barrier deposition preferentially occurred in updrift embayments prior to the accumulation of substantial deposits within the northern embayment [*Roy and Thom*, 1981].

Prior to MIS 7 the northern highstand embayment was dominated by an extensive backbarrier estuarine system, which was impounded by earlier highstand barrier systems that developed near the mouth of the embayment. This kind of setting is demonstrated in Figure 4.10a, in which a highstand barrier develops near the mouth

of the embayment. Weathered and compacted backbarrier muds that predate coastal barrier deposition underlie the Pleistocene strandplains and Holocene barrier system of the northern embayment [Fig. 2.21]. The fine texture of the mud deposits suggest accumulation in the central region of a broad estuarine basin, as would have developed behind an earlier barrier located near the mouth of the present highstand embayment. Although *Roy et al.* [1997] depict an undifferentiated estuarine sediment unit underlying both the Pleistocene and Holocene barrier deposits [Fig. 4.9a], it is likely that multiple phases of estuarine deposition occurred within the embayment during successive sea-level highstands. That is, the setting depicted in Figure 4.10a was likely repeated during multiple pre-MIS-5 highstands, which may have been characterised by lower eustatic sea levels relative to the MIS 5 and Holocene interglacial stages [Fig. 4.2]. This also appears to have been the case in the Port Stephens-Myall Lakes region to the immediate south [Fig. 2.8], where a thicker undifferentiated mud unit underlies coastal barrier deposits [*Thom et al.*, 1992]. During lower sea level conditions the estuarine muds were subject to sub-aerial weathering whilst barrier deposition occurred across the contemporary shelf [Fig. 4.10b].

The ages of barrier deposits shown in Figure 4.5 suggests that deposition of the western Pleistocene strandplain began during MIS-7 sea-level highstands. By this stage ongoing margin subsidence and global sea levels permitted, under this reasoning, barrier deposition within the northern embayment. The western Pleistocene strandplain occupies a bay-head position where barrier sands dating to MIS 7 [Tab. 2.2] onlap bedrock in the central section of the embayment. The error bars of the ages from these earliest barrier deposits do not allow for the isolation of strandplain initiation to any particular sea-level highstand, and perhaps suggest multiple phases of deposition. The onlapping relationship between regressive barrier sands and bedrock at the embayment head implies that backbarrier deposition was absent there, most likely having been restricted to narrow drainage valleys at the head of the embayment and the Wallamba and Wallingat palaeo-river valleys. Thus deposition of the western Pleistocene strandplain appears to have begun in a similar manner to the simulated deposition of the MIS-5a strandplain in the LG-M2 model, which is illustrated in Figure 4.10c. That is, the simulated overstepping of an antecedent barrier nearer to the embayment mouth caused an instantaneous shoreline migration to the embayment head, which was followed by strandplain progradation supplied by shoreface reworking of the antecedent barrier. Prior to MIS

5 tidal delta deposition likely dominated within the deeper southern embayment, with coastal barriers restricted to the bedrock topographic high between Cape Hawke and Green Point, thereby permitting deposition of the Cape Hawke dune field [Fig. 2.13].

4.6.2 Late Pleistocene

4.6.2.1 MIS 5e

The second age group of regressive barrier sands from the western Pleistocene strandplain date to between 131-147 ka [Tab. 2.2]. These deposits are interpreted to be associated with the MIS 5e sea-level highstand [Fig. 4.5]. The interface between MIS 7 and MIS 5e regressive barrier sands is not readily discernible in the GPR profile from the central section of the strandplain and heavy mineral mining across this section of the strandplain may have disturbed the upper section of the profile [Fig. 2.15]. Furthermore, similar to the MIS-7 barrier sands there is no evidence of backbarrier deposition associated with the MIS-5e barrier sands. It is therefore proposed that strandplain deposition recommenced within the northern highstand embayment during MIS 5e from the relict front of the MIS-7 strandplain. Barrier progradation continued for up to 1.5 km throughout MIS 5e. Deposition appears to have been more widespread alongshore during MIS 5e, with parts of the barrier developing around the mouths of the Wallamba and Wallingat Rivers, and several mainland beaches forming throughout the Forster-Tuncurry region [Fig. 2.13].

Deposition in the southern embayment during MIS 5e is less constrained. However, it is likely that the Wallis Lake barrier was initiated in the northern half of the embayment during this stage, reaching part of the way between Cape Hawke and Booti Hill [Fig. 2.13]. The alongshore extent of the barrier was most likely limited by both the variable bedrock topography and accommodation surplus within the southern embayment. That is, bedrock islands formed by Cape Hawke and Green Point provided a supporting framework for the barrier within the shallow northern half of the embayment. However, an opening to the ocean near the southern end of the embayment was most likely maintained due to only partial infilling of the deeply incised (c. -50 to -60 m PMSL) palaeo-river channels at that time, which drained the valleys during lower sea levels prior to MIS 5a. Thus the southern half of the embayment probably featured tidal delta complexes throughout MIS 5e. Considering the similar sea level curves of

the MIS-5e and Holocene interglacial phases, and global evidence for MIS-6 interstadial sea-level highstands similar to MIS 3 [Fig. 4.5], presumably the general distribution of shelf deposits at Forster-Tuncurry was comparable to the present situation. That is, falling-stage barrier systems may have partially filled mid-shelf palaeo-embayments, and a shelf sand body may have developed along the steeper inner shelf south of Cape Hawke during the latter stages of transgression.

4.6.2.2 MIS 5c

Significant coastal barrier systems developed within the northern and southern highstand embayments between the MIS-5e and Holocene interglacial sea-level highstands [Fig. 4.5]. Global sea level records imply that during this time sea level reached sufficient heights to penetrate the embayments only during MIS 5c and MIS 5a [Fig. 4.1]. The LG-M2 model suggests that the northern embayment MIS-5c highstand barrier developed near the mouth of the embayment, where it impounded a broad estuary in which backbarrier fill accumulated [Fig. 4.10a]. The MIS-5c barrier system was subsequently abandoned during sea-level fall into MIS 5b [Fig. 4.10b]. Barrier deposition appears to have extended along the full length of the southern embayment during MIS 5c. Drill hole DH4 contains a series of vertically stacked barrier and backbarrier deposits [Fig. 2.14]. At the base of the drill hole, barrier sands dating to 96.5 $\pm$ 12.2 ka overlie tidal channel fill dating to 115 $\pm$ 15 ka. Thus it appears that the lower barrier system in DH4 may have developed during MIS 5c, in which case the deeper southern section of the southern embayment would have been partially infilled with barrier deposits.

4.6.2.3 MIS 5a

The stratigraphy and distribution of ages from the eastern Pleistocene strandplain favour deposition during MIS 5a. Specifically, the eastern Pleistocene strandplain is composed of regressive barrier sands that date between 94-79 ka, which form a low strandplain between MIS 5e and Holocene coastal barrier deposits. As for the western composite strandplain, there is no stratigraphic evidence of backbarrier deposition associated with the eastern strandplain [Fig. 2.15]. Rather, it appears that progradation commenced from the relict front of the antecedent MIS-5e strandplain. Furthermore the LG-M2 model has shown that establishment of the eastern Pleistocene strandplain

during MIS 5a without transgressive deposition could occur where an antecedent bay-mouth barrier associated with lower MIS-5c sea levels is overstepped by the shoreline during sea-level rise into MIS 5a [Fig. 4.10c]. Thus it is proposed that deposition of the eastern Pleistocene strandplain occurred as was demonstrated in the LG-M2 model [Fig. 4.8]. Shoreline progradation during this phase in response to the deposition of about 26 x 10^3 m^3 of sand extended the strandplain up to 3 km further seaward.

Complete infilling of the southern embayment palaeo-river channels during MIS 5a allowed the contemporary barrier system to form, spanning the length of the embayment between Cape Hawke and Booti Hill. By this time the southern embayment palaeo-river channels were no longer in use. Drill hole DH4 penetrated one such palaeo-river channel, where two vertically stacked barriers overlie tidal channel fill deposits [Fig. 2.14]. The upper barrier sands date to 87 $\pm$ 8.6 ka and suggest that deposition of the Wallis Lake barrier was completed during MIS 5a. It is proposed that following abandonment during MIS 5b, the MIS 5c barrier was overtopped during MIS 5a, at which time the upper barrier accumulated atop. The southern half of the barrier is therefore inferred to be a separate feature composed of vertically stacked MIS-5c and MIS-5a barrier systems, which is distinct from the northern half that developed during MIS 7 and MIS 5. The total volume of the southern embayment barrier sands is estimated at 67 x 10^3 m^3 [*Roy et al.*, 1997].

Considering the relatively high elevations of the MIS 5d and 5b sea level lowstands [Fig. 4.4], many significant bedrock promontories updrift from the Forster-Tuncurry region would have remained influential throughout MIS 5. Thus it is likely that the sources of MIS 5c and MIS 5a barrier deposition within both embayments were within the region. Specifically, it was proposed by *Roy et al.* [1994] that during the sea-level fall that followed the MIS 5e interglacial, the erosion of shelf sand bodies that had established south from Cape Hawke released significant sediment volumes into the littoral transport system, which represent the majority contribution to barrier deposition in the coastal embayments during MIS 5c and 5a. This has been proposed to also explain the mineral deficient composition of the eastern Pleistocene strandplain in the northern embayment relative to MIS 7 and MIS 5e barrier sands [*Roy et al.*, 1997]. Specifically, these sources were already stripped of heavy minerals during prior sea level fluctuations.

4.6.2.4 MIS 3

Global sea levels during MIS 3 may have been characterised by a number of oscillations in which peak sea levels during successive interstadial highstands were progressively lower [Sec. 4.2]. Sea levels below -30 m PMSL left the highstand embayments in which MIS-7 and MIS-5 barrier deposition occurred stranded. Rather, coastal barrier deposition was focused on the contemporary inner-mid shelf, where falling-stage coastal barriers developed within mid-shelf embayments where the bedrock framework supported the accumulation of sediments. Following the impoundment of Wallis Lake due to completion of the southern embayment barrier during MIS 5a, the southern embayment drainage channels were no longer available to coastal rivers and streams during the lower sea levels of the last glacial period. In response to the altered conditions, the Wallingat River appears to have cut a more direct path through the northern composite strandplain, separating Wallis Island from the central part of the barrier [*Melville*, 1984]. During this time drainage of the southern embayment likely proceeded via the original Wallingat River mouth between Wallis Island and the then Cape Hawke tombolo.

In the northern mid-shelf embayment, the ages and elevations of the well-preserved falling-stage barrier systems suggest deposition during the first half of MIS 3 (i.e. 43-59 ka), although additional falling-stage deposits lower on the shelf are yet to be dated. As in the LG-M2 model, deposition of the first MIS-3 falling-stage barrier was preceded by significant highstand backbarrier deposition, which occurred around the interface between the highstand and mid-shelf embayment (-30 m and -40 m PMSL). This deposit has been sampled at the bases of FT13.3 and FT13.4 [Fig. 4.9c]. The arrangement of palaeo-shoreface reflectors within the falling-stage barriers show evidence of both normal and forced regression i.e. the overall down-stepping arrangement of strandplain deposits is interspersed with series of horizontally-stacked reflectors [Fig. 4.9c]. Furthermore, backbarrier fill between some reflector sets (e.g. vibrocore 13.8) suggests periods of stable or slowly rising sea levels. This evidence supports intermittent phases of transgressive and highstand barrier deposition during interstadial sea level conditions, within an overall falling sea-level trend. Age data from the deeper southern embayment falling-stage barriers suggest deposition during the second half of MIS 3 (30-37 ka BP). The preservation of only lower shoreface facies there suggests that any

earlier MIS 3 barriers that occupied higher elevations may have been entirely reworked during MIS-1 transgression.

Rather than continuous forced-regressive deposits therefore, the falling-stage barriers were deposited in multiple phases, each associated with separate MIS-3 highstands. Due to the temporal resolution of the model only two representative MIS-3 oscillations were considered in the simulations [Fig. 4.4]. Thus although the models depict representative falling-stage barrier systems, it unlikely that the full complexity of MIS-3 deposition has been simulated. That is, considering the nature of MIS-3 sea level fluctuations suggested by the records in Figure 4.4, the MIS-3ii and MIS-3i model sea-level highstands alone are expected to generate a simpler stratigraphic response than reality. The uncertainties surrounding MIS-3 sea level oscillations have been discussed in Section 2. The interpretation of *Roy et al.* [1997] shows two forced-regressive strandplain deposits occurring between -30 m to -60 m and -60 m to -80 m PMSL [Fig. 4.9a]. The stratigraphy of the upper barrier system can be seen in seismic line FT13 in Figure 4.9c. The sensitivity of coastal barrier deposition to MIS-3 sea level change is considered in further detail in Section 6.3. From that more detailed analysis, it can be concluded that the simulated MIS-3 stratigraphy in Figure 4.9b is representative of the upper falling-stage barrier system, whilst the lower barrier system would feature similar stratigraphic architecture had it been captured in the LG-M2 model.

Roy et al. [1997] proposed that deposition of the MIS-3 falling-stage coastal barrier systems involved a strong interaction with other depositional features of the Forster-Tuncurry region. For example, deposition of the northern embayment falling-stage barriers appears to have been augmented by the concurrent erosion of antecedent shelf sand bodies on the steeper updrift coast south of Cape Hawke. Prior to MIS 3 it is likely that an MIS-5 shelf sand body was partially reworked and redeposited during the rapid MIS 5c and MIS 5a sea level fluctuations. In response to more steady rates of sea-level fall during MIS 3 however, complete erosion of the shelf sand bodies would have released significant sediment volumes into the littoral transport system. Although *Cowell et al.* [1995] demonstrated that the volume of the falling-stage barrier deposits could have been mostly supplied by shoreface reworking of antecedent falling-stage barrier systems, it is likely that both concurrent erosion of the shelf sand bodies and reworking of the antecedent shelf substrate supplied the deposition of the falling-stage barrier systems. Thus the LG-M2 model would be improved by the inclusion of both

additional MIS-3 sea level oscillations and higher rates of external sediment supply to the northern mid-shelf embayment.

4.6.3 Holocene

4.6.3.1 Post-glacial transgression

Sea levels during the last glacial maximum (c. -130 m PMSL) imply that the Forster-Tuncurry coastline would have been located near the continental-shelf break, where the relatively continuous sandy coast would have been dominated by strong northward alongshore sediment transport [*Roy and Thom*, 1981]. As sea level rose through the post-glacial transgression however, northward sediment transport would have become increasingly interrupted as the coastline encountered bedrock outcrops at inner to mid shelf depths that project seawards from the contemporary headlands. Once sea level reached -60 m, the northern and southern embayments would have been divided into separate sedimentary compartments. At this time, growth of the Seal Rocks transgressive dune field and the deposition of the contemporary shelf sand body between Seal Rocks and Cape Hawke would have represented significant sinks in the alongshore transport system [*Roy et al.*, 1997].

Barrier deposition during the rapid sea-level rise was limited to the development and intermittent abandonment of transgressive barrier systems. The simulated strata of the LG-M2 model shows the remnants of overstepped transgressive barriers at about -60 m and -80 m PMSL, which appear as convex deposits of coarser barrier sands and backbarrier fill. The barrier remnants are found where the antecedent substrate steepened toward the MIS-3 falling-stage barriers [Fig. 4.9]. Higher up the shelf the upper sections of the MIS-3 falling-stage barriers were reworked. Sediment budget deficits in both the northern and southern embayments caused by the preferential filling of updrift compartments and transgressive shelf sand body growth had implications for the preservation of earlier barrier systems. It is estimated from previous computer modelling that the falling-stage shelf barriers of the northern embayment were lowered between 3-5 m by shoreface erosion during passage of the transgressive barrier [*Cowell et al.*, 1995]. A similar pattern of reworking is demonstrated in the LG-M2 model [Fig. 4.9b]. This process would have fueled the growth of the transgressive barrier sand body, which is estimated to have ultimately reached 28 x 10^6 m^3/m in volume.

The coarse inner-shelf sands that bury the MIS 3 falling-stage barriers between 20-50 m water depth [Fig. 4.9a] has been proposed to represent a lag deposit resulting from shoreface reworking during transgression [*Roy et al.*, 1997]. Evidence of transgressive lag deposits is found in the LG-M2 model in both the remnant overstepped barrier deposits and the occurrence of thin coarse-grained sand deposits across the inner shelf, such as at the top of W3.4 [Fig. 4.8c]. The preservation of only lower shoreface deposits in the southern embayment suggests that shoreface erosion during transgression was enhanced there, which was likely associated with the steeper substrate gradients encountered by the transgressing coastline as it approached the antecedent composite Pleistocene highstand barrier system [*Roy et al.*, 1994].

4.6.3.2 Highstand

At the termination of post-glacial sea-level rise the transgressive barrier stabilised seaward of the MIS 5a strandplain, with the two barriers being separated by the MIS-1 late-transgression backbarrier fill [Fig. 4.9]. Mid- to late-Holocene deposition within the northern embayment was investigated in detail in Chapter 3, and only a brief account is provided here for completeness. Rapid deposition of the shelf sand body between 6-4 ka BP suggests that the northern embayment experienced a stable or deficit sediment budget during that period, and inner shelf lowering was the dominant source of strandplain progradation [Sec. 3.5.1.1]. By 4 ka BP the surface of the shelf sand body appears to have aggraded to a sufficient depth to allow headland bypassing of sand around Cape Hawke and into the embayment. Initially however, the majority of sand supplied by alongshore transport was sequestered into Wallis Lake, as evidenced by the rapid formation of the flood-tide delta between 4-2 ka BP [*Roy et al.*, 1997]. By 2 ka BP the Wallis Lake flood-tide delta appears to have reached equilibrium with the tidal amplitude and basin dimensions, and thus alongshore supply to the northern highstand embayment resumed. The simulation findings demonstrate that given diminishing rates of shoreface sand supply from inner shelf lowering, sometime after 2 ka BP the headland bypassing of sediments around Cape Hawke surpassed inner shelf lowering as the dominant source of strandplain progradation [Fig. 3.8].

4.7 Conclusions

This chapter has investigated the deposition and preservation of last-glacial coastal barrier systems at Tuncurry using the BARSIM numerical stratigraphic model. The simulated stacking relationships and depositional architecture of the diverse highstand barrier systems were shown to be consistent with previous stratigraphic interpretations of the geological record. Coastal barrier deposition was found to be highly sensitive to last-glacial sea-level change, with a modified relative sea level curve required to achieve simulated stratigraphy consistent with the observed depositional record. The modified sea level curve featured MIS-5a and MIS-3 peak sea level between 10-15 m higher than indicated by many existing sea level records, which is consistent with the arrangement of dated palaeo-shoreface deposits at Tuncurry. However, the modified curve is consistent with a growing body of evidence that suggests the potential for higher than traditionally accepted sea levels at intermediate- to far-field sites during those particular stages.

The varying stratigraphy between the Pleistocene strandplains and Holocene barrier system were suggested to have emerged from alternative transgressive-barrier behaviours. The interaction between antecedent topography and sea-level rise appears to control the relationship between barrier volume and backbarrier dimensions, which supported barrier overstepping and barrier rollover at different sea level stages. The following general conclusions are drawn from the outcomes of the simulation experiments:

1. The development of composite coastal strandplains (e.g. as suggested by the age structures of the Tuncurry Pleistocene strandplains) associated with successive interglacial sea-level highstands appears to be possible without the preservation of related transgressive and backbarrier deposits.

2. Transgressive-barrier overstepping is one mechanism that supports cyclical coastal strandplain progradation without the preservation of transgressive-barrier and backbarrier deposits. At Tuncurry for example, the simulated flooding of the highstand embayment by sea-level rise into MIS 5a resulted in the overstepping of a bay-mouth transgressive barrier, and the switching of sub-aerial coastal deposition to the strandplain at the head of the highstand embayment. For rapid

sea-level rise typical of late-Quaternary transgression, barrier-overstepping may be caused by topographic inflections that support the rapid expansion of back-barrier dimensions.

3. Continuous transgressive-barrier rollover favours the development and preservation of transgressive and backbarrier facies within highstand coastal barrier systems. At Tuncurry for example, simulated coastal barrier evolution during mid-Holocene transgression was characterised by barrier-rollover behaviour, and thus the preservation of a transgressive barrier in the highstand embayment. For rapid sea-level rise typical of late-Quaternary transgression, continuous barrier rollover is supported by consistent substrate geometry and an adequate sediment supply.

4. Shoreface sand supply may play a critical role in coastal barrier evolution, particularly in autochthonous settings. The varying development of coastal barriers throughout the last-glacial simulations suggests that rates of onshore sand supply from shoreface erosion appear to be correlated with rates of sea level change. The findings suggest that active shoreface response varies significantly for rates of sea level change typical of late-Quaternary coastal evolution.

5. The distribution and elevations of dated coastal barrier deposits at Tuncurry, and the sensitivity of simulated coastal barrier evolution to the sea level histories considered, suggest that MIS-5a and MIS-3 sea levels in southeastern Australia may have been near-PMSL and approximately -30 m PMSL respectively, which is higher than indicated by many existing sea level records that have been derived from continuous indirect records and relative sea level indicators [Sec. 4.2].

The findings of the simulation experiments described in this chapter provide further motivation for the detailed investigations of sea level change and shoreface response in Chapters 5 and 6. Furthermore, the relationship between shoreface response and MIS-3 falling-stage barrier deposition at Tuncurry is considered in detail in Section 6.3.

4. ORIGINS AND CONTROLS OF STACKED COASTAL BARRIER SYSTEMS: LESSONS FROM NUMERICAL EXPERIMENTS AT FORSTER-TUNCURRY

5

Shoreface Response to Sea Level Change 1: Concepts

5.1 Introduction

5.1.1 Background

Although it has been suggested that the rate of sea-level change regulates the potential for wave processes to shape the shoreface surface, and thus generate reworked sediment volumes for coastal deposition [*Roy et al.*, 1994], little remains known about the influence of sea-level change on shoreface geometry [*Pilkey et al.*, 1993; *Thieler et al.*, 2000]. That is, further to controlling the rate of cross-shelf migration of the shoreface domain, the rate of sea-level change may also determine shoreface shape and dimensions, by controlling morphodynamic disequilibrium in the context of the inherited substrate. In the absence of a significant external sediment supply, the nature of shoreface disequilibrium is a primary control on shoreline migration, coastal evolution and stratigraphic preservation, because it determines the reworked ('autochthonous', after *Swift and Thorne* [1991]) sediment budget [*Storms et al.*, 2002; *Tortora et al.*, 2009a]. Considering the order-of-magnitude difference between upper and lower shoreface morphological relaxation timescales [*Stive and de Vriend*, 1995; *Cowell et al.*, 2003a], it stands to reason that disequilibrium-induced shoreface response is an important consideration for rates of sea-level change characteristic of late-Quaternary coastal evolution and potential future coastal response to climate change. Constraining shoreface response to sea-level change therefore, may provide an opportunity to improve the reliability of predictive

models that apply shoreface surface behaviour to solve for coastal evolution and shoreline migration.

At this point, a more detailed understanding of shoreface concepts is required to establish and examine the research questions of this chapter. In Section 5.2, existing shoreface definitions are reviewed in the context of depth-varying shoreface 'activity'. *Stive and de Vriend* [1995] coined the term 'active zone' to describe the shoreface area that satisfies the condition of time-invariant geometric behaviour for the setting and forcing scenario of interest. This can be differentiated from the remainder of the shoreface, which might be expected to be characterised by depth-dependent (hereafter h-dependent) shoreface response. The conceptual approach of *Stive and de Vriend* [1995] is adopted here as it provides a useful basis for exploring the relationship between shoreface response and sea-level change. The key shoreface domains considered here are defined by the upper-shoreface limiting depth (h_c), active-shoreface limiting depth (h_a), lower-shoreface limiting depth (h_i) and wave base (h_w). The nature of, and relationships between, these depth- and time-dependent domains are further described in Section 5.2.

5.1.2 Aims

The aim of this chapter is to explore the relationships between the rate of sea-level change (R), shoreface kinematic behaviour, and barrier-coast evolution, using a series of hypothetical model experiments that are based on the simulated evolution of the Tuncurry coastal barrier systems documented in Chapters 3 and 4. The overall objectives of the experimental design are to demonstrate and quantify the sensitivity of active shoreface extent and depth-dependent lower shoreface responses to the range of R typical of late-Quaternary coastal evolution and projected future sea-level rise. More specifically, the following questions are considered:

1. What range of variation in the active shoreface limiting depth (h_a) should be expected for the range of R typical of late-Quaternary coastal evolution and projected future sea-level rise?

2. For a typical value of R, is h_a sensitive to between-site variations in shelf gradient and complexity, and shoreface morphodynamic efficiency?

3. Are depth-diminshing (i.e. h-dependent) rates of shoreface response between h_a and wave base (h_w) sensitive to R?

4. For a typical value of R, is h-dependent shoreface response sensitive to between-site variations in shelf gradient and complexity, and shoreface morphodynamic efficiency?

5. What do the relationships between R, h_a, and h-dependent shoreface response suggested by the simulations imply regarding the evolution of shoreface geometry during sea-level change?

6. If the assumption of time-invariant shoreface geometry is restricted to the active shoreface domain [Sec. 5.2.3], does h-dependent shoreface response beyond h_a constitute significant and unaccounted for volume exchanges (for the timescales typical of late-Quaternary and future coastal change problems) in the context of geometric-equilibrium models?

The chapter begins with a concise review of shoreface concepts and definitions to establish the theoretical paradigms in which the experimental design is founded [Sec. 5.2]. These concepts are later reviewed in the context of the findings from simulation experiments, with revisions proposed to incorporate the implications of shoreface response to sea-level change for coastal evolution, shoreline migration, and stratigraphic preservation in shallow-marine depositional systems.

5.2 Shoreface definitions

The fundamental role of the shoreface in controlling coastal evolution in response to system forcing was briefly introduced in Section 1.1. Furthermore, the proposed dependence of shoreface response on the relationship between morphological relaxation (T_r) and system forcing timescales (T_f) was described in Section 1.3.3. In this chapter the ideas are quantitatively examined using the stratigraphic modelling approach. However, the quantitative investigation of shoreface response to sea-level change first requires a more detailed review of shoreface concepts to establish the status and limits of the present knowledge base. This will enable the consideration of R-dependent shoreface response within the context of the present theoretical framework.

5. SHOREFACE RESPONSE TO SEA LEVEL CHANGE 1: CONCEPTS

Beginning with *Johnson* [1919], numerous definitions of the shoreface depositional feature have been proposed from the study of coastal processes and evolution across various timescales of observation and interest. As a point of confusion, different authors from related disciplines have presented various ideas on the relationship between the shoreface and other coastal depositional environments, such as the surf zone and inner-continental shelf. For example, *Cowell et al.* [1999] note that *Niedoroda et al.* [1985b] and *Niedoroda and Swift* [1991] defined the shoreface as occurring between the surf zone and inner-continental shelf, whilst *Wright* [1995] regarded the shoreface as being synonymous with the inner-continental shelf. *Cowell et al.* [1999] reviewed shoreface definitions in the context of coastal morphodynamics theory [*Wright and Thom*, 1977; *Cowell and Thom*, 1994], focusing on the relationship between morphological behaviour and scale for timescales spanning days through millennia. Considering that the primary lines of enquiry in this chapter emerged from their conclusions, the morphodynamics definition of the shoreface is a natural starting point to address the questions under investigation here.

Thus the term shoreface herein refers to coastal domain spanning from the limit of wave runup on the beach face, seaward to the limiting depth of the effective influence of gravity waves in shaping seabed morphology [Fig. 5.1]. The shoreface morphodynamic domain comprises:

1. the upper shoreface, which extends from the limit of wave runup to a point somewhere beyond the surf zone where surface response rates (due to cross-shore sediment transport) become too gradual to support profile adjustment in response to annual wave climate variability, and

2. the lower shoreface, which extends from the limiting depth of the upper shoreface to a point beyond which cross-shore sediment exchanges are insignificant at the timescale of interest, where profile response rates progressively diminish toward wavebase.

The upper and lower shoreface definitions are necessarily vague to accommodate the diverse variety of settings in which the shoreface feature occurs, and the range of timescales of relevance to coastal evolution. The distinction between upper and lower

shoreface processes and timescales is discussed in further detail below, using the coastal-tract concept [*Cowell et al.*, 2003a,b] as a conceptual framework to understand process-morphology interactions across the relevant timescales. Furthermore, the 'active shoreface' and its relationship to morphodynamic scale are formally introduced.

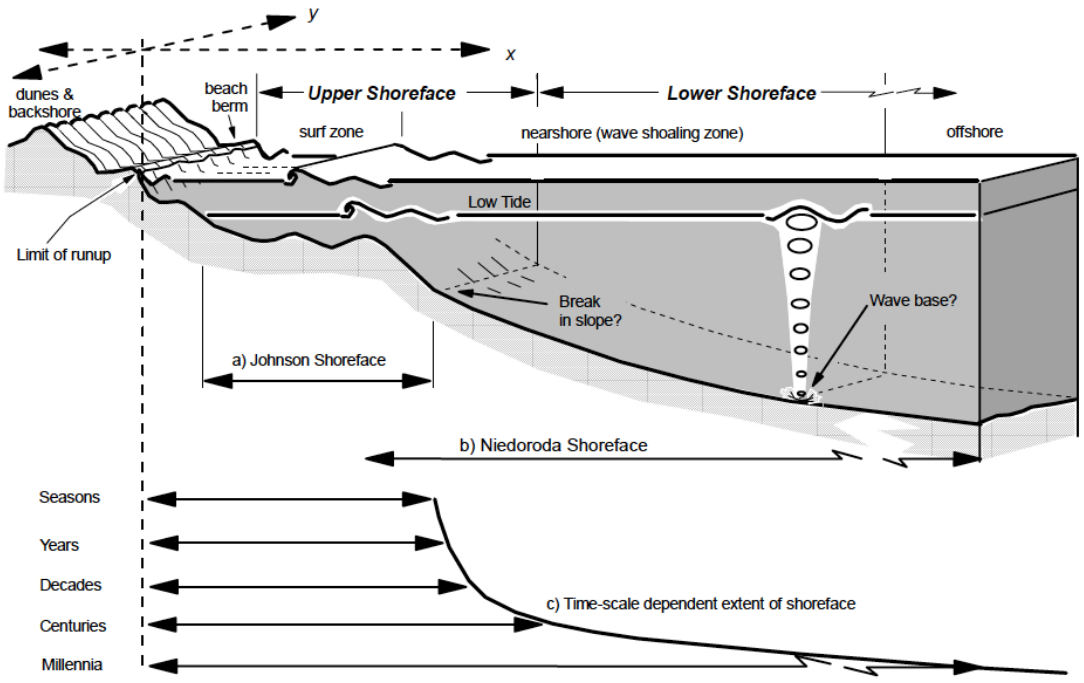

Figure 5.1: Morphodynamic definition of the shoreface - The shoreface as defined by *Cowell et al.* [1999] spans from the limit of wave runup to the effective limit of gravity-wave influence on seabed morphology. The surf zone is considered to be a nested morphological element within the upper shoreface domain. Lower shoreface response timescales increase with depth.

5.2.1 Upper shoreface

Consistent with the inverse relationship between water depth and wave-driven sediment entrainment and transport capacities, long-term shoreface survey datasets indicate that for annual to multi-year timescales vertical surface adjustments diminish across the upper shoreface with increased depth [*Birkemeier*, 1985; *Nicholls et al.*, 1998]. Therefore the seaward limit of the upper shoreface (h_c) is typically defined as the depth beyond which vertical surface adjustment due to wave agitation does not exceed a fixed-magnitude limit at measurement timescales. The specification of such a limit may be

used to constrain cross-shore sediment budgets and thereby provides the opportunity to investigate coastal evolution and shoreline migration using sediment-mass conservation principles. Accordingly, the collective colloquialism for upper shoreface depth limits is the 'depth of closure' (or 'closure depth'), which describes the depth beyond which cross-shore sediment exchanges are assumed to be negligible for *annual* timescales.

Under the above definition the surf zone represents a morphological element where surface response occurs at event timescales, which is nested within the upper-shoreface morphological unit, where surface response takes place at between event to annual timescales [*Cowell et al.*, 2003a]. Therefore h_c typically occurs at a point somewhere beyond the modal surf zone [Fig. 5.2]. Measured h_c is likely to vary between years due to inter-annual wave climate variability and the impacts of extreme events on upper shoreface profile geometry, and thus multi-decadal survey data may be required to reliably resolve the upper shoreface depth limit. Considering the scarcity of long-term survey datasets however, a relationship between h_c and mean wave climate is appealing. For example, *Hallermeier* [1981] proposed a 0.3 m fixed-magnitude limit of surface adjustment as a pragmatic measure of the inner shoal zone depth limit (d_l) for a typical year. Advancing that concept, Hallermeier also identified an analytical relationship between wave climate and d_l, which allowed prediction of the inner shoal zone limit for quartz sand in seawater using only wave climate statistics:

$$d_l = 2.28H_{sig} - 68.5\frac{H_{sig}^2}{gT_{sig}^2} \tag{5.1}$$

In Equation 5.1, H_{sig} and T_{sig} represent local (i.e. nearshore) significant wave height and significant wave period respectively. Due to the limited availability of such data however, Hallermeier also proposed the following approximation for d_l:

$$d_l \cong 2H_{sig} + 11\sigma \tag{5.2}$$

Hallermeiers inner shoal zone limit has since been relied upon as the predominant approach used to define the upper shoreface depth limit in engineering practice and for investigations of coastal response to sea-level change. Other studies however have suggested other relationships between wave climate and h_c [*Birkemeier*, 1985]. Notwithstanding contention over the most reliable relationship between wave climate and h_c for different settings, it is important to note that Hallermeiers equation (and likewise

others) is tied to the measurement timescales of the empirical datasets that were used to verify the relationship. Whilst few attempts have been made to accommodate longer timescales or variable rates of sea-level change, the datasets of *Birkemeier* [1985] and *Nicholls et al.* [1998] span inter-annual timescales. Because of the dependency of such relationships on measurement timescale therefore, predictive applications at timescales that exceed the observation dataset should be interpreted with caution. This is due to the increased potential for non-negligible cross-shore sediment transport residuals beyond the closure depth over longer timescales. Nonetheless, $h_c = d_l$ is adopted as a starting point here.

5.2.2 Lower shoreface

The differences in morphologic scale and response timescale between the upper and lower shoreface approach or exceed an order of magnitude [*Cowell et al.*, 1999; *Stive and de Vriend*, 1995]. Relative to the upper shoreface, the lower shoreface is essentially a lower-order morphological complex within the coastal tract cascade [*Cowell et al.*, 2003a]. As such upper shoreface processes may be regarded as noise at the timescales of lower shoreface response, and lower shoreface changes drive shore-normal upper shoreface translation. However, there exists little quantitative knowledge on which to found concepts of lower shoreface change. This is due to the logistical difficulties of working in shoreface waters, and limitations in the capacity of instruments to resolve the seabed to the levels of precision required to quantify gradual and imperceptible change. Although measurements of hydrodynamic process have been made across the lower shoreface, the outcomes (in terms of sediment transport) of complex interactions between the vast array of lower shoreface processes remain essentially unknown [*Niedoroda and Swift*, 1991]. Consequently, the representation of lower shoreface processes in predictive models is usually based on profile equilibrium theories [*Bruun*, 1954; *Dean*, 1977, 1991].

There is little empirical evidence to describe the lower shoreface depth limit (h_i). In his investigation of the relationship between wave climate and shoreface sediment transport, *Hallermeier* [1981] also identified an outer shoal zone limit d_i. The physical significance of d_i is based on the annual limit of significant onshore-offshore sand

transport due to waves, and is simply derived from mean wave climate statistics and shoreface sediment grain size at the location of $1.5d_l$:

$$d_i \cong (H_{sig} - 0.3\sigma)T_{sig}(\frac{g}{5000D})^{0.5} \tag{5.3}$$

Equation 5.3 is essentially a refined definition of wave base (h_w), which is typically defined as $h_w = L/2$ (where L is wavelength). That is, although waves may begin to interact with the seabed at h_w, the intensity of that interaction only becomes sufficient to manifest non-negligible cross-shore sediment transport above h_i [Fig. 5.2]. *Cowell et al.* [1999] demonstrate that Equation 5.3 returns values roughly equivalent to $0.5h_w$, except for wave climates where Ts is extremely high or low. Although the simple evaluation of d_i in relation to wave climate is appealing, in reality there does not usually exist a single representative shoreface sediment grain size, and thus the applicability of Equation 5.3 remains contingent on shoreface sediment grain-size distributions. Nonetheless, Equation 5.3 provides a general measure of the outer shoreface limit and thus $h_i = d_i$ is adopted here.

Although *Hallermeier* [1981] argued that d_i provides an appropriate morphological scale for the solution of coastal response to sea-level change using shoreface profile translation, *Cowell et al.* [1999] argued that it is unlikely that the assumption of time-invariant shoreface geometry is valid to d_i. Rather, they suggest that d_i might represent an appropriate cross-shore sediment budget closure depth, although shoreface response is likely to become timescale dependent between d_l and d_i for timescales relevant to coastal management (c. $10 - 10^2$ years). Considering that surface adjustment manifests from cumulative cross-shore sediment transport, shoreface response to sea-level change is naturally dependent on depth-diminishing sediment transport rates and the timescale or rate of change. The absence of temporal dependence suggests that the upper and lower shoreface definitions introduced above may be unnecessarily restrictive for the timescales and rates of sea-level change relevant to coastal evolution.

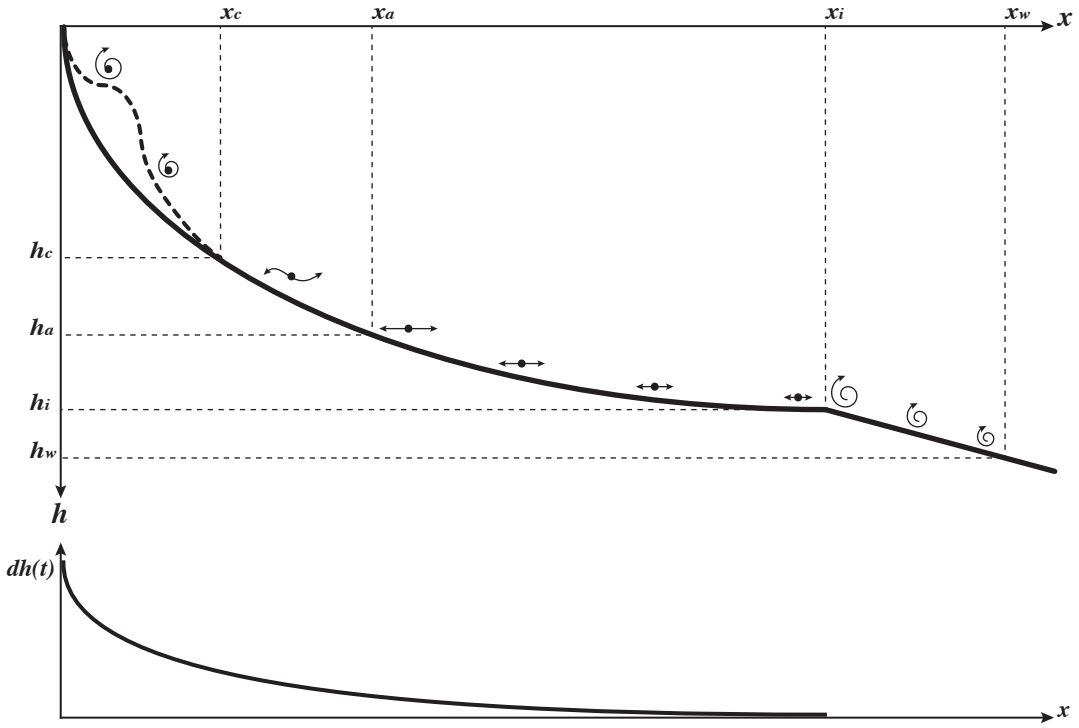

Figure 5.2: Limits of timescale- and depth-dependent shoreface response - The upper shoreface depth limit (h_c) specifies the limit of measurable surface change at annual timescales, and occurs somewhere beyond the modal surf zone (which is indicated by the dashed profile). The active shoreface depth limit (h_a) specifies the limit of time-invariant surface behaviour for a given substrate and rate of sea-level change. The lower shoreface depth limit (h_i) specifies the limit of significant depth-dependent surface response, beyond which waves action ceases to contribute to significant cross-shore sediment transport residuals. Wave base (h_w) defines the depth at which gravity waves begin to feel the seabed.

5.2.3 Active shoreface

The definitions for the upper- and lower-shoreface depth limits considered above appear to provide indicative limits for vertical shoreface adjustment and cross-shore sediment transport for stationary sea level conditions and annual timescales. During sea-level change however, the significance of h_c and h_i in terms of shoreface kinematics is less certain. That is, in the context of geometric modelling, h_c may not define an appropriate depth limit for application of the time-invariant shoreface assumption in all cases. For cases of gradual sea-level change for example, depth-dependent rates of lower shoreface response may well exceed the rate of sea-level change for some distance beyond h_c. Where substrate geometry is relatively uniform, surface response rates may then exceed the rate of physiographic inheritance across part of the lower shoreface, which would thus maintain time-invariant geometry. Thus the significance of h_c in cases of sea-level change may well be the exception as opposed to the standard, and an alternative definition for the responsive upper shoreface is required.

Therefore, the *active shoreface* is defined here as the shoreface region in which profile geometry exhibits statistical stationarity for the timescale and rates of change of interest. That is, although the active shoreface profile may be subject to vertical adjustment in response to individual storms and wave climate fluctuations, profile variance is constant about a stationary mean and may be considered noise. The depth at which this condition fails to be satisfied is defined as the active shoreface depth limit, h_a [Fig. 5.2]. The implication of this definition is that whilst active-shoreface relaxation timescales may increase from instantaneous at the shoreline to beyond event timescales with increasing proximity to h_a, rates of shoreface response for water depths less than h_a exceed the rate of physiographic inheritance due to sea-level change. The latter term is a product of the rate of sea-level change and the geometric departure of the substrate from the average gradient. Thus for a given wave climate, h_a is expected to vary with changes in the rate of sea-level change and substrate physiography.

The term 'active shoreface' is borrowed from *Stive and de Vriend* [1995], who described the active zone as the part of the shoreface that satisfies the condition of time-invariant geometry relative to mean sea level. Although the active zone definition derives from basic shoreface equilibrium concepts [*Bruun*, 1954, 1962; *Dean*, 1977], *Stive and de Vriend* [1995] made the fundamental observation that for multi-decadal

timescales the assumption of profile invariance should be restricted to the vicinity of the upper shoreface: i.e. where wave action is sufficient to maintain profile geometry for a given rate of sea-level change. By definition therefore, beyond the active shoreface rates of change in boundary conditions exceed surface response rates, which are regulated by the intensity of wave-driven cross-shore sediment transport processes. Implicit in that proposition is the concept of shoreface morphological relaxation (i.e. towards equilibrium), and time-lagged shoreface response: i.e. following the stabilisation of boundary conditions ongoing surface adjustment may persist beyond the active shoreface. Considering the diminished potential for wave-driven surface adjustment, it has been proposed that lower shoreface relaxation timescales are on the order of $10^2 - 10^3$ years [*Stive and de Vriend*, 1995; *Cowell et al.*, 2003a].

Although the relative differences between upper and lower shoreface morphological timescales have been previously described [*Cowell et al.*, 1999], there remains little quantitative evidence regarding lower-shoreface response timescales beyond the work of *Nicholls et al.* [1998], especially under dynamic boundary conditions. For example, the relationship between the active shoreface depth limit and rate of sea-level change remains largely unexplored. Between the surf zone and wave base cross-shore sediment transport is predominantly driven by the influence of shoaling waves, and this influence decreases with increased depth [*Niedoroda and Swift*, 1991]. Under static sea level conditions this may be readily observed as shoreface profile convergence in long-term measurement datasets, which is the basis of closure depth definitions in practice [Sec. 5.2.1]. Considering the progressive seaward reduction in rates of shoreface surface change however, it is intuitive that the active shoreface depth limit must vary for different rates of sea-level change. Specifically, the depth at which the rate of sea-level change exceeds rates of shoreface surface response should decrease for increased rates of change. Conversely, for slower rates of change the active shoreface is expected to extend to increasing depths.

5.3 Methods

The relationships between the active shoreface limiting depth (h_a), depth-dependent shoreface response, and the rate of sea-level change, were examined using the site-calibrated Tuncurry BARSIM model [Sec. 3.3.1]. Specifically, the model was used to

simulate coastal evolution in response to an 80 m linear relative sea level fall at rates of 10, 5, 2.5, 1 and 0.5 mm/a. An 80-m linear sea level fall was applied in all cases to eliminate any significant influence of the present-day shoreface geometry from the model findings. To isolate shoreface response to sea-level change, no external sediment supply was included in these idealised model experiments. Furthermore, the initial surface geometry of the models featured the present-day Tuncurry shoreface fronted by a linear 0.15° shelf, which is consistent with the gradient of the Tuncurry lower shoreface. Thus uniform profile geometry was maintained across the shoreface-inner shelf interface such that any potential influences of complex shelf physiography were excluded from these experiments. To investigate the influence of shelf gradient and complex shelf physiography on shoreface response, the 2.5 mm/a sea level fall scenario was subsequently applied to separate models that featured linear shelf gradients of 0.225° and 0.3°, and the surveyed bathymetry from the Tuncurry shelf (which has an average gradient of 0.225° between the shoreline and 80 m depth contour). Lastly, the influence of site-specific morphodynamic efficiency on shoreface response was considered using the site-calibrated Moruya BARSIM model, which was applied with a 2.5 mm/a sea level fall scenario and linear 0.3° shelf.

Considering the range of simulation durations required to achieve an 80-m relative sea level fall at the various rates examined, model time steps equivalent to 8-m relative sea level fall increments were plotted to allow for comparison between the different scenarios. For example, the model time increment required for an 80-m sea level fall at 10 mm/a was 8 ka, whilst the corresponding simulation time for the 0.5 mm/a relative sea level fall experiment was 160 ka. Therefore the 8-m model increments for the respective simulations represent model time steps of 1 ka and 16 ka. To isolate the extent of the active shoreface, depth-dependent shoreface response, and morphological inheritence throughout the simulations, the shoreface profiles corresponding to 8-m model increments were normalized within Lagrangian reference frames. That is, profiles were normalised for cross-shore and vertical shoreface translation by subtracting the strandplain progradation distance and sea level fall from profile coordinates at each model increment. This permitted direct comparison between shoreface geometry at progressive model increments in each simulation. Furthermore, Lagrangian-normalised shoreface profiles allowed for total surface adjustment to be calculated across the shoreface for

each simulation. Total shoreface adjustment was then compared with depth-dependent shoreface erosion rates to identify the extent of depth-dependent shoreface response.

The depth limits of the active shoreface and lower shoreface were also measured throughout the simulations. The depth limit of the active shoreface was defined using a fixed-magnitude depth limit applied to the Lagrangian-normalised shoreface profiles. Specifically, the limit of the active shoreface was measured at the depth beyond which shoreface profile variation relative to the initial (i.e. present-day) shoreface exceeded 0.3 m, after accounting for variable berm heights (i.e. shoreface origin) associated with the influence of the event-driven model wave climate. The measured active shoreface depth limit throughout each simulation was then compared against the sampled wave base depths, Hallermeiers d_i, and a rate-threshold surface change limit. Specifically, the timescale-independent shoreface depth limit was defined as the depth beyond which the rate of shoreface surface adjustment decreased to below 5 mm/a. The rate-based definition of the lower shoreface depth limit provided an objective measure of the shoreface extent between each simulation. Because the model wave climate, substrate geometry and sediment characteristics were kept the same between simulations, the lower shoreface depth limit remained relatively consistent between simulations.

After *Wolinsky* [2009], overall shoreface geometry was measured at each model timestep using the dimensionless order-one shape index, alpha [Sec. 3.3.1.3]. Alpha (α) measures shoreface shape where $0 < \alpha < 0.5$ indicates overall profile concavity and $0.5 < \alpha < 1$ profile convexity. Finally, shoreline trajectory (θ) relative to the initial shoreline was measured at each model timestep to investigate the influences of the rate of sea level fall, shoreface response and substrate gradient on strandplain deposition. Shoreline-trajectory analysis has been used as an interpretive tool to describe the evolution of coastal depositional systems in response to relative sea level fall and sedimentary regime [*Helland-Hansen and Martinsen*, 1996; *Helland-Hansen and Hampson*, 2009; *Tortora et al.*, 2009a,b]. Shoreline trajectories from the simulations carried out here were analysed to investigate the reliability of shoreline-trajectory analysis as a proxy for predicting depositional volumes and stratigraphic architecture.

5.4 Simulation results

5.4.1 Rate of sea-level change

Figure 5.3 shows the results of the -10 mm/a sea level fall scenario over the linear 0.15° shelf. Figure 5.3a shows that simulated coastal evolution (in 8-m model sea level increments) was characterized by deposition of a forced-regressive (F-R) strandplain of 22.5 km extent and 6 m thickness between 0 and -80 m PMSL. The F-R strandplain was sourced entirely from shelf sediments that were reworked by shoreface erosion processes. Figure 5.3b shows the evolution of shoreface geometry for the same model increments within a Lagrangian reference frame, from the initial shoreface (black line) to the final shoreface (red line). Shoreface geometry is seen to shoal rapidly during sea level fall across the initial shoreface surface at -10 mm/a, before rates of change decrease progressively during sea level fall across the linear 0.15° shelf. The extent of the active shoreface as defined on the basis of time-invariant profile geometry was limited to the uppermost shoreface for the duration of the simulation, as seen in the divergence of normalised shoreface profiles beyond 5 m shoreface depth [Fig. 5.3b].

Figure 5.3c demonstrates the active shoreface depth limit quantitatively using the definition $dh < 0.3$ m. It can be seen that following model warm-up the active shoreface depth limit stabilises at 4 m shoreface depth. The rate-threshold shoreface limit ($dh(t) < 5$ mm/a) decreased from about mean wave base to 32 m shoreface depth throughout the simulation. Also shown are depth-dependent shoreface erosion and total shoreface adjustment, and shoreface shape and shoreline trajectory throughout the simulation [Fig. 5.3d-e].

Comparison of model results from the -10 mm/a sea-level-fall simulation [Fig. 5.3] with the corresponding model outputs from the -5 mm/a [Fig. 5.4], -2.5 mm/a [Fig. 5.5], -1 mm/a [Fig. 5.6] and -0.5 mm/a [Fig. 5.7] sea-level-fall scenarios shows the influence of the rate of sea-level change on coastal evolution, the active shoreface depth limit and depth-dependent shoreface response. Whilst the widths of the F-R strandplains (i.e. 22.5 km) remained consistent between simulations, strandplain volume increased with decreasing rates of sea-level change [Figs. 5.3-5.7a]. Specifically, F-R strandplain thickness for the -5, -2.5, -1 and -0.5 mm/a sea-level-fall scenarios were 12, 18, 24 and 30 m respectively. Comparison of the Lagrangian-normalised shoreface profiles between experiments demonstrates the seaward extension of the active shoreface and decrease

in depth-dependent surface adjustment across the shoreface for decreasing rates of sea-level change [Figs. 5.3-5.7b]. This is further demonstrated by the progressive increase in h_a towards d_i and h_w for decreasing rates of sea-level change. Specifically, h_a increased progressively from 4 m to approximately 10 m, 15 m, 25 m and 32 m for the -5, -2.5, -1 and -0.5 mm/a sea-level change scenarios respectively [Figs. 5.3-5.7c]. In contrast, the location of the rate-threshold shoreface depth limit remained more or less uniform between each simulation, decreasing from about mean wave base to 32-36 m shoreface depth throughout the simulation [Figs. 5.3-5.7c].

By definition [Sec. 5.2.3], total shoreface adjustment was negligible across the active shoreface. Therefore total shoreface adjustment extended across the shoreface with h_a for decreasing rates of sea-level change [Figs. 5.3-5.7d]. Beyond h_a, shoreface adjustment was depth-dependent and decreased with decreasing rates of sea-level change [Figs. 5.3-5.7d]. Comparison of shoreface erosion between simulations shows that depth-dependent shoreface erosion rates decreased with increased h_a and decreased rates of sea-level change [Figs. 5.3-5.7d]. That is, the seaward extension of the active shoreface (and time-invariant shoreface behaviour) supported maintenance of a deeper shoreface profile (comparable to the initial profile), which resulted in reduced depth-dependent shoreface erosion rates. The area beneath both the shoreface erosion and total adjustment curves represents the sum of depth-dependent cross-shore sediment transport residuals beyond the active shoreface. Comparison between Figures 5.3-5.7d therefore indicates that depth-dependent cross-shore sediment transport residuals per unit time decreased for decreasing rates of sea-level change.

Shoreface shape also varied with the rate of sea-level change, with profiles becoming progressively more concave for increased h_a and slower rates of change [Figs. 5.3-5.7e]. For the -5 and -10 mm/a sea level scenarios shoreface shape became progressively more convex relative to the initial shoreface profile. For the -2.5, -1 and -0.5 mm/a sea level scenarios shoreface shape became progressively more concave relative to the initial shoreface profile. Shoreline trajectory was also sensitive to the sea level scenarios examined [Figs. 5.3-5.7e]. For rapid rates of sea level fall (e.g. -10 and -5 mm/a) shoreline trajectories varied with the shape of the initial shoreface profile [Figs. 5.3-5.4e]. For slower rates of sea level fall shoreline trajectories were more constant throughout simulations [Figs. 5.5-5.7e], converging at the terminal trajectory at an earlier stage of sea level fall. In all simulations terminal shoreline trajectories converged on 0.2°.

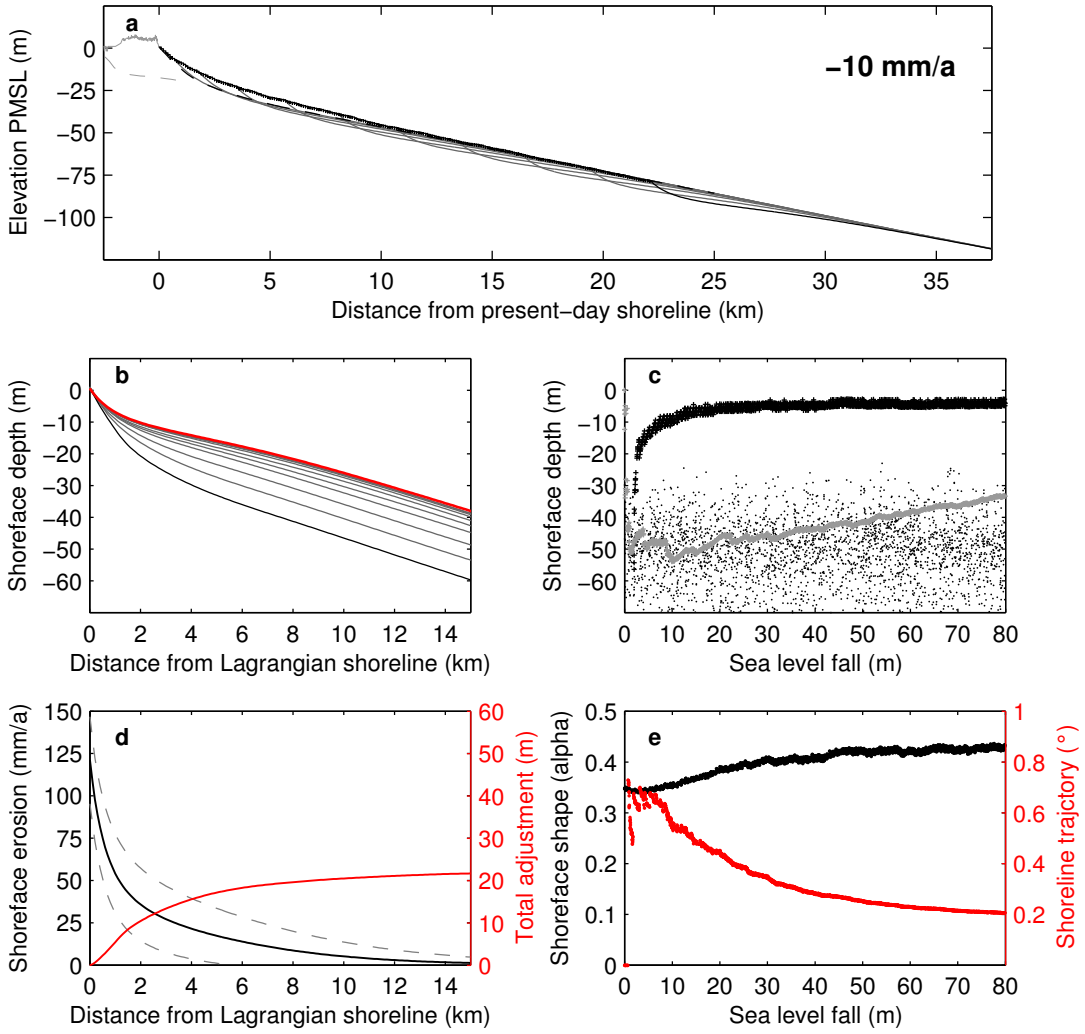

Figure 5.3: Tuncurry 80-m sea level fall at -10 mm/a for shelf gradient 0.15° - (a) Simulated coastal evolution at 8-m model increments; (b) Lagrangian-normalised shoreface profiles for 8-m model increments; (c) sampled active shoreface depth limit (black +), lower shoreface depth limit (grey +) and wave base (.) throughout simulation; (d) average depth-dependent erosion (black solid) ± one standard deviation (grey dashed), and total shoreface response (red); (e) shoreface shape factor alpha (black) and shoreline trajectory (red) throughout simulation.

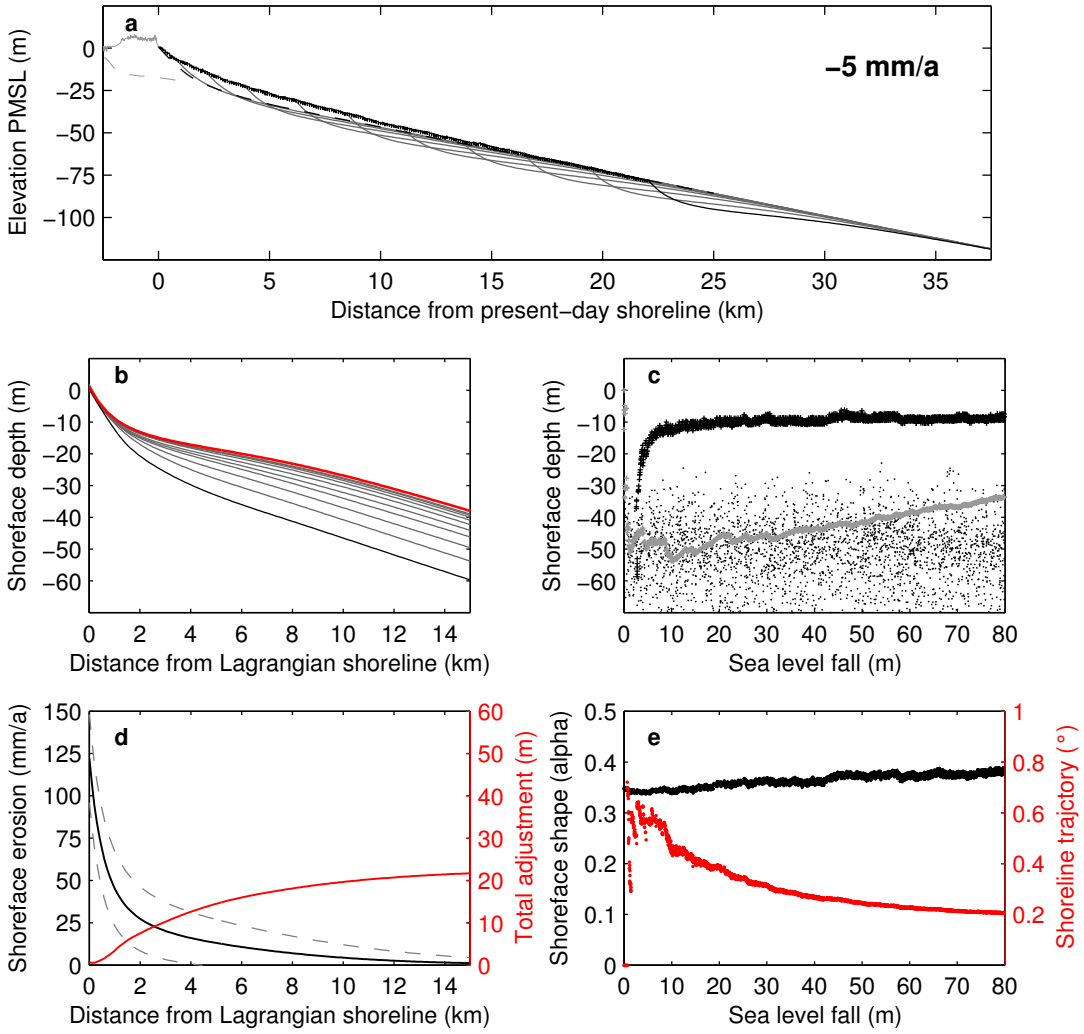

Figure 5.4: Tuncurry 80-m sea level fall at -5 mm/a for shelf gradient 0.15° - (a) Simulated coastal evolution at 8-m model increments; (b) Lagrangian-normalised shoreface profiles for 8-m model increments; (c) sampled active shoreface depth limit (black +), lower shoreface depth limit (grey +) and wave base (.) throughout simulation; (d) average depth-dependent erosion (black solid) ± one standard deviation (grey dashed), and total shoreface response (red); (e) shoreface shape factor alpha (black) and shoreline trajectory (red) throughout simulation.

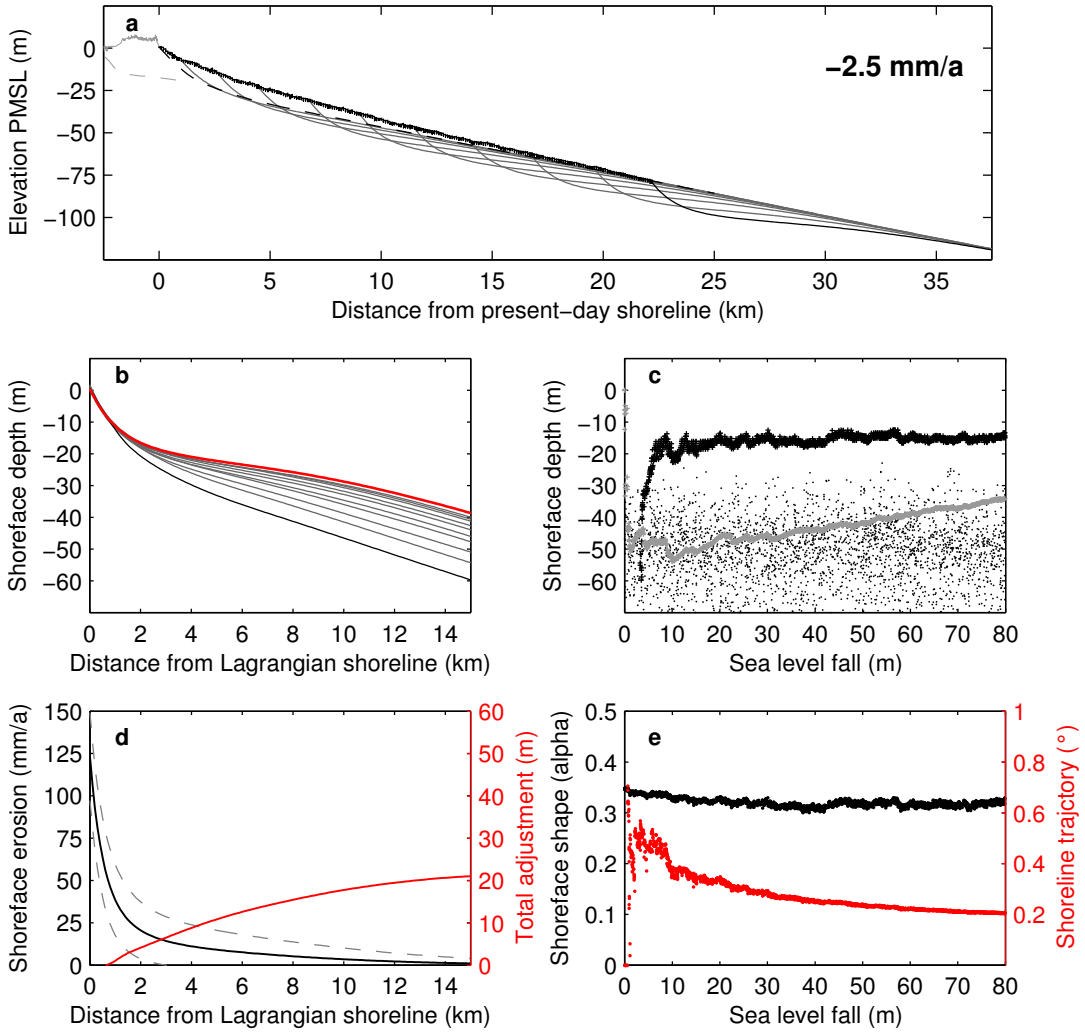

Figure 5.5: Tuncurry 80-m sea level fall at -2.5 mm/a for shelf gradient 0.15° - (a) Simulated coastal evolution at 8-m model increments; (b) Lagrangian-normalised shoreface profiles for 8-m model increments; (c) sampled active shoreface depth limit (black +), lower shoreface depth limit (grey +) and wave base (.) throughout simulation; (d) average depth-dependent erosion (black solid) ± one standard deviation (grey dashed), and total shoreface response (red); (e) shoreface shape factor alpha (black) and shoreline trajectory (red) throughout simulation.

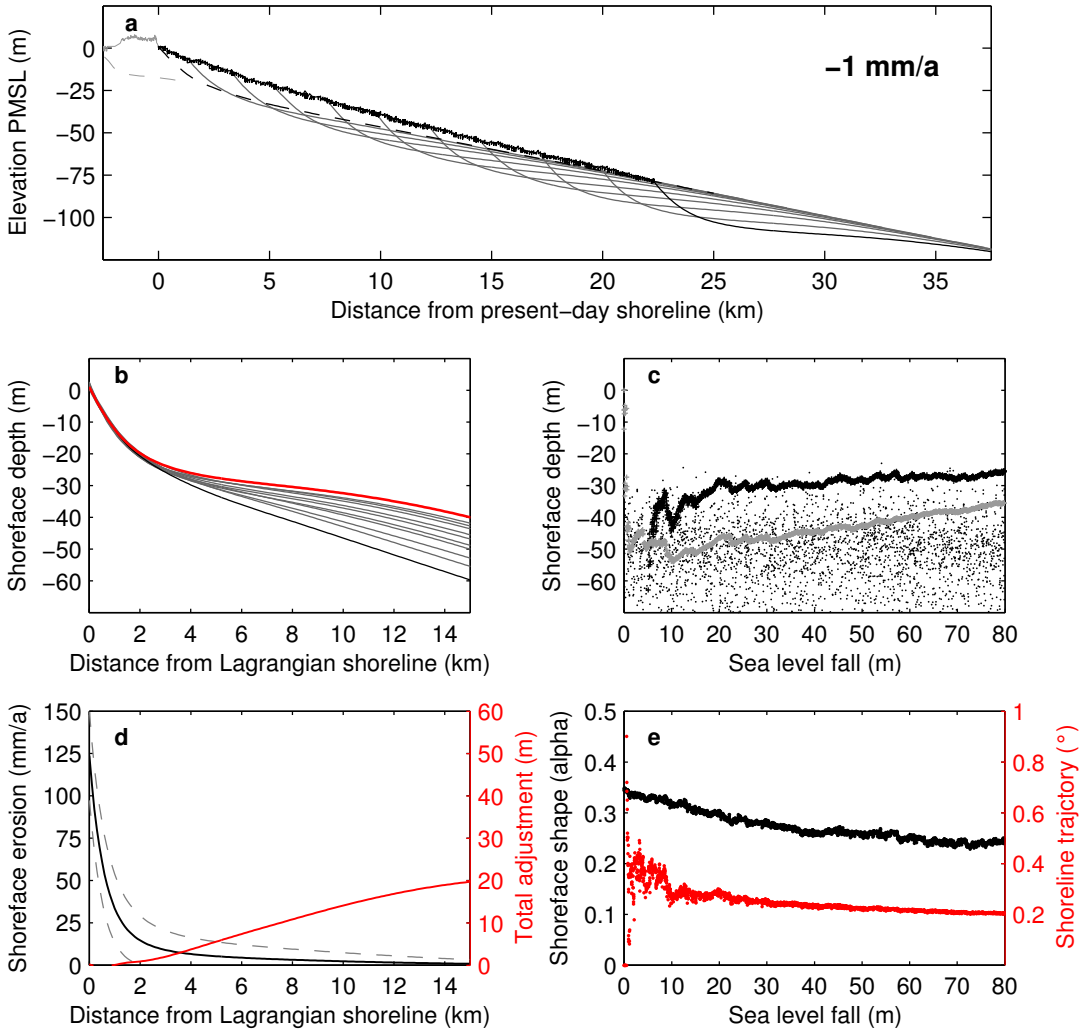

Figure 5.6: Tuncurry 80-m sea level fall at -1 mm/a for shelf gradient 0.15° - (a) Simulated coastal evolution at 8-m model increments; (b) Lagrangian-normalised shoreface profiles for 8-m model increments; (c) sampled active shoreface depth limit (black +), lower shoreface depth limit (grey +) and wave base (.) throughout simulation; (d) average depth-dependent erosion (black solid) ± one standard deviation (grey dashed), and total shoreface response (red); (e) shoreface shape factor alpha (black) and shoreline trajectory (red) throughout simulation.

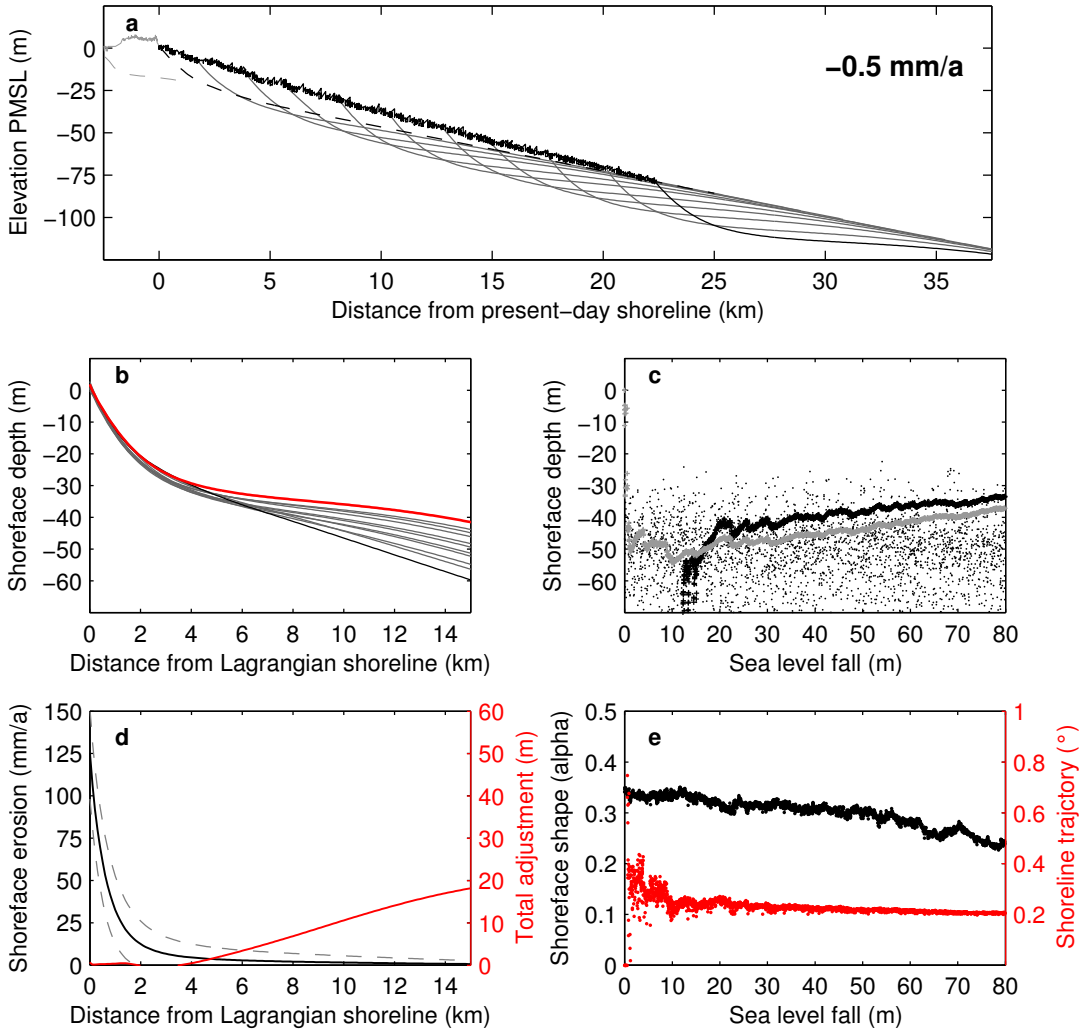

Figure 5.7: Tuncurry 80-m sea level fall at -0.5 mm/a for shelf gradient 0.15° - (a) Simulated coastal evolution at 8-m model increments; (b) Lagrangian-normalised shoreface profiles for 8-m model increments; (c) sampled active shoreface depth limit (black +), lower shoreface depth limit (grey +) and wave base (.) throughout simulation; (d) average depth-dependent erosion (black solid) ± one standard deviation (grey dashed), and total shoreface response (red); (e) shoreface shape factor alpha (black) and shoreline trajectory (red) throughout simulation.

5.4.2 Substrate gradient

The influence of substrate gradient on shoreface response and coastal evolution is considered in Figure 5.8 and Figure 5.9, in which the same simulation as in Figure 5.5 was carried out for shelf gradients of 0.225° and 0.3° respectively. Comparison between Figures 5.5, 5.8 and 5.9 thus demonstrates that for the -2.5 mm/a sea-level-change scenario, the active shoreface was not sensitive to variations in substrate gradients. Rather, time-invariant shoreface geometry persisted to approximately 15 m shoreface depth throughout each simulation. The shelf gradients considered are representative of variation in profile geometry across the entire continental shelf at Tuncurry (where the average shelf gradient is 0.225°). Although the active shoreface depth limit remained uniform between the simulations, strandplain volume, shoreface shape and lower shoreface response varied between the 0.15°, 0.225° and 0.3° simulations. In particular, depth-dependent rates of shoreface response decreased for steeper shelf gradient [Figs. 5.5b, 5.8b and 5.9b]. That is, although depth-dependent shoreface erosion rates remained constant between the models [Figs. 5.5d, 5.8d & 5.9d], shoreface response rates decreased for steeper shelf substrates. Accordingly, shoreface shape became increasingly convex due to the inheritance of steeper shelf substrates into the lower-shoreface geometry [Figs. 5.5e, 5.8e and 5.9e]. The changes to shoreface shape and depth-dependent response rates associated with steeper shelf gradients were accompanied by a reduced volume of strandplain deposition.

To examine the influence of complex substrates, the -10 and -1 mm/a sea-level-change scenarios were applied in separate models that featured substrates consistent with the surveyed continental shelf bathymetry at Tuncurry. Comparison between the complex substrate models [Figs. 5.10 and 5.11] and the respective linear 0.15° simple substrate models [Figs. 5.3 and 5.6] demonstrates the influence of complex shelf geometry on shoreface shape and depth-dependent response rates. However, similar to the linear substrate examples, the active shoreface was not sensitive to complex substrate geometry. Comparison between Figure 5.10 and Figure 5.11 demonstrates that the influence of complex substrates on shoreface shape and depth-dependent response rates were more apparent for rapid rates of sea-level change. Specifically, for the -1 mm/a complex substrate scenario, the inheritance of shelf physiography had negligible influence on cross-shore sediment transport residuals beyond h_a [Figs. 5.10d and 5.11d].

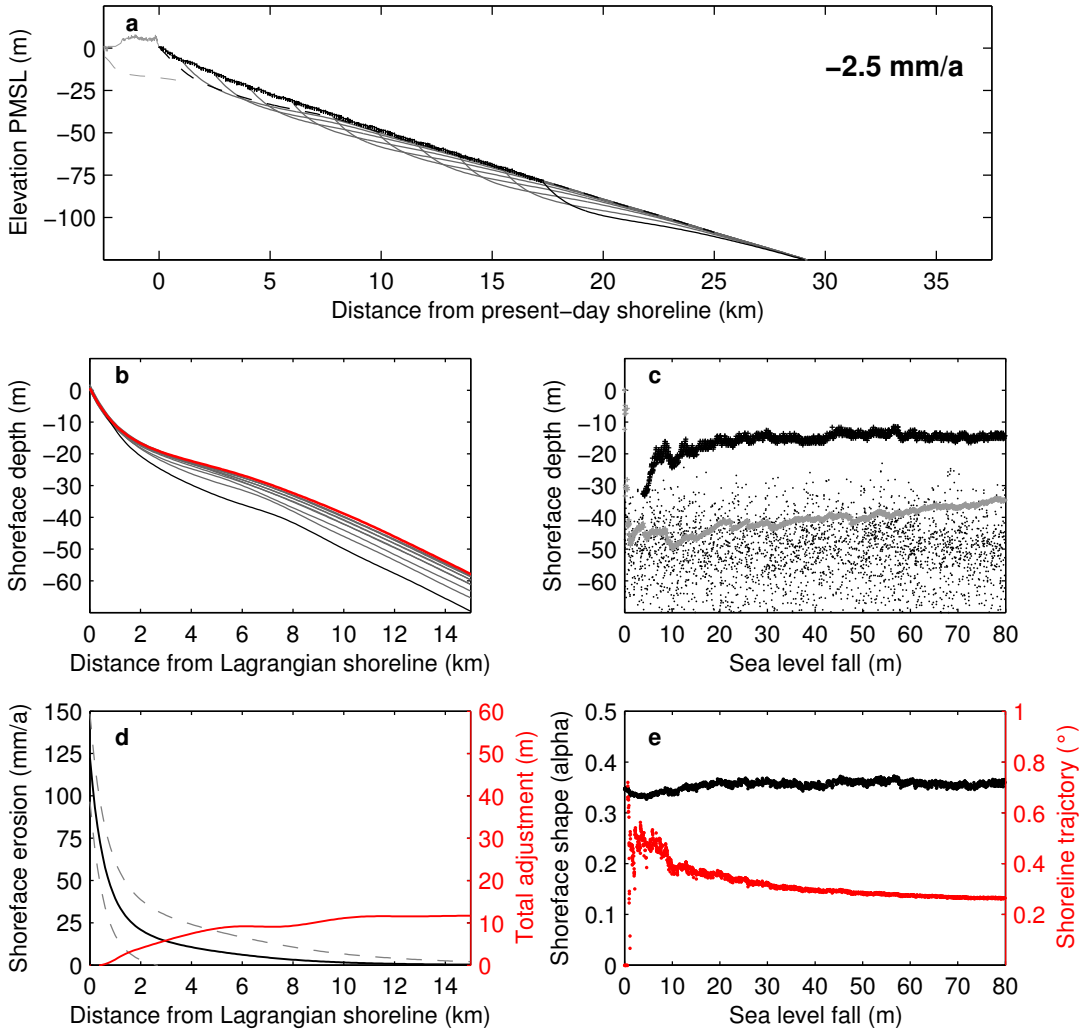

Figure 5.8: Tuncurry 80-m sea level fall at -2.5 mm/a for shelf gradient 0.225° - (a) Simulated coastal evolution at 8-m model increments; (b) Lagrangian-normalised shoreface profiles for 8-m model increments; (c) sampled active shoreface depth limit (black +), lower shoreface depth limit (grey +) and wave base (.) throughout simulation; (d) average depth-dependent erosion (black solid) ± one standard deviation (grey dashed), and total shoreface response (red); (e) shoreface shape factor alpha (black) and shoreline trajectory (red) throughout simulation.

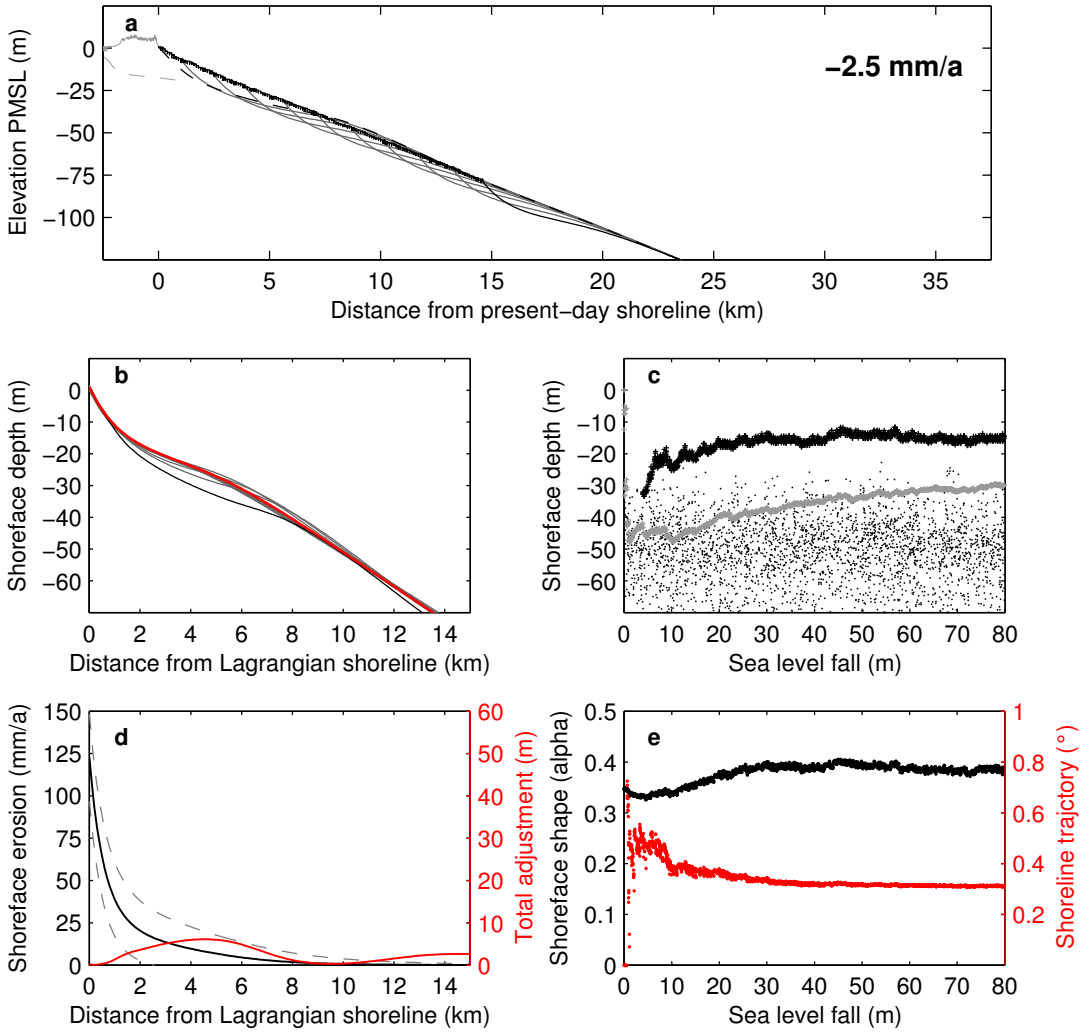

Figure 5.9: Tuncurry 80-m sea level fall at -2.5 mm/a for shelf gradient 0.30° - (a) Simulated coastal evolution at 8-m model increments; (b) Lagrangian-normalised shoreface profiles for 8-m model increments; (c) sampled active shoreface depth limit (black +), lower shoreface depth limit (grey +) and wave base (.) throughout simulation; (d) average depth-dependent erosion (black solid) ± one standard deviation (grey dashed), and total shoreface response (red); (e) shoreface shape factor alpha (black) and shoreline trajectory (red) throughout simulation.

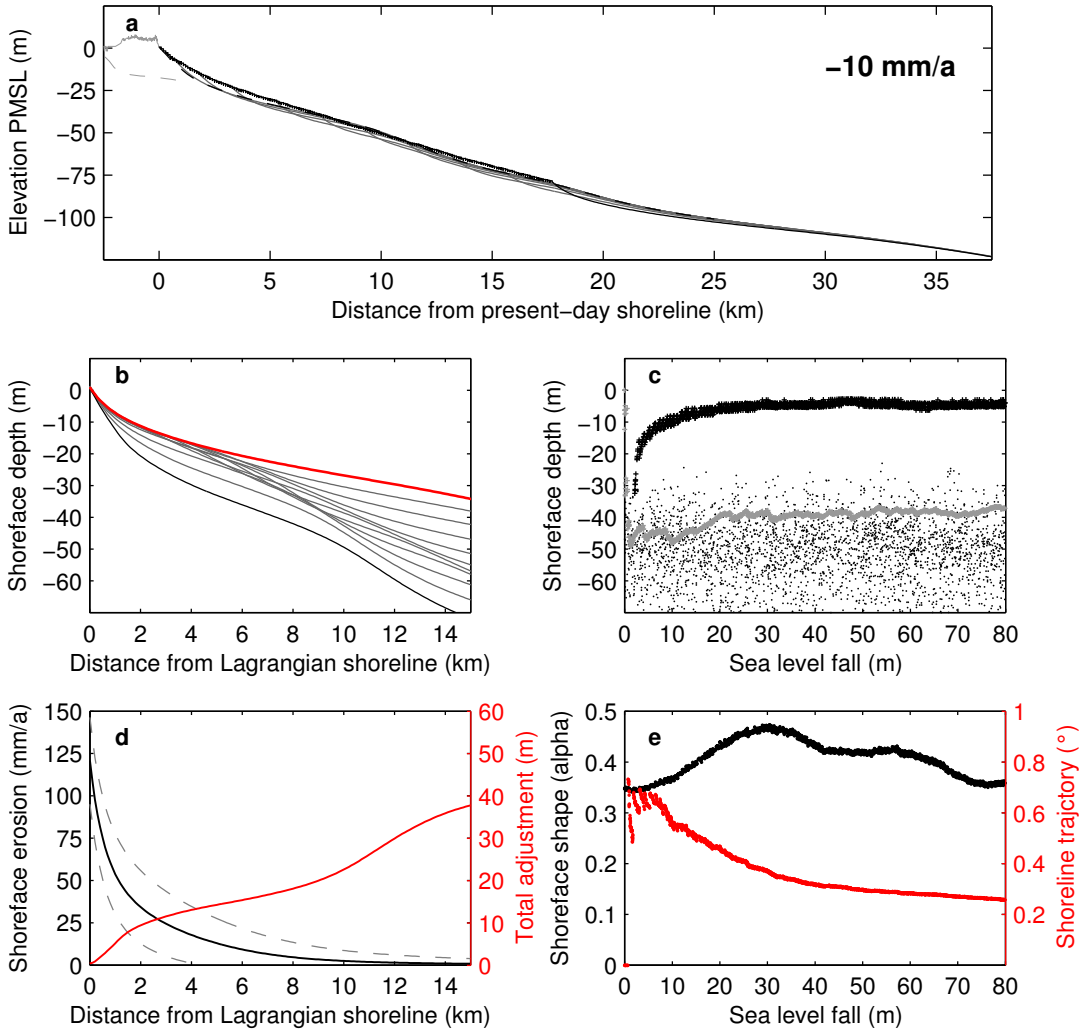

Figure 5.10: Tuncurry 80-m sea level fall at -10 mm/a for surveyed shelf - (a) Simulated coastal evolution at 8-m model increments; (b) Lagrangian-normalised shoreface profiles for 8-m model increments; (c) sampled active shoreface depth limit (black +), lower shoreface depth limit (grey +) and wave base (.) throughout simulation; (d) average depth-dependent erosion (black solid) ± one standard deviation (grey dashed), and total shoreface response (red); (e) shoreface shape factor alpha (black) and shoreline trajectory (red) throughout simulation.

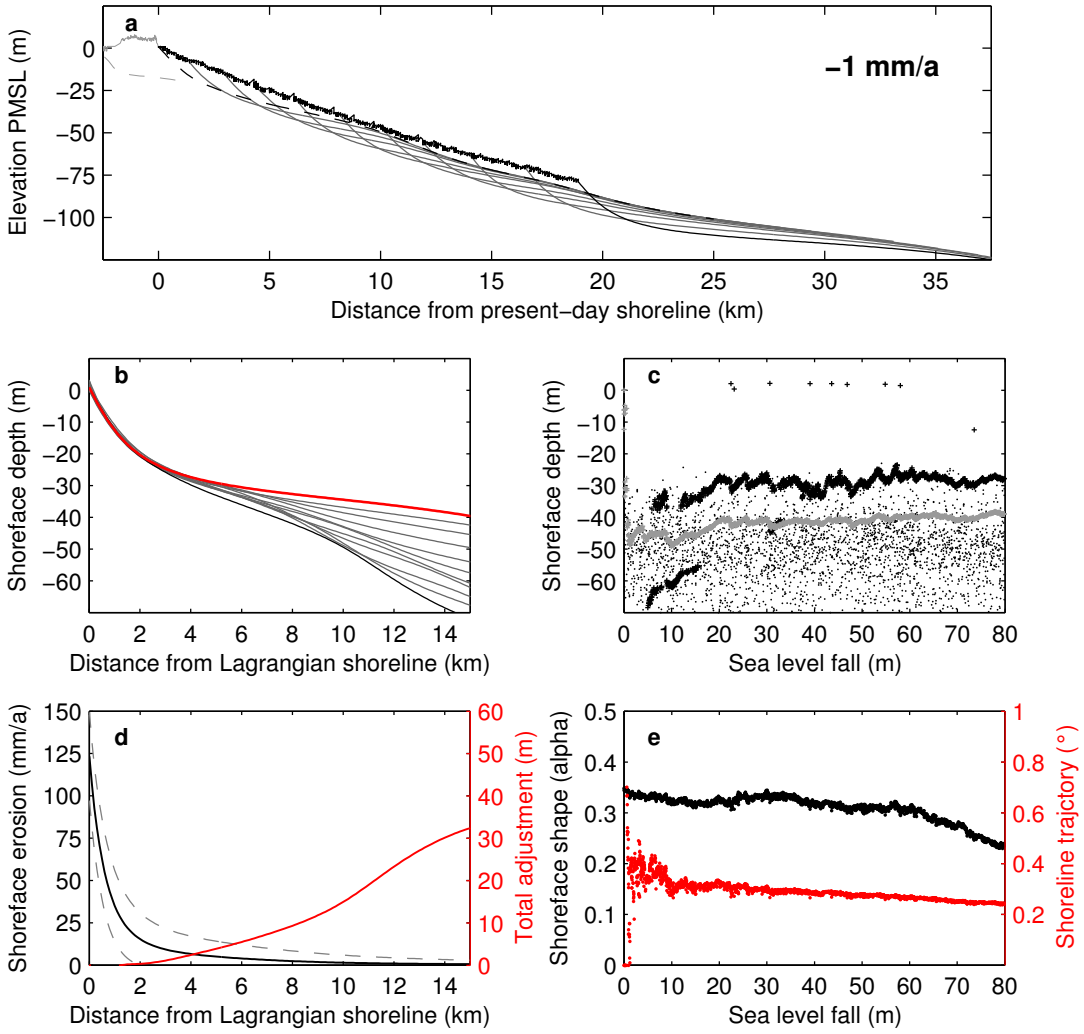

Figure 5.11: Tuncurry 80-m sea level fall at -1 mm/a for surveyed shelf - (a) Simulated coastal evolution at 8-m model increments; (b) Lagrangian-normalised shoreface profiles for 8-m model increments; (c) sampled active shoreface depth limit (black +), lower shoreface depth limit (grey +) and wave base (.) throughout simulation; (d) average depth-dependent erosion (black solid) ± one standard deviation (grey dashed), and total shoreface response (red); (e) shoreface shape factor alpha (black) and shoreline trajectory (red) throughout simulation.

5.4.3 Site morphodynamic efficiency

The 2.5 mm/a sea-level-fall scenario was also applied in a separate experiment that featured a linear 0.3° shelf, present-day shoreface morphology at Moruya, and the Moruya BARSIM model configuration. The objective of the simulation was to examine the role of site-specific morphodynamics on shoreface response to rapid sea-level change. Comparison between Figure 5.9 and Figure 5.12 shows that for the Moruya BARSIM model h_a extended to 20 m depth, whilst under the same sea level scenario and shelf gradient h_a was only 15 m depth for the Tuncurry BARSIM model. Furthermore, as the 0.3° linear shelf is equivalent to the present-day (initial model) lower-shoreface gradient there was no inheritance of complex shelf physiography into the shoreface within the Moruya BARSIM model [Fig. 5.12b]. In accordance with differences between the active shoreface and depth-dependent shoreface response between the Moruya and Tuncurry models, strandplain volume, shoreface shape and shoreline trajectory also varied between the two simulations.

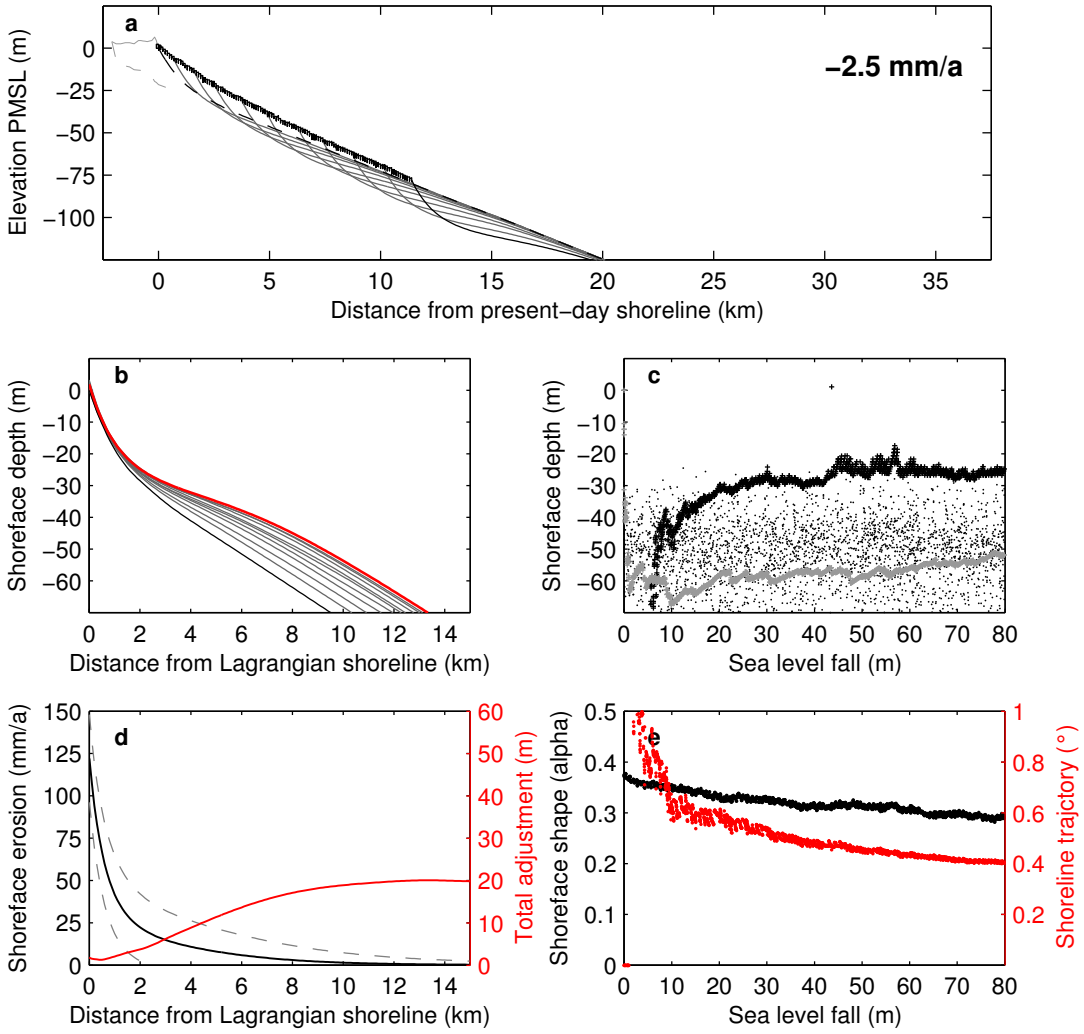

Figure 5.12: Moruya 80-m sea level fall at -2.5 mm/a for shelf gradient 0.30° - (a) Simulated coastal evolution at 8-m model increments; (b) Lagrangian-normalised shoreface profiles for 8-m model increments; (c) sampled active shoreface depth limit (black +), lower shoreface depth limit (grey +) and wave base (.) throughout simulation; (d) average depth-dependent erosion (black solid) ± one standard deviation (grey dashed), and total shoreface response (red); (e) shoreface shape factor alpha (black) and shoreline trajectory (red) throughout simulation.

5.5 Discussion

5.5.1 R-dependent shoreface response

The findings of the simulation experiments [Sec. 5.4.1] suggest that complete time-invariant shoreface response (i.e. $h_a = h_i$) is only supported for the slowest rates of sea-level change considered here [e.g. Fig. 5.7]. This suggests that late-Quaternary coastal evolution and potential future coastal change are characterised by R-dependent shoreface response. That is, coastal evolution in response to sea-level change at rates between 1-10 mm/a is described by R-dependent shoreface response. This finding raises further questions regarding the behaviour of the active shoreface and the significance of h-dependent lower-shoreface response rates for different rates of sea-level change. Furthermore, the prevailence of R-dependent shoreface response raises questions about the use of geometric equilibrium models in the geomorphology and coastal engineering disciplines. These issues are considered in further detail below.

5.5.1.1 Active shoreface depth limit

The hypothetical simulation experiments demonstrate that the active shoreface depth limit (h_a) varies significantly for rates of sea-level change characteristic of late-Quaternary coastal evolution and future coastal change. Specifically, complete time-invariant shoreface response was only valid for $R < 0.5$ mm/a [e.g. Fig. 5.7]. Put into context, a 100-m sea-level change at that rate would require 200,000 years to achieve. Late-Quaternary sea levels fluctuated beyond that range at approximately 100-ka periodicity [Fig. 4.2]. However, the rates of sea-level change experienced during the rapid oscillations into and out of glacial and interglacial maxima exceeded 15 mm/a. That is, actual rates of late-Quaternary sea-level change were about an order of magnitude greater than generalised third-order sea level cycles. Considered in the context of the findings [Sec. 5.4.1], the assumption of complete time-invariant shoreface response does not seem to be applicable to late-Quaternary coastal evolution. Furthermore, current projections of sea-level rise due to anthropogenic global warming range between 0.5-1.5 m over the next century [*Meehl et al.*, 2007; *Rahmstorf*, 2007], which for the case of a simple linear rise is equivalent to values of R between 5-15 mm/a. In reality, rates of sea level rise are expected to accelerate through that period in line with the lagged response of oceans to

warming. Thus the assumption of complete time-invariant shoreface response appears to be similarly inappropriate for predicting future coastal change.

However, the time-invariant shoreface assumption appears to hold relevance for the stratigraphy paradigm, where geometric equilibrium models are routinely applied with little consideration for shoreface response timescales. For example, relative sea-level change driven by tectonic responses and eustatic sea-level change driven by evolving ocean basin dimensions typically occurs at rates less than 0.01 mm/a . Thus for the geological timescales at which ancient depositional sequences formed, the time-invariant shoreface assumption is certainly applicable. Even for such long timescale problems however, it may indeed be the case that geometric equilibrium models only afford an order-of-magnitude estimation of shoreline migration and shallow-marine deposition. This may be the case, for example, where the resolution to which boundary conditions are resolved dilutes the actual rates of change. That is, within the prolonged duration of basin-scale change, there are most likely other active influences on relative sea levels that may contribute to higher-frequency fluctuations in shoreface response and shallow-marine deposition. However the depositional responses to such change may be below the resolution of ancient stratigraphic records. This suggests that although geometric equilibrium models ignore coastal evolution in response to higher order changes in boundary conditions, they may be suited to some applications.

For rates of sea-level change relevant to late-Quaternary coastal evolution and future coastal change, the results demonstrate that the active shoreface extends seaward (i.e. h_a increases) for decreasing rates of sea-level change [Figs. 5.3-5.7]. Conversely, h_a decreases for increased R. The relationship between h_a and R is summarised in Figure 5.13a. The black profile represents a benchmark case for R-dependent shoreface response, in which h_a occurs at a depth shallower than h_i. For faster rates of sea-level change the active shoreface becomes constricted and the shoreface profile may shoal as the significance of h-dependent shoreface response rates increases. For slower rates of sea-level change h_a approaches h_i and the shoreface profile becomes deeper and more concave. Panels (b) and (c) in Figures 5.3-5.7 demonstrate the relationship between h_a and R, whilst panel (e) shows the influence of h_a on shoreface shape.

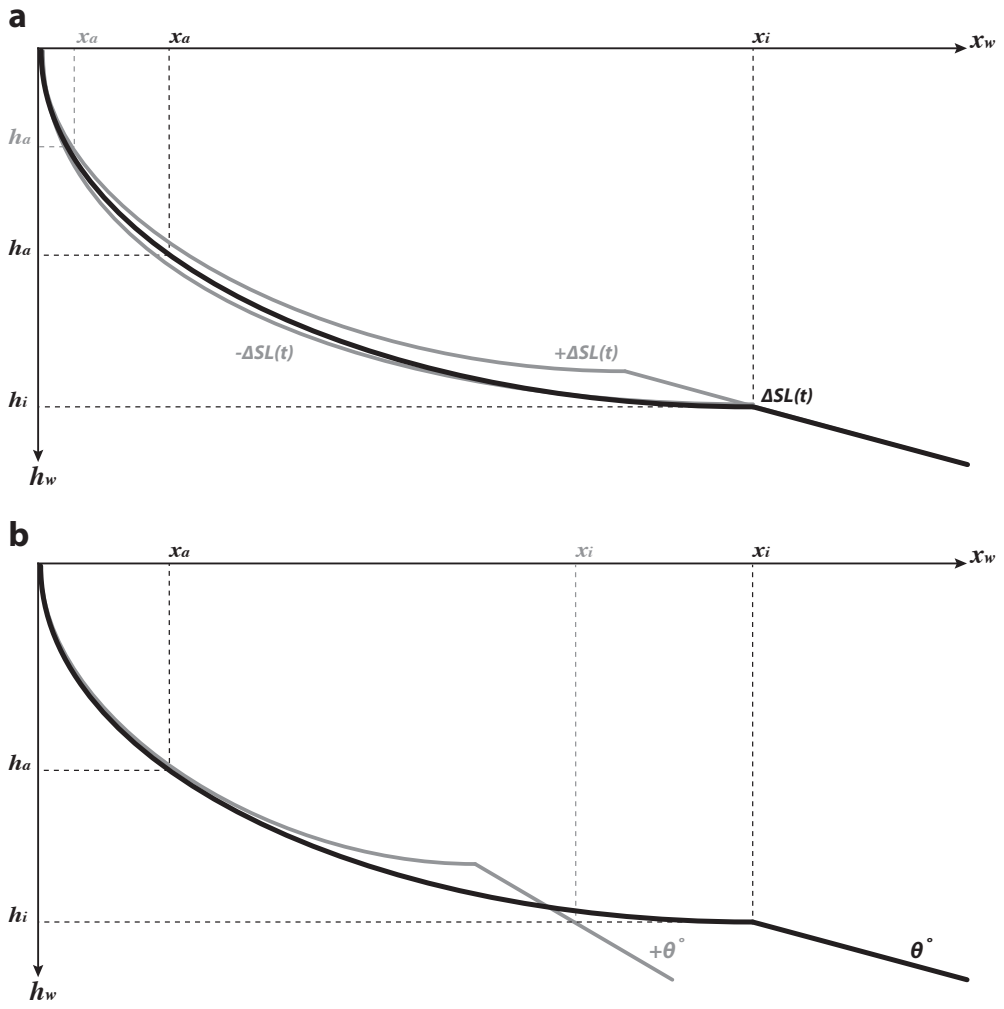

Figure 5.13: Controls on shoreface response to sea-level change - (a) The shoreface becomes shallower and the concave profile narrower for increased rates of sea-level change, due to restriction of the active shoreface and lower shoreface domains. In contrast, the shoreface becomes deeper for increased rates of sea-level change with the expansion of the active shoreface domain towards the shoreface toe. (b) The active shoreface depth limit (h_a) and lower shoreface depth limit (h_i) are insensitive to changes in shelf slope. For steeper slopes the lower shoreface becomes restricted due to decreased x_i, whilst for gentler slopes the lower shoreface expands due to increased x_i.

As illustrated in Figure 5.13b, the active shoreface depth limit was insensitive to substrate gradient and the geometric complexity of the surveyed Tuncurry shelf. Specifically, h_a was approximately 15 m for $R = 2.5$ mm/a and linear shelf gradients of 0.15, 0.225 and 0.3° [Figs. 5.5, 5.8 & 5.9]. Furthermore, h_a was approximately 5 m for $R = 10$ mm/a and both the 0.15° linear shelf and Tuncurry survey shelf [Figs. 5.3 & 5.10]. Rather, h_a was only sensitive to the rate of sea-level change as discussed above and site morphodynamic efficiency, as demonstrated by comparison of the Moruya and Tuncurry 0.3° linear shelf models [Figs. 5.9 & 5.12]. This finding may be significant, as it implies that if h_a is known for a given R and morphodynamic setting, it should be applicable to comparable settings where similar wave climate and sediment characteristics prevail. Thus for settings where stratigraphic preservation is low, a regional h_a value may be derived from a singular geological record in which shoreface response and coastal evolution has been preserved. Furthermore, the dependence of h_a only on R and morphodynamic efficiency suggests that a relationship between h_a and d_l may exist.

The seaward extension of h_a beyond h_c for decreasing R demonstrates the inconsistency between existing shoreface definitions [Sec. 5.2] and sea-level change. For example, the alignment of the 'surf zone', 'upper shoreface' and 'active shoreface' domains, which are sometimes used interchangeably, appears to be a fortuitous occurrence arising from stable boundary conditions and brief observational timescales. Although traditional upper shoreface definitions are derived from arguments based on wave dissipation and morphodynamic equilibrium [*Bruun*, 1962; *Dean*, 1977], in practice h_c is often derived from measured shoreface profiles [Sec. 5.2.1]. At measurement timescales (c. 10^0-10^1 years) h_a may be restricted to the vicinity of h_c, as suggested by a geometric profile inflection [*Inman et al.*, 1993] or the extent of measurable profile change [*Birkemeier*, 1985; *Nicholls et al.*, 1998]. However, differentiation between the upper and lower shoreface on that basis is not relevant to coastal evolution across all timescales. For example, Figures 5.3-5.4 demonstrate that for rates of sea-level change greater than 2.5 mm/a, h_a falls within the limits of h_c. However, Figures 5.6-5.7 show that for rates of sea-level change less than 2.5 mm/a, h_a extends beyond h_c and approaches h_i. The simulation experiments therefore suggest that whilst R-dependent shoreface response is characteristic of sea-level change typical of late-Quaternary coastal evolution and future coastal change, shoreface T_r may exceed T_f across much of the shoreface.

The findings from the simulation experiments suggest that for $R < 5$ mm/a there is no relationship between the active shoreface and the surf zone. Rather, the surf zone represents a nested morphological element within the active shoreface, which responds to high-frequency fluctuations in boundary conditions that drive higher-order sediment transport processes [*Cowell et al.*, 2003a]. The geometry of the surf zone profile may be distinctive from overall upper shoreface geometry [*Inman et al.*, 1993], because the profile is regulated by wave breaking and surf zone processes, as opposed to wave shoaling [Fig. 5.2]. Therefore if the upper shoreface is by definition synonymous with the active shoreface, any relationship between the upper shoreface and the surf zone is simply an artefact of the measurement timescale. In Section 5.5.2, a revised shoreface definition is proposed that uses the constrained active shoreface behaviour as a basis to transcend morphodynamic scales. For $R \geq 10$ mm/a [Fig. 5.3] the simulation findings suggest that the active shoreface is restricted to the surf zone. Because surf zone processes are beyond the scope of the BARSIM stratigraphic model, estimates of shoreface response for $R > 10$ mm/a are considered unreliable. Nonetheless the dynamic nature of the surf zone at observational timescales implies that the breaker point likely defines the upper range of h_a.

5.5.1.2 Depth-dependent shoreface response

By definition, rates of shoreface erosion between the active-shoreface depth limit (h_a) and wave base (h_w) decrease with increasing depth, and beyond the lower-shoreface depth limit (h_i) the contribution of shoreface erosion to coastal sediment budgets is negligible [Sec. 5.2]. The simulation experiments demonstrate the influence of depth-diminishing erosion rates on shoreface response beyond h_a. That is, h-dependent shoreface response varied with the rate of sea-level change and thus h_a [Figs. 5.3-5.7d]. For a given h_i (i.e. morphodynamic efficiency), increased h_a for decreased R [e.g. Fig. 5.6] implies that $h_i - h_a$ becomes smaller (i.e. the active shoreface expands whilst the lower shoreface contracts). The effect of lower-shoreface contraction and thus reduced h-dependent shoreface response is that the potential for passive shoreface response due to morphological inheritance decreases. For rapid sea-level change [e.g. Fig. 5.3], reduced h_a allows expansion of the lower-shoreface domain and thus the potential for shoreface inheritance is high. This is demonstrated in comparison between panel (b) of Figures 5.3-5.7, which shows that the departure of Lagrangian model shorefaces from

the initial shoreface increases with both increased R and increased shoreface depth. Furthermore, comparison between panel (e) of the same figures shows that shoreface shape (measured to $h_i = 35$ m) becomes increasingly concave for decreased R, as indicated by decreasing α. Passive shoreface response due to morphological inheritance was driven by the shallow shelf gradient used in the simulations, which reflected the lower-shoreface gradient at Tuncurry (i.e. 0.15°), not the average shelf gradient (i.e. 0.225°). The relationship between R and passive shoreface response is summarised in Figure 5.13a, which shows that for increased R, substrate inheritance increases with expansion of the lower shoreface (increasing $h_i - h_a$).

Perhaps contrary to basic intuition, h-dependent shoreface erosion rates *decreased* for slower rates of sea-level change. That is, seaward extension of the active shoreface (i.e. increased h_a) resulted in reduced rates of h-dependent erosion across the lower shoreface (i.e. beyond h_a). This is seen in the increasing concavity of the erosion rate curves in panel (d) of Figures 5.3-5.7 for reduced R. Similarly, comparison of the Lagrangian shoreface profiles (i.e. panel (b) in Figures 5.3-5.7) between simulations shows that for decreasing R and increasing h_a, model shorefaces became deeper and more concave, with geometry approaching that of the initial (black) profile. Considering the inverse relationship between wave-induced shoreface erosion rates and depth (as reproduced in BARSIM [Sec. 1.5]), for a given morphodynamic-efficiency rate, a deeper shoreface is characterised by lower erosion rates beyond h_a. This suggests that as h_a approaches h_i (e.g. -0.5 mm/a sea level scenario in Figure 5.7), the significance of h-dependent lower-shoreface response decreases due to both increased h_a and diminishing rates of h-dependent shoreface erosion. Furthermore, the potential for morphological inheritance is low due to high h_a. This is illustrated in Figure 5.13a, in which reduced R toward the benchmark case results only in increased shoreface concavity as h_a approaches h_i. For rapid sea-level change where $h_a << h_i$ however, h-dependent lower shoreface response may be significant.

Beyond h_a, the significance or otherwise of h-dependent cross-shelf sediment transport to predictions of geometric equilibrium models also depends on the timescale of the application. For example, Table 5.1 shows residual lower-shoreface erosion volumes for the simulations in Figures 5.3-5.7. The residuals equate to total lower-shoreface erosion volume between h_a and h_i throughout the simulations, and were calculated

in units of time (m^3/a) and sea-level change (m^3/mSL) per metre of shoreline. Table 5.1 demonstrates that residual lower-shoreface erosion per unit time *decreased* for decreasing R, which is consistent with increased h_a and reduced rates of h-dependent shoreface erosion. However, when expressed as volume per metre of sea-level change, residual lower-shoreface erosion *increased* for reduced R to a peak of 39,164 m^3/mSL for the 2.5 mm/a sea level fall scenario [Tab. 5.1]. For $R < 2.5$ mm/a, residual lower-shoreface erosion then *decreased* [Tab. 5.1]. This demonstrates that for a given magnitude sea-level change, residual lower-shoreface erosion volumes are sensitive to the combined influence of h-dependent shoreface erosion and timescale (T). The significance of residual lower-shoreface erosion volumes for predicting coastal evolution is considered further in Section 5.5.2.

Table 5.1: Residual shoreface response volumes - Depth-dependent lower shoreface erosion volumes calculated between the active shoreface depth limit (h_a) and lower shoreface depth limit (h_i) for the simulations shown in Figures 5.3-5.7.

R (mm/a)	h_a (m)	Residual volume (m^2/a)	Residual volume (m^2/m_{SL})
10	5	2.19	219
5	10	1.51	302
2.5	15	0.97	392
1	25	0.38	385
0.5	32.5	0.15	302

For the 2.5 mm/a sea level fall scenario the active shoreface was insensitive to shelf gradient and extended to $h_a = 15$ m depth in each case [Figs. 5.5c, 5.8c and 5.9c]. However, the lower shoreface domain contracted and h-dependent shoreface erosion rates diminished more rapidly for steeper shelf gradients (panels (b) and (d) in Figures 5.5, 5.8 and 5.9). Consistent with lower shoreface contraction, morphological inheritance of shelf physiography decreased for steeper shelf gradients [Figs. 5.5b, 5.8b and 5.9b]. Thus although active shoreface dimensions were insensitive to shelf gradient [Sec. 5.5.1.1], h-dependent shoreface erosion beyond h_a diminished more rapidly for steeper slopes. This resulted in a reduced sediment flux available for deposition, which was reflected in lower strandplain volumes for the 0.225° [Fig. 5.8a] and 0.3° [Fig. 5.9a] linear substrates, compared to the 0.15° substrate [Fig. 5.5a]. Therefore the general behaviour for increasing substrate gradient may be characterised by contraction

of the lower shoreface and reduced autochthonous sediment supply. This was also described in the simulations as an increase in shoreface convexity (i.e. increased α) for steeper substrates [Figs. 5.5e, 5.8e and 5.9e]. The general behaviour is illustrated in Figure 5.13b, which shows that for typical concave shoreface geometry, whilst h_i is insensitive to shelf slope, x_i decreases for steeper substrates and increases for more gently sloping substrates. Considering all of the above, for a given R, h-dependent lower-shoreface erosion occurs at both higher rates and across a wider domain for gently sloping substrates, which results in a greater sediment flux for coastal deposition.

The importance of the relationship between shoreface slope and substrate slope, in controlling the mode of coastal response and the distribution of shoreface erosion and deposition during sea-level change, has been demonstrated previously [*Roy et al.*, 1994; *Cowell et al.*, 1995; *Tortora et al.*, 2009a,b]. As seen in Figure 5.14, they found that substrates steeper than the shoreface slope favoured a shift in deposition from the upper shoreface (coast) to beyond the lower shoreface toe (shelf). The simulation findings presented here build on their work by demonstrating that for the range of shelf gradients typical of barrier coasts (i.e. where deposition may be directed onshore), the erosive capacity of the lower shoreface becomes increasingly limited for steeper substrates, and thus total volumes of shoreface erosion and coastal deposition decrease. The findings therefore imply that for sea-level change in barrier-coast settings, coastal barrier deposition will decrease across steeper sections of the shelf. It has been shown that this behaviour emerges from a combination of contraction of the lower shoreface domain and reduced h-dependent erosion rates (i.e. reduced erosive capacity), and increasingly offshore-directed deposition demonstrated by *Roy et al.* [1994].

Comparison between Figure 5.9 and Figure 5.12 shows that for a given shelf gradient (0.3°), site morphodynamic efficiency also controls the depositional response to sea-level change. Intuitively, higher morphodynamic efficiency contributes to higher shoreface erosion rates and an increased sediment flux available for coastal deposition.

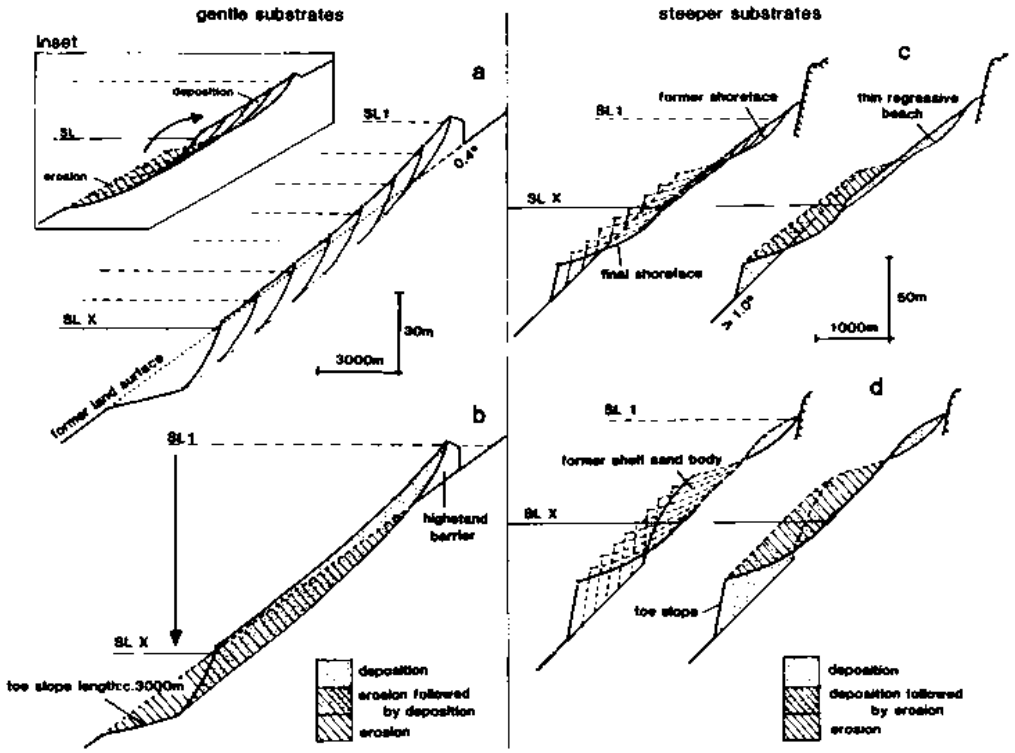

Figure 5.14: Influence of substrate slope on coastal barrier deposition during sea-level fall - For gentle substrate slopes shoreface sand supply due to erosional reworking is directed onshore (upper shoreface). Sub-aerial coastal deposition is limited for the case of steep substrate slopes, with shoreface sand supply directed offshore (lower shoreface). From *Roy et al.* [1994].

5.5.2 Scale-transcending shoreface definition

Collectively, the R-dependent active shoreface, h-dependent lower shoreface response, and site-dependent wavebase hint at the existence of a relationship between shoreface response and coastal evolution that spans the the spectrum of morphodynamic scales [Fig. 1.1]. This suggests that the varying relationships between h_c, h_i, h_a and h_w may provide a useful framework for describing coastal evolution across the scale divisions that separate typical problems in coastal engineering, geomorphology and stratigraphy [*Wolinsky*, 2009]. *Wolinsky and Murray* [2009] contemplated the issue of scale in the context of modelling long-term shoreline migration and coastal evolution. Specifically, they developed an approach based on the shoreline Exner Equation to reconcile alternative shoreline trajectories predicted by the Bruun rule and passive inundation models. However, the investigation of R- and h-dependent shoreface response was beyond the scope of their study, and their simplified approach assumed a time-invariant shoreface profile and fixed closure depth. However, the broadly defined scales of shoreline migration proposed by *Wolinsky* [2009] appear to be equally reconcilable with the nature of R- and h-dependent shoreface response described here. Therefore, his definitions of microscale, mesoscale and macroscale shoreline migration, which derive from the hierarchical nature of coastal geomorphic systems [*Cowell et al.*, 2003a,b], are extended here to include dynamic shoreface response. The relationship between scale-dependent coastal evolution and shoreface response may be described as follows:

1. *microscale* (e.g. $10^0 - 10^1$ years), in which the active shoreface depth limit is constrained to the surf zone or within the *Hallermeier* [1981] limit of annual profile activity ($h_a \leq h_c$), and, for the timescale of the problem, h-dependent lower-shoreface response does not accumulate to sufficient cross-shelf sediment transport residuals to impair predictions of geometric equilibrium models;

2. *mesoscale* (e.g. $10^2 - 10^5$ years), in which the active shoreface depth limit occurs between the Hallermeier inner and outer limits ($h_c < h_a < h_i$), and, for the timescale of the problem, h-dependent lower-shoreface response does not accumulate to sufficient cross-shelf sediment transport residuals to impair predictions of geometric equilibrium models; and

3. *macroscale* (e.g. 10^6+ years), in which the active shoreface depth limit approaches the Hallermeier outer limit ($h_a \approx h_i$), and thus h-dependent lower-shoreface response is absent and wave-induced cross-shelf sediment transport residuals between the shoreface toe (h_i) and wave base (h_w) are negligible.

Table 5.2 summarises the relationship between shoreface response and the morphodynamic scales of coastal evolution. Microscale coastal evolution encompasses short-term coastal engineering problems where the timescale of interest implies that shoreface activity and associated cross-shore sediment transport is limited to the upper shoreface [*Dean and Dalrymple*, 2002]. For example this could include the calculation of sand nourishment volumes for temporary beach protection from storms [*Dean*, 2002]. Morphokinematic models applied to microscale problems may be restricted to the upper shoreface. Mesoscale coastal evolution includes many problems of relevance to the coastal management/planning and geomorphology disciplines. For example, unravelling coastal evolution in response to late-Quaternary sea level fluctuations and predicting future shoreline retreat due to projected sea level rise [*Stive*, 2004; *FitzGerald et al.*, 2008; *Nicholls and Cazenave*, 2010] appear to be mesoscale problems. Morphokinematic models applied to mesoscale problems should consider the potential for R-dependent shoreface response. Macroscale change refers to coastal evolution at geological timescales of relevance to the study of ancient depositional systems, for which higher order fluctuations in boundary conditions and associated depositional responses are poorly constrained. Morphokinematic models applied to macroscale problems may be simplified to geometric equilibrium models that assume complete time-invariant shoreface behaviour [*Cant*, 1991; *Nummedal et al.*, 1993; *Kim et al.*, 2006].

Table 5.2: Scales of coastal evolution and indicative shoreface response - Suggested relationships between scales of coastal evolution problems and the nature of R-dependent shoreface response. Note that the significance of h-dependent lower-shoreface transport residuals varies with both timescale and setting. Modified from *Wolinsky* [2009].

Scale	Time	Space	Field	h_a	h-dependent residual
Microscale	years	10^0 km	engineering	$h_a \leq h_c$	insignificant
Mesoscale	ka	10^2 km	geomorphology	$h_c < h_a < h_i$	significant
Macroscale	Ma	10^3 km	stratigraphy	$h_a \approx h_i$	absent

5.5.3 Implications for late-Quaternary coastal barrier evolution

The findings of the simulation experiments presented in this chapter have implications for the investigations of Holocene coastal strandplain progradation [Ch. 3] and late-Quaternary coastal barrier evolution [Ch. 4]. For example, review of the geological evidence (i.e. RSL indicators) and physical reasoning for late-Holocene sea level fall in southeastern Australia [Sec. 3.2.1] suggested that a relative sea level fall of about 1.5 m beginning between 3 ka to 1.5 ka BP is the most representative scenario (i.e. between HL-2 and HL-3 in Figure 3.5). This implies an average rate of late-Holocene sea level fall between 0.5 mm/a and 1 mm/a. Comparison with the 0.5 mm/a [Fig. 5.7] and 1 mm/a [Fig. 5.6] simulation experiments described in this chapter, then suggests an active shoreface depth limit of 25 m $< h_a <$ 32.5 m for the Tuncurry site [Tab. 5.1]. Furthermore, multiplication of the associated annual residual h-dependent shoreface response volumes for the 3 ka and 1.5 ka durations suggests lower-shoreface sand supply volumes beyond h_a on the order of 0.151-0.385 m^3/a, or a total supply volume of 453-578 m^3 (per metre of shoreline). Combined with the total active-shoreface sand supply volumes for h_a = 25 m and h_a = 35 m [Tab. 3.3], this implies a total potential contribution of relative sea level fall to late-Holocene strandplain progradation of $1,877 + 453 = 2,330$ m^3 for the 0.5 mm/a scenario, or $1,443 + 578 = 2,020$ m^3 for the 1 mm/a scenario. Thus increased R is characterised by a reduced sand supply from the active shoreface (i.e. decreased h_a) and increased significance of h-dependent lower-shoreface erosion residuals.

For the last-glacial cycle simulation experiments described in Chapter 4, the findings from this chapter provide further insights on variability in the deposition and preservation of coastal barrier systems associated with different sea level stages. For example, whilst coastal barrier deposition was more or less continuous at Tuncurry through the last glacial cycle, preservation was mostly limited to MIS-5 sea-level highstands and the MIS-3 falling stage [Fig. 4.9]. The sea level reversals experienced during interglacial and interstadial highstands would have been characterised by stable to slowly changing sea levels during which shoreface morphodynamic disequilibrium would have driven high rates of onshore shoreface sand supply, comparable to conditions experienced early in the Holocene highstand [Ch. 3]. In contrast, during the post-glacial marine transgression sea level rose 120 m in about 12,000 years [Fig. 4.4], implying

an average R on the order of 10 mm/a. Figure 5.3 suggests that the active shoreface would have been limited to the vicinity of the surf zone during rapid sea level rise, restricting the autochthonous sediment flux available for deposition. The limited depth of shoreface erosion would have supported preservation of the antecedent MIS-3 falling stage barrier systems, and transgression was most likely characterised by a combination of barrier rollover and overstepping, due to low rates of coastal deposition and variable backbarrier dimensions enforced by the inherited substrate physiography [Fig. 4.10].

5.5.4 Potential for model dependence

In this chapter, the BARSIM models developed in Chapter 3 were applied in a series of exploratory simulations to investigate the nature of shoreface response to sea level change. Acknowledging that the adopted model configurations represent only one possibility in the spectrum of uncertainty regarding shoreface response rates, Section 3.5.3 discussed the key sources of model uncertainty and their potential influence on the conclusions drawn in Chapter 3. Whilst the simulation findings presented in this chapter are subject to the same sources of uncertainty, the potential for model dependence on the conclusions drawn in Section 5.6 should be considered. Furthermore, although quantitative findings are presented to facilitate conceptual discussions on simulated shoreface behaviour, expression of the predicted behaviour using the shoreface definitions described in Section 5.2 - e.g. the discussion of scale-transcending shoreface concepts in Section 5.5.2 - provides an informative approach to generalising the outcomes of the BARSIM model experiments.

First, it must be acknowledged that the quantified rates of shoreface response and values of h_a in the simulation experiments described in this chapter would vary for a different shoreface erosion function or value of m. Similarly, potential volumes of strandplain progradation due to relative sea-level fall calculated in Section 5.5.3 are also valid for the adopted model configuration only. This is because model predictions are contingent on an assumption of exponentially depth-diminishing shoreface erosion rates (and onshore sand transport rates within a balanced sediment budget) and the erosion-efficiency calibration procedure used to derive suitable values of m [Sec. 3.3.1.3]. Given that the calibration procedure only considered stable sea levels, the model configurations applied may not necessarily be optimal for rates of sea level change and substrate slopes investigated in this chapter. Nonetheless, considering that the scaling

exponent m is used in the models to reflect local erosion efficiency (i.e. for the wave climate and sediment characteristics), application of the m values derived in Chapter 3 seems reasonable in lieu of any relevant observational data.

However, the qualitative shoreface behaviour described in this chapter, including the relative relationships between key shoreface depths, is anticipated to be largely independent of the m value. That is, similar behaviour would be expected for the range of feasible m values for the Tuncurry and Moruya settings, although the rates of shoreface erosion and values of m would vary between calibrations. This is because, for the balanced sediment budgets considered in this chapter, the cumulative effect of depth-dependent erosion rates implies larger volumes of coastal deposition for slower rates of sea level change. The erosion-efficiency calibration procedure that was described in Section 3.3.1.3 identified relevant m values for the two sites, based on the average inner-continental shelf gradients, and the relationship between the respective wave climates and sediment characteristics that was not captured by other model parameters. Thus the qualitative conclusions presented in this chapter may be applicable to comparable settings where exponentially depth-diminishing shoreface erosion rates (and onshore sand transport rates) are a valid assumption. Considering the arguments above, the conclusions presented in Section 5.6 that are potentially subject to model dependence are distinguished from those that are expected to be generally robust.

5.6 Conclusions

Conclusions about the relationship between shoreface response and sea-level change can be drawn from the results of a series of idealised and exploratory simulation experiments reported in this chapter. The sensitivity of shoreface behaviour to the individual depositional controls examined in the simulations demonstrate the relationship between shoreface behaviour and sea-level change, as a consequence of variation in active shoreface response (i.e. erosion) and morphological inheritance. Ultimately, during sea-level change on barrier coasts, shoreface response manifests in the shoreline trajectories and the volumes of coastal deposition. Thus consequences for coastal barrier deposition are implicit in the findings presented in this chapter.

As in Chapter 3 aspects of the conclusions may be model dependent [see Sec. 5.5.4] have been *italicised*. This is not to imply that the suggested behaviours are incorrect,

but that quantitative estimates are dependent on the BARSIM algorithms and model configurations. The key conclusions regarding shoreface response to sea level change include:

1. The extent of time-invariant shoreface response, as defined by the active shoreface depth limit (h_a), was shown to be independent of the upper-shoreface depth limit (h_c). This is reasonable as h_c is derived from wave climate statistics [Eq. 5.1], whereas h_a is a function of the relationship between h-dependent shoreface erosion rates and R. *For increasing R within the range considered (i.e. 0.5-10 mm/a), h_a contracted from the lower-shoreface depth limit (h_i) to the surf zone.*

2. *For R = 2.5 mm/a, h_a was insensitive to substrate gradient within the range of slopes considered (i.e. 0.15-0.3°). Furthermore, for the range of R considered, h_a was insensitive to complex substrate geometries. Rather, h_a was only sensitive to R and site morphodynamic efficiency (defined by m).* Considering that wave energy varies with shelf gradient, due to increased or moderated attenuation during shoaling, h_a may in fact be sensitive to significant variations in shelf gradient. In the model experiments presented here, altered wave energy attenuation beyond the geometric considerations of the BARSIM erosion function [Eq. 1.3], and the calibration of m for slopes other than the average shelf gradient at each site, was beyond the scope of the investigation.

3. For a given h_i and decreasing R, the lower shoreface domain contracts as h_a approaches h_i, and thus the contribution of h-dependent lower-shoreface response to the shoreface sediment flux decreases accordingly. The volume of h-dependent lower-shoreface erosion decreases due to both contraction of the lower-shoreface domain (i.e. reduced surface area), and reduced rates of shoreface erosion imposed by deeper and more concave shoreface geometry. Consequently, the potential for shoreface morphological inheritance also decreases for decreasing R.

4. Whilst active shoreface dimensions were insensitive to substrate gradient in the model experiments considered here, the lower-shoreface contracted for increased substrate slope. This is reasonable as h_i is derived from wave climate statistics and sediment grain size [Eq. 5.3], whereas h_a is a function of the relationship

between h-dependent shoreface erosion rates and R. *For increasing substrate gradient, whilst increased shoreface convexity sustained mid-shoreface erosion rates, beyond h_a, h-dependent erosion rates diminished more rapidly across the lower shoreface, causing reduced shoreface sediment flux. That is, both a reduction in lower-shoreface shore-normal extent, and reduced h-dependent lower-shoreface erosion rates, contributed to reduced shoreface sand supply to the coast.* This is reasonable assuming exponentially depth-diminishing shoreface erosion rates.

5. Conclusions 1-4 suggest that for a given h_i, slower rates of sea level change (i.e. low R) is characterised by deeper and more concave shoreface geometry associated with h_a approaching h_i. This shoreface geometry is less sensitive to variable substrate physiography, and supports higher gross autochthonous sand supply for a given sea level change, although lower instantaneous rates of onshore sand supply. For increasing R, shoreface geometry is typically shallower and more convex in shape, due to decreased (shallower) h_a. This shoreface geometry is more susceptible to morphological inheritance of the antecedent substrate. Whilst shallower shoreface geometry supports higher instantaneous rates of onshore sand supply, the gross autochthonous sand supply for a given sea level change is lower, contributing to reduced volume coastal barrier systems. This is consistent with the demonstrated relationship between h_a and R.

6. The nature of h_a may provide a conceptual measure with which to categorise timescale-dependent coastal evolution, which may also have practical significance for the design of modelling approaches. For example: *microscale* coastal evolution (c. $10^0 - 10^1$ years) may be characterised by $h_a \leq h_c$; *mesoscale* coastal evolution (c. $10^2 - 10^5$ years) may be characterised by $h_c < h_a < h_i$; and, *macroscale* coastal evolution (c. 10^6+ years) may be characterised by $h_a \approx h_i$. An improved understanding of the relationship between h_a and R has the potential to inform the design and development of new modelling approaches that account for h-dependent shoreface erosion and R-dependent shoreface response.

7. The significance of h dependent lower-shoreface response (i.e. the cumulative sediment transport residuals that originate from beyond h_a) appear to be greatest for mesoscale coastal evolution, which includes both late-Quaternary and anticipated

future coastal change associated with climate change projections. For such problems, cross-shelf sand transport characterised by h-dependent shoreface response may accumulate to significant (and unaccounted for) residuals at the timescale of interest, in the context of geometric-equilibrium modelling approaches.

This chapter considered the nature of shoreface response to sea level change and potential implications for coastal deposition through a series of idealised and exploratory simulation experiments. The potential implications of R-dependent shoreface response for late-Quaternary coastal evolution and future coastal change are explored in further detail in Chapter 6.

6

Shoreface Response to Sea Level Change 2: Examples

6.1 Introduction

The simulation experiments documented in Chapter 5 investigated shoreface response to sea-level change (i.e. R-dependent shoreface response) for conditions and settings typical of late-Quaternary and potential future coastal change on barrier coasts. Consideration of the findings in the context of traditional approaches to predicting coastal evolution and shoreline migration [Sec. 1.4.1] suggest potential implications for approaches and predictions. This chapter is organised into three sections that investigate the implications of R-dependent shoreface response, as described in Chapter 5, for typical problems encountered in the coastal management/planning, geomorphology, and stratigraphy disciplines. The aims, methods and research findings specific to each problem of interest are described and discussed in each section. A synthesis of the principal conclusions from each section is provided in Section 6.5.

6.2 Predicting coastline response to climate change

Physics-based global climate modelling suggests that by the end of the present century, anthropogenic global warming will have contributed to a rise in global mean sea levels of between 0.4 to 0.8 m above 1990 levels, due to thermal expansion of the oceanic water mass and melt water additions from ice caps and glaciers [*Meehl et al.*, 2007]. Furthermore, semi-empirical models suggest the potential for a higher sea-level rise

(i.e. up to 1.5 m above 1990 levels) within the same timeframe, due to alternative radiative forcing scenarios and/or faster than anticipated rates of ice sheet response [*Overpeck et al.*, 2006; *Rahmstorf*, 2007; *Horton et al.*, 2008; *Jevrejeva et al.*, 2012]. Where projected rates of sea-level rise exceed persisting tectonic or isostatic uplift of the coast, barrier coasts may be expected to respond by shoreline retreat, with potentially significant impacts for coastal settlements [*Stive*, 2004; *FitzGerald et al.*, 2008; *Nicholls and Cazenave*, 2010; *Woodroffe and Murray-Wallace*, 2012]. Aside from uncertainties regarding future greenhouse-gas emissions and rates of sea level response to global warming [*Meehl et al.*, 2005, 2007], shoreface response to projected sea-level rise represents a fundamental source of uncertainty in the context of predicting when and at what rates shoreline retreat may occur [*Cowell et al.*, 2006]. Even with robust projections of future sea-level rise therefore, managing and planning for climate-change driven shoreline retreat remains a significant challenge due to the poorly constrained scope of potential future coastal responses.

The simulation experiments documented in Chapter 5 demonstrated the sensitivity of shoreface response to the rate of sea-level change and geomorphic setting. That is, considering the shoreface morphological relaxation time (T_r) for a given setting, active shoreface response decreases for increasing rates of sea-level change, as seen in the contraction of the active shoreface domain and increased significance of depth-dependent lower shoreface response. Contraction of the active shoreface is associated with reduced shoreface erosion, and thus a decrease in cross-shore sediment exchanges between coast and shelf. For accelerated rates of sea-level rise therefore, it may be anticipated that active shoreface dimensions may decrease as the rate of sea level forcing continues to exceed shoreface relaxation timescales. This may potentially mitigate the shoreline retreat commitment for the coming century, due to decreased cumulative sediment losses from the coast to the shoreface for faster rates of sea-level rise. In such a case, the ultimate slowing or cessation of sea-level rise may then lead to increased onshore shoreface sediment supply, due to lagged shoreface response to morphological disequilibrium stress. The potential significance of shoreface response to future coastal change remains to be explored in detail. Considering the above, this section addresses the following questions:

1. How may active shoreface dimensions vary in response to projected accelerating sea-level rise over the coming century?

2. What are the implications of the anticipated shoreface response for predictions of shoreline retreat within and beyond that timeframe?

3. Do predictions of future shoreline retreat that consider R-dependent shoreface response vary from predictions generated by geometric equilibrium-profile models, in which time-invariant shoreface response is assumed?

6.2.1 Methods

6.2.1.1 Accelerating sea-level rise scenario

As described above [Sec. 6.2], projections of sea-level rise due to global warming over the coming few centuries vary depending on the adopted greenhouse-gas emission scenario and the assumed rates of ice sheet response (i.e. melt water input). As such there is considerable variability in global mean sea level projections for the typical planning horizon of 2100. Relative to historical measurements of sea-level change however [*Church and White*, 2006; *Church et al.*, 2008; *Church and White*, 2011], most projections may be characterized by accelerated sea-level rise through the present century, followed by the subsequent slowing of sea-level rise beginning at some point during the 22$^{\text{nd}}$ or 23$^{\text{rd}}$ centuries, and ultimate stabilisation perhaps occurring around 2500 [*Meehl et al.*, 2005, 2007; *Jevrejeva et al.*, 2012]. The period of accelerated sea-level rise implies a significant change in rates of sea level forcing, which may be expected to contribute to timescale-dependent shoreface response over the coming centuries, based on the simulation results documented in previous chapters.

The simulation experiments carried out here consider both historical measurements of sea-level rise and the period of projected acceleration in sea-level rise to 2100. Specifically, the reconstructed global mean sea level curve of *Church and White* [2011] was used to construct the scenario from 1880 to 2010 [Fig. 6.1]. The period of slowed sea-level rise experienced during the 1960s was not considered in the adopted sea-level rise scenario as decadal-scale variability was beyond the scope of the simulations. That is, the experiments were designed to investigate shoreface response to mean-trend change in the rate of sea-level rise. The 95-percentile high range of the IPCC A1FI scenario was adopted for the future component (i.e. 2010-2100) of the sea level curve [Fig. 6.2a]. The decision to adopt the IPCC's upper range projection reflects both recent

observations that suggest global mean sea level has followed the upper range projection [Fig. 6.2b], and the potential for faster rates of sea-level rise than were predicted using physics-based climate models and the IPCC AR4 emission scenarios [Sec. 6.2]. Figure 6.3 shows the complete sea level curve that was used to drive the simulation experiments that are described in Section 6.2.1.2.

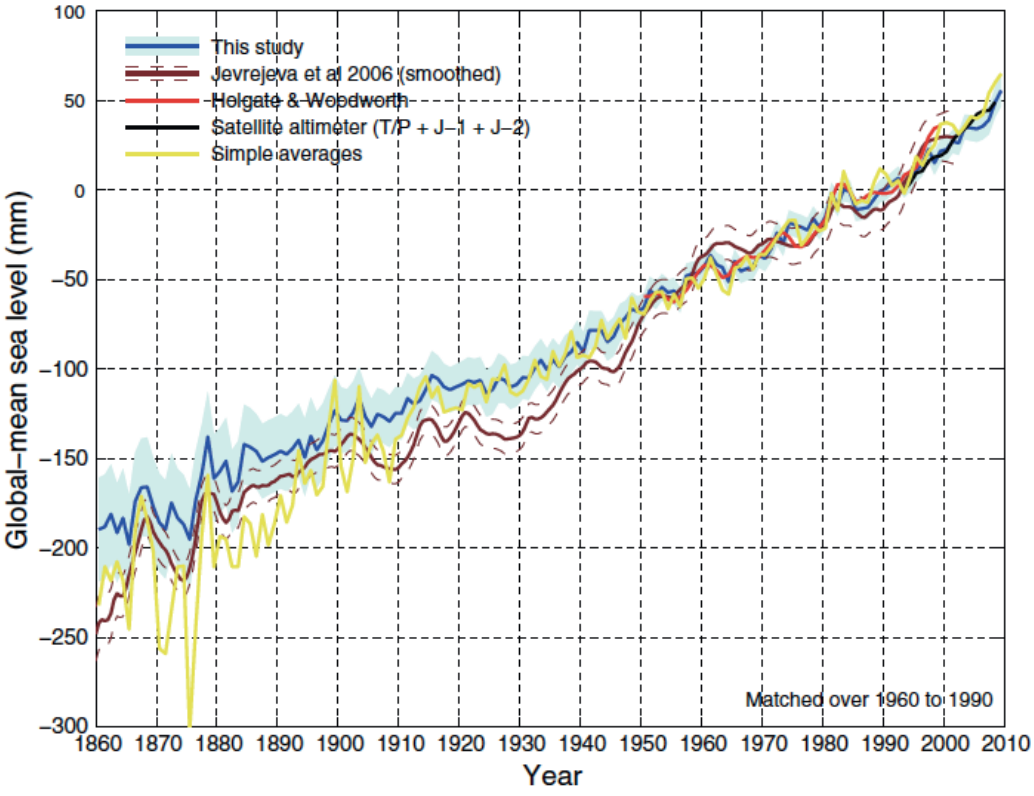

Figure 6.1: Historical record of global mean sea-level change - Corrected measurements from tide gauge data and satellite altimetry suggest that global mean sea level rose 0.15 m over the period 1890-1990, and a further 0.06 m to 2010. From *Church and White* [2011].

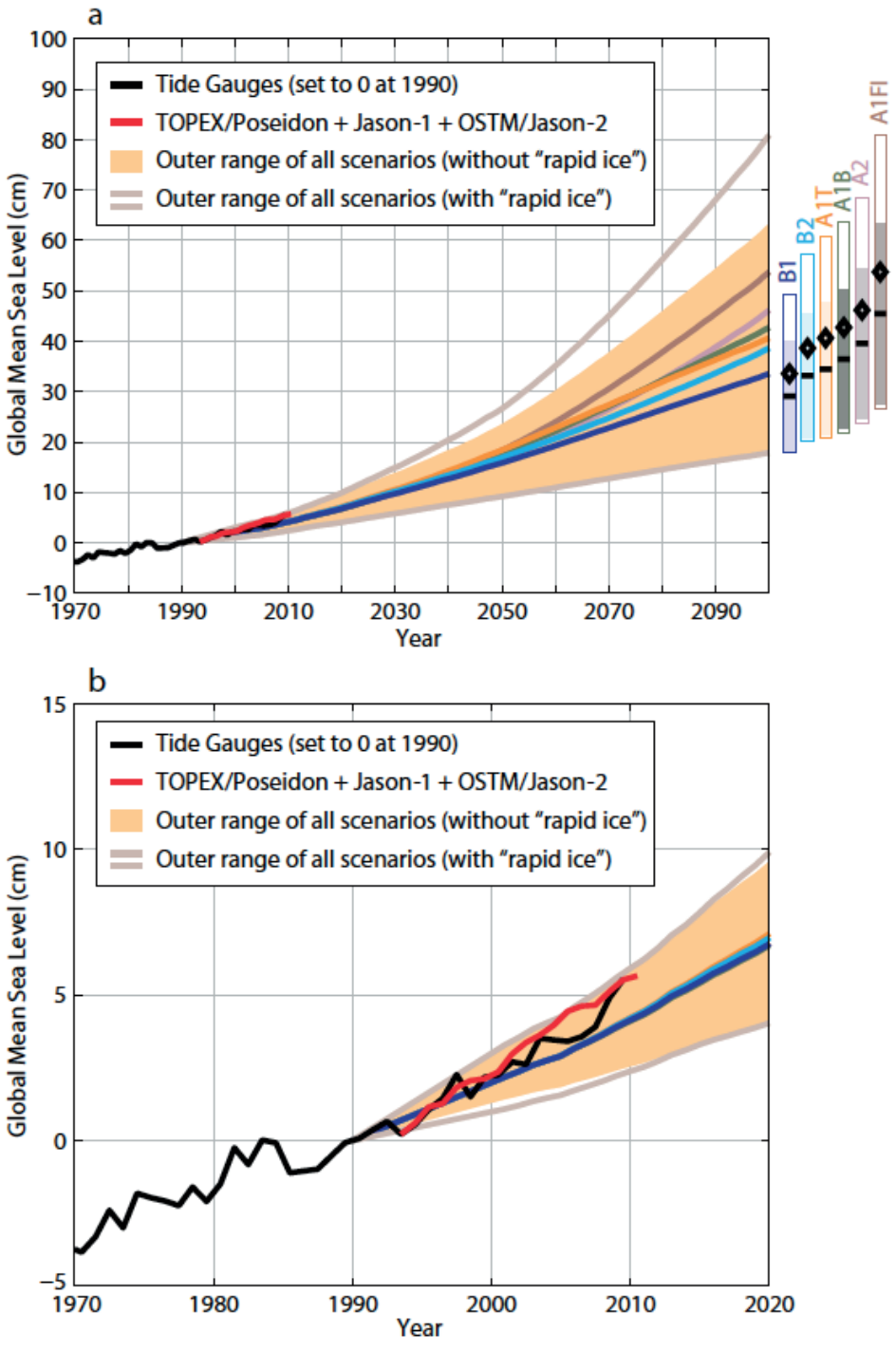

Figure 6.2: Projected global mean sea-level rise relative to measurement data - (a) Range of projected sea-level rise to 2100 based on the emission scenarios and modelling adopted in IPCC AR4, with and without rapid ice loss; (b) Tide gauge and satellite altimetry records suggest that global mean sea-level rise followed the upper range of IPCC projections over the period 1990-2010. From *Church et al.* [2011].

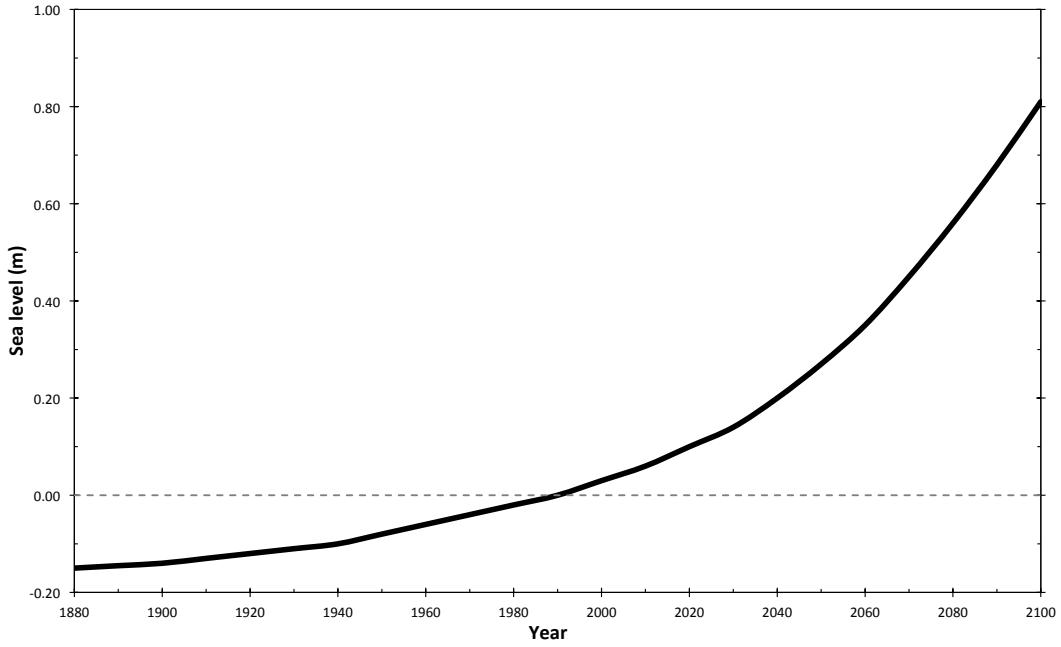

Figure 6.3: Accelerating sea level scenario applied in sea-level rise models - Climate-change induced sea-level rise scenario applied in morphokinematic models to predict potential future shoreline retreat. The scenario is based on historical observations [Fig. 6.1] and physics-based climate model projections based on the IPCC AR4 A1FI (upper range with rapid sea ice) emission scenario [Fig. 6.2].

6.2.1.2 Simulation experiments

A time-dependent morphokinematic modelling approach was adopted to investigate shoreline retreat in response to the adopted sea-level rise scenario [Sec. 6.2.1.1] at the two study sites. This allowed for absolute control over the simulated shoreface response to assess the range of potential outcomes. Previous studies and datasets describing the coastal geomorphology and stratigraphy at Tuncurry [Sec. 2.7] and Moruya [Sec. 2.6] were used to guide the design of site terrain models for the experiments. The individual Tuncurry drilling transect [Fig. 2.13] and central Moruya transect [Fig. 2.10] were used as representative profile locations. For each model, the shoreface profile was obtained from hydrographic survey data and the dune profile was extracted from field survey (Tuncurry) and LIDAR (Moruya) datasets.

The shoreface origin was defined at the position of the 'winter' beach berm (at 2.5 m PMSL), to account for fluctuations in beach width associated with the strong seasonal and inter-annual variability in the southeast Australian wave climate [*Short and Trenaman*, 1992; *Harley et al.*, 2010]. That is, whilst the average range of beach variability was removed from the site terrain models, the potential for further cyclical shoreline retreat and advance, due to extreme storm-induced beach erosion, was preserved. In this way the models provide estimations of potential future change in modal shoreline position (and not the maximum extent of beach erosion). The purpose of these simulations was to consider the sensitivity predicted shoreline retreat to R-dependent shoreface response and thus the shoreline origin is not particularly important. In assessing potential shoreline retreat for management and planning purposes, it would be more appropriate to define the shoreface origin at the maximum potential storm cut. Linear beach face gradients between the shoreface origin (i.e. beach berm) and the surveyed fore-dune scarp were 0.8° at Tuncurry and 0.7° at Moruya.

For a standardised comparative reference, the simulation was first carried out using a static geometric-equilibrium (i.e. time-invariant) shoreface model, in which complete active shoreface response was assumed to a fixed and constant closure depth. As this approach is the basis of the standard Bruun rule of coastal erosion [*Bruun*, 1962, 1983, 1988], using this approach the model generates shoreline retreat that is more or less consistent with Bruun Rule predictions (see Section 1.4.1 for further discussion of the Bruun rule). For a given setting, the key input parameter in this approach is the profile closure depth, which defines the absolute seaward limit of implied cross-shore sediment transport. To investigate the sensitivity of predicted shoreline retreat a range of potential closure depths were investigated for each site, including:

1. the typical upper shoreface depth limit for open-coast settings in southeastern Australia [*Cowell et al.*, 1999] 12 m;

2. the suggested profile closure depth for a 100-year response timescale, derived from the analysis of bathymetric survey data from the Gold Coast, Queensland [*Patterson*, 2012] 17 m;

3. the typical surficial sediment transition between finer regressive shoreface sands and the coarser inner-shelf transgressive sand sheet in southeastern Australia [*Roy et al.*, 1997] 22 m; and

4. the typical lower shoreface depth limit for open-coast settings in southeastern Australia [*Cowell et al.*, 1999] 35 m.

A summary of the various approaches that may be used to define the upper and lower shoreface depth limits has been provided in Section 5.2.

The simulation experiments were then repeated using dynamic shoreface models, in which shoreface geometry was guided by the outcomes of the BARSIM experiments documented in Chapter 5. Shoreface geometry was defined using the standard equilibrium shoreface function $h = Ax^m$, after [*Bruun*, 1954; *Dean*, 1977, 1991]. The active shoreface depth limits determined for the 0.5 to 10 mm/a sea-level fall experiments in Section 5.4.1 were used as a guide to fit the shoreface function in the morphokinematic modelling approach. Specifically, the approach involved the dynamic specification of shoreface geometry that reflected discrete model phases designed to reflect the increasing rate of sea-level change [Fig. 6.3].

Model sea-level change for each decadal time-step, and the corresponding shoreface parameters adopted for each phase of the Tuncurry and Moruya models, are provided in Table 6.1. For each model phase, the shoreface shape (defined by m in the equilibrium shoreface function) was fitted to provide the closest representation of the lower portion of the active shoreface, accounting for the evolving shoreface toe position relative to the initial shoreface morphology. This was intended to provide a realistic representation of the transitional inflection between the active shoreface and (passive) lower shoreface-inner shelf profile. A linear shoreface-shelf ramp that extended to $h_a + 1$ m was also included to enable a realistic shoreface-inner shelf transition characteristic of depth-diminishing shoreface response in the vicinity of profile closure.

Table 6.1: Shoreface dimensions applied in the dynamic shoreface models - The accelerating sea-level rise scenario was based on Figure 6.1 and Figure 6.2 (A1FI with rapid ice) and resulted in a total 0.96 m rise between 1880-2100. The dynamic shoreface models featured six phases between which shoreface geometry was varied based on the average rate of sea-level change within each phase. The Bruun factor (BF) is shown for each shoreface phase assuming an average dune height of 6 m at both sites.

Step	Year	Sea Level	Phase	Moruya			Tuncurry		
				x_a	h_a	BF	x_a	h_a	BF
0	1880	-0.15	0	0	0	0	0	0	0
1	1890	-0.145	1	3100	35	77	5700	35	140
2	1900	-0.14	1	3100	35	77	5700	35	140
3	1910	-0.13	2	1800	27	56	3500	27	108
4	1920	-0.12	2	1800	27	56	3500	27	108
5	1930	-0.11	2	1800	27	56	3500	27	108
6	1940	-0.10	2	1800	27	56	3500	27	108
7	1950	-0.08	3	900	17	41	1500	17	67
8	1960	-0.06	3	900	17	41	1500	17	67
9	1970	-0.04	3	900	17	41	1500	17	67
10	1980	-0.02	3	900	17	41	1500	17	67
11	1990	-0.00	3	900	17	41	1500	17	67
12	2000	0.03	4	600	12	36	1000	12	58
13	2010	0.06	4	600	12	36	1000	12	58
14	2020	0.10	4	600	12	36	1000	12	58
15	2030	0.14	4	600	12	36	1000	12	58
16	2040	0.20	5	400	9	30	700	9	50
17	2050	0.27	5	400	9	30	700	9	50
18	2060	0.35	5	400	9	30	700	9	50
19	2070	0.45	6	300	6	29	500	6	46
20	2080	0.56	6	300	6	29	500	6	46
21	2090	0.68	6	300	6	29	500	6	46
22	2100	0.81	6	300	6	29	500	6	46

6.2.2 Results

To evaluate the sensitivity of predicted shoreline retreat to the active shoreface extent, the sea-level rise experiment was first attempted using a time-invariant shoreface model with a fixed active shoreface depth limit (i.e. profile closure depth). Figure 6.4 shows the coastline response predicted for Moruya using the time-invariant shoreface model with closure depths of 12 m [Fig. 6.4a], 17 m [Fig. 6.4b], 22 m [Fig. 6.4c] and 35 m [Fig. 6.4d]. The total shoreline retreat predicted by 2100 for each of the four cases was 49.7 m, 56 m, 56.9 m and 82 m respectively [Fig. 6.5a]. For all cases the rate of shoreline retreat increased throughout the scenario [Fig. 6.5a], and the rates of retreat were proportional to the rate of sea-level rise [Fig. 6.5b]. The predicted shoreline retreat increased for deeper profile closure depths [Fig. 6.5]. For closure depths of 12-22 m the average beach berm position was predicted to retreat to the toe of the contemporary foredune [Fig. 6.4]. For a closure depth of 35 m shoreline retreat was predicted to extend into the dune system [Fig. 6.4]. Negligible difference was observed between the outcomes of the 17 m and 22 m closure depth models [Fig. 6.5].

Figure 6.6 shows the coastline response predicted for Tuncurry using the time-invariant shoreface model with closure depths of 12 m [Fig. 6.6a], 17 m [Fig. 6.6b], 22 m [Fig. 6.6c] and 35 m [Fig. 6.6d]. The total shoreline retreat predicted by 2100 for each of the four cases was 73.7 m, 80.4 m, 95.4 m and 142 m respectively [Fig. 6.7a]. For all cases the rate of shoreline retreat increased throughout the scenario [Fig. 6.7a], and the rates of retreat were proportional to the rate of sea-level rise [Fig. 6.7b]. The predicted shoreline retreat increased for deeper profile closure depths [Fig. 6.7]. For closure depths between 12-35 m the average beach berm position was predicted to retreat into the dune system in all cases [Fig. 6.6]. More specifically, the model predicted that the contemporary foredune would be removed for a fixed closure depth of 12 m, whilst almost 1 km of the dune system would be eroded assuming a fixed closure depth of 35 m [Fig. 6.6].

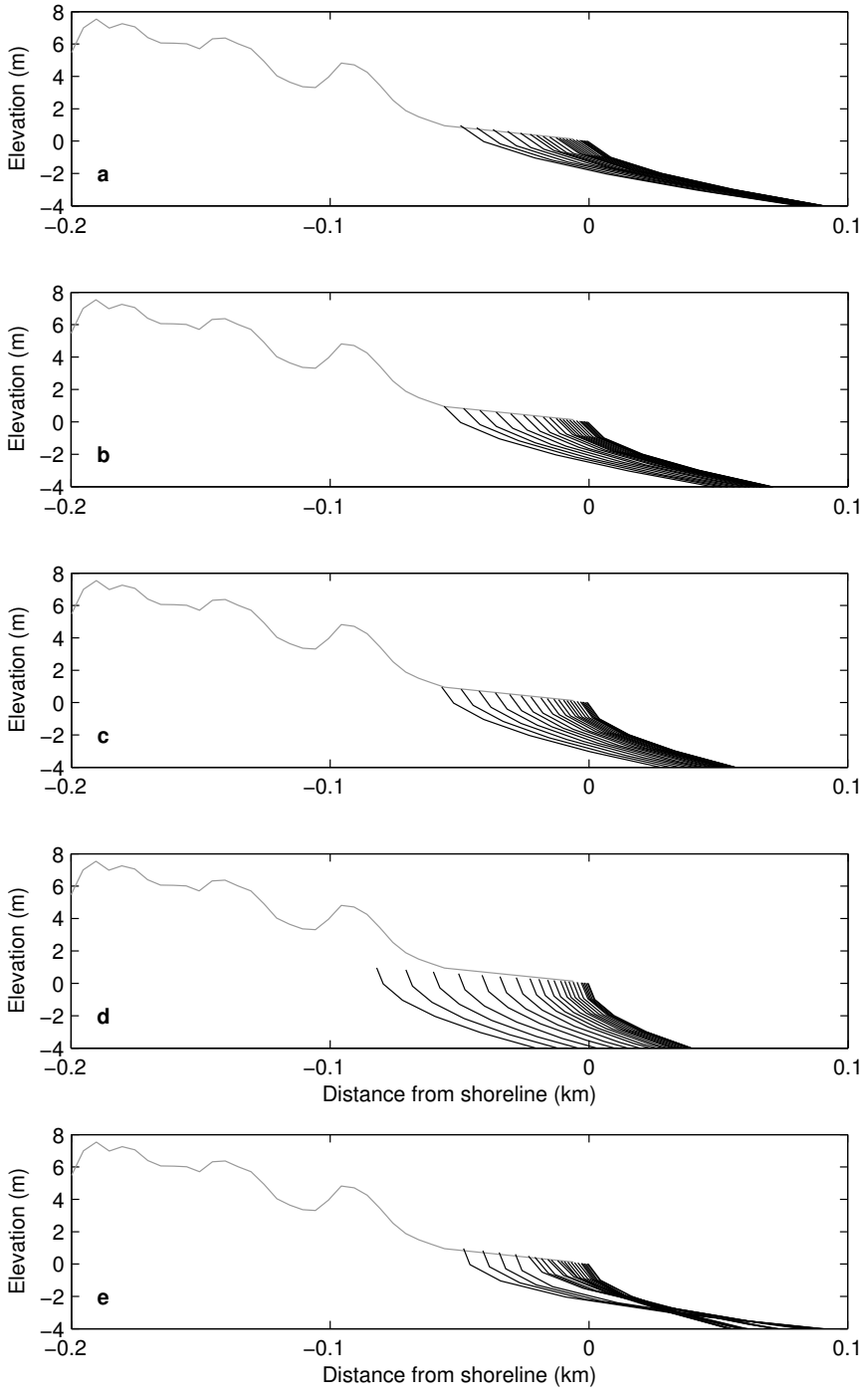

Figure 6.4: Simulated coastline response at Moruya, 1880-2100 - Simulated coastline response to a 0.96 m sea-level rise [Fig. 6.3] at Moruya between 1880 and 2100. The results of time-invariant shoreface models with fixed active shoreface depth limits of (a) 12 m, (b) 17 m, (c) 22 m and (d) 35 m are shown with the outcome of (e) the dynamic shoreface model [Tab. 6.1].

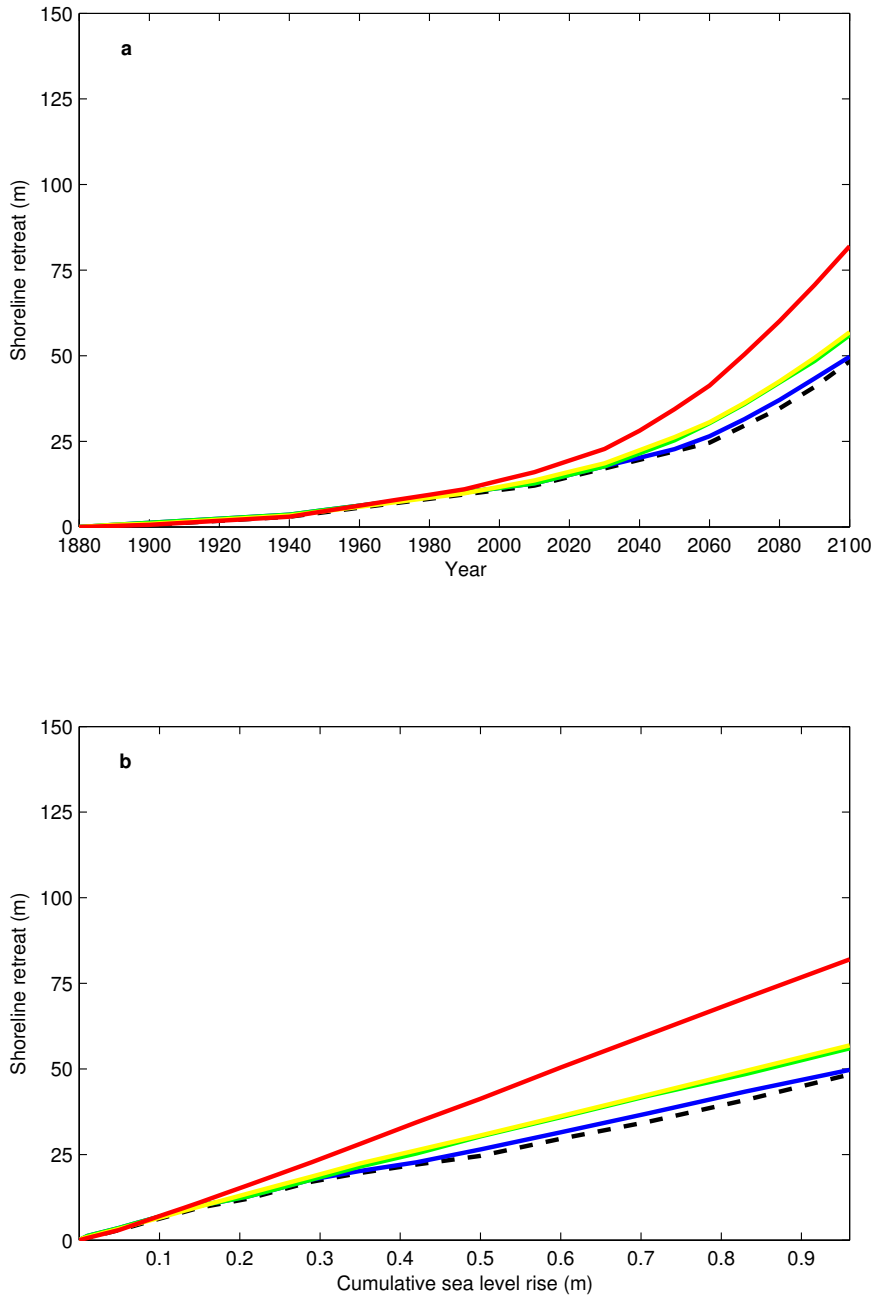

Figure 6.5: Predicted shoreline retreat at Moruya, 1880-2100 - Predictions of shoreline retreat at Moruya for the period 1880-2100 in relation to (a) time and (b) cumulative sea-level rise. Model predictions from the 12 m (blue), 17 m (green), 22 m (yellow) and 35 m (red) time-invariant shoreface models and the dynamic shoreface model (dashed black) are shown. See Figure 6.4 for model outputs.

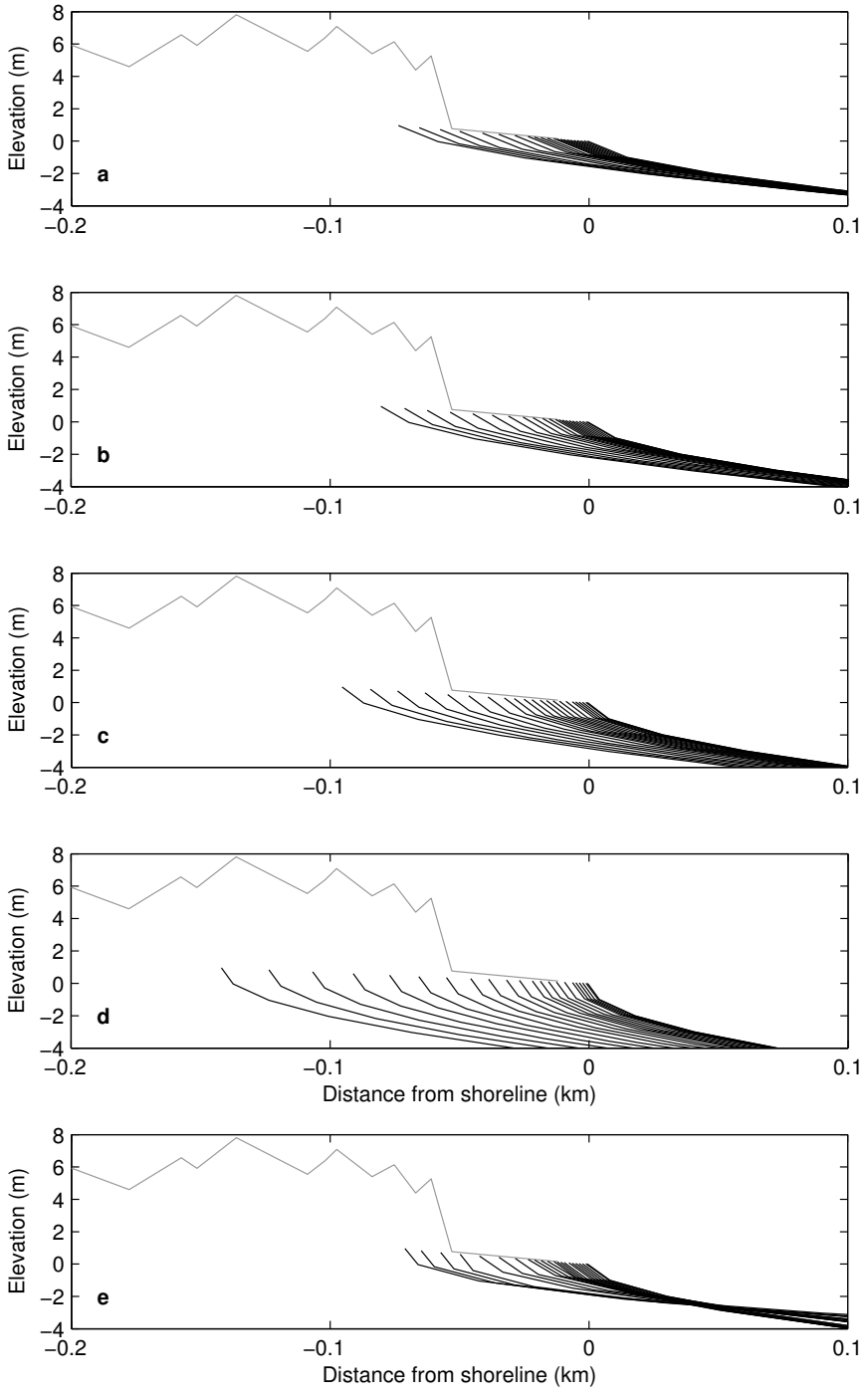

Figure 6.6: Simulated coastline response at Tuncurry, 1880-2100 - Simulated coastline response to a 0.96 m sea-level rise [Fig. 6.3] at Tuncurry between 1880 and 2100. The results of time-invariant shoreface models with fixed active shoreface depth limits of (a) 12 m, (b) 17 m, (c) 22 m and (d) 35 m are shown with the outcome of (e) the dynamic shoreface model [Tab. 6.1].

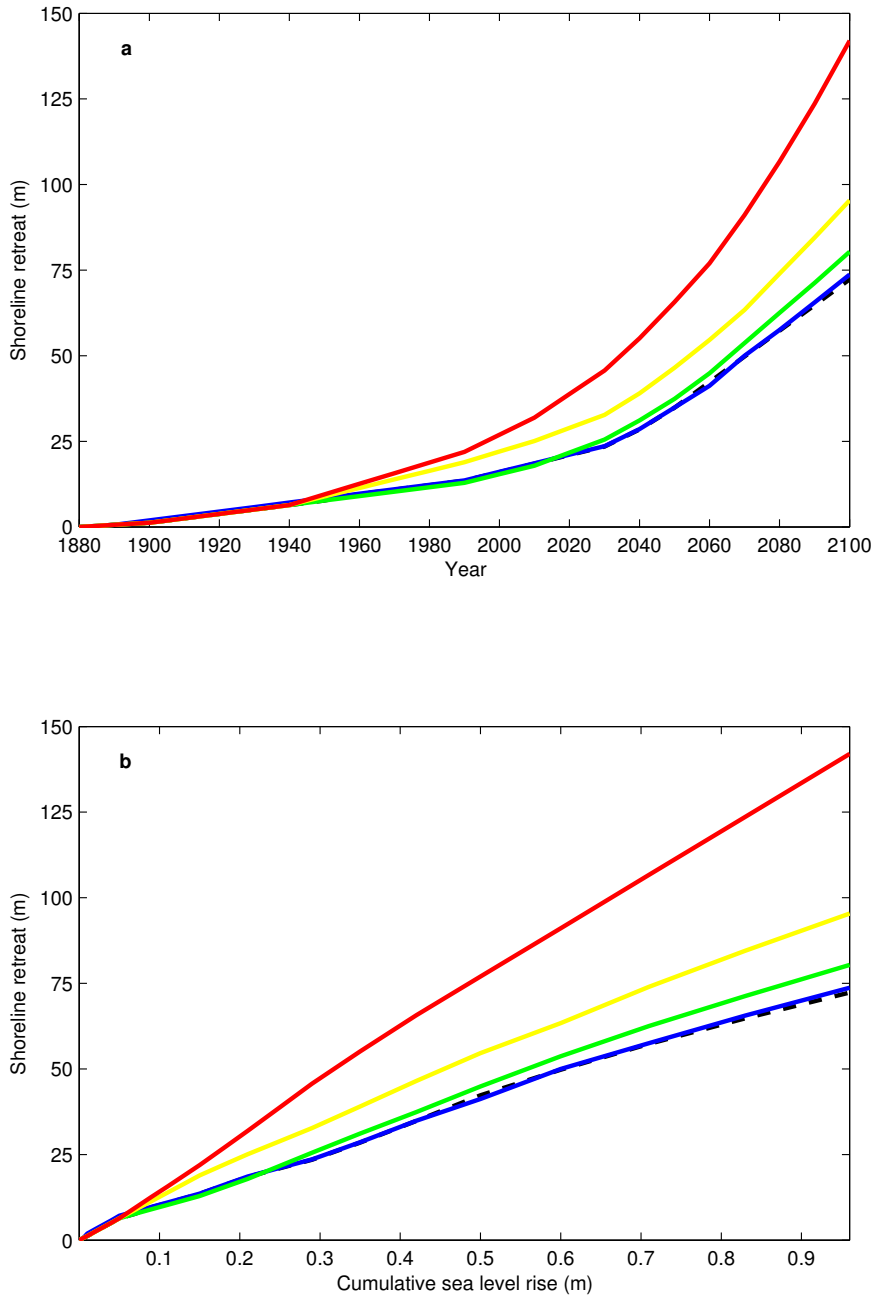

Figure 6.7: Prediction shoreline retreat at Tuncurry, 1880-2100 - Predictions of shoreline retreat at Tuncurry for the period 1880-2100 in relation to (a) time and (b) cumulative sea-level rise. Model predictions from the 12 m (blue), 17 m (green), 22 m (yellow) and 35 m (red) time-invariant shoreface models and the dynamic shoreface model (dashed black) are shown. See Figure 6.6 for model outputs.

The findings of the BARSIM experiments presented in Chapter 5 demonstrated that active shoreface dimensions are sensitive to the rate of sea-level change. Given that the rates of sea-level change considered in Chapter 5 reflect the range of historical and projected rates of sea-level rise, the findings from Chapter 5 were used to guide active shoreface dimensions throughout the sea-level rise scenario for the dynamic shoreface models. That is, the active shoreface depth limits were derived from the simulation findings presented in Figures 5.3-5.7. Table 6.1 shows the active shoreface dimensions that were adopted for each phase of the dynamic shoreface models. Each model phase represents a discrete period of the sea-level rise scenario [Fig. 6.3] for which a relatively constant rate of sea-level rise persists, and thus a fixed active shoreface depth limit may be applied. Table 6.1 shows that based on the findings of Chapter 5, progressively shallower profile closure depths were required to simulate coastal response to the accelerating rate of sea-level rise shown in Figure 6.3.

Figure 6.4e shows the coastal response predicted for Moruya using the dynamic shoreface model with the active shoreface dimensions adopted for each model phase [Tab. 6.1]. The total shoreline retreat predicted by 2100 was 48.5 m [Fig. 6.5]. Whilst the total shoreline retreat was similar to that predicted by the 12 m fixed closure depth model, Figure 6.5 suggests that decadal rates of shoreline retreat differed between the fixed and dynamic shoreface models. Figure 6.6e shows the coastal response predicted for Tuncurry using the dynamic shoreface model with the active shoreface dimensions adopted for each model phase [Tab. 6.1]. The total shoreline retreat predicted by 2100 was 71.1 m [Fig. 6.7]. Similar to the Moruya example, the coastline response predicted by the dynamic shoreface model closely resembled the outcome of the 12 m fixed closure depth model.

6.2.3 Discussion

The outcomes of the time-invariant shoreface models presented in Section 6.2.2 demonstrate the sensitivity of predicted coastline response to the chosen profile closure depth, although in principle this sensitivity depends on the geometry (degree of concavity) of the shoreface. For the range of potentially relevant closure depths, predicted shoreline retreat varied by up to 32 m at Moruya [Fig. 6.4] and 68 m at Tuncurry [Fig. 6.6]. The increase in predicted shoreline retreat for deeper closure depths can be explained by the extension of the active shoreface domain across the inner shelf, which invokes

a greater exchange of sediments between coast and shelf within geometric closed sediment budget models. In the standard Bruun Rule, active shoreface dimensions are simply described by the 'Bruun factor', which represents the inverse of the linear slope between the dune system and closure depth. Adopting a representative dune height of 6 m for both sites, Table 6.1 also shows the corresponding Bruun factors for the range of fixed profile closure depths considered here. For a given sea-level rise therefore, the effect of typical concave-up shoreface geometry is that shoreline retreat predicted by the standard Bruun Rule increases with the chosen closure depth, for concave shorefaces.

Comparison between the Moruya and Tuncurry sites demonstrates the influence of shelf gradient and shoreface shape on predicted shoreline retreat. As demonstrated by the site bathymetry [Figs. 2.10 & 2.13], the Moruya shelf (0.45°) is roughly twice as steep as at Tuncurry (0.225°). For a given profile closure depth therefore, the Tuncurry shoreface is approximately twice as wide, which results in twice the shoreline retreat predicted by the fixed geometry closed sediment budget model. The influence of x_a on model predictions is best observed in comparison of the 17 m and 22 m fixed closure depth models. For the Moruya example negligible difference is observed between model predictions [Fig. 6.4] due to the relatively small change in x_a associated with increasing h_a from 17 to 22 m [Tab. 6.1]. At Tuncurry however, the same variation in h_a results in a comparatively larger increase in x_a [Tab. 6.1] and a more noticeable increase in predicted shoreline retreat [Fig. 6.6]. Rather, the difference between the 12 m and 17 m fixed closure depth models is less apparent at Tuncurry [Fig. 6.6].

It was established in Chapter 5 that active shoreface dimensions are sensitive to the rate of sea-level change. The adoption of a fixed profile closure depth therefore implies that application of the Bruun Rule inherently assumes a uniform rate of sea-level rise over the planning period of interest. However, projections of future sea-level change suggest accelerating sea-level rise throughout the present century [Fig. 6.2]. Comparison of historical and projected future rates of sea-level rise with the findings of Chapter 5 suggests that active shoreface dimensions are likely to contract over the duration of the typical 100-year planning period considered in coastal management [Tab. 6.1]. Thus shoreline retreat predictions made using the fixed closure depth models would be representative of a uniform 0.96-m sea-level rise at the average rate for the corresponding model phase [Tab. 6.1].

For both sites, shoreline retreat predicted by the dynamic shoreface model was comparable with the predictions of the 12 m fixed closure depth model. Specifically, the difference in predicted shoreline retreat by 2100 was -1.2 m at Moruya [Fig. 6.5] and -2.6 m at Tuncurry [Fig. 6.7]. From Table 6.1 it can be seen that the dynamic profile closure depth varied from 35 m to 17 m for the period 1890-1990, and from 12 m to 6 m for the period 1990-2100. However, the total sea-level rise over the same two periods was 0.15 m and 0.81 m respectively [Tab. 6.1]. Thus although the active shoreface extent was more than halved over the first eleven model steps, the relatively small change in sea level resulted in a near negligible difference in predicted shoreline retreat. Indeed Figure 6.5a and Figure 6.7a show only a minor difference between all model predictions for the first half of the scenario at both sites. In contrast, whilst the total sea-level change over the second half of the scenario was much greater, the reduction in h_a from 12 m to 6 m resulted in a comparatively smaller decrease in active shoreface dimensions. More specifically, the reduction in active shoreface dimensions was less significant because of smaller reductions in both h_a and x_a, due to the steeper gradient of the upper shoreface.

Experimentation with dynamic active-shoreface dimensions based on the findings presented in Chapter 5 suggests that for the case of accelerating sea-level rise to 2100 [Fig. 6.3], h_c may in fact represent an appropriate profile closure depth for application of the Bruun Rule. That is, $h_a = h_c$ may offer a reasonable approximation of the average shoreface response timescale for the rates and duration of sea-level rise relevant to historical and projected future sea-level change. The restriction of h_a to the vicinity of h_c for predictions of coastline response to sea-level rise over the coming century is consistent with previous suggestions that lower shoreface response timescales are on the order of millennia [*Stive and de Vriend*, 1995]. For example, geological evidence for net onshore sand supply in southeastern Australia throughout the Holocene has been linked to an ongoing disequilibrium-stress response across the lower shoreface [*Cowell et al.*, 2001, 2003b; *Daley*, 2012]. The validity of that concept was further examined and strengthened through the simulations presented in Chapter 3.

More recently, *Patterson* [2012] derived an empirical relationship for depth-dependent shoreface T_r from the analysis of repeat survey data from a shoreface sediment lobe at the Gold Coast. As seen in Figure 6.8, the extrapolation of measured shoreface response over the 41-year survey dataset suggest that T_r increases from 15 years at about

12 m water depth to 100 years at 17 m depth and 200 years at 18 m depth. Thus, for gradually rising sea level conditions between 1966-2007 [Fig. 6.3], it would take 200 years to achieve the equilibrium profile at 18 m water depth. The empirical shoreface response timescales presented by *Patterson* [2012] provide further evidence for depth-dependent shoreface T_r and onshore shoreface sand supply. However, they make no allowance for accelerating rates of sea level forcing and thus are representative of stable or slowly rising sea level conditions. Thus $T_r = 200$ years at 18 m depth does not necessarily imply that the relevant profile closure depth for the 220-year sea-level rise scenario considered here would be 18 m. Rather, as described above, the effect of the rate of sea-level change on active shoreface dimensions suggests that a representative fixed closure depth for the scenario considered here would be 12 m.

An interesting and unanticipated implication of the dynamic shoreface model experiments was the potential for enhanced onshore shoreface sand supply upon the slowing and stabilisation of sea-level rise. For example, if active shoreface response were restricted to above h_c for the rest of this century, the shoreface at 2100 would feature an inflection beyond the active shoreface domain, due to encroachment of the active shoreface into the upper shoreface. This feature would be most pronounced in low-gradient settings due to the relationship between shelf gradient and shoreline migration during sea-level change [*Roy et al.*, 1994]. This mid-shoreface sand body might then provide for increased rates of onshore sand supply upon stabilisation of sea-level rise, due to the time lag in active shoreface response associated with enhanced shoreface disequilibrium stress. The potential response would be similar to the Holocene coastal evolution documented in Chapter 3, albeit at a smaller scale. This then suggests that the realised coastal response to sea-level rise at centennial timescales may be highly sensitive to inter-decadal fluctuations in wave climate. For example, a predominantly constructive wave climate following a slowing of sea-level rise may moderate shoreline retreat through enhanced onshore sand supply. However, a predominantly destructive wave climate could result in the redistribution of the mid-shoreface sand body across newly generated accommodation space on the lower shoreface.

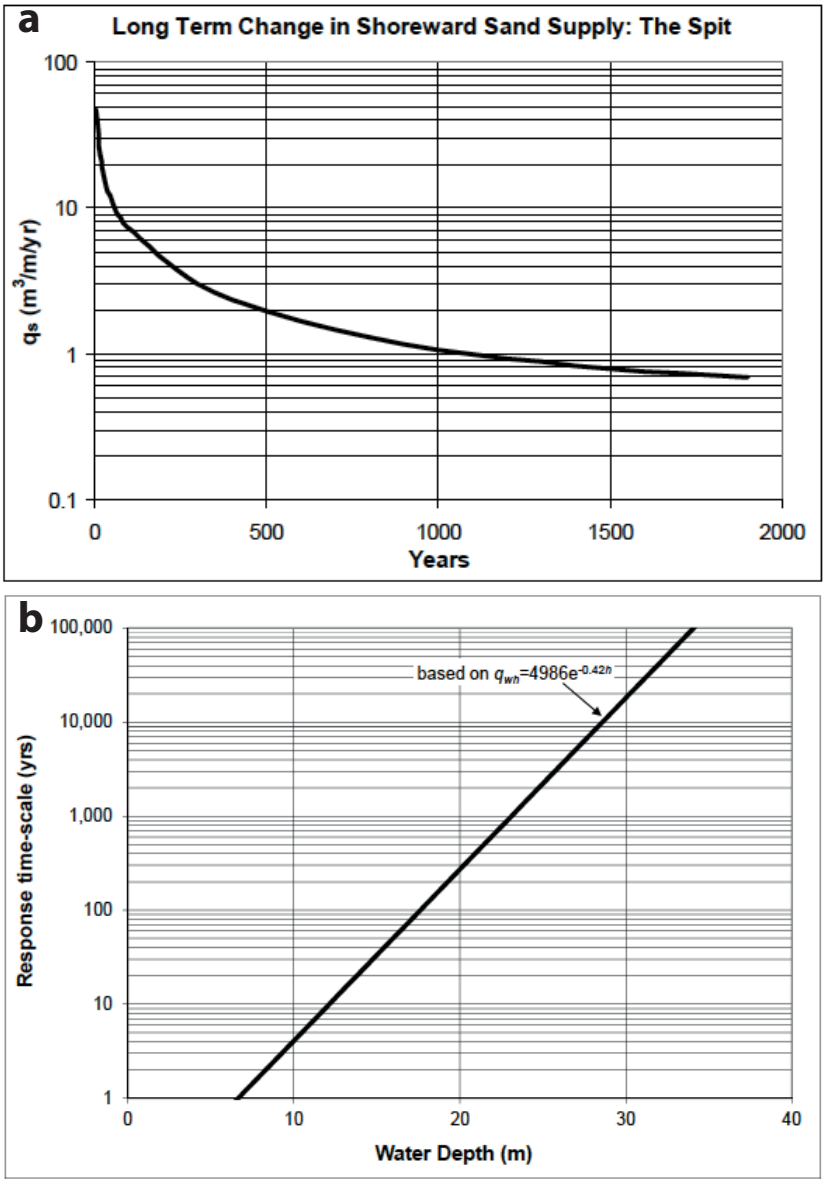

Figure 6.8: Extrapolated shoreface response timescales from Gold Coast dataset - Empirical relationship for depth-dependent shoreface morphological relaxation timescale (T_r) derived from the analysis of a 41-year (1966-2007) repeat survey dataset of a shoreface sediment lobe at the Gold Coast, Australia. From *Patterson* [2012].

Instantaneous profile response across the active shoreface for each decadal model time step was assumed in the simulations described here. No allowance was made for active h-dependent lower-shoreface response due to ongoing disequilibrium-stress response or the generation of lower-shoreface accommodation. Whilst $h_a = h_c$ may represent an appropriate limit for complete time-invariant shoreface response, the restriction of closure depth to h_c implicitly ignores the potential for ongoing shoreface adjustment (and shoreline change) beyond the slowing or stabilisation of sea-level rise. That is, lagged shoreface response due to morphodynamic disequilibrium implies that shoreface adjustment may continue if rates of sea-level rise were to slow or stabilise. Potential shoreline migration in response to lagged adjustment could be characterised by shoreline progradation or shoreline retreat, depending on the nature of shoreface morphodynamic disequilibrium at the time of sea level stabilisation. Whilst the relatively low-gradient settings of barrier coasts suggests the potential of maintained onshore shoreface sand supply, typically concave-up shoreface geometry implies that potential remains for cumulative offshore losses of coastal sediments due to accommodation generation across the mid to lower shoreface. Thus there may exist a threshold sea-level rise for a given setting beyond which any persisting onshore sediment supply is diminished and net shore-normal sediment transport is directed offshore.

The simulation experiments described here were largely exploratory, and were designed for the primary purpose of investigating the potential influence of R-dependent shoreface response on predictions of shoreline retreat due to sea-level rise. Although a profile survey record exists for the Moruya site [*Thom and Hall*, 1991], model verification was not pursued as the dataset does not suggest a trend of shoreline retreat for the sampling period (i.e. 1972 to present). This is a typical limitation of historical beach survey datasets, in which periodic (e.g. ENSO) and event timescale (storms) high-magnitude shoreline change signals mask any mean-trend change signal that may be present [*Cowell et al.*, 2003a]. Given the low rates of shoreline change predicted by the models for this period [Fig. 6.5a], it is possible that a subtle signal of shoreline retreat could be hidden in the survey record. However, potential ongoing onshore sand supply at Moruya due to shoreface D-S response [Sec. 3.4.1] suggests that the shoreface there may be initially insensitive to sea level rise. [*Cowell et al.*, 2001, 2003a].

6.3 Falling-stage coastal barrier deposition

Section 6.2 considered the potential significance of R-dependent shoreface response for predicting future coastal change. However, the rates of sea-level change and thus the range of shoreface response considered in Chapter 5 also has implications for late-Quaternary coastal evolution, which was characterised by periods of rapid sea-level change [Fig. 4.5]. For example, the balance of coastal barrier deposition supplied by active shoreface response and external sediment supply is fundamental to understanding coastal dynamics in autochthonous shelf settings. BARSIM has been previously applied to investigate coastal dynamics during post-glacial rapid sea-level rise on the northern Adriatic shelf of Italy [*Storms et al.*, 2008]. Whilst the simulation experiments documented in Chapter 4 provided new insights into highstand coastal barrier deposition in particular, the temporal resolution of the models limited the analysis of barrier deposition during rapid sea level oscillations. Thus coastal barrier deposition during the MIS-3 interstadial stage is further investigated in this chapter to consider shoreface response to rapid late-Quaternary sea-level change, and the origins of falling-stage barrier systems at Tuncurry. The following questions are addressed:

1. Was falling-stage coastal barrier deposition at Tuncurry primarily driven by relative sea-level fall, external sand supply, or onshore shoreface sand supply driven by shoreface morphodynamic disequilibrium?

2. Is it likely that MIS-3 sea-level change supported complete time-invariant shoreface response (i.e. $h_a = h_i$)?

3. Which potential MIS-3 sea level scenario is best supported by the depositional evidence from the Tuncurry falling-stage barrier systems?

6.3.1 Methods

6.3.1.1 MIS-3 sea-level rise scenarios

Whilst global sea level change throughout the last glacial cycle is relatively well constrained in the context of geological timescales, significant uncertainties remain regarding the magnitude and timing of interglacial and interstadial sea-level highstands [Sec. 4.2]. Regarding sea-level change during the MIS-3 interstadial stage (i.e. 60-30 ka),

the timing and magnitude of periodic sea level fluctuations, which were superimposed on an overall falling trend, varies between records [Fig. 4.2], and remains contested [*Rohling et al.*, 2008]. In reviewing the evidence for fluctuating MIS-3 sea levels from eighteen key records, *Siddall et al.* [2008] made the following conclusions:

1. Sea level rose to an average of -60 m PMSL by 60 ka, and fluctuated around that level for the first half of MIS 3, before falling to an average of about -80 m PMSL for the remainder of MIS 3.

2. The difference in average sea levels during the first and second half of MIS 3 is correlated with a comparable drop in 65° North June Insolation.

3. Four sea level fluctuations on the order of 20-30 m were likely superimposed on the general trend described in Point 1.

4. Sea level fluctuated predominantly to an Antarctic rhythm, and thus rose during periods of cooling in Greenland and warming in Antarctica.

As described in Section 4.2 however, there is evidence from southern Australia and abroad to suggest that MIS-3 sea levels may have been up to 30 m higher than depicted in the Red Sea record [*Siddall et al.*, 2003]. Furthermore, the elevations and arrangement of falling-stage coastal barrier systems at Forster-Tuncurry provide further evidence of higher MIS-3 sea levels, which appear to be more consistent with the upper range of the *Lambeck and Chappell* [2001] envelope [Fig.4.5].

Four alternative sea level scenarios were examined to explore the sensitivity of shoreface response and coastal barrier evolution to steady or oscillating MIS-3 sea-level fall. Figure 6.9 shows the four scenarios in relation to a selection of sea level records that are representative of the range of available evidence. The rationale for the four sea-level scenarios is summarised below:

1. Linear sea-level fall between 60 and 32 ka at a steady rate of -1 mm/a, which is representative of the average rate of MIS-3 sea-level fall (FS-1).

2. Two interstadial sea-level highstands, one in the first half and one in the second half of MIS 3 (FS-2). This scenario is equivalent to the modified sea level scenarios applied in the Tuncurry last-glacial cycle models [Fig. 4.4].

3. Four interstadial sea-level highstands arranged in two pairs, with one pair occurring in the first half and one pair in the second half of MIS 3 (FS-3). This scenario is representative of the *Waelbroeck et al.* [2002] composite curve.

4. Five interstadial sea-level highstands, arranged as an early MIS-3 pair, mid MIS-3 individual, and late MIS-3 pair (FS-4). This scenario is representative of the trend suggested by both the *Lambeck and Chappell* [2001] and *Siddall et al.* [2003] curves, which show similar phasing [Fig. 6.9].

Peak sea levels attained during MIS-3 interstadial highstands in each of the four scenarios were consistent with the modified sea level scenarios (i.e. LG-M1 and LG-M2) applied in the Tuncurry last-glacial models, which were guided by the observed elevations of preserved falling-stage barrier systems at Tuncurry [Fig. 4.5]. Peak MIS-3 sea levels were thus about 10 m higher than suggested by the selected continuous records, and best represented by the *Lambeck and Chappell* [2001] Huon envelope [Fig. 6.9].

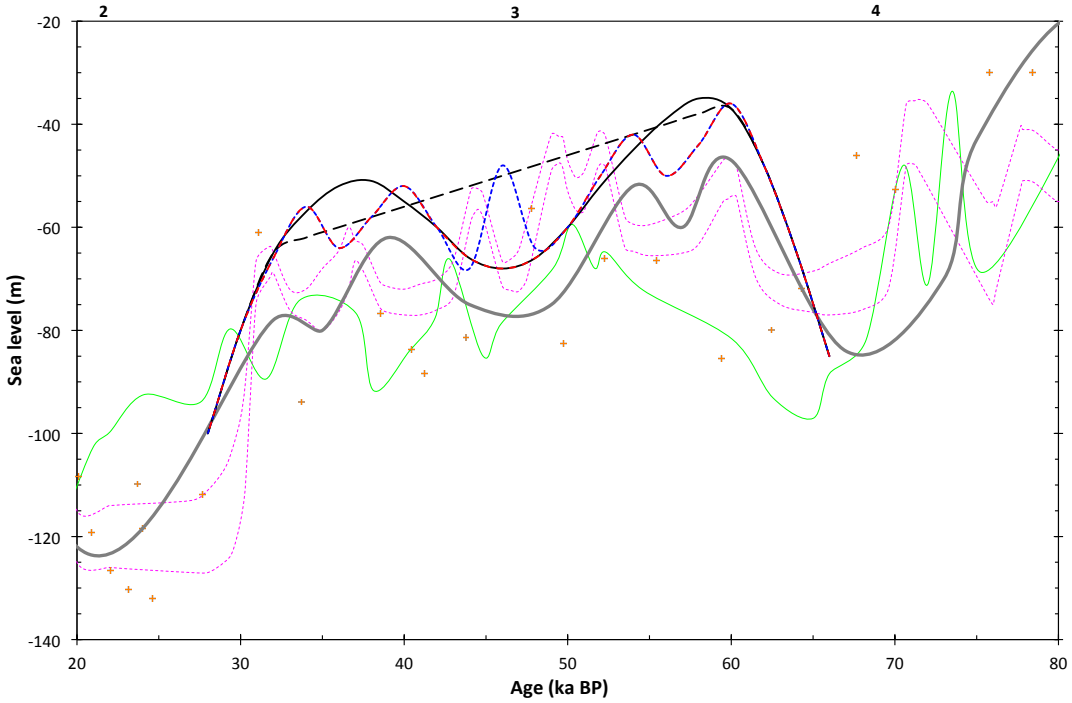

Figure 6.9: Sea level scenarios applied in Tuncurry MIS-3 falling-stage models - Sea level scenarios applied in the MIS-3 falling-stage stratigraphic models at Tuncurry, including the SL-FS1 (dashed black), SL-FS2 (solid black), SL-FS3 (dashed red) and SL-FS4 (dashed blue) scenarios. The scenarios represent progressively increasing temporal resolution of MIS-3 sea-level change, from a linear sea-level fall at a steady rate of 1 mm/a (i.e. SL-FS1), to oscillating scenarios featuring 2 (SL-FS2), 4 (SL-FS3) and 5 (SL-FS4) interstadial sea-level highstands. The SL-FS2 scenario is equivalent to the MIS-3 sea levels applied in the last-glacial cycle simulations [Sec. 4.3.2.1]. A selection of sea level records is shown for comparison - see Figure 4.4 for a description of the datasets.

6.3.1.2 Simulation experiments

The Tuncurry BARSIM model that was applied in the last-glacial cycle experiments [Sec. 4.3.2.2] was again used to simulate shoreface response to sea-level change and coastal barrier deposition at Tuncurry during MIS 3. The calibration procedure used to tune the BARSIM erosion-efficiency scaling exponent to be representative of the local morphodynamic regime has been described in Section 3.3.1. Model wave climate parameters, sediment characteristics and internal parameters were maintained as per the Tuncurry last-glacial cycle simulations. The model configuration was described in Section 3.3.1, and was guided by datasets that have been described in descriptions of the regional setting [Sec. 2.2] and Tuncurry site [Sec. 2.7]. The initial model substrate was also maintained, featuring inner- and mid-shelf embayments, separated by a transitional profile inflection that is enforced by the bedrock framework.

The model was run four times, once for each of the sea level scenarios described in Section 6.3.1.1. Each simulation spanned a 38 ka period from the end of the MIS-4 lowstand (66 ka) to the transition into the MIS-2 lowstand (28 ka), as indicated by the model sea level scenarios shown in Figure 6.9. External sediment supply rates were maintained uniform between each simulation and were guided by the geological evidence collected by *Roy et al.* [1997], which has been described in Section 2.7. Specifically, model external sediment supply rates were 0 m^3/m for the period 66-60 ka, 2 m^3/m for the period 60-34 ka, and 1 m^3/m for the period 34-28 ka. The increased rate of supply to the Tuncurry mid-shelf compartment during the MIS-3 sea level oscillations reflects the observation that a prominent and protruding reef structure at the northern extremity of the present-day embayment would have acted as a significant sand trap during intermediate sea levels [*Roy et al.*, 1997]. Thus it has been proposed that falling-stage barrier deposition was fuelled by both shoreface erosion and littoral drift into the mid-shelf embayment associated with the erosion of updrift shelf sand bodies [*Roy et al.*, 1994].

6.3.2 Results

Figure 6.10a shows the simulated stratigraphy generated by the Tuncurry BARSIM model and the FS-1 sea level scenario. A transgressive barrier system comprising

medium-coarse sands and extensive backbarrier facies was deposited at the upper extremity of the mid-shelf embayment during sea-level rise into MIS 3. Steady sea-level fall throughout MIS 3 at a rate of 1 mm/a resulted in the deposition of an extensive forced-regressive strandplain across the mid-shelf embayment. The strandplain was 20-25 m thick, relatively uniform in dimensions and surface gradient, and was characterized by densely stacked uniform time-interval reflectors. The reflectors were concave-up, seaward dipping and were arranged in offlapping relationships, as is typical for the case of forced-regressive deposits. Accelerated sea-level fall into MIS 2 resulted in a reduction in strandplain volume, although coastal deposition continued for the remainder of the scenario to -100 m PMSL.

Figure 6.10b shows the simulated stratigraphy generated by the Tuncurry BARSIM model and the FS-2 sea level scenario. A transgressive barrier system comprising medium-coarse sands and extensive backbarrier facies was deposited at the upper extremity of the mid-shelf embayment during sea-level rise into MIS 3. The twin sea-level highstands of the FS-2 scenario resulted in the deposition of two strandplains. The earlier strandplain associated with the first highstand was between 10-15 m thick and extended to -70 m PMSL. The younger strandplain was deposited atop the earlier strandplain from 50 m PMSL, and was comparatively thinner at 5-10 m. The two strandplains were separated in the upper half of the section by a thick deposit of finer-grained sediments representative of backbarrier facies that were deposited during sea-level rise into the second higstand. A lens of coarser transgressive sands separated the younger strandplain from the backbarrier facies.

Figure 6.10c shows the simulated stratigraphy generated by the Tuncurry BARSIM model and the FS-3 sea level scenario. A transgressive barrier system comprising medium-coarse sands and extensive backbarrier facies was deposited at the upper extremity of the mid-shelf embayment during sea-level rise into MIS 3. Simulated strandplain stratigraphy generated by the FS-3 scenario was similar to that of the FS-2 model, with the strandplain being separated into an earlier inner section and younger outer section. However, each section was again divided into two strandplain components, representative of the twin sea-level highstand peaks. Transgressive and backbarrier facies separating the twin components were minimal, with only a thin lens of finer sediments preserved within each strandplain, and transgressive-barrier deposits separating

the strandplain components at the surface. The strandplains associated with the earlier highstand were thicker relative to the later strandplains.

Figure 6.10d shows the simulated stratigraphy generated by the Tuncurry BARSIM model and the FS-4 sea level scenario. A transgressive barrier system comprising medium-coarse sands and extensive backbarrier facies was deposited at the upper extremity of the mid-shelf embayment during sea-level rise into MIS 3. The FS-4 scenario generated a series of five strandplains that were relatively evenly spaced at the surface and organised in a down-stepping arrangement. Transgressive and backbarrier deposits between each strandplain were limited and generally restricted to coarser sands within the upper parts of the section.

Lagrangian-normalised shoreface profiles were also extracted from each of the BARSIM model runs to compare shoreface response to each of the four MIS-3 sea level scenarios. Figure 6.11 shows Lagrangian shoreface profiles at 0.5-ka temporal resolution for each scenario. The plots are colour-coded to differentiate between shoreface profiles associated with different sea level conditions. For all scenarios the shoreface profiles demonstrate that barrier-overstepping behaviour dominated during transgression into MIS 3, as indicated by the black profiles. Steady sea-level fall throughout MIS 3 in the FS-1 model supported extension of the active shoreface to about 30 m shoreface depth [Fig. 6.11]. In response to the fluctuating sea level scenarios (i.e. FS-2, FS-3 and FS-4) the active shoreface became restricted, with higher frequency sea level fluctuations resulting in shallower shoreface profiles [Fig. 6.11b-d]. For all scenarios the shoreface experienced rapid shoaling in response to accelerated sea-level fall into MIS 2 [Fig. 6.11].

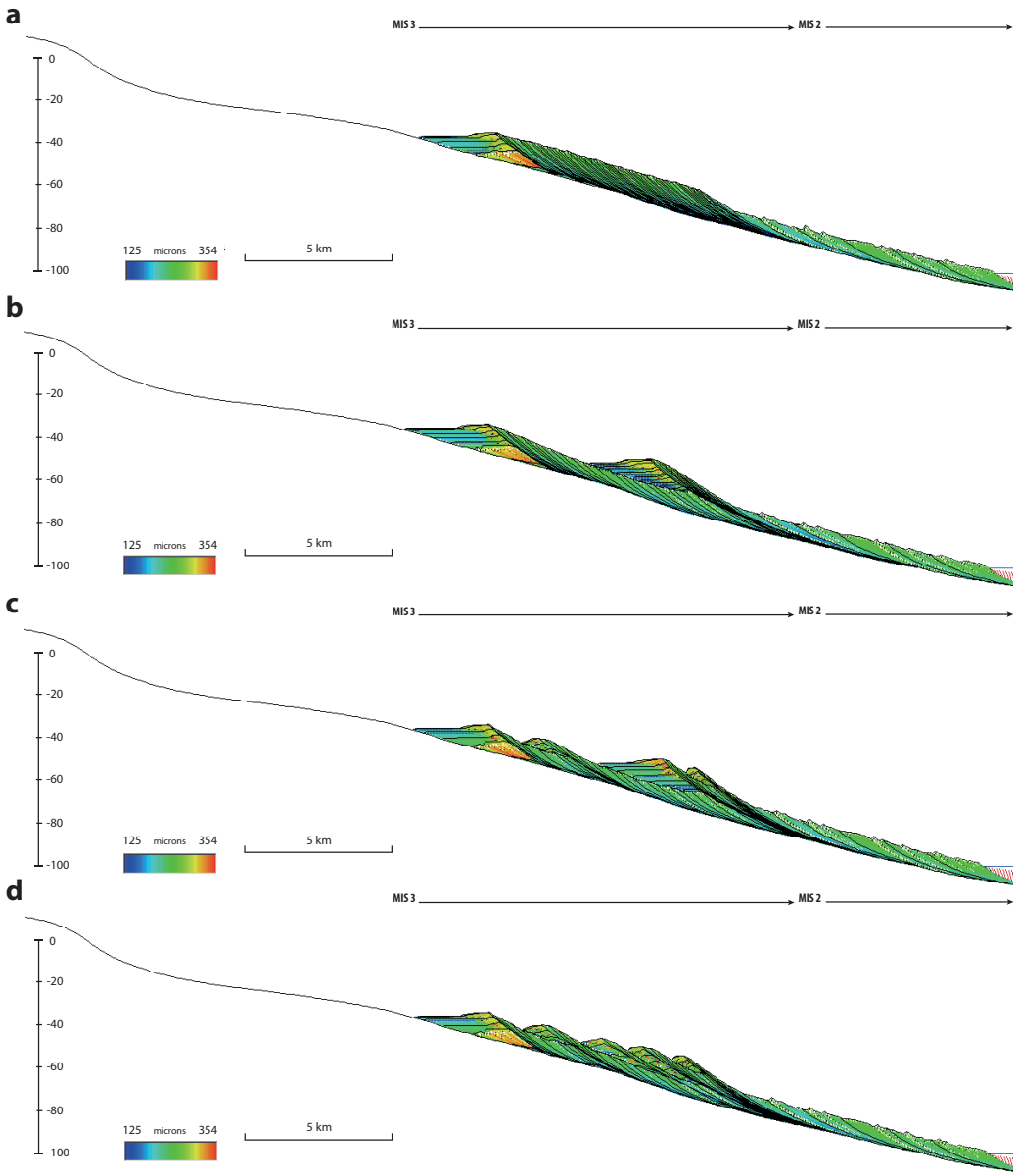

Figure 6.10: Simulated falling-stage coastal barrier deposition at Tuncurry - Simulated coastal barrier deposition at Tuncurry in response to the (a) SL-FS1, (b) SL-FS2, (c) SL-FS3 and (d) SL-FS4 MIS-3 sea level scenarios. The complexity of MIS-3 falling-stage coastal barrier deposition increase with the sea level scenarios, from an individual forced-regressive strandplain (FS1), to up to five composite highstand/forced-regressive strandplains organised in a down-stepping arrangement (FS4). In each model, early transgression into MIS-3 was characterised by barrier-overstepping, whilst late transgression was characterised by barrier-rollover, resulting in the deposition of transgressive and backbarrier facies at the landward end of the shelf embayment. See Figure 6.9 for a description of the sea level scenarios.

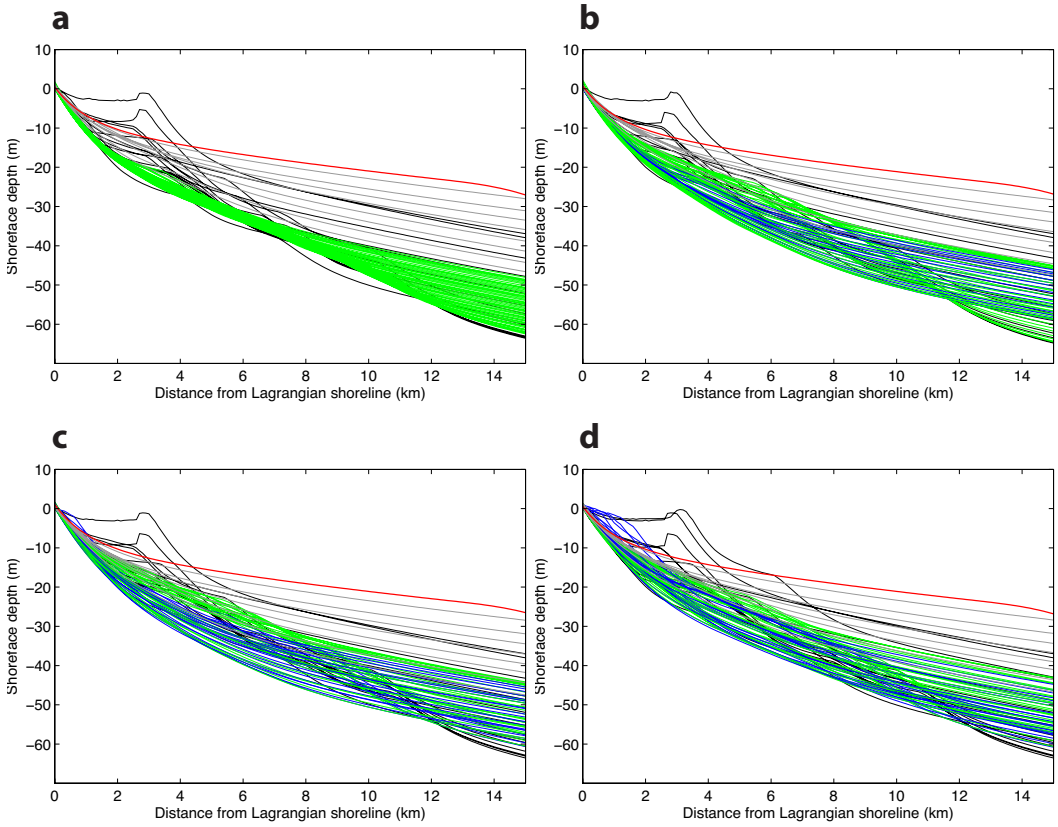

Figure 6.11: Lagrangian shoreface profiles from Tuncurry MIS-3 simulations - Lagrangian-normalised shoreface profiles from Tuncurry BARSIM models forced by the (a) FS-1, (b) FS-2, (c) FS-3 and (d) FS-4 MIS-3 sea level scenarios [Fig. 6.9]. Profiles are colour-coded to differentiate between different stages. Black profiles correspond to the rapid transgression into MIS-3 (i.e. pre-60 ak BP), and grey profiles correspond to rapid sea-level fall into MIS 2 (i.e. post-30 ka BP). Within MIS 3 (i.e. 60-30 ka BP), blue profiles correspond to rising sea level whilst green profiles correspond to falling sea level.

6.3.3 Discussion

The outcomes of the stratigraphic modelling allows for a review of falling-stage coastal barrier deposition at Tuncurry. *Cowell et al.* [1995] briefly investigated the deposition of the Tuncurry falling-stage strandplains using a geometric equilibrium model, which assisted in the interpretation of the geological evidence [*Roy et al.*, 1994, 1997]. Their simulations were similar to the FS-1 model used here [Fig. 6.10a], in that a steady rate

of sea-level fall and time-invariant shoreface geometry was assumed for the duration of strandplain deposition. The outcome of the FS-1 model here supports their assumption that a fully active (i.e. time-invariant) shoreface form is feasible for the average rate of sea-level fall experienced during MIS 3 [Fig. 6.11a]. This is also in agreement with the hypothetical forward simulations that were described in Chapter 5, which suggest that the active shoreface depth limit at Tuncurry is 25 m for the case of sea-level change at 1 mm/a [Sec. 5.5.1.1]. However, as is suggested by the sea level records shown in Figure 6.9, the assumption of steady sea-level fall at a uniform rate of 1 mm/a is only a gross approximation of sea-level change throughout MIS 3. Therefore, both the previous findings of *Cowell et al.* [1995] and the FS-1 model here only provide a first-order approximation of coastal barrier deposition at Tuncurry during MIS 3.

From a review of eighteen key records, *Siddall et al.* [2008] concluded that MIS-3 sea levels were most likely characterised by four sea level fluctuations, two in the first half of MIS 3 when sea levels averaged -60 m PMSL, and two in the latter half when sea levels averaged -80 m PMSL. That pattern is most consistent with the FS-3 scenario applied here, and is also captured in the *Waelbroeck et al.* [2002] composite sea level curve [Fig. 6.9]. Figure 6.12 compares the simulated barrier stratigraphy from the FS-3 model with the interpreted Tuncurry shelf stratigraphy of *Roy et al.* [1997]. The simulated stratigraphy shows two twin-barrier systems that are associated with early and late MIS-3 sea level fluctuations [Fig. 6.12b]. A thick backbarrier deposit associated with transgression into the first of two late-MIS-3 highstands separates the twin barrier systems from one another [Fig. 6.12b]. This is consistent with the interpretation of *Roy et al.* [1997] which shows two falling-stage barrier systems separated by backbarrier deposits [Fig. 6.12a]. Furthermore, closer inspection of the high-resolution seismic stratigraphy suggests that there is evidence for two falling-stage barrier systems within line FT-13 [Fig. 6.12c]. As indicated in Figure 6.12, the stratigraphy shown in line FT-13 represents the earlier of the two twin-barrier systems that were generated in the model. Thus rather than being a continuous forced-regressive strandplain as has been suggested in previous studies [*Cowell et al.*, 1995; *Roy et al.*, 1994, 1997], the Tuncurry falling-stage barriers appear to comprise at least four down-stepping coastal barrier systems that are associated with four MIS-3 interstadial sea-level highstand events.

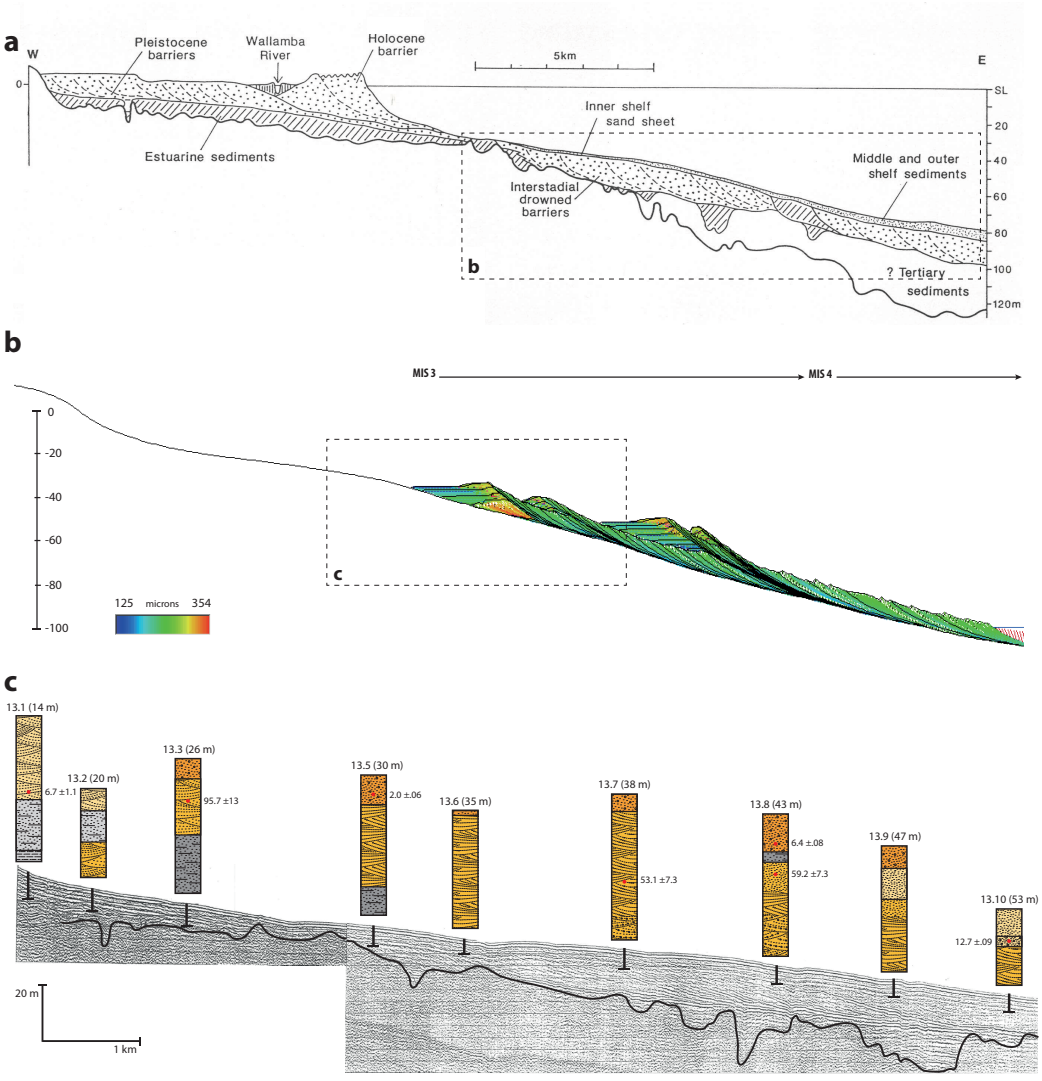

Figure 6.12: Interpreted and simulated MIS-3 stratigraphy at Tuncurry - (a) Interpreted stratigraphy of the Tuncurry embayment from Roy et al. (1997), (b) simulated stratigraphy from the FS3 model as shown in Figure 6.10c, and (c) shallow-marine seismic line FT13 with interpreted vibrocores as shown in Figure 2.18. The dashed box in (a) shows the domain of the simulated stratigraphy in (b), whilst the dashed box in (b) shows the approximate domain of the seismic profile in (c).

This revised interpretation of falling-stage coastal barrier evolution at Tuncurry has implications for shoreface response to MIS-3 sea-level change and its role in coastal barrier deposition. Whilst the FS-1 model implied the potential for complete active shoreface response, the fluctuating sea level models suggest R-dependent shoreface response dominated during MIS-3, with shoreface profiles becoming shallower during higher frequency fluctuations, and thus faster rates of sea-level change [Fig. 6.11]. Furthermore, the Lagrangian shoreface profiles shown in Figure 6.11 suggest that the range of shoreface response was broadly equivalent during sea-level rise and sea-level fall. This is to be expected given the roughly symmetrical geometry (and thus comparable rates of sea-level rise and fall) of the interstadial sea level fluctuations in the FS-2, FS-3 and FS-4 scenarios [Fig. 6.9]. The range of shoreface response observed in the fluctuating sea level models implies similar variation in rates of onshore sand supply from shoreface reworking [Sec. 5.5.1].

The potential dominance of R-dependent shoreface response has implications for the coastal sediment budget at Tuncurry during MIS-3. Specifically, R-dependent shoreface response implies that shoreface erosion may have perhaps played a less significant role in falling-stage coastal barrier deposition than was previously thought [*Cowell et al.*, 1995]. In that case, deposition of the extensive falling-stage barrier systems would have required a significant supplementary external sand supply. This is consistent with the interpretation of *Roy et al.* [1997], who proposed that the falling-stage barrier systems at Tuncurry were partly sourced from the erosion of the updrift shelf sand body [Sec. 4.6], which was exposed to active shoreface reworking during MIS-3 sea-level fall [Sec. 2.7.4]. Here, an external sediment supply rate of 2 m^3/a was adequate to reproduce model stratigraphy consistent with the volumes of falling-stage coastal barrier systems at Tuncurry.

The necessary condition of an external sediment supply does not negate the role of shoreface erosion in falling-stage coastal barrier deposition at Tuncurry, but demonstrates that the contribution of shoreface erosion would have been most significant during times when shoreface morphodynamic disequilibrium was greatest (and reduced during rapidly fluctuating sea-level change). At Tuncurry, shoreface sand supply would have peaked during and shortly after interstadial sea-level highstands, when shoreface D-S response and erosion rates were highest. This reasoning suggests that D-S induced shoreface sand supply was the primary source of coastal barrier deposition during and

after interstadial sea-level highstands, whilst external sand supply, presumably sourced from the alongshore transport system, was more dominant during rapid sea-level change between sea-level reversals.

Potentially similar depositional behaviour is apparent in the stratigraphy of comparable drowned barrier systems of the northern NSW inner-continental shelf, which provide further evidence that falling-stage coastal barrier deposition was closely related to a series of down-stepping interstadial sea-level highstands [Fig. 6.13]. For the drift-aligned northern NSW setting, it is less likely that the trapping of sand from the longshore transport system would have been a significant factor in coastal deposition, and thus the prospective MIS-3 coastal barrier systems shown in Figure 6.13 may further support the significance of R-dependent shoreface response in falling-stage coastal barrier evolution.

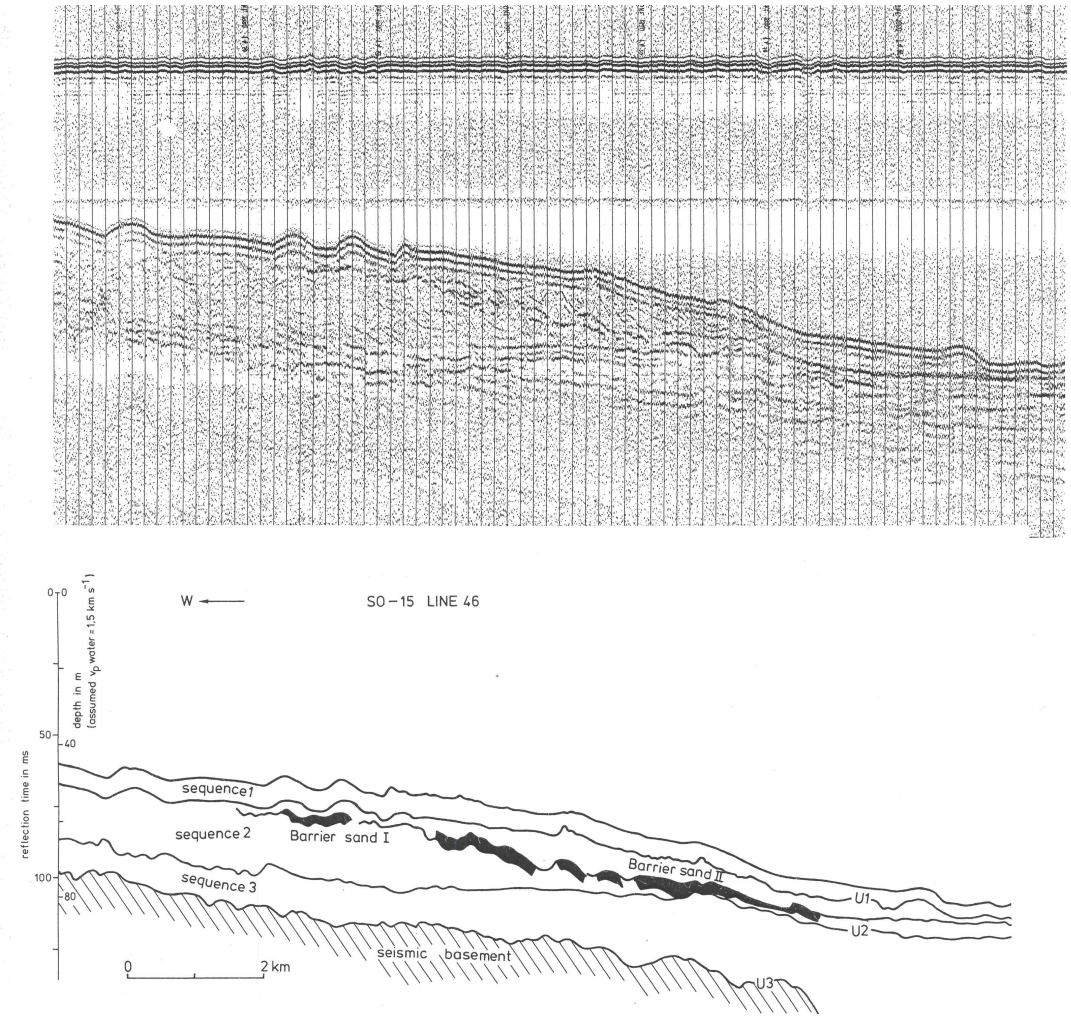

Figure 6.13: Seismic reflection line across the continental shelf off Ballina - This line from the northern New South Wales shelf appears to show at least two drowned coastal barrier systems that are similar to the MIS-3 falling-stage coastal barrier systems at Tuncurry, and located at comparable depths. From *Schluter* [1982].

6.4 Shoreline trajectories and highstand barrier stacking

The analysis of shoreline trajectories provides a simple and useful descriptive tool for characterising shallow-marine deposition in response to dynamic forcing [*Helland-Hansen and Martinsen*, 1996; *Helland-Hansen and Hampson*, 2009]. However, whilst shoreline trajectories have been considered in the context of the geohistorical variables [Sec. 1.3.1], their sensitivity to R-dependent shoreface response remains untested. Therefore, in this section the following questions are considered:

1. Are shoreline trajectories sensitive to R-dependent shoreface response?
2. If so, what are the potential implications for coastal barrier deposition?

The simulation experiments presented in Chapter 5 considered the sensitivity of shoreline trajectories to dynamic shoreface response. For example, panel (e) in Figures 5.3 to 5.7 demonstrates the decreasing sensitivity of shoreline trajectories to the geometry of the inherited shelf substrate for decreasing R. Specifically, for high R the shoreline trajectory closely follows the geometry of the initial shelf surface, resulting in a decreasing trajectory angle throughout the simulation [Fig. 5.3]. For low R however, the shoreline trajectory maintains a steady trend that is defined by the average gradient of the shoreface-inner shelf surface [Fig. 5.7]. This is consistent with the proposition that the antecedent substrate drives shoreline trajectories during long-term sea-level change [*Wolinsky and Murray*, 2009]. Furthermore, comparison between relative volumes of the forced-regressive strandplains (a) and the Lagrangian-normalised shoreface profiles (b) in Figures 5.3 to 5.7 shows that decreasing sensitivity of shoreline trajectories to the inherited shelf substrate for decreasing R is driven by increased h_a and a greater autochthonous sediment supply available for strandplain deposition. Thus for decreased R-dependency and increased h_a, ample shoreface sand supply volumes have the effect of reducing the sensitivity of shoreline trajectories to the inherited shelf substrate. Rather, shoreline trajectories are sensitive only to gross changes in substrate geometry (i.e. average shelf gradient).

6.4.1 Methods

An idealised example of the influence of R-dependent shoreface response on shoreline trajectories and coastal barrier stacking was generated using a morphokinematic mod-

elling approach. Again, the Tuncurry site model was used as a representative barrier-coast setting. Two model scenarios were compared, each comprising a 60-m sea-level fall from present-day initial conditions, which was followed by a 60-m sea-level rise back to PMSL. Both the sea-level fall and sea-level rise simulations were implemented in 5-m sea-level change increments. The two scenarios are differentiated as follows:

1. Complete time-invariant shoreface (i.e. $h_a = h_i$) response during both sea-level fall and sea-level rise

2. Dynamic shoreface response involving 8-m shoaling of h_a during sea-level fall, followed by complete time-invariant shoreface response identical to scenario 1 during sea-level rise

Thus the only difference between scenarios 1 (S1) and 2 (S2) was the reduction of h_a by 8 m during sea-level fall in S1, which was implemented in 1-m steps over the first eight model increments. Scenario 1 was designed to characterise R-dependent shoreface response for the case of an accelerating sea-level fall, relative to the case of constant R as demonstrated in S2. That is, S1 was characterised by an R value that did not support complete time-invariant shoreface response throughout sea-level fall. In both scenarios sea-level rise was characterised by complete time-invariant shoreface response based on identical shoreface geometry, and thus the only difference between scenarios was the inherited substrate resulting from the preceding sea-level fall. As the aim was to consider only the depositional response to shoreface behaviour and associated autochthonous sand supply, both simulations featured zero external sediment supply.

6.4.2 Results

Figure 6.14 shows the depositional response to sea-level fall for complete time-invariant shoreface response (S1), and dynamic shoreface response involving an 8-m shoaling of h_a (S2). As suggested by the findings presented in Chapter 5, forced-regressive strandplain deposition was characterised by a constant shoreline trajectory as a result of the steady sea-level fall in S1. Furthermore, the shoreline trajectory is visibly consistent with the average shoreface-inner shelf gradient [Fig. 6.14a]. The resulting forced-regressive strandplain was 20 m thick and extended 12.87 km from the initial shoreline. Deposition in response to S2 featured a comparatively lower-volume forced-regressive strandplain,

which was characterised by a steeper shoreline trajectory relative to S1 [Fig. 6.14b]. Specifically, the resulting forced-regressive strandplain was 15 m thick and extended 12.08 km from the initial shoreline. A change in shoreline trajectory is discernible at the eighth model increment in S2, where shoreface shoaling in response to accelerating sea-level fall ceased.

Figure 6.15 shows the subsequent depositional response to sea-level rise assuming complete time-invariant shoreface response, for substrates generated by the S1 and S2 sea-level fall scenarios. Again the only difference between the S1 and S2 sea-level rise simulations was the initial shelf substrate, which was inherited from the corresponding sea-level fall simulations [Fig. 6.14]. The S1 scenario was characterised by transitional behaviour from encroachment to barrier roll-over behaviour involving the progressive growth of a significant coastal barrier complex. This is indicated by the transition from lower-shoreface to coastal deposition throughout the simulation. The barrier complex was entirely sourced from erosion of the underlying forced-regressive strandplain [Fig. 6.15a]. Strandplain erosion was considerable during the first few model increments, although the rapid transition from encroachment to barrier roll-over behaviour and growth of the barrier complex contributed to high preservation of the antecedent strandplain. The final shoreline in the S1 scenario was over 2 km seaward of the initial shoreline, and the transgressive shoreline trajectory was therefore steeper than the forced-regressive shoreline trajectory.

In contrast, transgression during the S2 scenario was predominantly characterised by encroachment behaviour, with only a low-volume sub-aerial barrier complex and no backbarrier environment forming [Fig. 6.15b]. Deposition was concentrated across the lower shoreface throughout the simulation and was entirely sourced from upper-shoreface erosion of the antecedent forced-regressive strandplain. The final shoreline in the S2 scenario was identical to the initial shoreline, and the average shoreline trajectory during transgression was therefore comparable to the forced-regressive shoreline trajectory.

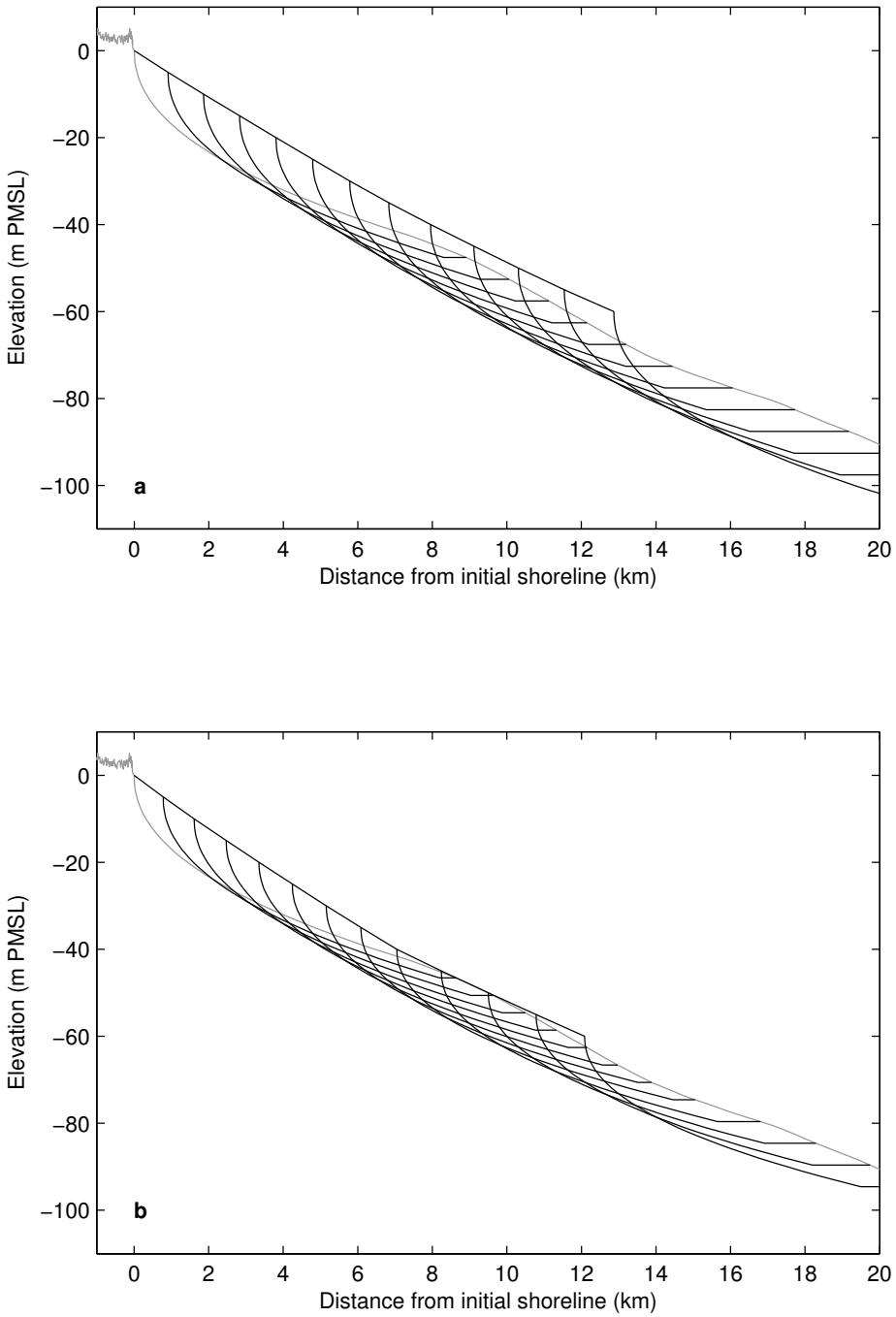

Figure 6.14: Depositional response to 60-m sea-level fall based on complete time-invariant and dynamic shoreface responses - Predicted shoreline trajectories and forced-regressive strandplain deposition in response to the (a) S1 and (b) S2 scenarios.

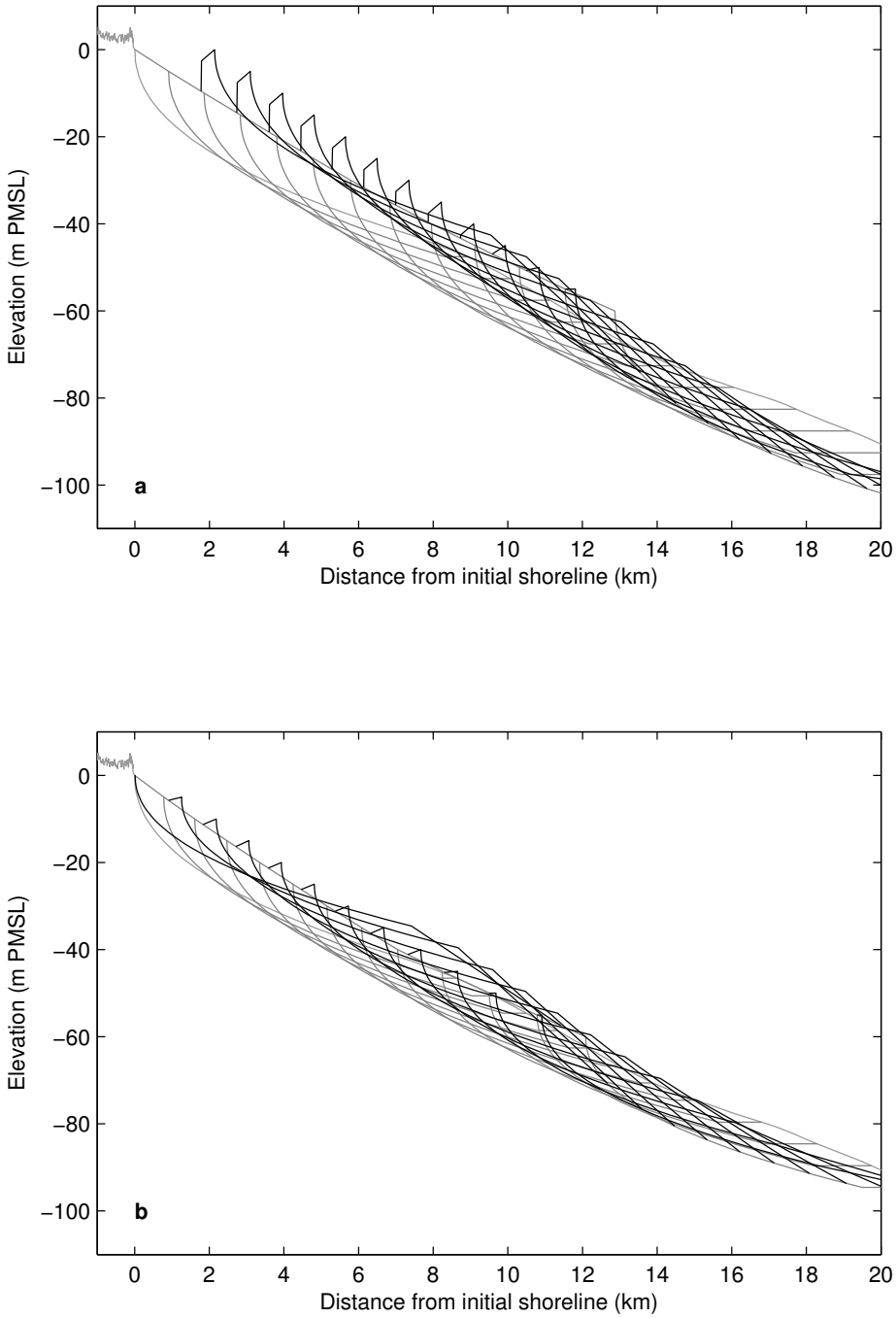

Figure 6.15: Depositional response to 60-m sea-level rise based on complete time-invariant shoreface response - Predicted transgressive-barrier behaviour in based on complete time-invariant shoreface response and the (a) S1 and (b) S2 shelf substrates as inherited from the corresponding models shown in Figure 6.14.

6.4.3 Discussion

The idealised simulations presented in Section 6.4.2 demonstrate the sensitivity of shoreline trajectories to R-dependent shoreface response as was suggested by the findings from Chapter 5. Specifically, for the case of a closed sediment budget, complete time-invariant shoreface response is characterised by linear shoreline trajectories associated with a constant rate of autochthonous sediment supply. In contrast, R-dependent shoreface response results in variable shoreline trajectories due to the dynamic nature of h_a, increased significance of h-dependent shoreface response, and thus increased potential for passive shoreface response driven by morphological inheritance.

Whilst R-dependent shoreface response is captured in the high-resolution BARSIM shoreline trajectories presented in Figures 5.3 to 5.7, the average shoreline trajectories do not vary between the models, and thus do not capture the varying shoreface response between the simulations. That is, in each case the final shoreline trajectory converged on -0.2°, which was consistent with the establishment of R-dependent equilibrium response with a linear shelf substrate. Thus, once the variable gradient of the shoreface domain was passed, long-term shoreline migration followed the linear geometry of the inherited shelf substrate. This is further supported by the outcomes of the variable substrate simulations, which demonstrated that the overall shoreline trajectories also converged on the average shelf gradients for the 0.225° [Fig. 5.8] and 0.3° [Fig. 5.9] linear substrate simulations, and both the 10 mm/a and 1 mm/a Tuncurry survey (approx. 0.225°) simulations [Fig. 5.10 & 5.11]. These findings suggest that the average shoreline trajectory may not be indicative of R-dependent shoreface response for the case of complex substrates. Given the relationship between R-dependent shoreface response and autochthonous sediment supply [Ch. 5], therefore, care should be taken when using shoreline trajectories to interpret depositional responses to sea-level change.

The outcome of alternative shoreline trajectories (and thus substrate gradients) for coastal barrier evolution during cyclical sea-level change is readily apparent in comparison between the S1 and S2 scenarios in Figure 6.15. Whilst average shoreline trajectories for the S1 and S2 sea-level fall scenarios (and thus the inherited substrates for the sea-level rise simulations) were comparable (0.27° and 0.28° respectively), the two scenarios resulted in alternative transgressive-barrier behaviours. Specifically, the S1 substrate supported the progressive transition from encroachment to barrier-rollover

behaviour, which resulted in the horizontal stacking [Sec. 2.4.2] of highstand coastal barriers [Fig. 6.15a]. Whilst the initial and final shorelines were both located at elevations 0 m PMSL, the final shoreline was about 2 km seaward of the initial shoreline, and was separated by the barrier complex and backbarrier environment [Fig. 6.15a]. Whilst rates of sea-level rise during the Holocene transgression on the order of 10 mm/a would not have supported complete time-invariant shoreface response [Sec. 5.5.3], the general transgressive-barrier behaviour of the S1 scenario is representative of late-transgressive barrier deposition, which contributed to horizontal barrier stacking at Tuncurry [Fig. 4.9].

In contrast, the increase in substrate gradient from 0.23° to 0.33° at -40 m PMSL in the S2 scenario supported transgression by continuous encroachment, which resulted in the absence of highstand coastal barrier development at the termination of transgression [Fig. 6.15b]. Whilst in the S2 example the initial and final shorelines coincided, this is not requisite of transgressive encroachment behaviour, and therefore it is tempting to suggest a link between that behaviour and the occurrence of vertical barrier stacking [Sec. 2.4.3]. That is, considering that vertically-stacked highstand barrier systems are typical of the southern sector of the southeast Australian margin [Fig. 2.7], which is characterised by steeper inner shelf topography [Sec. 2.2], it may be the case that (Holocene) late-transgressive behaviour there featured shoreline encroachment into pre-existing MIS 5 barrier systems. Given the preservation of antecedent forced-regressive strandplain deposits in the S2 example [Fig. 6.15b], such behaviour may have supported the burial and preservation of any MIS-5 barrier deposits. Whilst the examples provided do not allow for the advancement of this idea beyond a hypothesis, the observed behaviour provides a potential explanation for the restriction of vertically-stacked highstand barrier systems to only those parts of the margin that feature a steep inner shelf.

6.5 Conclusions

This chapter explored potential implications of the R-dependent shoreface response described in Chapter 5, in the context of: (1) predictions of future coastal change; (2) the role of shoreface response in late-Quaternary coastal barrier deposition; and, (3) the use of shoreline trajectories to characterise depositional responses to sea level change. The examples provided were only sufficient to illustrate the major arguments arising from the model findings presented in Chapter 5, and their necessarily limited scope raises prospects more detailed subsequent investigations.

As for previous chapters, potential model dependence is considered here by identifying conclusions that may vary if an alternative model or BARSIM configuration were used. Conclusions potentially subject to model dependence have been *italicised*.

Regarding the predictions of coastline response to climate change explored in Section 6.2, the following conclusions are made:

1. Accelerating rates of projected sea-level rise under future climate change scenarios may exceed morphological relaxation timescales (i.e. $T_f > T_r$) across the lower-shoreface domain. *Comparison of global mean sea level observations with model predictions suggests that present rates of (global) sea level rise (c. 3 mm/a) may already exceed shoreface response rates across much of the lower shoreface.*

2. *Accordingly, $h_a \approx h_c$ may in fact represent a reasonable approximation of the* ***active shoreface*** *extent for accelerating sea-level rise through the present century.* This is consistent with a recent analysis of depth-dependent shoreface response timescales using long-term bathymetric survey data from the Gold Coast, Queensland [*Patterson*, 2012], which suggested that centennial shoreface response timescales were exceeded beyond about 17 m water depth.

3. However, there nonetheless remains the potential for enhanced onshore sand supply (or the cumulative offshore loss of coastal sediments during storm conditions) beyond h_a, which may become significant around the slowing or stabilisation of sea-level rise. Geometric equilibrium-profile models based on a closure depth of h_c do not consider this effect. The significance of lower-shoreface response is likely to depend on the nature of shoreface disequilibrium beyond h_a, and thus the continental-shelf setting.

4. Predictions of coastline response to climate change for coastal management and planning purposes should consider both the extent of active-shoreface response and lagged R-dependent shoreface response for a given setting.

Regarding shoreface response and coastal evolution to rapidly fluctuating sea-level change, the following conclusions are made:

1. R-dependent shoreface response may be a significant control on coastal barrier deposition during rapid sea-level fluctuations. For example, rates of MIS-3 sea-level change as suggested by existing sea level records imply that complete time-invariant shoreface response was most likely unattainable at Tuncurry for the estimated forcing conditions.

2. *The Tuncurry falling-stage barrier systems were most likely sourced primarily from disequilibrium-stress induced shoreface sand supply during MIS-3 interstadial highstands, and additionally from a supplementary external sediment supply (i.e. the longshore transport system) during fluctuating sea levels.* This is consistent with the interpretation of *Roy et al.* [1997], who argued that the erosion of updrift shelf sand bodies during sea level reversals would contribute high rates of sand supply to the Tuncurry embayment.

Regarding shoreface response and coastal evolution to steady and prolonged sea-level change, the following conclusions are made:

1. The cumulative effects of R-dependent shoreface response on coastal sediment budgets may contribute to alternative shoreline trajectories that reflect the relationship between forcing and coastal dynamics. However the alternative trajectories may not necessarily be reflected in the average shoreline trajectory of a depositional sequence, meaning that the average shoreline trajectory may not capture R-dependent shoreface response.

2. The role of R-dependent shoreface response in the modification of the shelf substrate during cyclical sea-level fall may contribute to alternative highstand barrier-stacking arrangements, due to the modification of inner-shelf gradients that control the subsequent transgressive-barrier behaviour.

7

Conclusions and Future Work

7.1 Research conclusions

Two primary and interrelated themes of barrier-coast evolution have been considered in this thesis: (1) controls on the evolution of late-Quaternary coastal barrier systems; and, (2) the sensitivity of shoreface response to sea level change. Concepts and evidence from both themes were tested in numerical simulation experiments in an attempt to build on the existing knowledge base regarding sea level change, coastal dynamics, and coastal evolution. A range of conclusions have been drawn from the outcomes of those experiments, which address outstanding issues from both themes. The major research conclusions are summarised here in two sections, which reflect the two primary themes. Where relevant, references are made between the themes to emphasise the fundamental role of shoreface response to sea level change in barrier-coast evolution.

In presenting the conclusions of this thesis it must be acknowledged that some of the research findings, in particular quantitative constraints on shoreface behaviour and coastal deposition (where insufficient geological records exist), may be subject to model dependence. That is, the predicted rates of shoreface response and volumes of deposition may vary if a different model or model configurations were used. The issue of model dependence, and the methods used to verify model predictions, is further considered in Section 7.2. To aid in the interpretation of the conclusions, those aspect that may be subject to model dependence have been *italicised*.

7.1.1 Evolution of barrier coasts

Regarding barrier-coast evolution during sea-level highstand, as demonstrated by the simulated evolution of Holocene coastal strandplains in southeastern Australia [Sec. 3], the following conclusions are made:

1. Along the tectonically stable accommodation-dominated barrier coast of southeastern Australia, mid- to late-Holocene (6-0 ka BP) strandplain progradation was primarily a response to onshore shoreface sand supply, driven by morphodynamic disequilibrium-stress response associated with ongoing lower-shoreface morphological relaxation. Where active, external sand sources (e.g. longshore transport system), and relative sea-level fall related to glacio-hydro-isostatic margin response, contributed comparatively lower supplementary sediment volumes to supply Holocene strandplain progradation.

2. The disequilibrium-stress-induced onshore sand transport that supplied strandplain progradation was most likely sourced from the erosion of mid- to lower-shoreface sand bodies. Accordingly, rates of onshore sand supply diminished throughout the late Holocene due to the reduced rates of depth-dependent shoreface erosion associated with deeper and more concave shoreface geometries. *At Moruya and Tuncurry, for example, these sand bodies may have featured maximum thicknesses of between 7-9 m at around 20 m water depth.*

3. Regardless of the timing and rate of relative sea level change, sea-level fall from a potential mid-Holocene (i.e. 7 ka BP) highstand of +1.5 m PMSL would have been insufficient to supply interpreted volumes of mid- to late-Holocene strandplain progradation. Even for the most conservative scenario considered here (i.e. 1.5 m fall from 6-0 ka BP at 0.25 mm/a), which BARSIM simulations suggested would have supported complete time-invariant shoreface response (i.e. $h_a = h_i$), onshore sand supply due to relative sea level fall at Moruya and Tuncurry could only have supplied a maximum 15% of strandplain progradation. Furthermore, a review of the evidence for mid- to late-Holocene sea level change in southeastern Australia favours the commencement of sea-level fall sometime after 3 ka BP, in conjunction with the decline of melt-water input rates below hydro-isostatic response rates. *For the HL2 (i.e. a 1.5 m fall from 3-0 ka BP at 0.5 mm/a) and HL3 (i.e. a*

1.5 m fall from 1.5-0 ka BP at 1 mm/a) scenarios, the potential sediment-volume contributions (i.e. active shoreface response and h-dependent shoreface response) to strandplain progradation at Moruya and Tuncurry were less than 10%.

4. Model experiments support previous assertions that a time-varying external sand supply was necessary to reproduce the steady rates of late-Holocene strandplain progradation at Tuncurry, and that the longshore transport regime supplied about 20% of the total strandplain volume: this figure is consistent with the geological evidence reported by *Roy et al.* [1997]. Specifically, conclusions 2 & 3 imply that sustained steady rates of late-Holocene (i.e. 3-0 ka BP) strandplain progradation required a secondary external sediment supply. Geological evidence from Tuncurry points to the establishment of an alongshore sand-supply to the embayment from around 3 ka BP, following the filling of updrift sediment sinks and establishment of a littoral transport pathway [Sec. 2.7.4].

5. *In the absence of a mid- to lower-shoreface sand body as an initial condition, high volumes of shoreface accommodation space resulted in simulated strandplain progradation to much greater depths than is suggested by the geological evidence, thereby necessitating a much larger external sand supply volume to achieve the interpreted progradation distances.* The necessary rates of external sand supply are inconsistent with the geological evidence and the updrift-sink model [Sec. 2.7.4], which further supports the significance of disequilibrium-stress-induced shoreface sand supply for Holocene barrier deposition.

Regarding barrier-coast evolution in response to late-Quaternary sea level change, as demonstrated by the simulated evolution of coastal barrier systems at Forster-Tuncurry, the following conclusions are made:

1. The deposition of composite coastal strandplains (e.g. the Tuncurry Pleistocene strandplains), by means of successive and intermittent phases of barrier progradation during consecutive sea-level highstands, is possible without the deposition of significant transgressive facies. Specifically, late-transgressive barrier overstepping supports the cyclical deposition of regressive barrier facies during successive highstands, without the preservation of significant transgressive facies.

2. The stacking relationships of highstand coastal barrier systems is, in part, determined by the nature of late-transgressive barrier behaviour. That is, transgressive-barrier overstepping supports cyclical strandplain progradation without the preservation of transgressive barrier (and backbarrier) deposits, whilst transgressive-barrier rollover favours the deposition and preservation of transgressive and backbarrier facies within highstand coastal barrier systems.

3. In gently sloping shelf settings (e.g. Tuncurry), the transgressive-barrier behaviours described above contribute to the horizontal stacking of coastal barrier systems. In steeper shelf settings, enhanced upper-shoreface erosion and reduced barrier volumes may contribute to vertically-stacked barrier systems.

4. Drowned last-glacial falling-stage strandplains that have been preserved in contemporary inner-shelf settings are most likely composite (interstadial) highstand barrier systems that developed in response to fluctuating MIS-3 sea levels, rather than uniform forced-regressive deposits. *At Tuncurry, for example, model experiments suggest that falling-stage barrier deposition was sourced from onshore sand supply driven by both relative sea level fall (forced regression)* ***and*** *disequilibrium-stress induced shoreface lowering under relatively stable sea levels (normal regression), and, a supplementary sediment supply from the longshore transport system.*

5. Collectively, the distribution and elevations of dated coastal barrier deposits at Tuncurry, and the sensitivity of simulated coastal barrier evolution to sea-level change, both suggest that sea levels in southeastern Australia during MIS 5a and MIS 3 may have been 10-15 m higher than typically indicated by late-Quaternary global sea level records. Regardless of the limitations of the dating methods used, the chrono-stratigraphic evidence is consistent with a growing body of evidence from intermediate and far-field sites, which suggests that MIS-5a and MIS-3 sea levels were higher than depicted in many existing sea level records.

7.1.2 Sensitivity of shoreface response to sea level change

Regarding the sensitivity of shoreface response to sea level change, and the role of active shoreface response (erosion) in coastal and shallow-marine deposition, the following conclusions are made:

1. At the onset of the Holocene sea-level highstand (i.e. 7 ka BP), shoreface morphodynamic disequilibrium in southeastern Australia likely persisted at depths beyond about h_c (i.e. 12-15 m). At Moruya and Tuncurry, shoreface geometry may have been characterised by convex mid- to lower-shoreface sand bodies that supplied mid- to late-Holocene strandplain progradation.

2. Interpreted rates of Holocene strandplain progradation and the findings of simulation experiments suggest that *peak rates of shoreface lowering of 2-3 mm/a (i.e. 2-3 m per millennia) between 6-5 ka BP, decreasing to less than 1 mm/a between 1-0 ka BP, would have been sufficient to supply strandplain progradation given the Tuncurry and Moruya settings. Peak rates of shoreface lowering occurred at mid-shoreface depths of around 18 m and decreased with increasing depth.* Associated rates of onshore sand supply rapidly decreased from up to 8 m^3/m/a between 6-5 ka BP to below 5 m^3/m/a from 5-4 ka BP onwards. The simulated shoreface behaviour is consistent with the concept of depth-diminishing onshore sand transport by wave processes.

3. Onshore shoreface sand supply is likely to persist in settings like Moruya and Tuncurry today, although at rates less than about 1 m^3/m/a. Therefore, any ongoing strandplain progradation may be difficult to discern in historical datasets, and may be diluted by the effects of periodic wave climate variations and storm events. Similarly, onshore sand supply from late-Holocene sea-level fall would be difficult to discern from sustained onshore sand supply due to ongoing shoreface morphological relaxation arising from the inheritance of an under-fit shelf regime following post-glacial marine transgression.

4. *For increasing rates of sea level change within the range typical of late-Quaternary and projected future sea level change (i.e. 0.5 to 10 mm/a), the active shoreface limiting depth (h_a) decreases from the lower-shoreface depth limit (h_i) to the surf zone. That is, shoreface response to sea level change varies from complete time-invariant response to complete depth-dependent response. For a given shelf gradient, h_a varies depending on morphodynamic efficiency: that is, the relationship between the energy climate and sediment characteristics. For a given setting, h_a is not sensitive to variations in shelf gradient, although the active-shoreface*

domain increases with reduced shelf gradient, and therefore the autochthonous sediment supply increases accordingly. The general relationship between h_a, h_c and h_i is expected to be generally robust assuming depth-diminishing shoreface erosion rates. However the quantitative relationship between h_a and R will vary for different erosion functions and model configurations.

5. The nature of h_a may provide a conceptual measure with which to categorise timescale-dependent coastal evolution, which may also have practical significance for the design of modelling approaches. For example: *microscale* coastal evolution (c. $10^0 - 10^1$ years) may be characterised by $h_a \leq h_c$; *mesoscale* coastal evolution (c. $10^2 - 10^5$ years) may be characterised by $h_c < h_a < h_i$; and, *macroscale* coastal evolution (c. 10^6+ years) may be characterised by $h_a \approx h_i$. An improved understanding of the relationship between h_a and R has the potential to inform the design and development of new modelling approaches that account for h-dependent shoreface erosion and R-dependent shoreface response.

6. The significance of depth-dependent shoreface response for coastal sediment budgets is most significant for mesoscale coastal evolution, which is characterised by R-dependent shoreface response (i.e. $h_c < h_a < h_i$). That is, collectively, h-dependent shoreface erosion and the timescales of interest suggest a non-negligible contribution to the sediment budget from lower-shoreface erosion. As h_a approaches h_i, h-dependent sediment transport residuals reduce due to the combined effects of increased h_a (lower-shoreface contraction) and lower rates of h-dependent shoreface erosion associated with a deeper and more concave shoreface. The significance of h-dependent transport residuals for coastal sediment budgets increases for both decreasing h_a and increased x_a (i.e. reduced shelf gradient). For microscale coastal evolution, the contribution of h-dependent shoreface erosion to coastal sediment budgets may be negligible for the timescale of the problem.

7. *The simulation experiments suggest that shoreface dimensions varied considerably for the late-Quaternary rates of sea level change.* Qualitatively, assuming depth-diminishing rates of shoreface erosion, the active shoreface would have contracted in response to the rapid sea level change experienced during sea level oscillations, and expanded during highstand and lowstand reversals, when low rates of forcing

would have supported development of the shoreface profile. Without significant external sand supply (and a means to trap it), therefore, coastal barrier deposition was most likely limited during rapid sea level change, with significant features developing only around the times of sea level reversals.

8. Geometric equilibrium-profile models, in which time-invariant shoreface response to a fixed closure depth is assumed, are most likely only capable of approximating late-Quaternary coastal evolution. This is because the relatively rapid rates of sea level change suggested by global sea level records imply time-varying shoreface geometry. For example, the simulation experiments in Section 6.3 suggested that MIS-3 falling-stage barrier systems at Tuncurry formed in response to progressively decreasing fluctuating sea levels, during which profile geometry across the majority of the shoreface may have varied considerably.

9. Considering the simulated relationship between the active shoreface depth limit and the rate of sea level change, accelerating sea-level-rise through the previous and present century imply contraction of the active shoreface. *The simulation experiments suggest that for southeast Australian settings, h_a may have decreased to h_c from around the year 1990 onwards, and thus a profile closure depth comparable to h_c may be representative of the time-averaged active shoreface response.* However, the application of h_c as the closure depth in geometric equilibrium-profile models does not consider two other important factors: (1) the potential for h-dependent shoreface erosion, which may be significant for mesoscale problems; and, (2) the potential generation of new accommodation space beyond h_a, which may contribute to the progressive 'permanent' loss of sand from coastal sediment budgets during storms.

10. Shoreline trajectories are sensitive to R-dependent shoreface response due to the relationship between shoreface erosion and onshore sand supply volumes. Thus the sensitivity of shoreline trajectories to shoreface response is likely to be most significant in autochthonous shelf settings. This suggests that where detailed shoreline trajectories are preserved, they may provide an indirect proxy measure of shoreface response to sea level change and active shoreface dimensions (where the nature of geohistorical variables [Sec. 1.3.1] can be reasonably constrained).

7.2 Limitations and opportunities for future research

It was established at the beginning of this thesis, that depth-dependent shoreface erosion rates and timescale-dependent shoreface response, suggest that historical measurement datasets provide little opportunity to constrain rates of surface response to changing boundary conditions [Sec. 1.3.3]. That is, measurement records only provide a partial insight into coastal dynamics, which is largely limited to the upper shoreface domain and microscale problems, and thus little is known about the coastal dynamics that affect mesoscale problems of interest to coastal engineers and geomorphologists alike [Sec. 1.1]. In an attempt to overcome these issues, a numerical process-response modelling approach was adopted in this thesis, which was applied with stratigraphic records of coastal barrier evolution to explore the sensitivity of shoreface response and coastal evolution to mesoscale forcing scenarios. Therefore the research findings presented in this thesis are subject to limitations arising from the geological datasets and the design of the modelling approach.

7.2.1 Available datasets

Although the Forster-Tuncurry dataset is the most comprehensive study of coastal barrier systems in southeastern Australia, in terms of deposition during different late-Quaternary sea level stages, some aspects of the dataset remain subject to uncertainty. For example, the limited number of age samples from the Pleistocene coastal strandplains, and the single transect in the centre of the northern embayment, may limit the applicability of the interpretations throughout the embayment. Also the thermoluminescence (TL) dating technique [Sec. 2.5.3], which has been used to date samples beyond the limits of radiocarbon dating, implies a degree of uncertainty regarding the absolute timing of deposition. Whilst the relative timing of deposition has been established, their remains potential for alternative interpretations should additional or revised data become available.

Therefore, although the conceptual evolutionary model presented in Section 4.6 is a rigorous reconstruction based on the available data and previous interpretations [*Melville*, 1984; *Roy et al.*, 1997], which has been further revised based on the outcomes of numerical modelling experiments presented in Chapter 4, some aspects of the evolutionary model remain better constrained than others. An obvious opportunity

for future work would be to gather additional stratigraphic and age data from the Forster-Tuncurry region to further inform the evolutionary model. In particular, the model would benefit from revised and more comprehensive age data for both the Pleistocene and Holocene highstand coastal barrier systems, perhaps using more reliable optically-stimulation luminescence (OSL) and Amino-acid racemisation (AAR) dating techniques.

Other data limitations relate to the use of observational data to simulate coastal evolution over geological timescales. For example, the BARSIM erosion function was calibrated using deep-water wave climate statistics that have been derived from waverider buoy measurements in southeastern Australia over the past few decades. It is unlikely that these wave climate statistics adequately describe wave climate during the mid- to late-Holocene, let alone throughout the last glacial-interglacial cycle. For example, previous investigations suggest that the southeast Australian wave climate experiences significant fluctuations in wave climate intensity and directionality associated with a range of climatic cycles of varying frequencies. [*Goodwin*, 2005; *Goodwin et al.*, 2006]. Whilst the consideration of these aspects was beyond the scope of the research presented here, future work may develop a statistical wave climate that is more representative of the periodic wave climate variability that is preserved in the geomorphology of coastal barrier systems.

7.2.2 Modelling approach

As for any modelling approach, the numerical simulations described in this thesis necessitated a series of simplifying assumptions, to represent complex and partially unresolved reality in a reliable and efficient approach. The BARSIM numerical stratigraphic model applies a series of process-response behaviour rules [*Storms et al.*, 2002], in an attempt to overcome the theoretical (i.e. non-linear morphodynamics) and computational barriers to up-scaling the predictions of process-based sediment transport models [Sec. 1.4.1]. The model parameterisation of physical reality has been covered in Section 1.5. Furthermore, the key assumptions of the modelling approach have been described in Section 3.3.1.

Whilst site-specific wave climate and sediment distribution data were applied in BARSIM configurations used here, verification of the sediment transport rules for the settings of interest was beyond the scope of the research. Evaluation of the model

transport rules using local empirical investigations could be pursued in future to refine model predictions. Although the absence of non-erodible strata was not deemed to have impaired the simulated coastal behaviour in a qualitative sense (i.e. depositional sensitivity to the bedrock framework at Tuncurry was captured in the substrate morphology), addition of non-erodible strata to BARSIM may improve quantitative predictions of coastal evolution. Similarly, the consideration of aeolian losses to dune systems, and the influence of dune morphology on coastal deposition may also improve quantitative model predictions.

Whilst the approach considered the contrasting depositional settings at Moruya and Tuncurry, and more generally idealised barrier-coast settings of southeastern Australia, the findings may not fully capture the behaviour of all barrier coasts. For example, the Moruya and Tuncurry sites are representative of embayed coasts, which support rapid and vast development of coastal barrier morphologies, due to the trapping of coastal sediments from internal and external sources. However, this capacity may be impaired in drift-aligned settings, where uninterrupted coastlines support balanced sediment budgets. The preservation of comparable coastal barrier stratigraphies in the drift-aligned setting at Ballina [Sec. 6.3.3] suggests that some aspects of the simulated behaviour may be generally applicable. Furthermore, records of barrier-rollover and barrier-overstepping behaviour exist in low-gradient drift-aligned barrier-coast settings elsewhere [*Leatherman*, 1983; *Niedoroda et al.*, 1985b; *Swift et al.*, 1985; *Storms et al.*, 2008].

Similarly, although the simulations considered a range of substrate gradients relevant to barrier coasts (e.g. 0.15-0.45°), and the natural substrates from Moruya and Tuncurry, the simulated shoreface responses may not be representative of steeper barrier-coast settings. For example, *Roy et al.* [1994] demonstrated that for steep substrate slopes (e.g. $> 1°$), deposition shifts from the coast to the lower shoreface-inner shelf environment. On this note, the ubiquity of the research findings could be extended through application of the approach to other barrier-coast settings where geological evidence of coastal evolution has been preserved. In doing so, regionally applicable relationships between morphodynamic efficiency, active-shoreface limiting depth, and depth-dependent rates of shoreface response could be obtained.

7.2.3 Potential for model dependence

The qualitative shoreface-response and depositional behaviours presented in this thesis are contingent on the assumption that exponentially depth-diminishing shoreface erosion (and onshore sand supply rates), conceptually due to depth-decaying wave-orbital-velocity skewness, is the primary driver of shoreface sediment transport. This is of course a gross simplification of reality, in that shoreface morphodynamics are characterised by a complex array of three-dimensional sediment transport processes [*Niedoroda et al.*, 1985a; *Niedoroda and Swift*, 1991]. For the wave-dominated barrier coast settings considered here, the concave contemporary shoreface geometries suggest that depth-decaying wave influences are a significant control on shoreface behaviour, and thus the assumption may provide a reasonable approximation for simplifying complex and unknown shoreface dynamics. The simulated shoreface response is also contingent on the empirically-derived grain-size dependent sediment travel distances used in BARSIM. These rules were derived from field experiments carried out at Terschelling, The Netherlands, and have not been further verified for the settings considered here.

The quantitative model predictions presented in this thesis are undeniably contingent on the BARSIM model algorithms and model configurations used. In particular, simulated rates of shoreface response and coastal deposition would undoubtedly vary if a different erosion function were used, or if different parameter settings were used with the existing BARSIM erosion function [Eq. 1.3]. Therefore the quantitative predictions of shoreface behaviour presented here can only be considered subjective approximations that inherit the limitations of the model parameterisation, and, the uncertainties associated with the procedure used to calibrate the erosion-efficiency scaling exponent (m) for the Moruya and Tuncurry settings [Sec. 3.3.1.3]. Where they are not constrained by the available geological datasets, the quantitative predictions of coastal deposition presented in this thesis also should only be considered approximations. In presenting the conclusions of this thesis, an attempt has been made to differentiate between those that are considered generally robust, and those that may be model dependent.

Assuming that the assumption of exponentially depth-diminishing shoreface erosion rates is reasonable for the settings considered, the calibration procedure aimed to tune the simplistic BARSIM erosion function for any local influences on the relationship between the energy regime and sediment transport, beyond the application of regional

wave climate statistics and sediment grain-size distributions. However, the calibration procedure itself was subject to uncertain initial conditions (i.e. shoreface geometry), and due to the limited available constraints on Holocene environmental forcing and coastal barrier deposition, could only be carried out for the case of stable sea level [Sec. 3.5.3]. Thus the calibration procedure in no way ensures that simulated shoreface dynamics in BARSIM provided an accurate depiction of reality at Tuncurry and Moruya; only that the model configurations were capable of generating stratigraphy and contemporary shoreface morphology consistent with the interpreted stratigraphic record, based on the uncertain initial conditions. Furthermore, the reliability of the geological evidence and process data applied in the models introduces further uncertainty into model predictions. Thus the potential remains that comparable coastal behaviour could emerge from non-unique combinations of initial conditions, system forcing variables, and parameterised coastal dynamics.

Although the research presented here was limited in scope to application of the existing BARSIM model to the southeast Australian settings considered, future research should consider the sensitivity of model predictions to the BARSIM erosion and deposition functions in more detail. That is, whilst the process-response approach provides a viable framework for simulating mesoscale coastal behaviour, sensitivity testing could be carried out to investigate a wider range of potential shoreface erosion parameterisations. Further to alternative calibrations of the existing erosion function, this could also include the consideration of complex shoreface functions that represent more discrete breaks in morphological relaxation timescales [*Inman et al.*, 1993; *Cowell et al.*, 1999]. These complex shoreface functions have emerged from observational evidence of contemporary shoreface geometry, and the acknowledgement of fundamentally different upper- and lower-shoreface sediment transport processes. The investigation of a range of potential erosion functions, in particular, would allow further qualification of the general applicability of the research findings presented in this thesis.

References

Aagaard, T., and P. Sorensen (2012), Coastal profile response to sea level rise: a process-based approach, *Earth Surface Processes and Landforms*, *37*(3), 354–362. 16, 18

Aagaard, T., R. Davidson-Arnott, B. Greenwood, and J. Nielsen (2004), Sediment supply from shoreface to dunes: linking sediment transport measurements and long-term morphological evolution, *Geomorphology*, *60*(1-2), 205–224. 100, 103

Abad, M., J. Rodrguez-Vidal, K. Aboumaria, M. N. Zaghloul, L. M. Cceres, F. Ruiz, A. Martnez-Aguirre, T. Izquierdo, and S. Chamorro (2013), Evidence of MIS 5 sea-level highstands in Gebel Mousa coast (Strait of Gibraltar, North of Africa), *Geomorphology*, *182*(0), 133–146. 162

Amoudry, L. O., and A. J. Souza (2011), Deterministic coastal morphological and sediment transport modeling: a review and discussion, *Rev. Geophys.*, *49*(2), RG2002. 16

Anthony, E. J., M. Mrani-Alaoui, and A. Hquette (2010), Shoreface sand supply and mid- to late Holocene aeolian dune formation on the storm-dominated macrotidal coast of the southern North Sea, *Marine Geology*, *276*(1-4), 100–104. 100

Baker, R. G. V., and R. J. Haworth (1997), Further evidence from relic shellcrust sequences for a late Holocene higher sea level for eastern Australia, *Marine Geology*, *141*(1-4), 1–9. 98

Baker, R. G. V., and R. J. Haworth (2000a), Smooth or oscillating late Holocene sea-level curve? Evidence from cross-regional statistical regressions of fixed biological indicators, *Marine Geology*, *163*(1-4), 353–365. 98

Baker, R. G. V., and R. J. Haworth (2000b), Smooth or oscillating late Holocene sea-level curve? Evidence from the palaeo-zoology of fixed biological indicators in east Australia and beyond, *Marine Geology*, *163*(1-4), 367–386. 98

Baker, R. G. V., R. J. Haworth, and P. G. Flood (2001), Inter-tidal fixed indicators of former Holocene sea levels in Australia: a summary of sites and a review of methods and models, *Quaternary International*, *83-5*, 257–273. 98

REFERENCES

Banfield, L. A., and J. B. Anderson (2004), *Late Quaternary evolution of the Rio Grande Delta*, in *Late Quaternary Stratigraphic Evolution of the Northern Gulf of Mexico Margin*, edited by J. B. Anderson and R. H. Fillon, pp. 289–306, Society for Sedimentary Geology, Tulsa. 162

Bateman, M. D., A. S. Carr, A. C. Dunajko, P. J. Holmes, D. L. Roberts, S. J. McLaren, R. G. Bryant, M. E. Marker, and C. V. Murray-Wallace (2011), The evolution of coastal barrier systems: a case study of the Middle-Late Pleistocene Wilderness barriers, South Africa, *Quaternary Science Reviews*, *30*(1-2), 63–81. 55, 162, 184

Belknap, D. F., and J. C. Kraft (1985), Influence of antecedent geology on stratigraphic preservation potential and evolution of Delaware barrier systems, *Marine Geology*, *63*(1-4), 235–262. 12

Bird, E. C. F. (1965), The evolution of sandy barrier formations on the East Gippsland coast, *Proccedings of the Royal Society of Victoria*, *79*, 75–88. 53

Birkemeier, W. A. (1985), Field data on seaward limit of profile change, *Journal of Waterway, Port, Coastal and Ocean Engineering, ASCE*, *111*(3), 598–602. 19, 211, 212, 213, 237

Boyd, R., K. Ruming, and J. J. Roberts (2004), Geomorphology and surficial sediments of the southeast Australian continental margin, *Australian Journal of Earth Sciences*, *51*(5), 743–764. 31, 33

Browne, I. (1994), Seismic stratigraphy and relict coastal sediments off the east coast of Australia, *Marine Geology*, *122*(1-2), 81–107. 31, 43, 57

Bruun, P. (1954), Coastal erosion and the development of beach profiles, *Technical memorandum no. 44*, Beach Erosion Board, USACE. 101, 145, 213, 216, 258

Bruun, P. (1962), Sea level rise as a cause of shore erosion, *Journal of Waterways and Harbors Division, ASCE*, *88*, 117–130. 3, 10, 17, 145, 148, 216, 237, 257

Bruun, P. (1983), Review of conditions for uses of the Bruun Rule of erosion, *Coastal Engineering*, *7*(1), 77–89. 3, 10, 17, 145, 257

Bruun, P. (1988), The Bruun Rule of erosion by sea-level rise - a discussion on large-scale two- and three-dimensional usages, *Journal of Coastal Research*, *4*(4), 627–648. 10, 17, 145, 257

Bryant, E. (1992), Last interglacial and Holocene trends in sea-level maxima around Australia - implications for modern rates, *Marine Geology*, *108*(2), 209–217. 97

Bryant, E. A., R. W. Young, D. M. Price, and S. A. Short (1994), Late Pleistocene dune chronology: near-coastal New South Wales and eastern Australia, *Quaternary Science Reviews*, *13*(3), 209–223. 57, 58, 66, 68, 69, 70

Bryant, E. A., R. W. Young, and D. M. Price (1997), Late Pleistocene marine deposition and TL chronology of the New South Wales, Australian coastline, *Zeitschrift Fur Geomorphologie*, *41*(2), 205–227. 58, 66, 69, 70

Cann, J. H., A. P. Belperio, V. A. Gostin, and C. V. Murray-Wallace (1988), Sea-level history, 45,000 to 30,000 yr BP, inferred from benthic foraminifera, Gulf St Vincent, South Australia, *Quaternary Research*, *29*(2), 153–175. 162

Cann, J. H., A. P. Belperio, and C. V. Murray-Wallace (2000), Late quaternary paleosealevels and paleoenvironments inferred from foraminifera, Northern Spencer Gulf, South Australia, *Journal of Foraminiferal Research*, *30*(1), 29–53. 162

Cant, D. J. (1991), Geometric modelling of facies migration: theoretical development of facies successions and local unconformities, *Basin Research*, *3*(2), 51–62. 10, 17, 244

Caputo, R. (2007), Sea-level curves: Perplexities of an end-user in morphotectonic applications, *Global and Planetary Change*, *57*(3-4), 417–423. 161, 162, 165, 167

Cattaneo, A., and R. J. Steel (2003), Transgressive deposits: a review of their variability, *Earth-Science Reviews*, *62*(3-4), 187–228. 41, 46

Chappell, J., A. Omura, T. Esat, M. McCulloch, J. Pandolfi, Y. Ota, and B. Pillans (1996), Reconciliation of late Quaternary sea levels derived from coral terraces at Huon Peninsula with deep sea oxygen isotope records, *Earth and Planetary Science Letters*, *141*(1-4), 227–236. 161

Charvin, K., K. Gallagher, G. L. Hampson, and R. Labourdette (2009), A Bayesian approach to inverse modelling of stratigraphy, part 1: method, *Basin Research*, *21*(1), 5–25. 2, 21, 27

Church, J. A., and N. J. White (2006), A 20th century acceleration in global sea-level rise, *Geophysical Research Letters*, *33*(1), 4. 253

Church, J. A., and N. J. White (2011), Sea-Level Rise from the Late 19th to the Early 21st Century, *Surveys in Geophysics*, *32*(4-5), 585–602. 253, 254

Church, J. A., N. J. White, T. Aarup, W. S. Wilson, P. L. Woodworth, C. M. Domingues, J. R. Hunter, and K. Lambeck (2008), Understanding global sea levels: past, present and future, *Sustainability Science*, *3*(1), 9–22. 21, 253

Church, J. A., J. M. Gregory, N. J. White, S. M. Platten, and J. X. Mitrovica (2011), Understanding and Projecting Sea Level Change, *Oceanography*, *24*(2), 130–143. 255

Clark, R. M. (1975), A calibration curve for radiocarbon dates, *Antiquity*, *49*, 251–266. 58

Cowell, P. J., and B. G. Thom (1994), *Morphodynamics of coastal evolution*, in *Coastal Evolution: Late Quaternary shoreline morphodynamics*, edited by R. W. G. Carter and C. D. Woodroffe, pp. 33–86, Cambridge University Press, Cambridge. 1, 13, 15, 93, 101, 210

REFERENCES

Cowell, P. J., P. S. Roy, and R. A. Jones (1995), Simulation of large-scale coastal change using a morphological behavior model, *Marine Geology*, *126*(1-4), 45–61. 2, 17, 20, 41, 43, 100, 187, 194, 201, 202, 241, 279, 280, 282

Cowell, P. J., D. J. Hanslow, and J. F. Meleo (1999), *The shoreface*, in *Handbook of beach and shoreface morphodynamics*, edited by A. D. Short, p. 392, John Wiley, New York. 1, 9, 14, 101, 139, 145, 151, 153, 210, 211, 213, 214, 217, 257, 258, 306

Cowell, P. J., M. J. F. Stive, P. S. Roy, G. M. Kaminsky, M. C. Buijsman, B. G. Thom, and L. D. Wright (2001), Shoreface sand supply to beaches, *27th International Coastal Engineering Conference*, pp. 2495–2508. 12, 14, 93, 100, 113, 154, 267, 270

Cowell, P. J., M. J. F. Stive, A. W. Niedoroda, H. J. de Vriend, D. J. P. Swift, G. M. Kaminsky, and M. Capobianco (2003a), The coastal-tract (part 1): A conceptual approach to aggregated modeling of low-order coastal change, *Journal of Coastal Research*, *19*(4), 812–827. 1, 3, 14, 16, 18, 93, 101, 207, 211, 212, 213, 217, 238, 243, 270

Cowell, P. J., M. J. F. Stive, A. W. Niedoroda, D. J. P. Swift, H. J. de Vriend, M. C. Buijsman, R. J. Nicholls, P. S. Roy, G. M. Kaminsky, J. Cleveringa, C. W. Reed, and P. L. de Boer (2003b), The coastal-tract (part 2): Applications of aggregated modeling of lower-order coastal change, *Journal of Coastal Research*, *19*(4), 828–848. 2, 9, 12, 16, 17, 18, 41, 100, 101, 154, 211, 243, 267

Cowell, P. J., B. G. Thom, R. A. Jones, C. H. Everts, and D. Simanovic (2006), Management of uncertainty in predicting climate-change impacts on beaches, *Journal of Coastal Research*, *22*(1), 232–245. 14, 20, 252

Curray, J. R. (1964), *Transgressions and Regressions*, in *Papers in marine geology*, edited by R. L. Miller, pp. 175–203, Macmillan Press, New York. 1, 10, 12, 39, 93

Daley, M. (2012), Disequilibrium-stress induced shoreface evolution, Phd thesis, the university of sydney. 100, 101, 102, 113, 267

Dean, R. G. (1977), Equilibrium beach profiles: U.S. Atlantic and Gulf coasts, *Ocean engineering report no. 12*, Department of Civil Engineering, University of Delaware. Newark, Delaware. 1, 101, 145, 213, 216, 237, 258

Dean, R. G. (1991), Equilibrium Beach Profiles - Characteristics and Applications, *Journal of Coastal Research*, *7*(1), 53–84. 1, 10, 20, 101, 145, 213, 258

Dean, R. G. (2002), *Beach nourishment: theory and practice*, 399 pp., World Scientific, River Edge, NJ. 9, 18, 244

Dean, R. G., and R. A. Dalrymple (2002), *Coastal processes: with engineering applications*, 475 pp., Cambridge University Press, New York. 16, 18, 19, 244

Dean, R. G., and E. M. Maurmeyer (1983), *Models for beach profile response*, in *CRC handbook of coastal processes and erosion*, edited by P. D. Komar, pp. 151–166, CRC Press, Boca Raton. 3

Dillenburg, S. R., P. S. Roy, P. J. Cowell, and L. J. Tomazelli (2000), Influence of antecedent topography on coastal evolution as tested by the shoreface translation-barrier model (STM), *Journal Of Coastal Research*, *16*(1), 71–81. 12, 55

Dorale, J. A., B. P. Onac, J. J. Fornos, J. Gines, A. Gines, P. Tuccimei, and D. W. Peate (2010), Sea-Level Highstand 81,000 Years Ago in Mallorca, *Science*, *327*(5967), 860–863. 162, 166

Evans, M. W., A. C. Hine, D. F. Belknap, and R. A. Davis (1985), Bedrock controls on barrier-island development - West-Central Florida Coast, *Marine Geology*, *63*(1-4), 263–283. 12

Fagherazzi, S., and I. Overeem (2007), Models of deltaic and inner continental shelf landform evolution, *Annual Review of Earth and Planetary Sciences*, *35*, 685–715. 16

Ferland, M. A., and P. S. Roy (1997), *Southeastern Australia: a sea-level dependent, cool-water carbonate margin*, in *Cool-water carbonates*, vol. Special Publication 56, edited by N. P. James and J. A. D. Clarke, pp. 37–52, Society of Economic Petrologists and Mineralogists (SEPM) Society for Sedimentary Geology, Tulsa. 45

Ferland, M. A., P. S. Roy, and C. V. Murraywallace (1995), Glacial Lowstand Deposits on the Outer Continental-Shelf of Southeastern Australia, *Quaternary Research*, *44*(2), 294–299. 31, 45

FitzGerald, D. M., M. S. Fenster, B. A. Argow, and I. V. Buynevich (2008), *Coastal impacts due to sea-level rise*, in *Annual Review of Earth and Planetary Sciences*, *Annual Review of Earth and Planetary Sciences*, vol. 36, pp. 601–647, Annual Reviews, Palo Alto. 18, 29, 244, 252

Frey, R. W., and J. D. Howard (1988), Beaches and beach-related facies, Holocene barrier islands of Georgia, *Geological Magazine*, *125*(6), 621–640. 55

Gagan, M. K., D. P. Johnson, and G. M. Crowley (1994), Sea-level control of stacked late Quaternary coastal sequences, central Great-Barrier-Reef, *Sedimentology*, *41*(2), 329–351. 53

Gaina, C., D. R. Muller, J. Y. Royer, J. Stock, J. Hardebeck, and P. Symonds (1998), The tectonic history of the Tasman Sea: A puzzle with 13 pieces, *Journal of Geophysical Research-Solid Earth*, *103*(B6), 12,413–12,433. 33

Gardner, J. V., P. Dartnell, L. A. Mayer, J. E. H. Clarke, B. R. Calder, and G. Duffy (2005), Shelf-edge deltas and drowned barrier-island complexes on the northwest Florida outer continental shelf, *Geomorphology*, *64*(3-4), 133–166. 45

REFERENCES

Gardner, J. V., B. R. Calder, J. E. H. Clarke, L. A. Mayer, G. Elston, and Y. Rzhanov (2007), Drowned shelf-edge deltas, barrier islands and related features along the outer continental shelf north of the head of De Soto Canyon, NE Gulf of Mexico, *Geomorphology*, *89*(3-4), 370–390. 45

Gelfenbaum, G., and G. M. Kaminsky (2010), Large-scale coastal change in the Columbia River littoral cell: An overview, *Marine Geology*, *273*(14), 1–10. 4

Gill, E. D., and D. Hopley (1972), Holocene sea levels in eastern Australia - a discussion, *Marine Geology*, *12*, 223–242. 97

Goodwin, I. D. (2005), A mid-shelf, mean wave direction climatology for southeastern Australia, and its relationship to the El Nino-Southern Oscillation since 1878 AD, *International Journal of Climatology*, *25*(13), 1715–1729. 34, 303

Goodwin, I. D., and N. Harvey (2008), Subtropical sea-level history from coral microatolls in the Southern Cook Islands, since 300 AD, *Marine Geology*, *253*(1-2), 14–25. 100, 114

Goodwin, I. D., M. A. Stables, and J. M. Olley (2006), Wave climate, sand budget and shoreline alignment evolution of the Iluka-Woody Bay sand barrier, northern New South Wales, Australia, since 3000 yr BP, *Marine Geology*, *226*(1-2), 127–144. 34, 50, 303

Grossman, E. E., S. L. Eittreim, M. E. Field, and F. L. Wong (2006), Shallow stratigraphy and sedimentation history during high-frequency sea-level changes on the central California shelf, *Continental Shelf Research*, *26*(10), 1217–1239. 2

Gutierrez, B. T., N. G. Plant, and E. R. Thieler (2011), A Bayesian network to predict coastal vulnerability to sea level rise, *Journal of Geophysical Research-Earth Surface*, *116*. 14

Hails, J. R. (1964), Coastal depositional features of southern Queensland, *Australian Geographer*, *9*, 207–217. 50

Hallermeier, R. J. (1981), A Profile Zonation For Seasonal Sand Beaches From Wave Climate, *Coastal Engineering*, *4*(3), 253–277. 19, 145, 150, 151, 212, 213, 214, 243

Hampson, G. J., and J. E. A. Storms (2003), Geomorphological and sequence stratigraphic variability in wave-dominated, shoreface-shelf parasequences, *Sedimentology*, *50*(4), 667–701. 2, 27

Hanson, H., S. Aarninkhof, M. Capobianco, J. A. Jimenez, M. Larson, R. J. Nicholls, N. G. Plant, H. N. Southgate, H. J. Steetzel, M. J. F. Stive, and H. J. de Vriend (2003), Modelling of coastal evolution on yearly to decadal time scales, *Journal of Coastal Research*, *19*(4), 790–811. 16

Harley, M. D., I. L. Turner, A. D. Short, and R. Ranasinghe (2010), Interannual variability and controls of the Sydney wave climate, *International Journal of Climatology*, *30*(9), 1322–1335. 34, 105, 257

Hayes, D. E., and J. Ringis (1973), Sea-floor spreading in the Tasman Sea, *Nature*, *244*(5408), 454–458. 33

Hayes, M. O. (1994), *The Georgia Bight barrier system*, in *Geology of Holocene barrier island systems*, edited by R. A. Davis, pp. 233–304, Springer-Verlag, Berlin. 55

Helland-Hansen, W., and G. J. Hampson (2009), Trajectory analysis: concepts and applications, *Basin Research*, *21*(5), 454–483. 12, 18, 219, 285

Helland-Hansen, W., and O. J. Martinsen (1996), Shoreline trajectories and sequences: Description of variable depositional-dip scenarios, *Journal of Sedimentary Research*, *66*(4), 670–688. 12, 219, 285

Hinton, C. L., and R. J. Nicholls (2007), *Shoreface morphodynamics along the Holland Coast*, in *Coastal and shelf sediment transport*, vol. Special Publications, 274, edited by P. S. Balson and M. B. Collins, pp. 93–101, Geological Society of London, London. 9

Horton, R., C. Herweijer, C. Rosenzweig, J. P. Liu, V. Gornitz, and A. C. Ruane (2008), Sea level rise projections for current generation CGCMs based on the semi-empirical method, *Geophysical Research Letters*, *35*(2), 5. 252

Hunt, D., and R. L. Gawthorpe (2000), *Sedimentary responses to forced regressions*, vol. Special Publication, 172, Geological Society, London. 42

Inman, D. L., and C. E. Nordstrom (1971), On the tectonic and morphologic classification of coasts, *Journal of Geology*, *79*(1), 1–21. 37, 46

Inman, D. L., M. H. S. Elwany, and S. A. Jenkins (1993), Shorerise and bar-berm profiles on ocean beaches, *Journal of Geophysical Research-Oceans*, *98*(C10), 18,181–18,199. 1, 237, 238, 306

Jenkin, J. J. (1968), The geomorphology and Upper Cainozoic geology of south-east Gippsland, Victoria, *Tech. rep.*, Geological Society of Victoria, Memoir 27. 53

Jevrejeva, S., J. C. Moore, and A. Grinsted (2012), Sea level projections to AD2500 with a new generation of climate change scenarios, *Global and Planetary Change*, *80-81*, 14–20. 252, 253

Johnson, D. W. (1919), *Shore processes and shoreline development*, 584 pp., John Wiley and Sons, New York. 1, 210

Jones, B. G., R. W. Young, and I. G. Elliot (1979), Stratigraphy and chronology of receding barrier-beach deposits on the northern Illawarra coast of New South Wales, *Journal of the Geological Society of Australia*, *26*, 255–264. 97

Jones, H. A., J. Lean, and H.-U. Schluter (1982), *Seismic reflection profiling off the east coast of Australia, Newcastle to Cape Hawke*, in *Heavy mineral exploration of the East Australian*

shelf. "Sonne" Cruise SO-15, 1980, vol. 56, edited by U. von Stackelburg, pp. 69–75, Geologisches Jahrbuch, Reihe D, Heft. 43

Kim, W., C. Paola, V. R. Voller, and J. B. Swenson (2006), Experimental measurement of the relative importance of controls on shoreline migration, *Journal of Sedimentary Research*, *76*(1-2), 270–283. 2, 18, 244

Komar, P. D. (1998), *Beach processes and sedimentation*, 544 pp., Prentice-Hall, New Jersey. 16

Komar, P. D., N. Lanfredi, M. Baba, R. G. Dean, K. Dyer, T. Healy, A. C. Ibe, J. H. J. Terwindt, and B. G. Thom (1991), The response of beaches to sea-level changes - a review of predictive models, *Journal of Coastal Research*, *7*(3), 895–921. 3, 19

Kooi, H., and C. Beaumont (1996), Large-scale geomorphology: Classical concepts reconciled and integrated with contemporary ideas via a surface processes model, *Journal of Geophysical Research-Solid Earth*, *101*(B2), 3361–3386. 19

Lambeck, K. (2002), *Sea-level change from mid Holocene to recent time: an Australian example with global implications*, in *Ice Sheets, Sea Level and the Dynamic Earth. Geodynamic Series 29*, *Geodynamic Series*, vol. Geodynamic Series 29, edited by J. X. Mitrovica and B. L. A. Vermeersen, pp. 33–50, American Geophysical Union. 100, 114

Lambeck, K., and J. Chappell (2001), Sea level change through the last glacial cycle, *Science*, *292*(5517), 679–686. 98, 161, 168, 169, 272, 273

Lambeck, K., and M. Nakada (1990), Late Pleistocene and Holocene sea-level change along the Australian coast, *Palaeogeography Palaeoclimatology Palaeoecology (Global and Planetary Change Section)*, *89*(1-2), 143–176. 97, 98, 114

Lambeck, K., and A. Purcell (2005), Sea-level change in the Mediterranean Sea since the LGM: model predictions for tectonically stable areas, *Quaternary Science Reviews*, *24*(18-19), 1969–1988. 161

Lambeck, K., C. Smither, and P. Johnston (1998), Sea-level change, glacial rebound and mantle viscosity for northern Europe, *Geophysical Journal International*, *134*(1), 102–144. 161

Lambeck, K., Y. Yokoyama, and T. Purcell (2002), Into and out of the Last Glacial Maximum: sea-level change during Oxygen Isotope Stages 3 and 2, *Quaternary Science Reviews*, *21*(1-3), 343–360. 161

Lambeck, K., A. Purcell, P. Johnston, M. Nakada, and Y. Yokoyama (2003), Water-load definition in the glacio-hydro-isostatic sea-level equation, *Quaternary Science Reviews*, *22*(2-4), 309–318. 98, 161

Langford-Smith, T., and B. G. Thom (1969), Coastal morphology of New South Wales, *Journal of the Geological Society of Australia*, *16*, 572–580. 47

Larson, M., and N. C. Kraus (1991), Mathematical-modeling of the fate of beach fill, *Coastal Engineering*, *16*(1), 83–114. 16

Leatherman, S. P. (1983), Barrier Dynamics And Landward Migration With Holocene Sea-Level Rise, *Nature*, *301*(5899), 415–417. 46, 188, 304

Lewis, S. E., R. A. J. Wst, J. M. Webster, and G. A. Shields (2008), Mid-late Holocene sea-level variability in eastern Australia, *Terra Nova*, *20*(1), 74–81. 98, 100

Lewis, S. E., C. R. Sloss, C. V. Murray-Wallace, C. D. Woodroffe, and S. G. Smithers (2013), Post-glacial sea-level changes around the Australian margin: a review, *Quaternary Science Reviews*, (0). 98

Lister, G. S., M. A. Etheridge, and P. A. Symonds (1986), Detachment faulting and the evolution of passive continental margins, *Geology*, *14*(3), 246–250. 33, 195

Lorenzo-Trueba, J., and A. D. Ashton (2014), Rollover, Drowning, and Discontinuous Retreat: Distinct modes of barrier response to sea-level rise arising from a simple morphodynamic model, *Journal of Geophysical Research: Earth Surface*, p. 2013JF002941. 21

Marshall, J. F., and B. G. Thom (1976), The sea level in the last interglacial, *Nature*, *263*(5573), 120–121. 189

Mauz, B., and U. Hassler (2000), Luminescence chronology of Late Pleistocene raised beaches in southern Italy: new data of relative sea-level changes, *Marine Geology*, *170*(1-2), 187–203. 162

Medina-Elizalde, M. (2013), A global compilation of coral sea-level benchmarks: Implications and new challenges, *Earth and Planetary Science Letters*, *362*, 310–318. 161, 162, 164

Meehl, G., T. F. Stocker, W. D. Collins, P. Friedlingstein, A. T. Gaye, J. M. Gregory, A. Kitoh, R. Knutti, J. M. Murphy, A. Noda, S. C. B. Raper, I. G. Watterson, A. J. Weaver, and Z.-C. Zhao (2007), *Global Climate Projections*, in *Climate Change 2007: The Physical Science Basis. Contribution of Working Group I to the Fourth Assessment Report of the Intergovernmental Panel on Climate Change*, edited by S. Solomon, D. Quin, M. Manning, Z. Chen, M. Marquis, K. B. Averyt, M. Tignor, and H. L. Miller, pp. 747–845, Cambridge University Press, Cambridge and New York. 234, 251, 252, 253

Meehl, G. A., W. M. Washington, W. D. Collins, J. M. Arblaster, A. X. Hu, L. E. Buja, W. G. Strand, and H. Y. Teng (2005), How much more global warming and sea level rise?, *Science*, *307*(5716), 1769–1772. 252, 253

Meleo, J. F. (1994), Shoreface variability in Southeastern Australia, Honours thesis. 145, 151

REFERENCES

Melville, G. (1984), Headlands and offshore islands as dominant controlling factors during late Quaternary barrier formation in the Forster-Tuncurry area, New South Wales, Australia, *Sedimentary Geology*, *39*(3-4), 243–271. 57, 66, 194, 200, 302, 346, 347

Mitrovica, J. X., and G. A. Milne (2002), On the origin of late Holocene sea-level highstands within equatorial ocean basins, *Quaternary Science Reviews*, *21*(2022), 2179–2190. 100

Mitrovica, J. X., and W. R. Peltier (1991), On postglacial geoid subsidence over the equatorial oceans, *Journal of Geophysical Research-Solid Earth*, *96*(B12), 20,053–20,071. 100

Moore, L. J., J. H. List, S. J. Williams, and D. Stolper (2010), Complexities in barrier island response to sea level rise: Insights from numerical model experiments, North Carolina Outer Banks, *Journal of Geophysical Research*, *115*, F03,004. 2, 17, 20, 148

Mountain, G. S., R. L. Burger, H. Delius, C. S. Fulthorpe, J. A. Austin, D. S. Goldberg, M. S. Steckler, C. M. McHugh, K. G. Miller, D. H. Monteverde, D. L. Orange, and L. F. Pratson (2007), *The long-term stratigraphic record on continental margins*, in *Continental Margin Sedimentation: From Sediment Transport to Sequence Stratigraphy*, vol. Special Publication Number 37 of the International Association of Sedimentologists, edited by C. A. Nittrouer, J. A. Austin, M. E. Field, J. H. Kravitz, J. P. M. Syvitski, and P. L. Wiberg, pp. 381–458, Blackwell Publishing, Oxford. 36

Muhs, D. R., K. R. Simmons, and B. Steinke (2002), Timing and warmth of the Last Interglacial period: new U-series evidence from Hawaii and Bermuda and a new fossil compilation for North America, *Quaternary Science Reviews*, *21*(12-13), 1355–1383. 162

Murray-Wallace, C. V., A. P. Belperio, V. A. Gostin, and J. H. Cann (1993), Amino-acid racemization and radiocarbon dating of interstadial marine strata (Oxygen Isotope Stage 3), Gulf St-Vincent, South-Australia, *Marine Geology*, *110*(1-2), 83–92. 162

Murray-Wallace, C. V., M. A. Ferland, P. S. Roy, and A. Sollar (1996), Unravelling patterns of reworking in lowstand shelf deposits using amino acid racemisation and radiocarbon dating, *Quaternary Science Reviews*, *15*(7), 685–697. 31, 45

Murray-Wallace, C. V., M. A. Ferland, and P. S. Roy (2005), Further amino acid racemisation evidence for glacial age, multiple lowstand deposition on the New South Wales outer continental shelf, southeastern Australia, *Marine Geology*, *214*(1-3), 235–250. 31, 45

Nicholls, R. J., and A. Cazenave (2010), Sea-Level Rise and Its Impact on Coastal Zones, *Science*, *328*(5985), 1517–1520. 18, 29, 244, 252

Nicholls, R. J., W. A. Birkemeier, and G. H. Lee (1998), Evaluation of depth of closure using data from Duck, NC, USA, *Marine Geology*, *148*(3-4), 179–201. 9, 19, 211, 213, 217, 237

Niedoroda, A. W., and D. J. P. Swift (1991), *Shoreface processes*, in *Handbook of Coastal and Ocean Engineering*, vol. 2, edited by J. B. Herbich, pp. 735–770, Gulf Publishers, Houston. 9, 93, 139, 151, 154, 210, 213, 217, 305

Niedoroda, A. W., D. J. P. Swift, T. S. Hopkins, and C. M. Ma (1984), Shoreface morphodynamics on wave-dominated coasts, *Marine Geology*, *60*(1-4), 331–354. 93, 154

Niedoroda, A. W., D. J. P. Swift, and T. S. Hopkins (1985a), *The Shoreface*, in *Coastal Sedimentary Environments*, edited by R. A. Davis, pp. 533–624, Springer-Verlag. 1, 305

Niedoroda, A. W., D. J. P. Swift, A. G. Figueiredo, and G. L. Freeland (1985b), Barrier-island evolution, middle Atlantic shelf, USA 2: evidence from the shelf floor, *Marine Geology*, *63*(1-4), 363–396. 46, 188, 210, 304

Niedoroda, A. W., C. W. Reed, D. J. P. Swift, H. Arato, and K. Hoyanagi (1995), Modeling shore-normal large-scale coastal evolution, *Marine Geology*, *126*(1-4), 181–199. 100

Nielsen, A. F., and P. S. Roy (1981), Age contamination of radiocarbon dates on shell hash from coastal sand deposits: southeast australian examples, *5th Australian Conference on Coastal and Ocean Engineering*, pp. 177–182. 57

Nummedal, D., G. W. Riley, and P. L. Templet (1993), *High-resolution sequence architecture: A chronostratigraphic model based on equilibrium profile studies*, in *Sequence Stratigraphy and Facies Associations*, vol. Special Publication No. 18 of the International Association of Sedimentologists, edited by H. W. Posamentier, C. P. Summerhayes, B. U. Haq, and G. P. Allen, pp. 55–68, Blackwell Scientific Publications, Oxford. 11, 17, 19, 244

Oertel, G. F. (1985), The barrier-island system, *Marine Geology*, *63*(1-4), 1–18. 1

Overpeck, J. T., B. L. Otto-Bliesner, G. H. Miller, D. R. Muhs, R. B. Alley, and J. T. Kiehl (2006), Paleoclimatic evidence for future ice-sheet instability and rapid sea-level rise, *Science*, *311*(5768), 1747–1750. 252

Patterson, D. C. (2012), Shoreward sand transport outside the surf zone, northern gold coast, australia, *33rd International Conference on Coastal Engineering*, p. 15. 103, 257, 267, 268, 269, 292

Persano, C., F. M. Stuart, P. Bishop, and T. J. Dempster (2005), Deciphering continental breakup in eastern Australia using low-temperature thermochronometers, *Journal of Geophysical Research-Solid Earth*, *110*(B12). 33

Pilkey, O. H., R. S. Young, S. R. Riggs, A. W. S. Smith, H. Y. Wu, and W. D. Pilkey (1993), The concept of shoreface profile of equilibrium - A critical review, *Journal of Coastal Research*, *9*(1), 255–278. 207

Plint, A. G., and D. Nummedal (2000), *The falling stage systems tract: recognition and importance in sequence stratigraphic analysis*, in *Sedimentary responses to forced regressions*, vol. Special Publications, 172, edited by D. Hunt and R. L. Gawthorpe, pp. 1–17, Geological Society, London. 36, 42

Posamentier, H. W., and W. R. Morris (2000), *Aspects of the stratal architecture of forced regressive deposits*, in *Sedimentary responses to forced regressions*, vol. Special Publications, 172, edited by D. Hunt and R. L. Gawthorpe, pp. 19–46, Geological Society, London. 39, 42, 185

Posamentier, H. W., and P. R. Vail (1988), *Eustatic controls on clastic deposition II - sequence and systems tract models*, in *Sea level change - an integrated approach*, vol. Special Publication 42, edited by C. K. Wilgus, B. S. Hastings, C. G. St. C. Kendall, H. W. Posamentier, C. A. Ross, and J. C. Van Wagoner, pp. 125–154, Society of Economic Paleontologists and Mineralogists (SEPM), Tulsa. 36, 37, 42, 45, 46

Posamentier, H. W., M. T. Jervey, and P. R. Vail (1988), *Eustatic controls on clastic deposition I - conceptual framework*, in *Sea level change - an integrated approach*, vol. Special Publication 42, edited by C. K. Wilgus, B. S. Hastings, C. G. St. C. Kendall, H. W. Posamentier, C. A. Ross, and J. C. Van Wagoner, pp. 110–124, Society of Economic Paleontologists and Mineralogists (SEPM), Tulsa. 10, 17

Posamentier, H. W., G. P. Allen, D. P. James, and M. Tesson (1992), Forced regressions in a sequence stratigraphic framework: concepts, examples, and exploration significance, *AAPG Bulletin-American Association of Petroleum Geologists*, *76*(11), 1687–1709. 39, 45, 95

Price, D. M., B. P. Brooke, and C. D. Woodroffe (2001), Thermoluminescence dating of aeolianites from Lord Howe Island and South-West Western Australia, *Quaternary Science Reviews*, *20*(5-9), 841–846. 58

Rahmstorf, S. (2007), A semi-empirical approach to projecting future sea-level rise, *Science*, *315*(5810), 368–370. 234, 252

Ranasinghe, R., R. McLoughlin, A. Short, and G. Symonds (2004), The Southern Oscillation Index, wave climate, and beach rotation, *Marine Geology*, *204*(3-4), 273–287. 34

Rodriguez, A. B., J. B. Anderson, L. A. Banfield, M. Taviani, K. Abdulah, and J. N. Snow (2000), Identification of a - 15 m middle Wisconsin shoreline on the Texas inner continental shelf, *Palaeogeography Palaeoclimatology Palaeoecology*, *158*(1-2), 25–43. 162

Roelvink, D., A. Reniers, A. van Dongeren, J. V. de Vries, R. McCall, and J. Lescinski (2009), Modelling storm impacts on beaches, dunes and barrier islands, *Coastal Engineering*, *56*(11-12), 1133–1152. 16

Rohling, E. J., K. Grant, C. Hemleben, M. Kucera, A. P. Roberts, I. Schmeltzer, H. Schulz, M. Siccha, M. Siddall, and G. Trommer (2008), New constraints on the timing of sea level fluctuations during early to middle marine isotope stage 3, *Paleoceanography*, *23*(3). 163, 272

Rohling, E. J., K. Grant, M. Bolshaw, A. P. Roberts, M. Siddall, C. Hemleben, and M. Kucera (2009), Antarctic temperature and global sea level closely coupled over the past five glacial cycles, *Nature Geoscience*, *2*(7), 500–504. 161

Roy, P. S. (1994), *Holocene estuary evolution - stratigraphic studies from southeastern Australia*, in *Incised valley systems: origin and sedimentary sequences*, edited by R. A. Dalrymple, R. Boyd, and B. A. Zaitlin, pp. 241–263, Society of Economic Petrologists and Mineralogists (SEPM) Society for Sedimentary Geology, Tulsa. 55

Roy, P. S., and E. A. Crawford (1980), Quaternary geology of Newcastle Bight inner continental shelf, New South Wales, Australia, *New South Wales Geological Survey - Records*, *19*, 145–188. 189

Roy, P. S., and C. Peat (1973), Estuarine investigation - Tuggerah Lake: The bathymetry and bottom sediments of Tuggerah, Budgewoi and Munmorah Lakes, and the subsurface stratigraphy of Tuggerah Lake, *Tech. rep.*, Geological Survey of New South Wales, Department of Mineral Resources. 55

Roy, P. S., and B. G. Thom (1981), Late Quaternary marine deposition in New South Wales and southern Queensland - An evolutionary model, *Journal of the Geological Society of Australia*, *28*(3-4), 471–489. 12, 31, 32, 33, 34, 47, 94, 195, 202

Roy, P. S., and B. G. Thom (1991), *Cainozoic shelf sedimentation model for the Tasman Sea margin of southeastern Australia*, in *The Cainozoic in Australia: A re-appraisal of the evidence*, vol. Special Publication 18, edited by M. A. J. Williams, P. de Deckker, and A. P. Kershaw, pp. 119–136, Geological Society of Australia. 33, 94, 195

Roy, P. S., B. G. Thom, and L. D. Wright (1980), Holocene sequences on an embayed high-energy coast: an evolutionary model, *Sedimentary Geology*, *26*(1-3), 1–19. 31, 34

Roy, P. S., P. J. Cowell, M. A. Ferland, and B. G. Thom (1994), *Wave dominated coasts*, in *Coastal Evolution: Late Quaternary shoreline morphodynamics*, edited by R. W. G. Carter and C. D. Woodroffe, pp. 121–186, Cambridge University Press, Cambridge. 1, 2, 11, 12, 32, 37, 38, 39, 40, 41, 43, 44, 46, 94, 105, 112, 194, 199, 203, 207, 241, 242, 268, 275, 279, 280, 304

Roy, P. S., W. Y. Zhuang, G. F. Birch, P. J. Cowell, and L. Congxiang (1997), Quaternary geology of the Forster-Tuncurry coast and shelf southeast Australia, *Tech. rep.*, Geological Survey of New South Wales, Department of Mineral Resources. 43, 57, 58, 66, 69, 70, 71,

72, 73, 74, 77, 79, 81, 83, 84, 86, 88, 89, 90, 94, 105, 112, 113, 140, 142, 143, 156, 157, 160, 172, 183, 184, 194, 196, 199, 201, 202, 203, 257, 275, 279, 280, 282, 293, 297, 302

Schluter, H.-U. (1982), *Results of a reflection seismic survey in shallow water areas off east Australia, Yamba to Tweed Heads*, in *Heavy mineral exploration of the East Australian shelf. "Sonne" Cruise SO-15, 1980*, vol. 56, edited by U. von Stackelburg, pp. 77–95, Geologisches Jahrbuch, Reihe D, Heft. 31, 43, 284

Schwab, W. C., W. E. Baldwin, C. J. Hapke, E. E. Lentz, P. T. Gayes, J. F. Denny, J. H. List, and J. C. Warner (2013), Geologic Evidence for Onshore Sediment Transport from the Inner Continental Shelf: Fire Island, New York, *Journal Of Coastal Research*, pp. 526–544. 100, 103

Searle, D. E. (1982), *Seismic reflection profiling off the east coast of Australia, South Stradbroke Island to Tweed Heads*, in *Heavy mineral exploration of the East Australian shelf. "Sonne" Cruise SO-15, 1980*, vol. 56, edited by U. von Stackelburg, pp. 97–104, Geologisches Jahrbuch, Reihe D, Heft. 43

Sen, A., C. G. S. Kendall, and P. Levine (1999), Combining a computer simulation and eustatic events to date seismic sequence boundaries: a case study of the Neogene of the Bahamas, *Sedimentary Geology*, *125*(1-2), 47–59. 18

Shackleton, N. J. (2000), The 100,000-year ice-age cycle identified and found to lag temperature, carbon dioxide, and orbital eccentricity, *Science*, *289*(5486), 1897–1902. 162, 163, 166

Short, A. D., and N. L. Trenaman (1992), Wave climate of the Sydney region, an energetic and highly variable ocean wave regime, *Australian Journal of Marine and Freshwater Research*, *43*(4), 765–791. 34, 105, 257

Siddall, M., E. J. Rohling, A. Almogi-Labin, C. Hemleben, D. Meischner, I. Schmelzer, and D. A. Smeed (2003), Sea-level fluctuations during the last glacial cycle, *Nature*, *423*(6942), 853–858. 161, 169, 272, 273

Siddall, M., E. J. Rohling, W. G. Thompson, and C. Waelbroeck (2008), Marine Isotope Stage 3 sea level fluctuations: data syntehsis and new outlook, *Reviews of Geophysics*, *46*(4). 163, 272, 280

Simms, A. R., R. DeWitt, A. B. Rodriguez, K. Lambeck, and J. B. Anderson (2009), Revisiting marine isotope stage 3 and 5a (MIS3-5a) sea levels within the northwestern Gulf of Mexico, *Global and Planetary Change*, *66*(1-2), 100–111. 162

Sircombe, K. N. (1999), Tracing provenance through the isotope ages of littoral and sedimentary detrital zircon, eastern Australia, *Sedimentary Geology*, *124*(1-4), 47–67. 94

Sloss, C. R., B. G. Jones, C. V. Murray-Wallace, and C. E. McClennen (2005), Holocene sea level fluctuations and the sedimentary evolution of a barrier estuary: Lake Illawarra, New South Wales, Australia, *Journal of Coastal Research*, *21*(5), 943–+. 55

Sloss, C. R., B. G. Jones, C. E. McClennen, J. de Carli, and D. M. Price (2006a), The geomorphological evolution of a wave-dominated barrier estuary: Burrill lake, New South Wales, Australia, *Sedimentary Geology*, *187*(3-4), 229–249. 55

Sloss, C. R., C. V. Murray-Wallace, and B. G. Jones (2006b), Aminostratigraphy of two Holocene wave-dominated barrier estuaries in southeastern Australia, *Journal of Coastal Research*, *22*(1), 113–136. 55

Sloss, C. R., C. V. Murray-Wallace, and B. G. Jones (2007), Holocene sea-level change on the southeast coast of Australia: a review, *Holocene*, *17*(7), 999–1014. 98, 99, 115

Sloss, C. R., B. G. Jones, A. D. Switzer, S. Nichol, A. J. H. Clement, and A. W. Nicholas (2010), The Holocene infill of Lake Conjola, a narrow incised valley system on the southeast coast of Australia, *Quaternary International*, *221*(1-2), 23–35. 55

Sloss, L. L. (1962), Stratigraphical models in exploration, *Journal of Sedimentary Petrology*, *32*, 415–422, sloss variables. 10, 11

Stive, M. J. F. (2004), How important is global warming for coastal erosion? An editorial comment, *Climatic Change*, *64*, 27–39. 18, 29, 244, 252

Stive, M. J. F., and H. J. de Vriend (1995), Modeling Shoreface Profile Evolution, *Marine Geology*, *126*(1-4), 235–248. 3, 9, 14, 93, 100, 207, 208, 213, 216, 217, 267

Stolper, D., J. H. List, and E. R. Thieler (2005), Simulating the evolution of coastal morphology and stratigraphy with a new morphological-behaviour model (GEOMBEST), *Marine Geology*, *218*(1-4), 17–36. 2, 17, 20

Storms, J. E. A. (2003), Event-based stratigraphic simulation of wave-dominated shallow-marine environments, *Marine Geology*, *199*(1-2), 83–100. 22, 24, 25, 27

Storms, J. E. A., and G. J. Hampson (2005), Mechanisms for forming discontinuity surfaces within shoreface-shelf parasequences: Sea level, sediment supply, or wave regime?, *Journal of Sedimentary Research*, *75*(1), 67–81. 19, 27

Storms, J. E. A., and D. J. P. Swift (2003), Shallow-marine sequences as the building blocks of stratigraphy: insights from numerical modelling, *Basin Research*, *15*(3), 287–303. 19, 27

Storms, J. E. A., G. J. Weltje, J. J. van Dijke, C. R. Geel, and S. B. Kroonenberg (2002), Process-response modeling of wave-dominated coastal systems: Simulating evolution and stratigraphy on geological timescales, *Journal of Sedimentary Research*, *72*(2), 226–239. 9, 22, 27, 41, 207, 303

Storms, J. E. A., G. J. Weltje, G. J. Terra, A. Cattaneo, and F. Trincardi (2008), Coastal dynamics under conditions of rapid sea-level rise: Late Pleistocene to Early Holocene evolution of barrier-lagoon systems on the northern Adriatic shelf (Italy), *Quaternary Science Reviews*, *27*(11-12), 1107–1123. 9, 21, 22, 26, 27, 45, 188, 189, 271, 304

Swift, D. J. P., and J. A. Thorne (1991), *Sedimentation on continental margins I: a general model for shelf sedimentation*, in *Shelf Sand and Sandstone Bodies - Geometry, Facies and Sequence Stratigraphy*, vol. Special Publication No. 14 of the International Association of Sedimentologists, edited by D. J. P. Swift, G. F. Oertal, R. W. Tillman, and J. A. Thorne, pp. 3–31, Blackwell Scientific Publications, Oxford. 1, 10, 207

Swift, D. J. P., A. W. Niederoda, C. E. Vincent, and T. S. Hopkins (1985), Barrier-island evolution, middle Atlantic shelf, USA 1: shoreface dynamics, *Marine Geology*, *63*(1-4), 331–361. 1, 188, 304

Swift, D. J. P., S. Phillips, and J. A. Thorne (1991), *Sedimentation on continental margins IV: lithofacies and depositional systems*, in *Shelf Sand and Sandstone Bodies - Geometry, Facies and Sequence Stratigraphy*, vol. Special Publication No. 14 of the International Association of Sedimentologists, edited by D. J. P. Swift, G. F. Oertal, R. W. Tillman, and J. A. Thorne, pp. 89–152, Blackwell Scientific Publications, Oxford. 11, 12, 46

Switzer, A. D., C. R. Sloss, B. G. Jones, and C. S. Bristow (2010), Geomorphic evidence for mid-late Holocene higher sea level from southeastern Australia, *Quaternary International*, *221*(1-2), 13–22. 98

Thieler, E. R., O. H. Pilkey, R. S. Young, D. M. Bush, and F. Chai (2000), The use of mathematical models to predict beach behavior for US coastal engineering: A critical review, *Journal of Coastal Research*, *16*(1), 48–70. 16, 207

Thom, B. G. (1960), The coastal geomorphology of the Port Stephens - Myall Lakes region, with particular reference to aeolian action, Ph.D. thesis. 51

Thom, B. G. (1965), Late Quaternary coastal morphology of the Port Stephens - Myall Lakes area, *Journal of the Royal Society of New South Wales*, *98*, 23–36. 47, 51

Thom, B. G. (1978), *Coastal sand deposition in southeast Australia during the Holocene*, in *Landform Evolution in Australasia*, edited by J. L. Davies and M. A. J. Williams, pp. 197–214, Australian National University Press, Canberra. 56, 94

Thom, B. G. (1984), Transgressive and regressive stratigraphies of coastal sand barriers in southeast Australia, *Marine Geology*, *56*(1-4), 137–158. 2, 31, 37, 41, 56, 94, 187, 190

Thom, B. G., and J. Chappell (1975), Holocene sea levels relative to Australia, *Search*, *6*, 90–93. 97

Thom, B. G., and W. Hall (1991), Behavior of beach profiles during accretion and erosion dominated periods, *Earth Surface Processes and Landforms*, *16*(2), 113–127. 144, 151, 270

Thom, B. G., and P. S. Roy (1985), Relative sea levels and coastal sedimentation in southeast Australia in the Holocene, *Journal of Sedimentary Petrology*, *55*, 257–264. 56, 94, 97, 100

Thom, B. G., J. R. Hails, and A. R. H. Martin (1969), Radiocarbon evidence against higher postglacial sea-levels in eastern Australia, *Marine Geology*, *7*, 161–168. 97

Thom, B. G., J. R. Hails, A. R. H. Martin, and C. V. G. Phipps (1972), Postglacial sea levels in eastern Australia - a reply, *Marine Geology*, *12*, 223–242. 97

Thom, B. G., H. A. Polach, and G. M. Bowman (1978), Holocene age structure of coastal sand barriers in New South Wales, Australia, *Tech. rep.*, Department of Geography, Faculty of Military Studies, The University of New South Wales. 51, 55, 58, 59, 65, 94

Thom, B. G., G. M. Bowman, and P. S. Roy (1981a), Late Quaternary evolution of coastal sand barriers, Port Stephens-Myall Lakes Area, central New South Wales, Australia, *Quaternary Research*, *15*(3), 345–364. 2, 31, 47, 50, 51, 52, 54, 94, 187, 189, 195

Thom, B. G., G. M. Bowman, R. Gillespie, R. Temple, and M. Barbetti (1981b), Radiocarbon dating of Holocene beach-ridge sequences in southeast Australia, *Tech. rep.*, University of New South Wales Faculty of Military Studies, Royal Military College, Duntroon, Monograph 11. 56, 57, 58, 59, 62, 63, 64, 65, 94, 124

Thom, B. G., M. Shepherd, C. K. Ly, P. S. Roy, G. M. Bowman, and P. A. Hesp (1992), *Coastal Geomorphology and Quarternary Geology of the Port Stephens-Myall Lakes Area*, Department of Biogeography and Geomorphology, Monograph No. 6, 407 pp., Department of Biogeography and Geomorphology, Monograph No. 6, ANU, Canberra. 51, 189, 196

Thom, B. G., J. B. Keene, P. J. Cowell, and M. Daley (2010), *East Australian marine abrasion surface*, in *Australian Landscapes*, vol. Special Publication 346, edited by P. Bishop and B. Pillans, pp. 57–59, Geological Society, London. 33

Thompson, W. G., and S. L. Goldstein (2006), A radiometric calibration of the SPECMAP timescale, *Quaternary Science Reviews*, *25*(23-24), 3207–3215. 161, 169

Thorne, J. A., and D. J. P. Swift (1991), *Sedimentation on continental margins II: application of the regime concept*, in *Shelf Sand and Sandstone Bodies - Geometry, Facies and Sequence Stratigraphy*, vol. Special Publication No. 14 of the International Association of Sedimentologists, edited by D. J. P. Swift, G. F. Oertal, R. W. Tillman, and J. A. Thorne, pp. 33–58, Blackwell Scientific Publications, Oxford. 11, 13

Tomazelli, L. J., and S. R. Dillenburg (2007), Sedimentary facies and stratigraphy of a last interglacial coastal barrier in south Brazil, *Marine Geology*, *244*(1-4), 33–45. 55

Tortora, P., P. J. Cowell, and K. Adlam (2009a), Transgressive coastal systems (1st part): barrier migration processes and geometric principles, *Journal of Mediterranean Earth Sciences*, *1*, 1–13. 2, 17, 46, 207, 219, 241

Tortora, P., P. J. Cowell, and K. Adlam (2009b), Transgressive coastal systems (2nd part): geometric principles of stratal preservation on gently sloping continental shelves, *Journal of Mediterranean Earth Sciences*, *1*, 15–32. 2, 12, 17, 46, 219, 241

Vousdoukas, M. I., O. Ferreira, L. P. Almeida, and A. Pacheco (2012), Toward reliable storm-hazard forecasts: XBeach calibration and its potential application in an operational early-warning system, *Ocean Dynamics*, *62*(7), 1001–1015. 16

Waelbroeck, C., L. Labeyrie, E. Michel, J. C. Duplessy, J. F. McManus, K. Lambeck, E. Balbon, and M. Labracherie (2002), Sea-level and deep water temperature changes derived from benthic foraminifera isotopic records, *Quaternary Science Reviews*, *21*(1-3), 295–305. 161, 167, 168, 169, 170, 171, 273, 280

Walker, M. J. C. (2005), *Quaternary Dating Methods*, 286 pp., John Wiley and Sons Ltd., West Sussex. 162

Walsh, I. L., and P. S. Roy (1983), Late Quaternary geology and coastal evolution near Yamba, north coast of NSW, *Tech. rep.*, Geological Survey of New South Wales, Department of Mineral Resources. 50

Ward, W. T., and I. P. Little (1975), Times of coastal sand accumulation in southeast Queensland, *Ecological Society of Australia, Proceedings*, *9*, 313–317. 50

Wehmiller, J. F., K. R. Simmons, H. Cheng, R. Lawrence Edwards, J. Martin-McNaughton, L. L. York, D. E. Krantz, and C.-C. Shen (2004), Uranium-series coral ages from the US Atlantic Coastal Plainthe "80 ka problem revisited, *Quaternary International*, *120*(1), 3–14. 162

Wolinsky, M. A. (2009), A unifying framework for shoreline migration: 1. Multiscale shoreline evolution on sedimentary coasts, *Journal of Geophysical Research-Earth Surface*, *114*. 4, 16, 17, 18, 19, 106, 112, 219, 243, 244

Wolinsky, M. A., and A. B. Murray (2009), A unifying framework for shoreline migration: 2. Application to wave-dominated coasts, *Journal of Geophysical Research-Earth Surface*, *114*. 2, 17, 243, 285

Woodroffe, C. D., and C. V. Murray-Wallace (2012), Sea-level rise and coastal change: the past as a guide to the future, *Quaternary Science Reviews*, *54*(0), 4–11. 4, 252

Wright, L. D. (1995), *Morphodynamics of Inner Continental Shelves*, 256 pp., CRC Press, Boca Raton, Florida. 3, 10, 93, 101, 210

Wright, L. D., and B. G. Thom (1977), Coastal depositional landforms: A morphodynamic approach, *Progress in Physical Geography*, *1*, 412–459. 1, 13, 210

Yokoyama, Y., K. Lambeck, P. De Deckker, P. Johnston, and L. K. Fifield (2000), Timing of the Last Glacial Maximum from observed sea-level minima, *Nature*, *406*(6797), 713–716. 161

Yokoyama, Y., P. De Deckker, K. Lambeck, P. Johnston, and L. K. Fifield (2001), Sea-level at the Last Glacial Maximum: evidence from northwestern Australia to constrain ice volumes for oxygen isotope stage 2, *Palaeogeography Palaeoclimatology Palaeoecology*, *165*(3-4), 281–297. 161

Appendix A

BARSIM Model Configurations

Table A.1: BARSIM model configurations for Moruya and Tuncurry - Standard configurations for BARSIM models applied to the Moruya and Tuncurry sites, based on calibrated models described in Section 3.3.1.

BARSIM Parameter	Moruya	Tuncurry
Number of grid cells	290	449
Grid cell width	100	100
Total simulation time	6000	6000
Minimum time step	0.5	0.5
Equilibrium runs	0	0
Storm wave threshold	2.5	2.5
Phase	1.5	1.5
Wavelength	10000	10000
Amplitude	0	0
Significant wave height	1.59	1.59
Standard deviation	0.4705	0.4705
Significant wave period	7.98	7.98
Standard deviation	0.5307	0.5307
Grain-size class 1	125	125
Grain-size class 2	177	177
Grain-size class 3	250	250
Grain-size class 4	354	354
Number of classes	4	4
Initial fraction 1	0.2	0.2
Initial fraction 2	0.2	0.2
Initial fraction 3	0.4	0.4
Initial fraction 4	0.2	0.2
Sea level rise fraction 1	0.2	0.2
Sea level rise fraction 2	0.2	0.2
Sea level rise fraction 3	0.4	0.4
Sea level rise fraction 4	0.2	0.2
Sea level fall fraction 1	0.2	0.2
Sea level fall fraction 2	0.2	0.2
Sea level fall fraction 3	0.4	0.4
Sea level fall fraction 4	0.2	0.2
Maximum height shoreline	3	3
Maximum height backbarrier side	4	4
Height restriction parameter shoreface	4	4
Height restriction parameter backbarrier	4	4
Fraction available for washover	0.25	0.25
Maximum island width	400	400
Tide amplitude	2	2
Fraction sand transported to tidal basin	0.1	0.1
Minimum tidal basin accumulation	20	20
Sediment erodibility factor	0.1	0.1
Erodibility substrate	1	1
Eevent erosion scaling wave height	1	1
Event erosion scaling shoreline-wavebase	2.7	4.5
Sediment travel distance corr. shoreface	1	1
Sediment travel distance corr. washover	0.1	0.1
Sediment travel distance corr. event	1.5	1.5

Appendix B

Holocene Relative Sea-Level Fall Simulation Outputs

B. HOLOCENE RELATIVE SEA-LEVEL FALL SIMULATION OUTPUTS

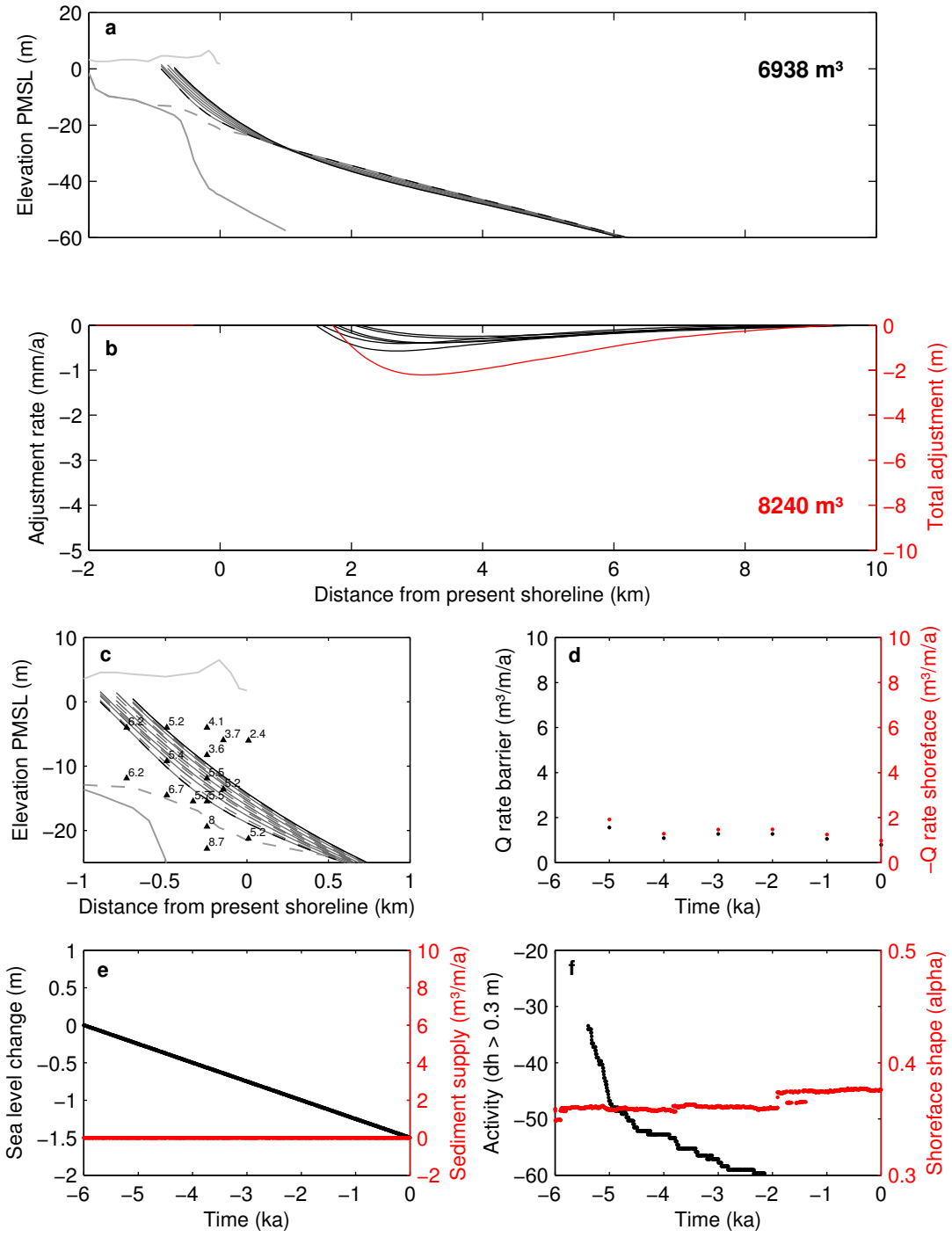

Figure B.1: MR-HL1 simulation experiment, see Table 3.1 - (a) Barrier & shoreface evolution at millennia-average increments & total barrier progradation volume; (b) millennia-average rates of depth-dependent shoreface lowering (black), total shoreface adjustment (red) & total shoreface erosion volume; (c) simulated evolution at 1-ka (solid) & 0.5-ka (dashed) increments with respect to C^{14} ages; (d) millennia-average rates of barrier deposition (black) & shoreface erosion (red); (e) sea level change & external sediment supply scenarios; (f) fixed-magnitude depth limit of shoreface activity (black) & dimensionless shoreface shape (red).

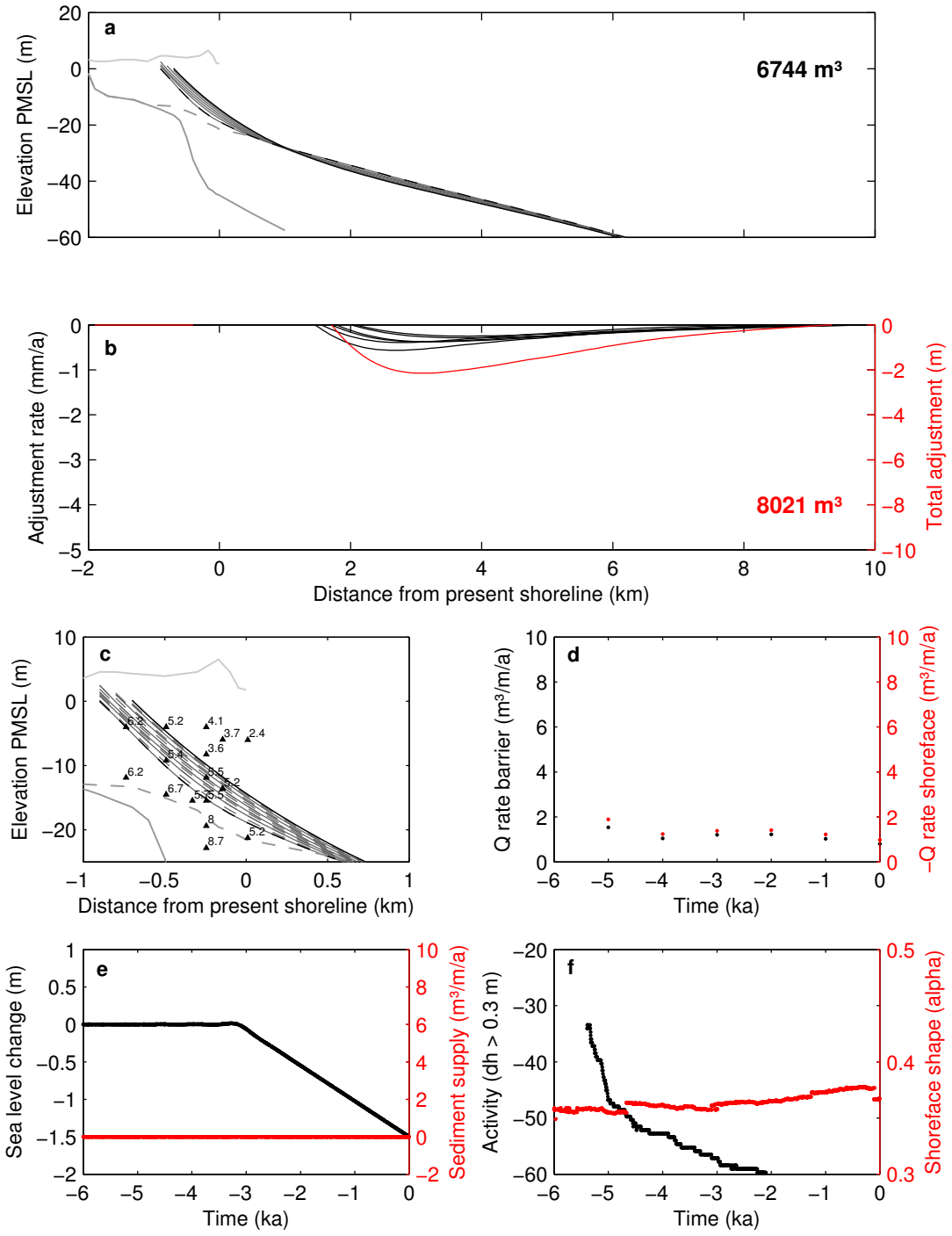

Figure B.2: MR-HL2 simulation experiment, see Table 3.1 - (a) Barrier & shoreface evolution at millennia-average increments & total barrier progradation volume; (b) millennia-average rates of depth-dependent shoreface lowering (black), total shoreface adjustment (red) & total shoreface erosion volume; (c) simulated evolution at 1-ka (solid) & 0.5-ka (dashed) increments with respect to C^{14} ages; (d) millennia-average rates of barrier deposition (black) & shoreface erosion (red); (e) sea level change & external sediment supply scenarios; (f) fixed-magnitude depth limit of shoreface activity (black) & dimensionless shoreface shape (red).

B. HOLOCENE RELATIVE SEA-LEVEL FALL SIMULATION OUTPUTS

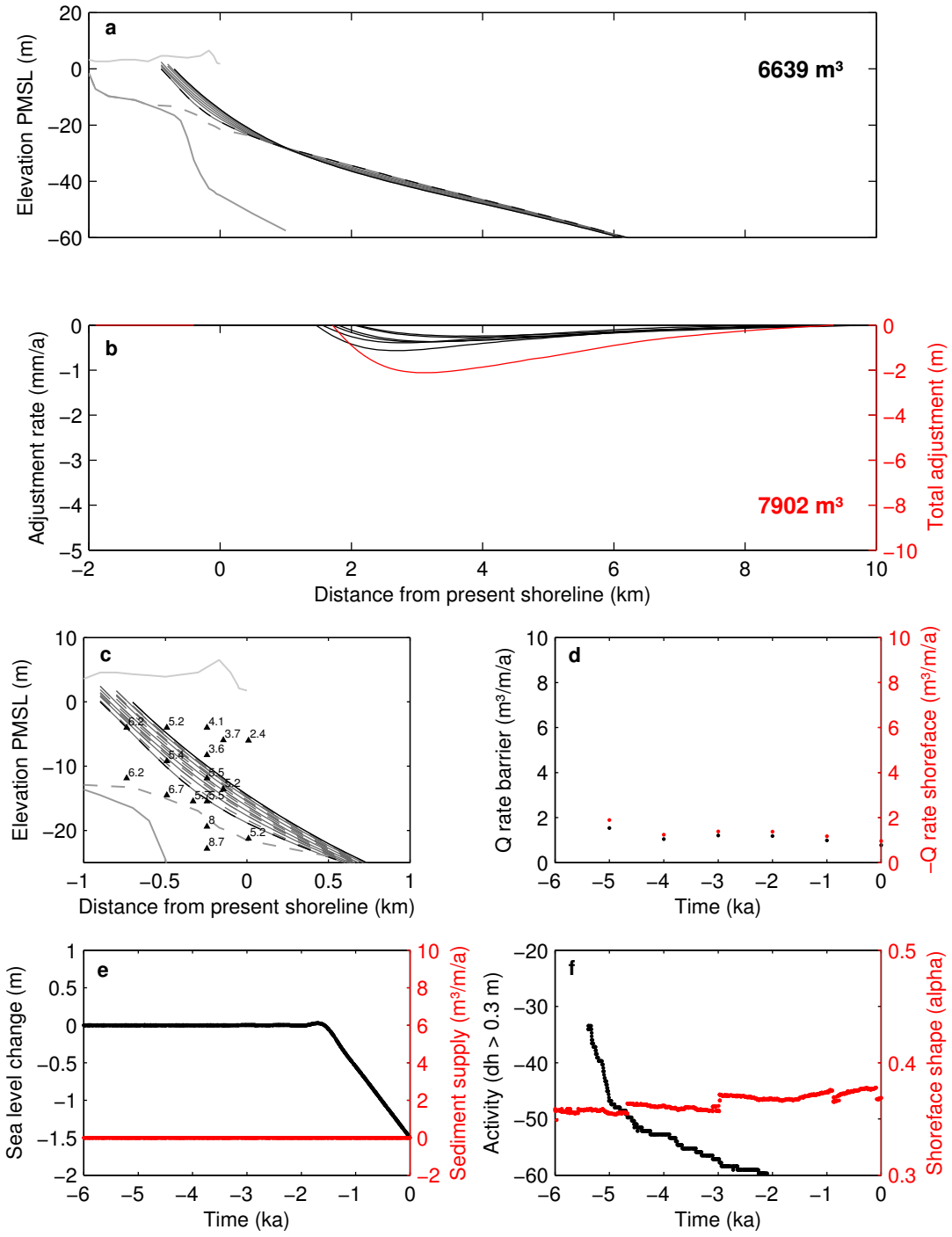

Figure B.3: MR-HL3 simulation experiment, see Table 3.1 - (a) Barrier & shoreface evolution at millennia-average increments & total barrier progradation volume; (b) millennia-average rates of depth-dependent shoreface lowering (black), total shoreface adjustment (red) & total shoreface erosion volume; (c) simulated evolution at 1-ka (solid) & 0.5-ka (dashed) increments with respect to C^{14} ages; (d) millennia-average rates of barrier deposition (black) & shoreface erosion (red); (e) sea level change & external sediment supply scenarios; (f) fixed-magnitude depth limit of shoreface activity (black) & dimensionless shoreface shape (red).

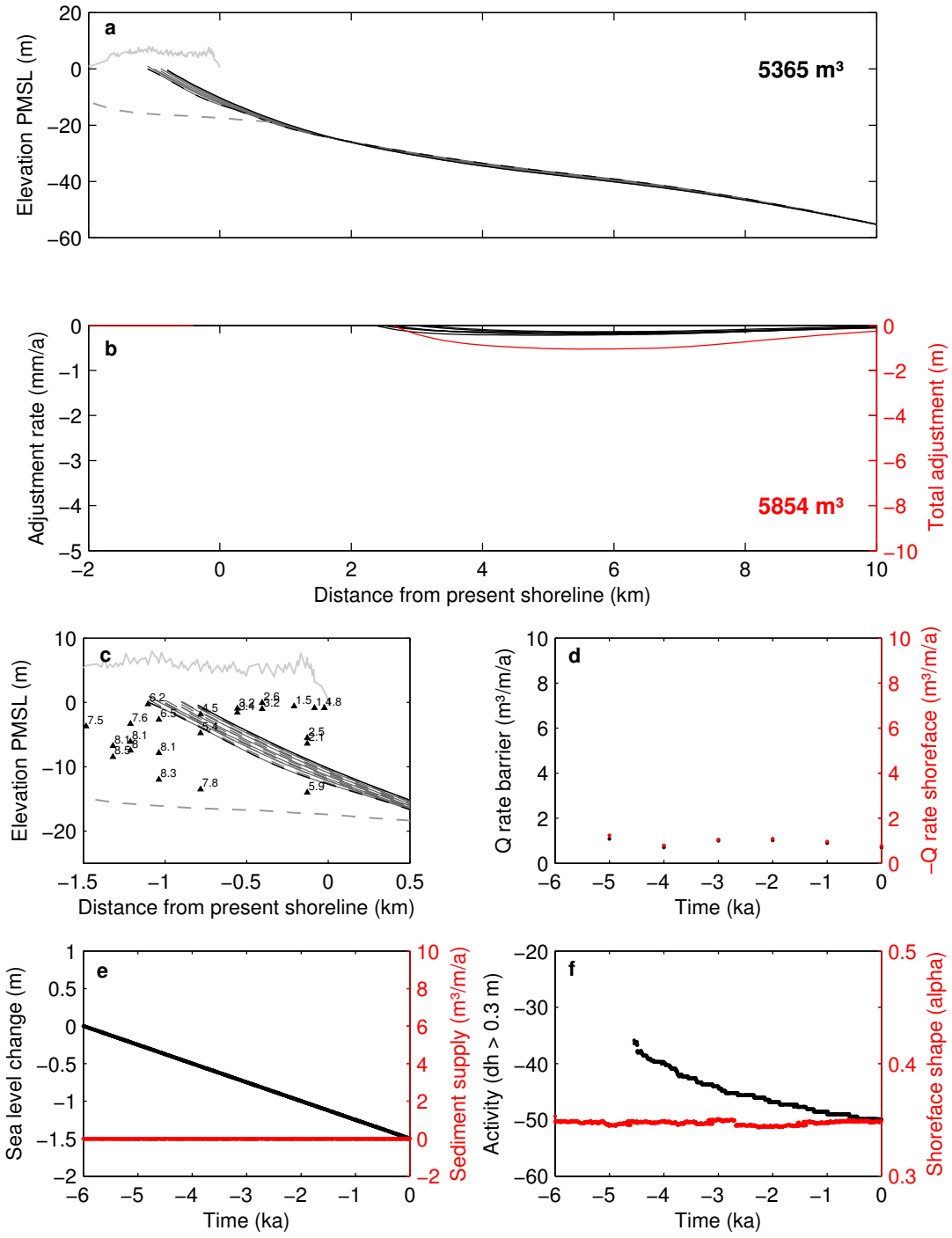

Figure B.4: TC-HL1 simulation experiment, see Table 3.1 - (a) Barrier & shoreface evolution at millennia-average increments & total barrier progradation volume; (b) millennia-average rates of depth-dependent shoreface lowering (black), total shoreface adjustment (red) & total shoreface erosion volume; (c) simulated evolution at 1-ka (solid) & 0.5-ka (dashed) increments with respect to C^{14} ages; (d) millennia-average rates of barrier deposition (black) & shoreface erosion (red); (e) sea level change & external sediment supply scenarios; (f) fixed-magnitude depth limit of shoreface activity (black) & dimensionless shoreface shape (red).

B. HOLOCENE RELATIVE SEA-LEVEL FALL SIMULATION OUTPUTS

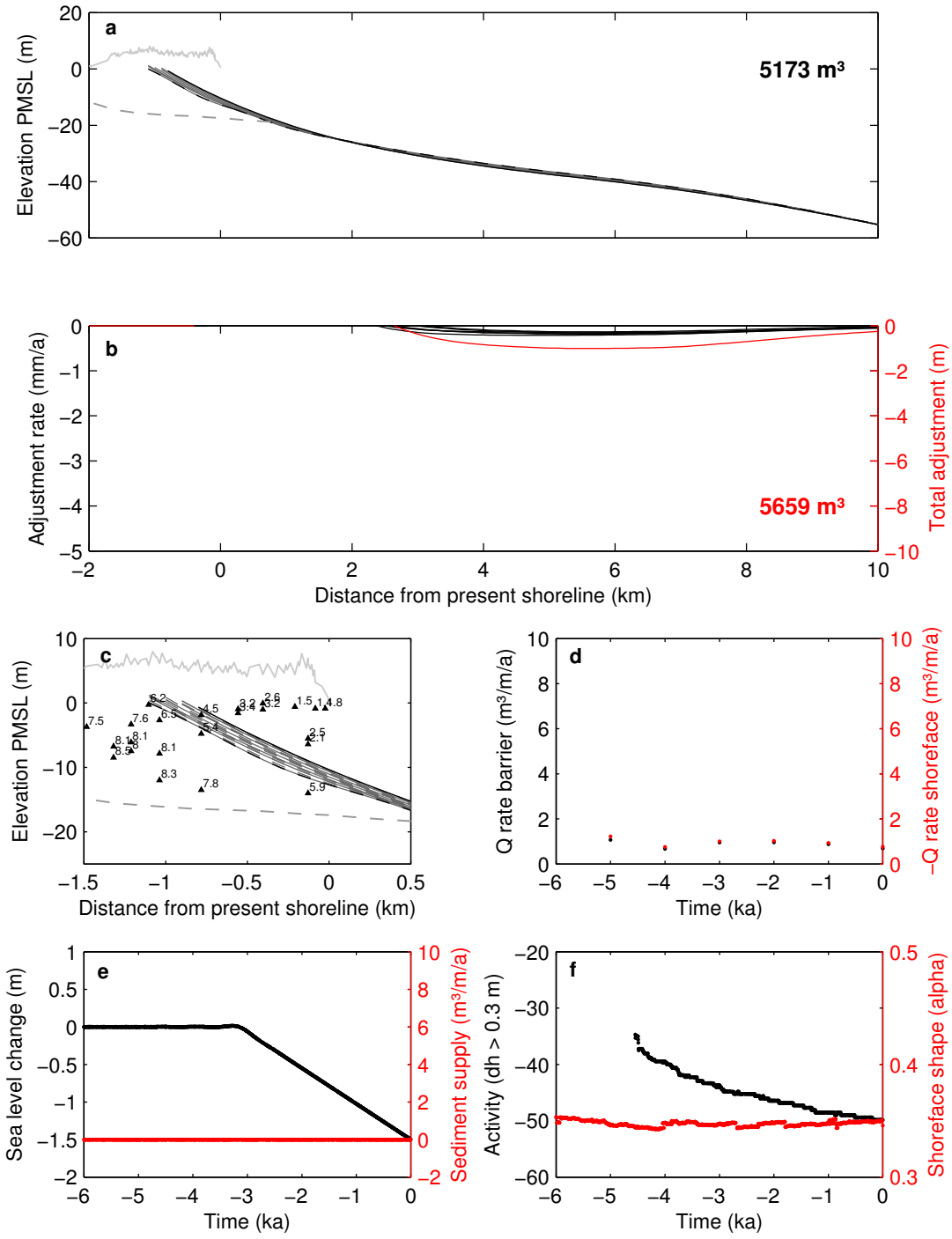

Figure B.5: TC-HL2 simulation experiment, see Table 3.1 - (a) Barrier & shoreface evolution at millennia-average increments & total barrier progradation volume; (b) millennia-average rates of depth-dependent shoreface lowering (black), total shoreface adjustment (red) & total shoreface erosion volume; (c) simulated evolution at 1-ka (solid) & 0.5-ka (dashed) increments with respect to C^{14} ages; (d) millennia-average rates of barrier deposition (black) & shoreface erosion (red); (e) sea level change & external sediment supply scenarios; (f) fixed-magnitude depth limit of shoreface activity (black) & dimensionless shoreface shape (red).

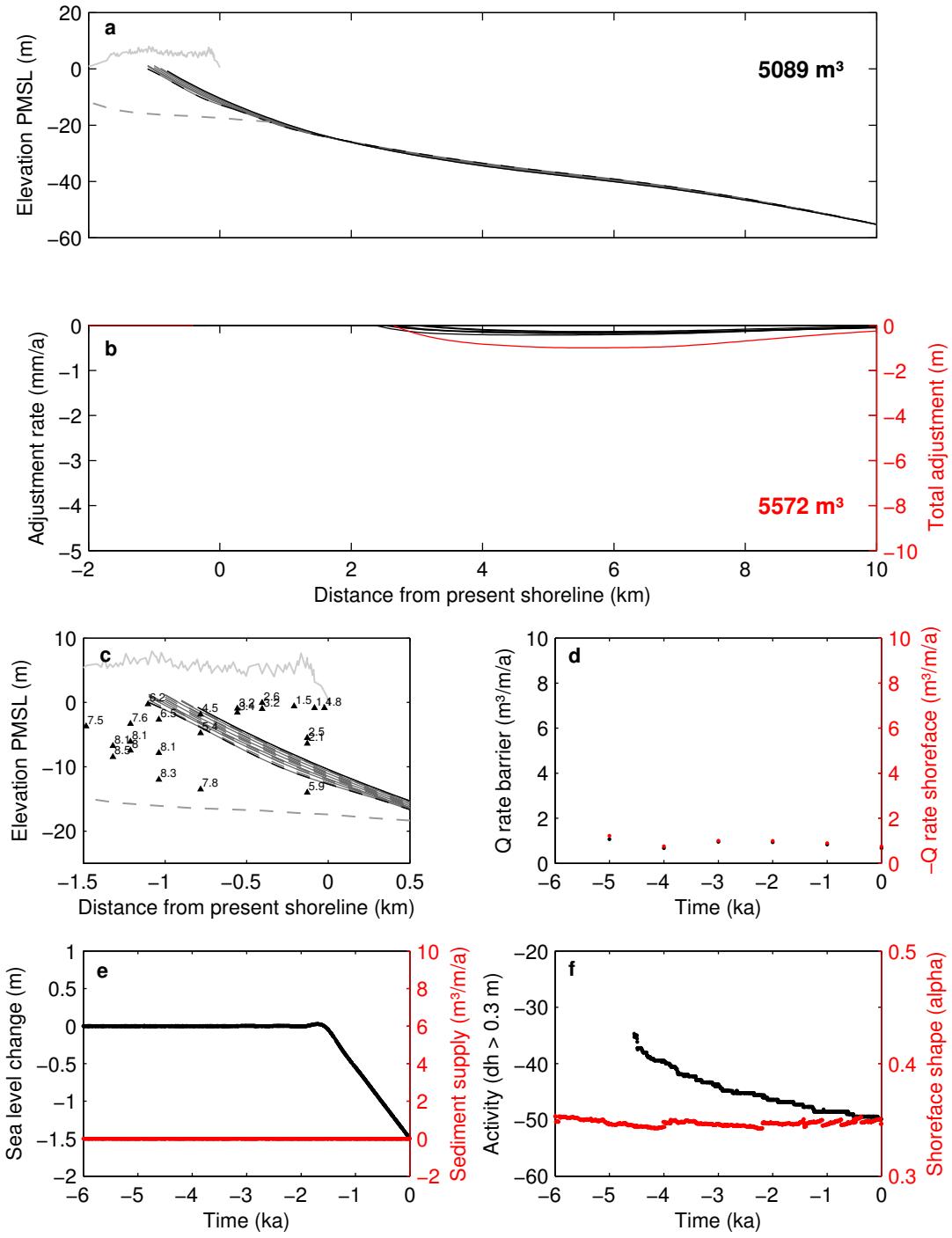

Figure B.6: TC-HL3 simulation experiment, see Table 3.1 - (a) Barrier & shoreface evolution at millennia-average increments & total barrier progradation volume; (b) millennia-average rates of depth-dependent shoreface lowering (black), total shoreface adjustment (red) & total shoreface erosion volume; (c) simulated evolution at 1-ka (solid) & 0.5-ka (dashed) increments with respect to C^{14} ages; (d) millennia-average rates of barrier deposition (black) & shoreface erosion (red); (e) sea level change & external sediment supply scenarios; (f) fixed-magnitude depth limit of shoreface activity (black) & dimensionless shoreface shape (red).

B. HOLOCENE RELATIVE SEA-LEVEL FALL SIMULATION OUTPUTS

Appendix C

Holocene Combined Forcing Simulation Outputs

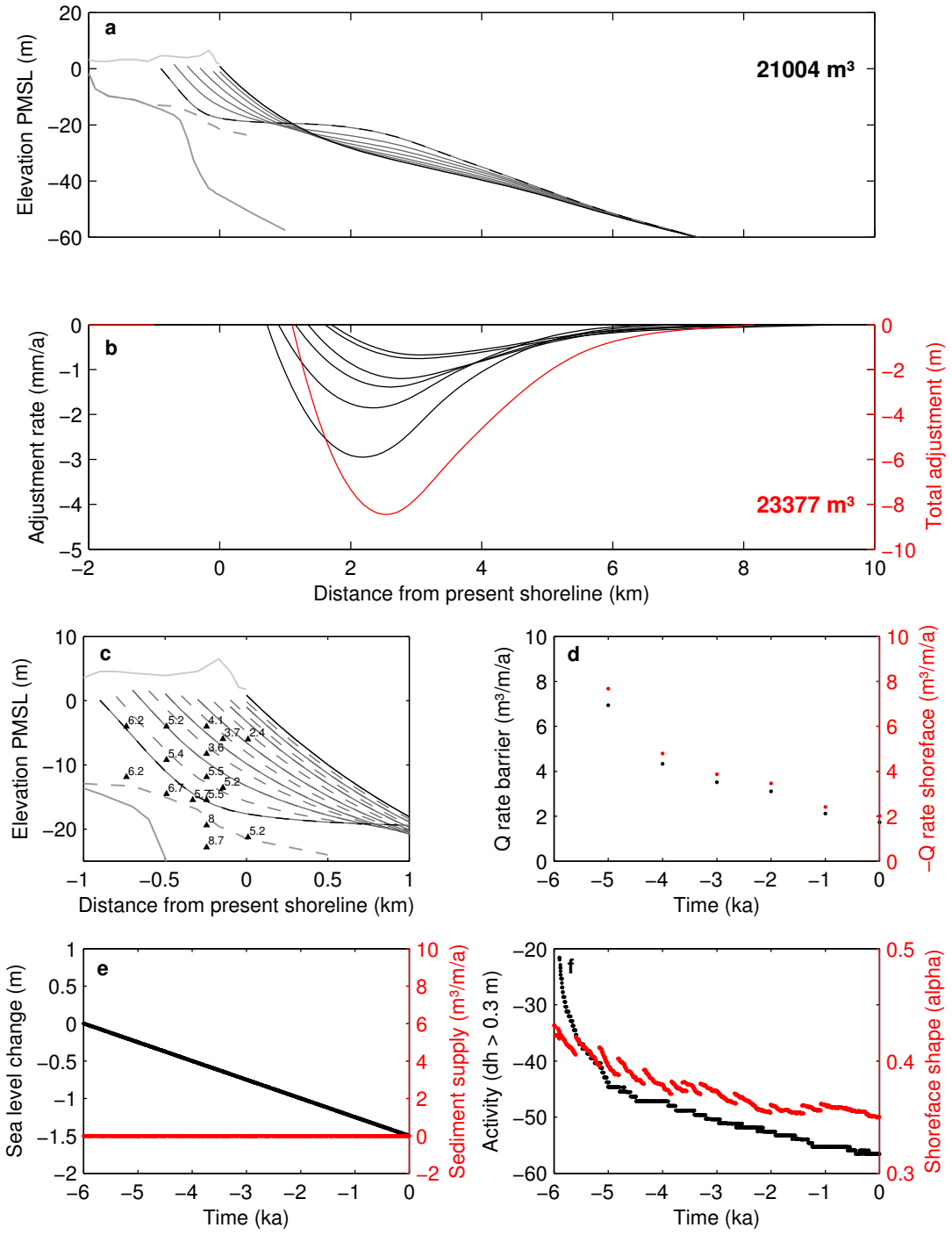

Figure C.1: MR-HL1-DS simulation experiment, see Table 3.1 - (a) Barrier & shoreface evolution at millennia-average increments & total barrier progradation volume; (b) millennia-average rates of depth-dependent shoreface lowering (black), total shoreface adjustment (red) & total shoreface erosion volume; (c) simulated evolution at 1-ka (solid) & 0.5-ka (dashed) increments with respect to C^{14} ages; (d) millennia-average rates of barrier deposition (black) & shoreface erosion (red); (e) sea level change & external sediment supply scenarios; (f) fixed-magnitude depth limit of shoreface activity (black) & dimensionless shoreface shape (red).

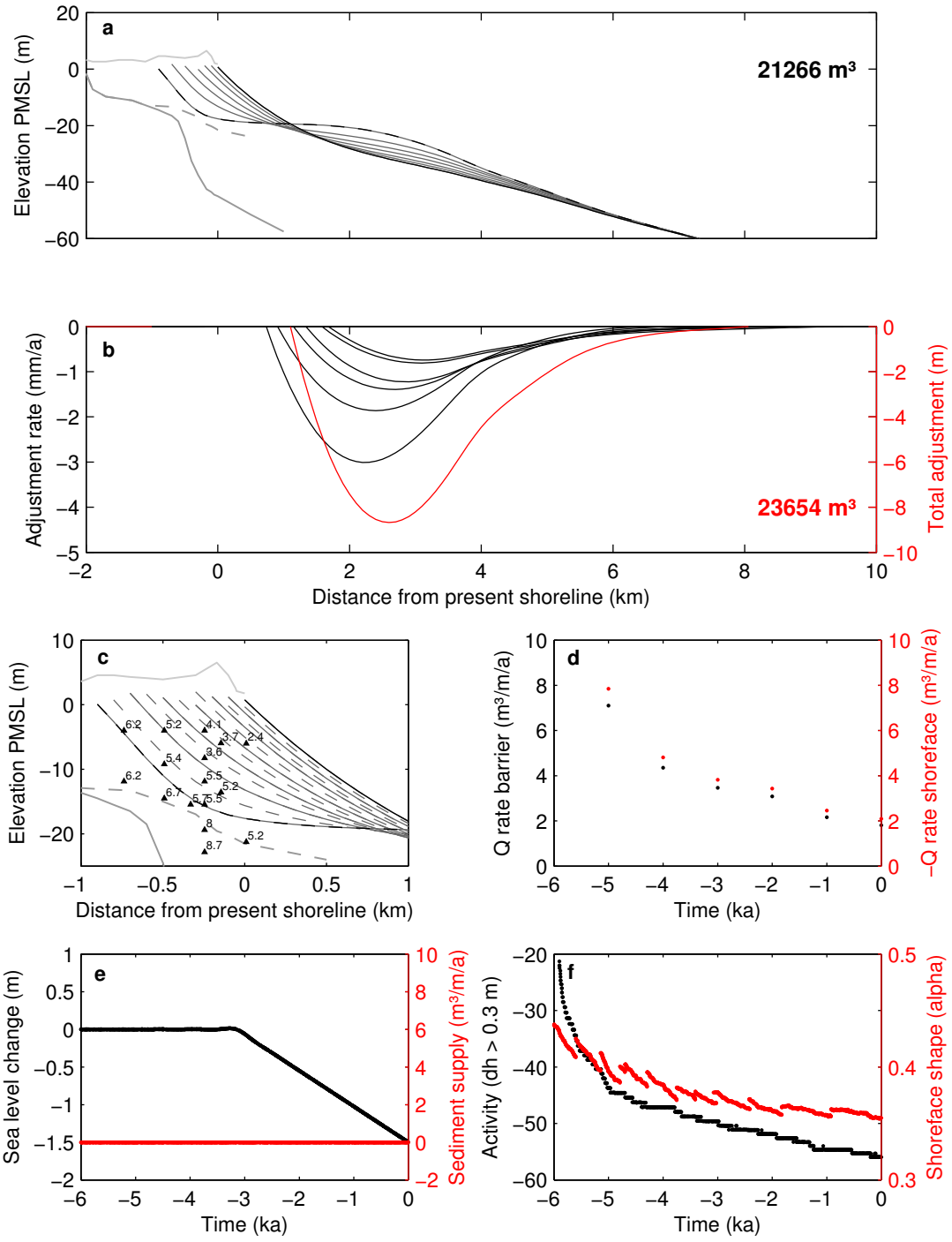

Figure C.2: MR-HL2-DS simulation experiment, see Table 3.1 - (a) Barrier & shoreface evolution at millennia-average increments & total barrier progradation volume; (b) millennia-average rates of depth-dependent shoreface lowering (black), total shoreface adjustment (red) & total shoreface erosion volume; (c) simulated evolution at 1-ka (solid) & 0.5-ka (dashed) increments with respect to C^{14} ages; (d) millennia-average rates of barrier deposition (black) & shoreface erosion (red); (e) sea level change & external sediment supply scenarios; (f) fixed-magnitude depth limit of shoreface activity (black) & dimensionless shoreface shape (red).

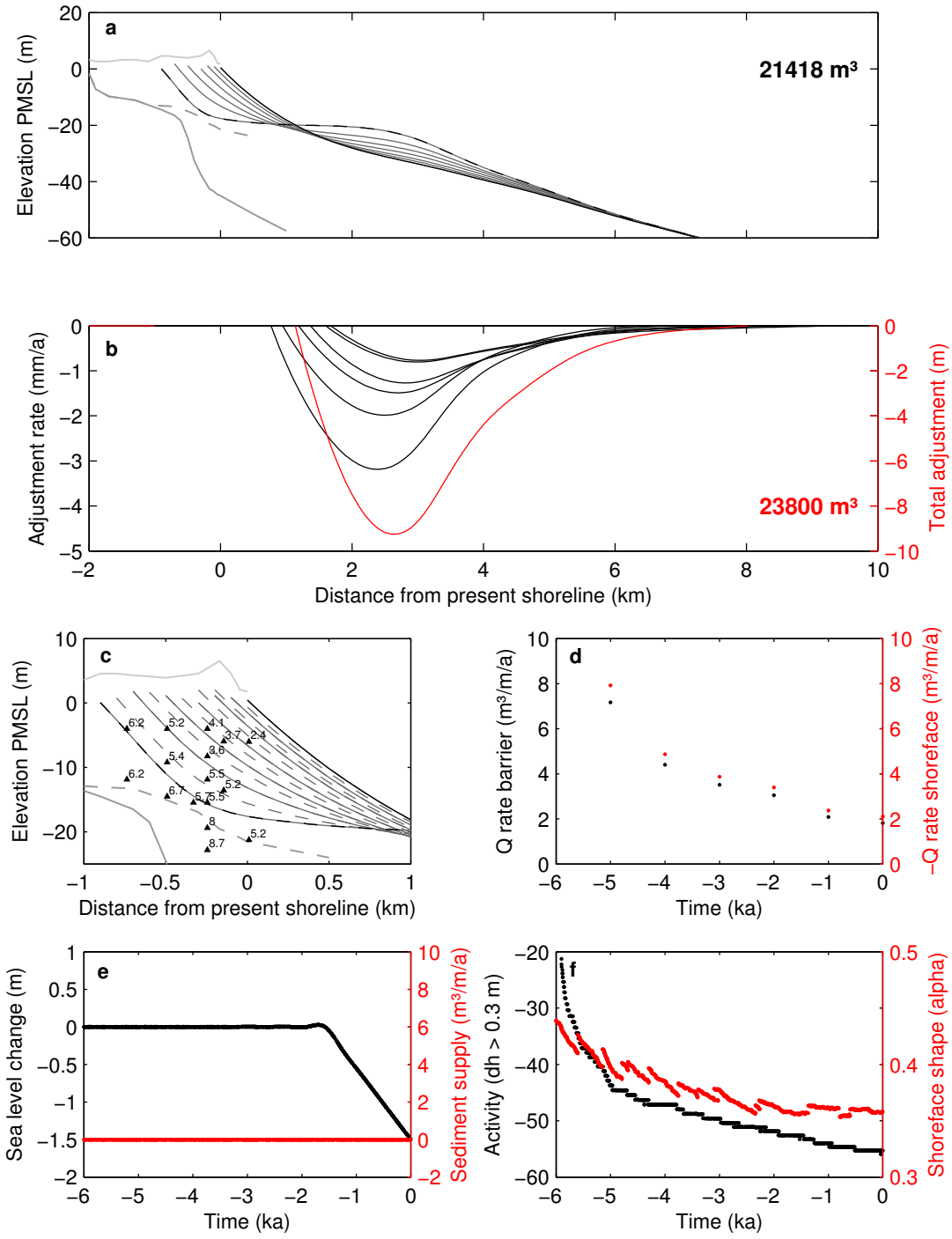

Figure C.3: MR-HL3-DS simulation experiment, see Table 3.1 - (a) Barrier & shoreface evolution at millennia-average increments & total barrier progradation volume; (b) millennia-average rates of depth-dependent shoreface lowering (black), total shoreface adjustment (red) & total shoreface erosion volume; (c) simulated evolution at 1-ka (solid) & 0.5-ka (dashed) increments with respect to C^{14} ages; (d) millennia-average rates of barrier deposition (black) & shoreface erosion (red); (e) sea level change & external sediment supply scenarios; (f) fixed-magnitude depth limit of shoreface activity (black) & dimensionless shoreface shape (red).

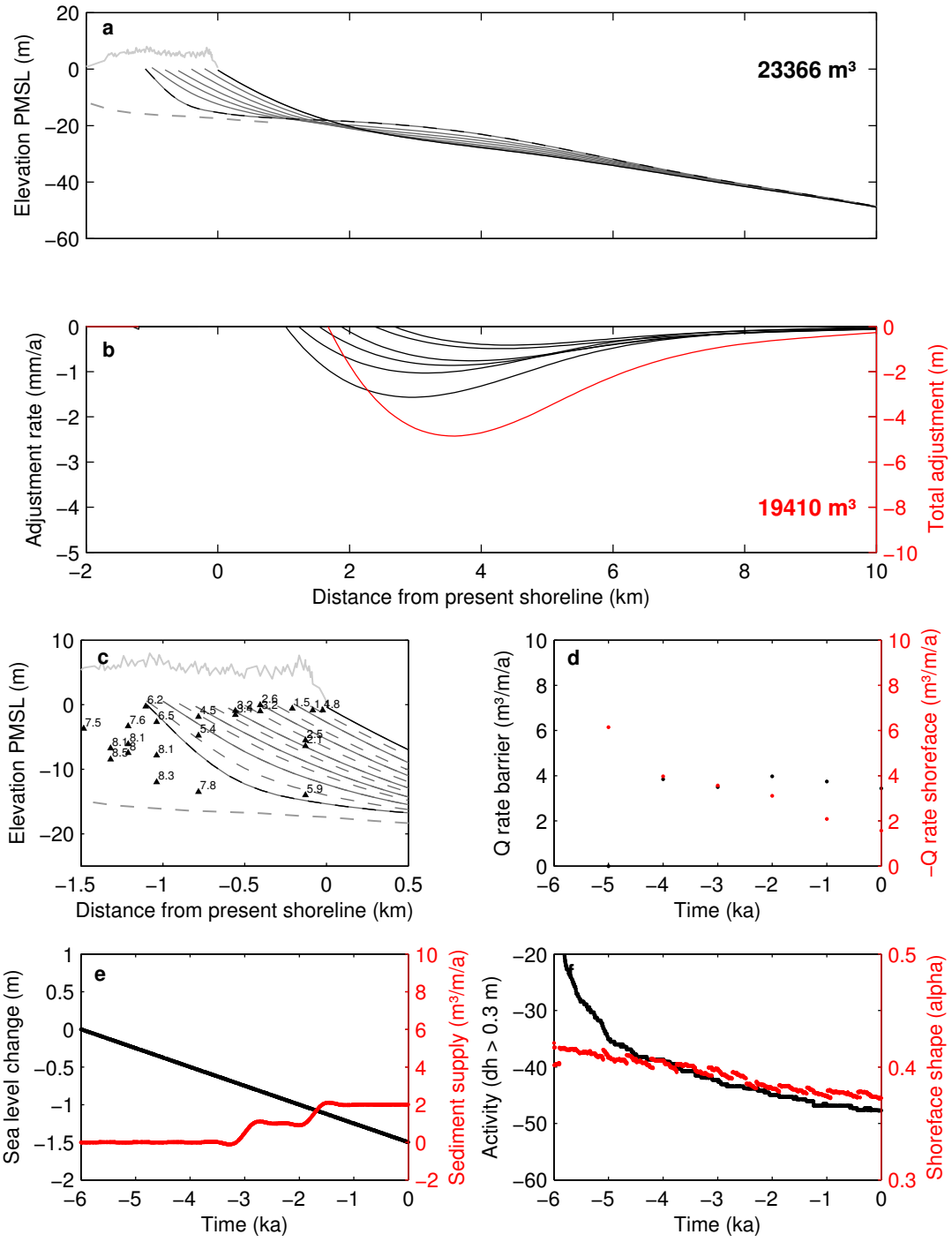

Figure C.4: TC-HL1-DS-Q2 simulation experiment, see Table 3.1 - (a) Barrier & shoreface evolution at millennia-average increments & total barrier progradation volume; (b) millennia-average rates of depth-dependent shoreface lowering (black), total shoreface adjustment (red) & total shoreface erosion volume; (c) simulated evolution at 1-ka (solid) & 0.5-ka (dashed) increments with respect to C^{14} ages; (d) millennia-average rates of barrier deposition (black) & shoreface erosion (red); (e) sea level change & external sediment supply scenarios; (f) fixed-magnitude depth limit of shoreface activity (black) & dimensionless shoreface shape (red).

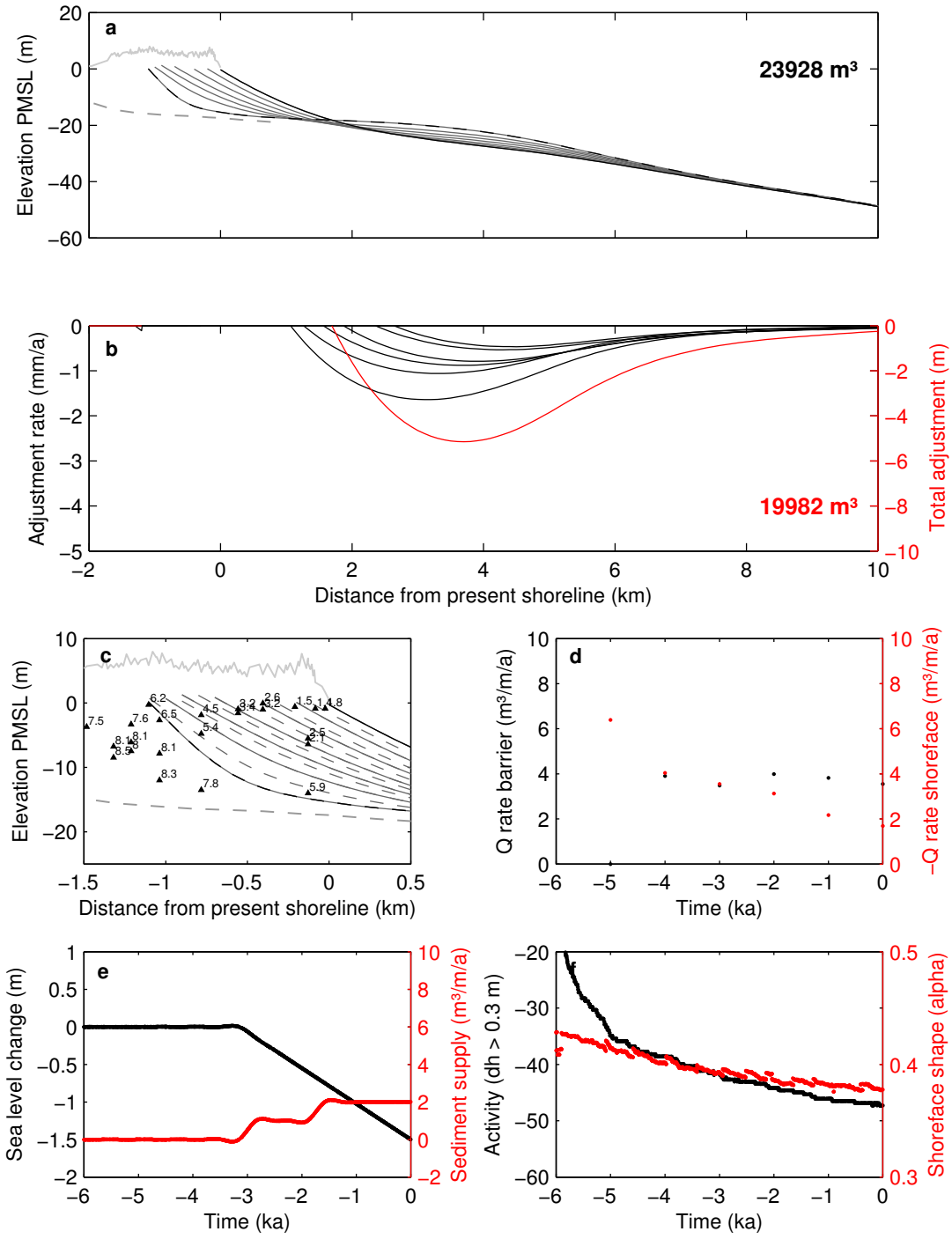

Figure C.5: TC-HL2-DS-Q2 simulation experiment, see Table 3.1 - (a) Barrier & shoreface evolution at millennia-average increments & total barrier progradation volume; (b) millennia-average rates of depth-dependent shoreface lowering (black), total shoreface adjustment (red) & total shoreface erosion volume; (c) simulated evolution at 1-ka (solid) & 0.5-ka (dashed) increments with respect to C^{14} ages; (d) millennia-average rates of barrier deposition (black) & shoreface erosion (red); (e) sea level change & external sediment supply scenarios; (f) fixed-magnitude depth limit of shoreface activity (black) & dimensionless shoreface shape (red).

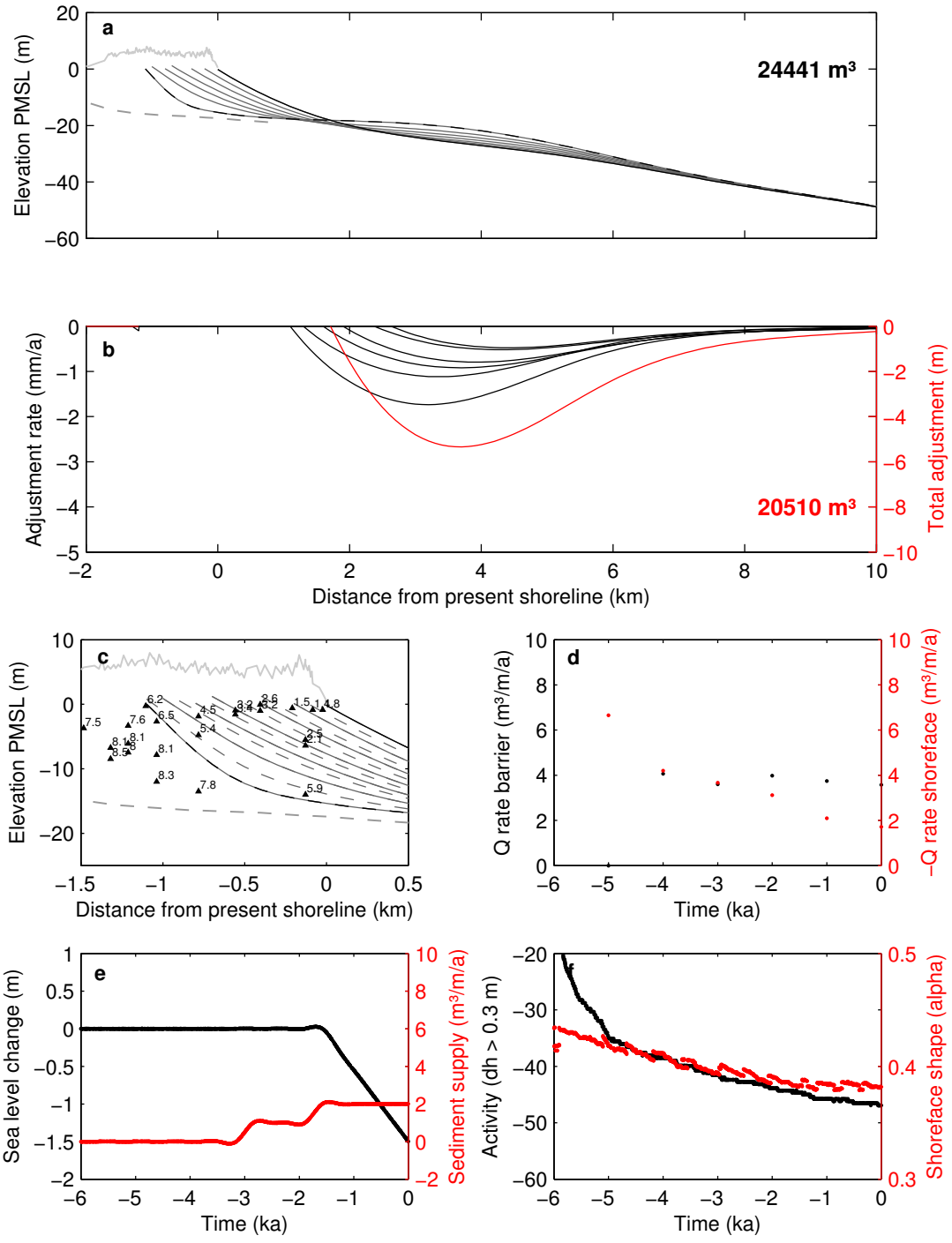

Figure C.6: TC-HL3-DS-Q2 simulation experiment, see Table 3.1 - (a) Barrier & shoreface evolution at millennia-average increments & total barrier progradation volume; (b) millennia-average rates of depth-dependent shoreface lowering (black), total shoreface adjustment (red) & total shoreface erosion volume; (c) simulated evolution at 1-ka (solid) & 0.5-ka (dashed) increments with respect to C^{14} ages; (d) millennia-average rates of barrier deposition (black) & shoreface erosion (red); (e) sea level change & external sediment supply scenarios; (f) fixed-magnitude depth limit of shoreface activity (black) & dimensionless shoreface shape (red).

Appendix D

Highstand Barrier Deposition at Forster-Tuncurry

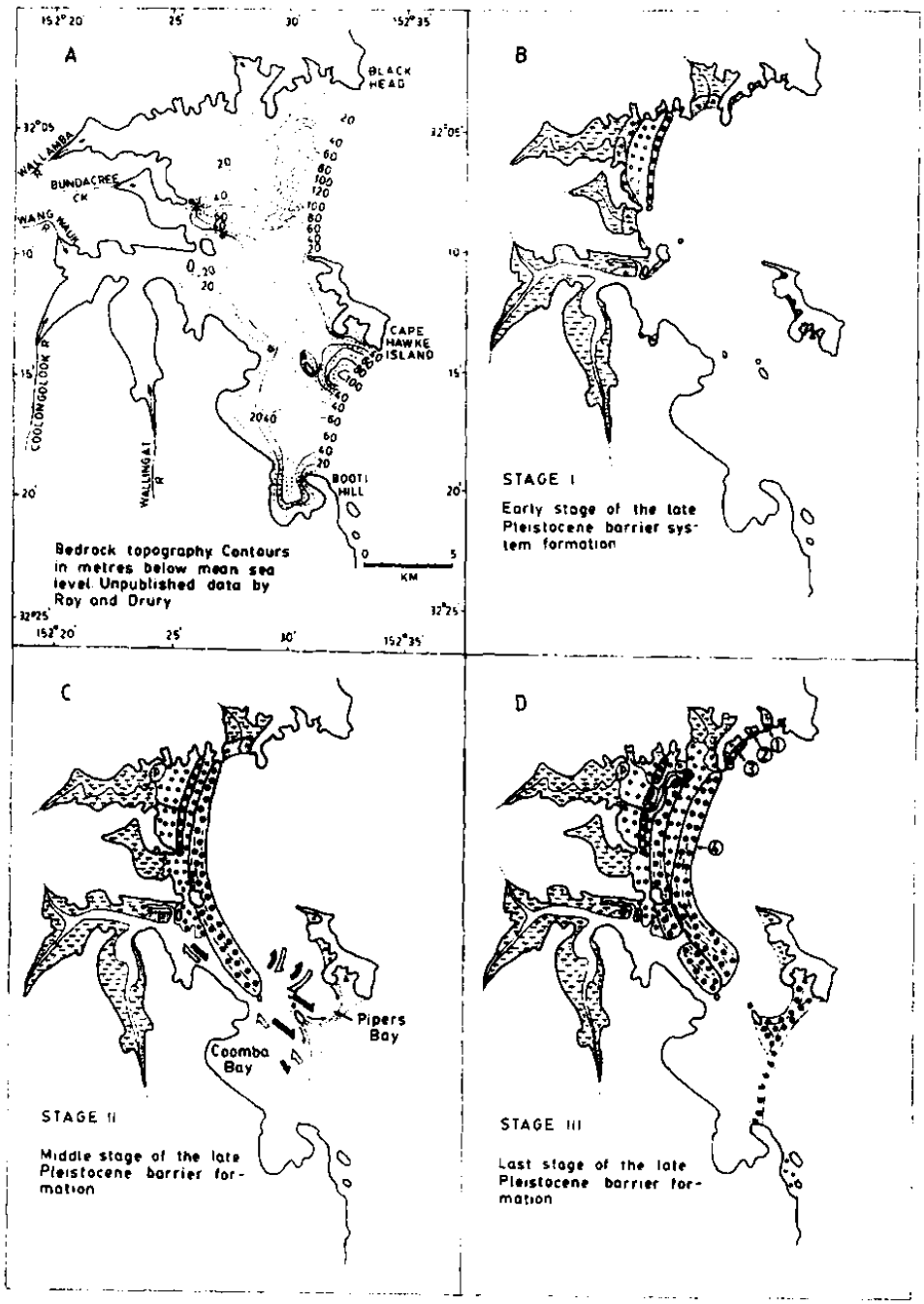

Figure D.1: Highstand barrier deposition at Forster-Tuncurry: Stages 1-3 - Evolutionary reconstruction of highstand coastal barrier deposition at Forster-Tuncurry, from *Melville* [1984].

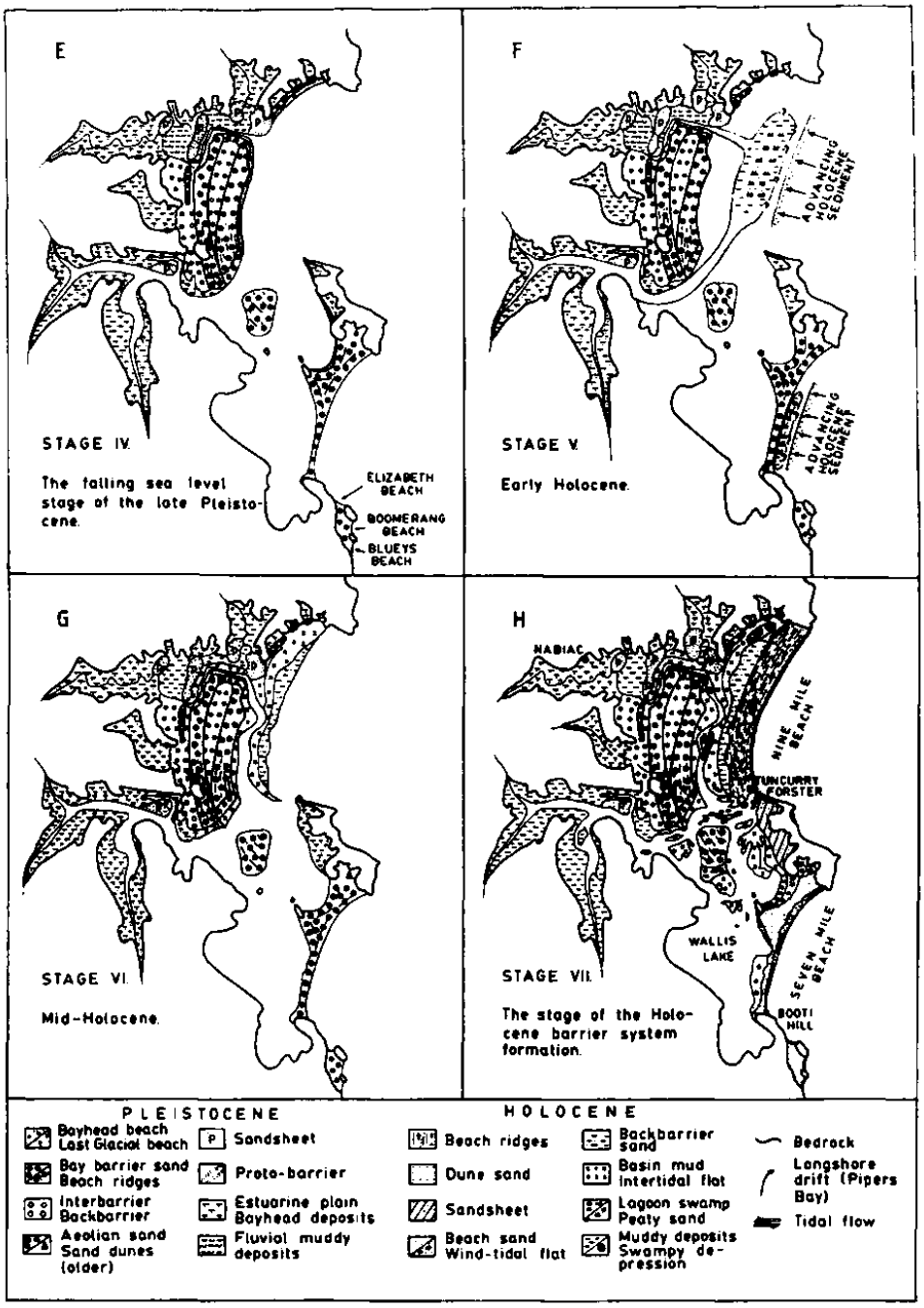

Figure D.2: Highstand barrier deposition at Forster-Tuncurry: Stages 4-7 - Evolutionary reconstruction of highstand coastal barrier deposition at Forster-Tuncurry, from *Melville* [1984].